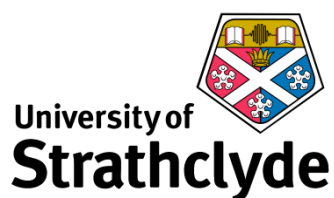


Synthesis and Biological Evaluation of Novel Small Molecule Bromodomain Inhibitors

Kayleigh Stafford



Department of Pure & Applied Chemistry, University of Strathclyde, 295 Cathedral Street, Glasgow G1 1XL

GSK Medicines Research Centre, Gunnels Wood Road, Stevenage, Hertfordshire, SG1 2NY

This thesis is the result of the author's original research. It has been composed by the author and has not been previously submitted for examination which has led to the award of a degree.

The copyright of this thesis belongs to GSK in accordance with the author's contract of employment with GSK under the terms of the United Kingdom Copyrights Acts. Due acknowledgment must always be made of the use of any material contained in, or derived from, this thesis.

Signed: Kayleigh Stafford

Date: 11th January 2019

The human biological samples were sourced ethically and their research use was in accord with the terms of the informed consents under an IRB/EC approved protocol.

All animal studies discussed within this thesis were ethically reviewed and carried out in accordance with Animals (Scientific Procedures) Act 1986 and the GSK Policy on the Care, Welfare and Treatment of Animals.

Acknowledgments

The preparation of this thesis would not have been possible without the support I have had throughout my PhD studies. First and foremost, I would like to extend my biggest thanks to my supervisors Dr Gemma Liwicki and Professor Glenn Burley, as well as Dr Jack Brown who began the journey with me. As well as this, I'd also like to thank Professor William Kerr and Professor Harry Kelly for all their hard work in putting the PhD programme together and for giving me the opportunity to take part in it.

As my industrial supervisor, I am grateful for Gemma's close supervision and guidance. I appreciate all the time given for proof-reading, as well as support when presenting my work. Throughout the PhD, she has continued to push me beyond my comfort zone which has enabled huge personal developments for which I will always be grateful.

I also extend my gratitude to Glenn, as my academic supervisor, for the advice and discussions throughout my PhD. Additionally, I am thankful for his meticulous proof reading of my key reports and final thesis.

I must also thank the ESM-iBET team who have been supportive throughout my PhD, as well as Katherine Jones who, as my line manager, has also been a great support. Furthermore, I am thankful to Laurence Morris-Moody, Juanjo Cabezas Giménez and Ross Thomas for a selection of preparative inputs.

Finally, many thanks go to my husband, Lee. His incredible, continuous support made the difficult times easier and I will be eternally thankful.

Abstract

Epigenetics is the study of changes in gene expression without changing the primary DNA sequence. Bromodomain-containing proteins are responsible for recognising acetylated residues on histone tails, recruiting transcriptional machinery and thus facilitating gene transcription. Small molecule bromodomain inhibitors prevent this recognition, thus downregulating the transcription of pro-inflammatory cytokines which could have therapeutic effects in immuno-inflammatory diseases such as RA.

A targeted approach, in which a drug is delivered selectively to target cell types associated with the disease, could minimise off-target toxicity and improve a therapeutic index. This thesis focuses on the development of an esterase sensitive motif (ESM) targeting strategy, which is selectively hydrolysed by the enzyme human carboxyesterase 1 (CES-1) to produce the biologically-active acid. Outside of the liver, this enzyme's expression profile is limited to the mononuclear monocyte and macrophage lineages, therefore providing the opportunity to treat immuno-inflammation diseases.

The investigation of two structurally differentiated series is described within this thesis. The starting point compound in the first series, in which the ESM is directed over a lipophilic groove formed by a tryptophan, proline and phenylalanine (termed the WPF shelf) suffered from high *in vitro* clearance (IVC) and lipophilicity. Replacement of the phenyl ring, which interacts with the WPF shelf, with five-membered heterocyclic rings was shown to be suboptimal resulting in reduced potency and poor metabolic stability (Figure 0.1). However, substitution of the six-membered ring and increasing the steric hindrance of the pyridyl core resulted in compounds with low microsomal and hepatocyte clearance (Figure 0.1). A lead molecule was identified from this series with improved physicochemical properties, and desirable potency and metabolic stability. The compound showed high selectivity for the BET family over non-BET bromodomain-containing proteins and off-targets and were shown to be substrates for CES-1.

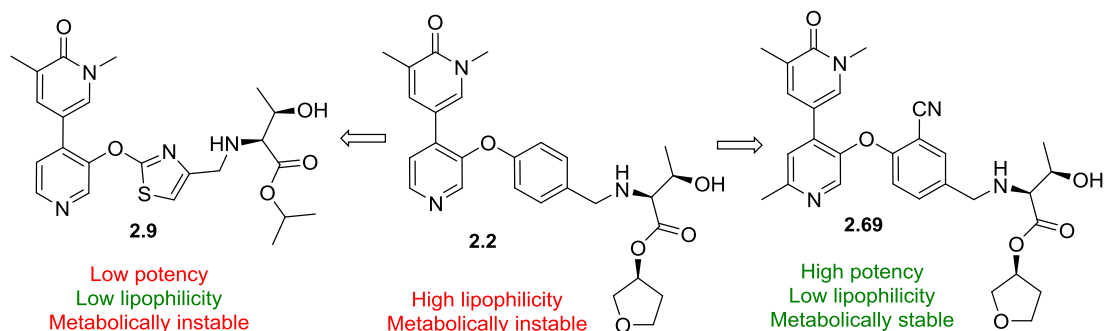


Figure 0.1. Replacement of the phenyl WPF shelf group of the initial lead **2.2** with 5-membered heteroaromatics produced molecules that exhibited low potency and high IVC, such as **2.9**. Mono-substitution of the phenyl ring and hindering the pyridyl core of **2.2** resulted in the lead molecule **2.69** which demonstrated high activity, low lipophilicity and metabolic stability.

The second part of this thesis focusses on the optimisation of a second structurally differentiated series with an alternative warhead, in which the ESM is directed through the ZA channel. Initial candidates showed an underlying issue with IVC. A range of substituents which acted as the shelf group were investigated. Employing the best shelf groups for IVC and replacing the phenyl ring with a pyridine or a diazine improved metabolic stability and resulted in compounds with desirable IVC profiles (Figure 0.2). Two lead molecules were identified from this series, both of which demonstrated high cellular activity and metabolic stability. They were selective for the BET family and were shown not to inhibit CYP3A4 in a time dependent manner, a common observed liability in this series.

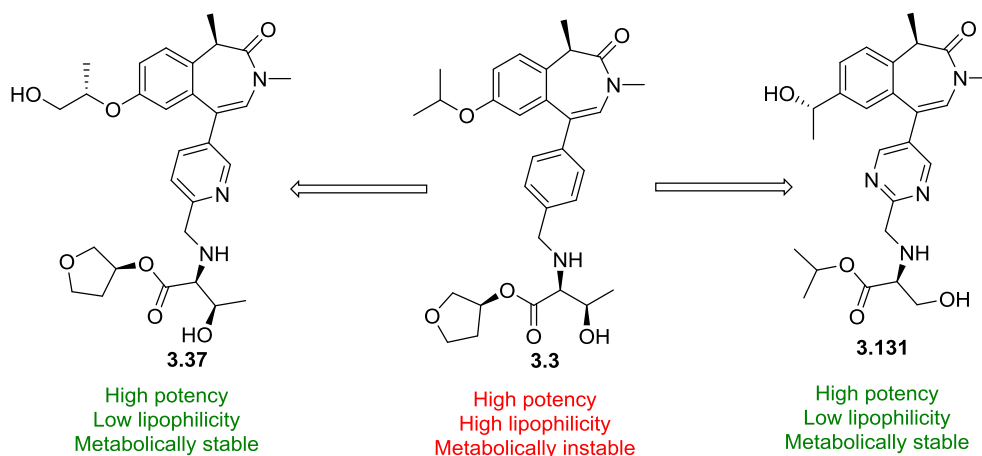


Figure 0.2. Replacement of the phenyl ZA channel group of **3.3** with 6-membered heteroaromatics and the isopropyl WPF shelf group with polar moieties produced molecules with high potency, low lipophilicity and low IVC. This led to the identification of the two lead molecules **3.37** and **3.131**.

Overall, work outlined in this report has taken molecules with high IVC and lipophilicity and optimised them into molecules with excellent potency, as well as desirable HLM and hepatocyte IVC and lipophilicity. Three molecules across both series were progressed into late stage cynomolgus monkey PK studies and were selected as the lead molecules for the series. Although the compounds were not progressed beyond the PK studies, they were key compounds for exemplifying that reducing cynomolgus monkey hepatocyte clearance, whilst maintaining a low lipophilicity and desirable metabolic stability, increased the oral bioavailability within cynomolgus monkeys.

Contents

1.0	Introduction.....	1
1.1	Structure and biological function of DNA.....	1
1.2	Biological mechanisms of epigenetic control of gene expression.....	5
1.2.1	DNA methylation.....	6
1.2.2	Overview of histone modifications.....	9
1.2.3	Bromodomains.....	14
1.2.4	BET bromodomains.....	16
1.3	Small molecule strategies for BET inhibition.....	18
1.3.1	First bromodomain inhibitor exemplars.....	19
1.3.2	BET inhibition as a strategy to treat rheumatoid arthritis.....	23
1.3.3	BET inhibitors: current state-of-the-art.....	29
1.3.4	Current limitations of BET inhibitors.....	32
1.4	Current state of the art of targeted drug delivery.....	33
1.4.1	Liposomal delivery system.....	34
1.4.2	Folate targeting agents.....	35
1.4.3	Pro-drug targeted delivery.....	37
1.5	Development of a targeted delivery strategy using an esterase sensitive motif.....	38
1.5.1	Human carboxylesterases as metabolic enzymes.....	39
1.5.2	ESM-containing inhibitors.....	42
1.6	Current state-of-the-art of BET inhibitor development within GSK.....	45
1.7	Screening cascade used to identify molecules with desirable profiles.....	48
1.8	Overall aims.....	52
2.0	Development of the “over the shelf” series as inhibitors for the BET family.....	56
2.1	Hypotheses to be tested in the OTS small molecule series.....	57
2.1.1	Bond angles of the ether linkage relative to the ESM influences the potency, IVC and CES-1 turnover.....	57

2.1.2	The substituted benzene moiety influences the potency, IVC and lipophilicity.....	60
2.2	Aims for the OTS series of small molecule inhibitors.....	62
2.3	Results and discussion.....	64
2.3.1	Investigating the bond angles of heterocyclic motifs in the first-generation series.....	64
2.3.2	Investigating substituted motifs interacting with the WPF shelf in the first-generation analogues.....	75
2.3.3	Further DMPK and selectivity profiling of lead compounds.....	96
2.3.4	Optimisation of the synthetic route to the lead OTS compound 2.69	100
2.3.5	<i>In vivo</i> cynomolgus monkey PK studies of the lead OTS molecule 2.69	106
2.4	Summary of the development of the OTS series for the use as BET inhibitors.....	107
3.0	Development of “benzazepinone” inhibitors of the BET family.....	111
3.1	Hypotheses to be tested within the BZP small molecule series.....	114
3.1.1	Incorporating polar moieties as the WPF shelf group reduces lipophilicity and IVC.....	114
3.1.2	Incorporating alternative ring systems as the ZA channel group reduces lipophilicity and IVC.....	115
3.2	Aims for the “BZP ZA” small molecule series.....	115
3.3	Results and discussion.....	117
3.3.1	Investigating polar moieties as the WPF shelf group.....	117
3.3.2	Investigating a 2,4-disubstituted pyridine as the ZA channel group.....	126
3.3.3	Investigating diazines as the ZA channel group.....	172
3.3.4	Further DMPK and selectivity profiling of lead compounds.....	186
3.3.5	Optimisation of the synthetic route to lead compounds 3.37 and 3.131	190

3.3.6	<i>In vivo</i> cynomolgus monkey PK studies of lead compounds 3.37 and 3.131	217
4.0	Conclusions.....	220
4.1	Future directions.....	229
5.0	Experimental.....	234
5.1	General experimental details.....	234
5.2	Procedures.....	237
6.0	References.....	340
7.0	Appendix 1: Assay protocols.....	348
8.0	Appendix 2: Measured IC ₅₀ values of compound 2.69 against closely related bromodomains.....	352
9.0	Appendix 3: <i>In vivo</i> PK data.....	353
10.0	Appendix 4: QSAR modelling supplementary information.....	354
10.1	All methods used to build the models.....	354
10.2	BRD4 BD1 QSAR model information.....	354
10.3	Human whole blood QSAR model information.....	355
10.4	Δ hWB QSAR model information.....	356
11.0	Appendix 5: NMR analyses of intermediate 3.96 and the corresponding diastereomer containing the (<i>S</i>)-configuration of the diol.....	358
11.1	NMR of the (<i>R</i>)-configuration of the diol synthesised in Scheme 3.16.....	358
11.2	NMR of the (<i>S</i>)-configuration of the diol synthesised by a colleague.....	358
12.0	Appendix 6: Chiral analysis and NMR interpretation of Intermediate 3.86	359
13.0	Appendix 7: NMR analyses to estimate diastereomeric excess.....	360

Abbreviations

ACR50	American College of Rheumatology, 50% of symptoms are relieved
ADA	Adalimumab
ADME	Absorption, distribution, metabolism and excretion
<i>allo</i> -Thr	<i>Allo</i> -Threonine
AMP	Artificial membrane permeability
AP	Aryl-pyridone
API	Active pharmaceutical ingredient
ApoA1	Apolipoprotein A1
BET	Bromodomain and extra-terminal
BMDM	Bone marrow-derived macrophages
Bp	Base pairs
BBr ₃	Boron tribromide
BZP	Benzazepinone
Cdk9	Cyclin-dependent kinase 9
CES	Human carboxylesterase
cChromLogD	Calculated ChromLogD
ChIP	Chromatin immunoprecipitation
ChromLogD	Chromatographic LogD
CLND	Chemiluminescent nitrogen detection
CRP	C-reactive protein
CTCL	Cutaneous T-cell lymphoma
CV	Column volume
CVD	Cardiovascular disease
CYPs	Cytochrome P450 enzymes
DCM	Dichloromethane
DIAD	Diisopropylazodicarboxylate
DMARD	Disease-modifying antirheumatic drugs
DMF	<i>N,N</i> -Dimethylformamide
DMR	Differentially methylated region
DMSO	Dimethylsulfoxide
DNA	Deoxyribonucleic acid
DNMT	DNA methyltransferases
ECFP	Extended connectivity fingerprint
ELT	Encoded library technology
EPR	Enhanced permeation and retention
ESI	Electrospray ionisation
ESM	Esterase sensitive motif
ESR	Erythrocyte sedimentation rate
ET	Extra-terminal
eXP	Enhanced cross-screening panel
FaSSIF	Fasted state simulated intestinal fluid
FCFP	Functional-connectivity fingerprint
FDA	Food and drug administration
FLS	Fibroblast-like synoviocyte
FR	Folate receptor
GSK	GlaxoSmithKline
H	Hours
HAC	Heavy atom count
HAT	Histone acetyltransferase

hCE	Human carboxylesterase
hCE-1	Human carboxylesterase 1
HBA	Hydrogen bond acceptor
HBD	Hydrogen bond donor
HDAC	Histone deacetylase
HDL	High-density lipoprotein
Heps	Hepatocytes
HLM	Human liver microsomes
HPLC	High performance liquid chromatography
HRMS	High resolution mass spectroscopy
HAS	Human serum albumin
hWB	Human whole blood
IC ₅₀	Half-maximal inhibitory concentration
IGF	Insulin-like growth factor
IL-1	Interleukin-1
IL-6	Interleukin-6
IR	Infrared
IVC	<i>In vitro</i> clearance
KAc	Acetyllysine
LBF	Liver blood flow
LCMS	Liquid chromatography mass spectroscopy
LDL	Low-density lipoprotein
LLE	Lipophilic ligand efficiency
LogD	Logarithm of the distribution coefficient
LogP	Logarithm of the partition coefficient
LPS	Lipopolysaccharide
MACE	Major adverse cardiac events
MCP-1	Monocyte chemoattractant protein-1
Min	Minute
MLA	Mouse lymphoma assay
MCP-1	Monocyte chemotactic protein-1
mRNA	Messenger RNA
MTD	Maximum tolerated dose
MTX	Methotrexate
MW	Molecular weight
NAD ⁺	Nicotinamide adenine dinucleotide
NADPH	Nicotinamide adenine dinucleotide phosphate
Nm	Nanometers
NMC	NUT midline carcinoma
NMR	Nuclear magnetic resonance
NUT	Nuclear protein in testis
OTS	Over the shelf
PCR	Polymerisation chain reaction
PEG	Polyethylene glycol
pIC ₅₀	- Log(IC ₅₀)
PK	Pharmacokinetic
PLS	Partial least squares
PRP	Predicted response property
PSA	Prostate specific antigen
P-TEFb	Positive transcription elongation factor b
PTM	Post-translational modification
PTT	Phenyltrimethylammonium tribromide
QSAR	Quantitative structure analysis relationship

RA	Rheumatoid arthritis
RES	Reticuloendothelial system
RMSE	Root mean squared error
RNA	Ribonucleic acid
Rt	Room temperature
SAH	S-Adenosyl-L-homocysteine
SAM	S-Adenosyl methionine
SAR	Structure-activity relationship
Ser	Serine
siRNA	Short interfering RNA
STAB	Sodium triacetoxyborohydride
TDI	Time dependent inhibition
THF	Tetrahydrofuran
THP	Tetrahydropyran
Thr	Threonine
TLC	Thin layer chromatography
TNF α	Tumour necrosis factor alpha
TPSA	Total polar surface area
TSS	Transcriptional start site
t _R	Retention time
UV	Ultraviolet radiation
WPF	Tryptophan, proline, phenylalanine
3'-UTR	Three prime untranslated region

Chapter 1

Introduction

1.0 Introduction

Immuno-inflammatory diseases encapsulate a group of common and often highly disabling conditions with an estimated prevalence of 5-7% in Western society.¹ Inflammation is a critical response to potential damage to the organs in the body. It plays an important role in providing protection against disease by identifying and killing pathogens.² An excessive response can cause the dysregulation of cytokines, a small group of proteins with a key role in cell signalling within the body.³ Furthermore, inflammation can be caused by the dysregulation of cytokines with significant evidence showing that certain cytokines are involved in the initiation and persistence of pathologic pain.⁴

Immuno-inflammatory diseases can be categorised as acute or chronic. Acute inflammation is part of the immediate immune response and prevents further damage whilst facilitating the healing process.⁵ However, when inflammation become self-perpetuating it can lead to long-term inflammation, termed chronic inflammation. Examples of immuno-inflammatory diseases include Crohn's disease and rheumatoid arthritis.⁵ Such diseases are typically characterised by the elevated levels of pro-inflammatory cytokines and cytokines as well as T-cells and B-cells. This overexpression of genes can be attributed to epigenetic changes to the deoxyribonucleic acid (DNA) chain, which affects the packing state of DNA and subsequent ability to be transcribed.

1.1 Structure and biological function of DNA

Deoxyribonucleic acid (DNA) carries the genetic information required for growth, development, functioning and reproduction of almost all living organisms.⁶ Therefore, the majority of cells contain a full, identical copy of the DNA of a specific organism. Mutations in the genetic code can lead to missing or malformed proteins, which may result in the onset of diseases. Such changes can be caused by DNA damage due to environmental factors, such UV radiation, chemicals, viruses, and DNA mutations.⁷

DNA predominantly exists as an anti-parallel duplex in which each strand is composed of four types of nucleotide subunits.⁶ A nucleotide comprises a nucleobase (also termed a nitrogenous base), a five-carbon deoxyribose sugar, and a phosphate group (Figure 1.4). The nucleotides are covalently linked together in a chain, forming a "backbone" of alternating sugar-phosphate units.⁸ The nitrogenous bases can be categorised into purines (adenine [A] and guanine [G]), each with two fused rings, and the pyrimidines (cytosine [C], thymine [T], and uracil [U]), each with a single ring (Figure 1.1).⁶

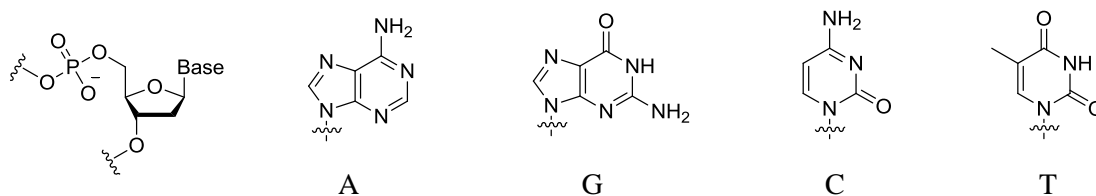


Figure 1.1. DNA is synthesised from four nucleoside triphosphates; adenine [A], guanine [G], cytosine [C], thymine [T]. A and G are categorised as purines, each with two fused rings, and C, and T are pyrimidines.

The two DNA strands self-assemble in an anti-parallel programmable fashion by hydrogen bonds between a purine and a pyrimidine base; adenine hydrogen bonds with thymine and cytosine with guanine to give two complementary base pairs of similar width (Figure 1.2).⁸

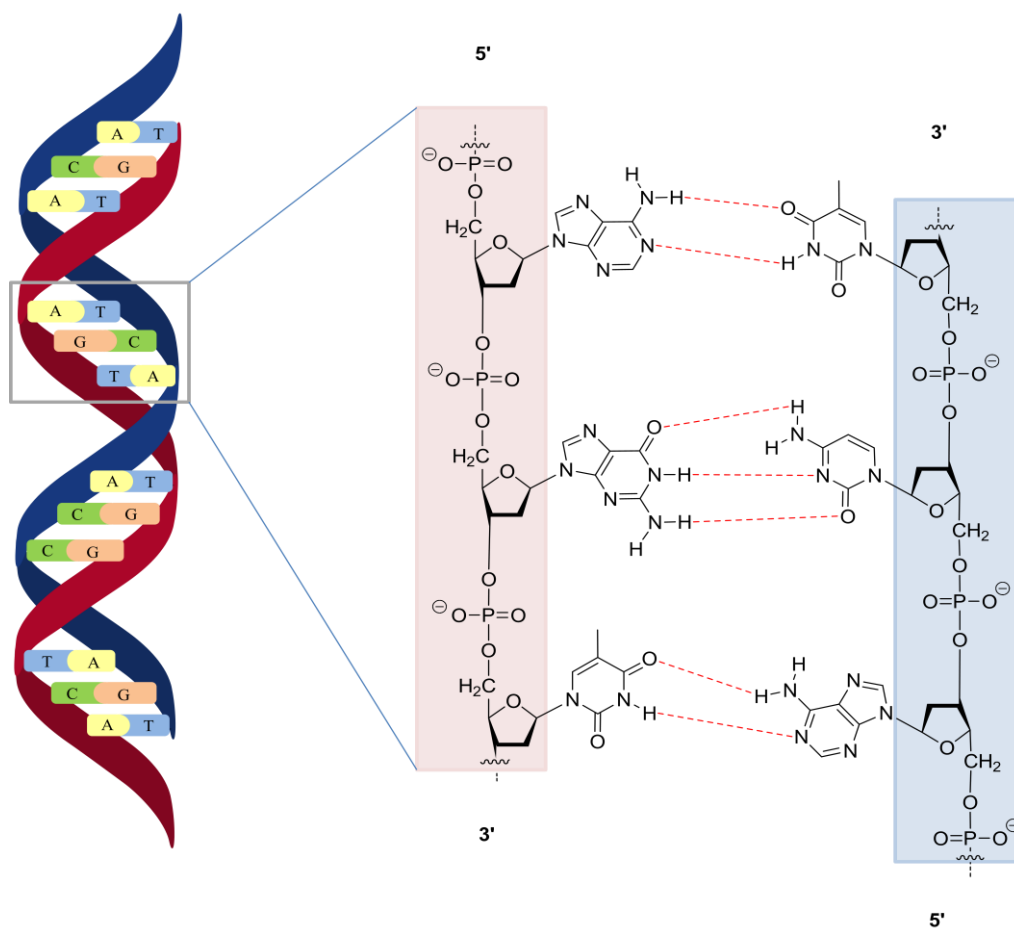


Figure 1.2. DNA adopts a B-type double helix conformation in which the two DNA strands are connected by hydrogen bonds between a purine and a pyrimidine base; adenine bonds with thymine and cytosine with guanine. The nucleotides are covalently linked together in a chain, forming a “backbone” of alternating sugar-phosphate units.

These hydrogen bonds, along with the restricted bond angles in the sugar-phosphate backbone, results in the double-stranded DNA adopting predominantly a B-type double helix formation with ten base pairs per helical turn (Figure 1.3).⁹ This arrangement maximises the efficiency of the base-pair stacking and maintains an equal distance between the two sugar-phosphate backbones along the DNA molecule. The outer edges of the nucleobases remain partially exposed and are available for potential hydrogen bonding. These hydrogen bonds provide easy access to the DNA for other molecules, including the proteins that play vital roles in the replication and expression of DNA.

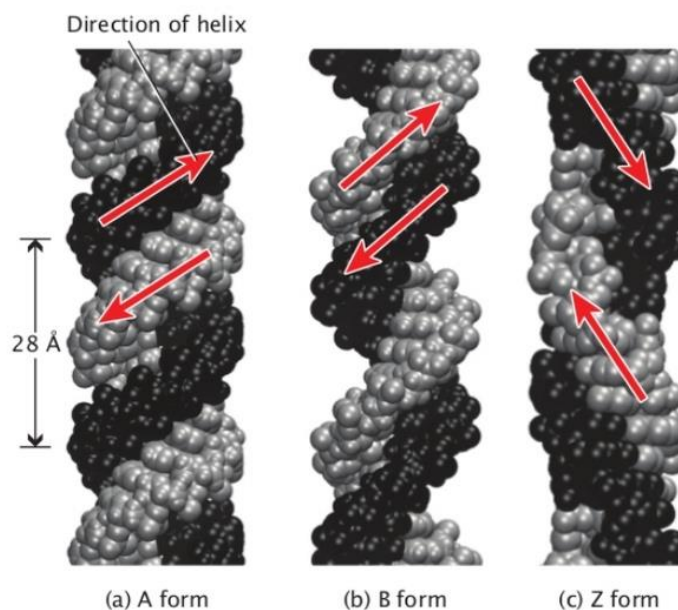


Figure 1.3. Duplex DNA can adopt three forms depending on the helix structure; A, B and Z. DNA in the cell functions as a B-form DNA, the most common type. Image was reproduced with permission from Pray, L. *Nature Education*, **2008**, *1*, 100.⁹

The DNA in each cell contains approximately 3 billion nucleotides and is ~1.6 m in length.¹⁰ As such, a high level of compaction is required in order for it to be contained within a nucleus of ~5 μm diameter. To achieve this, ~150 bases of DNA wrap around octameric histone proteins to form nucleosomes, the smallest structural unit of chromatin (Figure 1.4).¹¹ Further condensation produces a 30 nm chromatin fibre, which forms loops averaging 300 nm in length. Further compression forms a 250 nm wide fibre, which loops and coils around itself to form tightly wound chromatid. This is half of a chromosome and is transferred to daughter cells during cell division and replication.¹¹

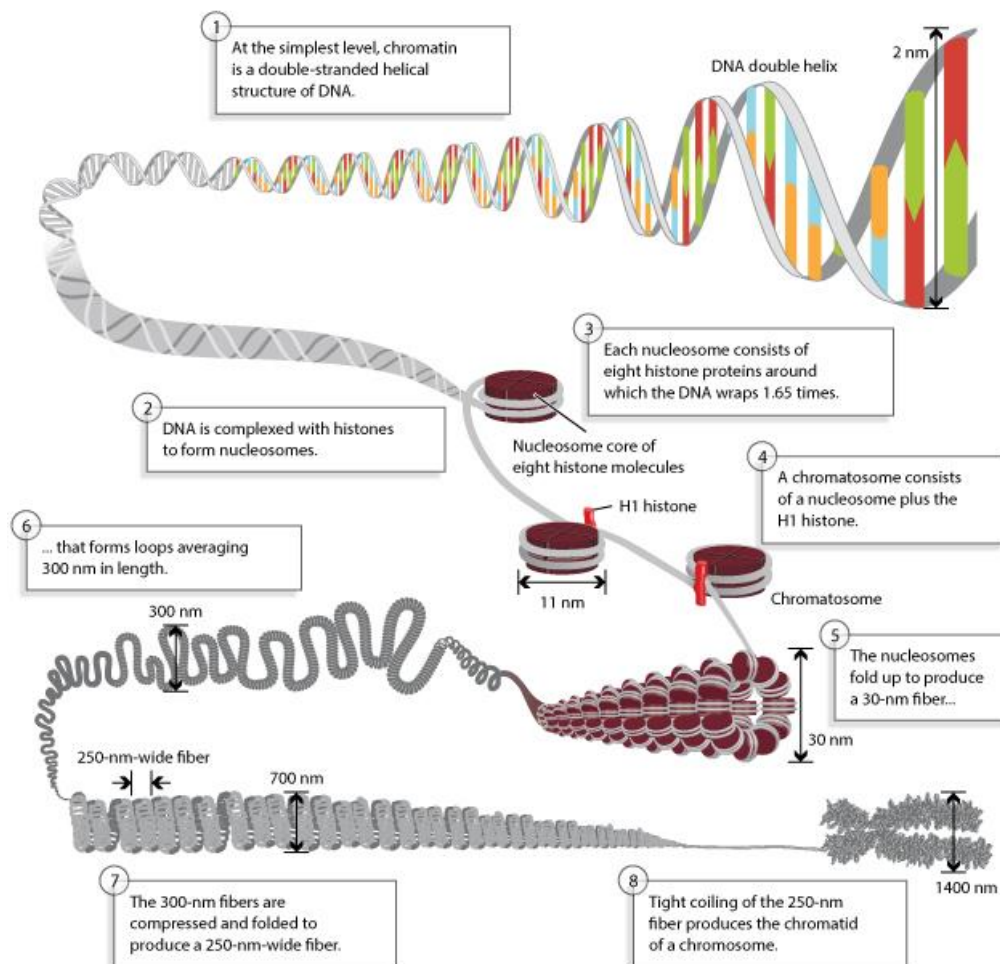


Figure 1.4. Duplex DNA is packaged inside nuclei by associating with histones. These are positively-charged proteins that form strong electrostatic interactions with negatively-charged DNA to form nucleosomes. Further condensation results in chromatin fibre loops, averaging 300 nm in length. These fibres are compressed and folded into a 250 nm wide fibre, which is tightly coiled into the chromatid of a chromosome. Image was reproduced with permission from Annunziato, A. *Nature Education*, 2008, 1, 26.¹¹

The packing of chromatin, known as the chromatin state, influences its ability to be transcribed or replicated. A closed chromatin structure, the most condensed and transcriptionally inactive form, is known as euchromatin.¹² During transcription or replication, the chromatin loosens to give an open chromatin structure, known as heterochromatin, in which sections of DNA are exposed. It is from this chromatin state that the synthesis of new proteins is possible. RNA polymerase II (RNA Pol II), along with one or more transcription factors, binds to the promoter region of DNA.¹³ A transcription bubble is formed, which breaks the hydrogen bonds between the nucleotides and separates the two strands of the DNA helix. RNA polymerase adds ribonucleotides and catalyses the production of messenger RNA (mRNA), a single-stranded ribonucleic acid.¹⁴ The mRNA is

complementary to the DNA strand and serves as a template for the protein's synthesis through translation.

DNA contains ~30,000 protein coding sequences, known as genes.¹⁵ A full copy of the DNA is present in the majority of cells, and therefore these cells have the potential to express every protein encoded by the genes. However, not all genes are expressed at the same time. This control over gene expression, which results in different combinations of genes being active at one time, allows the development of differentiated cell types from stem cells.¹⁶ Some genes are expressed continuously, as they produce proteins involved in basic metabolic functions. Otherwise, only the genes that are required for a particular function, which is dependent on the cell type, are expressed. Gene expression can be controlled by regulating the rate of transcription and translation, processes which can be influenced by epigenetic mechanisms.

1.2 Biological mechanisms of epigenetic control of gene expression

Epigenetics describes the stable and heritable changes in gene expression that are achieved without altering the underlying DNA sequence.¹⁷ The term comes from the Greek prefix 'epi' meaning 'above', thus literally means "above genetics". Epigenetics, essentially, affects how genes are read by cells, and subsequently how they produce proteins. Therefore, it is a crucial mechanism through which gene expression is regulated or altered.¹⁸ Epigenetics explains why genetically identical organisms can adopt different phenotypes. For example, it has been reported that the royal jelly fed to bee larvae influences the decreased DNA methylation levels observed in queen bees relative to the worker bees showing the epigenetic marker is critical for the differentiation of a bee caste (Figure 1.5).¹⁹



Figure 1.5. A queen honeybee, marked in white, surrounded by her worker bees. Reprinted with permission from Simpson *et al.*, *Curr. Biol.*, **2012**, 22, 738.¹⁹

There are several layers of regulation of gene expression. One way that genes are regulated is through the remodelling of chromatin.²⁰ If the way that DNA is wrapped around the histones changes, gene expression can change as well. There are two major epigenetic post-translational modifications which alter chromatin state: DNA methylation and histone protein alteration.²¹ Functionally, the patterns of epigenetic modifications can serve as epigenetic markers to represent gene activity and expression, as well as chromatin state. They are crucial for the packaging and interpretation of the genome under different physiological factors. As such, dysregulation of these modifications can lead to abnormal gene expression. This has fundamental implications within a multitude of diseases including cancer, neurodegenerative and autoimmune disorders. Consequently, modulation of epigenetic targets is emerging as an effective therapeutic treatment, with epigenetic therapies being widely researched.²²

1.2.1 DNA methylation

DNA methylation was the first recognised epigenetic modification and is the most well characterised. It is linked to transcriptional silencing and has a key role in gene regulation and tumourigenesis.²³ Cytosine is the most common substrate for DNA methylation in eukaryotes.²⁴ Methylation occurs at areas rich in cytosine-guanine dinucleotides, termed CpG islands, found within gene promoter regions.²⁵ The cytosine nucleobase is methylated at the C5 position by DNA methyltransferases (DNMT), (Figure 1.6). Subsequent recognition by the MBD reader proteins inhibits gene transcription of the adjacent gene. This is due to the MBD reader proteins containing a transcriptional repressor domain that facilitates the binding of the protein to a variety of repressor complexes, thus preventing gene transcription.²⁶

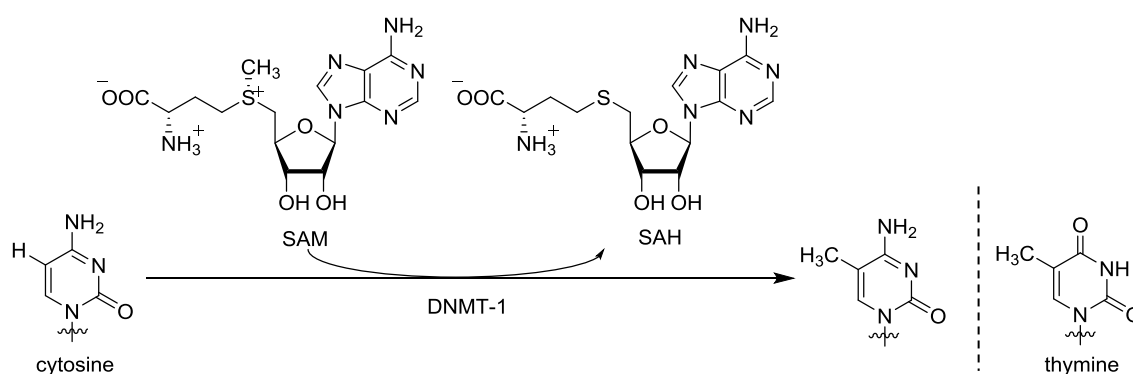


Figure 1.6. Cytosine is typically methylated in the C5 position by DNA methyltransferases. A methyl group is transferred from *S*-adenosyl methionine (SAM) to the cytosine C5, making it analogous to thymine and generating *S*-adenosyl-L-homocysteine (SAH).

Three functional DNMTs have been identified so far in the human genome.²⁷ These include the two *de novo* methyltransferases (DNMT3A and DNMT3B) and the maintenance methyltransferase (DNMT1), which is generally the most abundant and active of the three. All DNMTs employ a similar catalytic mechanism involving the covalent binding of the substrate base prior to methylation and, as such, the proteins are highly conserved.²⁸ The N-terminus contains a regulatory domain responsible for anchoring the DNMT in the nucleus and facilitating the recognition of nucleic acids or nucleoproteins. The C-terminus contains the catalytic domain, which is responsible for the enzymatic activity.²⁹ In addition to these three enzymes, the family also includes two extra members, DNMT2 and DNMT3L. DNMT2 is not currently considered a DNA methylase, but has a key role in the methylation of small transfer RNAs (tRNAs). Similarly, DNMT3L lacks the C-terminal catalytic site and, as such, cannot directly methylate DNA. However, it remains an important regulator of DNA methylation, operating through the heterotetrameric DNMT3L-DNMT3A form.²⁸

DNMT1 is responsible for duplication of the DNA methylation patterns during DNA replication and is essential for development and cancer cell growth.³⁰ Studies have shown that dysfunction of DNMT1 contributes to a wide range of malignancies, including colorectal and prostate cancer.³¹ Furthermore, knockout mice models, DNMT1^(-/-), demonstrated a 90% loss of DNA methylation as well as embryonic lethality.³² The key role of DNMTs as regulators of gene transcription and in carcinogenesis have caused them to be widely researched in the last decade as attractive targets for cancer therapies.³³

A normal DNA methylation pattern is established during development and maintained throughout an individual's lifetime. However, deviations from the expected methylation pattern can lead to abnormal gene expression. Promoter hypermethylation and genome-wide hypomethylation have been observed in many diseases, particularly cancer, due to the transcriptional inactivation of genes.¹⁷ It was first thought that all epigenetic markers were erased in primordial germ cells, precursors to sperm and eggs, but this does not account for epigenetic inheritance. Recent studies show that, in fact, a small proportion of DNA methylations remain intact during fertilisation.³⁴

As DNA methylation is a key epigenetic mechanism, and dysregulation is associated with a multitude of diseases, the inhibition of DNA methylation was thought to have potential as an efficient and broad therapy. DNA methylation is an epigenetic modification that can only be sustained by the presence of methylating enzymes and, as such, cellular replication in the presence of reduced levels of these enzymes results in significant demethylation in daughter cells, accompanied by gene reactivation.³⁵ Furthermore, whilst normal cells tend to survive

hypomethylation, cancer cells are either killed or stop proliferating upon reduced promoter methylation. This is thought to be due to the dependence of cancer cell survival on critical gene silencing. In particular, tumour suppressor genes in cancer cells are frequently silenced by promoter CpG methylation. As such, lower promoter methylation levels are often associated with the reactivation of tumour suppression genes and, consequently, slower proliferation. Therefore, DNA methylation inhibitors have been investigated as potential cancer therapeutics to reactivate these genes.²³

Over ten DNA methylation inhibitors have been approved for use in the clinic, with several more in late stage clinical trials.³⁶ The inhibitors broadly fall into two categories; nucleoside mimetics and non-nucleosides. A key example is azacitidine, commercially known as Vidaza (Figure 1.7).

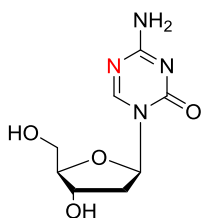


Figure 1.7. The structure of the known inhibitor azacitidine, a nucleoside mimetic. Azacitidine mimics cytosine but with the addition of the extra nitrogen (red) in place of the cytosine C5, therefore preventing methylation.

Azacitidine is an analogue of cytosine which inhibits DNA methylation through two mechanisms.³⁷ At low doses it inhibits DNMT, causing DNA hypomethylation. At high doses, it is incorporated into DNA, and to a larger extent, into RNA. Azacitidine's incorporation into RNA leads to the disassembly of polyribosomes, defective methylation and inhibition of the production of proteins. Its incorporation into DNA leads to covalent binding with DNA methyltransferases, which prevents DNA synthesis and subsequently leads to cytotoxicity. Of the two modes of action, DNMT inhibition is the most effective for preventing DNA methylation. However, inhibiting the enzyme does not direct the reactivation of a specific set of genes but, rather, results in a decrease in the overall level of methylation.³⁸ As such, a random selection of genes may be reactivated leading to a loss of specificity and a hypomethylation of the whole genome.³⁹ Therefore, more recent research has focussed on targeting histone modifications in an attempt to gain higher specificity and control over the outcomes.

1.2.2 Overview of histone modifications

Histones are the major structural proteins of chromosomes and consist of five major families; H1/H5, H2A, H2B, H3 and H4. H1/H5 are termed the linker histones whilst the remaining four families form the core histone. The core histones all exist as dimers which associate to form an octamer, (Figure 1.4 *vide supra*).⁴⁰ Protruding from histones are amino acid chains, termed histone tails, which are subject to post-translation modifications (PTM). These include, but are not limited to, methylation, acetylation, and phosphorylation (Figure 1.8).

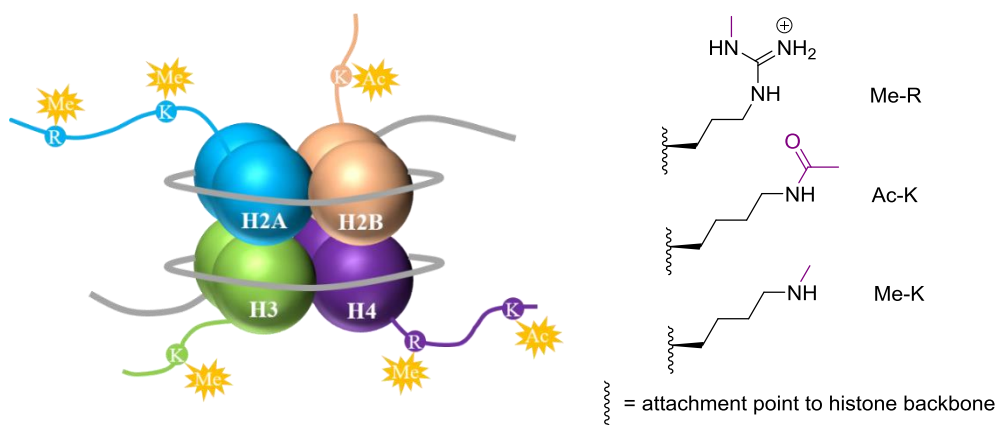


Figure 1.8. Octameric histones are the major structural proteins of chromosomes. Protruding histone tails can be post-translationally modified including arginine methylation (Me-R), lysine acetylation (Ac-K) and lysine methylation (Me-K) with the markers highlighted in purple.

A key histone modification is the acetylation of a terminal lysine residue on the histone tails. Lysine acetylation is a fundamental mechanism that regulates chromatin structure.⁴¹ Lysine is protonated at physiological pH, enabling strong ionic interactions with the negatively charged phosphate groups of the DNA backbone. This is associated with a tightly bound chromatin structure, known as euchromatin, which is transcriptionally inactive. Upon acetylation, the lysine is neutralised, thus reducing the electrostatic interactions. The DNA is less tightly bound to the histones resulting in a loose chromatin structure, or heterochromatin, which is now transcriptionally active. As such, aberrant lysine acetylation has implications in several diseases, making it an important biological target which could have an increased potential for therapeutic activity than DNMT.

There are three important classes of proteins that are involved with epigenetic modifications; writers, erasers and readers.⁴² Writer proteins are responsible for installing the modification, whilst erasers delete it. Finally, readers recognise the modification, thereby inducing

increased transcription and a subsequent change in gene expression. In the case of lysine acetylation, the writer and eraser proteins are known as histone acetyltransferases (HATs) and histone deacetylase (HDAC) proteins. The modification is recognised by bromodomains, proteins which have a vital role in the acetylation-dependent assembly of transcriptional regulator complexes (Figure 1.9).

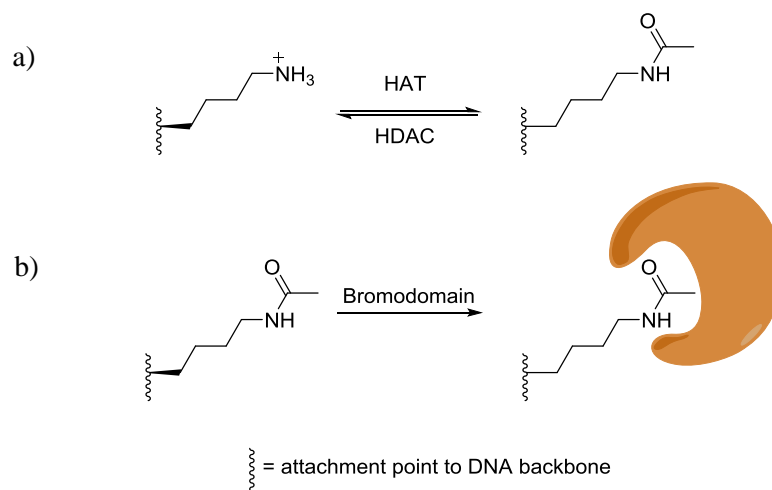


Figure 1.9. a) Writer proteins (e.g. HATs) are responsible for introducing modifications to the histone tails whilst eraser proteins (e.g. HDACs) delete the modification. b) Reader proteins (e.g. bromodomains) recognise and bind to the modification, resulting in gene transcription.

HAT enzymes introduce the acetyl group to the lysine from acetyl-CoA (*vide infra*, Figure 1.10a), causing remodelling of euchromatin to heterochromatin.⁷¹ The proteins are recruited at gene promoters by the binding of specific transcription factors, many of which also have intrinsic histone acetyltransferase activity, or activators.⁴⁴ The HATs comprises two major families, GNAT and MYST, split according to sequence homology and functional roles.⁴⁵ Furthermore, HATS are typically categorised into two classes, Type A and Type B, based on their subcellular localisation.⁴⁶ Type A HATs reside in the nucleus where they regulate gene expression through the acetylation of nucleosomal histones. Enzymes of this class contain a bromodomain, which aids in the recognition and binding of acetylated lysine residues on histones.⁴⁷ Type B HATs are found in the cytoplasm and have a key role in acetylating newly synthesised histones prior to their packing into nucleosomes. Unlike Type A HATs, proteins of this class lack a bromodomain as their targets are unacetylated and, as such, acetylated lysine recognition is not required. To date, Hat1 is one of the few known examples of Type B HATs. However, Type A are well characterised and a large number of members have been identified including p300/CBP-associated factor (PCAF) and Gcn5.

In the reverse process, lysine deacetylation is catalysed by HDAC proteins allowing the DNA and histones to reform euchromatin. There are two families of HDACs; silent information regulator 2 (Sir2)-related proteins (sirtuin) and classical HDACs, comprised of four classes of deacetylases (I-IV). Classes I, II and IV, comprising 11 proteins, have high sequence homology and catalyse the deacetylation via an active site Zn²⁺ dependent mechanism. In contrast, the seven members which form the class III HDACs show no sequence resemblance and use a nicotinamide adenine dinucleotide (NAD⁺) dependent mechanism of deacetylation (Figure 1.10b).⁴⁸

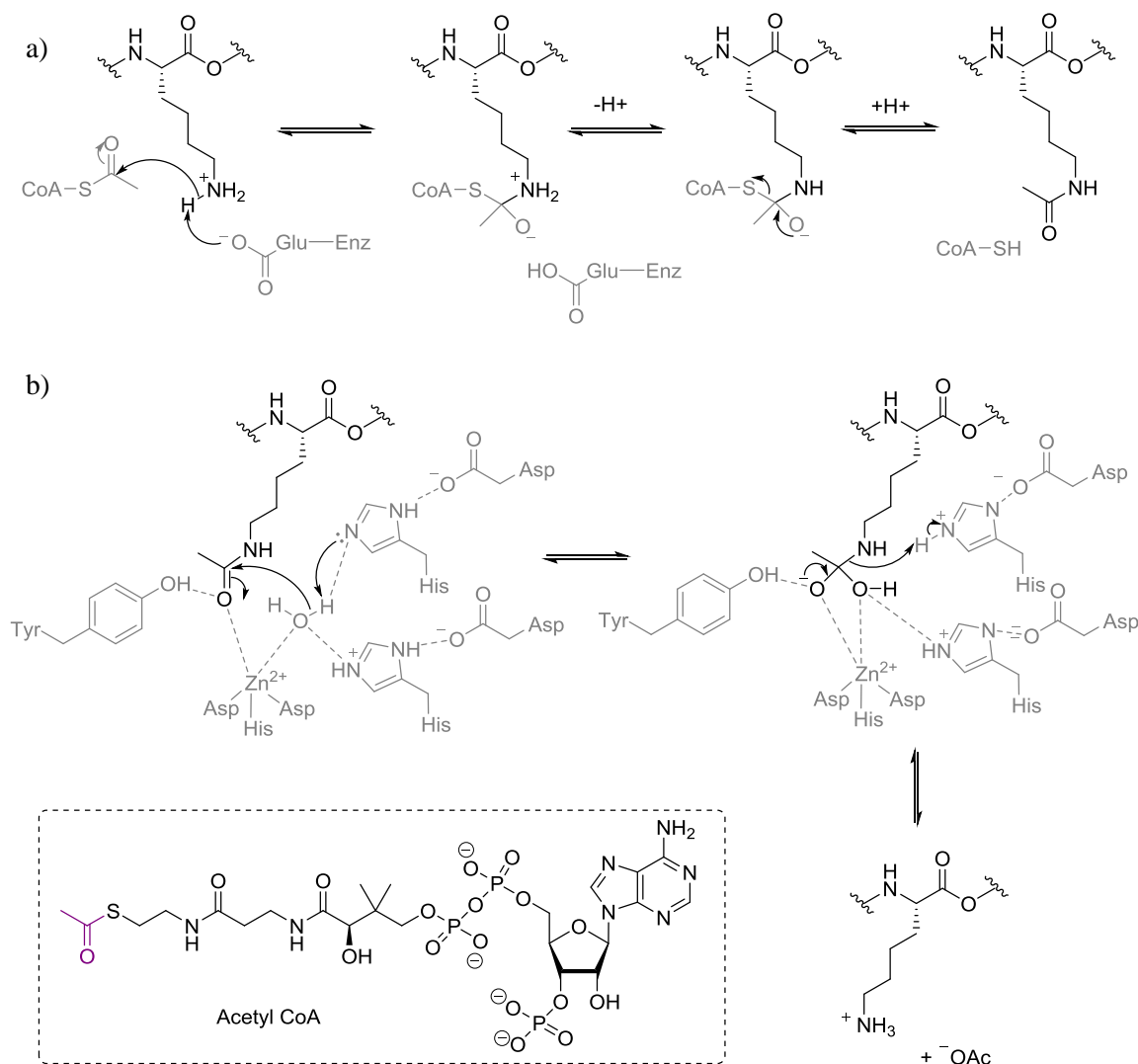


Figure 1.10. a) During lysine acetylation by HAT, a conserved glutamate residue deprotonates the amine, activating it for nucleophilic attack on the carbonyl group of acetyl CoA. The structure of acetyl CoA is shown, with the acetyl group that is transferred highlighted in purple. The resultant tetrahedral intermediate collapses to the acetylated lysine with the loss of coenzyme A. b) Lysine deacetylation by classes I, II and IV deacetylases is *via* an active site metal dependent mechanism. Coordination of the acetyllysine to key residues in the active site facilitates the nucleophilic attack of the water molecule, which is activated by deprotonation by a histidine residue.

HAT inhibition has not been widely researched within drug discovery as progress had initially been limited due to a lack of selective, drug-like molecules.⁴⁹ However, in 2018, a small molecule inhibitor of p300/CBP HAT, named A-485, was published by AbbVie. The compound is one of the first drug-like HAT inhibitors to be disclosed that exhibits selectivity, potency and oral bioavailability and, as such, could lead to a renewed interest in this area of research.⁴⁹ Meanwhile, HDAC inhibitors have proven to have therapeutic effects in a range of diseases. In particular, class I/II HDAC inhibitors have demonstrated

anticancer activities in preclinical studies and class III activators have been shown to suppress age-associated diseases e.g. obesity and type II diabetes.^{50,51} Approved by the FDA in 2006, suberoylanilide hydroxamic acid (SAHA or vorinostat) is a key example of the therapeutic potential of HDAC inhibition (Figure 1.11).⁵²

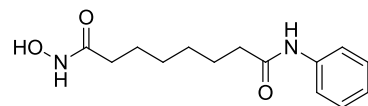


Figure 1.11. Structure of vorinostat.

Vorinostat is approved for the treatment of advanced primary cutaneous T-cell lymphoma (CTCL), underpinned by the 31% response rate observed in phase II clinical trials involving patients with stage 1B and higher CTCL and two failed systemic therapies.⁵² Since then, the use of vorinostat as a therapy for a range of solid and hematologic malignancies has been investigated, with >90 clinical trials currently ongoing.⁵³ Crystal structures of vorinostat bound to HDAC2 reveal it inhibits the HDAC classes I, II and IV by binding to the Zn^{2+} , which is crucial to the hydrolysis mechanism (Figure 1.12).⁵³

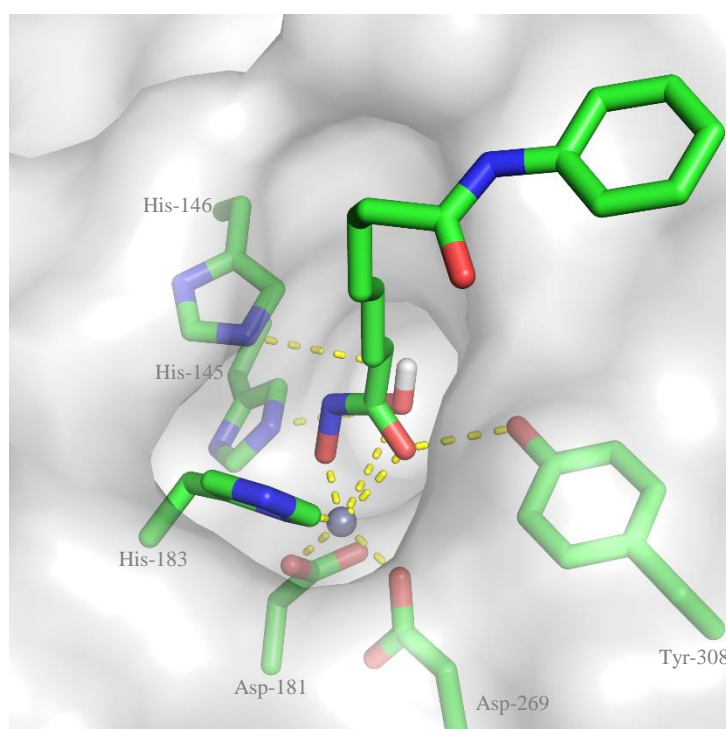


Figure 1.12. Crystal structure of vorinostat in HDAC2 (pdb: 4lxz).⁵⁴ The hydroxamic acid coordinates to the Zn^{2+} ion in the same way as the bound acetylated lysine, yielding a similar trigonal bipyrimidal intermediate, and does not impact the binding of the key water molecule.

Vorinostat chelates the zinc ion in a similar trigonal bipyramidal fashion, with almost identical positioning to the acetylated lysine. Furthermore, the alkyl chain of the inhibitor extends into the lipophilic channel, analogous to the binding of the lysine side chain. Whilst HDAC inhibitors have proven to have therapeutic effects in a range of diseases, particularly in T-cell lymphoma, inhibition of the reader proteins has also been widely researched.

1.2.3 Bromodomains

The first bromodomain was discovered in 1992 during studies of *Drosophila*.⁵⁵ It was found that the Brahma gene, hence the name bromodomain, was required for the activation of several homeotic genes, thereby having a role in gene expression. The first crystal structure of a bromodomain, contained within PCAF, was determined in 1999, both in the unbound (apo) form and in complex with an acetyllysine mimetic. Since then, more than half of the known bromodomains have had their structures identified.⁵⁶ The bromodomain fold is highly conserved and most share the same fundamental structure.⁵⁷ They have globular folds comprising a left-handed bundle of four alpha helices; A, B, C and Z (Figure 1.13a). The Z and A helices and the B and C helices are connected by two loops; the ZA and BC loops respectively. There are major sequence variations in the ZA and BC loops across the bromodomain family and, as such, the overall sequence similarity is not high despite the conserved structural fold.⁵⁸ However, the amino acid residues involved in acetyllysine binding are the most highly conserved in the family.

The packing of the ZA and BC loops creates a hydrophobic pocket which acts as the acetylated lysine (KAc) binding site. The recognition of acetylated lysine of the histone tail is driven by interactions with two conserved residues. The acetyl group forms a hydrogen bond with an asparagine residue on the BC loop and a through water hydrogen bond to a tyrosine residue on the ZA loops (Figure 1.13b). Within the binding pocket there are five water molecules, two of which have been recurrently found to interact with endogenous ligands and inhibitors in an analogous manner. These structural features are highly conserved and therefore it could be advantageous to interact with them with small molecule inhibitors.⁵⁹

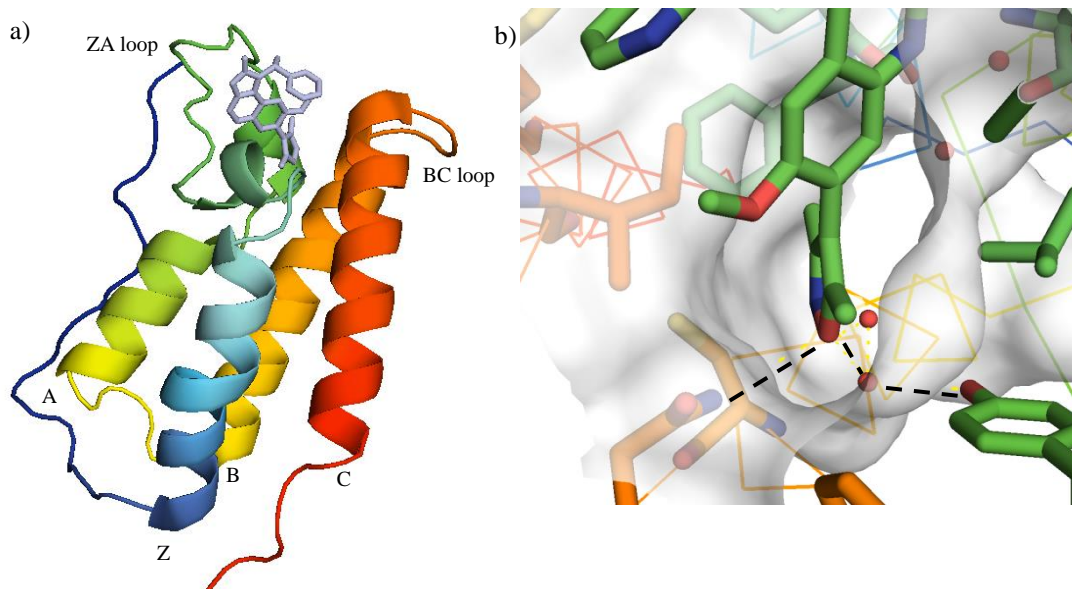


Figure 1.13. a) A crystal structure of BRD2 BD1 co-crystallised with the known BET inhibitor I-BET151 (pdb: 4alg).⁶⁰ Bromodomains have a highly conserved structure comprising a left-handed bundle of four alpha helices; A, B, C and Z. The A and Z helices are connected by the ZA loop and the B and C helices by the BC loop. The junction of the ZA and BC loop forms a lipophilic pocket which serves as the acetylated lysine (KAc) binding site. b) The ligand binds to the pocket *via* a hydrogen bond to an asparagine residue and a through-water hydrogen bond to a tyrosine residue.

There are currently 47 bromodomain-containing proteins with 61 unique bromodomains known in the human proteome.⁵⁶ These have been categorised into eight families according to structure homology and sequence (Figure 1.14). To date, the bromodomain families I, VI and VIII have been characterised and families II and IV nearly completed. However, several members of the families III, V and VII still lack structures. These proteins are atypical and exhibit unusual ZA loops and a different residue, typically threonine or tyrosine, in place of the conserved asparagine displayed in most bromodomains. Despite this, the proteins still bind histones in an acetylation-dependent manner, thus suggesting they use other methods for acetylated lysine recognition.

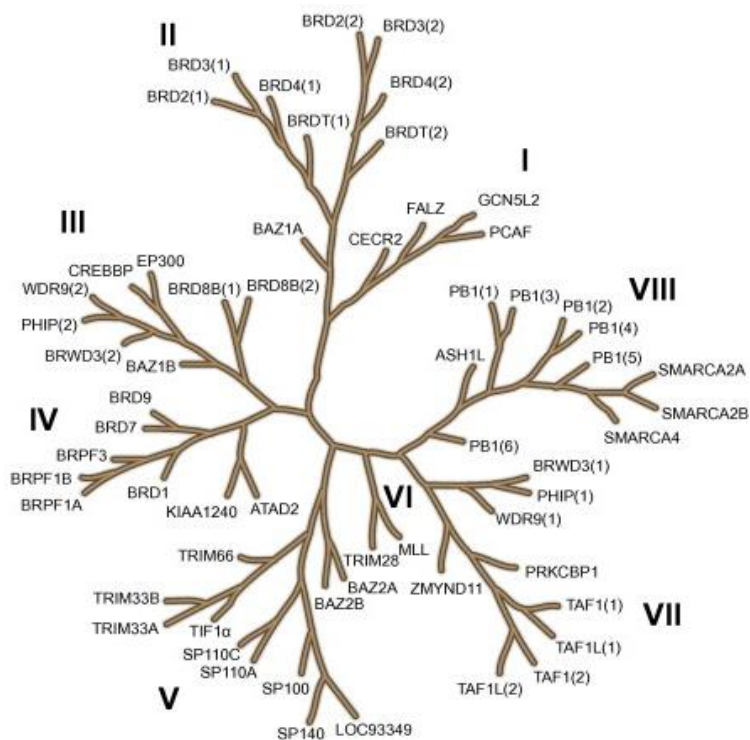


Figure 1.14. There are 47 bromodomain-containing proteins with 61 unique bromodomains. These have been categorised into eight families, as depicted in this phylogenetic tree, according to structure homology and sequence. Image was reproduced with permission from Filippakopoulos *et al.*, *FEBS Letters*, **2012**, 586, 2692.⁶¹

1.2.4 BET bromodomains

The Bromodomain and Extra-Terminal (BET) bromodomains consists of four proteins; BRD2, BRD3, BRD4 and BRDT. Each protein has two bromodomains, BD1 and BD2, thereby giving eight bromodomains in total.⁵⁹ The two bromodomains on the same protein show less sequence homology (~45%) than the corresponding bromodomain across the family (~75%). This offers the potential to gain bromodomain selectivity. However, the majority of existing small molecule BET inhibitors inhibit all eight bromodomains and are therefore termed pan-BET inhibitors.

Small molecule inhibitors bind to the KAc binding site through interactions with the conserved asparagine (N140) and tyrosine (Y97) (Figure 1.15). Selectivity and potency can be gained by extending into the adjacent regions; the WPF shelf and the ZA channel. BET proteins have a triad of amino acids, tryptophan (W81), proline (P82) and phenylalanine (F83), which create a lipophilic region, given the common name of the ‘WPF shelf’.⁶² This pocket is governed by a gatekeeper residue, isoleucine in BD1 and valine in BD2, which adopts a different conformation in the apo form than in the ligand-bound form of the

bromodomain.⁵⁸ The gatekeeper imposes spatial constraints on the size of the moieties that can access the WPF shelf, which can aid in gaining selectivity over other bromodomain-containing proteins.⁶³

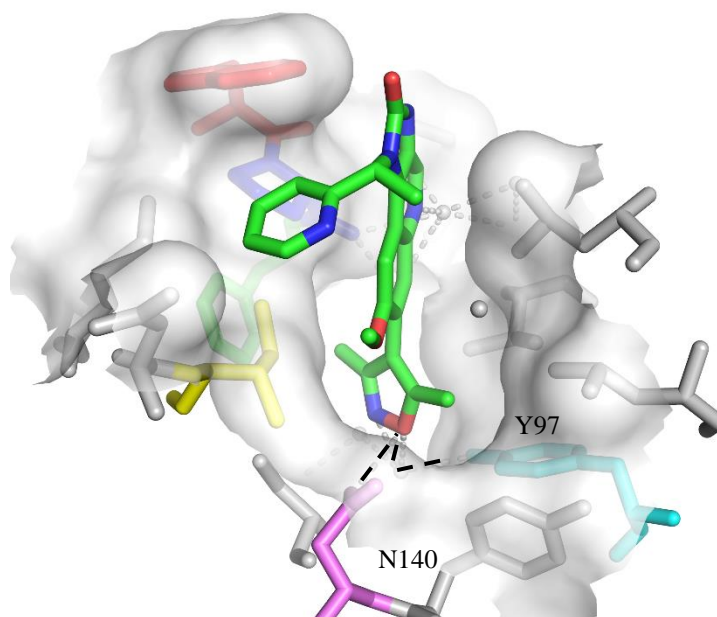


Figure 1.15. A crystal structure of BRD2 BD1 co-crystallised with the known BET inhibitor I-BET151 (pdb: 4alg).⁶⁰ Small molecule inhibitors bind to the KAc binding site through the conserved interactions with asparagine (magenta) and tyrosine (cyan). Selectivity and potency can be gained by extending onto the WPF shelf which is formed by a tryptophan (red), proline (dark blue) and phenylalanine (green) stack and a valine or isoleucine (yellow) gatekeeper.

In addition to gaining selectivity over other bromodomain-containing proteins, differences between the BD1 and BD2 pockets can confer selectivity between the bromodomains of each isoform. Although the bromodomains share ~95% sequence homology, two crucial residue differences, aside from the gatekeeper residues already mentioned, can be utilised when designing bromodomain selective inhibitors. For example, in the BRD4 isoform the BD1 residues Q85 and D144 are K378, and H437 residues respectively in BD2.⁶⁴ These subtle changes can have a significant impact on shape complementarity and interactions of inhibitors between the two bromodomains, thus allowing selectivity to be achieved. This can be advantageous as it has been demonstrated that selective inhibition of BD1 or BD2 can produce different transcriptional outcomes.⁶⁵ This is exemplified by olinone, the first example of a BD1 selective small molecule inhibitor, which promoted mouse oligodendrocyte differentiation.⁶⁶ The differentiation did not occur upon inhibition of both

bromodomains, thus suggesting that selective BD1 inhibition was required to exhibit the effect. Examples of BD2 selective inhibitors are also known (*vide infra*, Chapter 1.3.3) but to date, the majority of established small molecule inhibitors target the BET family in a pan-BET fashion.

1.3 Small molecule strategies for BET inhibition

The BRD2-4 BET proteins are ubiquitously expressed, whilst BRDT expression is limited to germ cells.⁶⁷ BET proteins interact with and function as scaffolds for a number of other molecules implicated in gene transcription. BRD2 is specifically recruited to acetylated lysines on H3 and H4, an interaction which is associated with active transcription and mitosis. Furthermore permissive RNA polymerase II (Pol II) transcription is facilitated by BRD2 and BRD3 recognition of the acetylated nucleosomes, with BRD4 playing a key role in the polymerase recruitment.^{68,69} The BD2 domain of BRD4 recognizes and interacts with the acetylated region of cyclin T1, which complexes with cyclin-dependent kinase 9 (Cdk9) to form the active form of the positive transcription elongation factor b (P-TEFb) (Figure 1.16).⁷⁰

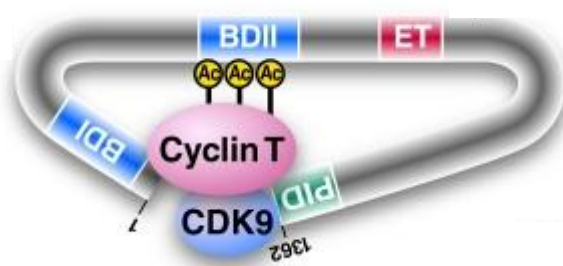


Figure 1.16. The active form of P-TEFb, depicted here by the cyclin T1 and Cdk9 complex, binds to BRD4 BD2 through the recognition of the acetylated Cyclin T segment of P-TEFb. Image reprinted with permission from Schroder *et al.*, *J. Biol. Chem.*, **2012**, 287, 1090.⁷⁰

The recruitment of active P-TEFb is crucial for the sustained presence of Pol II in active genes and for transcription initiation and elongation.⁷⁰ The expression of cell proliferation supporting genes, in particular the genes required in M to early G1 phase transition, is dependent on the recruitment of P-TEFb and Pol II by BRD4. The crucial role of the BET family in gene transcription and mitosis makes it an attractive biological target in a plethora

of diseases, including cancer, respiratory and immuno-inflammatory diseases, the latter of which is the particular concern of the work within this report.

1.3.1 First bromodomain inhibitor exemplars

The first selective BET inhibitors were reported in parallel in 2010. JQ1 and I-BET762 were developed by the Bradner group and GSK respectively and are both based on triazolodiazepine structures (Figure 1.17). The structures of the compounds were similar to those identified in a Mitsubishi Pharmaceuticals patent, published in 2009, in which triazolothienodiazepines were utilised for anti-inflammatory phenotypic screens.⁷¹

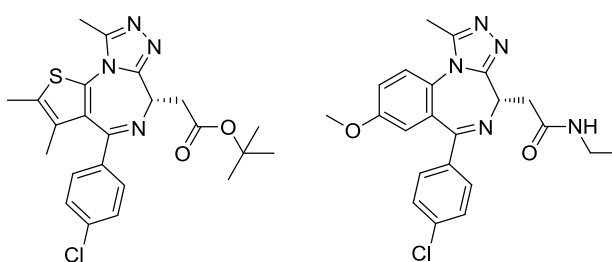


Figure 1.17. The structures of the known BET inhibitors JQ1 and I-BET762.

Apolipoprotein A1 (ApoA1) is the key protein in high-density lipoprotein (HDL). It has various atheroprotective functions, including cholesterol efflux from cells and anti-inflammatory effects.⁷² ApoA1 can inhibit monocyte activation and cytokine production and, as such, is an attractive drug target for therapies for inflammatory diseases. Upregulation of ApoA1 is associated with increased HDL levels and, therefore, anti-inflammatory properties. GSK completed a reporter phenotypic screen with the aim of finding hits that increased ApoA1 expression.⁷³ The human ApoA1 promoter and 3'-UTR were cloned flanking a luciferase reporter gene and transfected into HepG2 cells to generate a stable human HepG2 hepatocyte cell-line containing an ApoA1 luciferase reporter.⁷⁴ As such, increased ApoA1 expression also results in increased luciferase expression. Luciferases are a class of oxidative enzymes that enable the organisms that express them to bioluminesce (Figure 1.18).

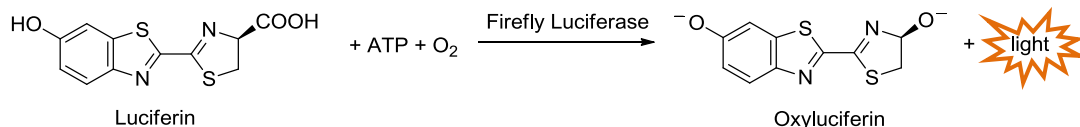


Figure 1.18. The luciferase catalysed conversion of luciferin to oxyluciferin which results in bioluminescence through the release of light.

A wide range of undisclosed chemotypes were identified from a phenotypic screen against the HepG2 cell-line.⁷⁴ From this effort, the triazolodiazepine series was discovered, of which several analogues demonstrated potent induction of the ApoA1 reporter gene. However, the biological target was still unknown and, as such, a chemoproteomics approach was employed. A potent analogue of the triazolodiazepine series was linked to a ReactiGel matrix to generate an affinity matrix. A control matrix using an inactive analogue was also created. Affinity chromatography was performed, in which HepG2 cell lysates were passed over the matrices, followed by extensive washing (Figure 1.19).

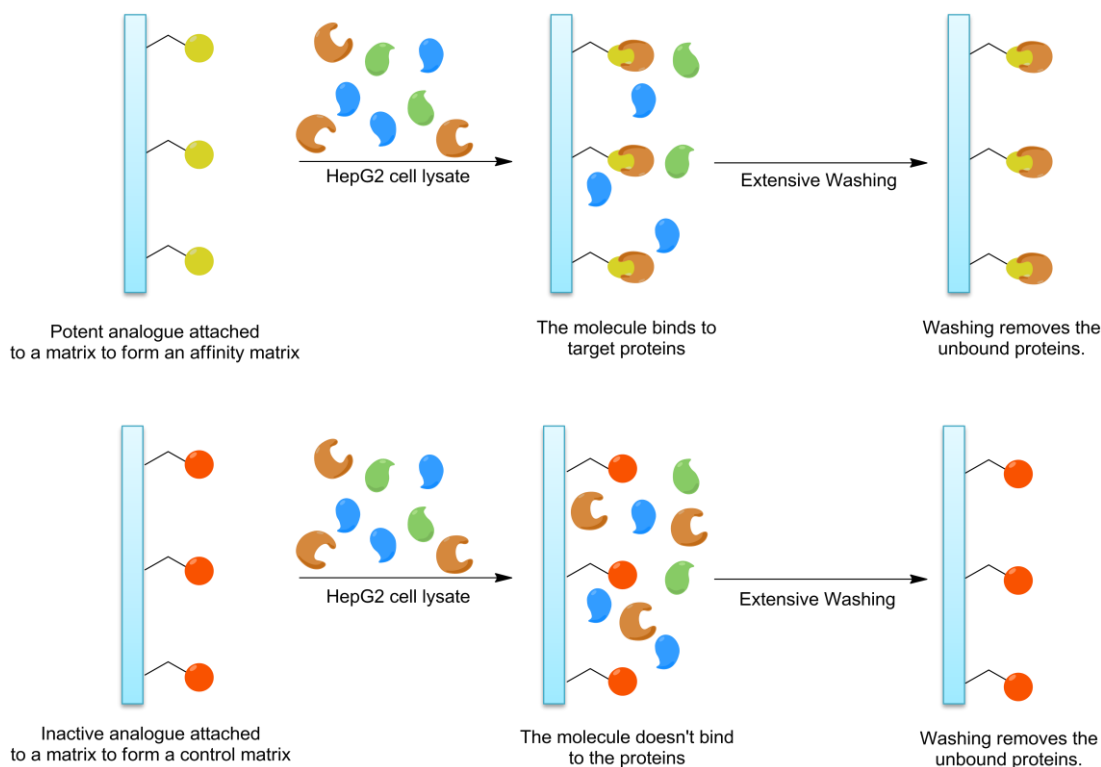


Figure 1.19. A potent analogue of the triazolodiazepine series was linked to a ReactiGel matrix to generate an affinity matrix. A control matrix using an inactive analogue was also created. HepG2 cell lysates were passed over the matrices and the potent analogue binds to target proteins whilst the inactive analogue doesn't bind. The matrices are extensively washed, removing all unbound proteins.

A consistent set of proteins were retained on the active matrix but not on the inactive matrix, suggesting they were the specific protein targets of the triazolodiazepine compound. Mass spectrometric analysis of the proteins captured on the active matrix by LC/MS/MS identified fragment peptides from just three proteins; BRD2, BRD3 and BRD4. The absence of other proteins on the matrix was an early indication that the triazolodiazepine analogues were highly selective for BET proteins. Mitsubishi Pharmaceuticals employed a similar approach in their discovery of JQ1.⁷³ Crystallography revealed that the triazole moieties of the triazolodiazepine series, including JQ1 and I-BET762, form hydrogen bonds with the conserved Asn residue and through-water hydrogen bonds with tyrosine, mimicking the natural acetylated lysine ligand (Figure 1.20). The pendant aryl rings are positioned on the WPF shelf and the fused aryl rings are directed through the ZA channel.

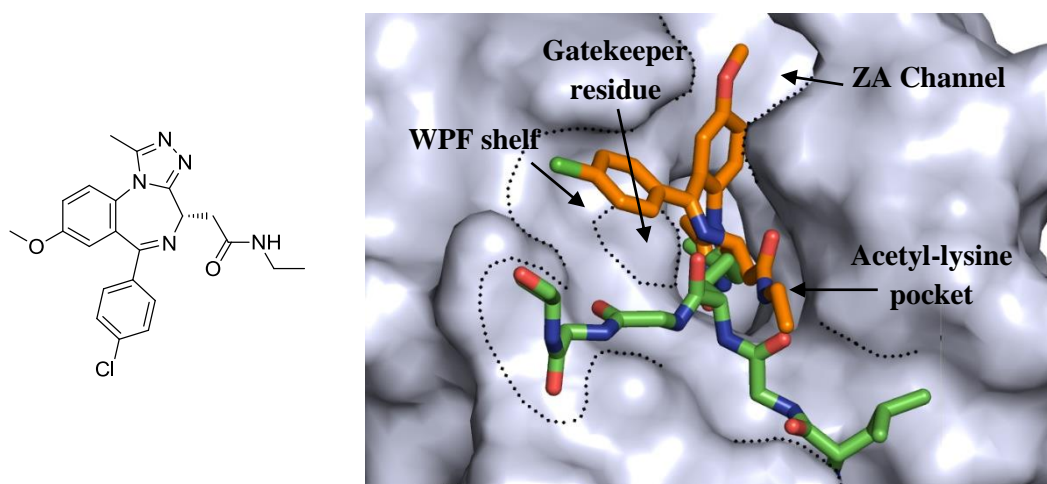


Figure 1.20. Structure of closely related analogue of I-BET762 (orange) bound to the acetyl-lysine binding pocket of BRD4-BD1 overlaid with acetylated histone H4 peptide. Reprinted with permission from Chung *et al.*, *J. Med. Chem.*, **2011**, *54*, 3827.⁷⁴

Despite being initially promising, JQ1 exhibits a short half-life in human hepatocytes and blood *in vitro*, reasons for which are not disclosed, which limited its progression into clinical trials. However, its high potency and selectivity for BET proteins has enabled it to become a powerful chemical probe. Meanwhile, I-BET762 is currently in phase I trials for the treatment of nuclear protein in testis (NUT) midline carcinoma, a rare and lethal form of cancer.⁷⁵ It has also been shown to inhibit T-cell mediated inflammation in a rat model to a similar level to that of the positive control, rapamycin. Furthermore, it was demonstrated that I-BET762 could be used to impact inflammation preclinically. Numerous inflammatory genes are upregulated upon the lipopolysaccharide (LPS) stimulation of bone marrow-

derived macrophages (BMDMs).⁷⁶ Pre-treatment of the BMDMs with I-BET762 prior to LPS stimulation resulted in a downregulation of LPS-inducible genes. In particular, the expression of key LPS-inducible cytokines and chemokines was suppressed, along with a number of transcription factors. This effect was highly selective with only specific cytokines and chemokines affected including tumour necrosis factor alpha (TNF α) and interleukin 6 (IL-6).⁶² In the absence of LPS stimulation, marginal effect on the upregulation of genes was observed. Furthermore, the expression of housekeeping genes and viability of BMDMs was not affected by I-BET762. These effects are similar to those demonstrated by the siRNA-mediated knockdown of inflammatory gene expression, therefore validating the anti-inflammatory potential of BET inhibitors.

Treatment of BMDMs with I-BET762 was shown to significantly reduce levels of associated proteins by a chromatin immunoprecipitation (ChIP) assay, a powerful technique for probing DNA-protein interactions, and can be used to identify multiple protein's transcription factors within a specific region of the genome e.g. transcriptional start sites (TSS).⁶² These studies revealed diminished levels of the BET proteins, as well as P-TEFb and RNA Pol II on TSS of genes affected by BET inhibition (sI-BET genes), when in the presence of I-BET762 relative to a DMSO control. This suggests that the lower levels are as a result of BET inhibition rendering the BET proteins incapable of recruiting the transcriptional machinery. However, whilst these effects were detected in sI-BET genes, pre-treatment of the BMDMs with I-BET762 did not result in diminished levels of the targets in genes not affected by BET inhibition (naI-BET), therefore implying key housekeeping genes would not be affected by BET inhibition.

A study investigating the genome-wide effects of I-BET762 on LPS-inducible genes gave insight into its selectivity. A marked difference between the levels of epigenetic markers was observed between the various genes, thus indicating that I-BET762 does not impact the gene expression of all LPS-inducible genes. It was found naI-BET genes exhibited elevated basal levels of histone acetylation, indicating they were already actively involved in transcription e.g. housekeeping genes.⁶² This exquisite selectivity suggests that downregulation of pro-inflammatory genes whilst maintaining levels of key housekeeping genes is possible, thus minimising the risk of the dysregulation of normal bodily functions. This would be of particular advantage to patients suffering with chronic immuno-inflammatory diseases, thus suggesting BET inhibition could be a viable therapeutic approach for the treatment of such diseases, for example rheumatoid arthritis.

1.3.2 BET inhibition as a strategy to treat rheumatoid arthritis

Rheumatoid arthritis is an immuno-inflammatory that characterised by elevated levels of key inflammatory cytokines including tumour necrosis factor alpha (TNF α), interleukin 6 (IL-6) and monocyte chemoattractant protein-1 (MCP-1).⁶² Therefore, the ability of the small molecule BET inhibitor I-BET762 to inhibit T-cell mediated inflammation in rat models, as well as down regulate key LPS-inducible cytokines and chemokines in pre-treated BMDMs prior to LPS stimulation suggests, that BET inhibition could potentially be used to treat rheumatoid arthritis.

1.3.2.1 Rheumatoid arthritis

Rheumatoid arthritis (RA) is the most common chronic immuno-inflammatory disease, affecting 0.5-1% of the human population with an incidence of 24-45/100,000 people per year.⁷⁷ It is primarily a disease that attacks the synovial joints, ultimately leading to joint degradation, but it can also affect many tissues and organs. As such, if incorrectly treated, RA can result in severe morbidity and disability.⁷⁸ RA onset increases in prevalence with age, typically occurring between 35-55 years of age and affecting females more than males.⁷⁹ The severity of RA means the majority of patients require continuous treatment to prevent disease progression. Furthermore, due to the destructive nature of RA on the joints, many patients also require surgery, such as hip or knee replacements.

Incidence and prevalence of RA varies significantly between populations of different geographic areas and over time. Genetic factors alone cannot explain these differences, rather a combination of environmental and gene-environmental factors is needed. Continuous monitoring of current trends in RA incidence is difficult due to the requirement of monitoring the disease profile over a long-time period. As such, the majority of incidence and prevalence studies are based on historic data, e.g. the 20th century. For example, a study completed on patients in Olmsted County, Minnesota suffering with RA between 1995-2007 is one of the more recent incidence studies for America.⁸⁰ The study comprised 466 patients, 66% female, with a mean age of 55.6 years. This study showed that the age-adjusted incidence was 53.1/100,000 and 27.7/100,000 for women and men respectively. While most studies show a slow reduction in RA incidence, including the USA, Finland and Japan, others have revealed an increasing incidence such as in Denmark.⁸¹⁻⁸³ The reduced incidence of RA has been reported to be influenced by the increased usage of hormonal contraception and the presence of a birth cohort effect, although there is no definitive evidence for this.⁸⁴

A recent study completed by Abhishek *et al.* examined the changes of incidence and prevalence of RA in the UK between 1990 and 2014.⁸⁴ The overall rates for each year were standardised to the 2014 population and the regional rates were standardised to the overall population. The study revealed the incidence and prevalence of RA in 2014 was 38.1/100,000 people per year and 0.67% respectively. Furthermore, the annual incidence of RA has decreased between 1990 and 2014 (Figure 1.21).⁸⁰

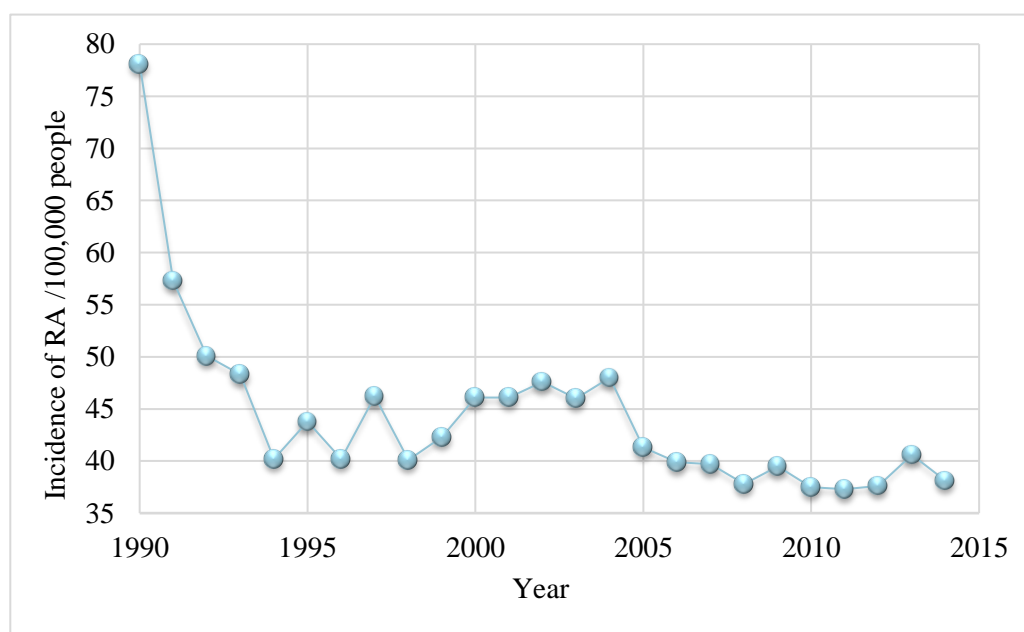


Figure 1.21. Incidence of RA in the UK between 1990 and 2014. This graph was recreated with permission using data from Myasoedova *et al.*, *Arthritis Rheum.*, **2010**, 62, 1576.⁸⁰

The diagnosis and assessment of RA is predominately based on semi-quantitative diagnostic methods, including symptoms, joint damage and physical function.⁷⁷ However, due to the commonality of symptoms across various types of arthritis, it can often delay the accurate prognosis of RA. Whilst most types of arthritis are due to general wear and tear, e.g. osteoarthritis, rheumatoid arthritis is an auto-immune disease in which the body incorrectly identifies the body's tissues as foreign tissues and attacks them.⁸⁵ This therefore leads to an elongated immune response relative to other arthritis types. RA is often monitored by radiographs or x-rays which allows the visualisation of the joints and synovial membranes. In addition, regular blood tests are taken in which levels of C-reactive protein (CRP) and the erythrocyte sedimentation rate (ESR), key indicators of the degree of inflammation, are measured. Clinical responses to treatment are often reported as ACR scores, named after the American College of Rheumatology, which show the difference in a measurable criterion,

e.g. ACR50 reflects a 50% improvement in patients.^{86,87} A treatment needs to achieve an ACR20 in patients to be clinically significant.

To date, there is no cure for RA and the successful management of the disease depends on early detection and severe treatment (Section 1.3.2.3, *vide infra*). This is in part due to the cause of the disease still remaining unknown, but also due to the complex molecular mechanisms involved with RA.⁷⁷

1.3.2.2 Pathogenesis of rheumatoid arthritis

The synovial membrane, termed the synovium, lines the joint capsule of all synovial joints where it reduces friction between the cartilage by secreting synovial fluid. The synovial membrane is formed of two layers: the outer layer (subintima) and the inner layer (intima). The intima is responsible for maintaining the inner joint homeostasis and mainly comprises specialised macrophages, termed macrophage-like synovial cells, and fibroblast-like synoviocytes (FLS).⁸⁸ Inflammation of the synovium, a hallmark of RA, causes an immune response which results in a unique inflammatory microenvironment, known as synovial hyperplasia.⁸⁹ This is characterised by increased levels of macrophages and FLS, as well as the recruitment of other innate immune cells including neutrophils, mast cells, dendritic cells and lymphocytes as well as adaptive immune cells such as T and B cells (Figure 1.22).⁹⁰ FLS accumulate to form a pannus tissue, which can display tumour-like invasive and destructive characteristics enabling them to attach to and invade cartilage and surrounding bones thus mediating their destruction. In addition, both the FLS and macrophages contribute further to the inflammatory microenvironment by directly producing pro-inflammatory factors.

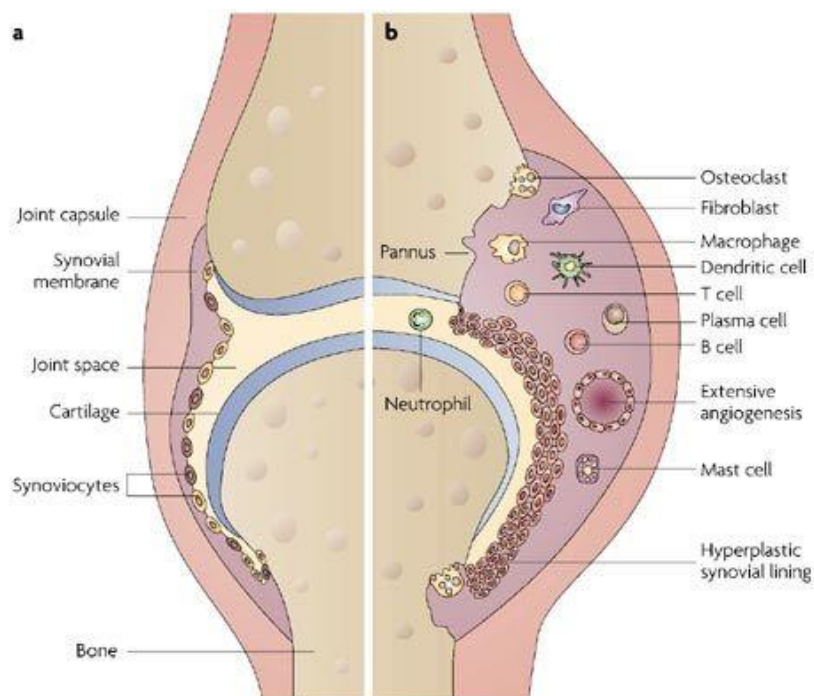


Figure 1.22. Comparison of a) a normal and b) RA synovial joint. The RA synovial joint features a pannus, containing innate and adaptive immune cells including macrophages, FLS, T cells and B cells. The joint is inflamed relative to the normal joint, and bone degradation is observed. Reprinted with permission from Strand *et al.*, *Nat. Rev. Drug Discov.*, **2007**, *6*, 75.⁹¹

Macrophages secrete cytokines and chemokines, the former of which mediate complex interactions amongst the inflammatory cells. As such, increased levels of cytokines are typically observed within RA patients. To add extra complexity, T cells within the synovium interact with dendritic cells, which are renowned for their antigen-presenting nature in the immune system. This interaction, along with interactions with monocytes and macrophages, triggers the production of several cytokines and chemokines by synovial macrophages including TNF α , IL-6 and MCP-1.⁹²

TNF α is a cytokine responsible for regulating immune cells. It is primarily secreted by myeloid lineage cells, such as macrophages and monocytes, but can also be produced by lymphocytes, neutrophils and mast cells.⁹³ TNF α promotes the inflammatory response and, as such, exacerbates RA symptoms further.⁹⁴ TNF α is a strong inducer of other cytokines and chemokines, including IL-6 and MCP-1, and induces FLS-proliferation.⁸⁹ Studies have showed blocking TNF α significantly reduced joint inflammation and cartilage degradation, thus confirming its key role in the pathogenesis of RA.⁹⁵

IL-6 is a multifunctional cytokine which has been found to be present in elevated levels within synovial fluid of RA patients.⁹⁶ Furthermore, the expression levels correlate with the

severity of bone and cartilage degradation. Within the synovium, IL-6 is produced by FLS and further promotes FLS proliferation. Its role within RA is exemplified by the lack of development of RA in multiple IL-6 deficient murine models.⁹⁷ Furthermore, the chemokine MCP-1 has been shown to have a fundamental role in recruiting monocytes to the synovium, again inducing further inflammatory response.⁹⁸

The secretion of MCP-1 by FLS or synovium cells is independent of cytokine stimulation and, as such, can promote myeloid cell accumulation in synovial joints prior to the elevation of cytokine levels. Overall, the pathogenesis of RA is extremely complicated, with each component playing multiple stimulatory roles. It is for this reason that the treatment and management of RA is reported to be difficult.

1.3.2.3 Treatment options for rheumatoid arthritis

At present, there is no cure for RA, with current treatments aimed at controlling inflammation and slowing down joint destruction. Three categories of therapies exist; corticosteroids, small molecule disease-modifying antirheumatic drugs (DMARDs) and biologic disease-modifying antirheumatic drugs. Corticosteroids are often prescribed on a short-term basis to relieve acute symptoms, e.g. reduce inflammation and pain. However, it is DMARDs that show the most efficacy and form the main treatment for RA. They have been significantly improved in the last decade with the emergence of several biologic agents and the re-examining of chemical agents in order to achieve higher efficacy.

The most common small molecule DMARD is methotrexate (MTX) which demonstrates the highest retention rates compared to other drugs (Figure 1.23).⁹⁹ Early efficacy studies showed 71% and 69% of patients demonstrated >50% reduction in the painful and swollen joint indices respectively. As its clinical efficacy has not been surpassed by other synthetic DMARDs, or by TNF α inhibitor monotherapies, methotrexate is often the first medication to be administered to RA patients.¹⁰⁰ Although the mechanism of action of methotrexate is not well understood, it has been shown to inhibit IL-1 and IL-6 activity, both of which are key proinflammatory cytokines in RA.¹⁰¹

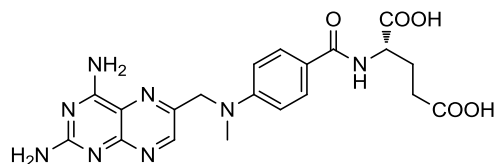


Figure 1.23. Structure of methotrexate.

Whilst small molecule DMARDs have proven to be efficacious and have therapeutic benefits, unfortunately, they are not suitable for all patients. In particular, methotrexate can result in hepatotoxicity or elevated liver enzymes, amongst other side effects, upon which the treatment cannot be sustained.¹⁰² In addition, the complex pathogenesis of RA means small molecule DMARDs are inactive in some patients due to alternative inflammatory processes stimulating the RA. Therefore, recent research has been focussed on the development of biologic DMARDs to modify the immune systems of patients who are not responding to small molecule DMARDs. These modern biologics, which are genetically engineered to mimic natural immune system proteins, have greatly improved treatment for many RA patients. Although they do not cure RA, they have been shown to dramatically slow its progression with reduced inflammation and joint damage observed. Furthermore, the development of the biologic DMARDs allows key proinflammatory cytokines, e.g. TNF α , to be targeted.¹⁰³ Their power can be seen in patients with early RA, where a similar clinical response was seen compared to methotrexate treatment but a significantly higher proportion of patients had no radiographic disease progression.

Although reduced radiographic disease progression is achieved by monotherapy biologic versus small molecule DMARDs, the similar clinical response led to research into combination therapies. Adalimumab (ADA) is an antiTNF α human monoclonal antibody approved by the FDA in 2008. It binds to TNF α , preventing its interaction with the TNF α receptor and thus reducing the inflammatory response. Whilst comparable ACR50 numbers, where a 50% reduction of RA symptoms is observed as defined by the American College of Rheumatology, were achieved for monotherapy adalimumab and methotrexate respectively, patients treated with methotrexate showed twice as much disease progression.⁷⁹ However, when the two therapies were co-administered, significant improvements in the clinical response was observed with a large proportion of patients achieving and maintaining the ACR50 for two years of treatment.¹⁰⁴

Whilst there have been major advancements in the treatment of RA, its complex pathogenesis means that there is still no cure. Not all patients respond to the treatments or maintain a clinical response over time. In such cases, patients need to switch to alternative

therapies, often within 24 months of therapy initiation. As RA treatments typically take 6-12 weeks to produce effects, this can lead to short term disease progression and joint damage. Furthermore, as small molecule DMARDs are immuno-suppressants, patients are at increased risk of infection as well as common side effects including nausea, abdominal pain and serious lung and liver toxicities.¹⁰⁵ Therefore, there is still a need for drugs with fewer side effects and increased success rates. One such way of doing this is to prevent the expression of cytokines rather than targeting the existing elevated levels observed within RA patients. This could be achieved by inhibiting bromodomain-containing proteins thus preventing the recognition of acetylated lysine residues and subsequent gene expression. As aforementioned, the BET family is a key family of bromodomain-containing proteins that has been extensively researched for a number of indications, with multiple small molecule inhibitors already progressing through the clinic.

1.3.3 BET inhibitors: current state-of-the-art

Since the discovery of JQ1 and I-BET762, a wide range of other KAc mimetics have been explored including, but not limited to, scaffolds which contain quinazolinones,¹⁰⁶ dimethylisoxazoles¹⁰⁷ and dimethyltriazole¹⁰⁸ (Figure 1.24).

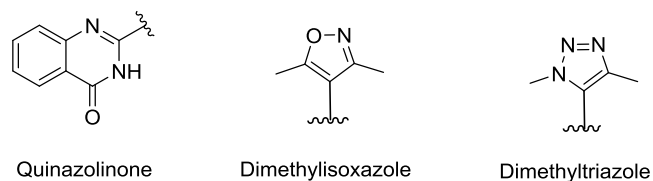
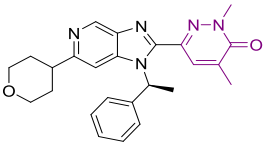
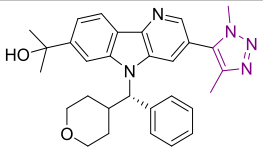
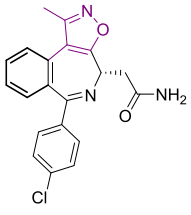
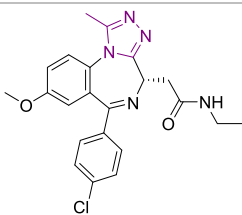
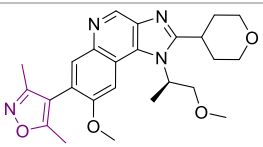


Figure 1.24. A wide range of acetylated lysine mimetics have been explored since the discovery of JQ1 and I-BET762. Some examples include the quinazolinone, dimethylisoxazole and dimethyltriazole.

At the point of writing this thesis, fifteen small molecule BET inhibitors have been progressed to the clinic, with thirteen currently in early phase trials (Table 1.1)^{109,64} Where the structures have been disclosed, the acetylated lysine mimetic is highlighted in purple to exemplify the large range of mimetics that have been discovered.

Compound	Sponsor	Disease	Phase	Identifier
 ABBV-075	AbbVie	Solid tumours and various cancers	I	NCT02391480
BAY1238097	Bayer	Solid tumours and lymphoma	I (terminated)	NCT02369029
 BI 894999	Boehringer Ingelheim	Solid tumours	I	NCT02516553
 BMS-986158	Bristol-Myers Squibb	Solid tumours	I/II	NCT02419417
 CPI-0610	Constellation Pharmaceuticals/ Roche	Various cancers Peripheral nerve sheath tumours II	I I	NCT01949883 NCT02157636 NCT02158858 NCT02986919
FT-1101	Forma therapeutics	AML, MDS	I	NCT02543879
GS-5829	Gilead	Various cancers and solid tumours	I /II	NCT02392611 NCT02983604 NCT02607228
 I-BET762	GlaxoSmithKline	Various cancers and solid tumours	I/II	NCT01943851 NCT01587703 NCT02964507
 GSK2820151	GlaxoSmithKline	Solid tumours	I	NCT02630251
INCB054329	Incyte	Hematologic	I/II	NCT02431260

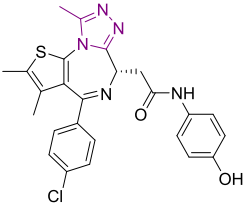
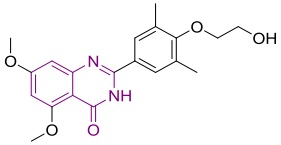
			malignancies, solid tumours		
	Merck/ Mitsubishi Tanabe	AML and solid tumours	I	NCT02698189 NCT02698176	
OTX015					
PLX51107	Plexxicon	Solid tumours, various cancers	I	NCT02683395	
	Resverlogix Corp	Type 2 diabetes mellitus patients with coronary artery disease	II (recruiting)	NCT0258615 5	
RVX-208					
TEN-010	Hoffman- LaRoche	AML, solid tumours	I	NCT02308761 NCT01987362	
ZEN003694	Zenith Epigenetics	Metastatic CRPC	I	NCT02705469	

Table 1.1. The candidates progressing through clinical trials as of April 2018.

The last five years has seen a significant increase in the number of small molecule BET inhibitors progressing to the clinic, with the majority of the clinical candidates being investigated as treatments for severe oncology indications. GSK developed a potent inhibitor, GSK2820151, incorporating a dimethylisoxazole warhead, which has improved pharmacological properties relative to I-BET762 in preclinical studies.¹¹⁰ RVX-208, developed by Resverlogix Corp, is the first example of a BD2 selective inhibitor. It is currently in phase III clinical trials for atherosclerosis and associated cardiovascular disease (CVD) where it has displayed profound effects in patients with established CVD. Treatment with RVX-208 resulted in increased HDL and ApoA1 levels and decreased the incidence of major adverse cardiac events (MACE).¹¹¹

A close analogue of JQ1 developed by OncoEthix, OTX015, is currently in phase I clinical trials for acute leukaemia.¹¹² It has been shown to inhibit proliferation in a wide range of hematologic malignancies and solid tumour cell lines *in vitro*. In *in vivo* studies, OTX015 inhibited tumour growth in a NUT midline carcinoma (NMC) model with a BRD4–NUT fusion.¹¹³ This initiated a phase I clinical trial for NMC patients, in which dramatic clinical and radiologic responses were observed in two of the four patients and stabilisation of the disease in a third. Also being investigated as a treatment for NMC and progressing through multiple phase I clinical trials is CPI-0610, discovered by Constellation Pharmaceuticals.¹¹⁴

The candidate TEN-010, developed by Tensha Therapeutics is also being investigated as a treatment for NMC and Bayer have completed a first time in man study with BAY1238097 for patients with solid tumours and lymphoma.⁴⁰ Unfortunately, the exact structure of the majority of the clinical compounds have not been disclosed, with companies preferring not to specify from their patents.^{39, 40, 114, 115}

Upon completion of the trials, a total of fifteen inhibitors would have been assessed in humans, providing a strong basis for considering the overall profiles of BET inhibitors in humans.

1.3.4 Current limitations of BET inhibitors

Pan-BET inhibition has been shown preclinically to result in on-target toxicities, particularly gastrointestinal (GI) effects. As such, the toxicities associated with pan-BET inhibitors have limited their therapeutic indications to severe diseases, with most of current preclinical pan-BET inhibitors having primary indications of cancer.¹⁸ During the clinical trials of OTX015, common toxic effects reported were thrombocytopenia, anaemia, neutropenia, fatigue and GI events including diarrhoea and nausea.¹¹⁶ Furthermore, despite the impressive clinical activity observed, the disease often progressed transiently after relatively short interruptions of BET inhibition. This implies that continuous dosing of the inhibitor is required to maintain the antitumour activity. As well as this, progressive disease states were observed after several months of treatment in a number of patients, suggesting that secondary resistance mechanisms are possible. This is supported by the recent study in which triple-negative breast cancer was shown to overcome BET inhibition through BRD4 phosphorylation, allowing it to remain associated with chromatin through interaction with MED1 (a mediator of RNA polymerase II).¹¹⁶

Furthermore, a recent study using an inducible and reversible transgenic RNAi mouse model, was used to demonstrate that strong inhibition of BRD4 in adult animals has dramatic effects in multiple tissues.¹¹⁷ BRD4-depleted mice displayed reversible epidermal hyperplasia, alopecia, and decreased cellular diversity and stem cell depletion in the small intestine. As well as this, the intestines became sensitive to organ stress and demonstrated impaired regeneration following irradiation. Therefore, it can be suggested that concurrent BRD4 inhibition and cytotoxic therapies may result in undesirable synergistic effects. As such, there is a demand for BET inhibitors with an improved safety profile and reduced toxicity, allowing their use as therapies in alternative indications.

The safety profiles of current BET inhibitors have limited their use to potentially fatal diseases, e.g. cancer, where the toxicities are considered acceptable due to the severity of the illness. However, for the use as a therapy in chronic diseases, an inhibitor with fewer side effects is required. It has been hypothesised that the toxicities observed with BET inhibitors are due to BD1 inhibition. As such, GSK are employing two approaches towards BET inhibitors for immuno-inflammation indications to try to mitigate the risks: BD2-selective molecules and a targeted drug delivery method using molecules incorporating an esterase sensitive motif (ESM). This report will focus on the latter approach.

1.4 Current state of the art of targeted drug delivery

A concept of targeted delivery of a drug to a specific target cell type would reduce drug-induced toxicities and increase the therapeutic index. However, this concept has a challenge on three fronts: identifying the desired target, developing the optimal drug and finding a suitable drug carrier.¹¹⁸ Once these factors have been established, four key aspects need to be optimised to create an effective targeted drug delivery system; retain, evade, target and release.¹¹⁹ The delivery vehicle must be able to transport efficient loadings of the drug in a stable form whilst avoiding immunogenic or metabolic machinery, thus giving it a sufficient residence time in the circulation. Furthermore, it must feature specific characteristics which direct the vehicle, and allow it to be retained, within the target site where it must release the drug within an appropriate timeframe to ensure effective function of the drug.

Targeted drug delivery systems can be classified into two categories of passive and active targeting. Passive targeting involves drug accumulation in areas with leaky vasculature around the target, e.g. tumours. This leads to enhanced permeation and retention (EPR), thus termed the EPR effect. This type of targeting is achieved by incorporating the drug into a nanoparticle or a macromolecule.¹²⁰ This area is widely researched which has led to the development of a multitude of delivery vehicles including liposome, nanotubes and dendrimers. Meanwhile, active targeting is the formation of specific interactions between the delivery system and the target cells, typically through ligand-receptor interactions, which are only possible at close proximities (<0.5 nm).¹²¹ This requires the drug to be conjugated to a tissue or cell specific ligand.¹²²

1.4.1 Liposomal delivery system

The most common vehicle employed for targeted drug delivery is the liposome. However, the concept of liposomes has also been extended to micelles, monolayer lipids rather than the bilayer as in liposomes, and dendrimers, which are also polymer-based spherical systems. Liposomes are non-toxic, non-hemolytic and non-immunogenic, which can increase their residence times.¹²³ They are also biocompatible and can be designed to evade clearance pathways e.g. metabolic inactivation, renal clearance or the reticuloendothelial system (RES). For example, liposomes were originally found to be subject to immediate uptake and clearance by the RES in *in vivo* studies. However, coating the liposomes with polyethylene glycol (PEG) limits this uptake and significantly increases their circulation time, whilst retaining the passive targeting nature.¹²⁴ Furthermore, the use of liposomes allows the cargo to be stored in the hydrophobic shell or the hydrophilic centre depending on the nature of the drug, thus broadening the scope of drugs that can be utilised.¹²⁵ Enhanced liposomal vehicles incorporating antibodies on the surface, termed immunoliposomes, have also been researched with great success (Figure 1.25).

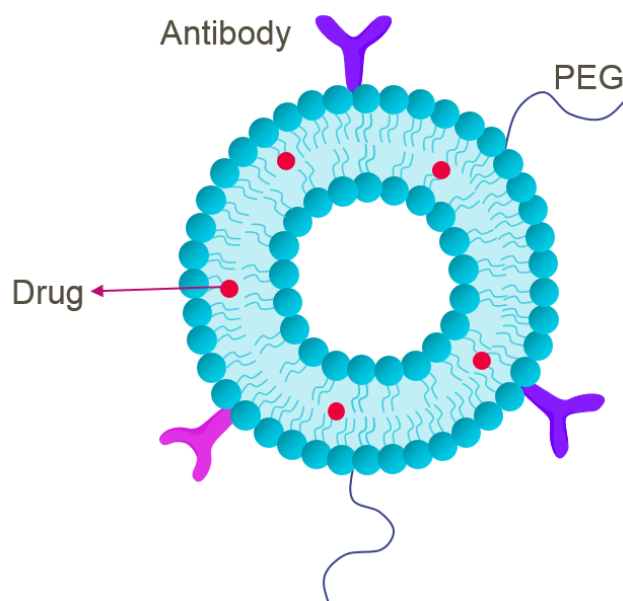


Figure 1.25. Structure of an immunoliposome in which the drug can be carried within the lipid bilayer or the hydrophilic centre depending on its properties. PEG attachments increase the circulation time by reducing RES uptake. Antibodies are attached to the surface of the liposome and direct the liposome to the target.

Liposomal delivery of drugs has been well researched, with multiple candidates progressing through clinical trials.¹²⁵ One example is the use of immunoliposomes to deliver doxorubicin to HER2 cells by incorporating anti-HER2 monoclonal antibodies into the liposome surface.¹²⁶ HER2 is a receptor tyrosine kinase that has a key role in the pathogenesis, associated with significant overexpression of HER2, in multiple cancers.¹²⁷ As such, HER2 is an attractive biological target and has already shown to be inhibited by doxorubicin.¹²⁸ Doxorubicin is a highly potent antineoplastic inhibitor that is used as a treatment for hematologic and solid cancers. However, its clinical use is limited by its toxicological profile which includes bone marrow toxicity, gastrointestinal problems and alopecia.¹²⁹

Initial studies with four different tumour xenograft models overexpressing HER2, showed significant growth inhibition and tumour regression upon dosing with doxorubicin contained within immunoliposomes (immunoliposome-dox). Furthermore, the cure rates reached 50%, whereas no cures were observed for free doxorubicin. Altogether, these results demonstrate that encapsulating doxorubicin in immunoliposomes greatly enhanced its therapeutic index as well as increasing the antitumour activity and reducing drug-associated toxicities.¹²⁶

1.4.2 Folate targeting agents

Folate targeting is another common delivery system, involving the conjugation of the vitamin folic acid (folate) to a drug. Folate has a natural high affinity for the folate receptor protein (FR), which is commonly expressed on the surface of tumour cells. Binding of folic acid to such cells, causes cellular uptake through endocytosis. The high affinity is retained for the drug-folate conjugates and, as such, allows the delivery of a drug directly to the tumour cells. This concept has resulted in four folate targeting drug delivery systems to enter the clinic, all of which are currently progressing through phase I/II trials. One such example is EC1456, a conjugate of folic acid and tubulysin which is undergoing assessment for solid tumours (NCT01999738) (Figure 1.26).¹²⁵

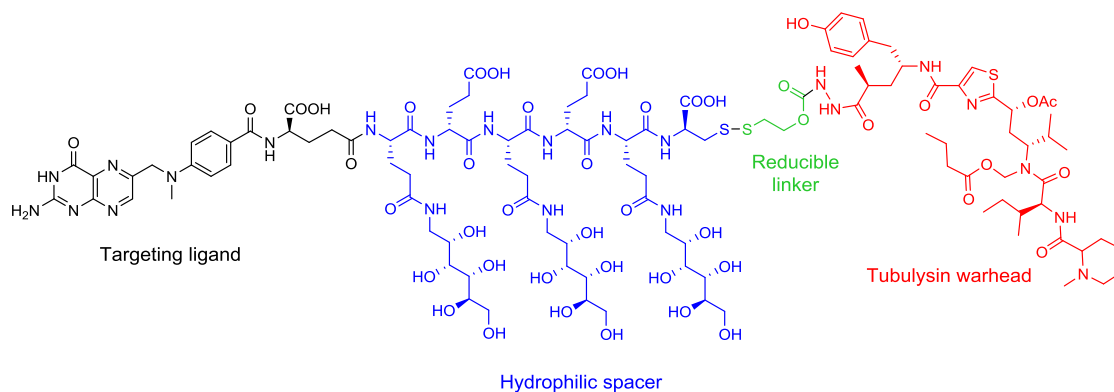


Figure 1.26. Structure of EC1456.

Tubulysins are naturally occurring cytotoxic tetrapeptides that demonstrate antimetabolic and antiproliferative activity against a multitude of cancers.¹³⁰ However, these properties also make them highly toxic in *in vivo* models.¹³¹ Therefore, it was thought that combining the drug with a targeted drug delivery vehicle would increase the therapeutic index and reduce the toxicities. Indeed, EC1456 has been shown to inhibit FR expressing cancer cell lines with nanomolar potencies, but is inactive in FR negative cell lines (Table 1.2).¹³²

Cell Line	Origin	FR Status	IC ₅₀ (nM)
KB	Human cervical carcinoma	+++	2.3
NCI	Human ovarian carcinoma	++	1.4
IGROV1	Human ovarian adenocarcinoma	+	0.72
MDA-MB-231	Human breast adenocarcinoma	+	0.47
A549	Human lung carcinoma	-	Inactive
H23	Human lung adenocarcinoma	-	Inactive
HepG2	Human hepatocellular carcinoma	-	Inactive
AN3CA	Human endometrial adenocarcinoma	-	Inactive
LNCaP	Human prostate adenocarcinoma	-	~850

Table 1.2. EC1456 is active in FR positive cell lines but inactive in FR negative cells lines. ‘+++’, ‘++’ and ‘+’ indicates high, moderate and low expression of the folate receptor respectively, whilst ‘-’ indicates no folate receptor expression.

In addition, *in vivo* murine models bearing FR positive human xenografts demonstrated complete remissions in 100% of the mice when dosed with EC1456.¹³³ Furthermore, no major organ tissue degeneration or noticeable weight loss, often seen with cancer treatments, were not observed thus showing the toxicities had been reduced, as hypothesised. As well as this, no significant anti-tumour activity was observed when mice were treated with a benign

folate ligand or free tubulysin B, thus showing that the effects of EC1456 were due to the uptake and accumulation within FR positive cell lines.¹³³ These preclinical studies show how powerful targeted drug delivery systems can be, with significant therapeutic advantages beyond the free drug.

1.4.3 Pro-drug targeted delivery

The term prodrug, first introduced in 1958 by Adrian Albert, is used to describe a molecule which has to be converted into the active drug before it has its biological effect.¹³⁴ Classical prodrugs typically consist of the drug molecule attached to a promoiety, which is transformed into the active drug through an enzymatic or chemical reaction. Prodrug methodology can be used to overcome issues such as bioavailability, solubility or toxicity. Furthermore, it has more recently discovered that it can be used to deliver drug molecules selectively to specific organs or cell lineages in a targeted approach.¹³⁴ In particular, targeting prodrugs to a specific membrane transporter or enzymes has potential in oncology indications. As aforementioned, targeted drug delivery often minimises the distribution of a drug within the body, thus reducing the quantity interacting with other tissues.¹¹¹ This may limit toxicity associated with off-target systemic toxicity. In addition, targeted delivery results in a higher concentration of the active molecule at the desired site and, as such, which often allows the dose to be reduced relative to non-targeted drugs. Therefore, targeted drug delivery using prodrugs can be used to improve therapeutic windows and reduce toxicity.

In an analogous method to the immunoliposomal delivery, a pro-drug approach has been investigated for the targeted delivery of doxorubicin.¹²⁹ Prostate cancer is the second most common cause of cancer-related deaths in males.¹³⁵ Its progression is associated with metastases in the bone and lymph nodes. Unfortunately, to date, there is no effective treatment for patients who no longer respond to hormone therapy. The use of chemotherapy is limited due to the lack of tumour selectivity and the observed toxicities.¹³⁶ As such, there is an unmet need for the development of a targeted drug delivery system that selectively transports the drug to the tumour and metastases.

Tumours are capable of trapping and degrading plasma proteins and using the degradation products to facilitate proliferation. Tumours uptake albumin through the EPR effect and, as such, human serum albumin (HSA) has had an increasing role as a drug carrier in a clinical setting in recent years.¹³⁷ This is possible due to a cysteine residue (Cys34) located in a hydrophobic groove of albumin, a feature which is unusual for extracellular proteins. As

such, this prevents the conjugation of the drug to other extracellular proteins, thus reducing selectivity issues. Therefore, doxorubicin was conjugated to albumin *via* a hydrolysable linker to form INNO-206 (Figure 1.27).¹³⁸

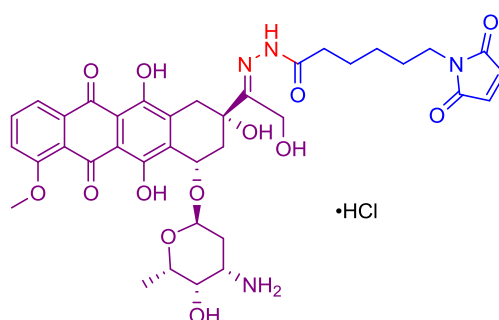


Figure 1.27. Structure of INNO-206 composed of doxorubicin (purple), a hydrolysable hydrazine linker (red) and a thiol-reactive linker (blue).

INNO-206 incorporates a maleimide that reacts rapidly with sulfhydryl groups through a Michael addition. This reaction is specific for sulfhydryl groups at physiological pH, thus increasing their selectivity for albumin. In addition, it contains an acid-labile hydrazine linker which facilitates the release of doxorubicin either extracellularly, in the slightly acidic environment present in tumour tissues, or intracellularly in acidic endosomal or lysosomal compartments.¹³⁹ *In vivo* murine renal cell carcinoma and mamma carcinoma xenograft models showed INNO-206 to be superior to free doxorubicin, with complete remissions of all models observed for INNO-206. Furthermore, the xenograft models revealed INNO-206 to have a maximum tolerated dose (MTD) of ~4 times higher than of free doxorubicin.^{138, 139} This significantly increased the therapeutic index relative to free doxorubicin. In addition, phase I studies showed a good safety profile and the ability of INNO-206 to induce tumour regression in cancers known to be doxorubicin-sensitive tumours.¹³⁸ To date, INNO-206 has progressed through seven phase I/II studies and recruitment is ongoing for an eighth phase I study, again emphasising the advantages of targeted drug delivery systems.

1.5 Development of a targeted delivery strategy using an esterase sensitive motif

An esterase sensitive motif (ESM) is another method that allows the molecules to act as targeted prodrugs, with the ester hydrolysed into the pharmacologically active acid *in vivo*. Interestingly, ESM-containing molecules are non-traditional pro-drugs in the sense that the parent molecule is also active. In 2006, Chroma Therapeutics released a patent which detailed the incorporation of an amino acid ester group within their drug molecules.¹⁴⁰ It was

postulated that the amino ester would increase the permeability of the molecule through the cell membrane compared to the parent acid (Figure 1.28). Intracellular hydrolysis by carboxyesterase enzymes would yield a pharmacologically active acid, which is charged and therefore not readily transported out of the cell. This would result in an increased localised concentration of the active molecule, therefore increasing the duration of action of the inhibitors in cells expressing specific carboxylesterases.

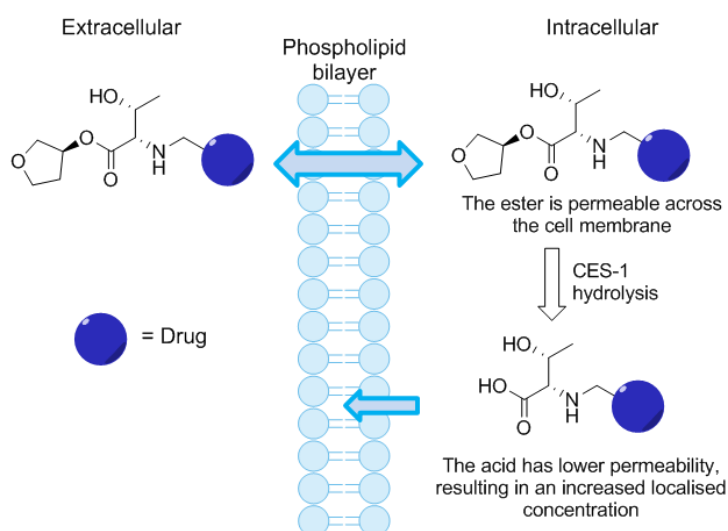


Figure 1.28. The ESM containing molecule was hypothesised to permeate through the cell membrane where it would be hydrolysed by CES-1. The resultant acid is less permeable, leading to retention and a higher localised concentration of the acid.

One of the recurring problems with drugs that act intracellularly is that their target enzymes are often part of signalling pathways that are active in most cells in the body.¹⁴¹ Therefore, toxic effects are often observed alongside the desired therapeutic effects. The range of drug dosages of a drug which can treat disease effectively without having toxic effects is commonly referred to as the 'therapeutic window'.¹⁰⁵ As such, selective delivery of drugs to specific cell types or cell lineages would have major advantages. The ESM technology is able to elicit such an effect as it shows specificity for human carboxylesterases (hCE).

1.5.1 Human carboxylesterases as metabolic enzymes

The carboxylesterase family are α,β -hydrolases comprising five isoforms which are responsible for the hydrolysis of esters and amides in xenobiotics, such as cocaine or heroin.¹⁴² The isoforms hCE1-5, classified based on sequence homology, with the majority

of the esterases falling into the hCE-1 and hCE-2 families. The hCE-1 isoform, otherwise known as CES-1, has a restricted expression profile in humans, with the highest levels found in hepatocytes, monocytes and macrophages. The CES-2 isoform is expressed mainly within the intestine, while CES-3 is found in the brain.¹⁴³ However, the expression profiles of CES-1 and CES-2 vary significantly across different species (Table 1.3).¹⁴⁴

Species	Isoform	Liver	Small Intestine	Kidney	Lung
Mouse	CES-1	+++	-	+++	+++
	CES-2	+++	+++	+++	-
Rat	CES-1	+++	-	+++	+++
	CES-2	-	+++	-	-
Beagle dog	CES-1	+++	-	NT	+++
	CES-2	++	-	NT	+
Monkey	CES-1	+++	++	-	NT
	CES-2	+	+++	+	NT
Human	CES-1	+++	-	+	+++
	CES-2	+	+++	+++	-

Table 1.3. CES expression profiles in different species where ‘+++’, ‘++’ and ‘+’ represent high, medium and low CES expression levels respectively, ‘-’ describes no expression and NT = not tested.

The most common drug substrates are ester prodrugs, typically used to enhance bioavailability, which must be hydrolysed to their active acid metabolite following absorption in the GI tract.¹⁴⁵ Although all carboxylesterases have broad substrate scopes, usually only one isoform predominates and forms the major metabolic enzyme. This is dependent on the structure of the substrate, in particular of the ester. Esters contain an acyl group and an alcohol group. The CES-1 enzyme prefers esters with a large, bulky acyl group and a small alcohol group, while CES-2 has the opposite preference, substrates with a small acyl group and a large alcohol group.

The CES enzymes comprise a central catalytic domain surrounded by α,β and regulatory domains. Structurally, the α,β -hydrolase-fold consists of a central β -sheet surrounded by α -helices and features a catalytic triad of serine, histidine and glutamic acid.¹⁴⁶ The triad is situated at the bottom of a 25 Å deep cleft, creating a hydrophobic active pocket and facilitating the metabolism of a wide range of hydrophobic substrates.¹⁴⁷ Adjacent to the active site in CES-1 is a large, flexible pocket on one side of the serine and a small, rigid

pocket on the opposite side. Next to the rigid pocket is an oxyanion hole, formed by two glycine residues.¹⁴⁴ Therefore, CES-1 has been proposed to prefer esters with large acyl moieties and small alcohol groups. A second hole is adjacent to the large pocket which facilitates the transport of small molecules in and out of the active site. The larger flexible pocket is lined by multiple non-polar residues and can accommodate larger molecules, whilst the smaller active site is lined with hydrophobic residues and prefers small methyl-ester or acetyl-type linkages. As such, the small, rigid pocket tends to be selective whilst the large, flexible pocket can tolerate a broad substrate scope. This is exemplified by the binding modes of cocaine versus heroin (Figure 1.29). Cocaine contains a large acyl group, the benzoylecgonine, which occupies the large, flexible pocket and a small methyl ester which sits in the small, rigid pocket. However, this does not stand true for heroin which has a small acetyl linkage and a large 6-monoacetylmorpholine alcohol moiety. Indeed, in this case, the acyl- and alcohol-binding pockets switch with the 6-monoacetylmorpholine occupying the large, flexible pocket.¹⁴⁶ This can be demonstrated by the crystal structures of structurally related analogues of cocaine and heroin, homatropine and naloxone respectively.

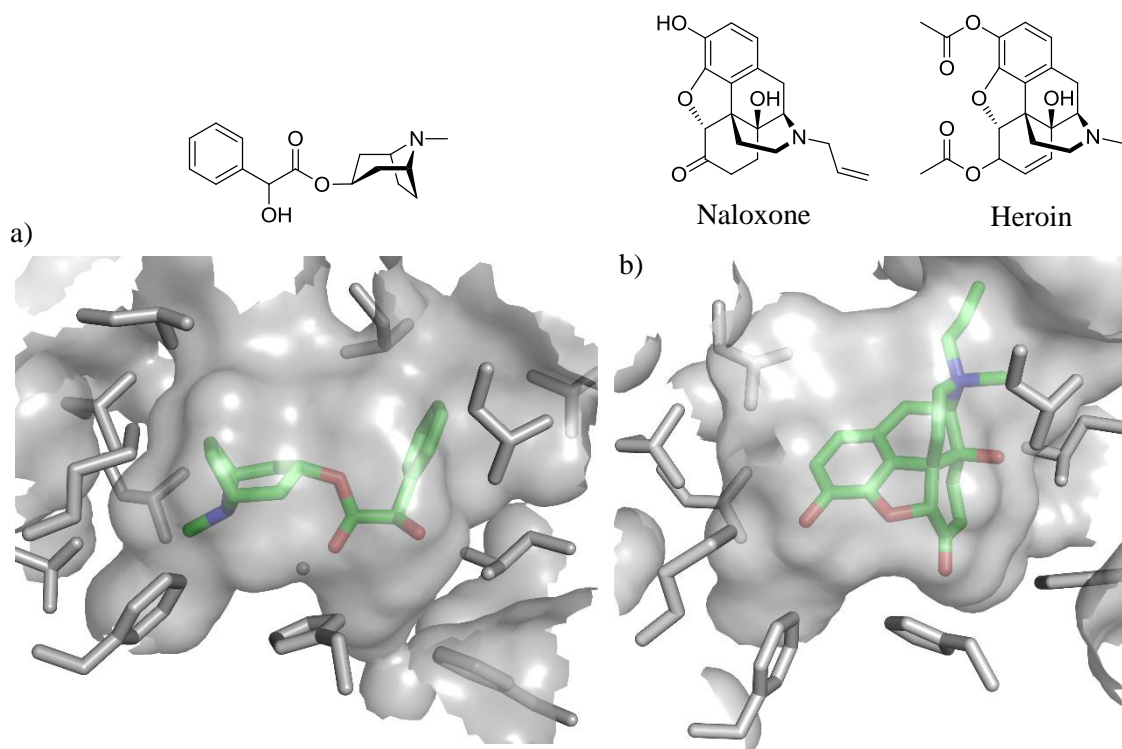


Figure 1.29. Crystal structures of a) Homatropine, an analogue of cocaine, in CES-1 (pdb: 1mx5). The acyl group is positioned in the flexible pocket. b) Naloxone, an analogue of heroin, in CES-1 (pdb: 1mx9) with the structure of heroin drawn for comparison. The phenol hydroxyl group of naloxone is directed towards the rigid pocket. The small methyl acyl group of heroin extends from this hydroxyl and thus would be positioned within the pocket, highlighting the binding mode can switch. Furthermore, significant movement in the residues of the flexible pocket can be seen between the two crystal structures, demonstrating further how the pocket can rearrange to accommodate a wide range of substrates.

1.5.2 ESM-containing inhibitors

Initial support for the proposed approach came from studies completed with the novel anticancer agent tosedostat, CHR-2797 (Figure 1.30). The phase II clinical candidate contains an amino acid ester motif that undergoes intracellular hydrolysis to the corresponding carboxylic acid.¹⁴¹

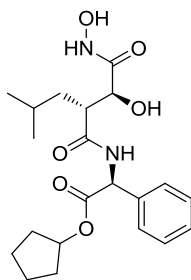
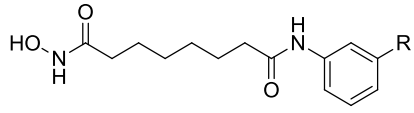


Figure 1.30. The structure of tosedostat, CHR-2797, a phase II clinical candidate that contains an amino acid ester motif.

In vitro and *in vivo* administration of tosedostat to human cells led to the intracellular build-up of the corresponding acid. This resulted in improved potency and increased duration of action.¹³⁸ However, the amino acid ester was hydrolysed by all three human carboxylesterases. It was concluded that in order to deliver an intracellularly acting drug to only CES-1 expressing cells, a CES-1-selective motif must be attached to a drug at a position which does not impede the target enzyme-inhibitor interaction. Further studies led to the discovery that an amine linkage, rather than the amide linkage found in tosedostat, led to ester hydrolysis in CES-1 positive, but not in CES-1 negative cells.¹⁴¹

Chroma investigated the effects of varying the ESM on a known HDAC inhibitor, vorinostat (SAHA, **1.1**, Table 1.4). The phenyl ring was substituted with different amino acid esters through an amine linkage. It was found that substitution remote from the hydroxamic acid binding site did not impact HDAC inhibition, as exemplified by the similar biochemical activity demonstrated by amino acid esters **1.2** and **1.3** relative to vorinostat, (Table 1.4).¹⁴¹ Furthermore, it was shown that unnatural amino acids were tolerated, with the unnatural amino acid phenyl glycine (**1.2**) and leucine (**1.3**) both demonstrating high potency in the enzyme and cellular assays. Most importantly, within CES-1-negative cell lines the antiproliferative potency of the HDAC inhibitors was similar to vorinostat, however, there was a 10- to 30-fold increase in potency in CES-1 positive cell lines, in particular MV4:11 cells, (Table 1.4). This is known as the 'ESM effect' and arises from the ester hydrolysis and subsequent acid retention within CES-1 positive cell lines.¹⁴¹ Interestingly, the *tert*-butyl ester (**1.4**) did not exhibit enhanced activity in the cellular activity, but rather displayed similar potency to vorinostat. This suggests that *tert*-butyl esters are not substrates for human carboxylesterases.



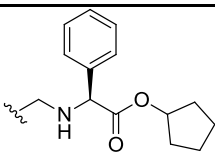
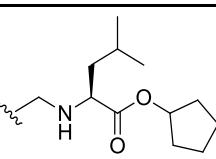
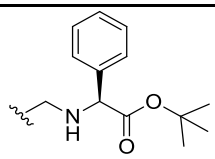
R	H (Vorinostat) 1.1	 1.2	 1.3	 1.4
Enzyme assay IC ₅₀ (nM)	78	53	75	132
Cellular assay IC ₅₀ (nM)	445	25	11	520

Table 1.4. Comparison of natural and unnatural amino acids as ESM in the HDAC enzymatic and hCE-1 positive MV4:11 cellular assays relative to the original inhibitor vorinostat.

These results indicate that amino acid ester-containing molecules can be selectively hydrolysed in CES-1 expressing cell lines to give enhanced potency. As CES-1 is thought to be expressed only in monocytes and macrophages, outside of the liver, an ESM-containing molecule could be used to direct therapeutic effects to the monocyte-macrophage lineage. Macrophages play a key role in inflammatory disorders in which they facilitate the release of pro-inflammatory molecules such as cytokines.¹⁴¹ They are the main cause of joint inflammation and joint destruction in rheumatoid arthritis. Consequently, targeting this cell type selectively could offer therapeutic treatments for immuno-inflammatory disorders. This was investigated by treating human blood with parent and ESM-substituted versions of HDAC inhibitors and monitoring their impact on protein acetylation.¹⁴¹ It was demonstrated that the incorporation of the ESM into known HDAC inhibitors produced extremely potent molecules with a wider therapeutic window than conventional HDAC inhibitors. In human blood, the effects of ESM-containing molecules on monocytes (CES-1 positive) were seen at concentrations 1000-fold lower than those on other cell types (CES-1 negative).¹⁴¹ Furthermore, it was reported that the use of secondary esters increases selectivity for CES-1 over the other two isoforms, whereas tertiary esters hinder hydrolysis completely. Therefore, esterase turnover can be fine-tuned by varying the ester group.

Similarly to HDAC proteins, the BET family of proteins play a key role in inflammatory responses. BET bromodomain inhibitors have been shown to suppress the expression of pro-inflammatory cytokines and chemokines in lipopolysaccharide (LPS)-stimulated macrophages *in vitro*.¹⁴¹ As such profound effects were observed with the ESM-containing

HDAC inhibitors, relative to their parent compounds, it was thought the same approach could be applied to BET inhibitors. Therefore, a medicinal chemistry programme focussed on ESM-containing BET molecules was instigated at GSK. The ESM programme is focussed on the selective delivery of BET inhibitors towards immune cells of the mononuclear myeloid lineage to deliver safer therapeutics.

1.6 Current state-of-the-art of BET inhibitor development within GSK

Upon starting research on the BET family of proteins within GSK, an encoded library technology (ELT) screen was initiated in order to find a lead compound for a pan-BET inhibitor. This approach uses combinatorial chemistry to produce a vast, chemotypically diverse library of DNA-encoded small molecules (Figure 1.31).¹⁴⁸ An affinity matrix is introduced to the mixture and all tagged targets are captured. The unbound molecules are washed away allowing the bound targets to be recovered and deconvoluted using polymerisation chain reaction (PCR) technology.¹⁴⁹ Finally the identified compounds are resynthesised in the absence of the DNA tag and tested within screening assays.

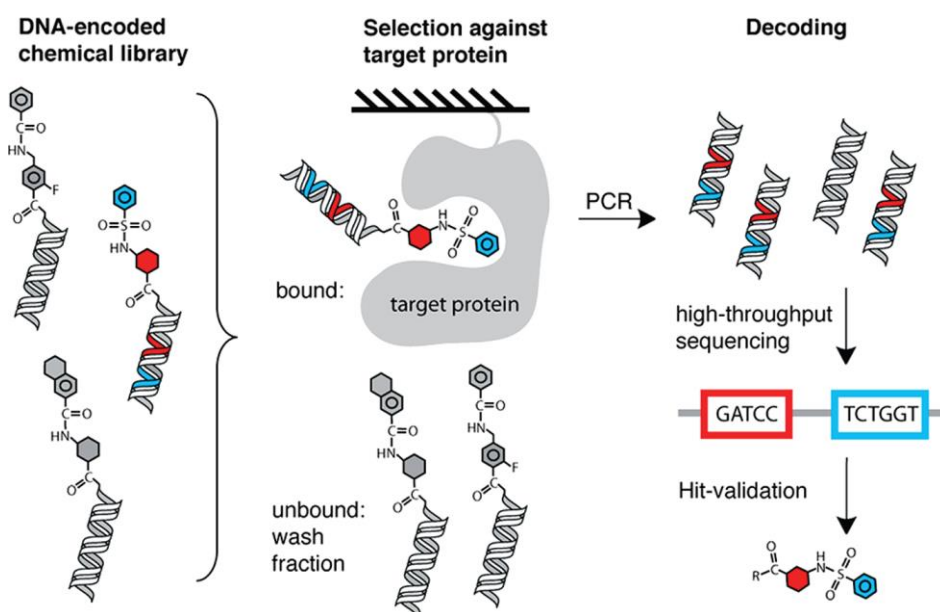


Figure 1.31. The DNA-encoded library is incubated with the target protein on a solid support. Washing cycles of the solid support removes unbound targets. The DNA codes of the bound molecules are amplified by PCR and the structures elucidated using high-throughput sequencing. Finally, the identified compounds are resynthesised in the absence of the DNA tag and tested within screening assays. Reprinted with permission from Encinas *et al.*, *J. Med. Chem.*, **2014**, *57*, 1276.¹⁴⁸

From the ELT screen, the hit compound **1.5** was identified which had properties for lead optimisation with moderate potency against BRD4 BD1 and 2 in the FRET biochemical assays and a solubility greater than the desired 100 µg/mL (Figure 1.32).

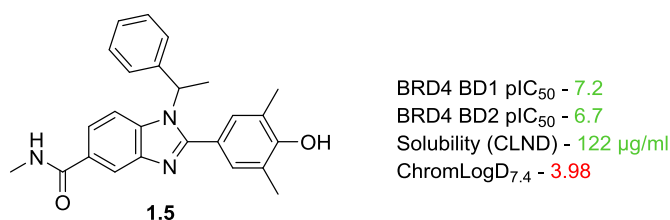


Figure 1.32. The ELT screen led to the discovery of the hit molecule, racemic **1.5**.

However, it suffered from high lipophilicity where the ideal ChromLogD_{7,4} for a typical small molecule inhibitor is usually <2.5. The phenol moiety itself is lipophilic and prone to phase II metabolism (e.g. glucuronidation of the alcohol).¹⁵⁰ Consequently, this is a potential metabolic hotspot which could result in high clearance *in vivo*. As such the pre-emptive decision was made to move away from this group. Therefore, priorities for lead optimisation were reducing the overall molecular lipophilicity and altering the warhead to prevent rapid metabolism. It was thought an alternative hydrogen bond donor (HBD) would be required in place of the phenol. However, in an attempt to protect the metabolic hotspot a carbonyl was investigated in the form of a pyridone (Figure 1.33). Addition of the second methyl, to form the *N*-methyl pyridone, gave a potency boost thus delivering the optimised pyridone warhead. Upon starting the ESM programme, a re-mining of in-house BET inhibitor templates was completed. It was found that the pyridone offered a good LE/LLE and, as such, was selected as the acetyllysine mimetic for this programme and has since been utilised in many other BET projects at GSK.

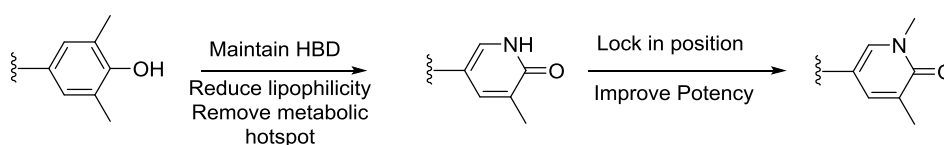


Figure 1.33. The optimised pyridone warhead designed to prevent phase II metabolism of the phenol warhead of the hit **1.5**. The dimethyl substituents were retained as they were shown to improve potency.

As shown in Figure 1.32, the initial hit incorporated an amide in the 5-position of the benzimidazole, to which the DNA tag was appended during the ELT. As such, it was thought

that the ESM moiety should be tolerated in this position. Indeed, molecules of this type exhibited high potency thus suggesting a good tolerance. Optimisation of this series resulted in the lead molecule **1.6**, which was candidate selected in 2016 and forms the first ESM-iBET inhibitor for GSK (Figure 1.34).

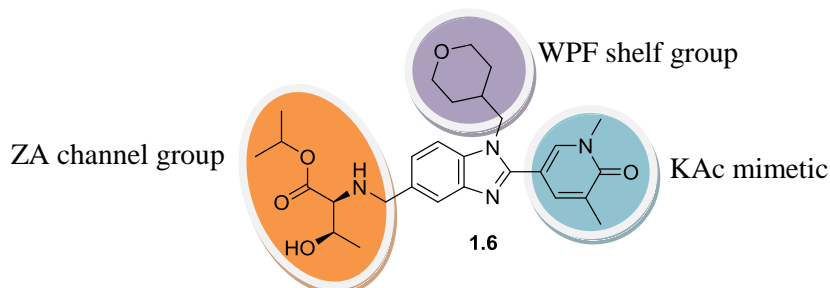
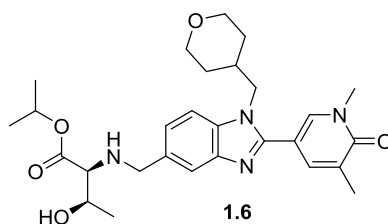


Figure 1.34. The first ESM candidate **1.6**.

The molecule incorporates the ESM in the 5-position which directs the motif through the ZA channel. In addition, the benzimidazole is substituted with a tetrahydropyran (THP) ring, which interacts with the WPF shelf and increases the potency of the molecule. The compound was found to be selective and exhibited a desirable profile (Table 1.5.)



		Cynomolgus monkey	1.6	Acid
ChromLogD _{7.4} / TPSA (Å ²)	3.0 / 108			
hWB pIC ₅₀ / Δ hWB	7.6 / +0.9			
Ester/Acid BD1 pIC ₅₀	7.3 / 6.8			
Permeability (AMP, nm/s)	73			
Solubility (CLND)	426 μM			
HLM IVC (+/- benzil)	0.9 / 1.5			
Hu Heps IVC (~LBF)	2.0 (73%)			
Cyno Heps IVC (~LBF)	1.0 (39%)			
		CL _{Total} (mL/min/kg)	35	-
		V _{SS} (L/kg)	1.1	-
		AUC _∞	502	82.6
		t _{1/2} (h)	0.4	0.9
		Acid: ester ratio	-	0.1:1
		C _{max} (ng/mL)	173	33.6
		AUC _∞	364	104
		Bioavailability (%)	24	-
		t _{1/2} (h)	1.2	1.5
		Acid: ester ratio	-	0.3:1

Table 1.5. Biological profile and cynomolgus monkey *in vivo* PK profile for **1.6**. IVC is measured in mL/min/g. For further details on the assays, refer to Chapter 1.7 (*vide infra*).

Molecule **1.6** demonstrated high biochemical potency with an increased whole blood activity and a high ΔhWB value, characteristics associated with the hydrolysis of the ester and subsequent retention of the acid within the cell i.e. the ESM effect. It exhibited a low TPSA, which combined with the ChromLogD_{7.4}, resulted in a desirable artificial membrane permeability (AMP) and solubility, as measure by chemiluminescent nitrogen detection (CLND). Furthermore, the *in vitro* clearance profile resulted in a desirable cynomolgus monkey PK profile in an IV/PO crossover *in vivo* study. Analogue **1.6** was dosed at 1 mg/kg in the IV portion and 3 mg/kg in the oral portion of the *in vivo* study. The pharmacokinetic parameters for **1.6**, and its acid metabolite, were both monitored following its administration. The compound exhibited a high clearance and a moderate volume of distribution. Although the oral bioavailability is low, considering the first pass extraction of the species, it suggests that the compound is well absorbed in the gut. Overall, the cynomolgus monkey *in vivo* profile was deemed desirable and the compound was eventually selected as the candidate for the pan-BET series.

1.7 Screening cascade used to identify molecules with desirable profiles

In a medicinal chemistry programme, compounds are progressed through a series of biological assays. The collected data allows differentiation of the compounds and shows their suitability to be potential clinical candidates. The screening cascade is formed of several tiers, designed to filter out compounds that do not meet the target profile. The target profile and screening cascade for the back-up molecule was based on the profile of **1.6** (Figure 1.35). The compounds can only be progressed to the next tier of tests if they meet the fulfilments of the current tier. Therefore, the number of compounds being screened decreases with each tier. The primary cascade focusses on the biological activity and pharmacokinetic profile of the compounds. The secondary cascade is run in parallel to the primary cascade but looks at the wider profile of the compounds e.g. non-BET bromodomain selectivity.

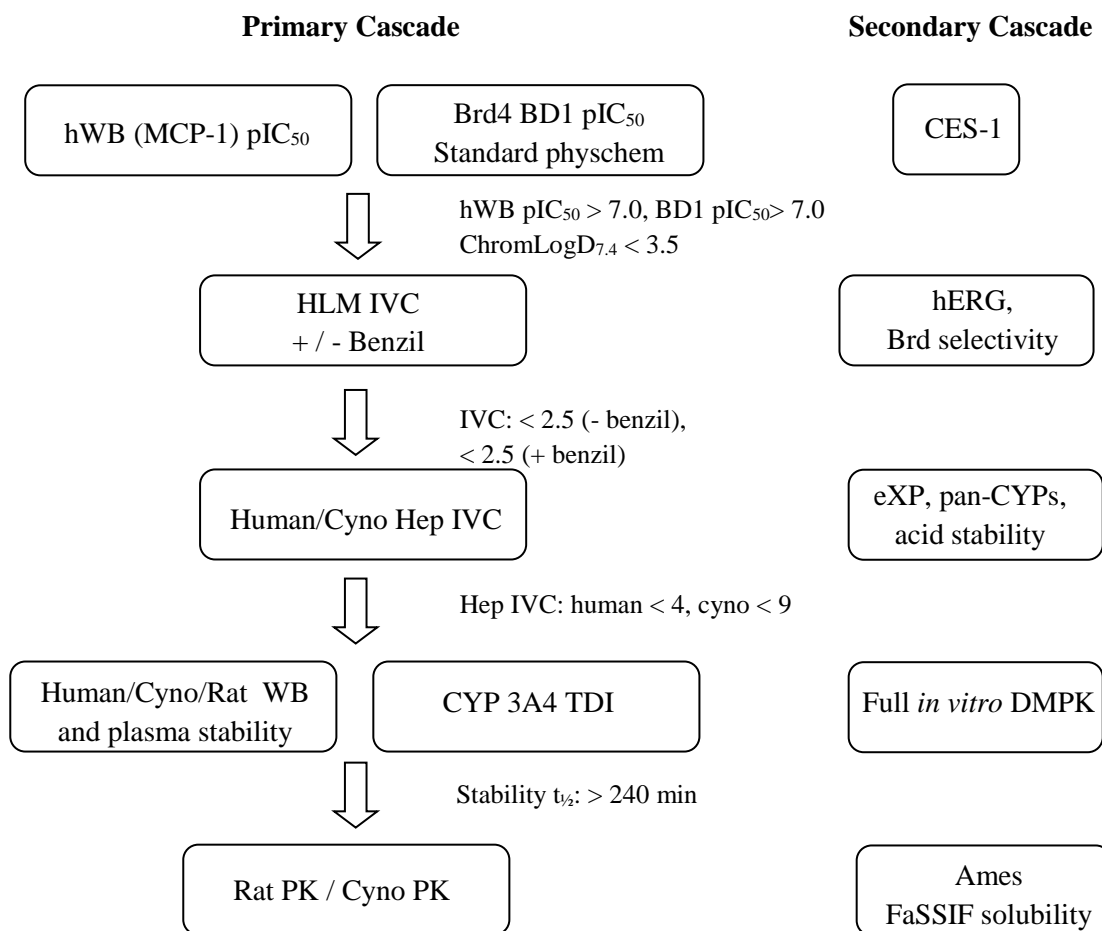


Figure 1.35. The screening cascade for the ESM-BET programme. The cascade is designed to filter out compounds that do not meet the target profile. The primary cascade considers the main properties of the molecule whilst the secondary cascade looks at the wider profile of the molecules. The assays are ordered in priority and ranked to form tiers. IVC values are quotes in mL/min/g.

The first tier involves the biochemical and human whole blood assays which measure the potency of the compound against BET. The biochemical assays use truncated protein as the substrate. The BRD4 BD1 protein has a single point mutation which causes BD2 to be defunct and vice versa. The human whole blood (hWB) assay is cell based and, as such, the permeability and protein binding of a compound has an impact. Therefore, a reduction in potency is usually observed between the biochemical and cellular assays. However, compounds incorporating an ESM should display enhanced hWB potency due to acid retention. The hWB assay observes the reduction in cytokine levels following stimulation by LPS, which induces an immune response. One such cytokine is MCP-1, known to recruit monocytes, memory T cells, and dendritic cells to the sites of inflammation.¹⁵¹ In order to see the potency gained from the ESM mechanism, the non-hydrolysable *tert*-butyl ESM is tested alongside the hydrolysable ESM in the hWB assay. The difference in potency between

the two molecules (ΔhWB) gives an indication of the effect from the ester hydrolysis and resultant localised concentration.

In parallel, the compounds are tested in a CES-1 assay. This is a complementary assay, designed to monitor the level of turnover by CES-1. The compounds are incubated with isolated CES-1 enzyme and the levels of ester and acid are measured at various time points. The rate of production of acid is then normalised against a known high turnover ESM containing compound, to account for variability across assays. At this stage, standard physchem parameters are also measured, including the AMP, ChromLogD_{7.4} and CLND solubility. Increasing lipophilicity of a molecule is associated with a higher permeability and, as such, an improved potency is usually observed. However, trading potency for lipophilicity has become a common problem within drug discovery and should try to be avoided.¹⁵² Increasing lipophilicity has been associated with lower aqueous solubility and higher promiscuity.¹⁵³ Only the soluble fraction of an orally active drug is available for absorption in the gut. Therefore, poor aqueous solubility can result in an insufficient systemic concentration of drug. Furthermore, increasing lipophilicity often results in increased non-specific binding rendering the compounds more promiscuous. As well as this, high MW and ChromLogD_{7.4} compounds are likely to be metabolised by the liver whereas low MW and LogD_{7.4} (<0) compounds tend to suffer from greater renal excretion.¹⁵³ As such, measuring these physicochemical parameters early on in the cascade, allows the prediction of whether a molecule will have a desired PK profile. To progress, compounds need to exhibit hWB pIC₅₀ > 7.0, BD1 pIC₅₀ > 7.0 and ChromLogD_{7.4} < 3.5.

The second tier investigates the microsomal stability of the compounds. The metabolism of the molecules is measured in an *in vitro* clearance assay (IVC) using isolated human liver microsomes (HLM). This assay gives an indication of the phase I metabolism, in which polar groups are introduced/unveiled through oxidation or reduction. In the case of ESM compounds, ester hydrolysis could also be a phase I metabolic pathway. Therefore, the HLM assay consists of two individual tests. In the first, the compounds are incubated with only HLM whereas in the second, an inhibitor is added. The inhibitor is a known esterase inhibitor, benzil, therefore removing the esterase component of the metabolism. This gives an indication on the level of non-esterase mediated metabolism.

For compounds exhibiting reasonable IVC, < 2.5 (- benzil) and < 2.5 (+ benzil), further metabolic studies are completed. In the third tier, the molecules are tested against human and cynomolgus monkey hepatocytes, capable of phase I and phase II metabolism. The latter involves the conjugation of polar molecules, e.g. glutathione or a sulphate, which promotes

excretion. The HLM and hepatocyte IVC combined give an insight into how the molecule may fare *in vivo* and is often used as a key decision point for the progression of a molecule. A drug with high clearance is unlikely to have a sufficient concentration at the site of action thus reducing efficacy. However, low clearance can lead to accumulation within the body which may increase toxicity risks, along with off-target inhibition. To gain perspective on the broader selectivity profile, screening against an enhanced cross-screening panel (eXP) of known biological liabilities, such as the human ether-à-go-go related gene (hERG), and pan-CYPs is performed.

The Cytochrome P450 family of enzymes (CYPs) are the major enzymes involved in drug metabolism.¹⁵⁴ CYP3A4, the most promiscuous family member, is primarily located in the liver and intestines, where it oxidizes small foreign organic molecules (xenobiotics).¹⁵⁵ It has been reported to metabolise over 75% of all marketed drugs and, as such, inhibition of CYP3A4 can impact the bioavailability and therapeutic index of an oral drug.¹⁵⁶ Therefore, the compounds are profiled in a 3A4 time dependent inhibition (TDI) assay at this stage, as well as a full *in vitro* DMPK study. Finally, the selectivity over non-BET bromodomains is determined. The stability of the compounds is further investigated in the fourth layer of the screening cascade, examining the human, rat and cynomolgus monkey blood/plasma stability. The rat and cynomolgus monkey form the two pre-clinical species and, as such, the stability in the blood/plasma needs to be understood in order to facilitate pharmacokinetic (PK) studies. The cynomolgus monkey is used due to the high homology of the cynomolgus monkey CES-1 gene and expression profile relative to the human gene (93%).¹⁵⁷

Finally, any remaining compounds are entered in a full rat and cynomolgus monkey IV-oral crossover (IV/PO) PK study. In parallel, the solubility is further investigated by testing compounds within the pharmacologically relevant fasted state simulated intestinal fluid (FaSSIF) solubility assay. The compounds are also tested for genotoxicity through the Ames assay. Typically, only one/two compounds from each series reach this stage, and if the data is promising it is selected as a pre-candidate. Following this, the compound is progressed into safety studies, e.g. a seven day rat toxicology study, and a broader biology package is collected. This package is bespoke to each individual molecule and is aimed at dispelling risks. One such assay is an in-depth human whole blood assay in which the effects of the compound on several chemokines and cytokines beyond MCP-1 is analysed. The solid form of the compound may be assessed as well as the broader selectivity of the molecule. If the data from these tests is desirable, then the compound can be selected as a clinical candidate.

1.8 Overall aims

BET inhibitors have been implicated in a plethora of diseases. The ubiquitous expression of the BET proteins means that all clinical BET inhibitors to date affect all cells, resulting in off-target toxicities which currently limits the majority of the inhibitors to severe indications such as cancer. The overall aim of the work discussed in this thesis is to develop a small molecule BET inhibitor with a suitable profile for chronic immuno-inflammatory diseases, such as RA. As discussed above, a targeted drug delivery approach, through the incorporation of an esterase sensitive motif in a small molecule series, could mitigate the currently challenging pre-clinical safety profile of a non-targeted BET inhibitor.

With **1.6** selected as the first ESM-containing candidate and progressing towards clinical trials as an inhibitor of the BET family for the treatment of rheumatoid arthritis (Table 1.5, *vide supra*), it was desirable that a second molecule with a desirable *in vitro* and *in vivo* cynomolgus monkey PK profile was developed. As there is a lack of *in vivo* human PK data for ESM-containing molecules, it is not currently known what profile these molecules will exhibit in human and whether efficacy and oral exposure can be achieved as well as no off-target toxicity. Therefore, it would be advantageous to have a second candidate molecule, with a similar or improved profile, in a structurally differentiated series in order to expand our knowledge surrounding monocyte-targeted small molecule inhibitor area. Furthermore, the optimised molecule could then replace the lead compound **1.6**, if toxicity or lack of efficacy was due to the molecular scaffold rather than the mode of action of the compounds.

At the beginning of this work, GSK had developed two series of molecules that incorporated the ESM technology; the benzimidazoles, from which **1.6** was developed, and the aryl-pyridone (AP) series (Figure 1.36). These two series showed that potent compounds with desirable pharmacological profiles can be achieved when the ESM is directed through the ZA channel. As well as this, *in vitro* studies suggested the compound **1.6** was retained within cells of the mononuclear monocyte lineage.

Crystallography indicates that the molecules belonging to the benzimidazole and AP series (Figure 1.36) bind in a similar mode to that of I-BET762 and I-BET151. Both series incorporate a pyridone motif (termed the warhead due to it being key for binding and potency) as the acetylated lysine mimetic (green) which binds in the KAc pocket (Figure 1.36). The tetrahydropyran (THP) ring of compound **1.6** and the ether moiety of the AP series interacts with the WPF shelf and, as such, is called the WPF shelf group (purple). The amino ester functionality (blue) is directed through the ZA channel from the central aryl ring

(red), known as the core. For both series, optimisation focussed predominantly on achieving selectivity for cells of the myeloid lineage by selective CES-1 hydrolysis, selectivity for non-BET bromodomains and desirable potency and metabolic stability by investigating different moieties as the WPF shelf (purple) and the ESM (blue).

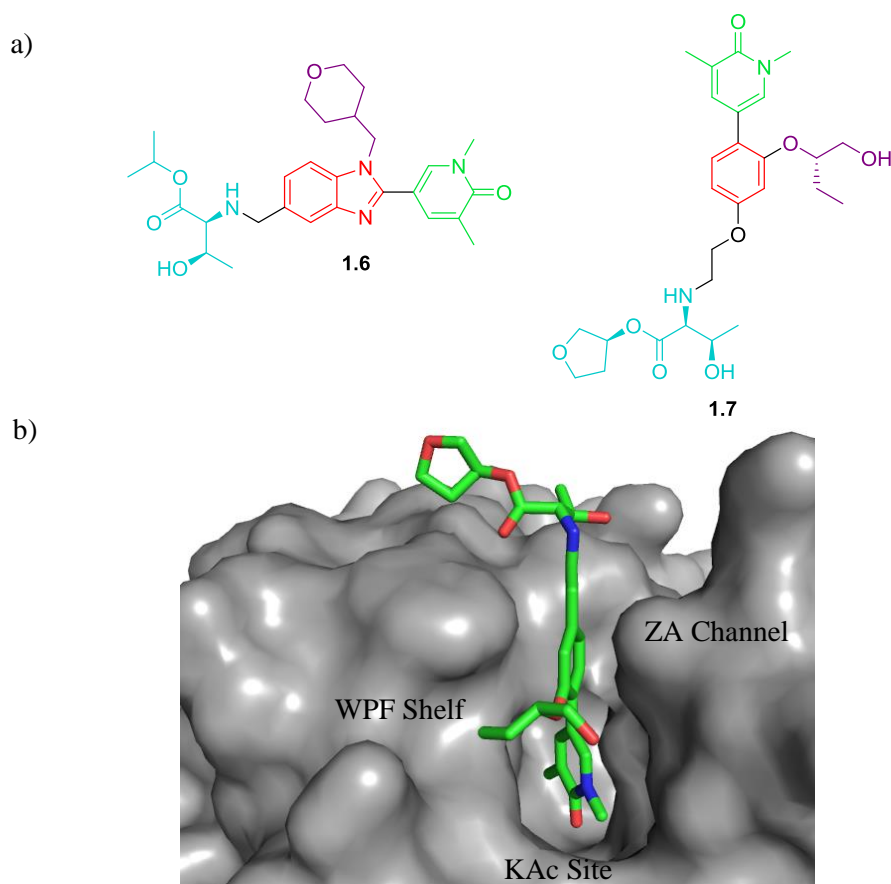


Figure 1.36. a) The structure of compound **1.6**, belonging to the benzimidazole series, and an exemplar analogue, **1.7**, from the AP series. Both series incorporate a dimethyl pyridone as the acetylated lysine mimetic (green) attached to a core (red) which occupies the ZA channel. Appended to the core is a moiety that interacts with the WPF shelf (termed the WPF shelf group, purple) which is a THP in **1.6** and an ether group in the AP series. The amino ester moiety (blue) is directed through the ZA channel. b) A crystal structure AP compound **1.7** in BRD4 BD1 exemplifying the ESM directed through the ZA channel and the ether group sitting on the shelf.

The work outlined in this thesis is based on the investigation of two further series, the over the shelf (OTS) series and the benzazepinone (BZP) series, with the aim of finding a lead molecule with a similar or improved profile relative to compound **1.6**. The first series to be discussed will be the OTS series and the main aim of investigating whether the ESM can be

directed over the WPF shelf to give potent, selective compounds with good physicochemical properties. The second part of this thesis will focus on the optimisation of the BZP series, based on an alternative scaffold, which aimed to develop molecules with the ESM directed through the ZA channel whilst adhering to the desired target profile (Figure 1.35, *vide supra*).

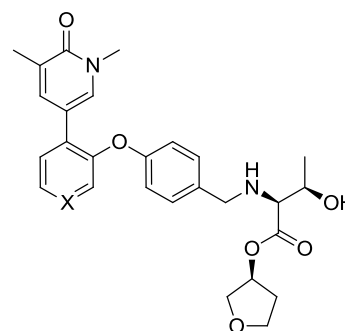
Chapter 2

Development of the “over the shelf”
series as inhibitors for the BET
family

2.0 Development of the “over the shelf” series as inhibitors for the BET family

The first series that was investigated within this thesis was the OTS series, which is structurally similar to the AP series. It can be seen in the crystal structure of compound **1.7** in BRD4 BD1 (Figure 1.36, Section 1.9), that it is possible to direct the ESM over the WPF shelf. This was attractive as all previous work focussed on the ESM directed through the ZA channel, thus offering the potential for achieving a different profile.

The first molecule synthesised in this series, compound **2.1**, was based on a phenyl core with a benzyl WPF shelf group (Table 2.1). SAR gathered elsewhere within the team showed that a pyridyl in place of the phenyl core, analogue **2.2**, reduced *in vitro* clearance (IVC). This is most likely due to the resultant decreased electron density in the ring, making it less nucleophilic and lipophilic. Therefore, the baseline compound **2.2** formed the starting point for this programme of work (Table 2.1).



	Desired Profile	2.1	2.2
X		CH	N
hWB pIC ₅₀ (MCP-1)	> 7.0	7.1	7.8
hWB ΔpIC ₅₀ (ESM- <i>t</i> Bu)	~ 1.0	+1.3	+1.1
Ester Brd4 BD1 pIC ₅₀	> 7.0	7.9	8.2
Acid Brd4 BD1 pIC ₅₀	> 6.5	6.8	6.6
HLM IVC (+/- benzil)	< 2.5 / < 2.5	7.0 / 12.6	4.5 / 8.3
Human blood / Cyno plasma t _{1/2} (min)	> 240	-	-
ChromlogD _{7.4}	< 3.5	4.4	2.8
TPSA (Å ²) / AMP (nm/s)	< 140 / > 30	99 / 260	112 / 22

Table 2.1. The desired profile of an ESM compound and the profile of the starting point, compounds **2.1** and **2.2**, for this project. IVC values are quoted in mL/min/g. Values depicted as – were not determined.

Analogue **2.1** displays high biochemical and moderate cellular potency, as well as a desirable CES-1 turnover as shown by the high ΔhWB (Δ = 1.3). As previously mentioned, the ΔhWB

is an indication of the effect from the ester hydrolysis and resultant localised concentration of the acid. It is the difference in potency between the hydrolysable ester **2.1** and the analogous biologically non-hydrolysable *tert*-butyl ester. If the ΔhWB is low, it is indicative of slow CES-1 turnover. If this is so, it can be assumed that once the ester has permeated into the macrophage-monocyte lineage cells, it is converted to the acid at a reduced rate. Therefore, a higher proportion of the ester is free to diffuse back out of the cells and results in a lower localised concentration of the acid in CES-1 positive cells. However, the acid potency is lower than desired and the IVC is too high, which may be somewhat due to the high lipophilicity of the ester. The direct analogue **2.2** has a lower ChromLogD_{7.4} and a lower IVC relative to **2.1**. However, the IVC is still higher than desired (optimal IVC is <2.5 mL/min/g), thus suggesting that the series has an underlying metabolic instability.

Therefore, the main objectives for the optimisation of this series were to reduce the IVC and improve the whole blood activity, whilst maintaining the high biochemical potency and good physicochemical properties. The physicochemical properties, including permeability, ChromLogD_{7.4} and solubility, are measured at an early stage of the screening cascade. These parameters can affect the promiscuity and oral bioavailability of a molecule, amongst other things, as well as allowing the prediction of whether a molecule will have a desired pharmacokinetic (PK) profile. The desired profile is largely based on the profile of **1.6** which resulted in good cynomolgus monkey PK data and it being taken into clinical studies (Table 1.5). As such, it was hypothesised that adhering to this profile increases the likelihood of a compound with a desirable cynomolgus monkey PK profile being identified. As **1.6** is currently the only known ESM-containing clinical compound, it is not yet known what the highest level of IVC is possible that will translate into desirable *in vivo* data. Therefore, human and cynomolgus monkey hepatocyte values of <4 and <9 mL/min/g (~80% liver blood flow) respectively.

2.1 Hypotheses to be tested in the OTS small molecule series

2.1.1 Bond angles of the ether linkage relative to the ESM influences the potency, IVC and CES-1 turnover

The WPF shelf is key for potency and gaining selectivity over non-BET bromodomains. The protein fold is such that the W81, P82 and F83 residues, located on the ZA loop, stack on top of each other to form a shallow hydrophobic groove (Figure 2.1).^{73,107} Furthermore, the gatekeeper, isoleucine (I146) in BD1 and valine (V435) in BD2, is also hydrophobic and

forms the bottom of the groove. Further into the pocket is a non-mobile methionine residue which causes a hump. Therefore, for molecules to extend deep into the WPF shelf, a mobile group is thought to be required in order to reach over the hump.

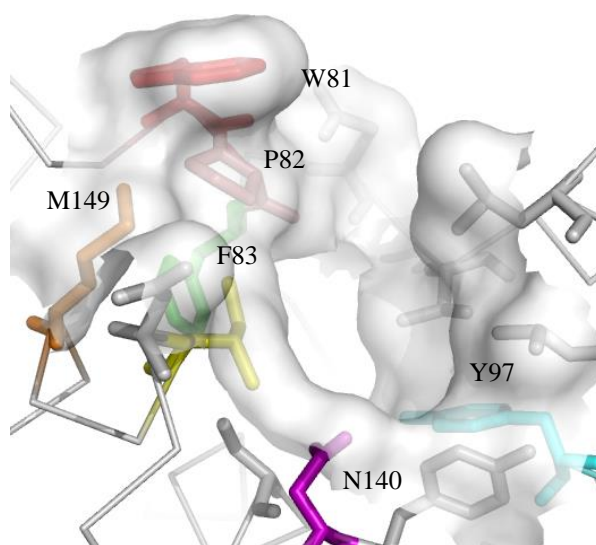


Figure 2.1. A crystal structure of BRD2 BD1 showing the key residues in the WPF shelf and KAc binding site (pdb: 4alg). The amino acids W81 (red), P82 (pink) and F83 (green) residues stack on top of each other to form a shallow hydrophobic groove. The non-mobile M149 creates a hump towards the back of the ledge. The residues Y97 (cyan) and N140 (purple) are the key binding residues in the KAc binding site.

The ESM moiety has a high degree of freedom and, as such, is very mobile. According to equation (1), with the same enthalpic interactions (ΔH), the higher the degree of freedom within a molecule, the larger the entropy (ΔS) loss is upon binding and therefore the lower the ΔG is. Consequently, a larger entropy loss will result in a lower binding affinity (equation 2).

$$\Delta G = \Delta H - T\Delta S \quad (1)$$

$$\Delta G = -RT \ln K_D \quad (2)$$

Equation 2.1. Mathematical equations for Gibbs free energy.

The ESM in the *para*-position is fairly constrained in the bound molecule due to the CH_2NH linker adopting a particular conformation which is needed to lift over the methionine residue (Figure 2.2a). This causes three bonds to be locked in position, which would result in an

entropy loss upon binding. Changing the bond angle vector could move the ESM away from the methionine residue. This could result in the bound molecule having more flexibility (Figure 2.2b). The higher degree of freedom within the linker could improve potency due to less entropic loss upon binding of the molecule. Furthermore, the change in bond angles could impact the rate of turnover by CES-1.

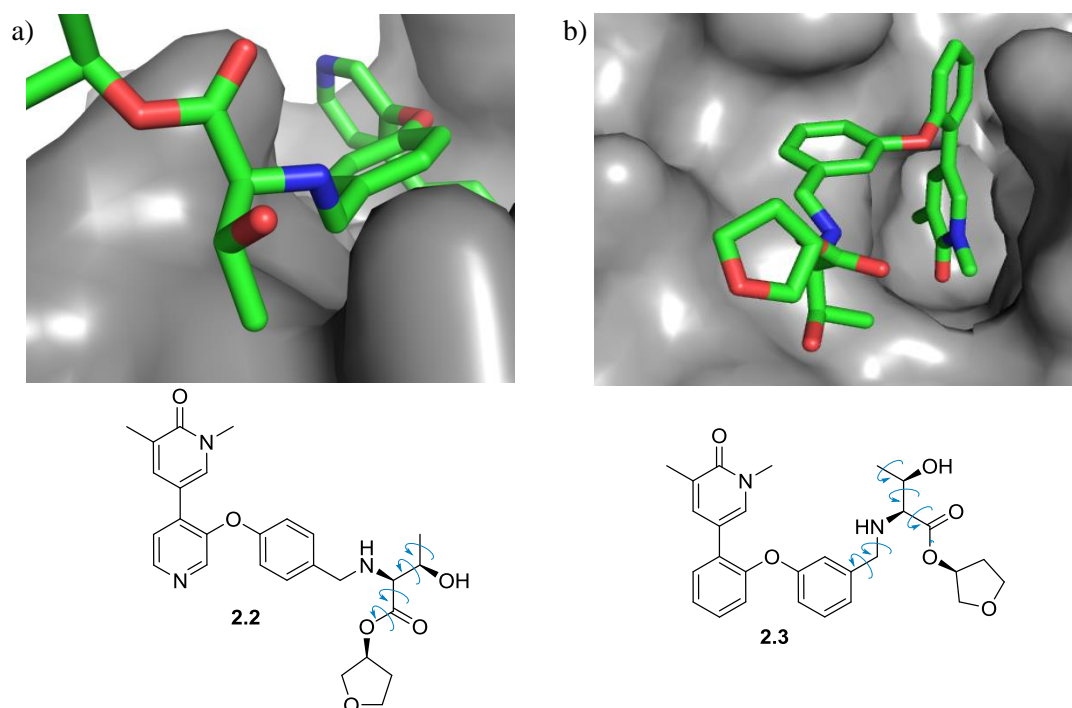


Figure 2.2. a) A crystal structure of **2.2** in BRD2 BD2 showing the ESM of lead compound **2.2** is fairly constrained due to the hump from the methionine residue causing the CH₂NH linker to adopt a particular conformation. This removes the degrees of freedom in these bonds, thus leading to an entropy loss upon binding. The blue arrows indicate the rotatable bonds. b) A crystal structure of **2.3**, an analogue of **2.2**, in BRD4 BD1 in which the ESM is directed through the solvent exposed channel adjacent to the WPF shelf. This region is unhindered and away from the methionine residue, allowing the ESM chain to have more flexibility as shown by the increased number of rotatable bonds.

Furthermore, as the area adjacent to the WPF shelf is solvent exposed, the ESM functionality is likely to be tolerated, as well as allowing a high degree of flexibility. Therefore, by changing the bond angle vectors the ESM could be directed through an adjacent cleft rather than over the WPF shelf. This could be achieved by replacing the benzene ring with five-membered heterocycles, which could also offer the advantage of lowering the lipophilicity, and therefore potentially IVC, of the compounds relative to **2.1**.

The hypothesis that will be explored in this small molecule series is that changing the bond angles to the ESM by incorporating five-membered heterocycles will improve the potency, by allowing more flexibility in the ESM linker, as well as reducing the IVC and lipophilicity.

2.1.2 The substituted benzene moiety influences the potency, IVC and lipophilicity

The tryptophan residue (W81) of the WPF shelf is in close proximity to the KAc binding site, making the WPF shelf easily accessible for substituents. A recent investigation was conducted, by Jung *et al.*, into the structural determinants for the interaction of BRD4 with inhibitors.¹⁵⁸ The effect of mutations in the BRD4 BD1 KAc binding pocket, WPF shelf group and BC loop on the recognition of JQ1 were evaluated. It was found that the hydrophobic interaction between JQ1 and W81 of the WPF shelf was as important as the interaction with the conserved tyrosine, Y97, and asparagine, N140, in the KAc binding pocket.¹⁵⁹ It has been found that aryl rings and ether moieties are the optimal substituents for occupying the WPF shelf and improving potency.⁶³

Crystal structures of BRD4 BD1 indicate a solvent exposed region adjacent to the WPF shelf (Figure 2.3). The area is unhindered at the surface of the bromodomain suggesting substitution of the benzene WPF shelf group would be tolerated. Furthermore, the solvent network is not in close proximity to the WPF shelf and, as such, small moieties may also be tolerated. Therefore, it was thought that substituting the ring and expanding into this region would improve the potency, whilst offering the opportunity to modulate the ChromLogD_{7,4} and reduce the IVC.

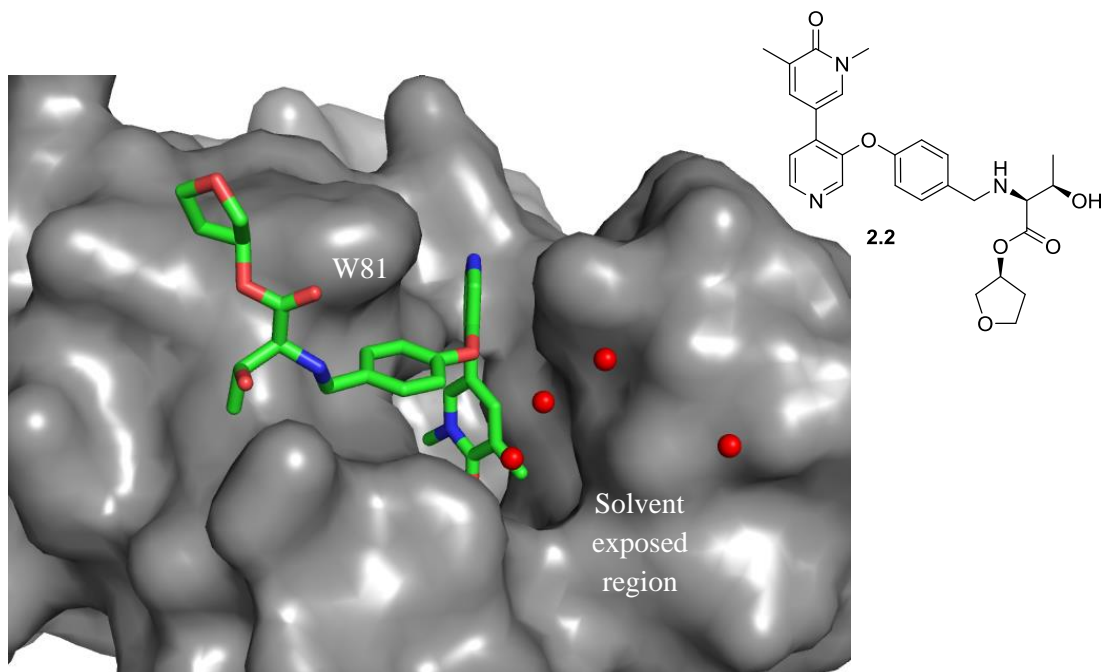


Figure 2.3. A crystal structure of the lead compound **2.2** in BRD2 BD2 showing the pyridine core directed through the ZA channel and the ESM directed over the shelf in close proximity to W81 of the WPF shelf. A solvent exposed region is adjacent to the WPF shelf, with the water network highlighted (red).

The use of substituted aryl rings as WPF shelf groups in the OTS series is an unexplored area. SAR gathered on the AP series focussed on ether moieties, with a small selection of heteroaromatics being synthesised. However, benzene or heteroaromatic rings are preferable in the OTS series as they allow for simple attachment of the ESM at the 4-position. Existing SAR was based on the otherwise unsubstituted benzene ring as a WPF shelf group, as in compound **2.2**. This could be a factor of the high IVC observed as well as the high lipophilicity, supported by the increased metabolic stability observed when replacing the otherwise unsubstituted aromatic ring of **2.1** with a pyridyl as in **2.2**. Lipophilic compounds tend to have a greater affinity for metabolising enzymes and, as such, increasing lipophilicity is associated with increased metabolism.¹⁶⁰ As well as this, the nucleophilic nature of unsubstituted aryl rings makes them prone to phase I metabolism, producing phenols which are then susceptible to phase II metabolism.¹⁶¹ Therefore, substituting the aromatic ring could offer the potential to reduce the lipophilicity, whilst also blocking metabolically vulnerable positions.

From the docking it was hypothesised that aromatic ring could be interacting with the tryptophan of the WPF shelf through parallel-displaced π - π stacking (Figure 2.4). As such, modulating the electronics of the WPF shelf group could strengthen this interaction, thus increasing potency. This could be achieved through the incorporation of functional groups

with strong mesomeric effects (e.g. ethers or amines). Alternatively, incorporating hydrogen bond acceptors or donors, such as amides or sulfonamides, may allow interaction with the solvent network through hydrogen bonding. Such interactions would fix the position of the aryl ring and increase the hydrophobic interaction with the WPF shelf.

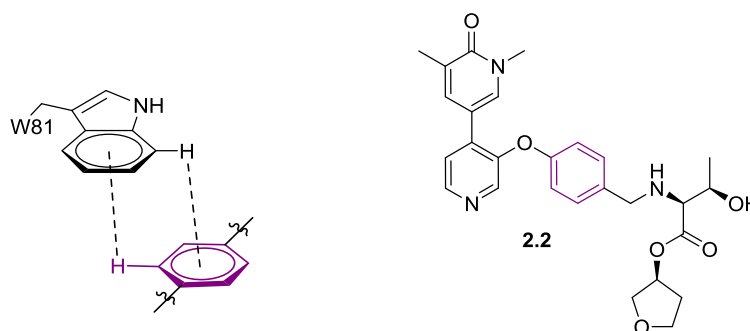


Figure 2.4. Proposed parallel-displaced π - π stacking between W81 of the WPF shelf and the WPF shelf group (purple) of analogue **2.2**.

2.2 Aims for the OTS series of small molecule inhibitors

SAR gathered on the aforementioned AP series focussed on the use of alkyl WPF shelf groups, therefore aromatic WPF shelf groups were relatively unexplored. In contrast, initial work within the OTS series focussed on a 6-membered aromatic ring with a 1,4-substitution pattern and, as such, a 180° bond angle between the ether linkage and ESM (Figure 2.2, *vide supra*). An unexplored area is changing the bond angles around the WPF shelf group in order to investigate the effect on potency and turnover by CES-1. Furthermore, it could offer the opportunity to reduce IVC and lipophilicity and therefore move towards the desired profile given in Table 2.1 (*vide supra*). In particular, the incorporation of five-membered heterocycles may offer a range of different bond angles with which to establish the SAR.

One of Lipinski's rule of five is that a molecular weight (MW) of <500 Daltons is desirable for oral molecules.¹⁵³ Therefore, as the aim is to develop an oral drug, the high MW of **2.2** (492 Daltons) restricts the possible substituents to small MW functional groups e.g. a methyl group. Furthermore, in order to assess the potential hydrogen bond interaction with the WPF shelf tryptophan, compounds with substituents exploring various electron-withdrawing and electron-donating effects will be synthesised. As well as this, polar hydrogen bond acceptors or donors will be explored with the aim of reducing the ChromLogD_{7.4} and interacting with the solvent network.

The specific aims of the work discussed in this chapter are to:

i) Synthesise a series of analogues of BET inhibitors based on the OTS scaffold, with five-membered heterocycles as WPF shelf groups. This enables exploration of how changing the bond angle between the ether and ESM linkages impacts potency of BET inhibition, as well as how the incorporation of heteroatoms affects IVC and lipophilicity. Examples of such heterocycles include furans and thiazoles, with bond angles of 120° and 130° respectively (Figure 2.5).

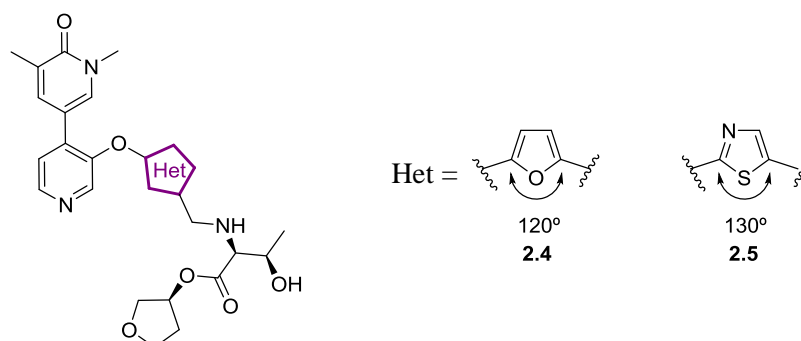


Figure 2.5. Five-membered aromatic heterocycles will be incorporated as the WPF shelf group (purple) in the OTS series to explore how changing the bond angle between the linkages to the ESM and the ether impacts potency of BET inhibition. The furan and the thiazole rings, compounds **2.4** and **2.5** respectively, would provide bond angles of 120° and 130° respectively.

ii) Synthesise analogues of **2.2** where mono-substitution of the aryl ring (purple, Figure 2.6) with small moieties such as amides and amines with the aim of impacting the potential hydrogen bond interaction whilst reducing IVC and lipophilicity and, as such, allow the progression towards the desired profile shown in Table 2.1 (*vide supra*) (Figure 2.6).

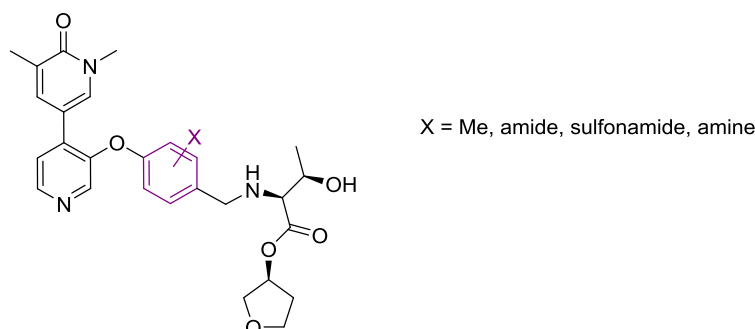


Figure 2.6. The design of the molecules focussed on mono-substitution of the aryl ring that forms the WPF shelf (purple).

iii) Combine knowledge from data generated from aims i) and ii) with structural changes, through rational design, to achieve the desired target profile outlined in Figure 1.35 (*vide supra*).

2.3 Results and discussion

2.3.1 Investigating the bond angles of heterocyclic motifs in the first-generation series

The Cambridge Structural Database of small molecule X-ray structures contains structural information on all published crystal structures. Therefore, a wealth of information is available on the angles between the two bond vectors of 5-membered aromatic rings in existing molecules. As it was desired to investigate how changing the angle between the ESM and ether linkage would impact potency, it was thought that this data could be used to infer which 5-membered aromatic systems would offer a range of angles to explore. Therefore, a statistical analysis was completed by a colleague at GSK in order to determine the characteristic bond angles of various 5-membered aromatic rings.¹⁶² The bond angle was defined as the angle between the two vectors *via* the shortest distance (Figure 2.7). As well as this, in order to be directly relevant to this series of molecules, a requirement that the vectors were acyclic was applied to the search. The 5-membered ring of each molecule retrieved by the search was converted to a SMILES sequence with * depicting the bonds entering or leaving the aromatic ring.

This data was used to generate box plots for each ring system, showing the spread of values, and the mean, for the angle between two bond vectors (Figure 2.7).

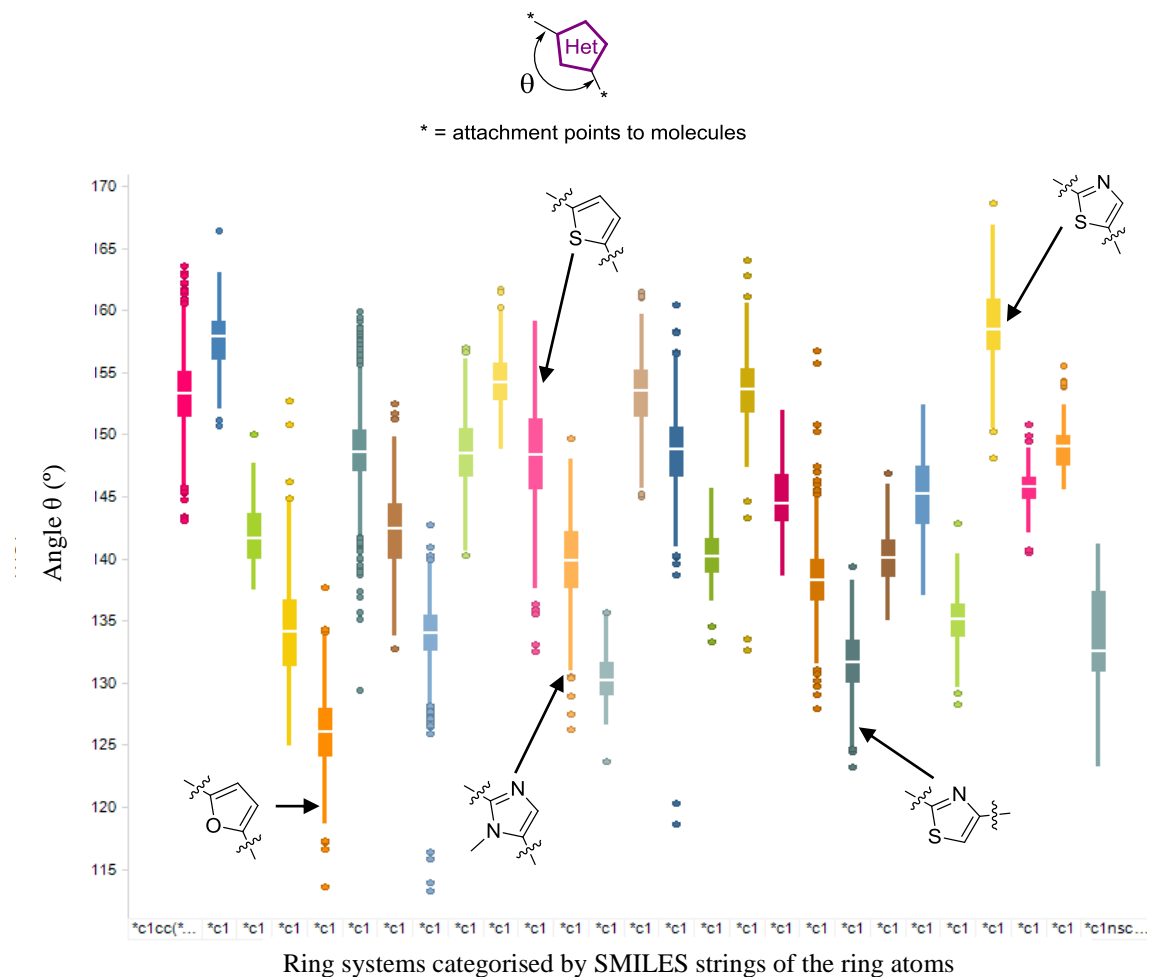
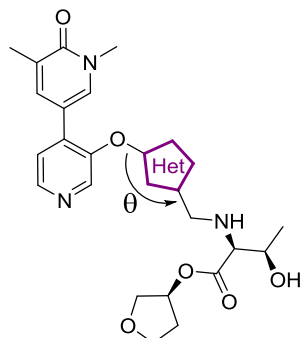


Figure 2.7. A statistical analysis of angles between bond vectors for five-membered rings on data derived from the Cambridge Structural Database of small molecule x-ray structures. The 5-membered rings were converted to SMILES strings and the vectors converted to generalised structures * to allow for comparison of the 5-membered ring across different molecules. Box plots were generated for each ring system, showing the spread of values, and the mean (as depicted by the central line within the box which represents the standard deviation), for the angle between two bond vectors. Highlighted are examples of some of the ring systems included in the analysis.

These data were used to design compounds **2.4-2.8**, incorporating five different 5-membered rings with angles that increased in approximately 10° increments, ranging from 120° to 160° degrees based on their mean values (Table 2.2). This would provide a detailed understanding of which angle between the two bond vectors, where the angle measured is the one created by the smallest distance between the two bonds, provides the optimal potency. Furthermore, using heterocycles may have the additional benefit of removing metabolic hotspots, reducing lipophilicity and modulating the electronics of the aromatic ring, thereby offering the potential to reduce IVC.



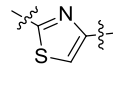
	Het	Approximate Angle (θ)
2.4		120°
2.5		130°
2.6		140°
2.7		150°
2.8		160°

Table 2.2. A statistical analysis of angles between bond vectors for five-membered and six-membered ring systems was completed. The data from the analysis were used to select five-membered rings with mean angles that increased in approximately 10° increments, ranging from 120° to 160°, to give compounds **2.4-2.8**.

Whilst there is a variety of methodology that can be employed to build bi-aryl ethers containing two 6-membered rings, there is little literature precedent for 6,5-bi-aryl ethers in which an ether linkage connects a 5-membered and 6-membered aromatic ring, such as in compounds **2.4-2.8**. A wide range of reaction conditions were used in an attempt to synthesise molecules **2.4** and **2.7** including Buchwald-Hartwig, Ullmann and Chan-Lam etherification conditions (Figure 2.8).

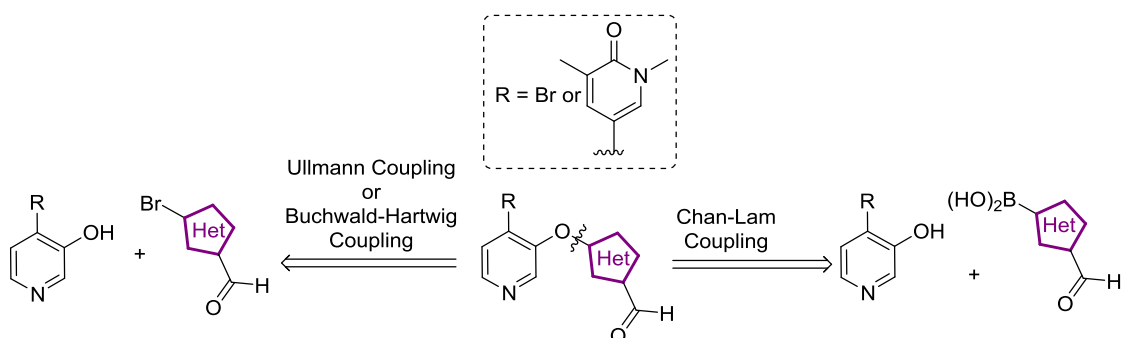


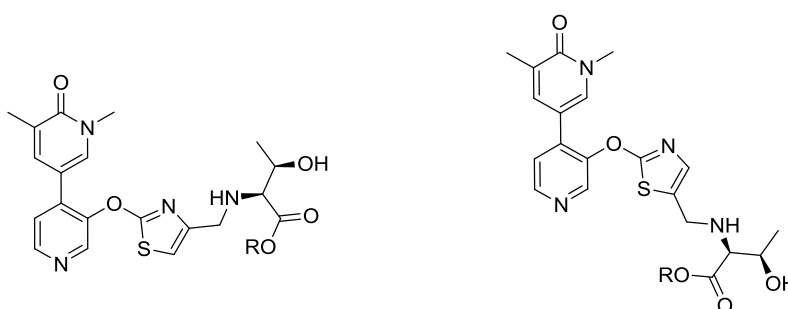
Figure 2.8. A wide range of Ullmann, Buchwald-Hartwig and Chan-Lam coupling conditions were employed in an attempt to synthesis molecules **2.4** and **2.7**.

However, none of the reactions were successful with either no or very minor formation of the ether linkage. Furthermore, attempts at S_NAr reactions to form the bi-aryl ether within

compound **2.6** were also unsuccessful despite employing a range of conditions and alternative starting materials. Therefore, unfortunately, due to synthetic challenges only the thiazole targets were synthesised and, as such, only these targets will be discussed within this thesis.

2.3.1.1 130° and 160° bond angles of the heterocyclic scaffold

As aforementioned, the 130° and 160° bond angles can be accessed by the 2,4- and 2,5-substituted thiazoles respectively. Therefore, the targets **2.5** and **2.8** were explored in parallel. Several ESM esters including the isopropyl Thr, THF Thr and ethanol Thr were profiled *in silico* (Table 2.3).

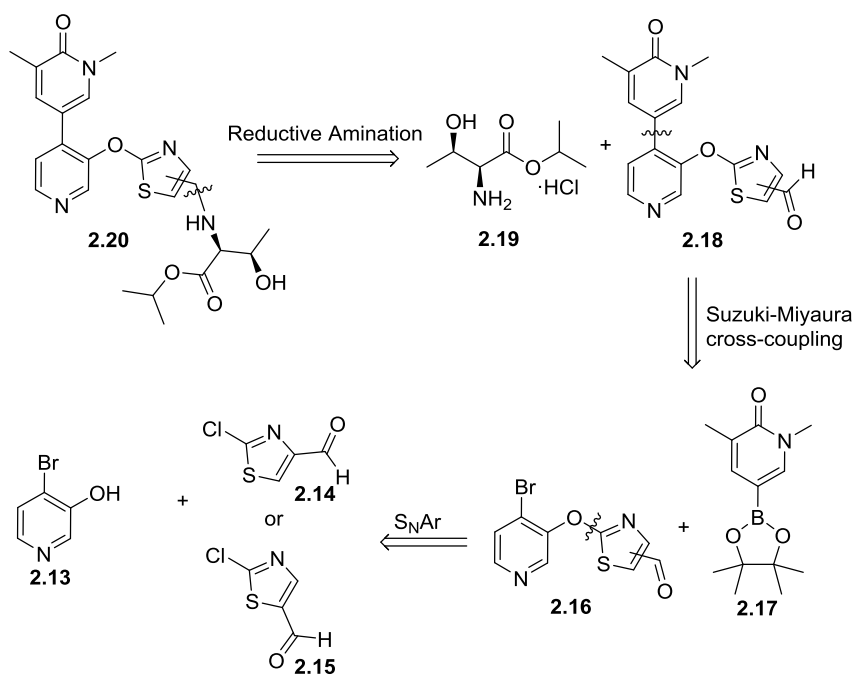


	2.5	2.9	2.10	2.8	2.11	2.12
R	THF	iPr	CH ₂ CH ₂ OH	THF	iPr	CH ₂ CH ₂ OH
ChromLogD _{7.4}	1.9	3.2	1.6	1.9	3.2	1.6
TPSA	125	115	136	125	115	136

Table 2.3. The calculated properties for the thiazole-containing analogues.

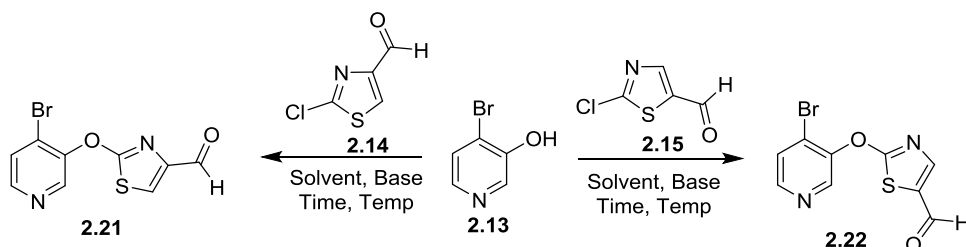
All of the analogues were predicted to have desirable TPSA (<140Å²). However, only the isopropyl Thr compounds **2.9** and **2.11** were predicted to have desirable ChromLogD_{7.4} values with compounds **2.5**, **2.10**, **2.8** and **2.12** predicted to be too polar, which could impact permeability and potency. Therefore, it was decided to synthesise analogues **2.9** and **2.11**.

A retrosynthetic analysis was applied to the generalised molecule **2.20** (Scheme 2.1). The C-N bond could be disconnected to the amino acid ester **2.19** and the formyl-thiazole intermediate **2.18**. An aryl-aryl disconnection could reach the commercially available boronic ester **2.17** and the corresponding bromo-aryl intermediate **2.16**. Finally, an O-aryl disconnection would yield the commercially available bromopyridinol **2.13**, 2-chlorothiazole-4-carbaldehyde **2.14** and 2-chlorothiazole-5-carbaldehyde **2.15**.



Scheme 2.1. Retrosynthetic analysis of the thiazole-containing targets **2.20**.

The first step in the forward synthesis was the etherification of pyridinol **2.13**. Initially, palladium and copper-catalysed reactions were trialled for both thiazoles (data not shown), although no conversion to the bi-aryl ethers was observed. Chlorothiazoles are known to undergo S_NAr reactions, although not commonly with an oxygen nucleophile. Therefore, various S_NAr conditions of pyridinol **2.13** and thiazoles **2.14** and **2.15**, to form intermediates **2.21** and **2.22** were attempted (Table 2.4). The conversion was estimated by the UV area/area observed by LCMS. As such, it is not an accurate measurement of conversion but rather a qualitative method to provide an idea of whether a low, moderate or high conversion was being achieved.

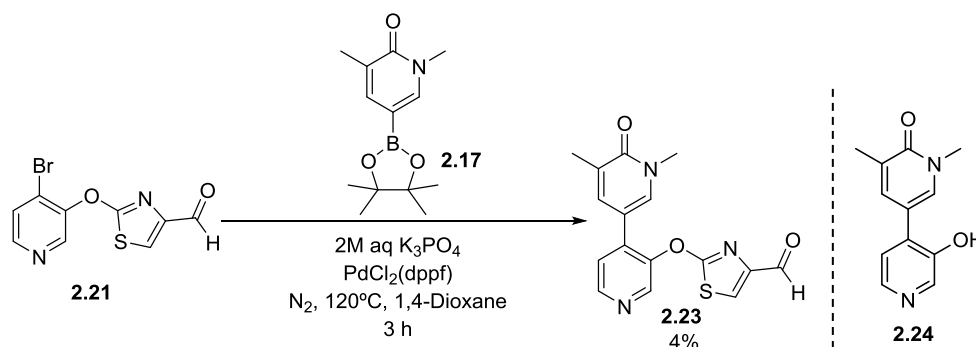


Entry	Product	Base	Solvent	Temp (°C)	Time (h)	Conversion (%)	Yield (%)
1	2.21	K ₂ CO ₃	DMF	120	16	60	10
2	2.21	NaH	THF	rt	6	14	-
3	2.22	K ₂ CO ₃	DMF	120	16	0	-
4	2.22	NaH	THF	rt	4	25	-
5	2.22	KO ^t Bu	MeCN	70	4	50	29

Table 2.4. Reaction conditions for the S_NAr reactions of **2.13** and thiazoles **2.14** and **2.15** to form intermediates **2.21** and **2.22** respectively. Conversion (%) was estimated by the UV area/area observed by LCMS.

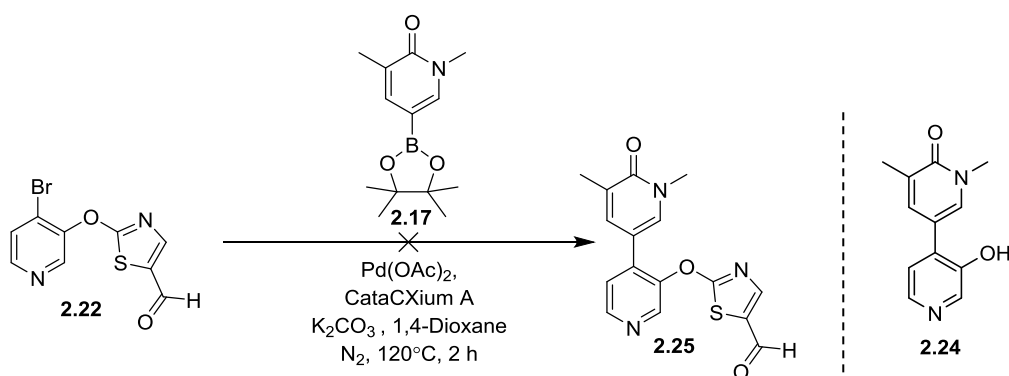
For both thiazoles, the classical K₂CO₃/DMF and NaH/THF S_NAr conditions (Entries 1-4) were employed first. Whilst a high conversion to the desired product using K₂CO₃/DMF was observed for thiazole **2.14**, there was no conversion for thiazole **2.15** using the same conditions (entries 1 vs. 3). On the other hand, NaH/THF (entries 2 and 4) resulted in low to moderate conversions and therefore was not pursued. As such, further reaction conditions were trialled for thiazole **2.15**. Employing KO^tBu in MeCN gave a good conversion to the desired product (**2.22**). Despite high conversions to **2.21** and **2.22** (entries 1 and 5), the work ups for both intermediates were particularly difficult, with a black emulsion formed along with an insoluble precipitate. Therefore, only poor isolated yields were obtained.

Intermediate **2.21** was then coupled to the pyridone boronic ester **2.17** through a Suzuki-Miyaura cross coupling reaction (Scheme 2.2).



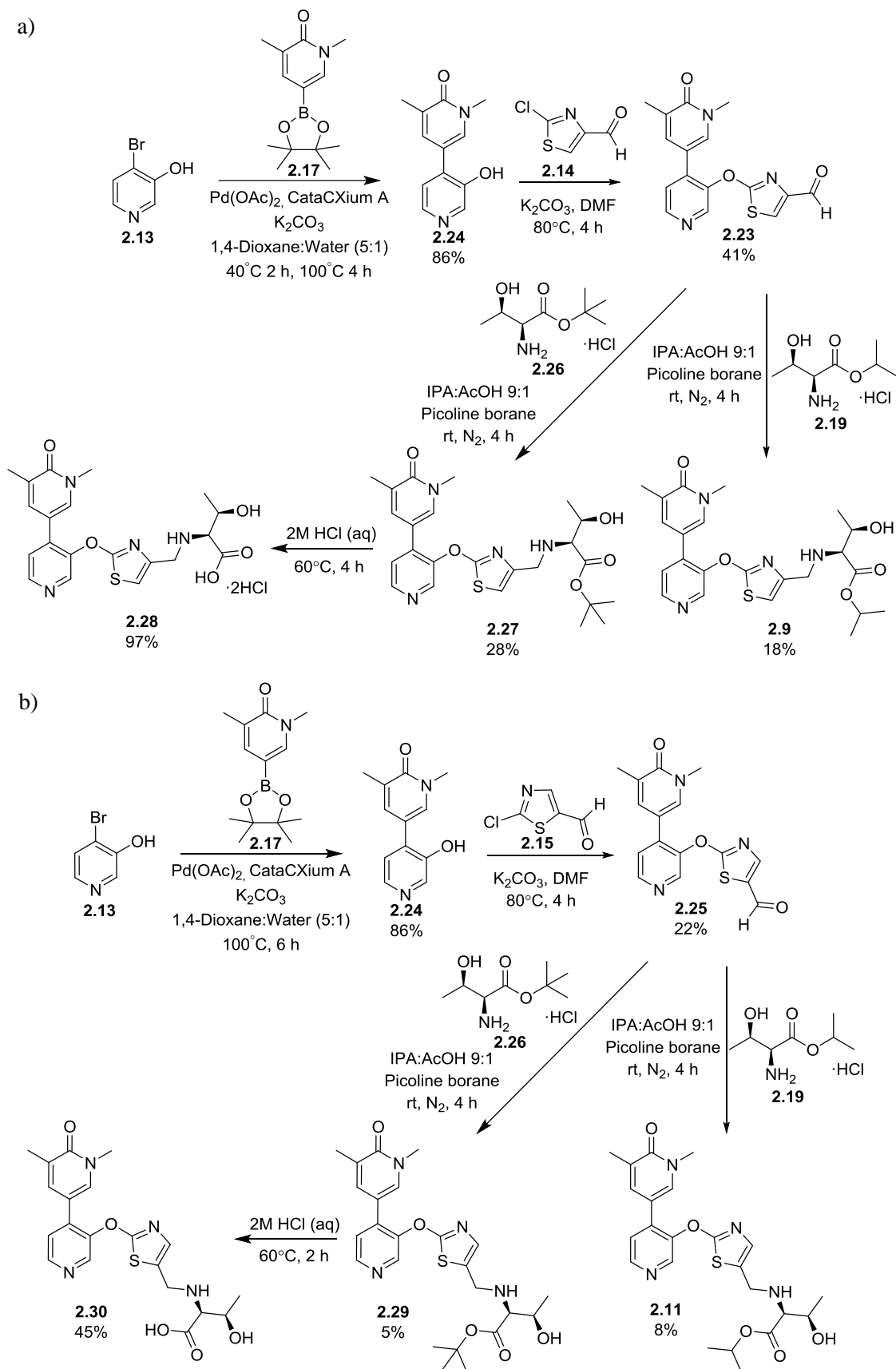
Scheme 2.2. Initial attempt of the Suzuki coupling on **2.21** which resulted in high conversion to **2.24**.

Surprisingly, the Suzuki reaction of intermediate **2.21** and boronic ester **2.17**, to form **2.23**, was low yielding with only 4% isolated yield obtained. Instead, the major component formed was the hydroxylated intermediate **2.24**, as determined by LCMS analysis, in which the thiazole has been displaced with a hydroxyl group. This was thought to be due to the aqueous solution of K_3PO_4 , therefore alternative conditions were attempted on intermediates **2.22** and to **2.17** form intermediate **2.25** (Scheme 2.3). Intermediate **2.24** was not isolated.



Scheme 2.3. Alternative Suzuki conditions for the coupling of **2.22** and **2.17**, which resulted in the high conversion to **2.24**.

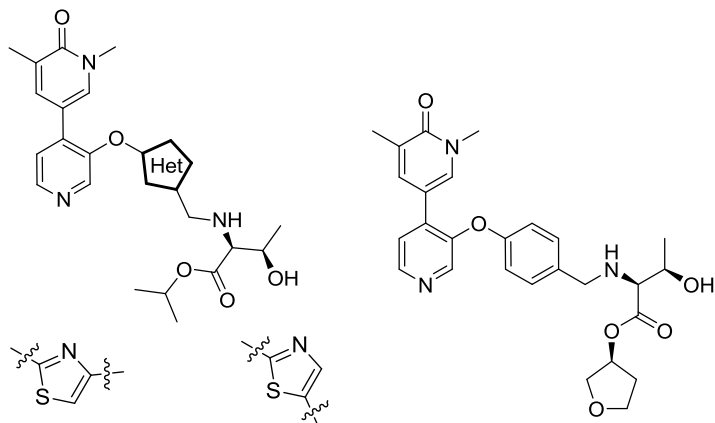
As before, the hydroxylated intermediate **2.24** was formed rather than the desired product **2.25**. Consequently, in order to avoid what was assumed to be the competitive hydroxylation of the intermediates, it was decided to attempt to synthesise the targets using intermediate **2.24** as the starting material (Scheme 2.4).



The Suzuki-Miyaura cross-coupling of pyridinol **2.13** and the boronic ester **2.17** provided intermediate **2.24** in 86% yield. The subsequent S_NAr reactions of intermediate **2.24** and thiazoles **2.14** and **2.15** proceeded well to give moderate yields of intermediates **2.23** (41%) and **2.25** (22%) respectively. Unlike the S_NAr performed on **2.13**, with the conditions in Table 2.4, there was no precipitate or emulsion formed. Therefore, the reaction mixtures were concentrated *in vacuo* and purified by mass directed auto prep (MDAP).

The reductive aminations of **2.23** with the amino acid esters **2.19** and **2.26** afforded the biologically hydrolysable **2.9** and non-biologically hydrolysable analogue **2.27** in low to moderate yields. This was also observed for the analogous reductive aminations with intermediate **2.25** to form **2.11** and **2.29**, despite high conversions to the products observed by LCMS analysis. The reaction mixtures were purified directly by mass directed auto prep (MDAP) using a basic modifier and so it is possible that the compounds could have been converted into the hydroxylated intermediate **2.24**, as previously observed during the Suzuki reactions in Scheme 2.2, during purification.

Subsequent hydrolysis of the *tert*-butyl esters **2.27** and **2.29** yielded the acids **2.28** and **2.30**. The clean LCMS reaction profile of **2.28** allowed the reaction mixture to be concentrated *in vacuo* to give the dihydrochloride salt with > 95% purity. However, during the hydrolysis of **2.29** to **2.30**, some conversion to the intermediate **2.24** was observed. Therefore, the reaction mixture was purified by MDAP, resulting in the free base of **2.30** in 45% yield. The amino acid esters and their corresponding acids were submitted for biological testing (Table 2.5). As the *tert*-butyl analogues are only used to determine the Δ hWB values, their biological profiles will not be displayed throughout the thesis.



X	2.9	2.11	2.2
hWB pIC ₅₀	6.5	6.9	7.8
Δ hWB	+0.9	+0.9	+1.1
Ester BD1 pIC ₅₀	6.0	6.5	8.2
Acid BD1 pIC ₅₀	5.5	5.8	6.8
HLM IVC (+/- benzil)	4.3 / 6.9	4.4 / 7.5	4.5 / 8.3
ChromlogD _{7.4}	3.2	3.1	2.8

Table 2.5. Biological data for thiazole WPF shelf groups **2.9** and **2.11**. IVC values are quoted in mL/min/g.

The thiazole analogues **2.9** and **2.11** were both found to be considerably less lipophilic than the initial lead compound **2.1** (3.2 and 3.1 vs. 4.4 respectively) whilst displaying similar ChromlogD_{7.4} values to that of **2.2**. Furthermore, they both displayed a desired ΔhWB of ~1, suggesting that the amino esters were being hydrolysed thus leading to retention of the compound within the cell. Unfortunately, the compounds exhibited a similar IVC profile relative to **2.2** and demonstrated low ester and acid biochemical activity. In an attempt to understand the potency differences, analogues **2.11** and **2.2** were submitted for x-ray crystallography in BRD2 BD2 (Figure 2.9).

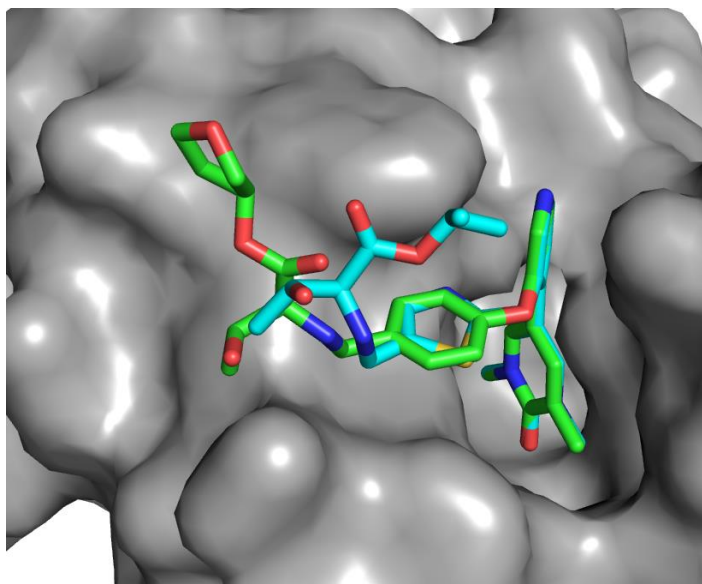


Figure 2.9. Overlaid crystal structures of lead compound **2.2** (green) and analogue **2.11** (blue) in BRD2 BD2.

The crystal structure of **2.2** and **2.11** in BRD2 BD2 shows the two compounds adopt very similar binding modes, with the main difference observed in the position of the ESM moiety. It can be seen that changing the bond angles by incorporating a five-membered heterocycle has caused the CH₂NH linker to move position, as hypothesised. However, instead of the ESM being directed through the adjacent cleft, in the case of the thiazole **2.11**, the ester folds back in towards the molecule, rather than extending into space as with the benzene analogue **2.2**. This could be due to the CH₂NH linker having to adopt a specific conformation to avoid a steric clash with an aspartate residue flanking the WPF shelf. This theory is supported by the ESM binding such that the hydroxy of its threonine residue is aligned with the aspartate, whilst the isopropyl of the ester is situated by the WPF stack. However, this also results in the polar ester group being in close proximity to the hydrophobic WPF stack, tryptophan in particular, which would be unfavourable. These interactions, along with the loss of entropy that would occur upon fixing the flexible ESM into a locked position, would make the binding of **2.11** less favourable than that of **2.2**. Furthermore, although the thiazole and benzene rings overlay well, the thiazole has less contact with the WPF shelf than the benzene group. As hydrophobic interactions with the WPF shelf are believed to be key for potency, this poorer contact of the thiazole with the shelf could rationalise the lower potency observed. Due to the low biochemical and cellular activity, the compounds were not progressed into cynomolgus monkey/human hepatocyte IVC assays and were not investigated further.

2.3.2 Investigating substituted motifs interacting with the WPF shelf in the first-generation analogues

In order to investigate the hypothesised π - π parallel displaced hydrogen bond between the WPF shelf group and W81 of the WPF stack, the electronics of the WPF shelf could be modulated which would impact the strength of the interaction (Figure 2.10).

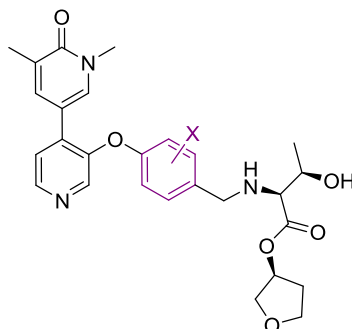


Figure 2.10. The electronics of the central aromatic ring, the WPF shelf (purple), can be modulated to impact the potential hydrogen bond with the shelf and reduce IVC and lipophilicity.

A *meta*- σ vs. *meta*- π Craig plot using the general scaffold in Figure 2.10 considers the inductive/mesomeric effects (σ) and the lipophilicity (π) effects of a *meta*-substituent compared to a hydrogen (Figure 2.11).¹⁶³ As such, the plot was used to identify substituents that would vary the electronics of the ring, as well as reduce the lipophilicity. It can be seen from Figure 2.11 that low lipophilicity groups include primary amide, amine, methyl sulfone and nitrile. Alternatively, halogens and fluorinated substrates would increase the lipophilicity of a compound relative to a hydrogen. Meanwhile, strongly electron withdrawing groups include the nitrile, sulfone and nitro groups while amines and small alkyl substituents are the most electron donating.

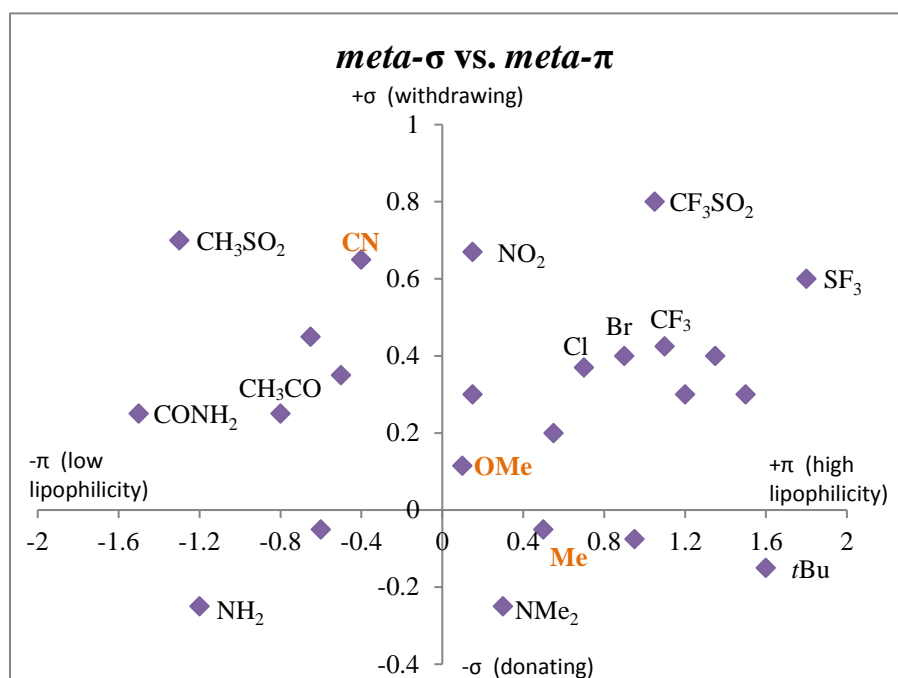


Figure 2.11. A *meta*- σ -*meta*- π Craig plot considers the inductive/mesomeric effects (σ) and the lipophilicity (π) effects of a *meta*-substituent compared to a hydrogen on aromatic rings. The substituents highlighted in orange provide a range of electronic effects whilst only having small effects on the lipophilicity.

Taking inspiration from the Craig plots, and the previous hypotheses, a range of substituents were profiled *in silico* including sulfones, amides, esters, amines, methyl, cyano and methoxy groups (Figure 2.12a). As previously mentioned, the target profile is TPSA <140Å² and a ChromLogD_{7.4} <3.5. As such, the data were plotted to allow for easier visualisation, with these values forming the boundaries for the analysis. It can be seen that a large proportion of the molecules fell outside of the desirable physicochemical space, mainly due to high TPSA values, and these analogues were therefore not synthesised. However, there were a number of compounds that were predicted to have desirable properties.

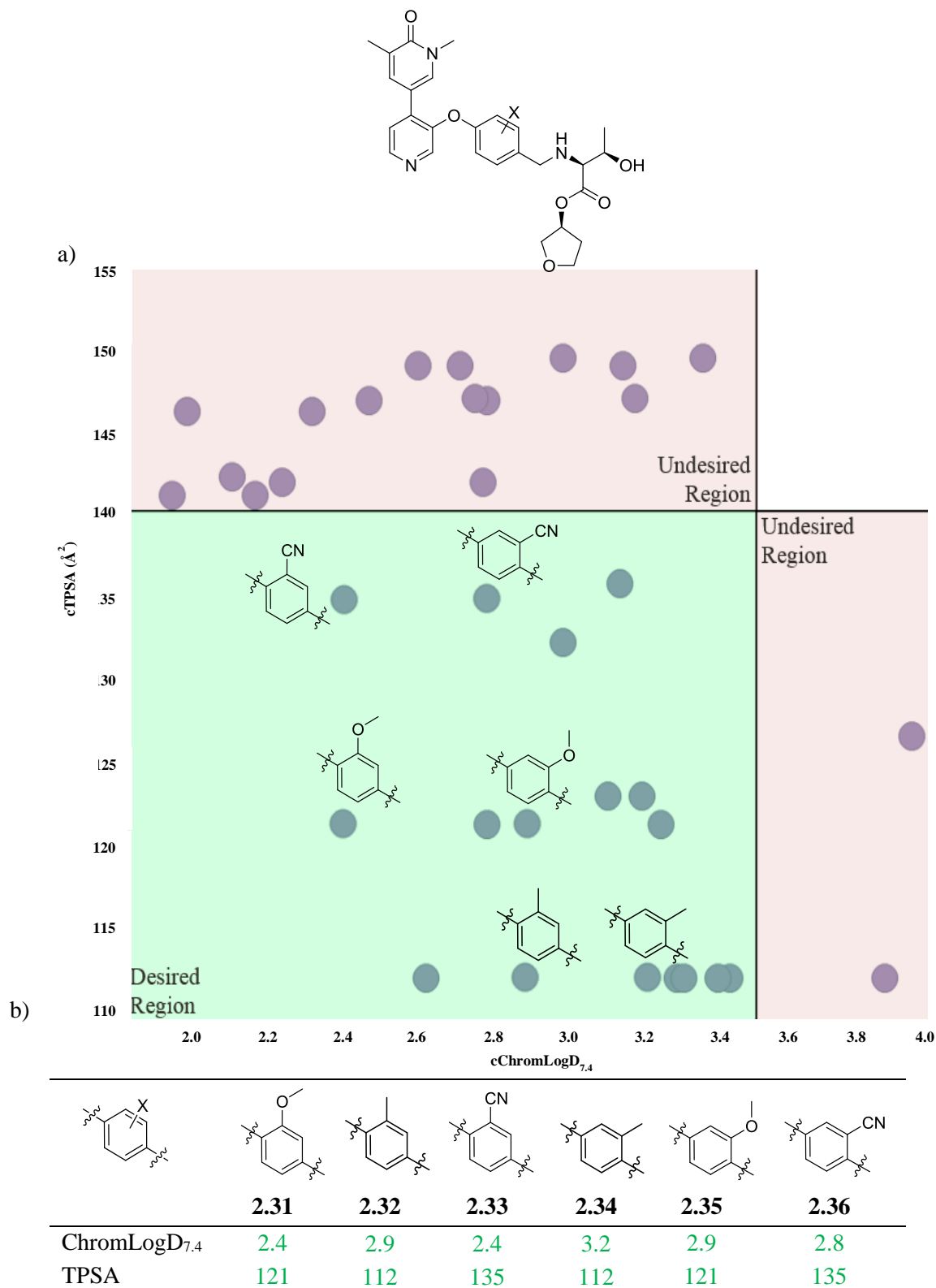
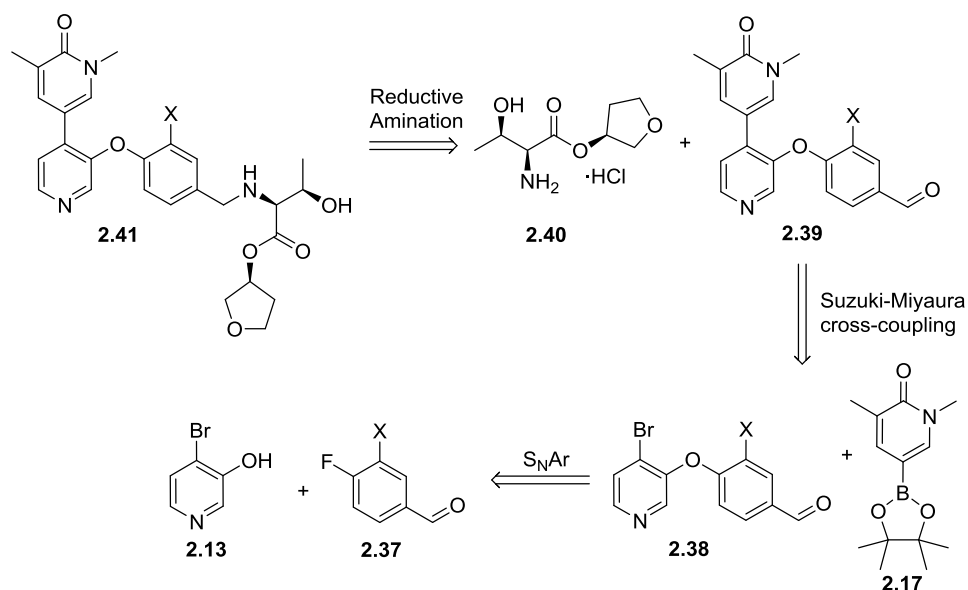


Figure 2.12. a) A plot of the calculated TPSA vs. calculated ChromLogD_{7.4} values for a range of substituents including sulfones, amides, esters, amines, methyl and methoxy groups. The lines depict boundaries (TPSA < 140 Å² and a ChromLogD_{7.4} < 3.5). b) *In silico* modelling predicted the methyl, methoxy and cyano substituents to give analogues with favourable physicochemical properties, with ChromLogD_{7.4} and TPSA values in the desired range (also highlighted on the plot). Therefore, these analogues were chosen for synthesis.

The *in silico* modelling predicted the methyl, methoxy and cyano substituents to give analogues with favourable physicochemical properties, with ChromLogD_{7.4} and TPSA values in the desired range of <3.5 and <140Å² respectively with a variety of ESMs (Figure 2.12b). Therefore, these substituents were chosen for exploration. However, the amides, sulfones and esters were outside of the desired range and not synthesised.

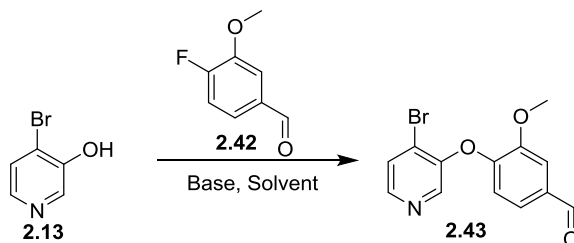
A retrosynthetic analysis was undertaken to investigate the route towards **2.31-2.36** (Scheme 2.5).



Scheme 2.5. A retrosynthetic analysis was completed on the generalised molecule **2.41** to investigate the synthetic route to the targets.

The retrosynthetic analysis outlined in Scheme 2.5 should be applicable to all of the desired targets. Firstly, the C-N bond can be disconnected to afford aldehyde **2.39** and the THF Thr ESM **2.40**. Next, aldehyde **2.39** can be formed through the Suzuki cross-coupling of the readily available boronic ester **2.17** and the bromide intermediate **2.38**. Finally, intermediate can be formed through the S_NAr reaction of pyridinol **2.13** and fluoro-aldehyde **2.37**.

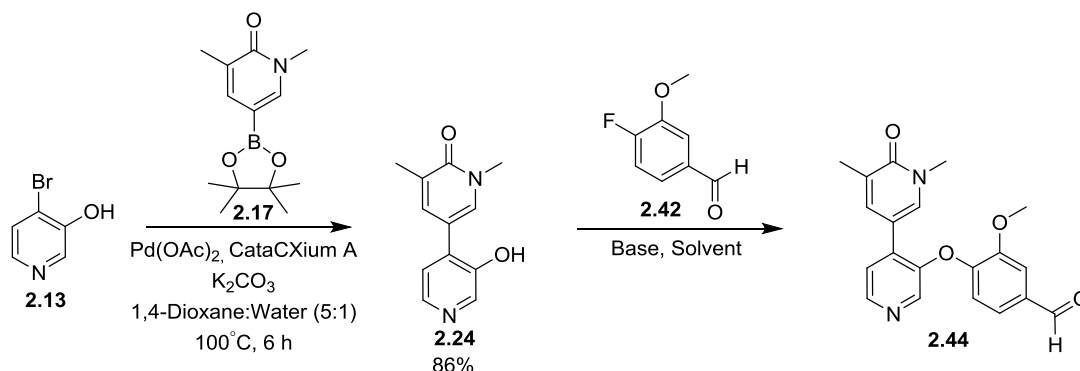
Synthetic efforts were initially focussed on the 2-methoxy compound **2.31**. The optimal reaction conditions were then to be applied to the other targets. The first step in the synthesis was the S_NAr of commercially available 4-bromopyridin-3-ol **2.13** and 4-fluoro-3-methoxybenzaldehyde (**2.42**) to form intermediate **2.43**. A range of reaction conditions were attempted (Table 2.6). The conversion was estimated by the UV area/area observed by LCMS.



Entry	Base	Solvent	Temp (°C)	Heating	Time (h)	Conversion (%)	Yield (%) 2.43
1	Cs ₂ CO ₃	DMSO	140	Microwave	1	18	-
2	KO ^t Bu	MeCN	70	Thermal	5	24	-
3	DIPEA	NMP	120	Microwave	0.5	0	-
4	K ₂ CO ₃	DMF	90-110	Thermal	20	11	-
5	K ₂ CO ₃	DMSO	160	Microwave	1	20	17%

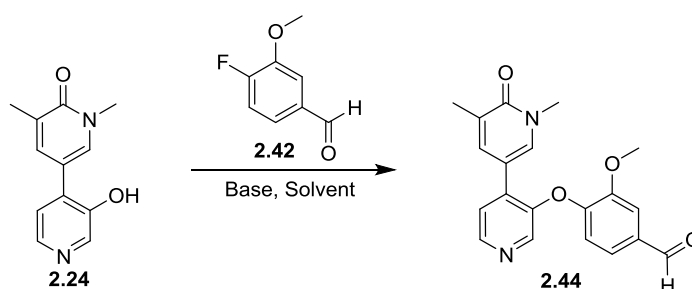
Table 2.6. Reaction conditions explored in the S_NAr reaction of 4-bromopyridin-3-ol **2.13** and 4-fluoro-3-methoxybenzaldehyde **2.42**. Conversion (%) was estimated by the UV area/area observed by LCMS.

All of the reaction conditions resulted in low conversion of **2.13** to the desired product **2.43**, which may be due to the electronics of pyridinol **2.13**. S_NAr reactions require a strong nucleophile, however, **2.13** is electron deficient and as such, exhibits poorer nucleophilicity. Furthermore, the *ortho*-methoxy substituent is likely to decrease the electrophilicity of the C-F carbon which, as the nucleophilic attack and breaking of aromaticity is the rate determining step, could have impacted the reactivity of the system. The highest conversion was observed with potassium *tert*-butoxide in acetonitrile (24% conversion, Entry 2), whereas DIPEA/NMP resulted in no conversion (Entry 3). As a result of the poor conversions, the order of steps was changed to perform the Suzuki cross-coupling to form the aryl-aryl C-C bond first (Scheme 2.6).



Scheme 2.6. A devised synthetic route in which the Suzuki cross-coupling to form the aryl-aryl bond is performed first, prior to the S_NAr reaction to install the ether linkage.

By reversing these two steps, it created a convergent synthesis in which intermediate **2.24** could be used as a building block for all six targets. Therefore, the synthetic route was reduced by one step. The Suzuki cross-coupling was performed with the ligand di(1-adamantyl)-*n*-butylphosphine (CataCXium A), which has been reported to facilitate the reaction with electron deficient aryl bromides. Although the reaction was high-yielding (86%), the protodeboronation of **2.17** was observed as a major by-product. The intermediate, **2.24**, was subsequently reacted with 4-fluoro-3-methoxybenzaldehyde **2.42** in an S_NAr reaction, yielding the bi-aryl ether **2.44** (Table 2.7).

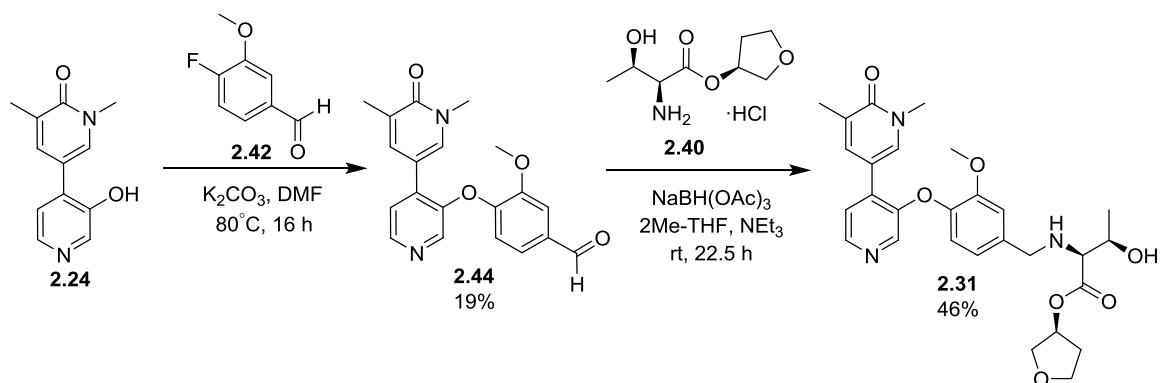


Entry	Base	Solvent	Temperature (°C)	Time (h)	Yield 2.44 (%)
1	K ₂ CO ₃	DMF	80	16	19
2	KO ^t Bu	MeCN	70	5	-

Table 2.7. Reaction conditions explored in the S_NAr reactions of intermediate **2.24** and 4-fluoro-3-methoxybenzaldehyde **2.42**.

The S_NAr reaction was poor yielding, and was not improved by alternative reaction conditions (data not shown), affording **2.44** in 19% yield (Entry 1, Table 2.7). Despite the low conversion to the bi-aryl ether **2.43** observed using KO^tBu/MeCN (24% conversion, Table 2.6, *vide supra*), **2.44** was not isolated using these conditions (Entry 2, Table 2.7).

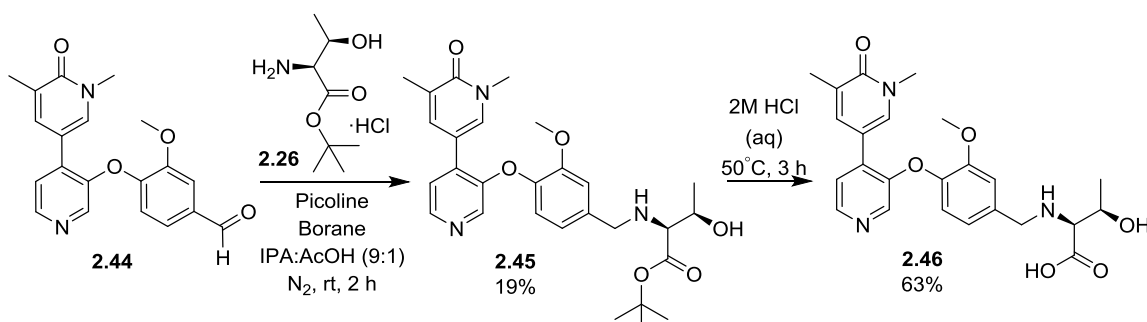
Finally, a reductive amination was performed on aldehyde **2.44** with the THF threonine ester (**2.40**) to give the final target **2.31**, with a moderate yield of 46%. The full synthetic route used to synthesise **2.31** can be found in Scheme 2.7.



Scheme 2.7. The synthetic route used to synthesise final target **2.31**.

The reductive amination proceeded very slowly and, despite the excess of sodium triacetoxyborohydride (STAB), the reaction stalled at various stages of the imine reduction. In total, ten equivalents of the reducing agent were necessary to complete the reductive amination. Therefore, 2-picoline borane in IPA/AcOH was utilised as the reducing agent for some of the remaining targets due to its stronger reducing ability.

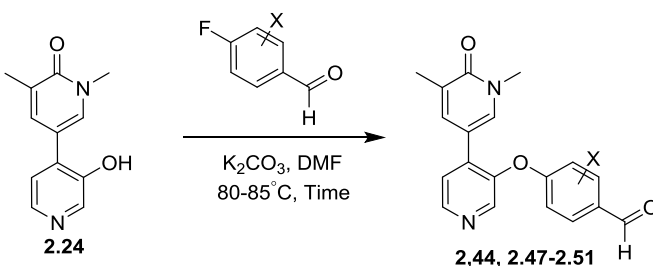
In order to assess the contribution of the ESM hydrolysis to the cellular potency, the biologically non-hydrolysable *tert*-butyl threonine ESM (**2.45**) was also synthesised through the reductive amination of aldehyde **2.44** with the *tert*-butyl Thr amino ester analogue (**2.26**) (Scheme 2.8). As the ester is hydrolysed intracellularly, the activity of the acid must also be optimised and assessed. Therefore, compound **2.45** was subsequently chemically hydrolysed to the acid (**2.46**).



Scheme 2.8. The biologically non-hydrolysable ESM **2.45** was also synthesised. It was subsequently chemically hydrolysed to the acid **2.46**.

The reductive amination of intermediate **2.44** and **2.26** resulted in high conversion by LCMS to the desired product **2.45**. However, an equipment error during MDAP purification caused the large majority of the sample being directed to the waste thus resulting in a poor recovery of the product. Subsequent hydrolysis with aqueous 2M HCl afforded the desired acid **2.46**.

The synthetic routes devised in Scheme 2.7 and Scheme 2.8 were used to synthesise the remaining analogues. The first step was the S_NAr reactions of **2.24** and the respective fluoro-aldehydes to give the aldehyde intermediates **2.47-2.51** (Table 2.8). Unfortunately, the 3-cyano analogue **2.51** was not able to be synthesised. Despite good conversion to the desired product, as shown by LCMS, the product degraded during the aqueous work up on several occasions and was unable to be isolated.



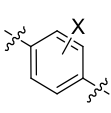
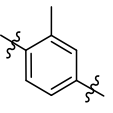
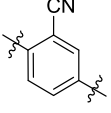
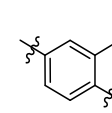
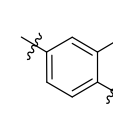
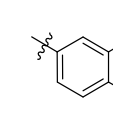
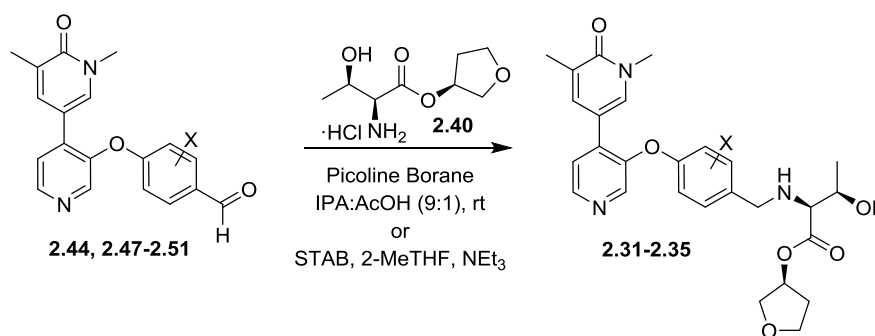
						
Time (h)	16	30	2.5	64	15	3
Temp (°C)	80	80	80	85	80	-
Yield (%)	19	16	33	27	22	-

Table 2.8. The reaction times and yields of the S_NAr reactions of **2.24** and the respective fluoro-aldehydes.

Next, reductive aminations of intermediates **2.47-2.50** with the THF amino ester **2.40** were performed to yield the biologically hydrolysable molecules **2.32-2.35** (Table 2.9).



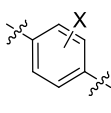
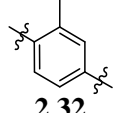
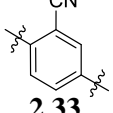
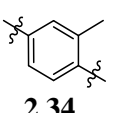
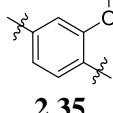
					
Yield	46 ^a	11 ^b	26 ^a	11 ^b	54 ^a

Table 2.9. The yields obtained for the reductive aminations to the final THF esters. ^aSodium triacetoxyborohydride, 2-MeTHF, NEt_3 ^b2-picoline borane, IPA, AcOH.

The intermediates **2.47-2.50** were also treated with the *tert*-butyl amino ester **2.26** under reductive amination conditions to yield the biologically non-hydrolysable *tert*-butyl esters **2.52-2.55** (Table 2.10).

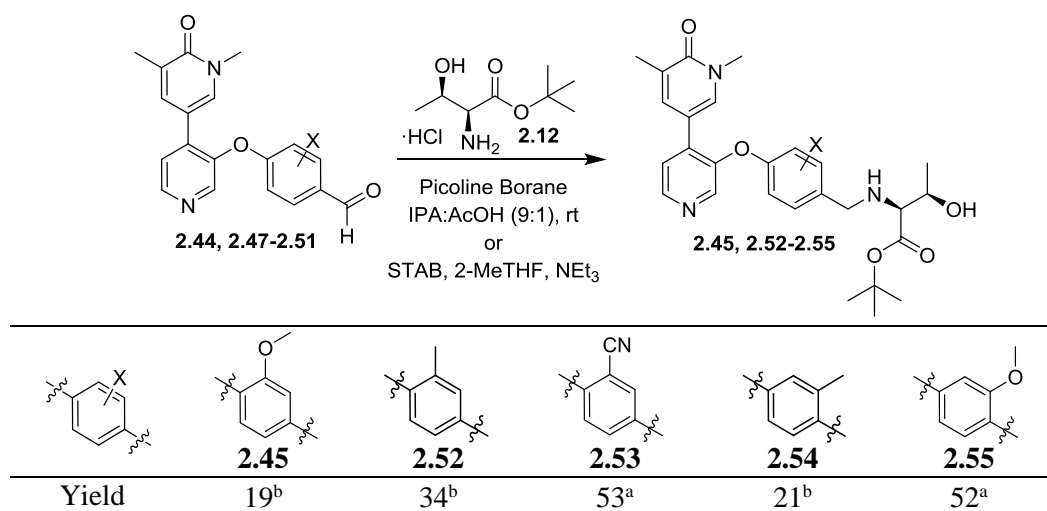


Table 2.10. The yields obtained for the reductive aminations to the final *tert*-butyl esters. ^aSodium triacetoxyborohydride, 2-MeTHF, NEt₃ ^b2-picoline borane, IPA, AcOH.

Finally, the *tert*-butyl analogues were hydrolysed to the acids **2.56-2.59** under acidic conditions (Table 2.11).

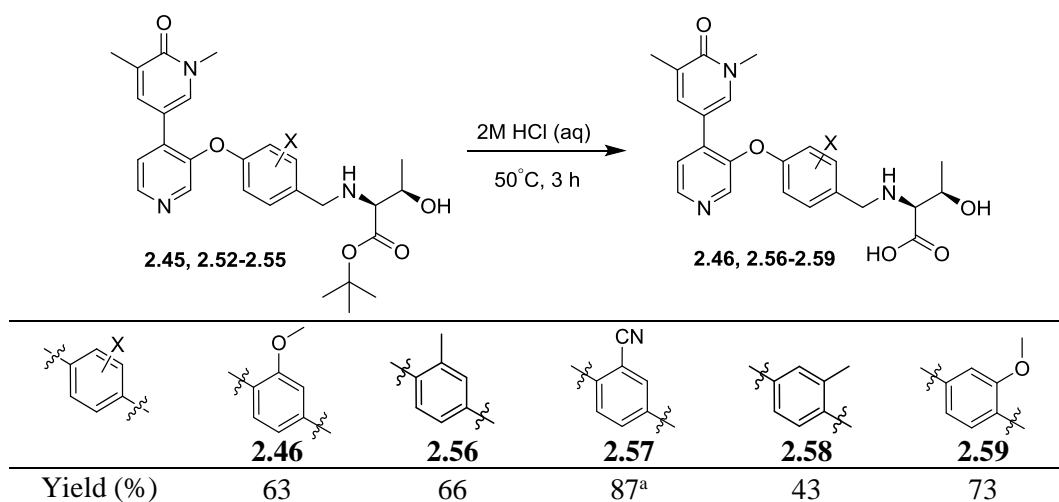
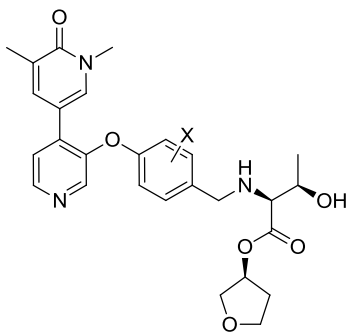


Table 2.11. The yields obtained for the chemical hydrolysis of the *tert*-butyl esters to the acids. ^a Isolated as the HCl salt.

The compounds were submitted for biological testing, the results of which can be found in Table 2.12.



	2.2	2.31	2.32	2.33	2.34	2.35
hWB pIC ₅₀	7.8	7.7	8.2	7.4	7.5	7.4
Δ hWB	+1.1	+0.6	+1.2	+0.3	+1.0	+1.0
Ester BD1 pIC ₅₀	8.2	7.8	7.8	8.0	7.6	7.3
Acid BD1 pIC ₅₀	6.8	6.7	6.9	6.7	6.3	6.2
HLM IVC (+/- benzil)	4.5 / 8.3	3.7 / 5.1	5.9 / 10.2	4.2 / 6.0	-	6.9 / 10.2
ChromlogD _{7.4}	2.8	2.9	3.3	2.8	3.4	3.0

Table 2.12. Profiles of the initial substituted WPF shelf group compounds. IVC values are quoted in mL/min/g. The ester pIC₅₀ relates to the THF ester.

All of the compounds synthesised displayed biochemical and cellular activities within the desired range. Furthermore, they showed similar activity relative to **2.2**, thus supporting the hypothesis that extending into the region adjacent to the WPF shelf would be tolerated. The binding of the substituent in the solvent exposed region adjacent to the shelf was confirmed by the crystal structure of **2.32** in BRD2 BD2 (Figure 2.13).

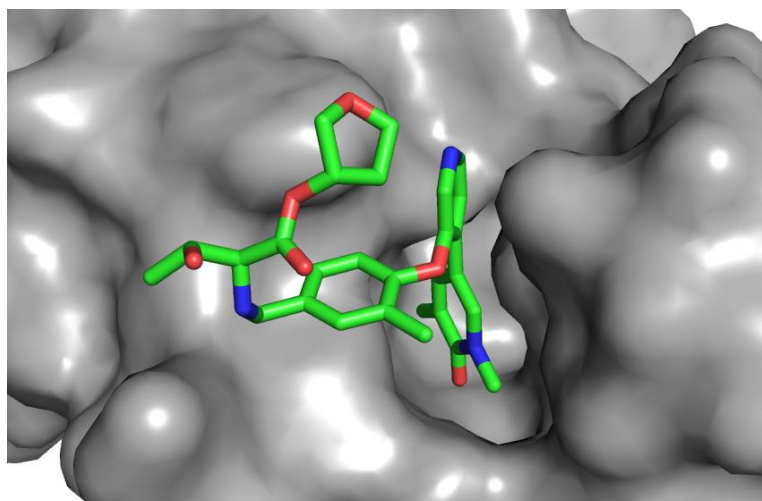


Figure 2.13. Crystal structure of **2.32** in complex with BRD2 BD2.

Compound **2.32** showed the highest whole blood activity and was > 0.5 log units more potent than the other analogues, which all displayed similar potencies. As well as this, the compounds exhibited similar inhibitory effects versus BRD4 BD1 in the biochemical assays, except for **2.35** which was half a log unit lower than the rest. Interestingly, the biochemical and cellular activities of **2.31** and **2.33** are similar. This shows that the activity is not influenced by the electronic nature of the WPF shelf group, thus suggesting that there is no parallel displaced π - π stacking with the tryptophan of the WPF shelf.

Whilst most compounds showed a desirable Δ hWB, the 2-methoxy and 2-cyano analogues, **2.31** and **2.33**, showed a lower effect from the ESM hydrolysis, Δ hWB = +0.6 and +0.3 respectively. In comparison, the 3-OMe analogue, **2.35**, shows a higher turnover, similar to that of the methyl analogue **2.34**. This suggests that substitution in the 2-position may slow down the rate of ester hydrolysis.

The compounds were submitted for HLM IVC assays. Analogues **2.31** and **2.33** showed increased microsomal stability compared to the baseline compound **2.2**. However, **2.32** and **2.35** displayed higher IVC, which may be due to the high lipophilicity of the compounds increasing its affinity for metabolic enzymes. Therefore, it was concluded that the methyl substituent is sub-optimal for IVC reduction, as is 3-substitution. Furthermore, even though a reduction in IVC was observed for some compounds, it was not sufficient to progress compounds **2.31** and **2.33** into *in vitro* hepatocyte assays. Therefore, further optimisation of the compounds was required.

2.3.2.1 Investigating the impact of the sterically hindered 2-methylpyridine and 2-pyridyl cores on IVC

Unsubstituted aryl rings are prone to metabolism due to their nucleophilic nature and inherent lipophilicity.¹⁶¹ Substitution of the WPF shelf group was shown to reduce HLM IVC, although not to the desirable level. The 3,4-substitution of the pyridine core means the nitrogen is relatively unhindered and, as such, could potentially readily undergo phase I and phase II metabolism.¹⁶⁴ Phase I metabolism involves the coordination of the pyridine nitrogen with Fe in the heme complex of P450 enzymes.¹⁶⁵ The coordination of unhindered pyridines, such as in **2.2**, is facile, resulting in high metabolic turnover. By sterically encumbering the nitrogen, the coordination to Fe should be slower, therefore reducing the rate of metabolism (Figure 2.14). Furthermore, the 6-position is susceptible to nucleophilic attack due to the ability of the *ortho*-nitrogen to stabilise the resultant negative charge.

Therefore, it was hypothesised within the chemistry team that substitution of the *ortho*-position would improve metabolic stability. In addition to this, the steric hindrance around the nitrogen can also be increased by synthesising the regioisomer, in which the nitrogen is *ortho* to the ether linkage.

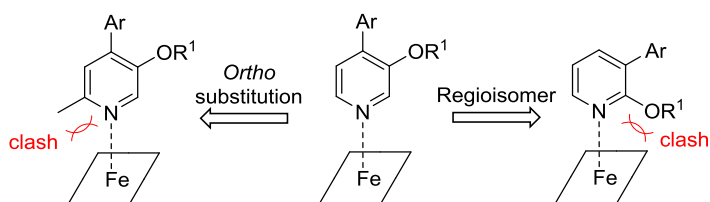


Figure 2.14. The coordination of unhindered pyridines to the Fe of the heme (depicted as the square) is relatively facile, thus leading to increased metabolic turnover. Substituting in the *ortho* position with a methyl, or synthesising the 2-pyridyl regioisomer, would introduce steric hindrance around the pyridyl nitrogen, therefore reducing the rate of coordination to Fe and subsequent metabolism.

To test this hypothesis, the methylpyridine¹⁶⁶ (**2.60**) and 2-pyridyl¹⁶⁷ (**2.61**) analogues were synthesised elsewhere in the team and profiled (Table 2.13).

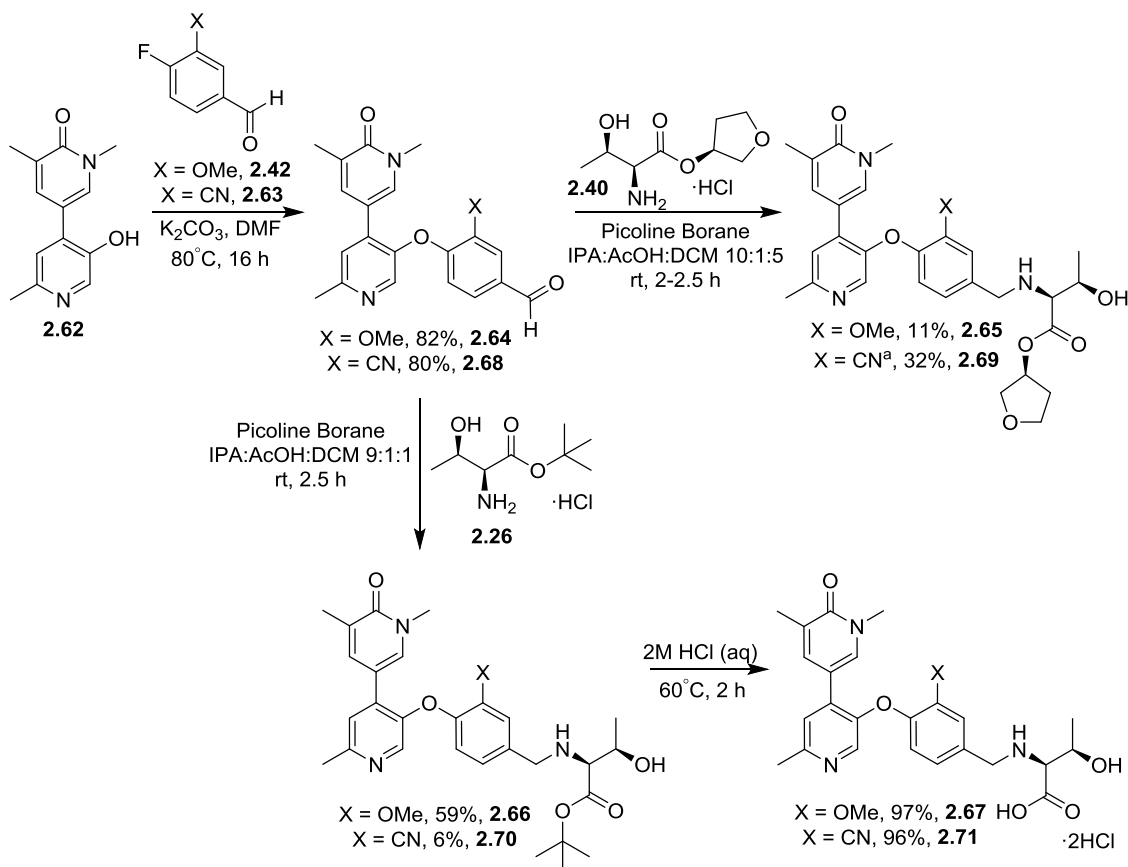
	2.2	2.60	2.61
hWB pIC ₅₀	7.8	7.3	7.6
Δ hWB	+1.1	+0.3	+0.7
Ester BD1 pIC ₅₀	8.2	7.7	7.6
Acid BD1 pIC ₅₀	6.6	6.8	6.4
HLM IVC (+/- benzil)	4.5 / 8.3	1.9 / 3.0	1.5 / 2.7
Heps IVC (Hu/cyno)	-	5.4 / 19.3	7.9 / 20.6
ChromlogD _{7.4}	2.8	3.2	3.2

Table 2.13. Profiles of the methylpyridine core, 2-pyridyl and unsubstituted pyridine cores synthesised elsewhere within the team. IVC values are quoted in mL/min/g.

The analogues **2.60** and **2.61** displayed lower cellular and biochemical activity compared to the baseline compound **2.2**, although the respective acids were equipotent against BRD4 BD1. However, the introduction of the methyl and the pyridyl regioisomer reduced the ΔhWB , suggesting that these changes were detrimental to CES-1 turnover relative to **2.2**. SAR gathered on the previous two series suggested the optimal ΔhWB is ~ 1 . A ΔhWB of $+0.3$ as seen for compound **2.60**, suggests that the rate of hydrolysis by CES-1 is slow. Although the 2-pyridyl core, **2.61**, also displayed a lower turnover compared to **2.2**, a moderate ESM effect was observed ($\Delta hWB = +0.7$). The HLM IVC was reduced to an acceptable level for both compounds, thus supporting the hypothesis that hindering the pyridyl nitrogen would decrease the rate of coordination to P450 enzymes and subsequent metabolism and allowing their progression into hepatocyte IVC. Unfortunately, the human and cynomolgus monkey hepatocyte stability was still not in the desired range.

The IVC values for compounds **2.60** and **2.61** suggest that sterically hindering the pyridine nitrogen, as well as blocking an activated position, through the substitution of the pyridine core and synthesising the regioisomer improved microsomal stability. Therefore, it was hypothesised that combining these cores with the preferred substituted WPF shelf groups would further reduce the IVC. As previously discussed, 2-methoxy and 2-cyano substitution increased microsomal stability whilst all other investigated substitutions offered no advantage. Therefore, only analogues with these substituents were synthesised.

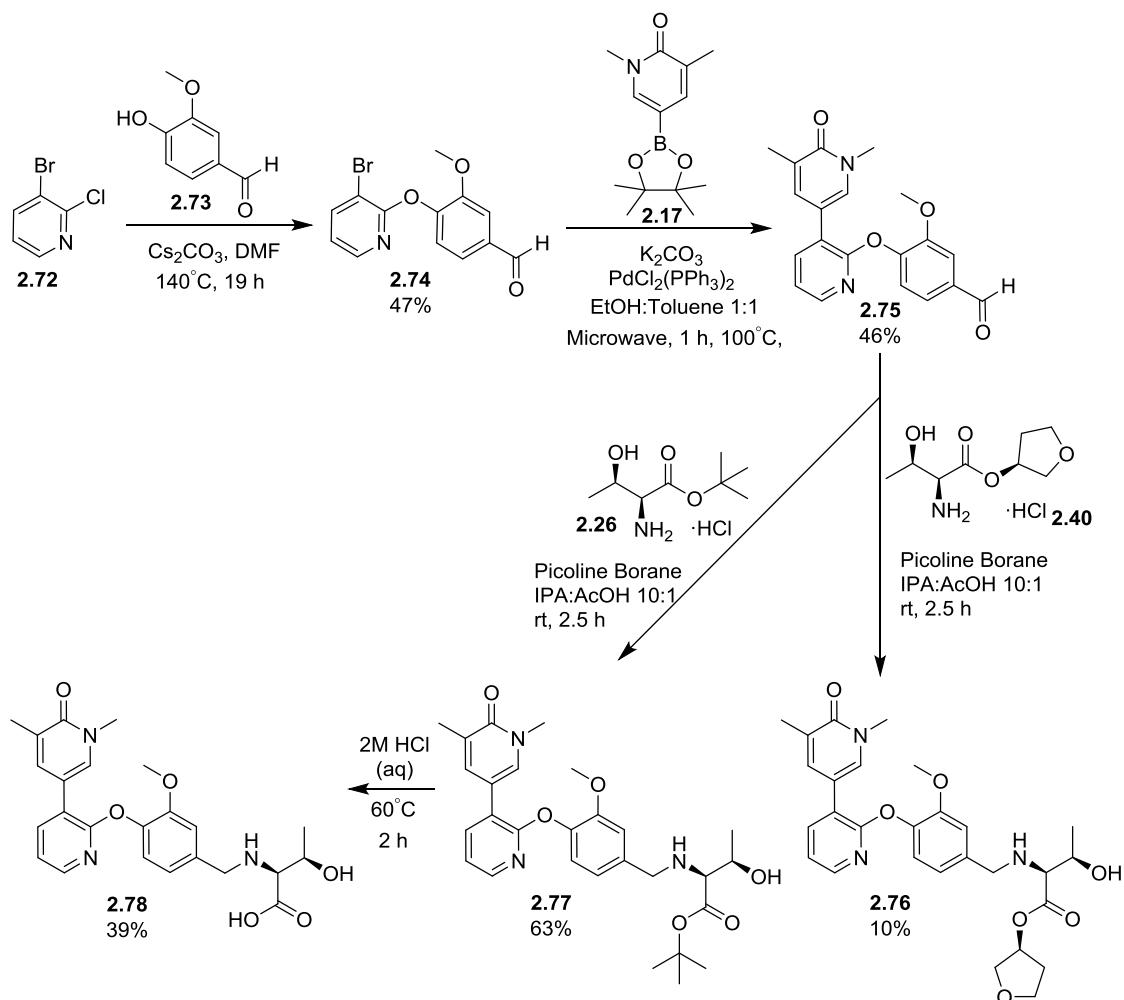
The methylpyridine analogues were synthesised through the same synthetic route utilised for the previous pyridyl compounds (Scheme 2.9).



Scheme 2.9. The synthetic route employed to synthesise the methoxy-substituted and cyano-substituted WPF shelf groups in the more efficient methyl pyridyl core, **2.65** and **2.69** respectively, along with their corresponding *tert*-butyl and acid analogues. ^a IPA:AcOH:DCM = 6:1:6.

Intermediate **2.62**¹⁶⁸ was reacted with aldehydes **2.42** and **2.63** under $\text{S}_{\text{N}}\text{Ar}$ conditions (Scheme 2.9). Higher yields were achieved than for the corresponding 6-*H* analogues **2.31** and **2.33** (Scheme 2.7 *vide supra*, >80% vs. 19% for **2.31** and 33% for **2.33**). Reductive aminations of **2.64** and **2.68** to yield the THF esters **2.65** and **2.69**, and the *tert*-butyl esters, **2.66** and **2.70**, were then performed. Intermediates **2.64** and **2.68** suffered with poor solubility in IPA, therefore, DCM was also added. Despite high conversions to all of the desired products, poor to moderate yields were obtained which suggests that the material was lost during purification, a common problem for compounds across the series. Subsequent hydrolysis of **2.66** and **2.70** yielded the acids **2.67** and **2.71**. The esters **2.66** and **2.70** were hydrolysed with an excess of aqueous 2M HCl, therefore, once the reaction was completed, the reaction mixture was concentrated *in vacuo* to afford the dihydrochloride salts of the acids **2.67** and **2.71** in high yield.

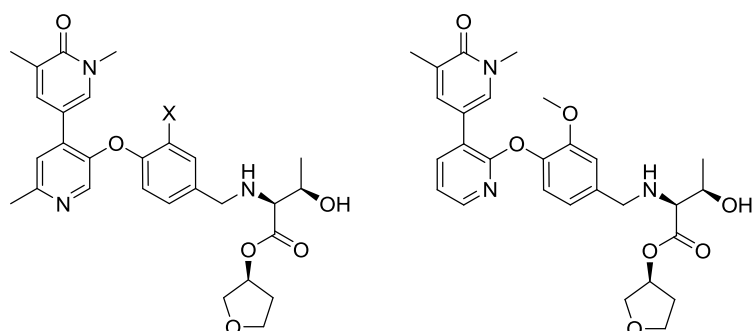
Following the synthesis of the methylpyridine analogues, the 2-pyridyl analogues were synthesised through an alternative route (Scheme 2.10).



Scheme 2.10. The synthetic route employed to synthesise the substituted WPF shelf groups in the more efficient 2-pyridyl core.

Initial attempts of the S_NAr reaction between chloropyridine **2.72** and the phenol aldehyde **2.73** using K_2CO_3 /DMF, as used in previous synthetic routes, were unsuccessful and only unreacted starting materials were observed by LCMS. However, switching the base to cesium carbonate and increasing the reaction temperature allowed the reaction to proceed, with a moderate isolated yield obtained. Following this, the Suzuki reaction of intermediate **2.74** and boronic ester **2.17**, to give **2.75**, was completed employing a $PdCl_2(PPh_3)_2$ catalyst and ethanol/toluene solvent system. Finally, the reductive aminations with amino acid esters **2.40** and **2.26** yielded the targets **2.76** and **2.77**. Unlike the methylpyridine intermediates **2.64** and **2.68**, aldehyde **2.75** was soluble in IPA and acetic acid. As such, the reaction mixtures were purified directly by MDAP, with no workups required. However, despite a good conversion to the desired product **2.76**, only a 10% isolated yield was obtained, again highlighting the problematic purification of compounds belonging to this series. Subsequent hydrolysis of **2.77** with aqueous 2M HCl produced the acid **2.78**. The esters and acids were

submitted for biological testing along with the methyl-pyridyl analogues synthesised in Scheme 2.9 (Table 2.14).



	2.65	2.69	2.76
X	OMe	CN	
hWB pIC ₅₀	8.0	7.7	7.8
Δ hWB	+0.7	+0.7	+0.7
Ester BD1 pIC ₅₀	8.1	8.1	7.5
Acid BD1 pIC ₅₀	7.1	6.7	6.8
HLM IVC (+/- benzil)	2.1 / 2.4	2.6 / 2.4	1.9 / 2.4
Hu Heps IVC (~LBF)	3.9 (85%)	2.2 (76%)	8.8 (92%)
Cyno Heps IVC (~LBF)	10.4 (88%)	4.6 (76%)	9.0 (87%)
ChromlogD _{7.4}	2.9	2.9	3.4

Table 2.14. Profiles of the substituted analogues in the methylpyridine core. IVC values are quoted in mL/min/g.

The 2-methoxy analogues, **2.65** and **2.76**, displayed higher ester biochemical potency relative to **2.31** (Table 2.12, *vide supra*), with **2.65** also demonstrating higher cellular activity (hWB pIC₅₀ = 7.7 for **2.31**). Meanwhile, the 2-cyano analogue **2.69** was equipotent compared to the desmethyl pyridyl analogue **2.33** (Table 2.12, *vide supra*), whilst displaying an improved ΔhWB (+0.7 vs. +0.3 for **2.33**). Interestingly, the lipophilicity of the methylpyridine compounds remained the same, despite the addition of the methyl group. The methyl group is inductively donating, which increases the basicity of the nitrogen. Therefore, the additional lipophilicity of the methyl is offset by the increase in nitrogen basicity. On the other hand, the 2-pyridyl analogue was more lipophilic relative to **2.31** (ChromLogD_{7.4} = 2.9).

As hypothesised, the methylpyridine and 2-pyridyl cores reduced the HLM IVC of the analogues. Therefore, the compounds were progressed into human and cynomolgus monkey

hepatocyte IVC. Pleasingly, the hepatocyte data was acceptable for all three analogues. Typically, a clearance of below ~33% liver blood flow (LBF) is desired for small molecule inhibitors. However, this is increased to ~85% for ESM containing compounds. This corresponds to human/cynomolgus monkey hepatocyte IVC values of <4 and <9 mL/min/g respectively, levels that were achieved for all three compounds. It was decided at this stage to complete no further work on **2.76** due to its high lipophilicity and poorer potency relative to **2.65** and **2.69**.

Despite displaying a moderate ΔhWB of +0.7, indicating reasonable CES-1 turnover, no difference was observed between the +/- benzil values of **2.65** and **2.69**. As previously mentioned, benzil is a known esterase inhibitor which removes the esterase component of the metabolism. Therefore, similar +/- benzil values suggests ester hydrolysis is not contributing to the IVC. However, the reasonable ΔhWB values suggest that the compound is being hydrolysed by CES-1. Therefore, **2.65** and **2.69** were submitted for analysis in a CES-1 assay to measure the actual rate of turnover by CES-1 (Table 2.15). In this assay, compounds are incubated with isolated CES-1 enzyme and the levels of ester and acid are measured at various time points. The rate of production of acid is then normalised against a known high turnover ESM containing compound, to account for variability across assay replicates.

	2.65	2.69
Specific activity ($\mu\text{M}/\text{min}/\mu\text{M}$)	0.02	0.08
Normalised activity	0.01	0.06

Table 2.15. CES-1 profiles of lead compounds **2.65** and **2.69**.

As expected, **2.65** and **2.69** exhibited slow turnover by CES-1 compared to the known inhibitor as shown by the low specific activities. The normalised values of 0.01 and 0.06 suggests that **2.65** and **2.69** are hydrolysed 100 times and 17 times slower respectively than the control compound. Therefore, it could be suggested that due to the slow rate of hydrolysis by CES-1, the esterase is only a minor contributing factor to the metabolism of the compounds which supports the similar +/- benzil values observed. However, although the specific activity of CES-1 is low, the data indicates that the compounds are indeed substrates for CES-1 thus suggesting the data agrees with the observed ΔhWB . Furthermore, the control compound is highly turned over by CES-1 and, as such, although **2.65** and **2.69** were hydrolysed at much slower rates, the rates observed were still considered acceptable. Overall, compounds **2.65** and **2.69** exhibit desired profiles with regards to potency and metabolic stability in human and cynomolgus monkey hepatocytes and, as such, were the

lead compounds from this generation. However, it was still desirable to obtain compounds with increased ΔhWB values and further investigations were undertaken.

2.3.2.2 Investigating esterase turnover in second generation compounds

Enzymes belonging to the same families tend to have highly conserved active sites, with catalytic residues in well-defined positions. This results in high specificity and, as such, the turnover of substrates is often related to the “fit” of the substrate.¹⁶⁹ This can be affected by factors such as steric bulk, chirality in close proximity to the site of reaction or simply suboptimal binding of the compound. As such, the turnover of **2.65** and **2.69** could be increased by varying the ESM group. To facilitate this, all data collected on the methylpyridyl and the 2-pyridyl series from across the team was collated and analysed. The data was converted into a ΔhWB vs. ChromLogD_{7.4} plot to allow for a simpler visualisation (Figure 2.15).

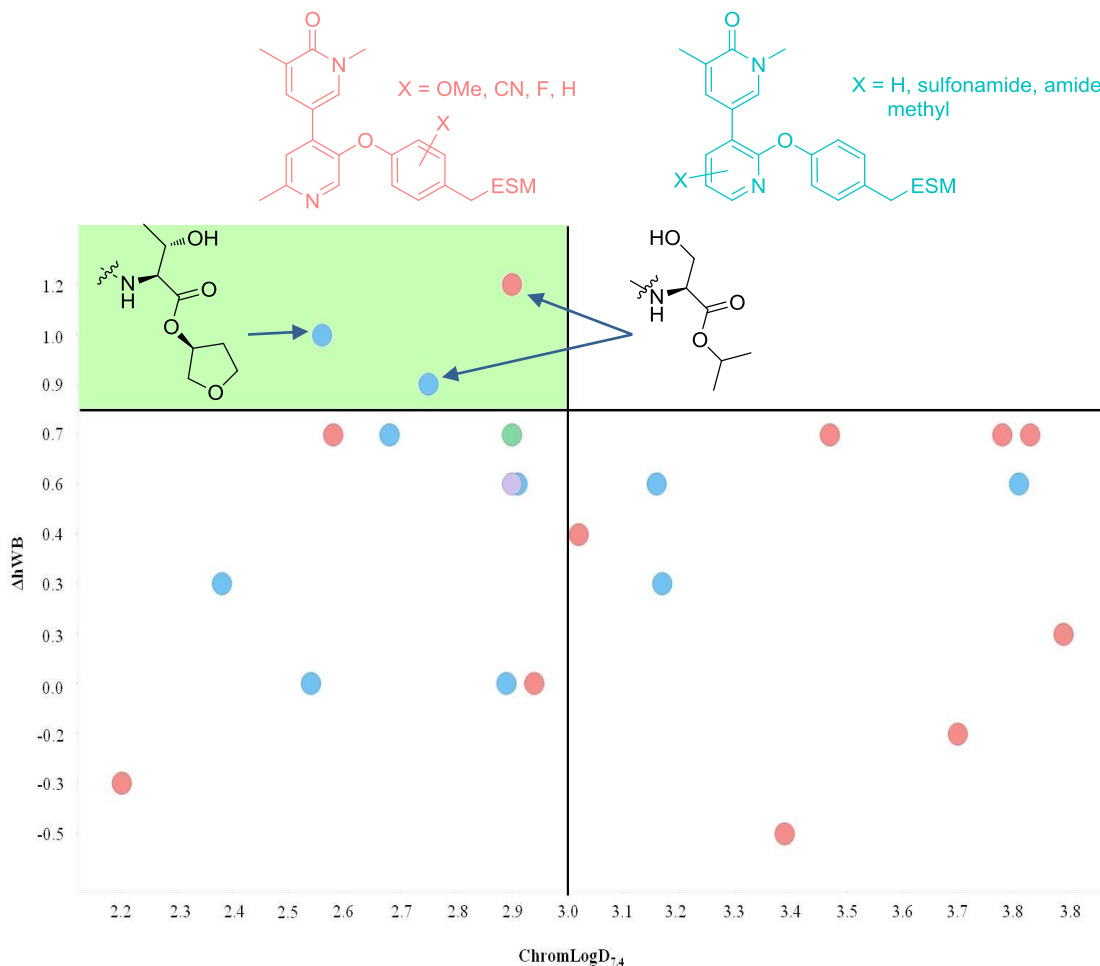
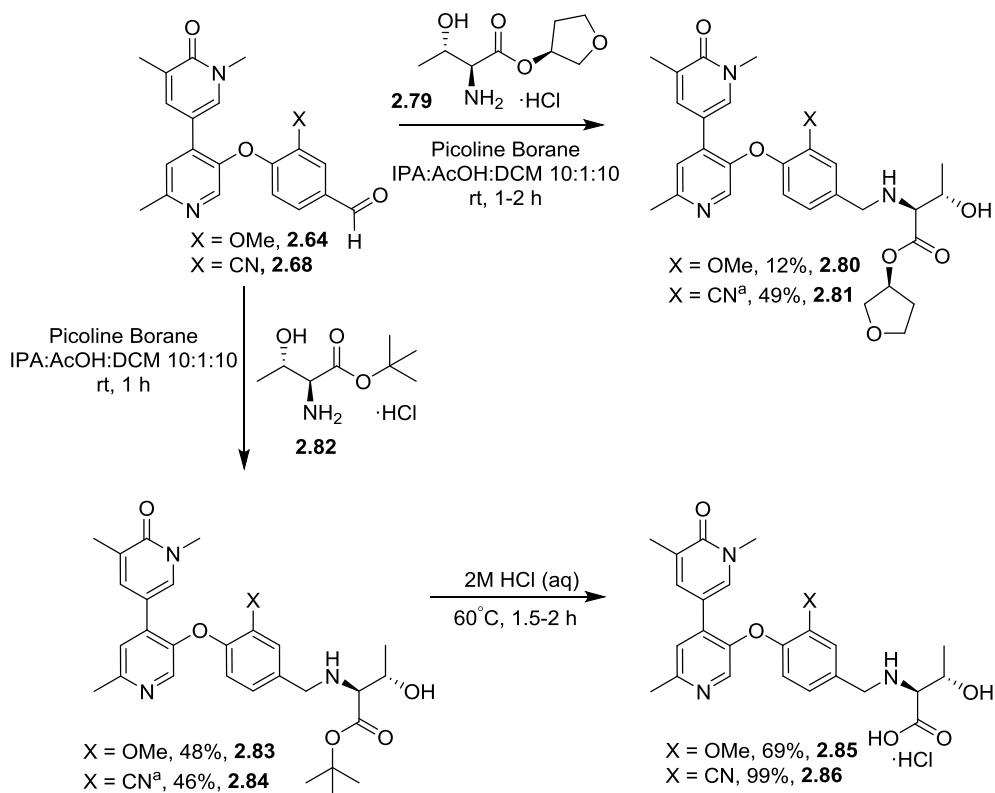
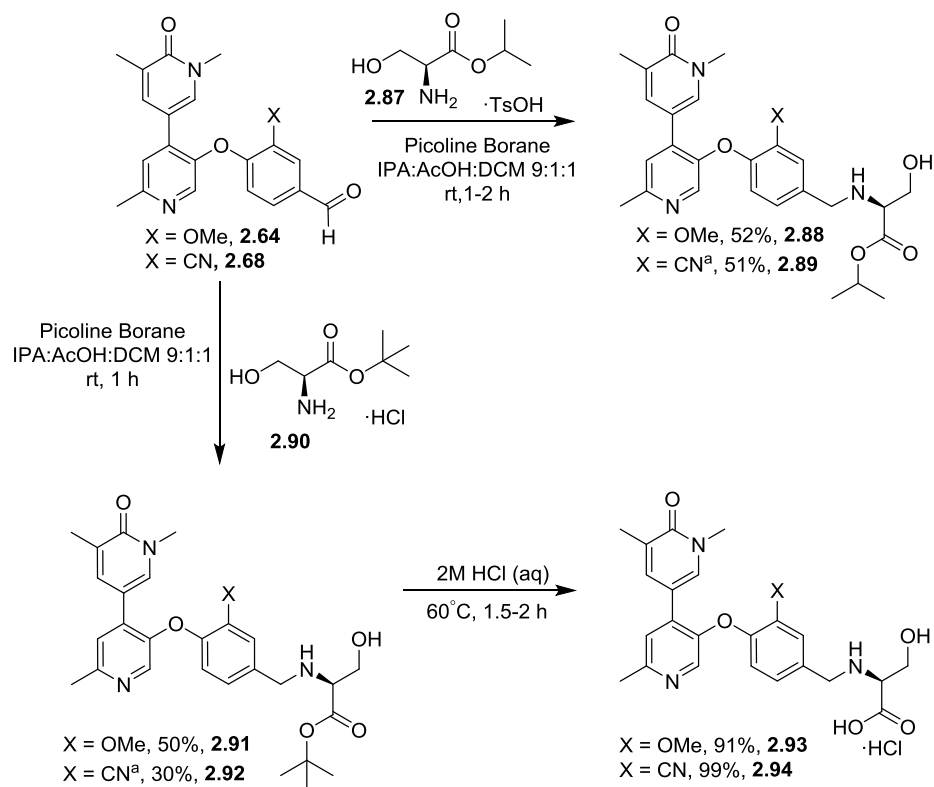


Figure 2.15. A ΔhWB vs. $ChromLogD_{7.4}$ plot of all data collected on the methyl pyridyl (pink) and the 2-pyridyl (blue) series, with the generalised core structures highlighted above. The lead compounds **2.65** (green) and **2.69** (purple) are also shown.

The visualisation indicated that a broad range of lipophilicity and turnover rates were obtained within the two series. The two boundaries $\Delta hWB > 0.8$ and $ChromLogD_{7.4} < 3$ were implemented on the plot to allow the identification of any compounds with desirable lipophilicity and a higher turnover rate than **2.65** and **2.69**. Three such compounds met these criteria and contained THF *allo*-Thr and isopropyl Ser ESM groups thus offering alternative options to the THF-Thr utilised in **2.65** and **2.69**. As such, it was hypothesised that incorporating these ESM groups into **2.65** and **2.69** would increase their turnover and ΔhWB to a desirable level. The analogues were synthesised using the synthetic route used for **2.65** and **2.69** (Scheme 2.11 and Scheme 2.12).

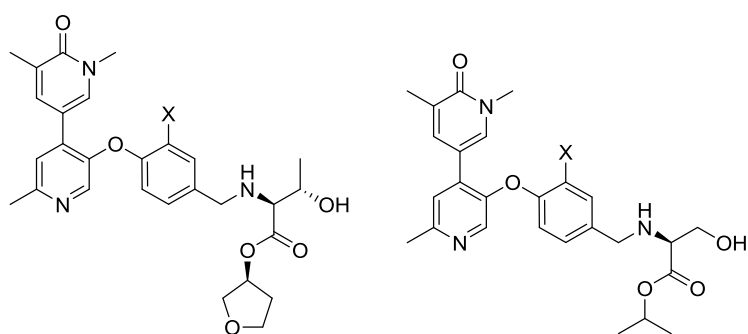


Scheme 2.11. The synthetic route employed to synthesise the *allo*-Thr analogues of **2.65** and **2.69**.^a IPA:AcOH:DCM = 6:1:6.



Scheme 2.12. Synthesis of the isopropyl Ser analogues of **2.65** and **2.69**.^a IPA:AcOH:DCM = 6:1:6

As aforementioned, **2.64** and **2.68** were poorly soluble in IPA, therefore, DCM was also added. The reductive aminations with the THF *allo*-Thr **2.79** and *tert*-butyl *allo*-Thr **2.82** to yield the THF esters, **2.80** and **2.81**, and the *tert*-butyl esters, **2.83** and **2.84**, respectively were then performed. In parallel, the reductive aminations with the isopropyl Ser ESM **2.87** and *tert*-butyl Ser ESM **2.90** to yield the isopropyl esters, **2.88** and **2.89**, and the *tert*-butyl esters, **2.91** and **2.92** were also performed. The esters were hydrolysed with an excess of aqueous 2M HCl, therefore, once the reaction was completed, the reaction mixture was concentrated *in vacuo* to give the monohydrochloride salts of the acids, **2.85**, **2.86**, **2.93** and **2.94**. These, along with the esters, were submitted for profiling (Table 2.16).



	2.80	2.81	2.88	2.89
X	OMe	CN	OMe	CN
hWB pIC ₅₀	7.9	7.7	8.5	7.6
Δ hWB	+0.8	+0.6	+1.1	+0.6
Ester BD1 pIC ₅₀	8.1	7.9	8.2	7.9
HLM IVC (+/- benzil)	1.5 / 2.0	2.5 / 2.6	1.4 / 3.0	1.6 / 1.9
Hu Heps IVC (~LBF)	1.8 (67%)	1.5 (67%)	20.5 (97%)	11.2 (94%)
Cyno Heps IVC (~LBF)	5.9 (80%)	4.2 (74%)	16.4 (92%)	4.8 (77%)
ChromlogD _{7,4}	2.8	2.8	3.1	3.2

Table 2.16. Profiles of the isopropyl Ser and THF *allo*-Thr analogues. IVC values are quoted in mL/min/g.

All of the compounds maintained their whole blood and biochemical potency relative to their Thr-THF analogues **2.65** and **2.69** (Table 2.14, *vide supra*). Pleasingly, the OMe analogue **2.88** exhibited a higher ΔhWB than its THF Thr comparator **2.65** (+1.1 vs. +0.7) and now meet the desired profile of ΔhWB ~ 1. Interestingly, although there was an increase in ΔhWB for the OMe analogue, no such effect was observed in the CN analogues **2.81** and **2.89** relative to their THF Thr analogue **2.69** (+0.6 vs. +0.7). This is reflected in the HLM IVC data in which the OMe analogues now display a difference in the +/- benzil values, indicating esterase metabolism, whilst no difference is seen for the CN analogues. Despite good microsomal stabilities, the isopropyl Ser analogues **2.88** and **2.89**, exhibited high

human hepatocyte clearance, with **2.88** also displaying poor cynomolgus monkey hepatocyte stability. In contrast, the THF *allo*-Thr analogues demonstrated human and cynomolgus monkey hepatocyte clearance below the desired 9 mL/min/g (~85% LBF). To assess the turnover in CES-1 further, the analogues were submitted to the CES-1 assay (Table 2.17).

	2.80	2.81	2.88	2.89
Specific Activity ($\mu\text{M}/\text{min}/\mu\text{M}$)	0.02	0.004	0.46	0.41
Normalised Activity	0.01	0.002	0.43	0.21

Table 2.17. CES-1 profiles of the analogues with THF *allo*-Thr and iPr Ser ESM groups.

The CES-1 data supported the ΔhWB data observed in the compounds, with similar or increased specific activities observed for **2.80** and **2.88** relative to **2.65**, whilst the specific activity for **2.81** remains low, reflecting its low ΔhWB . Despite a low ΔhWB , analogue **2.89** also displayed a high specific activity for CES-1 suggesting the isopropyl Ser is highly turned over by CES-1. However, due to its high IVC, no further work was completed on the isopropyl Ser analogues. Although the *allo*-Thr analogues displayed desirable profiles, they offered no advantage over analogues **2.65** and **2.69** which were much further down the screening cascade and, as such, it was decided to wait for data on these analogues before deciding whether to progress them further.

2.3.3 Further DMPK and selectivity profiling of lead compounds

The first generation substituted analogues **2.65** and **2.69** exhibited desirable profiles and were selected as the lead compounds for further investigation. The rat and cynomolgus monkey form the two pre-clinical species and, as such, the stability in the blood/plasma needs to be understood in order to facilitate pharmacokinetic (PK) studies. The cynomolgus monkey is used due to the high homology of the cynomolgus monkey CES-1 gene and expression profile relative to the human gene (93%).¹⁵⁷ Therefore, the stability of the compounds was further investigated by examining the human blood and cynomolgus monkey plasma stability (Table 2.18). In parallel, the compounds are profiled in a more advanced CYP3A4 time dependent inhibition (TDI) assay. The TDI assay investigates whether the molecule or a metabolite inhibits CYP3A4 over time *i.e.* irreversibly. The cytochrome P450 family of enzymes (CYPs) are the major enzymes involved in drug metabolism.¹⁵⁷ CYP3A4, the most promiscuous family member, is primarily located in the liver and intestines, where it oxidises xenobiotics.¹⁵⁸ It has been reported to metabolise over

75% of all marketed drugs and, as such, inhibition of CYP3A4 can impact the bioavailability and therapeutic index of an oral drug and lead to drug-drug interactions.¹⁵⁶

The assay is formed of three experiments; in the first there is no pre-incubation period prior to the enzyme, NADPH and known substrate being added. This measures the inhibition of CYP3A4 by the molecule of interest. In the second experiment, the molecule is pre-incubated for 30 minutes with the enzyme but without NADPH, after which NADPH and known substrate are added. Finally, in the third the molecule is pre-incubated for 30 minutes with the enzyme and NADPH, after which the known substrate and further NADPH is added. After the pre-incubation, the dose-reponse curves are generated for the metabolism of the known substrate midazolam (Figure 2.16).

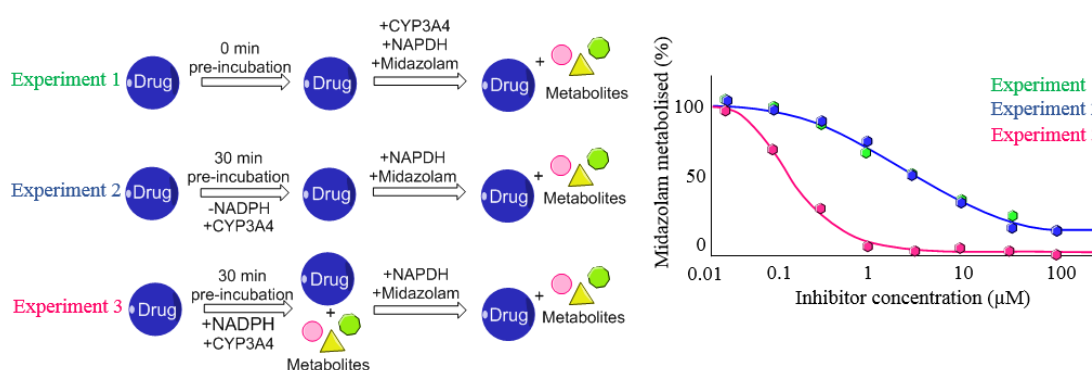
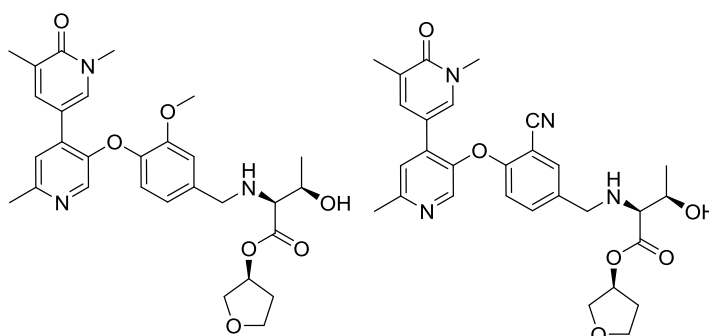


Figure 2.16. The TDI assay is formed of three experiments. In experiment 1, there is no pre-incubation period of the small molecule inhibitor prior to the addition of CYP3A4 enzymes, NADPH and the known substrate midazolam. In the second experiment, there is a 30-minute pre-incubation of the inhibitor with CYP3A4 in buffer prior to the addition of the other components. In the third experiment, the inhibitor is preincubated for 30 minutes with NADPH and the enzyme, which allows the generation of metabolites, prior to the other components being added. Once all reagents have been added, dose response curves are generated. If the parent compound is not an inhibitor of CYP3A4 itself, e.g. through covalent binding or a slow off rate, then experiments 1 and 2 should generate identical curves. If a metabolite formed in experiment 3 inhibits CYP3A4 enzymes then a shift will be observed in the dose response curve, indicating the metabolite is a more potent inhibitor of CYP3A4 enzymes than the parent compound.

NADPH is needed in order for the metabolism of the compound of interest to start and for metabolites to be formed. Therefore, in the first and second experiment there will be no metabolites present upon the addition of the enzyme and known substrate. Therefore, if the parent compound is not an inhibitor of CYP3A4 itself, e.g. through covalent binding or a slow off rate, then experiments 1 and 2 should generate identical curves. In the event that it does, the dose reponse curve for experiment 2 will be shifted to represent a higher binding

affinity. In the third experiment, metabolites will be present at the end of the 30 minute pre-incubation. If the metabolites inhibit CYP3A4, a shift in the dose-response curve would be observed, with the compound appearing more potent for the inhibition of the metabolism of the known substrate, relative to the other two curves. Shifts are quoted in log units with the lowest concentration quoted to allow comparison between various analogues.



	2.65	2.69
TDI fold shift (to lowest concentration)	4.3 (to 14 μM)	2.3 (to 42 μM)
$t_{1/2}$ human blood (min)	>745	>745
$t_{1/2}$ cyno plasma (min)	173	347

Table 2.18. Metabolic stability profiles of **2.65** and **2.69**.

Both analogues were shown to display TDI, with **2.65** being the more potent inhibitor. However, it was thought that this risk could be mitigated if the dose prediction was sufficiently low. Pleasingly, the compounds were stable in human blood with half-lives of >745 min observed. Furthermore, **2.69** exceeded the desired >240 min half-life in cynomolgus monkey plasma. Whilst the half-life of **2.65** was slightly shorter, it was still considered acceptable as ~3 hours should offer sufficient exposure of the compound.

Overall, the two analogues still exhibited attractive profiles following the stability investigations. To explore the selectivity of the compounds, they were screened against a panel of 32 closely related bromodomain-containing proteins (Figure 2.17). The assay employs an immobilised ligand (the control compound) which, when in the absence of test compounds, binds to the DNA-tagged bromodomains. When in the presence of test compounds, those that bind to the bromodomains prevent the binding of the bromodomain to the immobilised ligand. This results in a lower level of DNA-tagged bromodomain being detected on the immobilised ligand (termed percent control) relative to when test compounds are not present. Therefore, this ligand binding competition assay enables the quantitative measurement of the interactions between compounds of interest and the bromodomains.

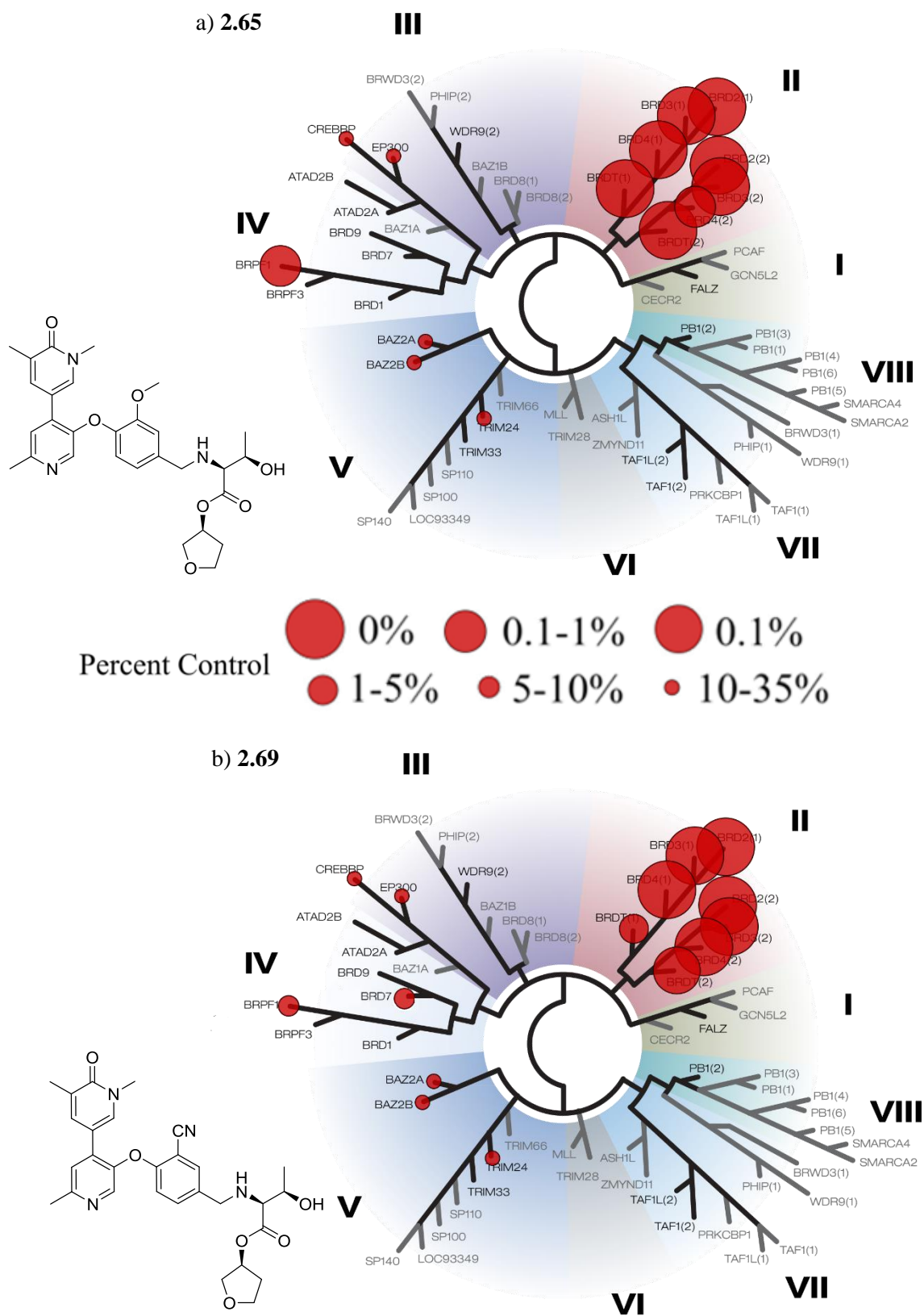


Figure 2.17. Selectivity profiles of a) **2.65** and b) **2.69** generated by screening the compounds at 10 μ M against 32 bromodomain-containing proteins. Responses of <35% control remaining are not shown.

Unsurprisingly, due to their analogous structures, **2.65** and **2.69** displayed very similar selectivity profiles. Overall, the compounds were highly selective for BET proteins, with only a small number of other proteins being inhibited. Outside of the BET family (family II in Figure 2.17), the strongest inhibition was observed for BRPF1, closely followed by BAZ2A and CREBBP. Although the profiles are relatively good, 30-fold selectivity over other bromodomain-containing proteins is desirable in order to reduce off-target toxicity. At a concentration of 10 μ M, it is not surprising that inhibition is observed at other bromodomain-containing proteins. Furthermore, it is difficult to quantify the inhibition relative to the inhibition at BET due to only a single concentration being dosed. Therefore, these assays are a valuable tool that can be used to highlight potential selectivity issues that need to be investigated further. As such, as the lead compound, **2.69** was submitted for full dose-response curves for CREBBP, BAZ2A, BRPF1 and EP300, as these all showed >80% inhibition, as well as BRD4 BD1 to contextualise the data. It was shown to exhibit >200-fold selectivity against all targets tested (refer to Appendix 2 for the data).

At this stage, the overall profiles of **2.65** and **2.69** were evaluated to determine whether there was any differentiation between the two compounds. Both analogues displayed identical biochemical and whole blood ester potencies and acid potency. Furthermore, the compounds exhibited similar lipophilicity, solubility and permeability. As well as this, there was little difference in the selectivity profiles against wider biological targets and also bromodomain-containing proteins. However, despite demonstrating similar HLM clearance, **2.69** displayed improved metabolic stability in hepatocytes across all species tested relative to **2.65**. Therefore, it was decided to progress **2.69** into a cynomolgus monkey PK study, whilst no further work was completed on **2.65**. However, to enable large quantities of material to be made, the synthetic route needed optimisation.

2.3.4 Optimisation of the synthetic route to the lead OTS compound 2.69

Across the ESM programme, the reductive amination involving the amino ester was found to be problematic, with poor yields obtained. Although these yields are deemed acceptable for a medicinal chemistry programme, late stage studies often require large quantities of product and, as such, they are not amenable to larger scale chemistry. Therefore, the reductive amination to form compound **2.69** was investigated further in an attempt to provide an insight into the issues and to improve the yields. The last decade has seen the emergence of imine reductases as a valuable new set of biocatalysts for the asymmetric synthesis of amines. Therefore, the reductive amination was first investigated using imine reductases.

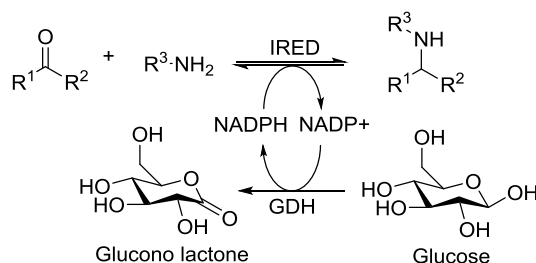
2.3.4.1 Imine reductase screen to identify an enzyme to perform a reductive amination

Chiral amines are key building blocks, with ~40% of all pharmaceuticals containing at least one amine moiety.¹⁷¹ Reductive aminations are the most common method of incorporating secondary and tertiary amines into drug-like molecules. However, these reactions often encounter different challenges, such as limited stability of the imine intermediate due to the reaction equilibrium disfavours imine formation unless water is removed. Furthermore, reducing reagents with high chemoselectivity are required due to the reducible nature of the carbonyl. On occasions, these factors can be overcome by employing organometallic catalysts such as ruthenium and iridium complexes.¹⁷² Biocatalysis is being increasingly applied to synthetic routes of APIs, due to their improved 'greenness' relative to chemical methods and scalability. Enzymes remove the need for toxic or heavy metal catalysts and are often extremely stereo- and regioselective whilst performing under mild, aqueous conditions.¹⁷³ The synthesis of chiral amines through transaminase and amine dehydrogenase biocatalysts are widely known. However, more recently, imine reductases (IREDs) have emerged as a valuable new set of biocatalysts for this transformation.¹⁷⁴

2.3.4.1.1 Imine reductases as chemoselective enzymatic reductive amination reagents

IREDs are NADPH-dependent oxidoreductases that catalyse the asymmetric reduction of prochiral imines to the corresponding amines. Müller *et al.* were the first to demonstrate that IREDs could be applied directly to reductive aminations, with the observation that they could reduce small quantities of imine formed by the condensation of a ketone and an amine in an aqueous reaction mixture.¹⁷⁵ This was possible due to the excellent chemoselectivity exhibited by the IREDs, which selectively reduce the imine but not the excess ketone substrate. More recently, Aleku *et al.* reported the enzymatic reductive amination of 1:1 stoichiometry of an amine and carbonyl when a homologue of the *Aspergillus oryzae* (AspRedAm) was employed.¹⁷⁶ Although this was a significant improvement from the small quantities observed by Müller *et al.*, the approach utilised purified protein, obtained *via* a costly and complex purification. Therefore, although higher activities were observed, and background reactions were minimised, the use of purified proteins was not desirable for substrate screening. A recent development saw the use of lyophilised whole cells successfully perform the reductive amination with identical stoichiometries, albeit with a limited substrate scope, thus increasing their applicability towards industrial application.¹⁷⁷

The reduction of imines is a physiological reaction in a number of biosynthetic pathways. As the imine intermediates are structurally distinct between the various pathways, a large number of functionally different IREDs, often with low sequence homology, exist.¹⁷⁴ With such a wide substrate scope, it was deemed feasible that an IRED could facilitate the reductive amination to form **2.69** (Scheme 2.13).

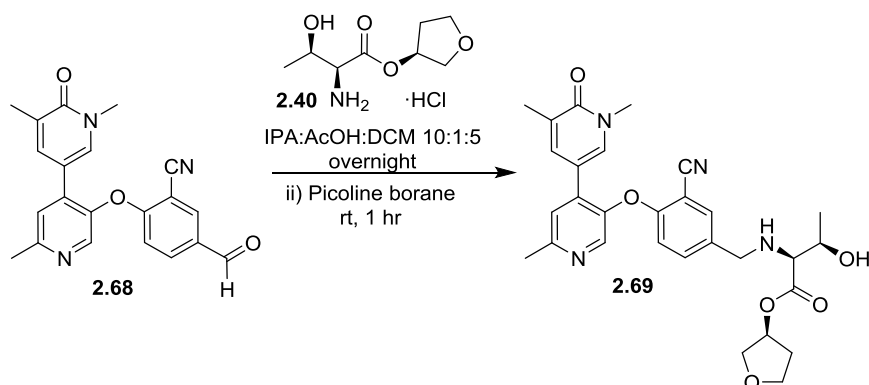


Scheme 2.13. General mechanism of the IRED catalysed reductive amination.

A panel of 85 enzymes, including AspRedAm, based on IRED sequences known in the literature or IRED database and novel putative IREDs with homology to known IREDs was developed by colleagues at GSK. The proteins are used as cell lysates in a 96-well plate format, which simplifies the process when screening new substrates. The IRED panel was employed to investigate its applicability to the reductive amination towards **2.69**. The screen was completed twice with two different enzyme: substrate loadings; 1:1 and 4:1. Unfortunately, neither screen produced any hits but rather showed complete conversion to the reduced aldehyde in all wells. This is analogous to similar findings with picoline borane conditions in Scheme 2.9 (*vide supra*) and thus, further exemplifies the difficult nature of the imine formation between amine **2.40** and aldehyde **2.68**. Therefore, additional investigations into the reductive amination employing chemical methods was necessary.

2.3.4.2 Reductive amination optimisation through chemical methods

As the IRED screen was unsuccessful, optimisation of the existing reductive amination conditions was needed (Table 2.19).

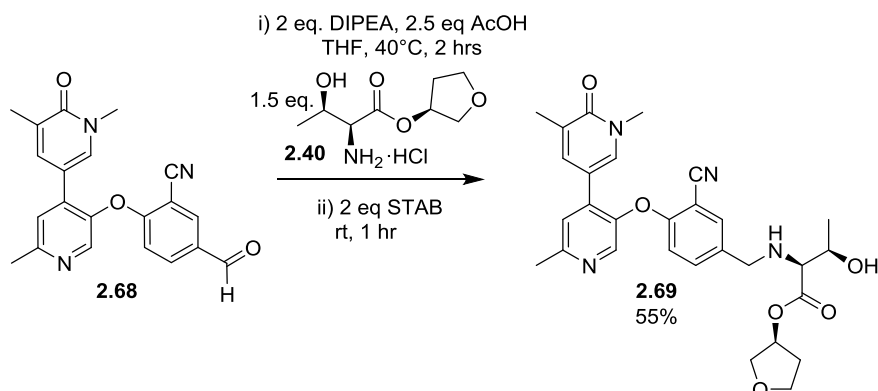


Entry	Amine 2.40 eq.	Isolated yield (%) 2.69
1	2	N/A
2	1.1	40
3*	1.1	7
4	2.5	51

Table 2.19. Reaction conditions employed during the investigation of the reductive amination to form compound **2.69**. * Contains molecular sieves.

Typically, reductive aminations employing 2-picoline borane are one pot syntheses or have short imine formation periods. As such, it is possible that full conversion to the imine is not being achieved prior to the introduction of the reducing agent. This is supported by the moderate conversion to the reduced aldehyde observed in these reactions. Therefore, it was hypothesised that increasing the quantity of imine formation would result in fewer side products, in particular the reduced aldehyde, and an improved yield. As such, the reaction mixtures in Table 2.19 were left to stir overnight, prior to the addition of 2-picoline borane, to promote imine formation. This was first attempted using the same conditions employed in Scheme 2.9 which afforded the product in a 32% yield (*vide supra*), but with a larger volume of DCM to aid solubilisation of the amino ester (Table 2.19, Entry 1). As expected, LCMS analysis suggested a higher conversion to the imine, however, the product was not isolated after reduction to the amine due to difficulties during the work up. Therefore, workups were avoided for the rest of the trial reactions. As this reaction resulted in an improved reaction profile compared to the original conditions, as observed by LCMS and TLC, the reaction was repeated utilising only 1.1 equivalents of **2.40** (Table 2.19, Entry 2). The amino ester is considered the most valuable starting material in this reaction and, as such, reducing the

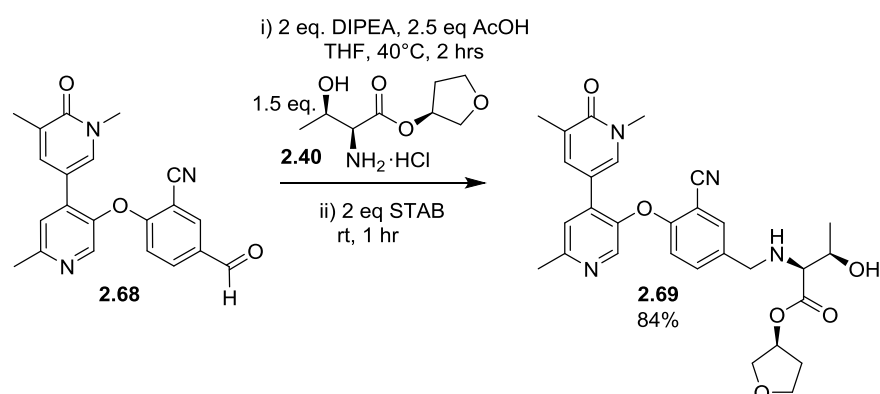
quantity needed is desirable. Following reduction, the reaction mixture was quenched and purified by flash column chromatography without an aqueous work up. A higher isolated yield of 40% was obtained relative to the original conditions. However, although not isolated, a moderate conversion to the reduced aldehyde was still observed by LCMS. This suggests that the conversion to the imine could be further improved. Imine formation is a reversible reaction, with water playing a key role in the imine hydrolysis. Therefore, it was hypothesised that removing the water, through the addition of molecular sieves, would prevent the hydrolysis and shift the equilibrium to the product (Table 2.19, Entry 3). However, this resulted in complete conversion to an unknown side product which was not able to be isolated despite attempts to do so. As water removal was not a viable route for driving forward the reaction, it was thought that increasing the equivalents of amino ester could offer another opportunity to do this (Table 2.19, Entry 4). Indeed, a higher isolated yield of 51% of **2.69** was obtained. Although this is improved relative to the conditions outlined in Scheme 2.9, it was desirable to increase it further. As such, alternative reaction conditions, suggested by colleagues, were employed (Scheme 2.14).



Scheme 2.14. Alternative reaction conditions for the reductive amination with purification by normal phase chromatography.

The reaction conditions outlined in Scheme 2.14 were discovered through a large screen of reductive amination conditions undertaken for a synthetic route optimisation towards a candidate molecule elsewhere within GSK. Imine formation, which is monitored by NMR analysis, is promoted by heating. Unlike the previous reactions, these conditions resulted in full conversion to the imine. Furthermore, upon the addition of sodium triacetoxyborohydride (STAB) only a low level of conversion to the reduced aldehyde was observed (~4% by NMR and LCMS analysis in comparison to ~30% with the original conditions). However, following purification by normal phase flash column chromatography,

only a 55% isolated yield was obtained. As complete imine formation, and thereafter full conversion to the product was observed, this suggests that material is being lost during purification. To test this theory, the reaction was repeated but instead of flash column chromatography, the reaction mixture was purified directly by MDAP using a basic modifier (Scheme 2.15). This would give an indication as to whether the material is being retained on the silica column. Pleasingly, through this method an isolated yield of 84% was obtained. Therefore, the moderate isolated yield in Scheme 2.14, obtained following normal phase column chromatography, can be attributed to issues in purification. This potentially could be overcome by a reverse phase column chromatography purification using a basic modifier, mimicking the MDAP conditions (Scheme 2.15).

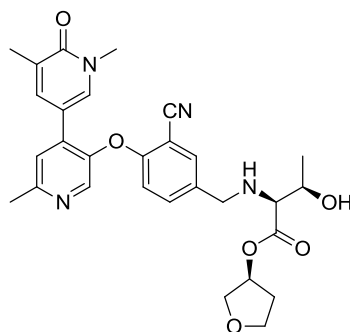


Scheme 2.15. Alternative reaction conditions for the reductive amination with purification by reverse phase chromatography.

Overall, the reductive amination step has been optimised from 32% to 84% using conditions outlined in Scheme 2.15. Heating the imine with increased equivalents of base and acid promoted complete conversion to the imine. This, along with employing STAB as a reducing agent rather than 2-picoline borane, resulted in a cleaner reaction profile with only minor conversion to the reduced aldehyde. Finally, purification by MDAP (or reverse phase chromatography) is preferred to normal phase chromatography, which results in the loss of material. This optimisation has resulted in an isolated yield of 84% compared to the starting point of 32%.

2.3.5 *In vivo* cynomolgus monkey PK studies of the lead OTS molecule 2.69

Following the route optimisation, the lead compound **2.69** was progressed into a cynomolgus monkey IV/PO crossover PK study. The analogue was dosed at 1 mg/kg in the IV portion and 3 mg/kg in the oral portion (Table 2.20).



		2.69	Acid
IV 1 mg/kg	CL _{Total} (mL/min/kg)	80.7	-
	V _{SS} (L/kg)	1.98	-
	t _{1/2} (h)	0.3	1*
	AUC _∞	209	54.5 [#]
	Acid: ester ratio	-	0.3:1
PO 3 mg/kg	C _{max} (ng/mL)	14.9	13.0
	Bioavailability (%)	1.2	-
	t _{1/2} (h)	0.3 [~]	-
	AUC _∞	8.8	8.2 [#]
	Acid: ester ratio	-	0.9:1

Table 2.20. Cynomolgus monkey *in vivo* PK data for **2.69** based on n=3. *n=1, [~]n=2, [#]AUC_{0-t}

The pharmacokinetic parameters for **2.69**, and its acid metabolite, were both monitored following its administration. The compound exhibited a high clearance (>100% LBF) and a moderate volume of distribution. Unfortunately, the high clearance resulted in a short half-life with both of these factors likely contributing to the poor bioavailability (1%), along with poor absorption as suggested by the low area under the curve (AUC) values demonstrated by the ester and acid.

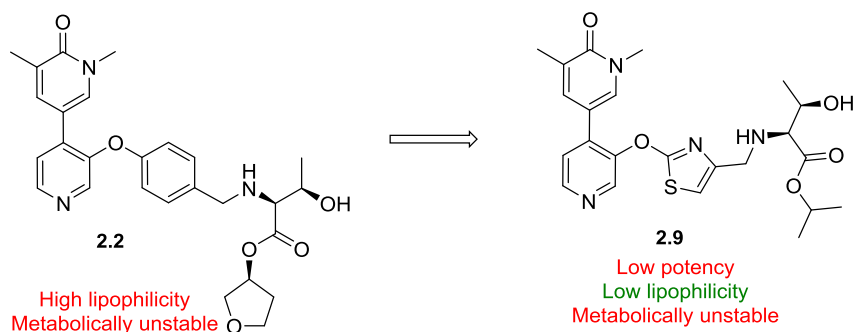
Although the compound did not meet the desired *in vivo* cynomolgus monkey profile as exhibited by analogue **1.6** (Table 1.5, *vide supra*), the molecule demonstrates high cellular activity, metabolic stability and physicochemical properties thus achieving the aims outlined at the beginning of the series. Furthermore, the *in vivo* cynomolgus monkey PK profile

revealed a key outcome that the target IVC profile originally outlined within the desired target profile for this series was too high to produce a molecule with desirable *in vivo* PK.

2.4 Summary of the development of the OTS series for the use as BET inhibitors

The work outlined in this chapter began with the identification of the starting point molecule **2.2**. The compound contains the same pyridone warhead contained within the candidate **1.6**, however, whilst **1.6** incorporates the ESM through the ZA channel vector, molecule **2.2** was the first to explore the extension of the ESM over the WPF shelf. The result was a potent compound with a desirable ΔhWB , but it unfortunately suffered with metabolic instability.

Crystal structures of BRD4 BD1 show a non-mobile methionine residue at the back of the WPF shelf which results in a hump in the surface. This was predicted to cause a restricted conformation of the CH₂NH linker of the ESM in order for it to lift over the hump, thus potentially increasing the loss of entropy upon binding. Therefore, the first approach taken was to investigate the impact of altering the bond angles between the ESM and the ether linkage to the core of the molecule. It was hypothesised that a smaller bond angle would move the ESM away from the methionine residue, thus reducing the loss of entropy upon binding and increasing potency. This was investigated through the exploration of 5-membered heteroaromatics as the WPF shelf group, which had the added benefit of the heteroatoms reducing lipophilicity and blocking possible metabolic hotspots. Therefore, these alternative WPF shelf groups also had the potential to increase metabolic stability. A statistical analysis of bond angle vectors for five-membered rings based on data derived from the Cambridge Structural Database was used to select five-membered rings with angles increasing in 10° increments from 120° to 180°. Due to synthetic tractability, only the 130° and 160° bond angles were accessed. However, the data gathered was sufficient to suggest that the 180° bond angle is the optimal, with both molecules displaying poor biochemical and cellular activity and no improvement in IVC (Scheme 2.16).



Scheme 2.16. Replacement of the benzene WPF shelf with 5-membered heteroaromatics were investigated with the aim of improving potency, by moving the ESM linker away from the non-mobile methionine residue and increasing metabolic stability by reducing lipophilicity and blocking potential metabolic hotspots. The synthesised molecules exhibited reduced potency and were shown to be metabolically unstable.

The second approach investigated the substitution of the WPF shelf group with the aim of improving potency and increasing metabolic stability. It was hypothesised that the benzene WPF shelf group of **2.2** was interacting with the tryptophan of the WPF shelf through parallel-displaced π - π stacking. A *meta*- σ *meta*- π Craig plot was used to identify substituents to modulate the electronics of the ring, as well as reduce lipophilicity, and methoxy, methyl and cyano moieties were selected to be investigated as substituents for the benzene ring. Initial data indicated the 2-OMe and 2-CN analogues, **2.31** and **2.33** respectively, showed improved metabolic stability and similar potencies relative to **2.2** (Table 2.12). However, as **2.31** and **2.33** display similar biochemical and cellular activities, showing that modulating the ring electronics does not impact potency, it suggests the molecules do not interact with the tryptophan of the WPF shelf in a parallel-displaced π - π hydrogen bond.

Although the analogues displayed a lower HLM IVC, a further reduction was required. Unhindered pyridines are known to be substrates for cytochrome P450 enzymes, and therefore the sterically encumbered methylpyridine, **2.65** and **2.69**, and 2-pyridyl, **2.76**, analogues were investigated (Scheme 2.17). Indeed, the HLM and hepatocyte IVC were reduced to a desirable level for all three analogues. Alternative ESM groups were investigated with the aim of increasing the Δ hWB of these three analogues could be increased, but they exhibited similar profiles and, as such, compound **2.69** was selected as the lead molecule for the series and was the only molecule of the series to be progressed into an *in vivo* cynomolgus monkey PK study. Overall, a molecule with metabolic instability (compound **2.2**) has been developed into a molecule with low lipophilicity, low HLM and hepatocyte IVC and a desirable profile in late stage DMPK profiling. Furthermore, analogue

Chapter 3

Development of “benzazepinone” inhibitors of the BET family

3.0 Development of “benzazepinone” inhibitors of the BET family

The continuing search for a backup molecule to analogue **1.6** has seen several series be developed with a pyridone acetyllysine mimetic (the warhead featured in **1.6**). As this clinical candidate is yet to be profiled in humans, little is known about how this acetylated lysine mimetic will compare *in vivo* to well established mimetics, such as the benzodiazepine motif of I-BET762 or the dimethylisoxazole of GSK2820151 (Table 1.1, section 1.4.2, *vide supra*). Therefore, a structurally differentiated scaffold was desirable as it would offer an alternative scaffold in the event that toxicity due to the structure of **1.6**, or the pyridone warhead, rather than mechanism is observed.

Elsewhere within GSK, a reminding of a HTS screen in the search for a pan-BET hit unveiled the ligand efficient benzazepinone (BZP) motif. Extensive SAR was gathered on this scaffold, resulting in the identification of the lead molecule **3.1** (Figure 3.1).

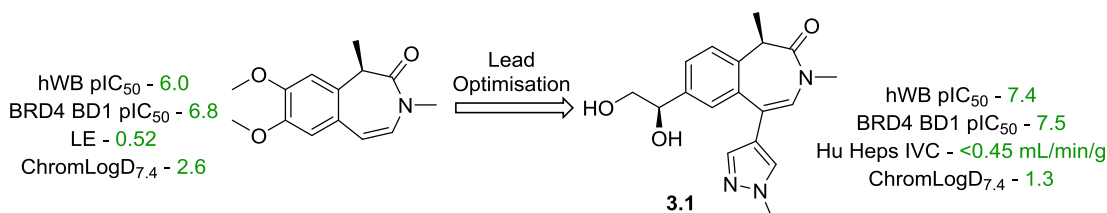


Figure 3.1. The BZP scaffold was discovered to be a hit for the BET family through a HTS reminding. It exhibited high biochemical activity and a high ligand efficiency (LE). Lead optimisation on the BZP scaffold resulted in the lead molecule **3.1**.

The lead compound **3.1** exhibits a desirable biochemical and cellular potency and was shown to be metabolically stable in *in vitro* assays and *in vivo* dog PK studies (data not shown). Therefore, it was decided to explore the BZP motif as an alternative scaffold for the ESM-containing molecules due to its favourable profile within the small molecule pan-BET series.

The scaffold has two diversity points, one of which can be used to access the WPF shelf and the ZA channel (Figure 3.2a). BZP molecules have a similar binding mode to the OTS compounds, with the azepinone acting as the acetyllysine mimetic (Figure 3.2b). The crystal structure shows that the ESM can be directed through the ZA channel or over the shelf.

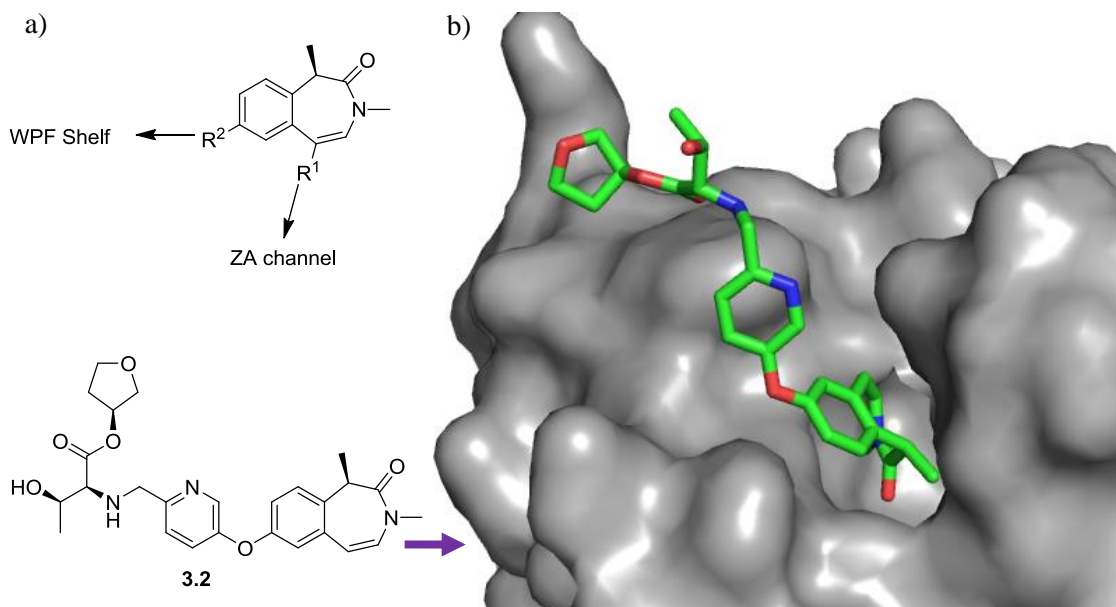


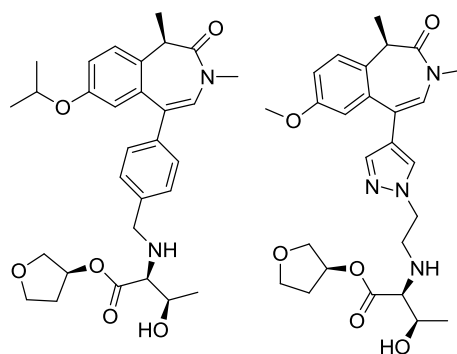
Figure 3.2. a) The BZP scaffold has two diversity points: R, which is a vector for the WPF shelf, and R¹ which can be used to access the ZA channel. The ESM can be directed through the ZA channel or over the shelf. b) A crystal structure of a BZP analogue **3.2** in complex with BRD2 BD2 showing the azepinone binding as the acetyllysine mimetic with the ESM directed over the WPF shelf.

This piece of work focusses on the optimisation of the lead molecule **3.3** to investigate whether the ESM can be directed through the ZA channel to achieve potent, selective molecules with good physicochemical properties and a desirable IVC profile. The overall aim of the series is to identify a compound with a similar or improved profile relative to the clinical candidate **1.6** (Table 1.5, *vide supra*), which would facilitate its selection as a lead molecule.

Compound **3.3**, the first compound to be synthesised as part of these investigations on the BZP ZA subseries, sees the ESM appended to a phenyl ring due to the known preference for aromatic or sp²-hybridised moieties to occupy the ZA channel. This resulted in a molecule with excellent biochemical and whole blood potency, but it suffered from high lipophilicity (Table 3.1). As increasing lipophilicity tends to lead to increased metabolism, due to lipophilic binding to metabolism enzymes, the compound could not be progressed into microsomal IVC studies. It was shown elsewhere in the group that exchanging the appended six-membered ring for a pyrazole and the isopropyl group for a methyl group, as in analogue **3.4**, decreased the lipophilicity but desirable metabolic stability was still not achieved.

Although the AP OTS compound **2.69** was not progressable due to the poor oral bioavailability observed in the *in vivo* cynomolgus monkey study (Table 2.20, *vide supra*), a key learning was that a cynomolgus monkey hepatocyte clearance of 4.6 mL/min/g is likely

too high for a desirable *in vivo* PK profile. As such, the desirable profile for the BZP series was amended to address this resulting in a new desirable cynomolgus monkey hepatocyte clearance of <1.5 mL/min/g (Table 3.1). Similarly to the AP OTS series, the biologically hydrolysable esters were submitted along with their biologically non-hydrolysable *tert*-butyl analogues so that the difference in whole blood (hWB) could be determined. As the *tert*-butyl analogues cannot be hydrolysed by CES-1 (Table 1.4, Section 1.62, *vide supra*), this difference can be attributed to the hydrolysis of the ESM and subsequent retention of the acid within the cells i.e. the ESM effect. As the *tert*-butyl analogues are only synthesised to generate the Δ hWB, their biological profiles will not be displayed. Furthermore, to assess the contribution of ester hydrolysis to the metabolism of the compounds, the analogues were tested in human liver microsomes (HLM) both in the absence and presence of benzil. As benzil is a known pan-esterase inhibitor, this allowed the underlying P450 metabolism to be measured.



	Desired Profile	3.3	3.4
hWB pIC ₅₀	> 7.5	8.1	7.5
Δ hWB	~ 1.0	+ 1.3	+0.9
Ester BD1 pIC ₅₀	> 7.0	7.9	7.0
HLM IVC (+/- benzil)	< 1.0 / < 1.5	- / -	3.4 / 3.5
Human/Cyno Heps IVC	< 1.5 / < 1.5	-	10.6 / 15.4
ChromLogD _{7.4}	< 3.5	5.8	3.2

Table 3.1. The desired profile of a BZP ESM compound and the profile of the starting points, compounds **3.3** and **3.4**, for this project. IVC values are quoted in mL/min/g.

3.1 Hypotheses to be tested within the BZP small molecule series

3.1.1 Incorporating polar moieties as the WPF shelf group reduces lipophilicity and IVC

Reducing the lipophilicity is a widely-used tactic to improve metabolic stability. This is thought to be due to reducing lipophilicity-driven binding to metabolic enzymes such as cytochrome P450 enzymes.¹⁷⁸ It was initially hypothesised that further reducing the lipophilicity of **3.4** would improve the HLM and hepatocyte clearance. Furthermore, the methoxy substituent may be a metabolic liability as this functionality is known to be prone to phase I metabolism. Therefore, the first approach to improving the IVC profile was to reduce the lipophilicity of the compounds by incorporating polar moieties in the vector that accesses the WPF shelf, which also added the benefit of removing the methoxy group (Figure 3.3). The WPF shelf is a lipophilic ledge and, as such, hydrophobic moieties are preferred. However, the adjacent cleft is solvent exposed and hydrogen bond acceptors and donors can also be tolerated. This means that the WPF shelf group can be used to tune the physicochemical properties of analogue **3.4**. Therefore, shelf groups incorporating both hydrogen bond acceptors/donors and hydrophobic elements could be used to maintain potency whilst reducing the lipophilicity and IVC.

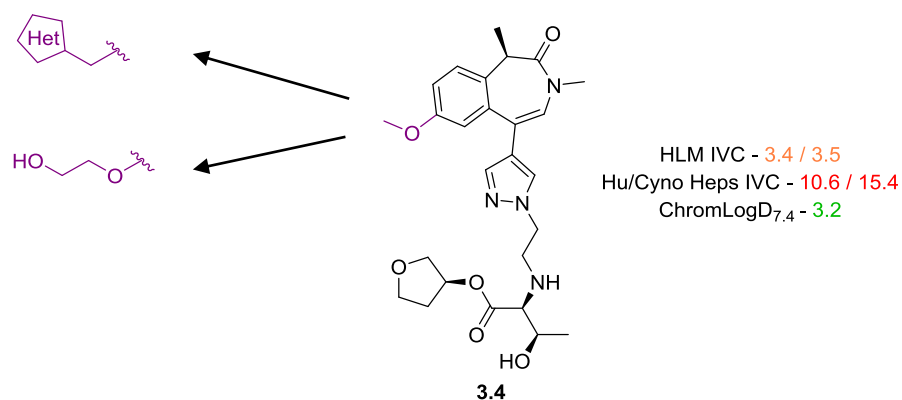


Figure 3.3. Compound **3.4** exhibits metabolic instability. Methoxy groups are known to be prone to phase I metabolism. Replacement of the methoxy moiety with polar functionalities such as aliphatic heterocycles or ether chains could reduce the lipophilicity, whilst removing a metabolically labile group, and thus increase the metabolic stability. IVC values are quoted in mL/min/g.

3.1.2 Incorporating alternative ring systems as the ZA channel group reduces lipophilicity and IVC

The ZA channel is a narrow, hydrophobic region which joins the Z and A helices. As such, moieties containing sp^2 hybridisation are preferred in substituents that act as the ZA channel group. Therefore, alternative ring systems were focussed on aromatic groups as opposed to saturated rings. Pyrazoles are activated to electrophilic addition in the C2/C5 positions and, as such, the C5 position of **3.4** is a potential metabolic hotspot. Benzene derivatives such as **3.3** are less susceptible to electrophilic addition and therefore, six-membered aryl rings could offer an alternative to the pyrazole. However, as observed in **3.3**, the benzene ring resulted in high lipophilicity as indicated by the high $\text{ChromLogD}_{7.4}$ of 5.8. This could be overcome by incorporating a 6-membered aromatic heterocycle rather than the benzene ring (Figure 3.4). As well as this, unsubstituted positions of aryl rings are known to be prone to phase I metabolism. Therefore, heteroatoms within the ring could act to block potential metabolic hotspots. Furthermore, the ring would be rendered less nucleophilic due to reduced electron density, thus potentially further deactivating it to phase I metabolic pathways.

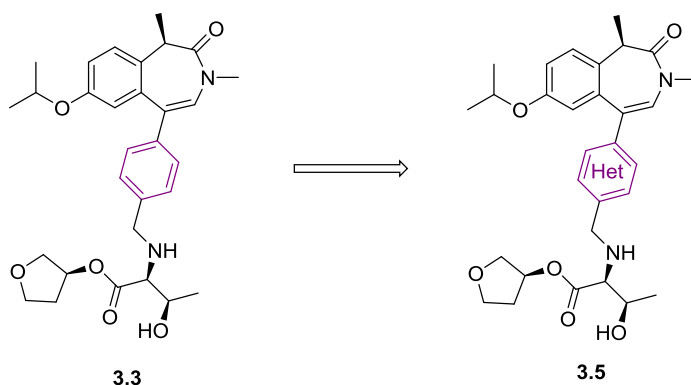


Figure 3.4. Replacing the benzene ring with 6-membered heteroaromatic rings, to give structures such as **3.5**, offers the potential to reduce lipophilicity and IVC through blocking potential metabolic hotspots.

3.2 Aims for the “BZP ZA” small molecule series

At the point of starting this work, only small methoxy and isopropyl groups had been explored with the pyrazole as the ZA channel group. Therefore, in order to interact with the WPF shelf whilst modulating physicochemical properties, shelf groups incorporating both hydrogen bond acceptors/donors and hydrophobic elements were to be investigated (Figure

3.5). Furthermore, the introduction of the extra polarity could offer the opportunity to reduce the IVC.

In addition, aside from the pyrazole ring, only the benzene ring had been explored as the ZA channel group at the onset of this work. This yielded a compound with high potency, but it suffered with high lipophilicity, as exemplified by compound **3.3** (Table 3.1, *vide supra*). The narrow nature of the ZA channel means sp² hybridisation of the moiety acting as the ZA channel group is preferred. Therefore, alternative 6-membered ring systems were to be investigated as ZA channel groups.

The specific aims of the project were:

i) Synthesise a series of analogues of compound **3.4** (Table 3.1, *vide supra*) with a range of alkyl-based moieties containing hydrogen bond acceptors and donors as WPF shelf groups. This would enable exploration of how introducing polar groups on the lipophilic WPF shelf impacts the potency of BET inhibition whilst potentially reducing the IVC and lipophilicity. Examples of such polar groups include carbamates and alcohol-containing ethers such as analogue **3.6** and **3.7** (Figure 3.5).

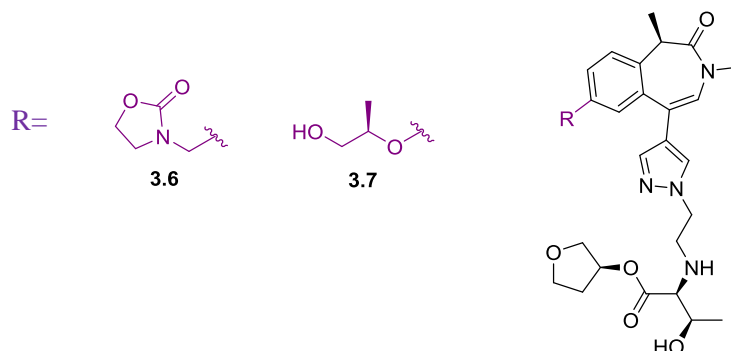


Figure 3.5. Examples of carbamate and ethereal substituents such as in analogues **3.6** and **3.7** that were to be investigated as the WPF shelf group (purple).

ii) Synthesise analogues of **3.3** with a pyridine or diazine ZA channel group (such as in **3.8** and **3.9**), with the aim of reducing lipophilicity, as well as IVC through blocking a potential metabolic hotspot, whilst maintaining potency (Figure 3.6).

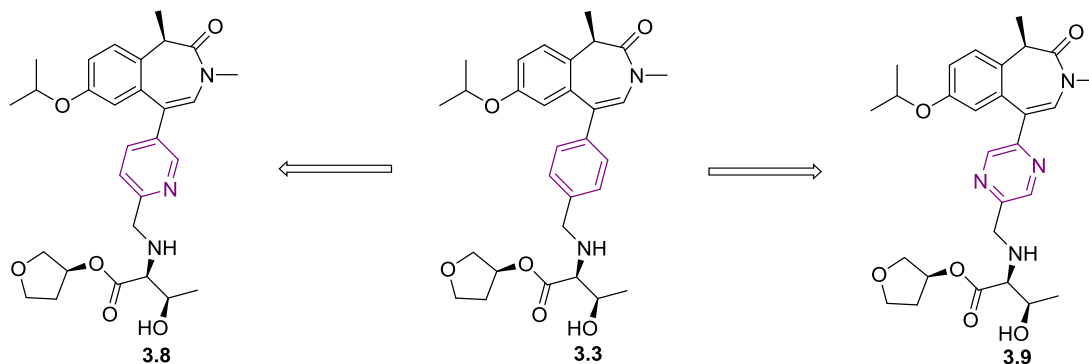


Figure 3.6. Examples of the replacement of the benzene ZA channel group (purple) in **3.3** with a pyridine or diazine, analogues **3.8** and **3.9**.

iii) Combine knowledge from data generated from aims i) and ii) with structural changes, through rational design, to achieve the desired target profile outlined in Table 3.1.

3.3 Results and discussion

3.3.1 Investigating polar moieties as the WPF shelf group

At the point of starting this piece of work, the BZP motif had been extensively explored in a pan-BET programme within GSK, meaning existing SAR surrounding the shelf group was available. As the first approach focussed on single point changes to the shelf group, the molecules would be consistently appended to the pyrazole as in **3.4**. Furthermore, X-ray crystallography evidence suggests that due to the attachment point of the ESM, it is unlikely to be involved in binding and, therefore, should not affect the potency (crystal structure not shown). As such, SAR gathered on the pan-BET molecules, in which the ZA group was an *N*-methyl pyrazole, was thought to be transferable to the ESM-BET analogues (Figure 3.7). This was supported by the initial lead **3.4** which exhibited high potency and low lipophilicity thus showing compounds with desirable physicochemical properties could be developed within this series.

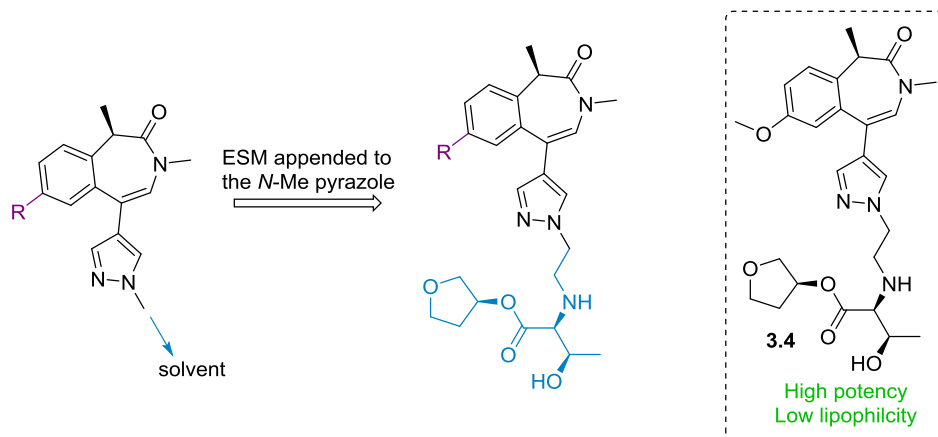


Figure 3.7. A pan-BET BZP series was explored elsewhere within GSK, of which a large number of compounds incorporated an *N*-methyl pyrazole as the ZA channel group. It was thought that when the ESM (blue) is appended to the *N*-methyl pyrazole, SAR surrounding the WPF shelf group (purple) from the pan-BET series could be translatable to the BZP ZA series to form compounds such as **3.4**.

Consequently, a plot of the human hepatocyte IVC vs. human whole blood potency was generated, based on all of the pan-BET analogues (Figure 3.8). Highlighted on the plot are compounds which incorporated the *N*-methyl pyrazole in the ZA channel. As a similar whole blood potency and $\text{ChromLogD}_{7.4}$ of **3.4** and reduced hepatocyte clearance was desired, the plot was coloured by $\text{ChromLogD}_{7.4}$ and boundaries of hWB $\text{pIC}_{50} = 7$ and IVC = 1.0 mL/min/g were installed. This allowed the identification of compounds which exhibited high potency and low IVC whilst being within the desired lipophilicity range. These shelf groups were profiled *in silico*, with the molecules that had parameters within the desired range, and therefore selected for synthesis, shown in Table 3.2.

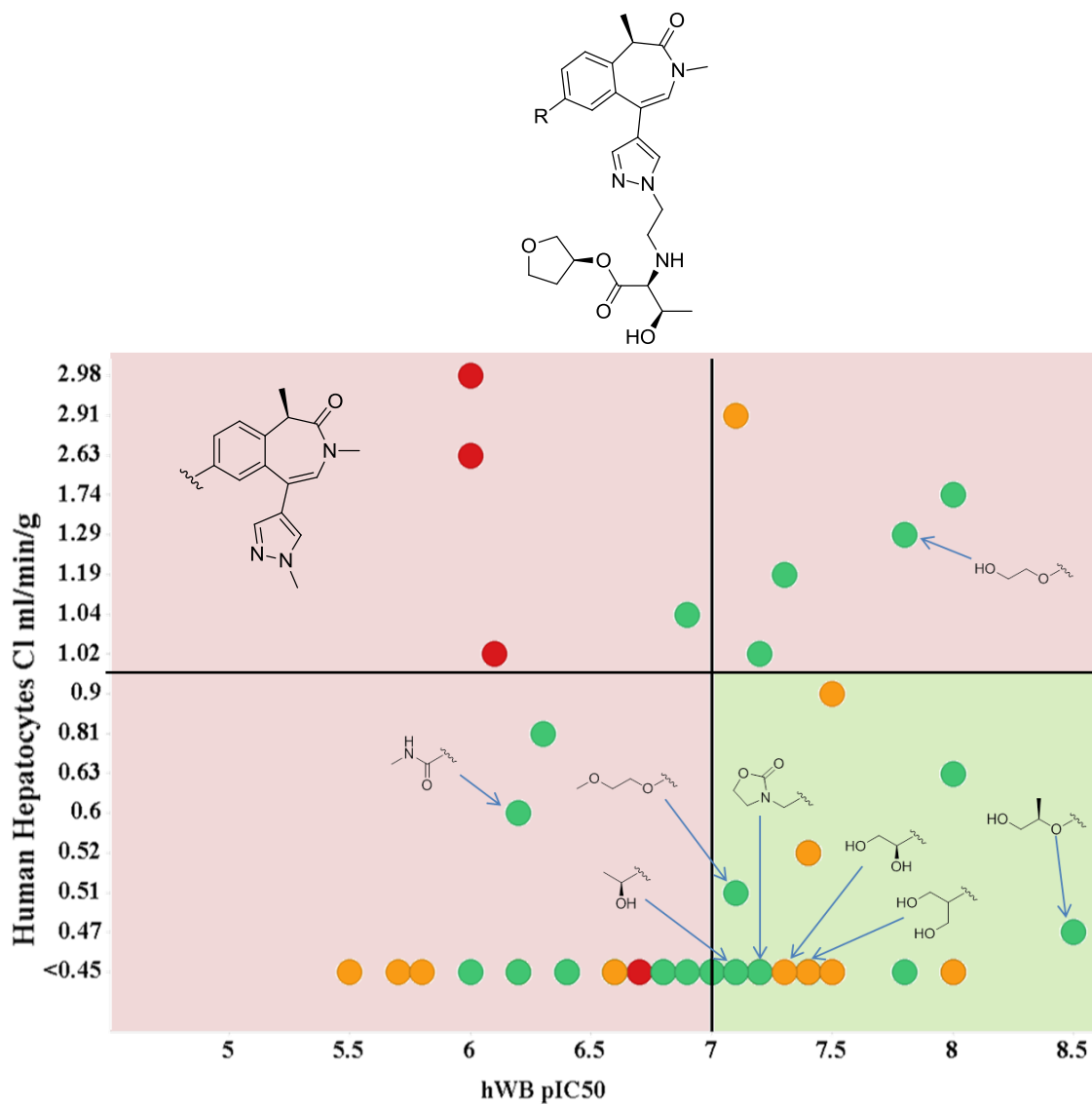
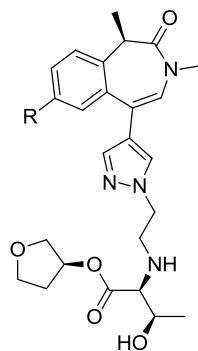


Figure 3.8. A plot of the human hepatocyte clearance vs. hWB potency of the pan-BET BZP analogues. Highlighted are a selection of the analogues containing an *N*-methyl pyrazole as the ZA channel group. The plot points are coloured by ChromLogD_{7,4}, where orange = <math>< 2.2</math>, green = $2.2 - 3.5$, red = > 3.5 and the boundaries depicting the lowest desired hWB and the highest desired human hepatocyte IVC.



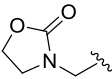
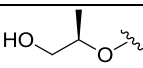
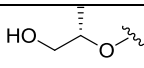
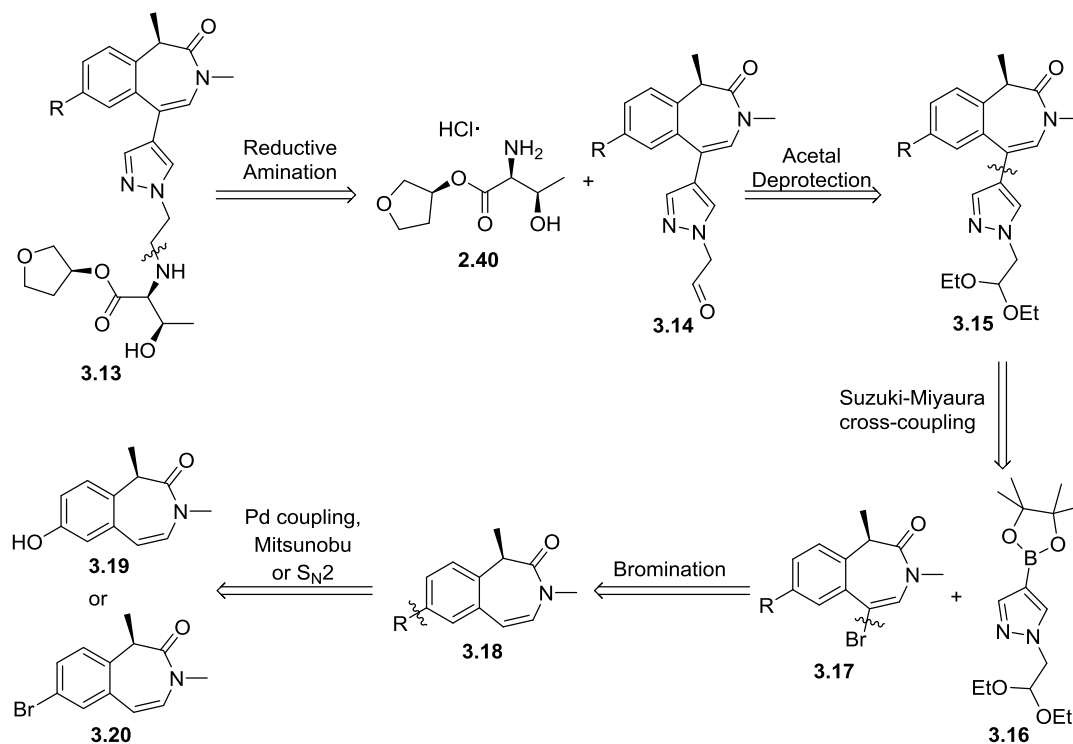
					
	3.6	3.7	3.10	3.11	3.12
ChromLogD _{7.4}	2.8	3.4	3.4	2.8	2.8
TPSA	136	135	135	126	126

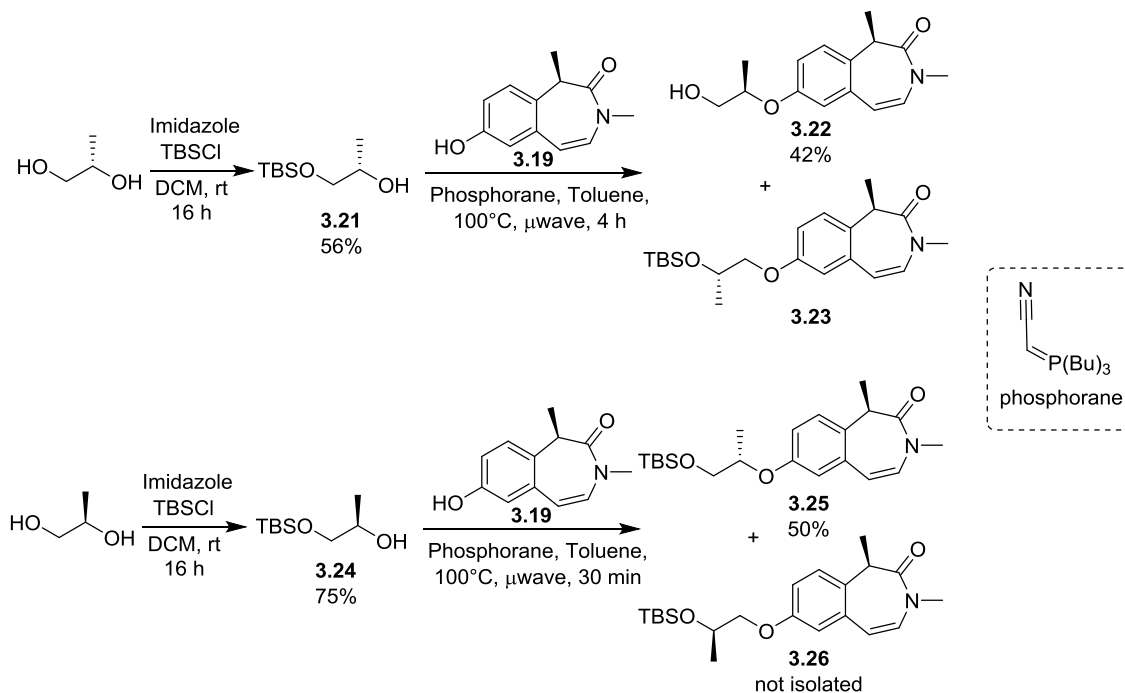
Table 3.2. The *in silico* data for the various WPF shelf groups.

A retrosynthetic analysis was undertaken on the generalised molecule **3.13**. Firstly, the C-N linkage to the ESM can be formed by a reductive amination of the THF ester **2.40** and aldehyde **3.14**. The aldehyde can be accessed from the diethyl acetal **3.15**, which can be formed through a Suzuki cross-coupling of readily available pyrazole boronic ester **3.16** and benzazepinone **3.17**. Next, a C-Br disconnection can be performed, to form **3.18**, and finally a C-R disconnection to yield the hydroxybenzazepinone **3.19** and the bromobenzazepinone **3.20** which can be used to access the O-linked and C-linked WPF shelf groups respectively (Scheme 3.1).



Scheme 3.1. A retrosynthetic analysis was completed to investigate the synthetic route to the targets.

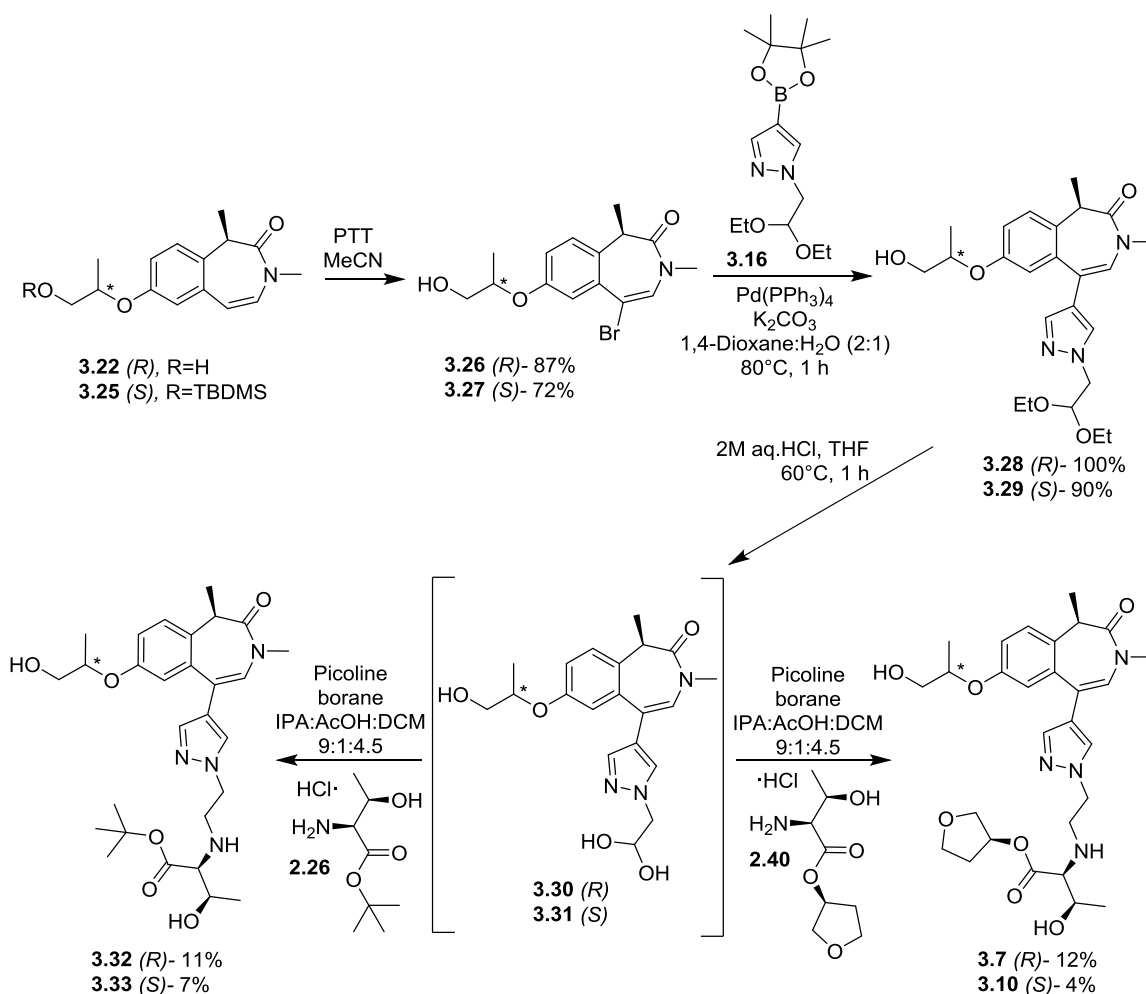
Analogues **3.6**, **3.11** and **3.12** (Table 3.2, *vide supra*) were synthesised by colleagues at GVK leaving only **3.7** and **3.10** to be synthesised. Propane-1,2-diol is commercially available as the chirally pure enantiomers and, as such, the desired diastereomers **3.22** and **3.25** could be accessed through Mitsunobu chemistry (Scheme 3.2). However, the starting material contains two alcohols; one primary and one secondary. Mitsunobu reactions involve the displacement of a hydroxyl group with a nucleophile, in this case benzazepinone **3.19**, in an S_N2 fashion. As such, the reaction should occur selectively on the primary alcohol of propane-1,2-diol due to sterics. Therefore, prior to the Mitsunobu reaction, the primary alcohol was protected as a *tert*-butyldimethyl silyl (TBS) ether.



Scheme 3.2. Intermediates **3.22** and **3.25** were achieved through a Mitsunobu reaction of **3.19** and TBS protected **3.21** and **3.24** respectively.

The primary alcohols were protected with the *tert*-butyl dimethyl silyl group (TBS) to afford **3.21** and **3.24** in moderate-high yields. Initially the Mitsunobu reaction was attempted with diisopropyl azodicarboxylate (DIAD) and triphenylphosphine but only moderate conversions to the desired products were observed despite large excesses of reagents. Therefore, the phosphorane 2-(tributyl-15-phosphanylidene)acetonitrile was employed which resulted in higher conversion to the products **3.22** and **3.25**. However, only moderate yields were obtained for both products due to the migration of the silyl group during the reaction from the primary alcohol to the secondary alcohol, thus forming the proposed side products **3.23** and **3.26** which were not isolated. Furthermore, as a result of an acidic workup during purification of **3.22**, the silyl group cleaved to afford the alcohol rather than the proposed silyl protected alcohol.

Following the isolation of the benzazepinones **3.22** and **3.25**, the rest of the synthesis was completed through the route outlined by the retrosynthetic analysis in Scheme 3.1 (Scheme 3.3).



Scheme 3.3. Synthetic route to afford the desired analogues **3.7** and **3.10** and the *tert*-butyl analogues **3.32** and **3.33**. * depicts the chiral centre with (*R*) and (*S*) defining the stereochemistry at that centre.

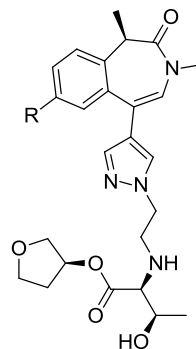
The bromination of **3.22** and **3.25** was achieved with phenyltrimethylammonium tribromide (PTT) in acetonitrile to afford **3.26** and **3.27** in high yields. Surprisingly, these reaction conditions also cleaved the TBS group and, as such, removed the need for a deprotection step in the synthetic route. The pyrazole was then inserted *via* a Suzuki cross-coupling with the readily available **3.16**, before the acetal was deprotected with aqueous 2M HCl in acetone. Interestingly, LCMS analysis implied the hydrate had been formed rather than the expected aldehyde, which suggests that the aldehyde is not stable or is highly reactive. This is supported by the observed degradation of the aldehyde during purification or if the material was not used immediately. Therefore, in order to remove the problematic aqueous work ups and purifications, the hydrates **3.30** and **3.31** were obtained by the concentration of the reaction mixture and was used as crude material.

Two thirds of the crude material **3.30** was reacted with the THF Thr ESM **2.40** and one third of the material was reacted with the *tert*-butyl ester **2.26** under reductive amination

conditions to give the desired biologically hydrolysable analogue **3.7** and non-biologically hydrolysable analogue **3.32**. In parallel, two thirds of the crude material **3.31** was reacted with the THF Thr ESM **2.40** and one third of the material was reacted with the *tert*-butyl ester **2.26** under reductive amination conditions to give the desired biologically hydrolysable analogue **3.10** and non-biologically hydrolysable analogue **3.33**. All of the reductive amination products were isolated in low yields which can be attributed to the significant conversion to an unknown side product, which was not isolated or characterised. Furthermore, conversion to the imine was slow, as observed by LCMS analysis, which suggests that the conversion of the hydrate into the aldehyde was slow.

Compound **3.12** was outsourced to colleagues at GVK who found that the secondary alcohol of the WPF shelf group was being displaced by a bromide during bromination. In addition, racemisation of the same alcohol chiral centre was observed during hydrolysis of the acetal, as a result of protonation and subsequent displacement with water. Finally, the reductive amination was poor yielding. The culmination of these problems means that only a minor amount of product was obtained, which meant resolution of the diastereomers was not possible. Based on the initial data on analogues **3.6**, **3.7** and **3.10-3.11**, which suggested this subseries was insufficient at reducing IVC to a desirable level, it was decided to not resynthesise this compound.

The desired compounds and their *tert*-butyl analogues were submitted for biological testing (Table 3.3). As the data of the *tert*-butyl analogues is only used to generate the Δ hWB values, their biological profiles will not be displayed or discussed.



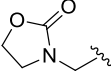
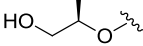
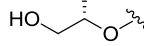
R				
	3.6	3.7	3.10	3.11
hWB pIC ₅₀	6.6	7.1	7.7	7.7
Δ hWB pIC ₅₀	+0.1	+0.3	+0.2	+0.9
Ester BD1 pIC ₅₀	7.0	7.4	7.4	7.4
HLM IVC (+/- benzil)	<0.45 / 3.5	2.3 / 2.7	1.7 / 2.5	3.5 / 4.2
Heps IVC (Hu/cyno)	-	-	<0.45 / 1.81	- / 0.89
ChromLogD _{7.4}	2.5	2.5	2.7	2.4

Table 3.3. Biological data for the various WPF shelf groups. IVC values are quoted in mL/min/g.

All of the analogues showed reduced lipophilicity relative to **3.4** (ChromLogD_{7.4} = 3.2) with **3.7-3.11** also displaying improved metabolic stability. Furthermore, compound **3.10** exhibits desirable human and cynomolgus hepatocyte clearance which is significantly reduced compared to **3.4**. Analogue **3.11** also displayed desirable cynomolgus monkey hepatocyte clearance, however, due to its higher than desired HLM IVC, it was not submitted for human hepatocytes and was not progressed further. The analogues maintained high biochemical and cellular potency, except for **3.6** which demonstrated a lower hWB potency than desired and was not progressed further. This may be attributed to the constrained nature of the group possibly preventing the ethylene component interacting with lipophilic WPF shelf to its full potential. Unfortunately, compounds **3.7** and **3.10** exhibited low ΔhWB which prevented further progression. All of the analogues displayed a lower ChromLogD_{7.4} than predicted by the *in silico* data in Table 3.2 (*vide supra*). As such, the majority of the compounds exhibited low ChromLogD_{7.4} values and low permeability. This may have affected the whole blood potency of the THF Thr analogues. This would therefore impact the ΔhWB, as the *tert*-butyl analogues have higher lipophilicities and permeabilities thus not impacting their cellular potency. As low lipophilicity is commonly associated with low permeability, it was hypothesised that the low permeabilities observed for the analogues were due to their low ChromLogD_{7.4} values.

3.3.2 Investigating a 2,4-disubstituted pyridine as the ZA channel group

To explore the pyridine as an alternative ZA channel group to the pyrazole, SAR was gathered with a range of WPF shelf groups. Firstly, in order to address the overcalculated ChromLogD_{7.4} values observed for the pyrazole analogues (*vide supra*), a plot of the measured vs. calculated ChromLogD_{7.4} values for all of the BZP compounds synthesised across the team was generated (Figure 3.9). The plot is coloured by the difference between the measured and calculated values, with darker colouring indicating higher differences. Furthermore, the points were shaped by the various WPF shelf groups that had been utilised.

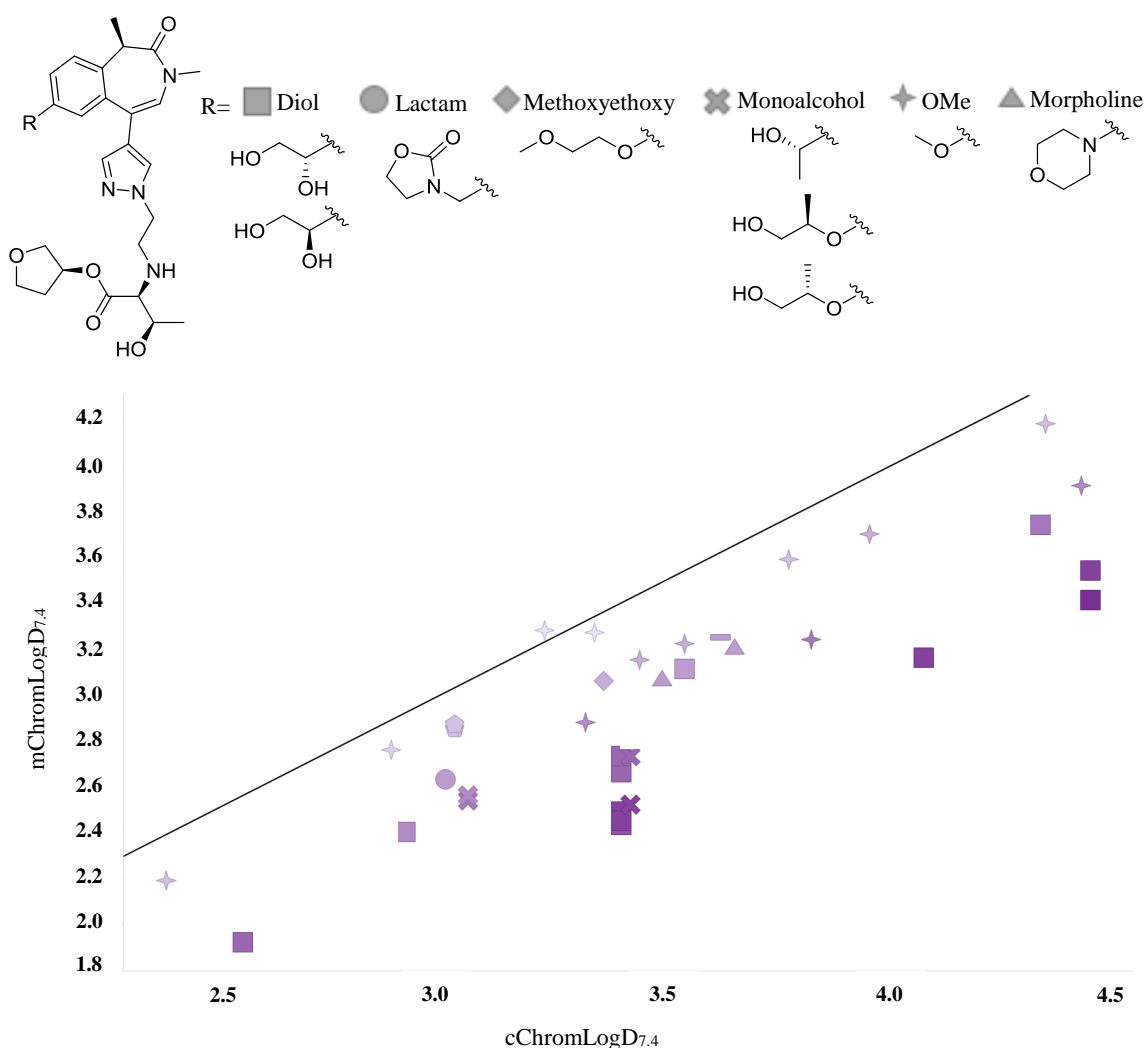
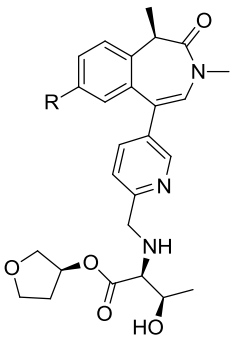


Figure 3.9. A plot of the measured ChromLogD_{7.4} values vs. calculated ChromLogD_{7.4} values with the line $y=x$ installed. The plot is coloured by the difference between the respective values, with darker colouring indicating higher differences, and shaped by various substituents.

The plot shows that the model is overpredicting the majority of the ChromLogD_{7.4} values. It can be seen that the lipophilicities for monoalcohols, as in **3.7**, **3.11** and **3.12** and shown in Figure 3.9, are poorly predicted with differences of 0.6 – 0.9 observed between the measured and calculated values. Furthermore, the methoxyethoxy shelf group (shown in Figure 3.9), which was previously discounted from the pyrazole sub-series due to a high predicted ChromLogD_{7.4}, was overpredicted by 0.4 log units. As such, the methoxyethoxy was modelled along with the monoalcohol shelf groups with a new upper ChromLogD_{7.4} boundary of 3.9 to account for the overprediction. The *in silico* data for the compounds can be found in Table 3.4.



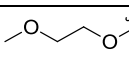
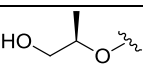
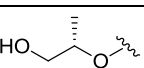
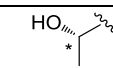
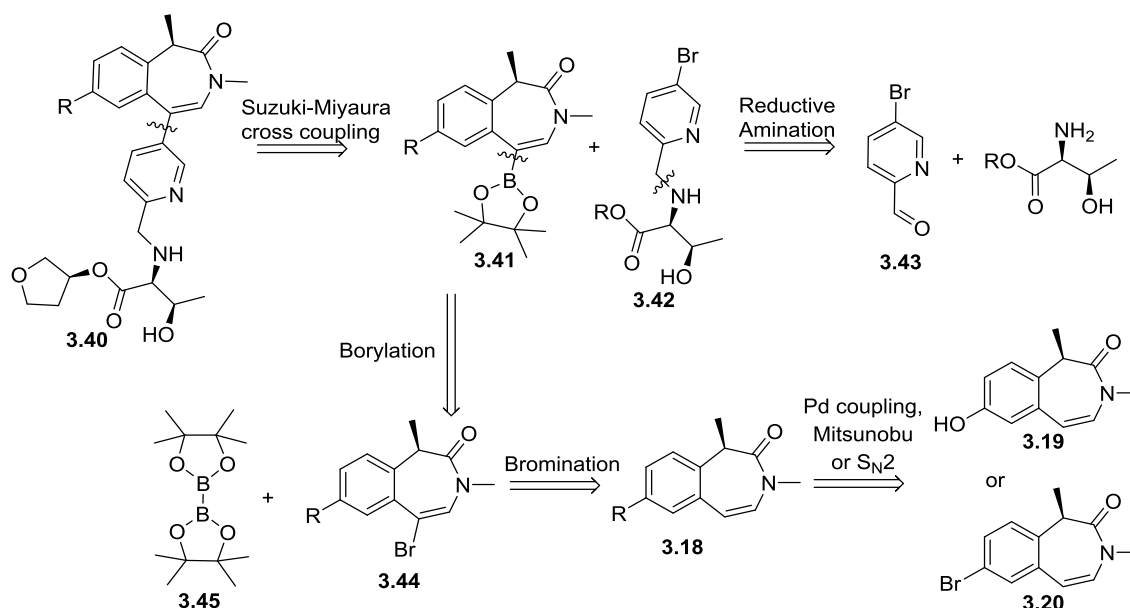
						
	3.34	3.35	3.36	3.37	3.38	3.39
ChromLogD _{7.4}	4.0	3.8	3.7	3.7	3.1	3.1
TPSA	110	120	131	131	121	121

Table 3.4. The *in silico* data for the various WPF shelf groups with pyridine as the ZA channel group

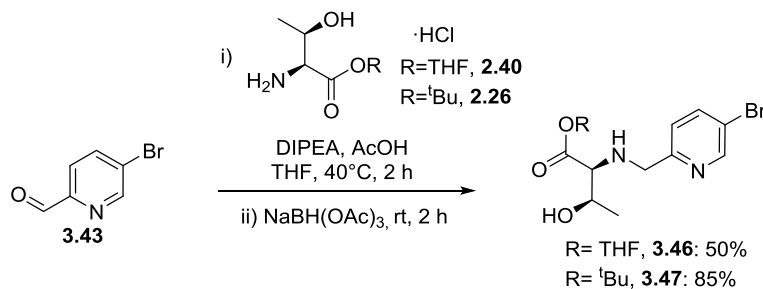
Although the methoxy analogue **3.34** was predicted to be lipophilic, it was synthesised by a colleague at GVK as it forms the direct analogue to **3.4**. A retrosynthetic analysis was undertaken on the generalised molecule **3.40** to investigate the route towards the remaining **3.35-3.39** (Scheme 3.4). Firstly, a C-C disconnection can be completed on the generalised product to yield boronic ester **3.41** and bromopyridine derivative **3.42**. Performing this disconnection first creates a convergent synthesis in which the two intermediates **3.41** and **3.42** are synthesised and then combined together to form the product *via* a Suzuki cross-coupling reaction. Intermediate **3.42** can undergo a C-N disconnection, with the bond being formed by a reductive amination, to give the commercially available 2-formyl-5-bromopyridine **3.43** and the relevant amino acid ester. Intermediate **3.41** can be formed by a Miyaura borylation of bromobenzazepinone **3.44** using bis(pinacolato) diboron **3.45**, which can in turn be synthesised through the bromination of benzazepinone **3.18**. Finally, if **3.18**

contains an O-linked WPF shelf group then it can be formed through the reaction of hydroxybenzazepinone **3.19**. Likewise, if **3.18** contains a C-linked WPF shelf, it can be accessed through the functionalisation of bromobenzazepinone **3.20**.



Scheme 3.4. A retrosynthetic analysis was completed to investigate the synthetic route to the targets.

The first step of the synthesis was the reductive aminations of **2.40** and **2.26** with commercially available **3.43** to form the building blocks **3.46** and **3.47** respectively (Scheme 3.5).

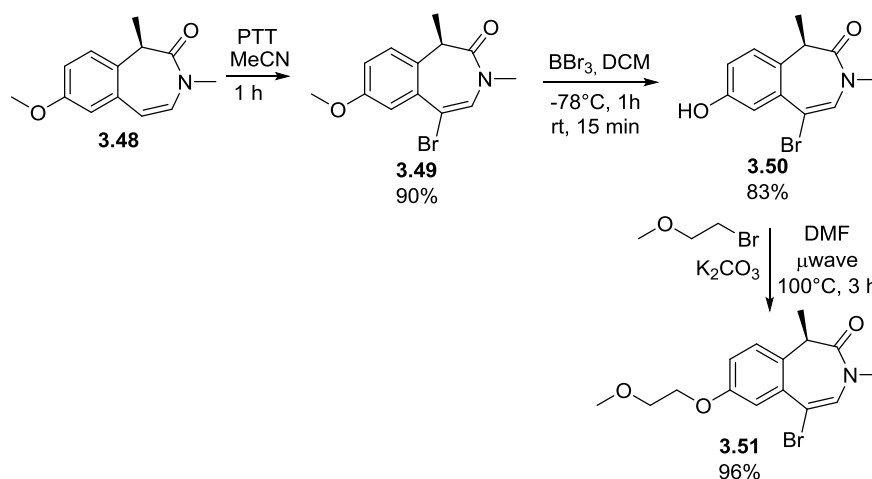


Scheme 3.5. Reductive amination conditions employed to form intermediates **3.46** and **3.47**.

The previously optimised reaction conditions (Scheme 2.14, section 2.3.4.2) were employed to form **3.46** and **3.47** in moderate to high yields. In both reactions, the LCMS reaction profile was very clean with minimal reduced aldehyde observed.

In parallel, the boronic ester coupling partners were synthesised. The 1-hydroxypropan-2-ol shelf group was synthesised as shown in Scheme 3.2. The synthesis was initially focussed on

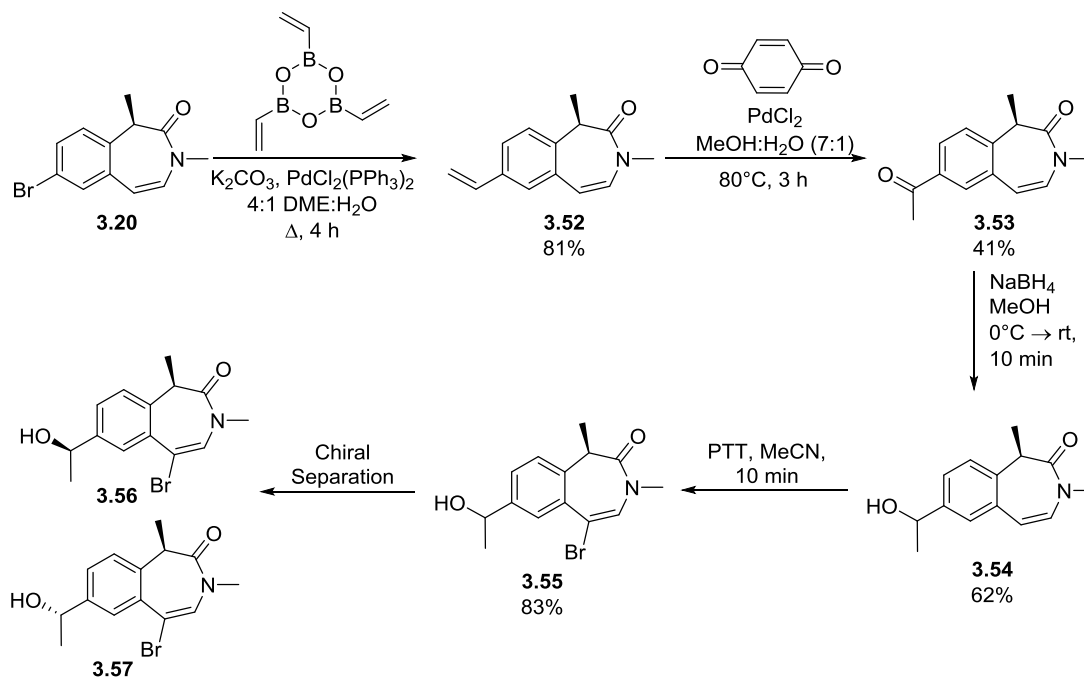
the methoxyethoxy WPF shelf group, as in **3.34**, due to its achiral nature simplifying the synthesis. At this stage of the project, the initial batch of hydroxybenzazepinone **3.19** had been depleted and only the methoxybenzazepinone **3.48** was available. As such, in order to access the hydroxy functionality, **3.48** was brominated and then demethylated. Next, the WPF shelf group was installed *via* a nucleophilic substitution reaction with 1-bromo-2-methoxyethane (Scheme 3.6).



Scheme 3.6. The synthetic route to obtain intermediate **3.51**.

Similarly to the previous analogues, the benzazepinone was brominated using PTT to afford **3.49** in high yield and with no purification required. Next, the demethylation to afford **3.50** was achieved by employing boron tribromide in DCM. The addition of BBr_3 causes an exotherm and, consequently, was completed at -78°C . However, the reaction did not proceed at this temperature and only a small amount of conversion to the desired product was observed by LCMS. Therefore, after addition of BBr_3 at -78°C and subsequent stirring for 1 hour, the reaction was stirred at room temperature for 15 minutes to afford the desired product in a high yield. Finally, the nucleophilic substitution reaction with 1-bromo-2-methoxyethane, using potassium carbonate as a base in DMF provided the desired intermediate **3.51**. Microwave heating was employed to facilitate the reaction and resulted in complete conversion to **3.51**. As such, the product was isolated as pure material in a very high yield following an aqueous work up.

Next, work focussed on the 2-propanol shelf group. As both configurations of the alcohol were desired, it was decided to synthesise the racemic alcohol and use flash column chromatography using a chiral stationary phase to obtain the diastereomers **3.56** and **3.57** (Scheme 3.7).

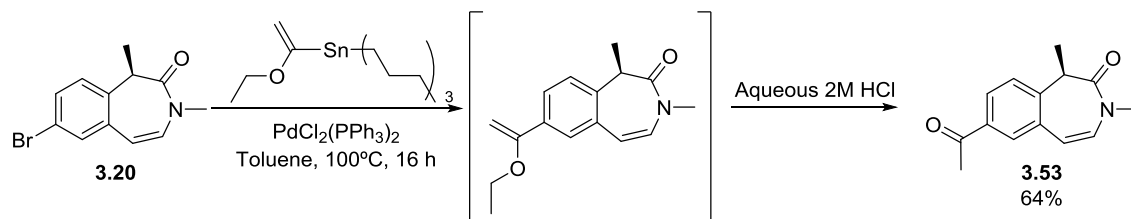


Scheme 3.7. The synthetic route towards intermediates **3.56** and **3.57**.

As aforementioned, C-linked shelf groups can be accessed through bromobenzazepinone **3.20**. As such, the first step of the synthesis was to install a terminal alkene *via* a Suzuki cross-coupling with vinylboronic anhydride to give **3.52**. Following this, the ketone was formed through a Wacker-Tsuji oxidation with benzoquinone to give **3.53** in moderate yield. This reduced yield may be due to the multiple side products formed during the reaction, as observed by LCMS analysis. Furthermore, purification by column chromatography proved to be difficult, with **3.53** being isolated at ~70% purity. Even so, the material was carried forward into the reduction with sodium borohydride in methanol to afford **3.55** in a moderate yield. Finally, bromination of **3.55** with PTT resulted in **3.55** containing the racemic alcohol. Initially, a reaction time of 1 hour was used which led to complete conversion to an undesired product in which the hydroxyl group had been displaced by the bromine. The HBr generated by PTT, following the bromination of the alkene, was able to facilitate this displacement. To reduce this side reaction, the reaction was repeated with a shorter reaction time of 10 minutes which resulted in a high isolated yield of **3.55**. Intermediate **3.55** was submitted for chiral separation which afforded the two chiral intermediates **3.56** and **3.57**.

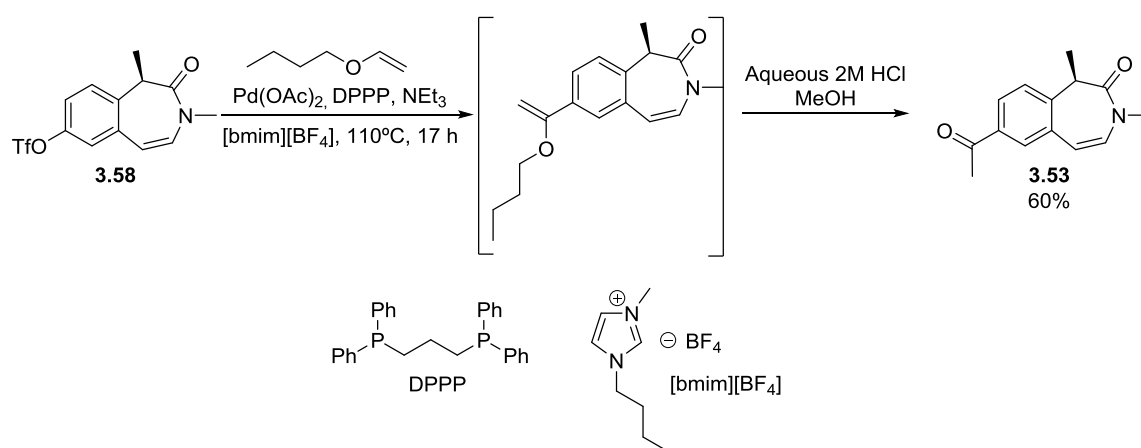
In an attempt to reduce the number of synthetic steps required to access **3.53**, and remove the suboptimal Wacker-Tsuji oxidation, alternative conditions were investigated. Aryl methyl ketones are a key class of carbonyls and act as a versatile building block. In 1987, Kosigu *et al.* reported the cross-coupling of an organostannane and an aryl bromide with ensuing

hydrolysis as a method for installing a methyl ketone. These conditions were applied to the synthesis of **3.53** (Scheme 3.8).



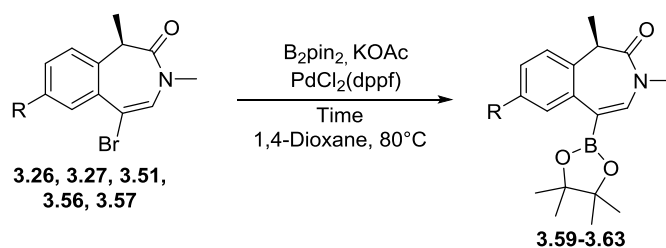
Scheme 3.8. Stille reaction to install the ketone.¹⁷⁹

The reaction employed tributyl(1-ethoxyvinyl)stannane as the organostannane which was reacted with the aryl bromide **3.20** in a palladium catalysed cross-coupling to form a vinyl ether intermediate, which was not isolated. Subsequent hydrolysis of the intermediate with aqueous 2M HCl resulted in **3.53**. This route improved the yield from 33% for the two steps to **3.53**, as shown in Scheme 3.7, to 64%, as well as reducing the synthetic route by one step. However, although this is a huge improvement, organostannanes are notoriously toxic reagents and their use should be limited where possible. Therefore, elsewhere within the team, efforts were made to find an alternative method. From this work, an optimised route to **3.53** was developed which employed an ionic liquid promoted Heck reaction first reported by Mo *et al.*¹⁸⁰ Similarly to the Stille reaction, the Heck reaction involves the palladium-catalysed vinylation of **3.20** followed by hydrolysis under acidic conditions to afford **3.53** (Scheme 3.9). Due to the limited availability of **3.20**, the conditions were optimised on the triflate **3.58** rather than the bromide **3.20**.



Scheme 3.9. Heck reaction to install the ketone.¹⁸¹ *DPPP = 1,3-bis(diphenylphosphanyl)propane, [bmim][BF₄] = 1-butyl-3-methylimidazolium tetrafluoroborate

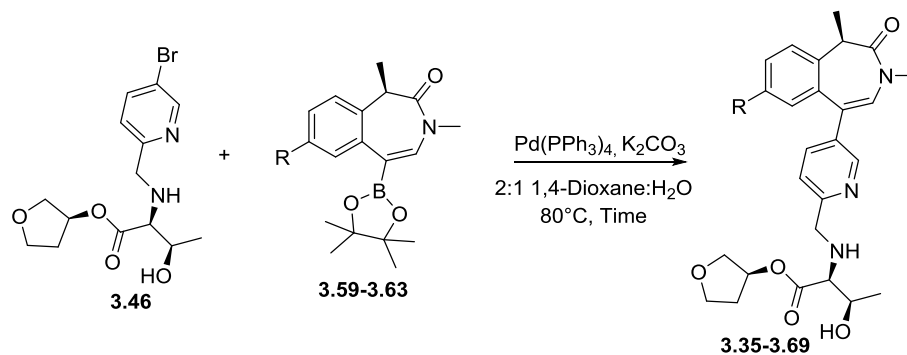
This procedure widely broadened the scope of the Heck reaction. Although an ionic liquid is not essential, Mo *et al.* found that the use of the ionic liquid 1-butyl-3-methylimidazolium tetrafluoroborate ([bmim][BF₄]) promoted the reaction by forming a hydrogen bond between the acidic C-H of the imidazole and the triflate ion, thus facilitating its dissociation from palladium.¹⁸⁰ This, along with the bidentate nature of the ligand 1,3-bis(diphenylphosphanyl)propane, affords high regioselectivity with minimal insertion on the vinyl α -carbon observed. Subsequent hydrolysis of the vinyl ether with aqueous 2M HCl produces the ketone in similar yields to the Stille reaction shown in Scheme 3.8. The next stage was the borylation of the bromide intermediates to generate the required boronic esters **3.59–3.63** (Table 3.5).



R					
Product	3.59	3.60	3.61	3.62	3.63
Br intermediate	3.51	3.26	3.27	3.56	3.57
Time (h)	16	16 ^a	2	4	1
Yield (%)	82	56	99	90	84

Table 3.5. The yields obtained for the Miyaura borylation to the boronic ester intermediates. ^a 75°C

Finally, the final compounds **3.35–3.39** were synthesised through the Suzuki cross-coupling of the ESM-containing **3.46** and **3.47** and the respective boronic esters **3.59–3.63** (Table 3.6).



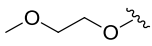
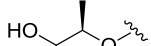
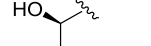
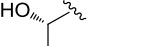
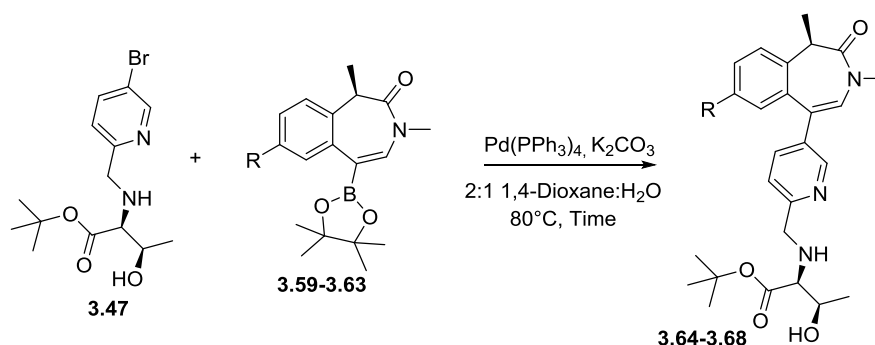
R					
Product	3.35	3.36	3.37	3.38	3.39
Boronic ester	3.59	3.60	3.61	3.62	3.63
Time (min)	60	60	120	10	10
Yield (%)	46	33	17	31	38 ^b

Table 3.6. The yields obtained for the Suzuki cross-couplings to the desired THF esters.

Similarly to what was observed with the AP OTS series, despite high conversions to the desired products, only low to moderate isolated yields were obtained following purification. This observation applies to all syntheses of the final compounds throughout the rest of this thesis, including those in Table 3.7.



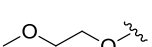
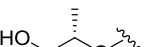
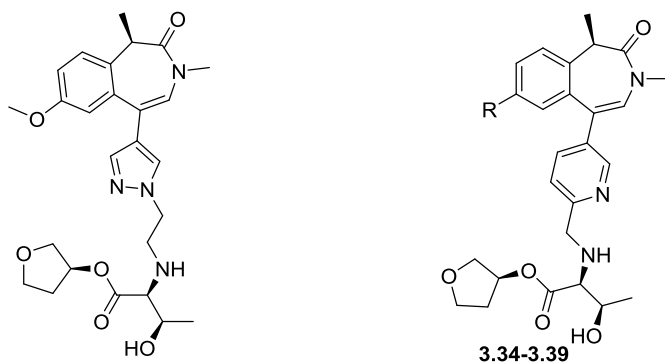
R					
Product	3.64	3.65	3.66	3.67	3.68
Boronic ester	3.59	3.60	3.61	3.62	3.63
Time (min)	60	60	60	10	10
Yield (%)	10	12	3	35	39

Table 3.7. The yields obtained for the Suzuki cross-couplings to the *tert*-butyl esters **3.64-3.68**.

The desired analogues were submitted for testing along with the biologically non-hydrolysable *tert*-butyl compounds (Table 3.8). Analogue **3.34**, which was synthesised by colleagues at GVK as a baseline compound was also submitted.

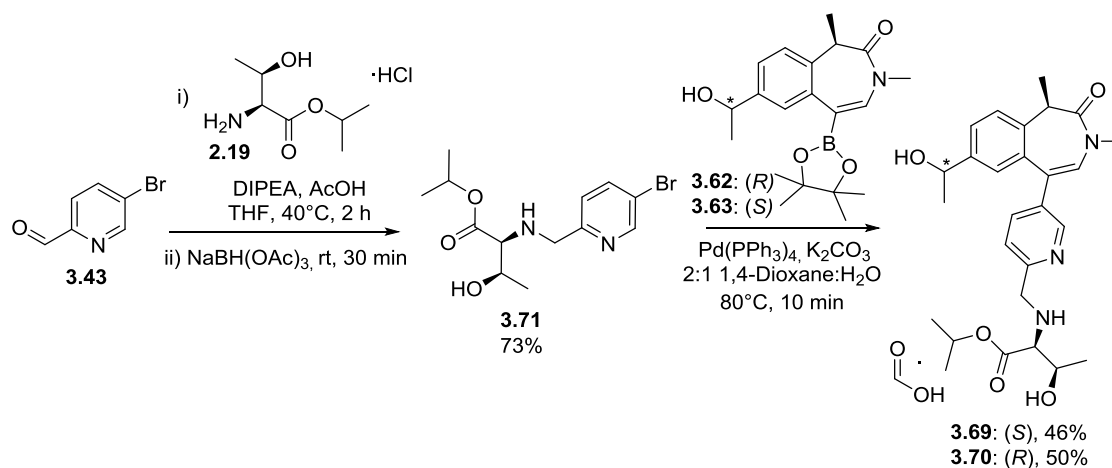


R							
Product	3.4	3.34	3.35	3.36	3.37	3.38	3.39
hWB pIC ₅₀	7.5	7.9	7.2	7.3	8.0	7.3	7.3
Δ hWB pIC ₅₀	+0.9	+1.4	+0.3	0.0	+0.6	+0.2	+0.1
Ester BD1 pIC ₅₀	7.0	6.4	6.7	7.1	7.5	6.9	6.8
HLM IVC (+/- benzil)	3.4 / 3.5	1.6 / 2.6	1.4 / 2.0	1.2 / 1.5	1.1 / 1.3	2.3 / 3.6	0.5 / 0.6
Hu Heps IVC (LBF)	10.6 (94%)	15.2 (91%)	1.5 (67%)	0.6 (45%)	0.5 (40%)	-	<0.45 (38%)
Cyno Heps IVC (LBF)	15.4 (91%)	37.2 (96%)	8.5 (85%)	1.4 (49%)	1.2 (45%)	1.5 (51%)	<0.89 (38%)
ChromLogD _{7.4}	3.2	3.7	3.5	2.8	2.8	2.5	2.6

Table 3.8. Biological data for the various WPF shelf groups with the pyridine as the ZA channel group. Compound **3.34** was synthesised by a colleague at GVK. IVC values are quoted in mL/min/g.

All of the analogues, except **3.34**, display desirable lipophilicity with the measured ChromLogD_{7.4} values being lower than the calculated values, as hypothesised from the data in Figure 3.9. Although **3.34** has a higher lipophilicity relative to its pyrazole analogue **3.4**, it displays improved microsomal stability. However, it also exhibits higher clearance in human and cynomolgus monkey hepatocytes. Analogue **3.34** also shows an increased hWB potency and ΔhWB compared to its pyrazole analogue **3.4**. Interestingly, exchanging the methoxy for alternative shelf groups, with the exception of **3.37**, decreases these values, suggesting a reduced turnover by CES-1. For analogues **3.36** and **3.39**, this is supported by the similar +/- benzil HLM values which suggests low levels of esterase mediated metabolism.

As hypothesised, analogues **3.35** to **3.39** all exhibit increased microsomal stability relative to **3.34**, with **3.36**, **3.37** and **3.39** also displaying an improved human and cynomolgus monkey hepatocyte clearance. This is also observed in analogue **3.38**, however, it also showed slightly poorer microsomal clearance than **3.34** and, therefore, was not progressed any further. Although compound **3.35** displayed improved human and cynomolgus monkey hepatocyte clearance compared to **3.34**, unfortunately the cynomolgus monkey clearance



Scheme 3.10. Synthetic route to the isopropyl Thr pyridine analogues.

As the synthetic route is convergent, the ESM-containing intermediate **3.71** was synthesised first through the reductive amination of 2-formyl-5-bromo pyridine **3.43** and the isopropyl Thr amino acid ester **2.19**. Subsequent Suzuki couplings with the relevant boronic esters **3.62** and **3.63** afforded the desired diastereomers **3.69** and **3.70** in moderate yields. As a result of purification by MDAP employing a formic acid modifier, the compounds were isolated as the formic acid salts. The analogues were submitted, along with their biologically non-hydrolysable *tert*-butyl analogues, **3.67** and **3.68** (Table 3.7, *vide supra*), were submitted for biological testing (Table 3.10).

	3.69	3.70
hWB pIC ₅₀	8.5	8.1
Δ hWB pIC ₅₀	1.3	1.0
Ester BD1 pIC ₅₀	7.1	6.7
HLM IVC (+/- benzil)	2.2 / 2.9	-
ChromLogD _{7.4}	3.6	3.6

Table 3.10. Biological profiles of the second generation isopropyl Thr pyridine analogues. IVC values are quoted in mL/min/g.

As hypothesised, reducing the size of the ester from the THF to the isopropyl ester increased the ΔhWB values to desirable levels (+0.2/+0.1 vs. +1.3/+1.0 for the THF ESM and iPr ESM analogues respectively). This resulted in higher whole blood potencies relative to the first-generation compounds. However, although the measured ChromLogD_{7.4} is lower than the calculated ChromLogD_{7.4}, the 0.6 log unit difference was not enough to bring the molecules into the desired region of <3.5. This, in combination with the undesirable HLM IVC of the THF analogue **3.38**, which also contains the stereoisomer with (*R*)-configuration at the 2-propanol group, meant compound **3.70** was progressed no further. However, the THF analogue of **3.69**, the direct comparator **3.39**, displayed low HLM and hepatocyte IVC. Therefore, it was decided that **3.69** was to be progressed into HLM studies on account that a slightly increased HLM profile would still be acceptable. Unfortunately, the HLM IVC was shown to be higher than desired which is most likely due to the high lipophilicity. Consequently, compound **3.70** was not progressed and it was decided that lower lipophilicity analogues were required.

In an attempt to indicate whether the increased ΔhWB values were indeed due to the reduced ester size, the THF and isopropyl analogues with (*S*)-configuration at the 2-propanol group, **3.39** and **3.69**, were docked into CES-1 by a colleague in computational chemistry (Figure 3.10).¹⁸²

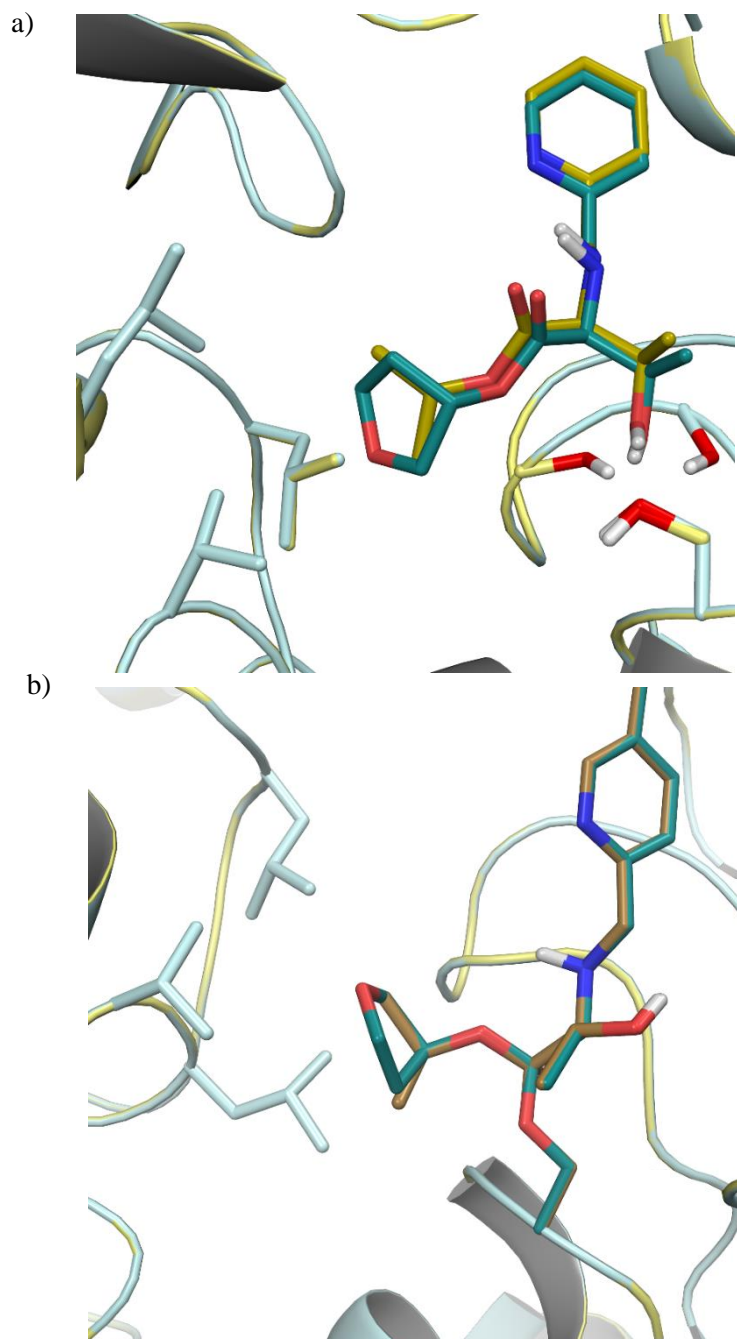


Figure 3.10. Overlaid dockings of the non-covalently bound **3.39** (teal) in CES-1 (light blue) and **3.69** (gold) in CES-1 (light yellow) with the catalytic serine residue. b) Overlaid dockings of the covalently bound **3.39** (teal) and **3.69** (gold) in CES-1 showing the tetrahedral intermediates formed by the backbone catalytic serine residue attacking the ester carbonyl during CES-1 hydrolysis of the ester (bottom). The structures overlay very closely which suggests that the ESM motif itself does not cause a change in the binding mode, and thus CES-1 hydrolysis. However, the THF ring changes conformation upon forming the tetrahedral complex and the oxygen of the ring is situated in a lipophilic region with several leucine residues. This suggests that the conformation change, and electrostatic penalties may make the binding of the THF ester less preferable.

The compounds were docked as both the non-covalently bound ligand and the covalently bound tetrahedral intermediate which is formed by the catalytic backbone serine residue attacking the ester carbonyl. Initial attempts at docking the non-covalently bound ligands proved difficult and they therefore had to be truncated and the BZP removed, in order to facilitate a reliable docking. The overlaid dockings of the two analogues show that, despite the bulkier size of the THF ring, the preferred binding modes are similar. Furthermore, the ester O-R bonds adopt the same position which places the isopropyl/THF group in the small, rigid hydrophobic pocket of CES-1. Two key residues in this pocket are leucines, highlighted in the docking, and these overlay perfectly between the two molecules in both the non-covalently bound ligand and covalent dockings. This suggests that the increased steric bulk of the THF ring is not impacting binding to CES-1 and, therefore, that the improved ΔhWB value may not be due to increased CES-1 turnover. To further investigate this, the computational colleague undertook energetic studies on the two molecules both in the non-covalently and covalently bound states (Figure 3.11).

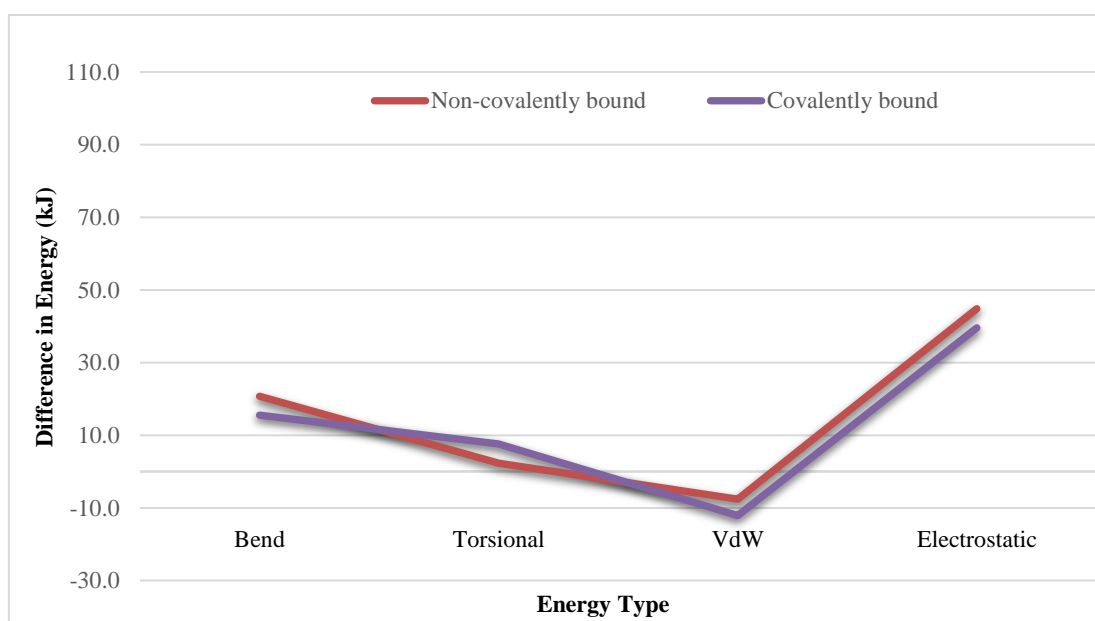


Figure 3.11. A plot of the differences in energy between the THF and isopropyl analogues, **3.39** and **3.69** respectively. The pink line depicts the difference in energies for the non-covalently bound analogues **3.39** and **3.69** in CES-1. The purple line shows the energy differences for analogues **3.39** and **3.69** when they are covalently bound to CES-1. Positive values indicate a preference for the isopropyl analogue whilst negative values suggest the THF ESM is preferred.

The computational chemist calculated the energies of **3.39** and **3.69** following minimisation of their structures in the CES-1 dockings (*vide supra*, Figure 3.10). The plot presents the

difference in energy observed between the THF ester **3.39** and the isopropyl ester **3.69**, with positive numbers indicating a preference for the isopropyl analogue and negative numbers the THF analogue. Although the absolute values are subject to significant errors, they can be used to infer a plausible reason for the difference in potency observed. The plot shows that in both the non-covalently bound and covalently bound substrates there are significant differences between the two molecules with regards to their electrostatic energy. The high positive electrostatic energy suggests that the binding of the isopropyl analogue **3.69** is preferred to the binding of the THF analogue **3.39**, both as a non-covalently bound substrate and covalently bound. This is most likely due to the ester group being situated in a lipophilic pocket and, therefore, the hydrophobic isopropyl group being preferred to the oxygen-containing THF ring.

In addition to this, given the very close overlay of the structures in the dockings, the moderate difference in the torsional energies of the unbound substrates imply a torsional strain is present. A comparison of the dockings of the non-covalently bound and covalently bound **3.39** in CES-1 show the THF ring has changed conformation between the unbound and bound states. As there is a small difference in torsional strain for the covalently bound substrates, this alludes to the torsional strain of the non-covalently bound substrate arising from the conformation of the THF ring as well as from the ester-THF bond. Based on small molecule X-ray data from the Cambridge crystallographic database, the computational chemistry colleague determined the preferred ester-THF bond angle is -47° , however, in the docking the angle is -40.8° . In comparison, the preferred ester-isopropyl bond angle is -32° and is suggested to be -32.7° by the docking. The large difference in preferred-predicted bond angles for the THF analogue **3.39** supports the hypothesis of torsional strain in the ester-THF bond, which could result in less favourable binding to CES-1 relative to the isopropyl analogue **3.69**.

At this stage of the investigations, a range of WPF shelf groups had been selected, based on previous SAR from a pan-BET series in which they demonstrated high hWB potency, and incorporated into the first generation pyridyl series. Although desirable lipophilicities and IVC profiles were exhibited by analogues **3.35-3.39**, small Δ hWB values were observed, except for analogue **3.37** which had a desirable Δ hWB of 0.8. It was hypothesised this was due to the THF Thr ESM causing reduced permeability of the compounds, thus impacting the hWB values observed relative to their hydrophobic *tert*-butyl analogues, as well as the steric bulk of the THF ring slowing down the rate of CES-1 turnover. As such, the second generation pyridyl analogues incorporated an isopropyl Thr ESM, with the aim of reducing

the steric bulk and reducing the TPSA of the molecules. Pleasingly, the analogues demonstrated desirable hWB potencies and increased Δ hWB values, but suboptimal IVC profiles due to their high lipophilicities. Together, these observations as well as the energies calculated from the dockings support the original hypothesis that the THF analogue **3.39** is a poorer substrate for CES-1, albeit not due to steric differences as initially thought but most likely electrostatics. To further investigate the differences in whole blood potency and Δ hWB values observed, QSAR modelling was performed.

3.3.2.1.1 QSAR Modelling to investigate the differences between the THF and ⁱPr Thr ESMs

The field of Quantitative Structure-Activity Relationship (QSAR) modelling was first founded over fifty years ago by Corwin Hansch.¹⁸³ Initially conceptualised as an extension of physical organic chemistry, significant advances in the last decade has led to it to becoming one of the most commonly employed computational tools in medicinal chemistry.¹⁸⁴ Once based on simple regression methods with applicability to a small series of congeneric compounds, its evolution now allows the analysis of very large datasets, comprising diverse molecular structures, using a wide range of statistical and machine learning algorithms. Computational chemistry depicts chemical structures as numerical models and simulates their behaviour through physics and quantum equations.¹⁸⁴ Within medicinal chemistry, QSAR modelling attempts to use these data to establish mathematical relationships linking chemical structure and pharmacological activity in a quantitative manner for a series of compounds.¹⁸⁵

A simple QSAR generally takes the form of the linear equation (1) which can be expanded to equation (2):

$$\text{Biological activity} = f(\text{molecular or fragmental properties}) \quad (1)$$

$$\text{Biological activity} = \text{Constant} + (C_1P_1) + (C_2P_2) + (C_3P_3) + \dots \quad (2)$$

The descriptor parameters P_n are computed for each molecule in the series. The coefficients C_n are calculated by fitting variations in the parameters and the biological activity through the application of advanced statistical techniques. This results in a numerical equation (a QSAR) which can be used to predict the activity of new compounds.¹⁸⁵ More complex machine learning algorithms, such as Random Forest or Support Vector Machines, are highly non-linear in nature and the mathematical formula describing the relationship between

activity and molecular description is not easily explained in an equation. However, the process of building and interpreting the models remains the same.

To enable QSAR modelling, a chemical dataset must first be simplified into the curated dataset which is then used to build and validate the model (Figure 3.12).¹⁸⁵

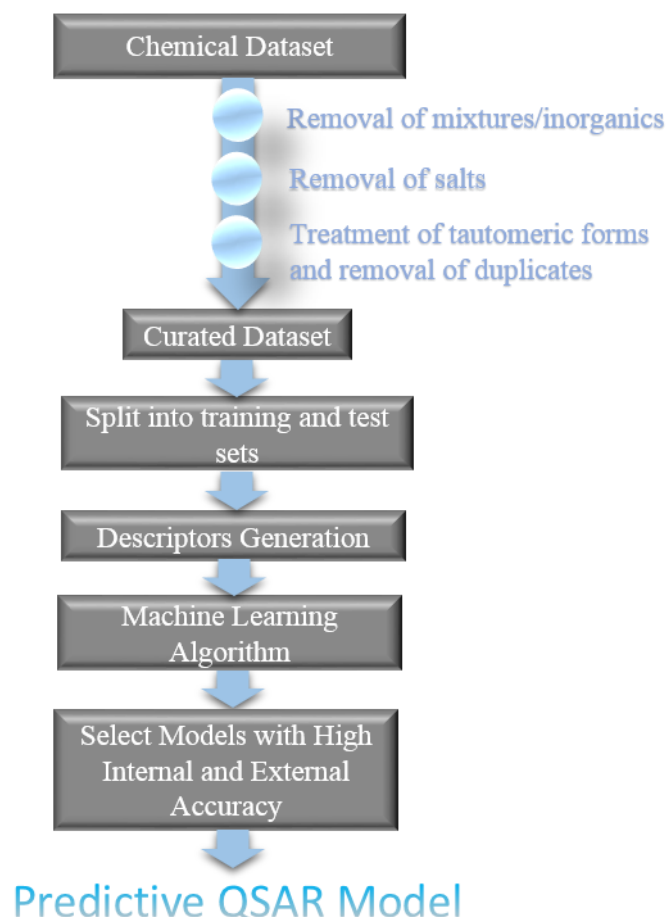


Figure 3.12. A flowchart depicting the process of building a predictive QSAR model.

Firstly, compound mixtures, inorganics and organometallics are removed from the dataset. Further removal of salts to give the parent compound, followed by treating tautomeric forms and deletion of duplicates, yields the curated dataset. Next, the data is split into a training set, which is used to build the model, and a test set, which is used to validate the model.

Following the splitting of the data, the descriptors required for equation (2) (P_n) are generated using the training set.¹⁸⁶ The descriptors can be categorised into four main classes; topological, geometrical, electronic and hybrid/three dimensional (3D) descriptors.¹⁸⁷ Topological descriptors are derived directly from the connection table representation of the

two dimensional (2D) structure, which contains information such as atom and bond counts, substructure counts and molecular connectivity indices.¹⁸⁸ In contrast, geometrical descriptors are derived from the 3D structure and include molecular volume and surface area, solvent-accessible surface area and charged partial surface area amongst other properties.¹⁸⁷ Electronic descriptors are used to characterise molecules with quantities such as dipole and quadrupole moments, polarizability and HOMO/LUMO energies.¹⁸⁹ Finally, hybrid/3D descriptors combine elements of the geometric and topological descriptors to describe pharmacophore fingerprints. In addition to these classes, macromolecular descriptors also exist which are concerned with the overall properties of the molecule for example the van der Waals surface area (VSA) and TPSA.¹⁹⁰

Once the descriptors have been generated, machine learning algorithms can be applied. There are three types of machine learning; supervised learning, unsupervised learning and reinforcement training.¹⁹¹ QSAR modelling within medicinal chemistry typically employs supervised learning algorithms in which a target variable (e.g. biological activity) is to be predicted from a given set of descriptors (independent variables).¹⁹¹ These variables are used to generate a function, such as equation (2), that maps inputs to desired outputs. This training process continues until the model achieves a desired level of accuracy on the training data. When achieved, the model is applied to the test data set. The accuracy and applicability of the model can be determined by plotting the predicted vs. actual value of interest. From the plot the determination coefficient (R^2) and the root mean squared error (RMSE) can be calculated.¹⁹² These are measurements of how tight the data is to the fitted regression line, with $R^2 = 1$ indicating the regression line perfectly fits the data, and how close the regression line is to the $y=x$ line respectively.

3.3.2.1.2 Structural Interpretation of QSARs

QSAR modelling is a powerful technique for building a model capable of predicting biological activity of designed molecules. However, it does not always provide an insight into what is driving the activity. Therefore, the last decade has seen significant advances in the structural analysis of QSAR models.¹⁹³ Such analyses could provide additional benefits, such as information on the mechanism of action and the elicitation of structural rules. This could enable the targeted design of new compounds or the structure optimisation of existing compounds to improve activity. One such structural interpretation method was disclosed by Polishchuk *et al* in 2013.¹⁹³ The technique focusses on investigating the contribution of a molecular fragment to the desired property, e.g. biological activity. It does this through

calculating the difference between the predicted property value for the molecule containing the fragment and the same molecule without the fragment. This results in a method that is capable of estimating contributions of any atom combinations or single atoms. As such, structural analysis can be incredibly powerful within medicinal chemistry by enabling the identification of fragments that are key for biological activity. For example, two congeneric compounds A-B and A-C have a common substructure A. Consequently, by using the QSAR model to predict the activity of A, ($P^{\text{pred}}(\text{A})$), and subtracting the value from the predicted values for A-B and A-C, ($P^{\text{pred}}(\text{AB})$) and ($P^{\text{pred}}(\text{AC})$) respectively, the contributions of B, ($P^{\text{pred}}(\text{B})$), and C, ($P^{\text{pred}}(\text{C})$), to the activity observed for the molecules can be estimated (Figure 3.13).¹⁹³

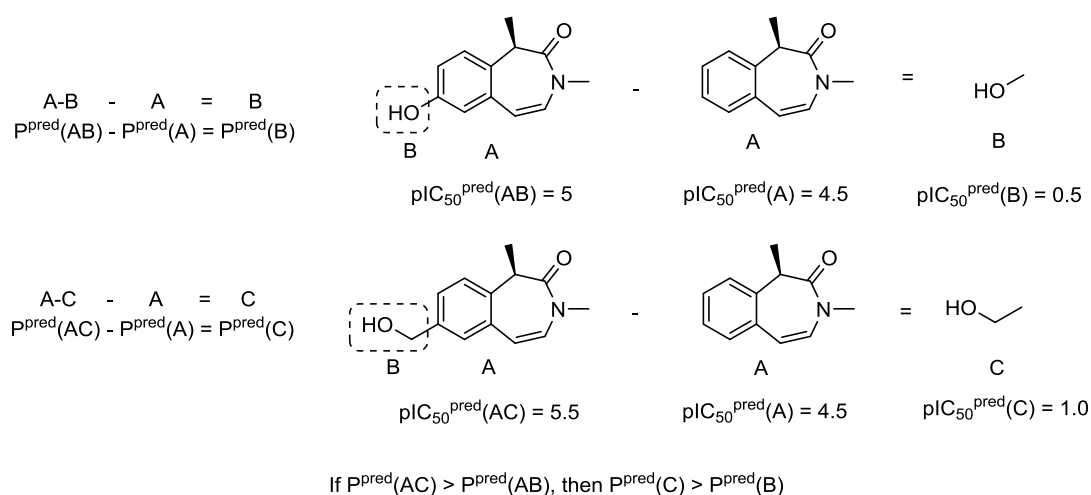


Figure 3.13. A structural interpretation of a QSAR can be used to elucidate what fragments contribute to the observed property by comparing congeneric compounds, here A-B and A-C. A QSAR model is used to predict the activity of A, ($P^{\text{pred}}(\text{A})$), which is subtracted from the value from the predicted values for A-B and A-C, ($P^{\text{pred}}(\text{AB})$) and ($P^{\text{pred}}(\text{AC})$) to give ($P^{\text{pred}}(\text{B})$) and ($P^{\text{pred}}(\text{C})$).

As can be expected, the contribution of the same fragment could vary between different molecules. Therefore, the fragment contribution to the biological activity is calculated for all molecules containing the same fragment within the dataset and the average taken. As aforementioned, the ability to know the contributions for a range of fragments can provide insight into what is key for potency as well as potentially providing a set of structural rules.

3.3.2.1.3 QSAR modelling on the analogues containing a 2,4-disubstituted pyridyl as a ZA channel group

As QSAR modelling has the capability to relate biological activity to chemical structures, it was thought that it could offer an alternative method to investigate the difference in Δ hWB observed between the first and second generation pyridyl analogues **3.39** and **3.69**. To enable this, models for BRD4 BD1 pIC₅₀, hWB pIC₅₀ and Δ hWB were desired. As well as creating models that could be used to predict values for new molecules, the structural interpretation would reveal whether identical fragments contribute to each function or if they differ. This would give an indication as to what structural components are important for the whole blood potency and Δ hWB, potentially allowing future molecules to be optimised. As aforementioned, the BZP has two vectors in which the amino acid ester can be positioned; the ESM can be directed over the shelf (BZP-OTS series) and through the ZA channel (BZP-ZA series). To facilitate these studies, data collected on all BZP-containing molecules synthesised (up to 14th December 2017) was collated. This provided a larger data set for the modelling, which increases the likelihood of a QSAR being determined and a successful model being generated. The data set comprised of 229 compounds for the BRD4 BD1 and whole blood modelling and contained 72 compounds with Δ hWB values for the Δ hWB modelling. The models were built and run by a colleague in computational chemistry.¹⁹⁴

To increase the likelihood of the generation of a reliable model, four splitting methods, five descriptor subsets and four machine learning algorithms were employed using QSAR workbench software, a commercial package available from Biovia.¹⁹⁵ This resulted in a total of 80 models being built. For the purpose of this report, only the selected models for the BRD4 BD1, whole blood and Δ hWB modelling will be discussed. However, further details can be found in the supporting information (Appendix 4). Validation of the QSAR models was done by comparing the actual vs. predicted pIC₅₀/ Δ hWB of the training dataset followed by the test set. Various statistical parameters such as the determination coefficient (R^2) and the RMSE were used to choose the best QSAR model for each property. Using the procedure disclosed by Polishchuk *et al*, GSK have built an in house algorithm to facilitate structural interpretations of QSARs, which utilises ChemAxon fragmentation software.^{193,195} Therefore, structural interpretation reports were also generated for the selected models. Each property and respective QSAR model will now be separately discussed in detail.

3.3.2.1.4 QSAR modelling to build a predictive model for BRD4 BD1 potency

Of the 80 models built, a model based on the Partial Least Squares Regression (PLS regression) was chosen as the best for predicting BRD4 BD1 potency. The curated dataset was split using a random split technique in which 20% of the dataset is randomly selected. The descriptor subset applied to the training dataset was ECFP_4, otherwise known as an extended-connectivity fingerprint.¹⁹⁶ Molecular fingerprints are collections of binary counts which encode the 2D or 3D features of molecules. Originally designed to assist in chemical database searching, they are now more commonly used for similarity searching or clustering.¹⁹⁷ As the binary counts are often of long lengths, they can encapsulate information on a wide range of structural or conformational features. The ECFP algorithm is an iterative process in which each atom in the molecule is initially assigned a numeric identifier.¹⁹⁶ This identifier contains information on at least six properties of an atom that do not depend on initial atom numbering. These properties include but are not limited to: the atomic number, the atomic mass, the atomic charge, the number of connections, the number of bonds to non-hydrogen atoms and the number of attached hydrogens. These values create an initial identifier, as exemplified in Figure 3.14, for each atom which is then converted to a binary value (0 or 1). Following this, the binary values for each atom are packed into a single 32-bit (or binary digit) integer value, where a maximum of 2^{32} numerical forms are possible (Figure 3.14).¹⁹⁶

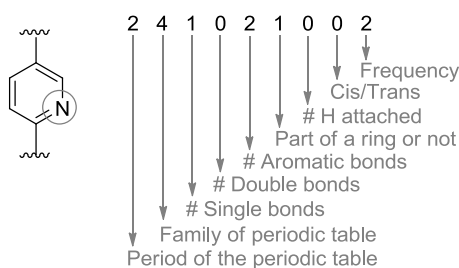


Figure 3.14. An example identifier based on a di-substituted pyridine ring. This identifier is then converted to a binary value of 0 or 1. The process is repeated on all atoms within the molecule and the resultant binary values packed together into a single 32-bit integer value.

Each successive iteration updates the existing identifier of each atom to reflect the identifiers of its neighbours, until all of the atoms have been disambiguated.¹⁹⁸ For example, the first iteration will look at the immediate neighbour, the second iteration will look at the neighbouring atom two bonds away and so forth. By doing this, each iteration builds up a picture of the functionality surrounding the atom (Figure 3.15).¹⁹⁸

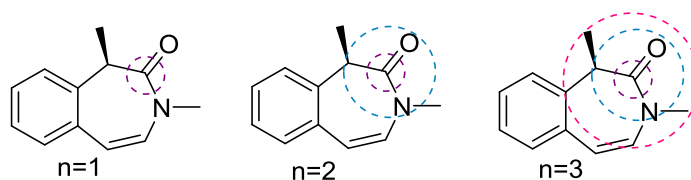


Figure 3.15. A binary identifier is generated for each atom within the molecule, exemplified above by the $n=1$ diameter around the carbonyl carbon, containing information properties such as the atomic number, the number of bonds to non-hydrogen atoms and the number of attached hydrogens etc. This identifier is then updated to reflect the identifier of the neighbours of the $n=2$ circle (blue). The newly generated identifier from this will then be updated to reflect the identifier of the neighbours on the $n=3$ radius (highlighted in pink). This process continues until a specified diameter is achieved and allows a picture to be built up of the functionality surrounding the atom in the $n=1$ diameter (purple).

Finally, duplicate binary digits (or bits) which represent the same feature or substructure are removed and the remaining bits transformed into a short fixed-length string (termed hashing). The hashing of the binary counts enables ECFPs to be rapidly calculated, whilst also containing a very large amount of information regarding structural and stereochemical features. It is the set of the resulting identifiers that defines the extended-connectivity fingerprint.¹⁹⁸

The machine learning algorithm employed was PLS regression. This technique generalises and combines features from multiple regression and principal component analysis.¹⁹⁹ However, whilst these methods search for the maximum variance between the response and independent variables, e.g. the biological activity and descriptor parameter terms in equation (2), PLS regression projects the predicted variables (x) and the observable variables (y) to a new dimension.¹⁹⁹ PLS is used to find the fundamental relationships between the two datasets, i.e. a latent variable (a variable that is not directly observed but is inferred from the observable variables).²⁰⁰ PLS regression models aim to identify the multidimensional direction in the X dataset that explains the maximum multidimensional variance direction in the Y dataset, thus accounting for the fact that several components may be contributing to the observed variable e.g. BRD4 BD1 potency is impacted by $\text{ChromLogD}_{7.4}$ and HBA count rather than just $\text{ChromLogD}_{7.4}$.²⁰⁰ PLS regression is particularly useful when the matrix of predictors (X matrix) has more variables than observations.

Validation of the model was completed by applying the model to the training dataset (183 compounds), after which it was used to predict the BRD4 BD1 potencies of the test dataset (46 compounds). A plot of the actual vs. predicted BRD4 BD1 $\text{pIC}_{50\text{s}}$ was generated for the test set (Figure 3.16).

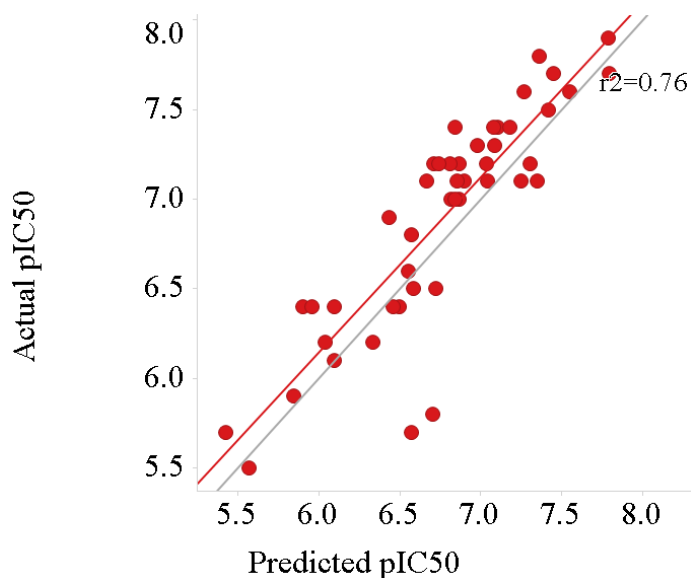


Figure 3.16. A plot of the actual vs. predicted BRD4 BD1 pIC₅₀s generated for the test set with the fitted regression line (red) and the y=x line (grey) plotted.

The plot indicates that the potencies in the test dataset are well predicted by the model, with a determination coefficient (R^2) = 0.76 and a root mean squared error (RMSE) = 0.33 observed. These values indicate that the model could be used to accurately predict the BRD4 BD1 potency of a novel compound. A structural interpretation of the QSAR was also completed. As previously mentioned, structural interpretation of a QSAR involves comparing the response gained from having a particular fragment present, across several molecules containing the same fragment. By doing this, it is possible to identify fragments which are key for potency, as well as those which are detrimental. This process is made easier by plotting the predicted response property (PRP), in this case predicted BRD4 BD1 potency, of the fragments. For a fragment to be considered, it must be present in at least 10 compounds which increases the reliability of the data. From the curated dataset, 25 fragments were plotted for both the highest PRP and lowest PRP. For the purpose of this thesis, only the top results for each model will be discussed (Figure 3.17).

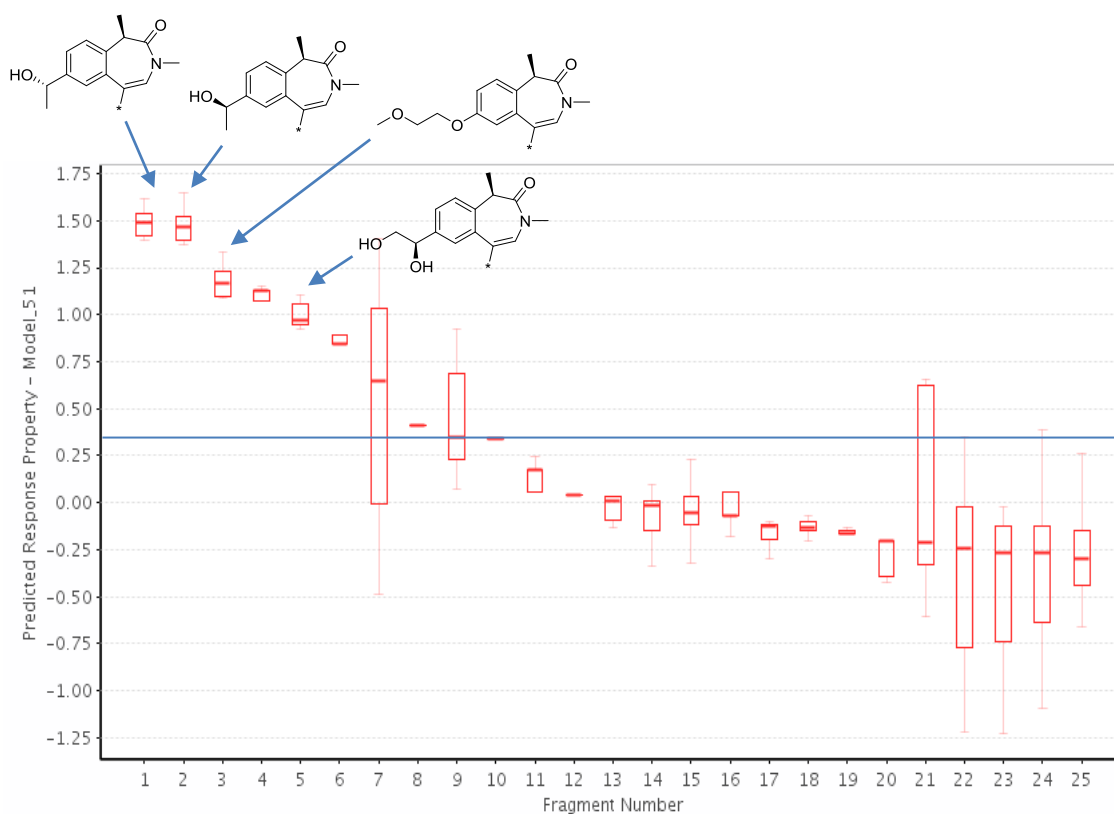


Figure 3.17. The structural interpretation of the BRD4 BD1 QSAR model with the line of significance ($\Delta pIC_{50} = 0.3$) and the structures of the fragments of interest highlighted. * is the attachment point to the molecules.

The resultant plot from the structural interpretation showed the PRP of 25 fragments. The error within biochemical assays is $\sim pIC_{50} = 0.3$, highlighted on the plot, and as such, PRP values above this were considered significant. As the curated dataset also contained BZP OTS compounds, some of the fragments displayed are related to that series. As such, only the fragments that were considered to contribute significantly to potency and corresponded to the BZP ZA sub-series have been highlighted. Pleasingly, the two fragments which were considered most potent were the enantiomers of the propan-2-ol shelf group which corroborates SAR observed thus far. Furthermore, a narrow range is observed for these box plots which shows that the presence of these fragments consistently resulted in high potency across all molecules that contained it. Furthermore, the diol has also been shown to demonstrate high potency (Table 3.13, *vide supra*) further supporting that the structural interpretation is consistent with known SAR.

3.3.2.1.5 QSAR modelling to build a predictive model for whole blood potency

The statistical analyses of the 80 models built revealed a model based on PLS regression to be the superior one for the whole blood potency QSAR modelling. This model utilised a clustering method (IndivClusters_80) to split the curated dataset into the training and test sets. The technique uses an algorithm to cluster compounds into subsets so that observations in each group are similar. It then allocates the group to either the training and test set until an approximate 80:20 ratio respectively is achieved. This technique resulted in a training set and test set of 156 and 67 compounds respectively. Following the creation of the training dataset, a functional-connectivity fingerprint (FCFP_4) descriptor subset was applied. This subset is an adaptation of the ECFP_4 set employed in the BRD4 BD1 model. As previously mentioned, the ECFP technique considers each atom individually and compares atomic properties, for example atomic number.²⁰¹ Whilst this has its advantages, it also means that atoms which are functionally similar in a drug-like molecule, e.g. a chlorine and bromine, are assigned different binary counts despite being functionally similar. This is accounted for in the FCFP-class fingerprint by swapping the atom characteristics for properties that relate to ligand binding, such as HBD count.²⁰¹ Finally, the PLS regression machine learning algorithm was applied and the model validated using the training set to afford the whole blood potency model. Following this, the model was used to predict the whole blood activities of the test set and the results compared to the actual data (Figure 3.18).

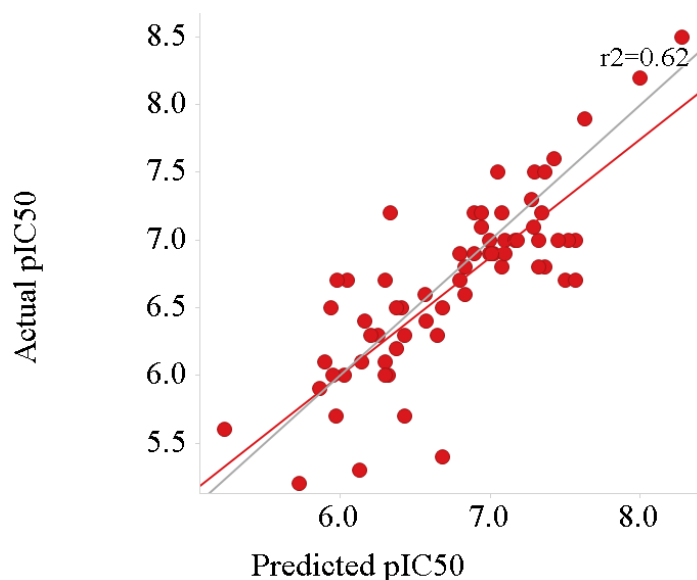


Figure 3.18. A plot of the actual vs. predicted whole blood pIC₅₀s generated for the test set along with the fitted regression line (red) and y=x line (grey).

The model for the whole blood potency was less accurate than the BD1 model when applied to the test data set, indicated by the poorer R^2 value of 0.62 and higher RMSE (0.43). However, based on these statistical parameters, although the model cannot be used to accurately predict whole blood potency, it could be used to rank compounds into predicted high, medium and low potencies. As such, the model could still be of value to the programme as it could assist in the prioritisation of targets. Similarly to the BRD4 BD1 model, a structural interpretation of the QSAR was completed using the ChemAxon fragmentation software (Figure 3.19).

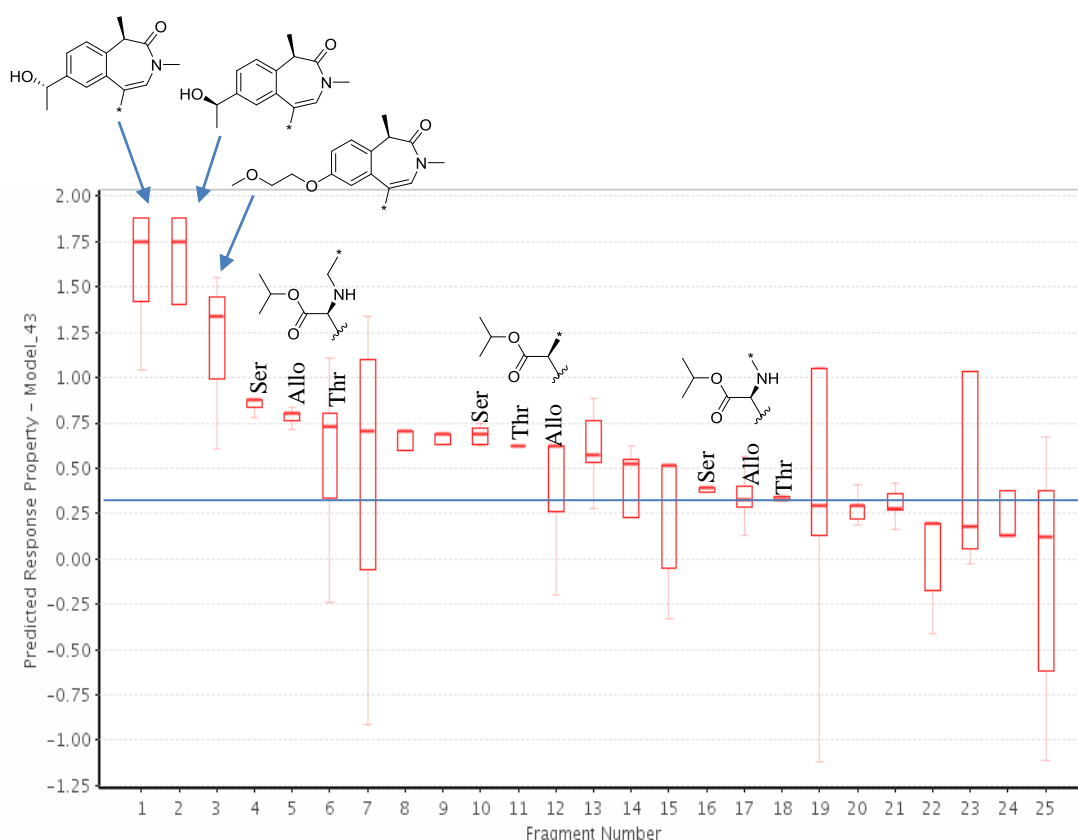


Figure 3.19. The structural interpretation of the whole blood QSAR model with the line of significance ($\Delta pIC_{50} = 0.3$) and the structures of the fragments of interest highlighted. * is the attachment point to the molecules.

Pleasingly, the top three fragments that were shown to increase whole blood activity were identical to those in the BRD4 BD1 model, further supporting the SAR observed in this thesis. However, more interestingly, the majority of the remaining fragments relate to amino acid ester fragments. The analysis indicated that the isopropyl Ser, *allo*-Thr and Thr ESMS, highlighted on the plot, were key for improving potency. This is an indicator that these

amino acid esters are being hydrolysed to the acid within the cell, leading to retention and increased activity. However, the lack of THF-Thr fragments suggested it does not positively impact the whole blood activity, thus implying slow CES-1 hydrolysis. This observation further supporting the SAR observed in this thesis in which the THF-Thr analogues consistently exhibit low ΔhWB values, whilst the isopropyl Thr analogues demonstrate ΔhWB desirable values.

3.3.2.1.6 QSAR modelling to build a predictive model for ΔhWB

Although a substantially smaller data set was used for the ΔhWB QSAR modelling than the BRD4 BD1 and whole blood models, pleasingly a model was developed. The dataset, consisting of 72 compounds, was ordered from the highest-lowest ΔhWB . It was then split into the training (80%) and test (20%) sets using a systematic method in which every 5th compound was selected for the test set. Unlike the other models, the optimal descriptors were physicochemical property based which included parameters such as HBA/HBD count, partial charges and number of Lipinski violations. Following this, a Random Forest machine learning algorithm was employed to perform the regression. This method is similar to a Decision Tree algorithm in that it utilises decision trees to model an end-point.²⁰² In the case of this model, the end-point is all compounds being split into groups of similar ΔhWB values. However, as an entire dataset is used to create a single decision tree, this method often results in overfitting and performs better with larger sample sizes.²⁰³ Random forest modelling is an ensemble approach and overcomes this by generating a large number of smaller decision trees on small subsets of the compounds and descriptors.²⁰² A single decision tree is considered to be a ‘weak learner’, however, a larger number of ‘weak learners’ can be used to generate a ‘strong learner’. In other words, increasing the number of decision trees improves the accuracy of the predicted outcome. The random subset is subjected to a series of questions which result in the dataset being split into two new nodes. At each node, a new question is asked which ultimately results in compounds being clustered together in similar groups.²⁰³ The decision tree in Figure 3.20 is a simplified exemplar of a decision tree.

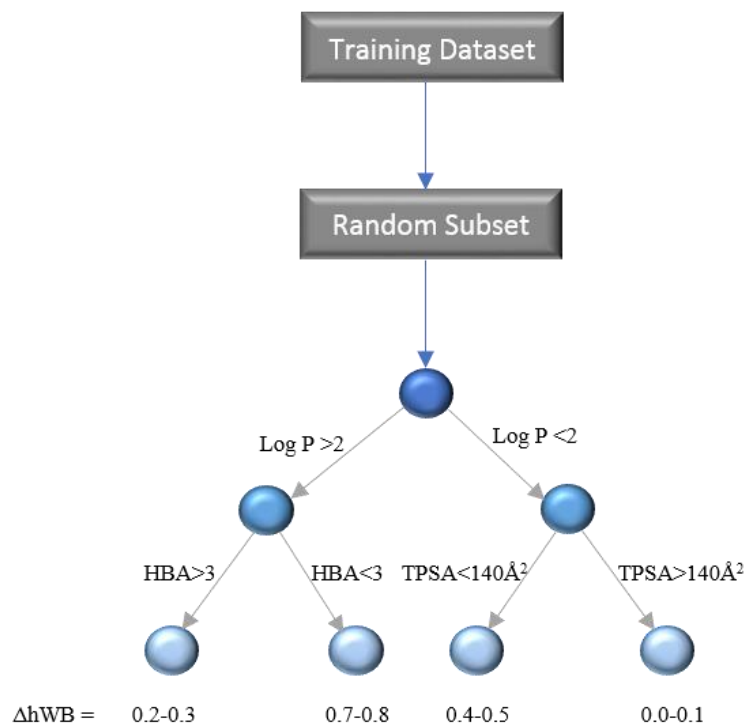


Figure 3.20. A simplified exemplar of a decision tree in which each node is split by the application of a parameter or question until an end-point is achieved.

The ΔhWB model was built such that 500 decision trees were generated based on small subsets of the training dataset. As a bagging ensemble method was employed, this resulted in 500 new training sets; one for each decision tree. Each new training set selects a sample of observations with replacement, termed bootstrap sampling, again from the original training dataset. Sampling with replacement means that observations may be repeated across the 500 training sets, thus increasing the accuracy of the outcome achieved when using the observation.²⁰³ With respect to this model, the observation is related to the physchem descriptors applied to the set e.g. number of rotatable bonds. At each node, \sqrt{D} predictor variables (where D = total number of descriptors) were randomly chosen and the split for each variable determined. The descriptor that resulted in the largest split, as well as the least variance in each subset following the split, was selected as the variable for that node. This process was repeated until the maximum depth level of 5 was achieved, after which the classifications of ΔhWB were formed. Finally, the model was validated with the full training set before it was used to predict the ΔhWB values of the test set. In order to do this, each compound of the test set was run through each of the 500 decision trees and the outcomes averaged to yield the final prediction. Following this, a plot of the actual vs. predicted ΔhWB values was created (Figure 3.21).

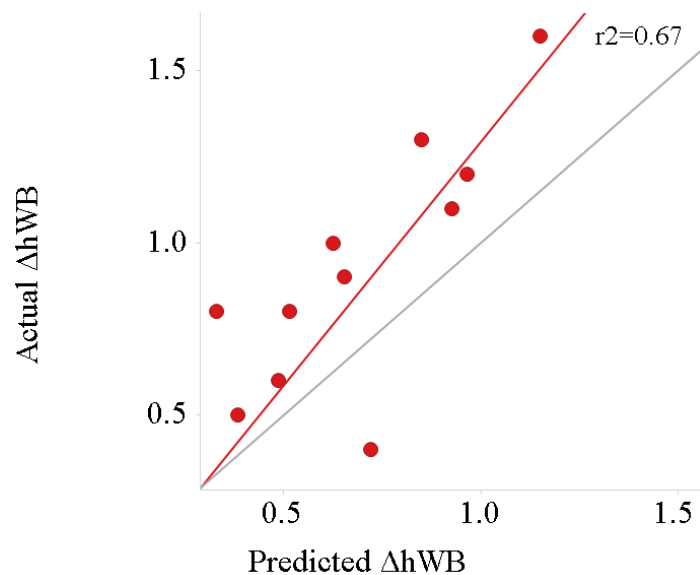


Figure 3.21. A plot of the actual vs. predicted ΔhWB values generated for the test set along with the fitted regression line (red) and the $y=x$ line (grey).

This model was the least predictive of all three models developed. Although statistically it is comparable to the whole blood model, with an $R^2 = 0.67$ and $RMSE = 0.30$, it can be seen by the plot that the fitted regression line lies significantly above the $y=x$ line. This shows that the model is underpredicting the ΔhWB values. However, similarly to the whole blood model, the statistical parameters suggest that the model could be used to predict whether novel compounds would have a high, medium or low ΔhWB . Finally, a structural interpretation was completed (Figure 3.22).

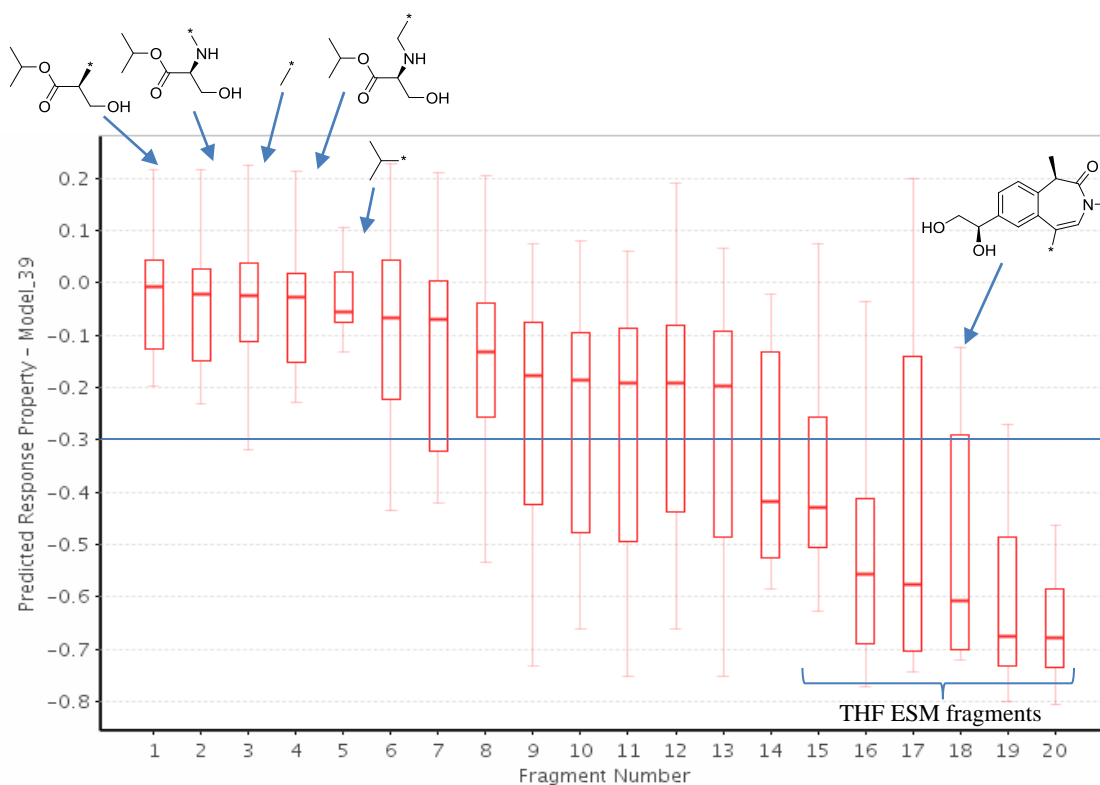


Figure 3.22. The structural interpretation of the ΔhWB QSAR model with the line of significance ($\Delta PRP = 0.3$) and the structures of the fragments of interest highlighted. * is the attachment point to the molecules.

Although the structural interpretation was completed in the same way, the plot differs for this model compared to the other two models. For this interpretation, the molecule with the highest ΔhWB (1.5) was selected as a reference compound. Rather than comparing the predicted potency gained/lost by a particular fragment, the predicted ΔhWB was compared instead. The predicted ΔhWB value was then compared to the reference compound. The difference in the two values is what forms the PRP axis for this model i.e. a value of -0.8 indicates the fragment resulted in a ΔhWB 0.8 log units lower than the reference compound. Pleasingly, this structural analysis is consistent with the observations in the whole blood model in that the isopropyl Ser ESM is key for high ΔhWB values. The analysis also showed that THF Thr ESM fragments caused the largest decrease in ΔhWB values relative to the reference compound. This supports the hypothesis that the THF Thr ESM is the least efficient ESM for increasing the ΔhWB and whole blood potencies, again suggesting it has low CES-1 turnover.

As part of the structural interpretation, various physicochemical properties were calculated and plotted for the fragments including TPSA, HBA and HBD count and Lipinski violations. This enabled the identification of any potential trends between the ΔhWB PRP in Figure

3.19 and particular physicochemical parameters. Of all the parameters investigated, only the TPSA plot suggested a possible trend (Figure 3.23).

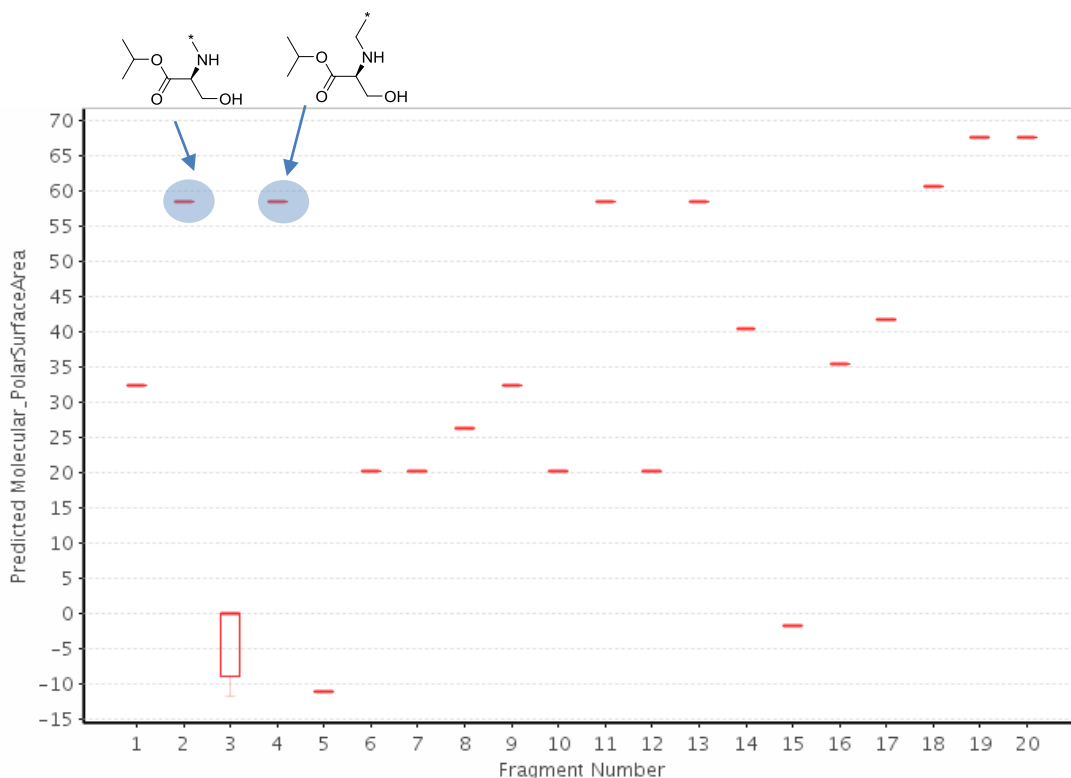


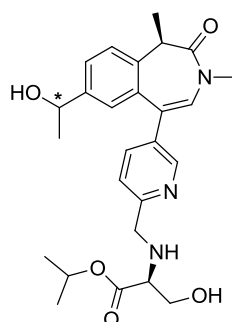
Figure 3.23. A plot of the TPSA produced during the structural interpretation of ΔhWB QSAR model with the structures of the fragments of interest highlighted. * is the attachment point to the molecules. The fragment numbers correspond to the same numbers in the PRP plot (Figure 3.22).

The fragment numbers of the TPSA plot correspond to the same fragments in the ΔhWB plot. Comparison of the plots show that fragments 2 and 4, highlighted on the plot, are isopropyl ESM fragments containing the NH. This results in the fragments having a high TPSA and, as such, should be considered as outliers. This reveals a negative correlation between TPSA and ΔhWB , with high TPSA causing low ΔhWB values. Pleasingly, this corroborates previous analyses, *vide supra*, which resulted in the desired profile of the molecules changing from TPSA $<140\text{\AA}^2$ to TPSA $<130\text{\AA}^2$. As previously discussed, this is thought to be due to the higher TPSA reducing the permeability of the THF Thr ESM across the cell membrane. Consequently, there could be a lower concentration of a THF Thr analogue relative to its corresponding isopropyl Thr analogue. As such, even if the CES-1 turnover was identical for the two compounds, which the CES-1 energetic studies suggest isn't the case, there would be a lower concentration of retained acid of the THF-Thr

compound thus resulting in a lower whole blood potency and ΔhWB . In conclusion, the CES-1 dockings and the QSAR modelling both suggest that the isopropyl ester ESMs are preferred over the THF Thr ESMs due to the energetics involved with the THF binding and the increased TPSA. The *in silico* modelling for the first-generation analogues show the compounds have TPSA $>130\text{\AA}^2$. As this resulted in poor permeability and low ΔhWB values, future compounds will be designed to have a TPSA $<130\text{\AA}^2$.

3.3.2.2 Third generation analogues with a 2,4-disubstituted pyridyl as the ZA channel group

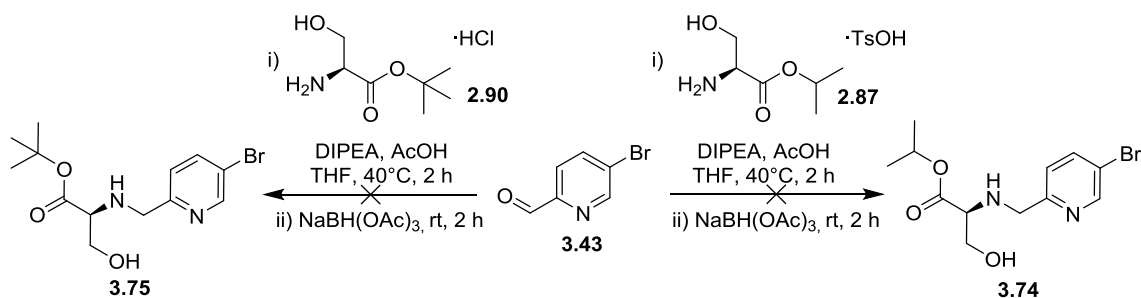
As demonstrated by the second generation pyridyl analogues, the isopropyl ester exhibited increased turnover by CES-1, as shown by the larger ΔhWB values in Table 3.10 and the QSAR modelling. Therefore, it was desired to incorporate this as the amino acid ester in the third-generation analogues with the hypothesis that truncating the isopropyl Thr to the isopropyl Ser would reduce the lipophilicity whilst maintaining the advantageous ΔhWB values. This was supported by the lower ChromLogD_{7.4} values calculated in the *in silico* analysis (Table 3.11).



Configuration at *	(S)	(R)
	3.72	3.73
TPSA	112	112
ChromLogD _{7.4}	3.4	3.4

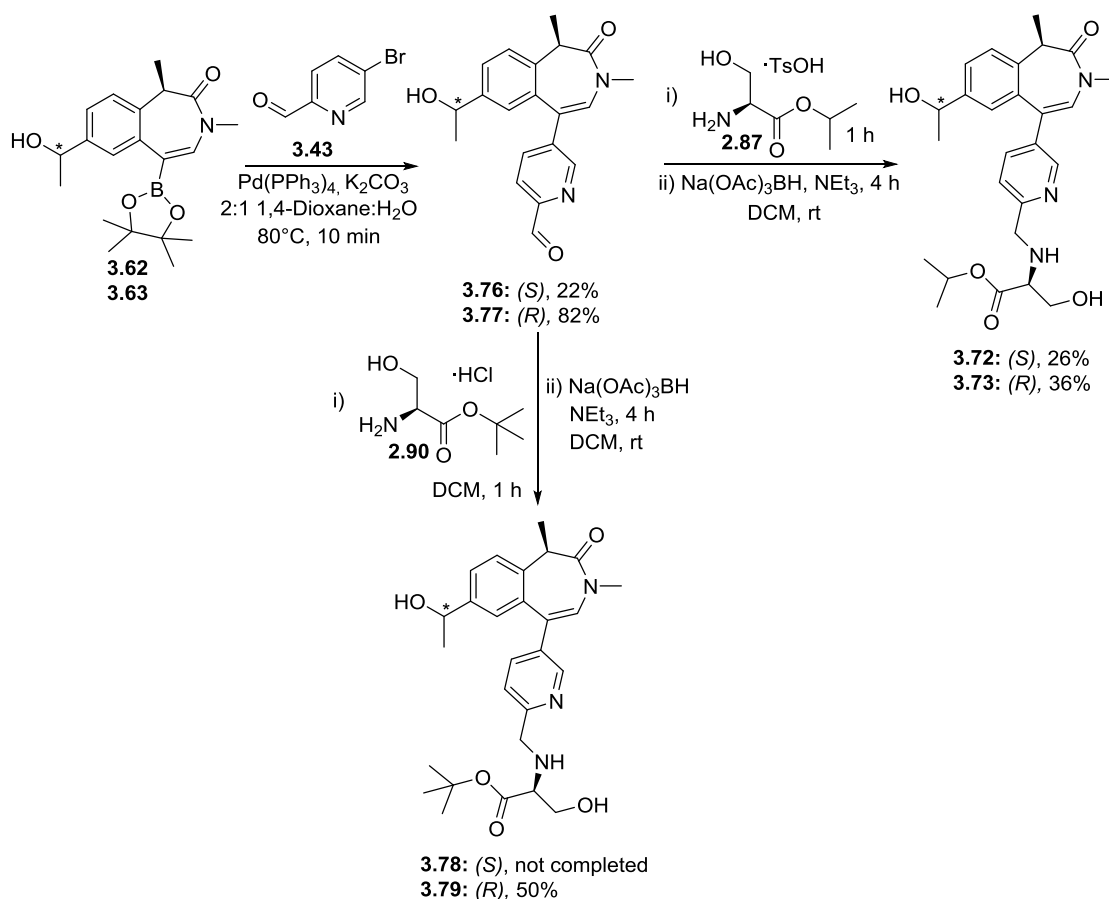
Table 3.11. *In silico* modelling of the third generation pyridyl analogues.

Due to the subtle change from the isopropyl Thr analogues, it was thought that the isopropyl Ser analogues could be synthesised by the same route employed in Scheme 3.10. The first step of the synthesis was the reductive aminations of aldehyde **3.43** and amino acid esters **2.87** and **2.90** to form the isopropyl and *tert*-butyl Ser intermediates **3.74** and **3.75** respectively (Scheme 3.11).



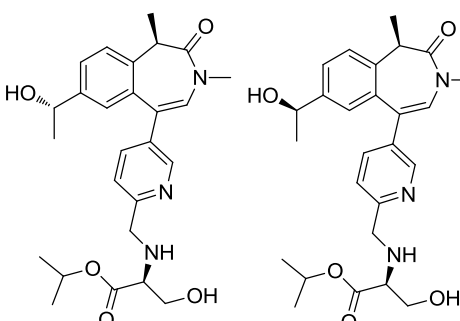
Scheme 3.11. Attempted reductive aminations to access the serine intermediates. Different salt forms of the amino acid esters were used based on availability of the reagents.

Interestingly, the reaction conditions employed to afford the isopropyl Thr analogue **3.71** (Scheme 3.10, *vide supra*) did not result in conversion to the product when applied to the Ser intermediates. Instead, LCMS analysis indicated high conversion to an unknown side product with no product observed. Therefore, the steps were reversed, so that the reductive amination was performed as the last stage, and different reaction conditions employed (Scheme 3.12).



Scheme 3.12. Synthetic route to the third-generation pyridine analogues. The (S) and (R) terminology refers to the stereochemistry at the stereogenic centre depicted by *.

The first step of the synthetic route was the Suzuki cross-coupling of the boronic esters **3.62** and **3.63** and pyridine **3.43** to afford the intermediates **3.76** and **3.77**, with **3.77** being isolated in high yields. The poor yield of **3.76** was due to a machine error during MDAP purification. Unfortunately, this only provided enough material to perform the reductive amination with the isopropyl Ser amino acid ester to afford the desired analogue **3.72**. Consequently, the *tert*-butyl analogue **3.78** was not synthesised at this stage. Fortunately, intermediate **3.77** was isolated in high yield, allowing both the isopropyl and *tert*-butyl Ser analogues **3.73** and **3.79** to be obtained in moderate yields following the reductive aminations of **3.77** with the respective amino acid esters. The desired isopropyl Ser analogues and their respective biologically non-hydrolysable *tert*-butyl analogues were submitted for biological testing (Table 3.12).



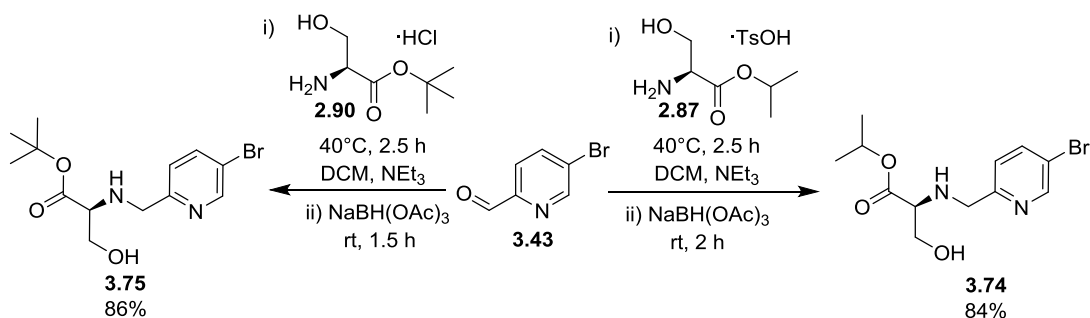
	3.72	3.73
hWB pIC ₅₀	7.8	7.7
Δ hWB pIC ₅₀	+1.1	+0.8
Ester BD1 pIC ₅₀	7.2	7.2
HLM IVC (+/- benzil)	0.7 / 1.0	2.1 / 2.7
Hu Heps IVC (LBF)	2.5 (78%)	-
Cyno Heps IVC (LBF)	<0.89 (38%)	1.8 (55%)
ChromLogD _{7.4}	3.1	2.9

Table 3.12. Biological profiles of the third-generation pyridine analogues. IVC values are quoted in mL/min/g.

As hypothesised the compounds have reduced lipophilicities relative to their isopropyl Thr analogues. Although not synthesised originally, route development (Scheme 3.14, *vide infra*) allowed the *tert*-butyl analogue **3.78** to be made, thus allowing the ΔhWB to be determined. The analogues exhibit desirable ΔhWB values and cellular and biochemical potency. Interestingly, there is a significant difference between the HLM IVC of the two diastereomers with the stereoisomer with (*S*)-configuration at the 2-propanol group, **3.72**, demonstrating improved an HLM IVC profile relative to the stereoisomer with (*R*)-

configuration at the 2-propanol group **3.73**. This difference is also observed with the THF Thr analogues **3.38** and **3.39**, thus suggesting that the (*S*)-configuration of the 2-propanol is inherently more metabolically stable than the (*R*)-configuration. This is further exemplified by the increased cynomolgus monkey hepatocyte clearance of **3.73** relative to **3.72**, for which the compound was not progressed further. On the other hand, **3.72** displayed desirable cynomolgus monkey hepatocyte IVC and was progressed into human hepatocyte assays. Unfortunately, the compound exhibited higher human hepatocyte clearance than anticipated but, due to its other favourable properties, it was selected for further profiling (section 3.3.4, *vide infra*).

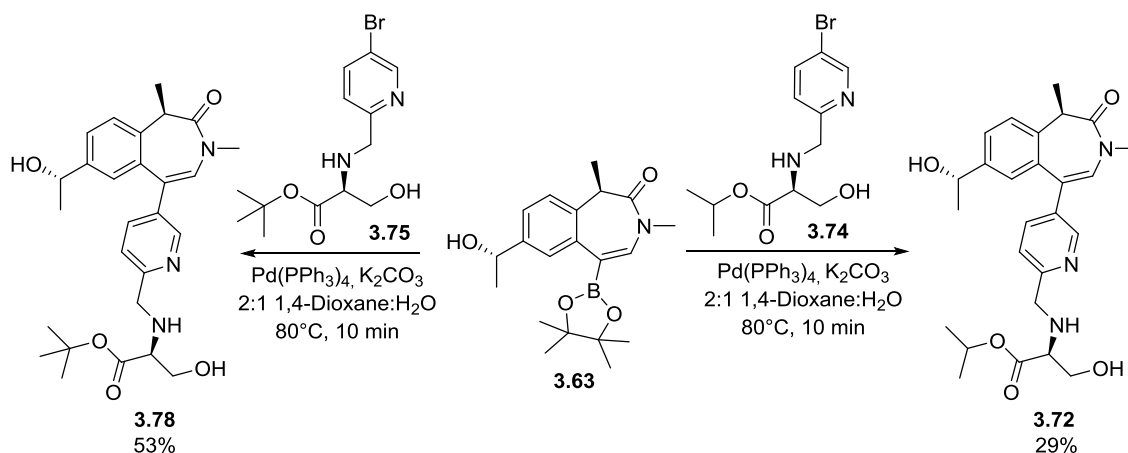
In order to facilitate further studies, a larger quantity of **3.72** was required. The BZP triflate building block **3.58** is synthesised from an 8-step synthetic route and was not readily available. Furthermore, due to the achiral ketone reduction, half of the material is lost during separation of the enantiomers. These combined factors meant a convergent synthetic route was desired as opposed to the linear route previously used (Scheme 3.12). As such, the reductive amination of aldehyde **3.43** and amino acid esters **2.87** and **2.90** was investigated further. In the first instance, the reaction conditions employed in Scheme 3.11 were simplified by removing acetic acid and exchanging THF for DCM (Scheme 3.13).



Scheme 3.13. Simplified reductive amination conditions to access the serine intermediates. Different salt forms were used based on availability of the reagents.

These reaction conditions resulted in high conversion to the imine, which was not seen with the original reactions (Scheme 3.11). Furthermore, upon addition of the reducing agent, complete conversion to the products **3.74** and **3.75** were observed for both the isopropyl Ser and *tert*-butyl Ser amino acid esters, **2.87** and **2.90** respectively. As such, the intermediates were obtained in high purity, negating the need for purification. In addition to this, the yields are increased relative to those obtained in the original synthesis towards the final target **3.72** (Scheme 3.10). These improved conditions meant the same convergent synthetic route used

to access the isopropyl Thr analogues (Scheme 3.10) could be employed. Therefore, the next step of the synthesis was the Suzuki cross-coupling of the intermediates **3.74** and **3.75** with boronic ester **3.63** (Scheme 3.14).



Scheme 3.14. Suzuki cross-couplings to access the serine analogues.

Despite high conversions by LCMS to the desired products (>80%), only low to moderate yields were obtained. This is consistent with yields obtained across this series for reactions involving ESM containing molecules and, as high conversions are observed, it is likely attributable to issues at the purification stage.

3.3.2.3 Fourth generation analogues with a 2,4-disubstituted pyridyl as the ZA channel group

As previously mentioned, the third generation analogue **3.72** exhibited a desirable profile except for the high human hepatocyte clearance. Consequently, it was hypothesised that exchanging the shelf group for other moieties, whilst retaining the pyridine ZA channel group and isopropyl Ser ESM, could result in a molecule with a similar profile to **3.72** but with improved hepatic stability. Therefore, it was decided to select a larger range of shelf groups in an attempt to identify a molecule with desirable human hepatocyte IVC. At the beginning of this project, a plot of the human hepatocyte IVC vs. human whole blood potency was generated, based on all of the pan-BET analogues previously synthesised (Figure 3.8). A remining of this data set identified three shelf groups that had not been previously investigated on the pyrazole sub-series due to unfavourable *in silico* data (Figure 3.24).

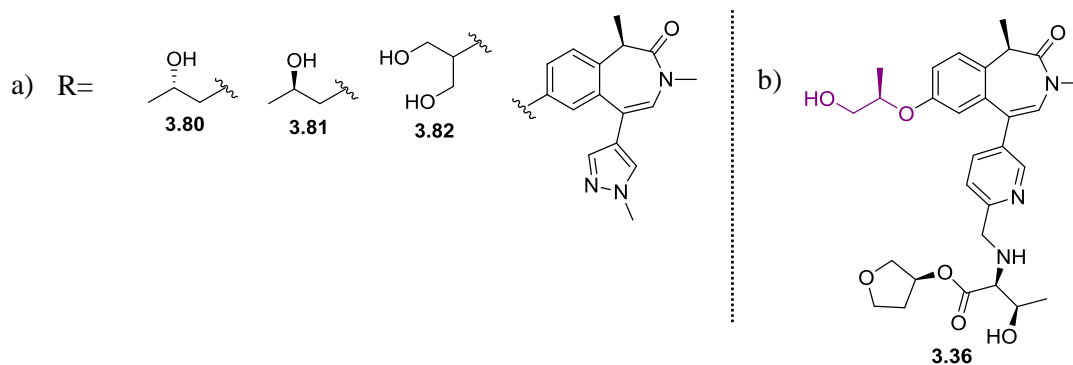
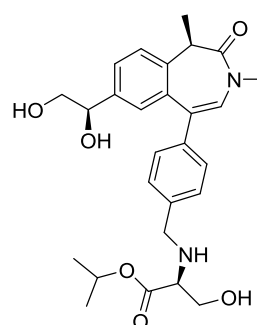


Figure 3.24. a) Three further shelf groups were identified from the remaining of SAR on the pan-BET *N*-methyl pyrazole series (Figure 3.8, *vide supra*); the monoalcohols **3.80** and **3.81** and the symmetrical diol **3.82**. b) The shelf group explored in the first-generation compound **3.36** (purple) exhibited a favourable profile except for a low Δ hWB, which was thought could be increased by the isopropyl Ser or THF *allo*-Thr ESMs.

In addition to these groups, due to the favourable profile displayed by **3.36**, this shelf group was selected. Furthermore, elsewhere in the team the 1,2-dihydroxyethyl group, also present on the aforementioned plot, had already been extensively explored and the lead molecule **3.83** with a desirable profile identified (Table 3.13).



	3.83
hWB pIC ₅₀	7.7
Δ hWB pIC ₅₀	1.1
Ester BD1 pIC ₅₀	7.0
HLM IVC (+/- benzil)	0.8 / 1.0
Hu Heps IVC (LBF)	1.3 (64%)
Cyno Heps IVC (LBF)	0.9 (38%)
AMP (nm / s)	30
ChromLogD _{7.4}	3.1

Table 3.13. Biological profile of the lead 1,2-dihydroxyethyl molecule **3.83**. IVC values are quoted in mL/min/g.

Although the compound displayed a desirable profile, it suffered from poor permeability and, therefore, the hepatocyte IVC may be artificially low. In an attempt to understand what may be driving the low permeability, a plot of the artificial membrane permeability versus the number of hydrogen bond acceptors was created. This was based on all of the existing molecules from the pan-BET series, all of which were used to generate the initial human hepatocyte clearance versus ChromLogD_{7.4} plot at the start of working on the series (Figure 3.8, *vide supra*) (Figure 3.25).

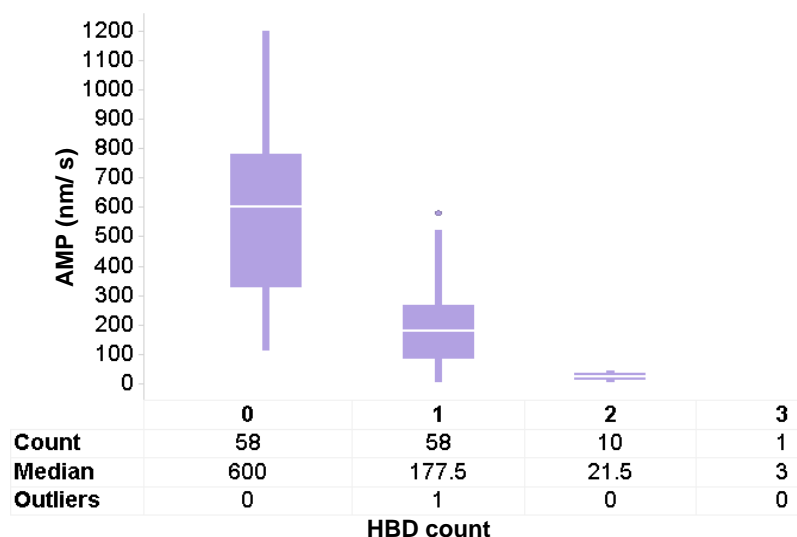
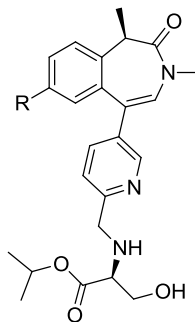


Figure 3.25. A box plot of the artificial membrane permeability versus the number of hydrogen bond acceptors for molecules belonging to the pan-BET series. Increased permeability, which is desirable, was observed for compounds with a lower HBD count.

As expected, the plot shows a negative correlation between the number of hydrogen bond donors and AMP. As such, it was hypothesised that reducing the number of hydrogen bond donors in the lead diol molecule would improve the permeability. As the isopropyl ESM has been shown to be optimal for potency and CES-1 turnover, it was decided to remove a hydrogen bond donor by methylating one hydroxyl group of the diol. As the diol is asymmetrical, both methylated products were deemed interesting shelf groups.

Altogether five alternative shelf groups were identified to expand on SAR gathered on the third generation pyridyl analogues (Table 3.14.)



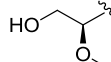
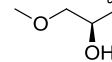
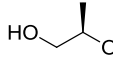
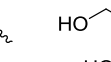
						
	3.84	3.85	3.86	3.87	3.88	3.89
ChromLogD _{7.4}	3.9	3.9	3.7	3.5	4.2	3.4
TPSA	112	112	121	121	121	132

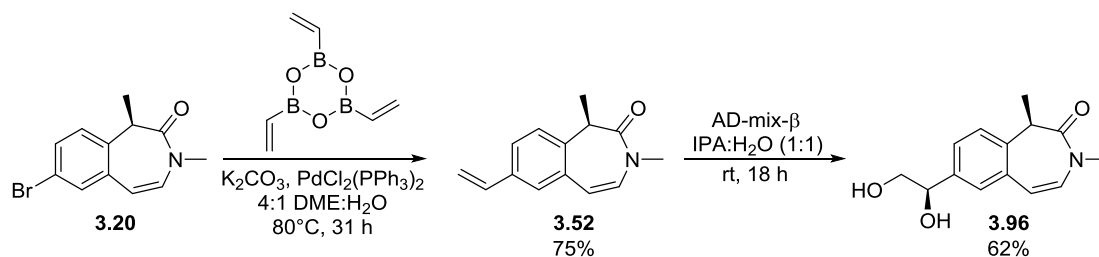
Table 3.14. The *in silico* data for the various WPF shelf groups with pyridine as the ZA channel group and the isopropyl Ser ESM.

As aforementioned, the measured ChromLogD_{7.4} of analogues belonging to this series is typically 0.5-1 log units lower than the calculated ChromLogD_{7.4} (Figure 3.9). Therefore, although some of the compounds were predicted to be highly lipophilic, it was hypothesised that the measured lipophilicity would be within the desired range. Compounds **3.85**, **3.88** and **3.89** were synthesised by a colleague within the team.

As only the shelf group has been altered, the convergent synthetic route shown in Scheme 3.4 can be applied to analogues **3.84**, **3.86** and **3.87**. Furthermore, as the pyridine-ESM intermediate **3.74** had already been produced (Scheme 3.13, *vide supra*), only the boronic ester counterparts had to be synthesised. It was also decided to prioritise the synthesis of the biologically hydrolysable esters and return to the synthesis of their respective *tert*-butyl analogues if the biological data demonstrated was of interest.

Compound **3.84** was synthesised first as the synthetic route also provided the intermediate required for analogue **3.85** (Scheme 3.15).

To allow diversity at a later stage, it was decided that analogues **3.86** and **3.87** would be synthesised from the selective methylation of diol **3.96** (Scheme 3.16).



Scheme 3.16. Synthesis of the diol intermediate **3.96**.

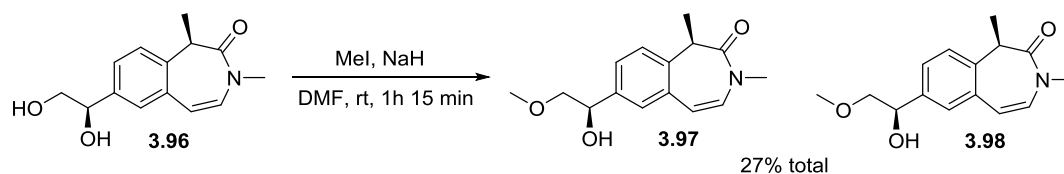
The first step of the synthesis was the Suzuki-Miyaura cross-coupling reaction of starting material **3.20** and vinylboronic anhydride to install the terminal alkene of intermediate **3.52**. The asymmetric dihydroxylation was achieved with AD-mix- β to selectively afford the desired diastereomer in moderate yield. As this reaction had been previously completed by a colleague and shown to be the diastereomer containing the (*R*)-configuration of the diol, it was assumed that this intermediate had the correct stereochemistry and was not tested for a diastereomeric excess (d.e). However, the two diastereomers are distinguishable by NMR and the diastereomer with the (*S*)-configuration of the diol was not present in the NMR of intermediate **3.96**, thus supporting that the asymmetric dihydroxylation selectively formed the desired diastereomer **3.96** (Appendix 5). Next, the selective methylation of the diol was attempted. Due to more literature precedence, albeit still limited, for the selective methylation of primary alcohols over secondary alcohols, it was decided to focus on the primary alcohol first. A range of reaction conditions were attempted. The conversion was estimated by the UV area/area observed by LCMS. As previously discussed, it is not an accurate measurement of conversion but rather a qualitative method to provide an idea of whether a low, moderate or high conversion was achieved on intermediate **3.52** (Table 3.15).



Entry	Conditions	Conversion (a/a%)
1	PhB(OH) ₂ , K ₂ CO ₃ , MeI, DMF, 48 h, 60°C	16
2	Ag ₂ CO ₃ , MeI, toluene, 48 h, 60°C	6
3	Fe(ClO ₄) ₃ ·H ₂ O, MeI, DCM, 21 h, rt	3

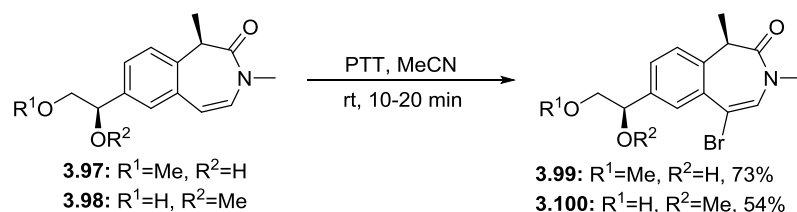
Table 3.15. Conversion (%) was estimated by the UV area/area observed by LCMS.

Although all three sets of literature conditions described high yielding reactions, only low conversions to intermediate **3.97** were observed. As there was less literature precedent for the methylation of the secondary alcohol, and attempts on the primary alcohol were unsuccessful, it was deemed unlikely that selective methylation would be achievable. Therefore, it was decided to attempt a classical methylation (Scheme 3.17).



Scheme 3.17. Methylation of the diol to the mono-ethers.

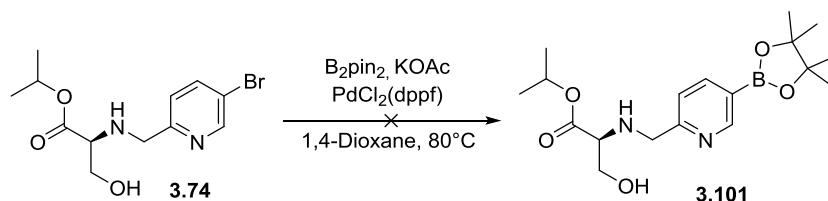
The methylation provided a mixture of both methylated alcohols in low yield which is due to the dimethylated diol also being formed. However, the regioisomers were separable by flash column chromatography employing a chiral stationary phase and intermediates **3.97** and **3.98** were obtained. Again, although the d.e. of these intermediates were not determined following the methylation, the undesired diastereomer containing the (*S*)-configuration of the diol is typically distinguishable by NMR and was not observed in the NMR. Furthermore, only two peaks were observed during the chiral analysis and subsequent purification, one per regioisomer, thus suggesting that epimerisation of the stereocentre had not occurred. The next step of the synthesis was the bromination of the intermediates (Scheme 3.18).



Scheme 3.18. Bromination of intermediates **3.97** and **3.98**.

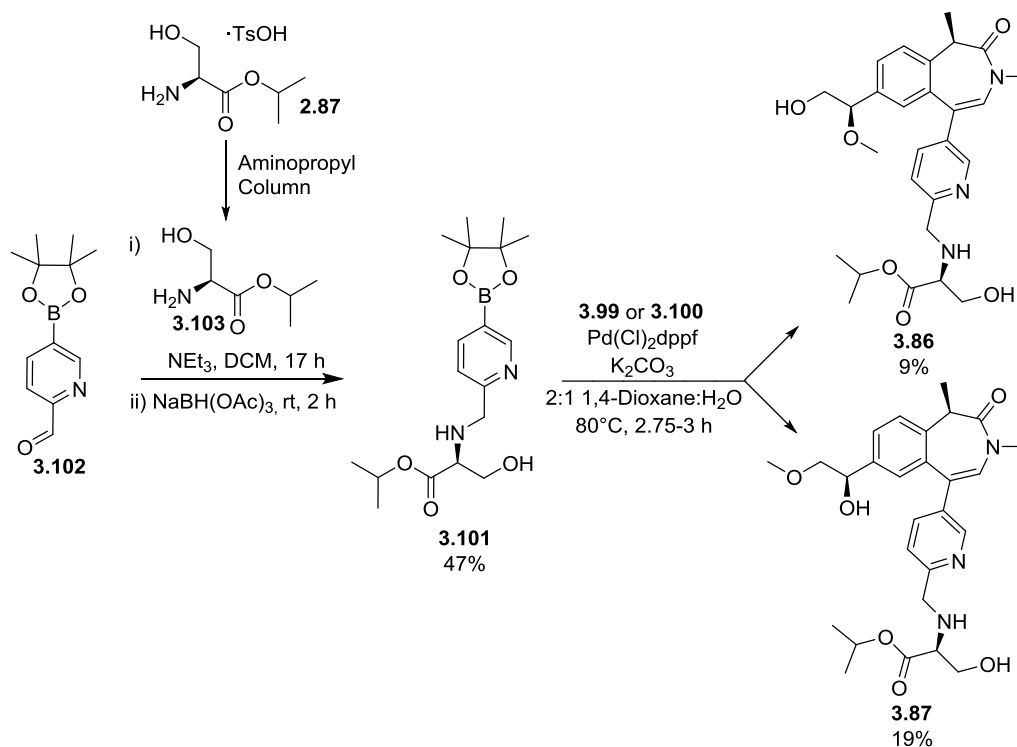
The brominations were achieved using PTT to afford the intermediates **3.99** and **3.100**. Despite high conversions by LCMS analysis (>95%) to the desired intermediates, they were only obtained in moderate-high yields. As the high conversions and clean profiles meant purifications were not required, it can be assumed that the material was lost during the work up stage. Unfortunately, these yields meant that there was an insufficient amount of material to borylate to form the boronic esters. Instead, it was decided to borylate intermediate **3.74**

and then perform the Suzuki-Miyaura cross coupling with intermediates **3.99** and **3.100** (Scheme 3.19).



Scheme 3.19. Attempted borylation of intermediate **3.74**.

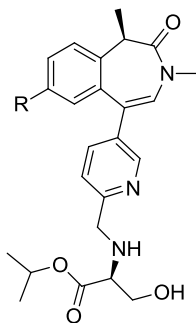
However, when attempted, low conversions to the borylated product **3.101** were observed by LCMS analysis and instead a multitude of side products were seen. Therefore, in an alternative approach, the borylated intermediate **3.101** was formed through the reductive amination of aldehyde **3.102** and the free base of the isopropyl Ser amino acid ester **2.87**, **3.103** (Scheme 3.20). Subsequent reaction with intermediates **3.99** and **3.100** gave the desired analogues **3.86** and **3.87**.



Scheme 3.20. Synthesis of the final compounds **3.86** and **3.87**.

Initial attempts at the reductive amination utilising the isopropyl Ser ESM **2.87** were low yielding due to the partial conversion of the boronic ester to the boronic acid during the reaction making its isolation difficult. As such, the amino acid ester was desalted using an aminopropyl ion exchange column to afford **3.103** prior to the reaction. The reductive amination was completed using the simplified reaction conditions employed in Scheme 3.13, to afford the desired intermediate **3.101** in moderate yield. Finally, the Suzuki-Miyaura cross-couplings of boronic ester **3.101** with the bromide intermediates **3.100** and **3.99** afforded the desired products **3.86** and **3.87** respectively. Similarly to other analogues in this series, despite high conversion to the desired products, as observed by LCMS analysis, poor yields were obtained following purification. Unfortunately, at this stage it was discovered through chiral analysis that the stereogenic centre of the isopropyl Ser ESM of **3.86** and **3.87** was racemic and, as such, the compound could not be progressed further than the whole blood assay. On further inspection of the NMR of these compounds, duplication of the doublets corresponding to the protons α to the ESM NH can be seen. Although the duplicated doublets overlap, integrating one peak of each doublet was found to result in a similar ratio (51:49) of the L- and D-Ser that was observed by chiral analysis (Appendix 6). Therefore, this was thought to be a suitable method for estimating the proportion of D-Ser present in samples. Using this technique, it was found that partial racemisation was also observed in **3.84**, which has already been submitted for the hWB assay (Appendix 7). Therefore, it was decided to use await the data before deciding whether to remake the analogue (Table 3.16).

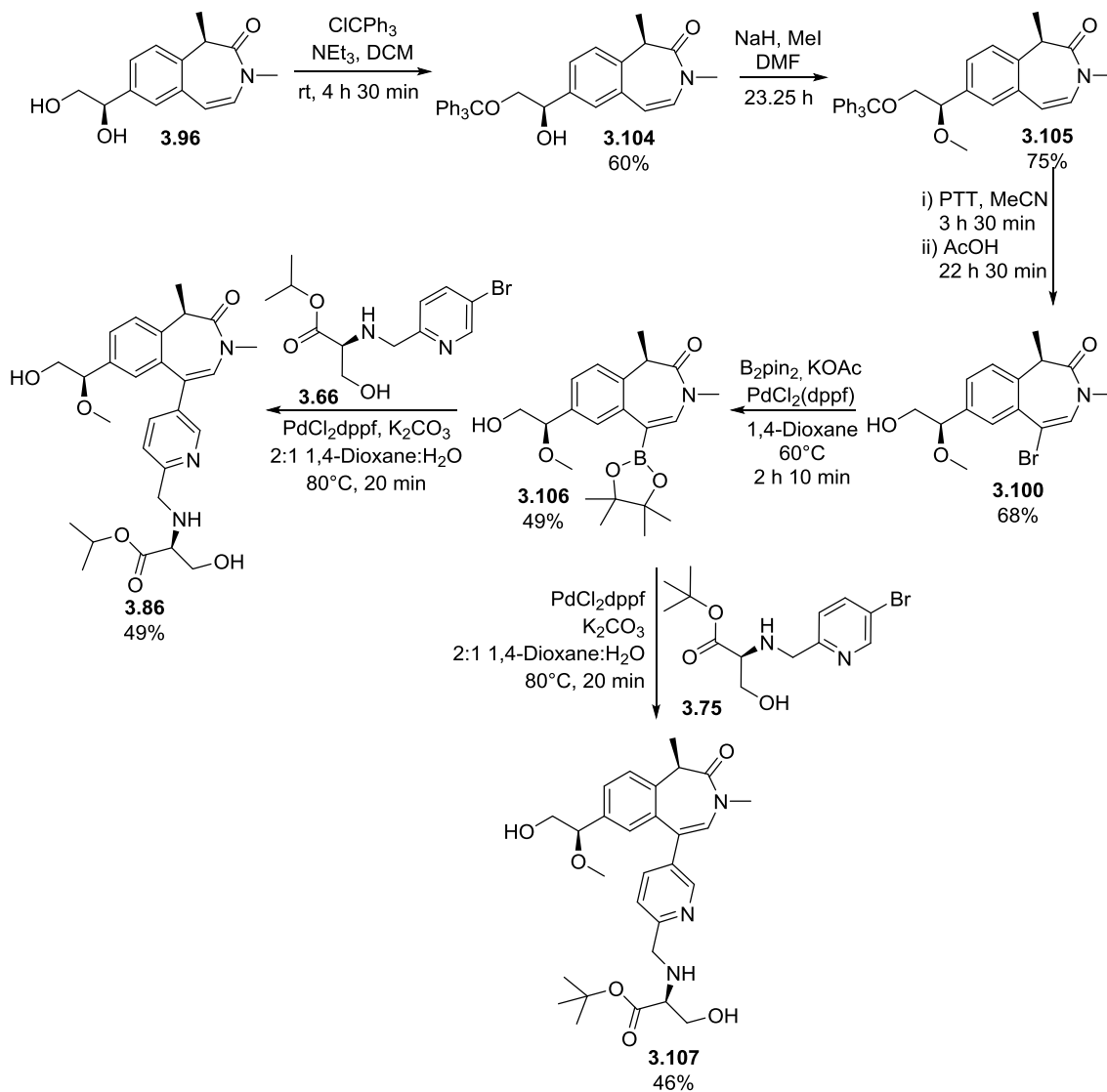
At this stage of the project, most compounds were demonstrating low HLM and hepatocyte IVC and therefore, the +/- benzil data was typically not being used to make decisions on the compounds. Therefore, it was decided to only submit compounds for the HLM (- benzil) assay due to its higher throughput and quicker turnaround times. As such, most compounds from here on will only have HLM (- benzil) data.



R						
	3.84	3.85	3.86	3.87	3.88	3.89
hWB pIC ₅₀	7.1	7.0	7.9	7.5	7.6	5.8
Ester BD1 pIC ₅₀	6.7	6.6	7.3	7.0	7.2	6.5
HLM IVC	-	-	-	-	2.4	-
Cyno Heps IVC (LBF)	-	-	-	-	<0.89 (<38%)	-
ChromLogD _{7.4}	3.2	3.2	2.8	3.0	3.1	2.1

Table 3.16. Biological profiles of the fourth generation pyridyl compounds. Analogues **3.86** and **3.87** are racemic at the * stereogenic centre of the ESM.

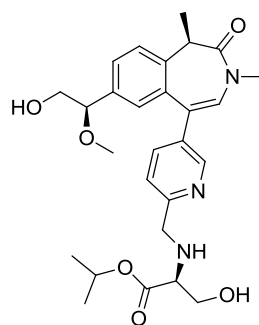
Interestingly, although the 1-hydroxypropan-2-ol and symmetrical diol shelf groups exhibited high whole blood potency in the pan-BET series, this did not translate into the BZP-ZA series with analogues **3.84**, **3.85** and **3.89** demonstrating low activity. Therefore, these compounds were not progressed into IVC studies and, as such, it was decided to not resynthesise **3.84**. Analogue **3.88** also exhibited desirable biochemical, whole blood potency and lipophilicity. Therefore, it was progressed into HLM and cynomolgus monkey hepatocyte IVC in parallel. Although the HLM IVC was too high, methylating the previous lead diol compound (Table 3.13, *vide supra*) increased the whole blood potency as observed in analogue **3.86**. Unfortunately, the material could not be investigated further due to the racemic centre. As such, the compound was resynthesised to facilitate its progression. As only **3.86** was of interest, the synthetic route was adapted so that chiral separation of the intermediates **3.97** and **3.98** could be avoided (Scheme 3.21).



Scheme 3.21. Alternative synthetic route to **3.86**.

As the secondary methyl ether was desired, the reactivity of the primary versus secondary alcohol could be taken advantage of in order to achieve the desired regiochemistry. Protection of the diol should be highly selective for the primary alcohol due to reduced steric hindrance. When this was attempted with a TBS protecting group, only an 80:20 primary:secondary protection ratio was observed. Therefore, the trityl group, which is more sterically hindered and often employed in carbohydrate chemistry, was attempted. This afforded **3.104** with only minor conversion to the protected secondary alcohol, which was separable by normal phase column chromatography. Subsequent methylation yielded **3.105** which was then brominated to give **3.100**. Borylation of this intermediate afforded **3.106** in a moderate yield. Finally, the Suzuki-Miyaura cross-couplings with the respective ESM-containing intermediates yielded the desired target **3.86** and its respective biologically non-hydrolysable analogue **3.107**.

The compound was submitted for further profiling (Table 3.17).



	3.86
hWB pIC ₅₀	7.3
Ester BD1 pIC ₅₀	6.8
HLM IVC	0.6
Hu Heps IVC (LBF)	0.8 (54%)
Cyno Heps IVC (LBF)	<0.89 (<38%)
ChromLogD _{7.4}	2.8

Table 3.17. Biological profile of **3.86**. IVC is measured in mL/min/g.

The compound exhibited excellent HLM and hepatocyte IVC and a desirable lipophilicity. Unfortunately, the compound demonstrated much lower potency relative to the racemised analogue, which displayed high potency (Table 3.16) and therefore further profiling was not carried out.

However, overall, from the investigations into using a pyridine as the ZA channel group, two lead molecules were developed and were of high interest to the programme. Therefore, they were progressed into late stage studies (*vide infra*).

3.3.3 Investigating diazines as the ZA channel group

As an alternative approach to reducing the IVC of the second generation analogues through lowering the lipophilicity by truncating the ESM, it was hypothesised that exchanging the pyridine for diazines would improve the IVC by reducing the electron density and also blocking a potential metabolic hotspot (Figure 3.26). The addition of the extra heteroatom was hypothesised to have an added benefit of reducing the lipophilicity of the compounds.

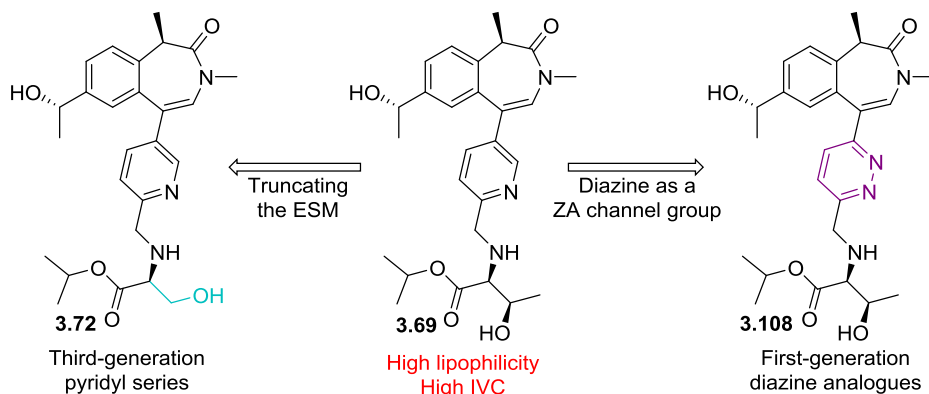
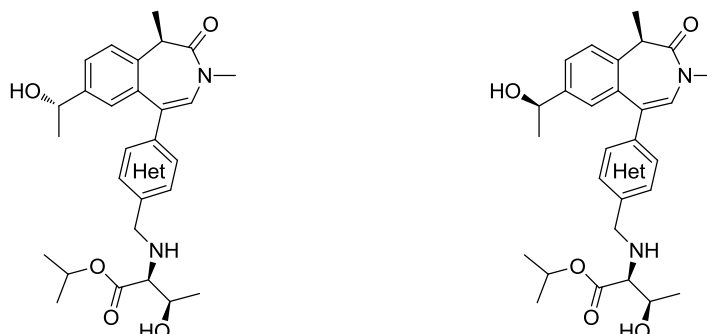


Figure 3.26. Reducing the high IVC of the second-generation compounds by truncating the isopropyl Thr ESM to the isopropyl Ser ESM (blue) and lowering lipophilicity, e.g. converting **3.69** to **3.72**, has already been investigated. An alternative approach is to incorporate a diazine as the ZA channel group (purple) rather than a pyridyl, such as the first-generation diazine analogue **3.108**, to reduce the electron density of the ring and blocking another potential metabolic hotspot.

Therefore, it was decided to investigate all four diazine rings and *in silico* modelling of the diazine-containing molecules was completed (Table 3.18).



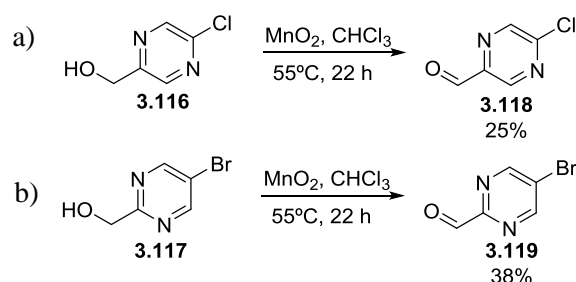
		3.108	3.109	3.110	3.111	3.112	3.113	3.114	3.115
TPSA		125	125	125	125	125	125	125	125
ChromLogD _{7.4}		3.9	3.8	3.7	4.1	3.9	3.8	3.7	4.1

Table 3.18. *In silico* modelling of the diazine containing molecules.

The *in silico* modelling predicts that, as hypothesised, the ChromLogD_{7.4} values of the diazine containing molecules **3.108-3.110** and **3.112-3.114** are lower compared to their corresponding pyridine analogues **3.69** and **3.70**. The analogues can be synthesised by the retrosynthetic route outlined in Scheme 3.4 (*vide supra*). Due to the limited availability of the boronic ester intermediates **3.62** and **3.63**, it was decided to prioritise the synthesis of the

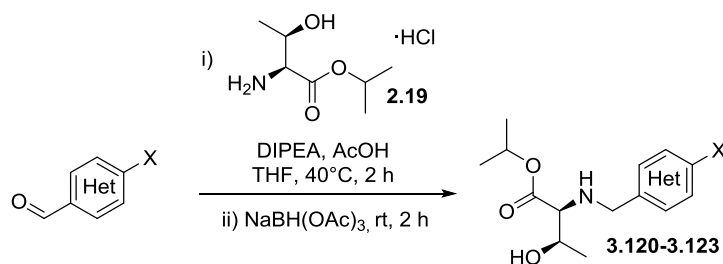
biologically hydrolysable esters and return to the synthesis of the respective *tert*-butyl analogues of compounds with a promising biological profile.

Whilst 3-bromo-5-formyl-pyridazine and 2-bromo-5-formyl-pyrimidine were commercially available, 2-chloro-5-formyl-pyrazine **3.118** and 2-formyl-5-bromopyrimidine **3.119** were not. Therefore, they were synthesised through the oxidation of the corresponding alcohols **3.116** (Scheme 3.22a) and **3.117** (Scheme 3.22b).



Scheme 3.22. The commercially available alcohols a) **3.116** and b) **3.117** were oxidised to the aldehyde using manganese dioxide.

The oxidations of **3.116** and **3.117** were achieved using manganese dioxide, a reagent that can be employed for benzylic or allylic alcohols, in moderate yields. Reductive aminations with the isopropyl amino acid ester **2.19** afforded the diazine intermediates (Table 3.19).

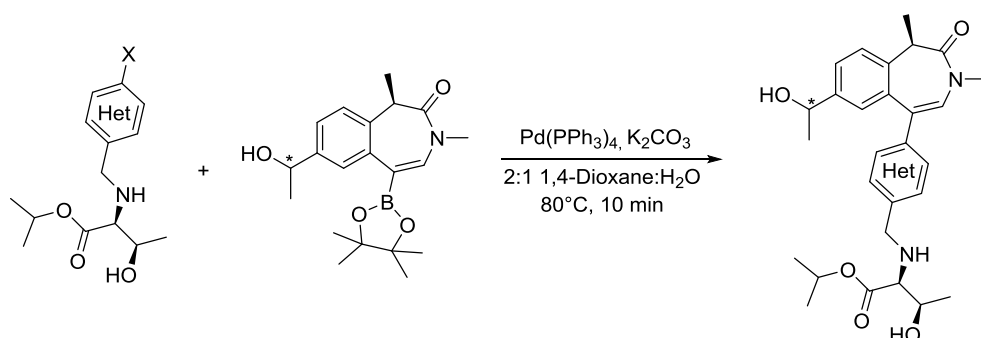


Het				
	3.120	3.121	3.122	3.123
X	Cl	Cl	Br	Cl
Yield (%)	46	22	28	78

Table 3.19. The yields obtained for the reductive amination to the ESM-containing intermediates.

As this work was completed in parallel to the third-generation pyridyl analogues, the unoptimised reductive amination conditions, as outlined in Scheme 3.10 (*vide supra*), were employed thus affording a range of poor to high yields. Interestingly, the two low yields were obtained on the two diazine rings whose aldehydes had to be synthesised following poor conversions to the desired products (Scheme 3.22).

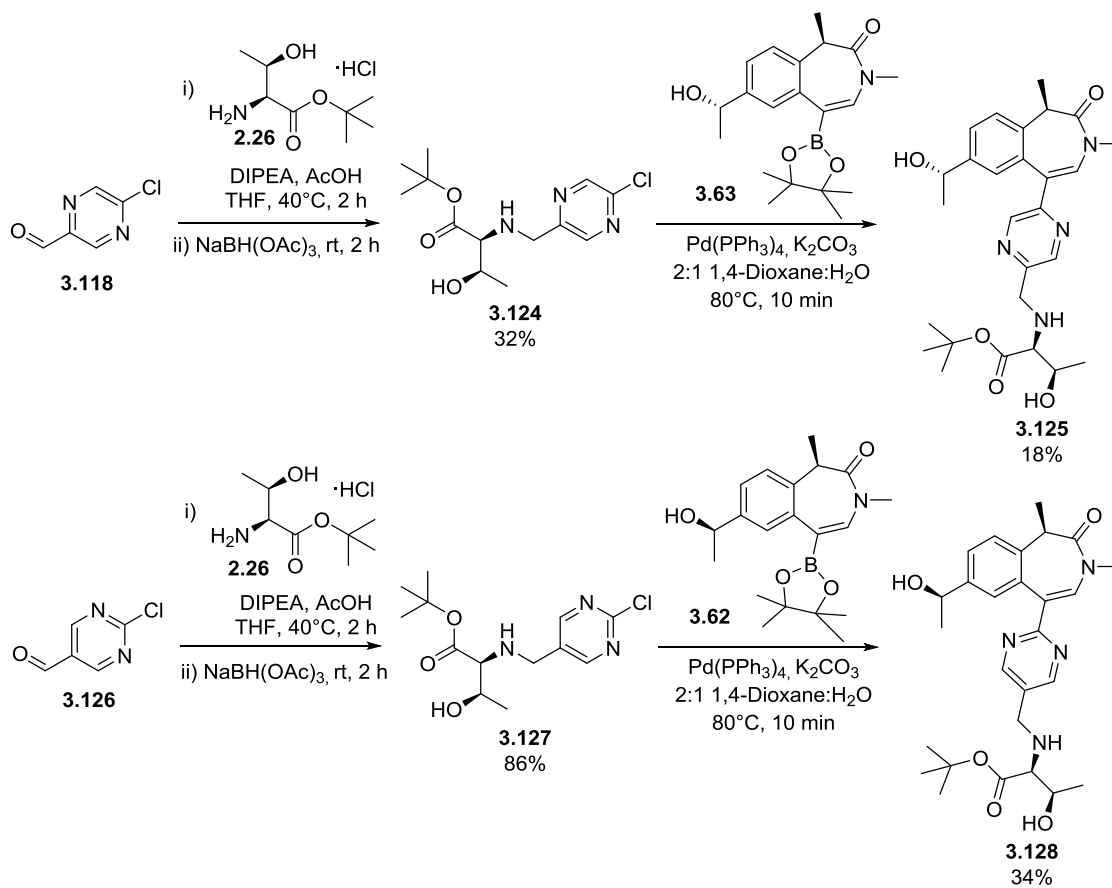
The final compounds **3.108-3.115** were achieved through the Suzuki cross-coupling of the boronic esters **3.62** and **3.63** with the corresponding amino acid ester intermediates **3.120-3.123** (Table 3.20). Prior to the synthesis of analogues **3.113** and **3.114**, which were the last two diazines to be synthesised, the decision was made to deprioritise the analogues containing the stereoisomer with the (*R*)-configuration of the 2-propanol group, as in **3.112-3.115**, and focus on compounds with the (*S*)-configuration, as in **3.108-3.111**, due to its improved metabolic stability as observed in the third generation pyridyl analogues. Therefore, **3.113** and **3.114** were not synthesised.



Product	3.108	3.109	3.110	3.111	3.112	3.113	3.114	3.115	
Br intermediate	3.120	3.121	3.122	3.123	3.120	3.121	3.122	3.123	
(<i>S</i>)/(<i>R</i>)	(<i>S</i>)	(<i>S</i>)	(<i>S</i>)	(<i>S</i>)	(<i>R</i>)	(<i>R</i>)	(<i>R</i>)	(<i>R</i>)	
Yield (%)	34	7	6	31	26	-	-	39	

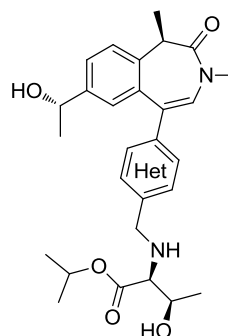
Table 3.20. The yields obtained for the Suzuki cross-couplings of boronic esters **3.62** and **3.63** with the bromide intermediates **3.120-3.123** to the desired isopropyl Thr esters **3.108-3.115**. (*S*)/(*R*) relates to the configuration of the chiral centre depicted *.

Following initial biological data (Table 3.21), the biologically non-hydrolysable *tert*-butyl analogues of **3.109** and **3.115** were also synthesised, **3.125** and **3.128** respectively (Scheme 3.23).



Scheme 3.23. Synthesis of the non-biologically hydrolysable *tert*-butyl analogues.

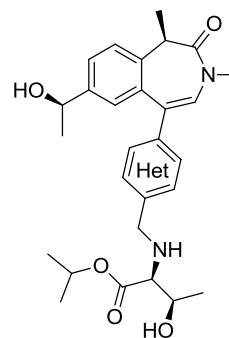
The desired analogues were submitted for biological testing (Table 3.21 and Table 3.22).



	3.69	3.108	3.109	3.110	3.111
hWB pIC ₅₀	8.5	6.7	7.5	7.9	6.8
Δ hWB pIC ₅₀	+1.3	-	+1.0	-	-
Ester BD1 pIC ₅₀	7.1	6.4	7.1	7.0	6.6
HLM IVC (+/- benzil)	2.2 / 2.9	-	- / 1.3	1.0 / 1.7	-
Hu Heps IVC (LBF)	-	-	2.8 (80%)	-	-
Cyno Heps IVC (LBF)	-	-	1.6 (52%)	3.1 (68%)	-
ChromLogD _{7.4}	3.6	3.0	3.4	3.2	3.4

Table 3.21. Profiles of the initial diazine containing compounds. IVC values are quoted in mL/min/g.

As hypothesised, all of the analogues demonstrated a lower ChromLogD_{7.4}. However, the diazine analogues all displayed lower hWB potency relative to **3.69**. This suggests that the compounds exhibit reduced levels of turnover by CES-1. Furthermore, **3.108** and **3.111** also showed lower biochemical potency and therefore were not progressed. Although lower than **3.69**, analogues **3.109** and **3.110** still displayed a desirable hWB potency and were submitted to HLM and hepatocyte IVC assays. As compound **3.109** displays a desirable ΔhWB value of 1, and an increased hWB potency relative to the biochemical potency, it was assumed that meaningful CES-1 hydrolysis was occurring. The analogues exhibited improved microsomal stability relative to **3.69**, but unfortunately the cynomolgus hepatocyte clearance of **3.110** was too high and therefore, was not progressed further. On the other hand, **3.109** displayed desirable cynomolgus monkey hepatocyte IVC and was progressed to human hepatocyte assays which unfortunately showed high clearance.



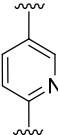
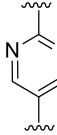
				
	3.70	3.112	3.115	
hWB pIC ₅₀	8.1	7.0	7.0	
Δ hWB pIC ₅₀	+1.0	-	+0.5	
Ester BD1 pIC ₅₀	6.7	6.5	6.6	
HLM IVC (+/- benzil)	-	1.9 / 2.6	1.1 / 1.4	
Hu Heps IVC (LBF)	-	-	-	
Cyno Heps IVC (LBF)	-	-	<0.89 (38%)	
ChromLogD _{7.4}	3.6	3.0	3.3	

Table 3.22. Profiles of the initial diazine containing compounds. IVC values are quoted in mL/min/g.

Analogues **3.112** and **3.115** displayed lower than desired hWB activity. However, compound **3.115** demonstrated a desirable IVC profile with low HLM and cynomolgus hepatocyte values observed. Although **3.112** exhibited undesirable HLM IVC, as its direct comparator **3.70** was not submitted for IVC assays it is not known whether it displays improved metabolic stability to the second generation pyridine analogue as hypothesised. Due to the low hWB potency of these compounds, they were not progressed through the screening cascade.

In an attempt to understand the potency differences between the various diazines, analogues **3.108** and **3.110** were docked into BRD4 BD1 (Figure 3.27).¹⁸²

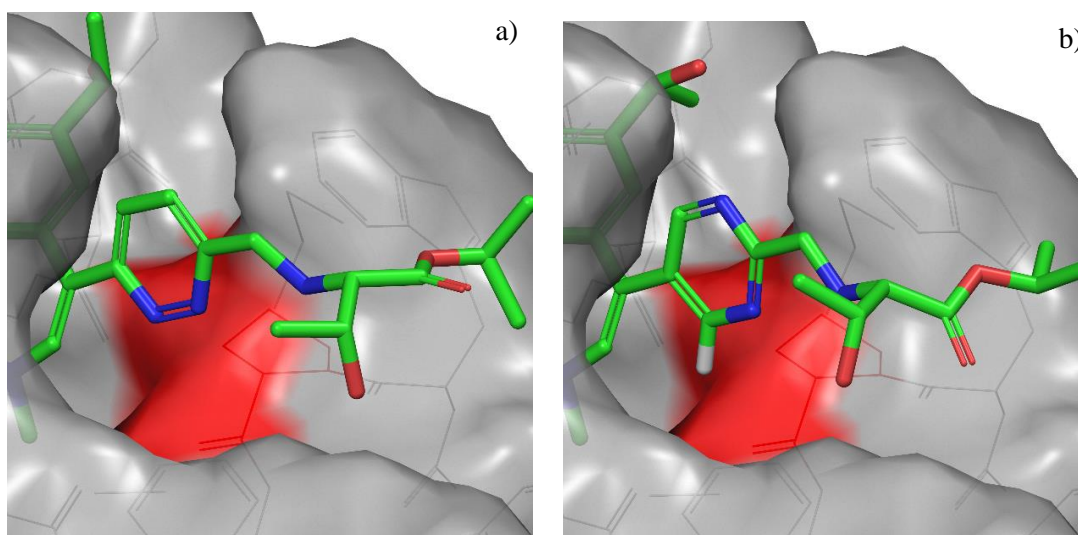


Figure 3.27. Dockings of a) **3.108** and b) **3.110** in BRD4 BD1. The red surface corresponds to the surface of a backbone proline residue (Pro371), the residue which was proposed to be conferring the potency difference. The pyridazine is proposed to adopt the shown conformation due to a preference for the pyridazine nitrogen *ortho* to the ESM and the ESM NH to have a syn orientation. This causes a clash between the lone pair of the pyridazine *ortho* to the BZP with the lone pair of the proline carbonyl. This clash does not occur in the pyrimidine where the N-lone pair is replaced with a C-H. Therefore, there is a lower preference for the binding of **3.108** relative to **3.110**.

Initial dockings of the diazines showed the two structures overlaid exactly, aside from the ESM which is mobile and tends to adopt different conformations. Therefore, one suggestion for the difference in potency could be due to unfavourable interactions with the protein rather than differences in the binding mode. In all of the poses of **3.108**, in which the energy has been minimised to find the lowest energy confirmation, the pyridazine is orientated as shown in Figure 3.27 as opposed to the two nitrogens being directed towards solvent. This is hypothesised to be due to a clash between the nitrogen lone pairs and a valine residue in the ZA channel, therefore making this an unpreferred binding mode. Furthermore, this orientation may be dictated by the preference of the ESM amine group to be orientated towards the ring nitrogen in the *ortho* position, which in turn allows the ESM to form favourable interactions with the water structure present in the ZA channel.

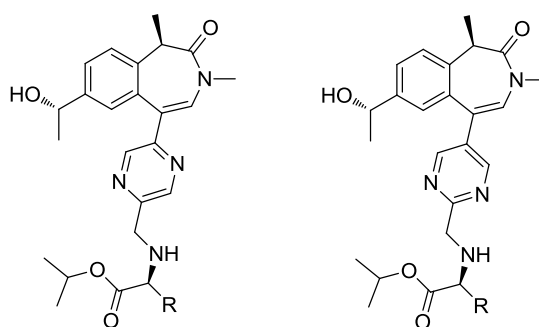
It can be seen from the dockings that the heteroaromatic ring is adjacent to the backbone proline residue (Pro371) of the WPF stack (red surface), placing the proline carbonyl in close proximity to the atom *ortho* to the BZP-aryl bond. Therefore, when this atom is a nitrogen, an electronic repulsion is introduced between the nitrogen and oxygen lone pairs, thus making the binding of the heteroaromatic ring in the ZA channel unfavourable. However, this is not the case for when the atom is a carbon as the attached hydrogen is directed

towards the carbonyl rather than a lone pair. This theory is supported by the low potency observed in **3.111**, in which both of the *ortho*-positions are occupied by nitrogen atoms, and the high potency of **3.109**, which contains the *ortho* C-H.

Consequently, based on the biological data and the docking models, no additional exemplars containing the pyrimidine and pyridazine were synthesised. However, the initial data suggested the diazine-containing subseries had the potential to produce a compound that met the outlined criteria (Table 3.1, *vide supra*). Therefore, further analogues of **3.109** and **3.110** were explored.

3.3.3.1 Second generation diazine analogues

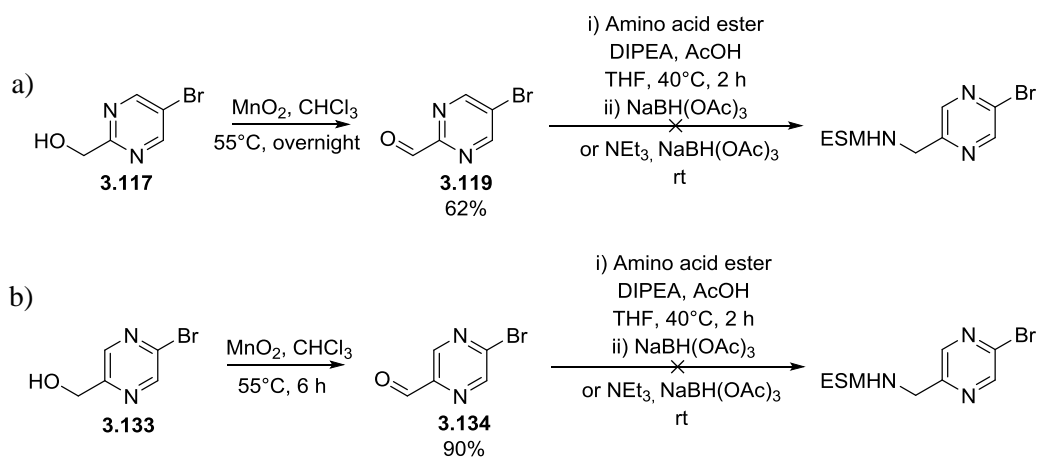
As demonstrated by the third generation pyridyl analogues (section 3.3.2.2, *vide supra*), incorporating the isopropyl Ser amino acid ester increased the metabolic stability relative to the isopropyl Thr compounds. Furthermore, it was demonstrated in the BZP-OTS series that replacing the isopropyl Thr with the isopropyl *allo*-Thr amino acid ester could achieve this. In addition to this, as observed with previous SAR and the QSAR modelling, these ESMs are desirable for whole blood potency. Therefore, it was hypothesised that incorporating the isopropyl Ser and isopropyl *allo*-Thr ESMs would reduce the IVC whilst maintaining the whole blood activity of the first-generation compounds. *In silico* modelling was completed for the proposed analogues (Table 3.23).



R	Ser	<i>allo</i> -Thr	Ser	<i>allo</i> -Thr
	3.129	3.130	3.131	3.132
TPSA	125	125	125	125
ChromLogD _{7.4}	3.0	3.8	3.0	3.8

Table 3.23. *In silico* modelling of the second generation diazine analogues.

In order to obtain the desired targets, further aldehyde intermediates needed to be synthesised. It is well known that aryl bromides are better substrates for Suzuki-Miyaura cross-couplings than aryl chlorides, due to the lower bond dissociation energy of the C-Br bond making palladium insertion easier. Therefore, at this stage it was decided to use 2-bromo-5-hydroxymethyl-pyrazine **3.133** as the starting material, rather than 2-chloro-5-hydroxymethyl-pyrazine **3.116** (Scheme 3.22), in an attempt to improve the yield of the Suzuki cross-coupling that was obtained in the first-generation compound **3.109** (7%). As discussed previously, the aldehyde intermediates **3.119** and **3.134** were synthesised in moderate yields through the oxidation of their respective hydroxymethyl starting materials **3.117** (Scheme 3.24a) and **3.133** (Scheme 3.24b) using manganese dioxide.

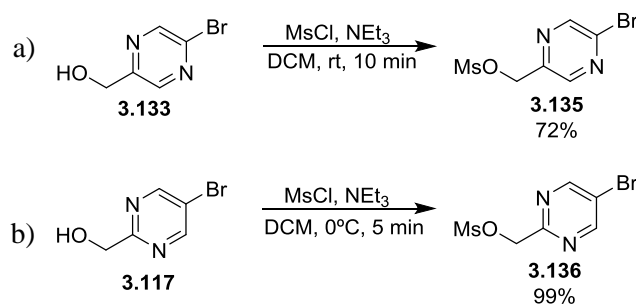


Scheme 3.24. Attempted synthesis of the ESM-containing intermediates. A modified work-up procedure was used for the isolation of a) **3.119** and b) **3.134**.

Due to the low availability and high cost of the starting materials, higher yields for the oxidation were desired. NMR analysis showed full conversion of the previous reaction mixtures to the aldehyde (Scheme 3.22, *vide supra*), suggesting that recovery of the product is the issue rather than the oxidation. Manganese dioxide is a heterogeneous reagent, with the oxidation occurring on the surface of the manganese. Therefore, it was proposed that the moderate yields could be a result of the compound being retained on the manganese. Typically, the reaction mixtures are cooled to room temperature prior to being filtered over Celite to remove the manganese residues, which were then washed with DCM. As such, in an attempt to increase the recovery, the reaction mixtures were filtered over Celite whilst they were at 55°C and the resultant manganese residues washed with 1:1 MeOH:DCM. This resulted in improved yields for both diazines which further suggests that the material was

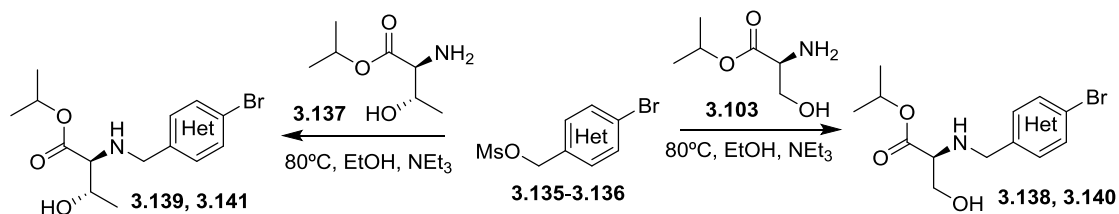
being retained on the manganese in earlier reactions. Due to the large volume of methanol used during the work up, the diazines were isolated as a mixture of the acetal and the aldehyde. This was problematic for the reductive aminations with the various amino acid esters and unfortunately poor imine and product formation was observed. This was not improved by the attempted deprotection of the acetal prior to the reductive aminations. Therefore, it was decided to investigate an alternative route.

Nucleophilic substitutions are a fundamental class of carbon-heteroatom bond forming reactions. In particular, the S_N2 reaction between an electron rich nucleophile and a haloalkane is a common transformation in synthetic chemistry. As demonstrated in the reductive amination reactions, the primary amine of the amino acid ester is capable of acting as a nucleophile. Therefore, by converting the alcohol of the diazines into a pseudohalide the desired products could be formed through an S_N2 reaction. A frequently used pseudohalide in such reactions is the mesylate group and, as such, this was attempted first (Scheme 3.25).



Scheme 3.25. Synthesis of the mesylate intermediates a) **3.135** and b) **3.136** from alcohols **3.133** and **3.117**.

The mesylations, with mesyl chloride and triethylamine, were successful with high yields being obtained for both diazines, **3.135** and **3.136**. Pleasingly, the reactions were quick and the products were isolated in sufficiently high purity following an aqueous work up meaning purification could be avoided. The next step of the synthesis was the S_N2 reactions with the respective desalted amino acid esters **3.103** and **3.137** (Table 3.24).



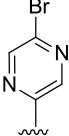
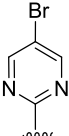
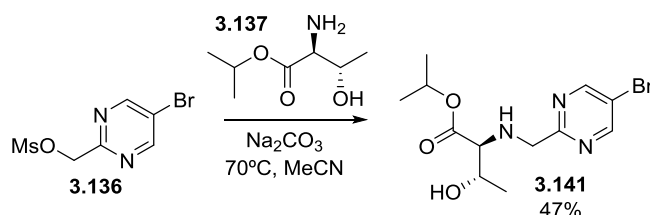
R				
	Ser	<i>allo</i> -Thr	Ser	<i>allo</i> -Thr
	3.138	3.139	3.140	3.141
Mesylate	3.135	3.135	3.136	3.136
Time (min)	20	120	60	120
Yield (%)	20	42	54	0

Table 3.24. Synthesis of the ESM-containing intermediates.

Intermediates **3.138-3.140** were isolated in low-moderate yields but unfortunately, low conversions to **3.141** was observed and it could not be isolated. As such, it was formed using alternative conditions employing a different base and solvent (Scheme 3.26).



Scheme 3.26. Alkylation of the mesylate to form **3.141**.

Finally, the Suzuki-Miyaura cross couplings of the bromide intermediates **3.138-3.141** and the boronic ester **3.63** afford the final compounds (Table 3.25).

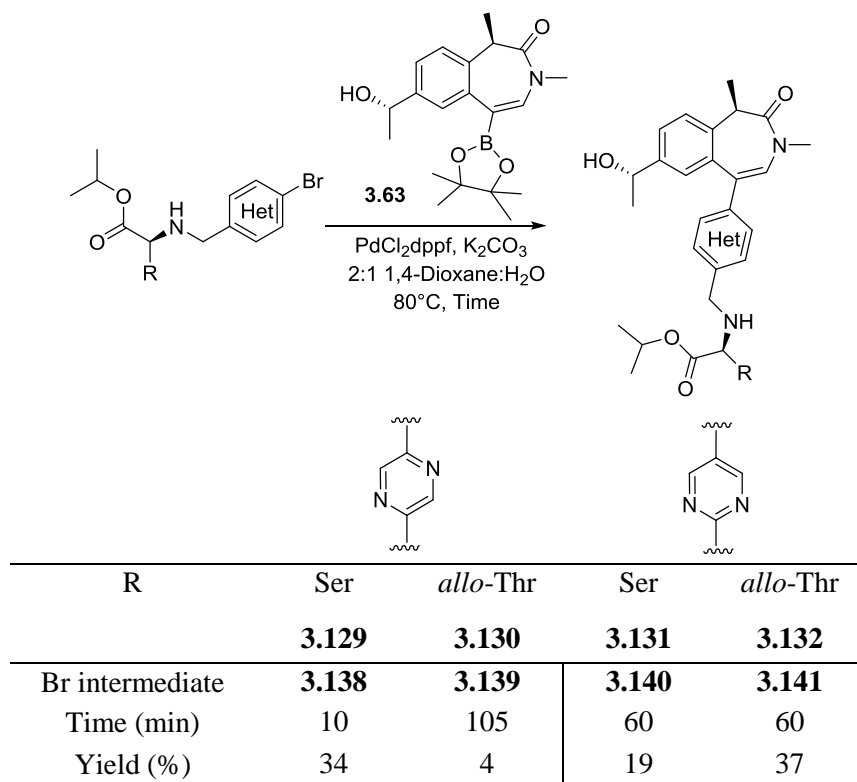
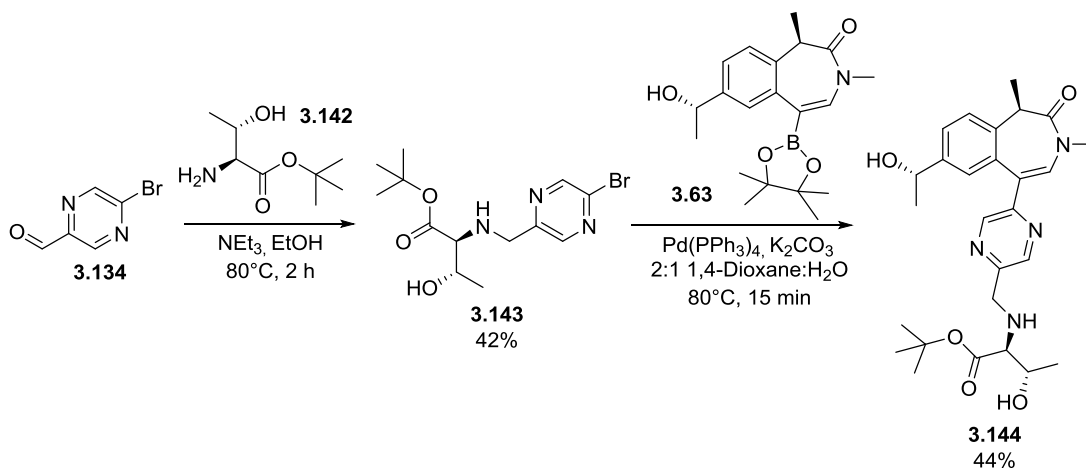


Table 3.25. Suzuki-Miyaura cross couplings to obtain the final compounds.

The final compounds were isolated in low-moderate yields despite high conversions by LCMS to the products. This is due to problematic purifications, as observed with previous compounds. All compounds had poor recovery following purification suggesting the compounds were being lost during this stage. The very low yield of compound **3.130** is due to the compound undergoing two purifications. As these analogues were made in parallel to the fourth generation pyridyl analogues, e.g. **3.84**, it was at this point that the epimerisation of the isopropyl Ser ESM was discovered (*vide supra*). Using the NMR technique described earlier, it was estimated that partial epimerisation had also occurred in analogues **3.129** and **3.131** (Appendix 7). As this was discovered after the compounds were submitted to biological assays, it was decided to use the data to determine whether a resynthesis was required (Table 3.26).

Following initial data, the biologically non-hydrolysable *tert*-butyl analogue of **3.130**, **3.144**, was synthesised (Scheme 3.27). Furthermore, the route optimisation discussed later in this thesis (*vide infra*, Chapter 3.3.4.1, Scheme 3.49), facilitated the synthesis of the *tert*-butyl analogue of **3.131**, **3.156**.



The desired analogues were submitted for biological testing (Table 3.26).

R	 3.129	 3.130	 3.131	 3.132
hWB pIC ₅₀	7.0	7.3	7.4	7.8
Δ hWB pIC ₅₀	-	+0.8	+1.1	-
Ester BD1 pIC ₅₀	6.9	7.3	6.8	6.9
HLM IVC	0.6	1.2	0.4	1.8
Hu Heps IVC (LBF)	0.8 (53%)	1.5 (68%)	1.1 (60%)	3.0 (80%)
Cyno Heps IVC (LBF)	<0.89 (<38%)	<0.89 (<38%)	<0.89 (<38%)	1.4 (49%)
ChromLogD _{7.4}	2.9	3.2	2.7	3.1

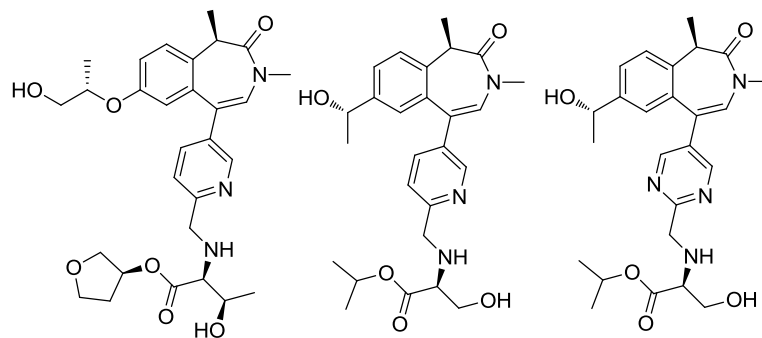
Table 3.26. Biological profiles of the second generation diazine analogues. IVC values are quoted in mL/min/g.

All of the analogues displayed desirable lipophilicities and were comparable to the first generation isopropyl Thr analogues (Table 3.21). Interestingly, the *allo*-Thr analogues maintained their whole blood potency compared to their first-generation analogues, whilst the isopropyl Ser compounds were ~0.5 log units less active but maintained a desirable

Δ hWB. Unfortunately, whilst compound **3.132** showed high whole blood potency, analogues **3.129-3.131** displayed lower than desired activity. However, all of the analogues did demonstrate equal or reduced HLM IVC relative to their isopropyl Thr comparators. All of the compounds were progressed into cynomolgus monkey hepatocyte assays. As hypothesised, all analogues were found to exhibit desirable IVC, with values below the lowest detection limit (0.89 mL/min/g) for analogues **3.129-3.131**. As such, they were then progressed into human hepatocyte IVC assays. Analogues **3.129-3.131** exhibited desirable human hepatocyte clearance, whilst **3.132** was higher than desired and as a result was terminated. Due to its desirable profile, **3.131** was selected as the lead diazine molecule and progressed into further studies. As well as this, route optimisation was undertaken to address the partial racemisation of the isopropyl Ser ESM (section 3.3.4.1, *vide infra*).

3.3.4 Further DMPK and selectivity profiling of lead compounds

The investigations into the incorporation of a pyridine or diazine ring as the ZA channel group for BZP-ZA compounds resulted in three molecules with desirable biological profiles: the first and third generation pyridine analogues **3.37** and **3.72**, and the second generation diazine analogue **3.131**. As such, the compounds were progressed into further profiling. The potency of the compounds against MCP-1 downregulation were measured in a lower throughput whole blood assay, which uses a different software that allows more control over the fitting of the curves to the data points. This data was used along with the human hepatocyte IVC and *in silico* prediction of the volume of distribution at steady state, V_{DSS} , to generate an early dose prediction. The calculation is based on achieving an IC_{90} for 4 hours and provides a prediction of the daily dosage that would be required for the respective compound. Furthermore, as previously mentioned, P450 enzymes are the major family involved in drug metabolism and inhibition of these enzymes would lead to increased levels of other drugs in the system of patients. This is of particular importance for RA patients, who tend to take multiple medications simultaneously. Therefore, the compounds were submitted for TDI assays in order to examine whether they, or their metabolites, inhibited CYP3A4 in a time dependent fashion. Furthermore, for compounds to enter late stage studies they must be dosed in an *in vivo* animal study. Therefore, to enable a cynomolgus monkey *in vivo* study, a molecule must exhibit a sufficient half-life in cynomolgus monkey blood in order to allow the various parameters, e.g. clearance, to be accurately measured. Furthermore, a sufficient half-life in humans is required for any oral drug molecule. Therefore, the stability of the compounds in human blood and cynomolgus monkey plasma was also assessed (Table 3.27).



	3.37	3.72	3.131
TDI (fold shift to lowest conc.)	1.4 fold to 112 μ M	1.9 fold to 73 μ M	0 fold to >500 μ M
hWB pIC ₅₀ (MCP-1) / Δ hWB	7.9 / +0.4	7.9 / +1.0	7.5 / +0.6
t _{1/2} human blood	686 min	542 min	>365 min
t _{1/2} cyno plasma	>745 min	>745 min	>365 min
Early dose prediction (mg QD)	16	165	100

Table 3.27. Further profiling of the lead molecules.

The compounds demonstrated desirable hWB activity and Δ hWB values. In the case of **3.37**, the high potency and low human hepatocyte IVC resulted in an excellent early dose prediction of 16 mg QD, much lower than the desired <100 mg QD. Furthermore, analogue **3.131** was also predicted to have a desirable early dose prediction of 100 mg QD. Although **3.72** was calculated to have early dose predictions of >100 mg QD, as it was only marginally above the desired value, and these predictions are subject to error, it was still deemed acceptable. Pleasingly, the compounds were stable in human blood and cynomolgus monkey plasma and, as such, were predicted to offer sufficient exposure in *in vivo* studies. Furthermore, analogues **3.37** and **3.72** were found to have acceptable TDI whilst **3.131** showed no TDI. As such, all three compounds were still of high interest.

In order to assess the wider selectivity profile of the compounds, they were screened against a panel of 32 closely related bromodomain-containing proteins (Figures 3.28 and 3.29). The assay employs an immobilised ligand (the control compound) which, when in the absence of test compounds, binds to the DNA-tagged bromodomains. When in the presence of test compounds, those that bind to the bromodomains prevent the binding of the bromodomain to the immobilised ligand. This results in a lower level of DNA-tagged bromodomain being detected on the immobilised ligand (termed percent control) relative to when test compounds are not present. Therefore, this ligand binding competition assay enables the quantitative measurement of the interactions between compounds of interest and the bromodomains.

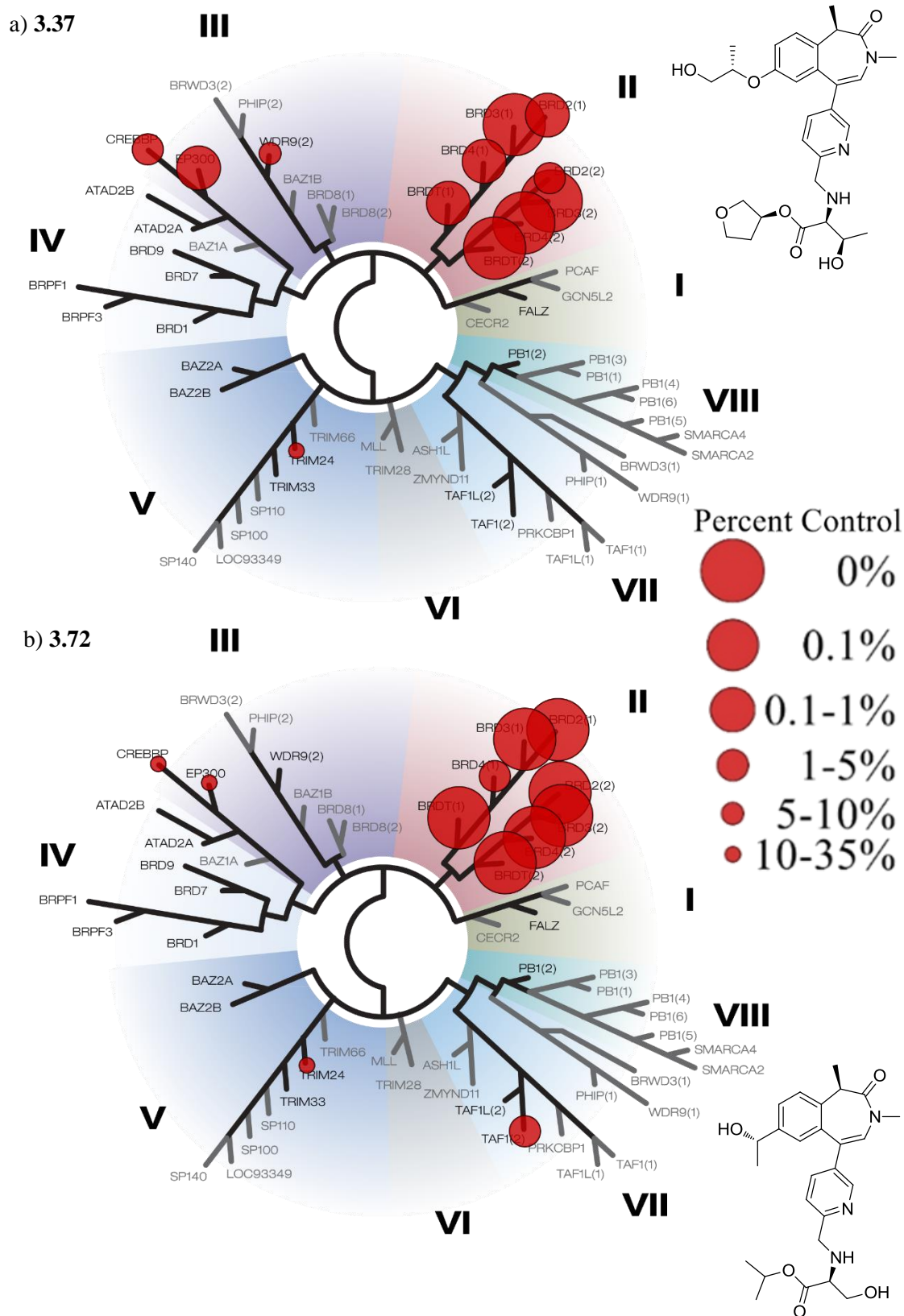
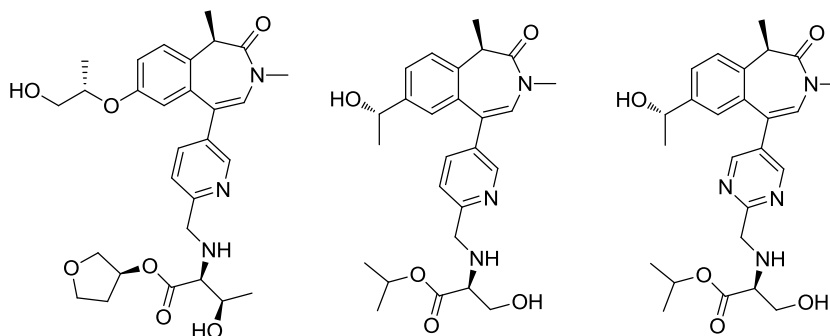


Figure 3.28. The selectivity profiles of a) 3.37, b) 3.72 and c) 3.131 generated by screening the compounds at 10 μ M against 32 bromodomain-containing proteins. *Continues on page 189.*



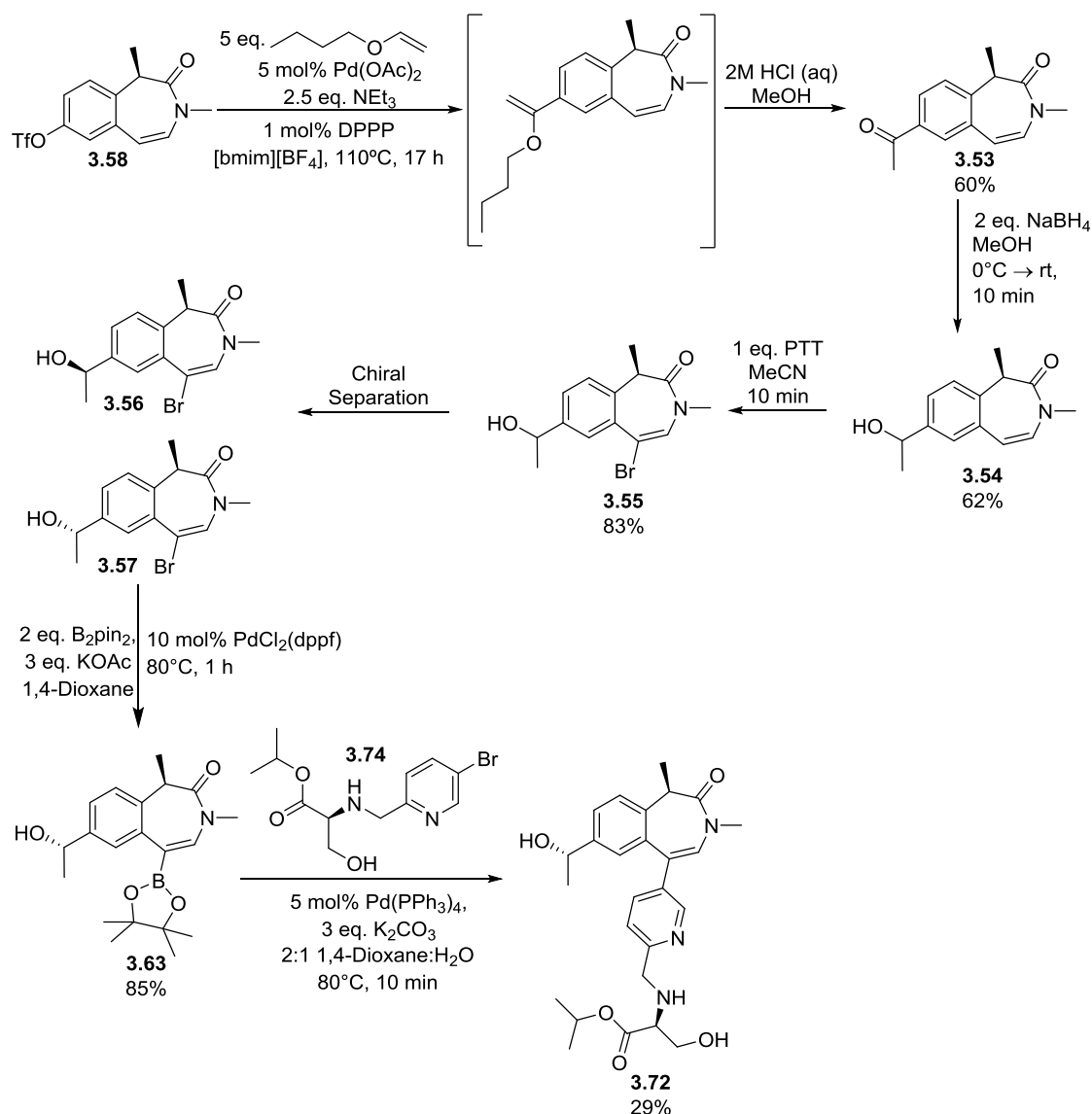
Target	3.37	3.72	3.131
CREBBP	27	161	-
EP300	22	-	21
WDR9(2)	480	-	-
TAF1(2)	-	>388	>240

Table 3.28. Fold selectivity over the bromodomain-containing proteins relative to the BRD4 BD1 IC₅₀ determined by full-dose response curves.

The IC₅₀ determinations showed **3.72** to have a desirable selectivity profile, whilst **3.37** and **3.131** demonstrated only ~20 fold selectivity over CREBBP/EP300 and EP300 respectively. Although this is lower than the desired 30-fold selectivity, it was thought that it could be mitigated by a low dose prediction, as well as further investigation into the definitive selectivity through isothermal titration calorimetry. As such, at this stage, the compounds were still of high interest, with the next step being *in vivo* PK and Ames studies. Any compound that still exhibited a desirable profile following these studies would need a large-scale synthesis to enable late stage profiling including safety studies and form investigations. As such, the synthetic routes of these compounds required optimisation to facilitate such a scale up. Due to the similar synthetic routes of **3.72** and **3.131**, efforts focussed on the optimisation of the synthesis of **3.72**, with the hypothesis that it could be directly applied to **3.131**, whilst the optimisation of the synthetic route to **3.37** was undertaken by colleagues.

3.3.5 Optimisation of the synthetic route to lead compounds **3.37** and **3.131**

To facilitate the PK studies and late stage investigations on the lead molecules, scale ups of each compound were required. However, prior to this, route optimisation was essential to ensure the scale up route was highly yielding thus minimising the amount of starting materials needed. The optimisation of **3.37** was completed by a colleague and, as such, only the investigations into **3.72** will be discussed within this thesis. The initial synthetic route towards **3.72** contained several suboptimal steps with low yields and the need for chiral column chromatography (Scheme 3.28).



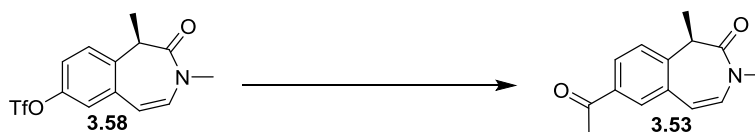
Scheme 3.28. Initial synthetic route to **3.72**.

The existing synthetic route to arrive at intermediate **3.53** contained a previously optimised Heck reaction to install the ketone from the triflate (Scheme 3.9). However, the ketone was still only obtained in moderate yields and thus needed further investigation. Once the ketone was isolated, it was reduced achirally to the alcohol **3.54** and brominated before undergoing chiral chromatography to retrieve the diastereomers. In addition to the moderate yield for the achiral reduction, the undesired diastereomer **3.56** was discarded following chiral separation thus leading to a further ~50% reduction in yield. Furthermore, the necessary column chromatography using a chiral stationary phase was lengthy due to a necessary low loading and, as such, was not desirable for large scale separations. Following the borylation of the core, the Suzuki cross-coupling of **3.63** with intermediate **3.74** gave the desired compound **3.72**. As previously discussed, despite high conversion to the product by LCMS (>90%),

difficulties with purification resulted in a poor yield. In addition to this, it was found that reductive amination of the isopropyl Ser amino acid ester **2.87** and pyridine **3.43**, to form **3.74**, resulted in partial racemisation of the chiral centre in the ESM. Therefore, the optimisation was to focus on improving the ketone installation and subsequent formation of the (*S*)-alcohol, as well as the synthesis of intermediate **3.74** and finally, the purification of the final compound **3.72**.

3.3.5.1 Optimisation of installing the ketone in the first synthetic step towards lead molecules **3.37** and **3.131**

The ketone installation was previously improved from two synthetic steps to one Heck reaction, using literature conditions, with similar yields obtained (*vide supra*, Scheme 3.9). Therefore, increased yields whilst maintaining the one step sequence was desired. Gøgsig *et al.* reported the use of nickel catalysis to transform a triflate to a ketone in 2012 using the same vinyl ether as the aforementioned Heck reaction.²⁰⁴ Furthermore, the original Heck conditions for this transformation employed a DMF solvent rather than the greener ionic liquid.²⁰² These conditions were applied to the synthesis of **3.53** (Table 3.29).



Entry	Conditions	Yield (%)
1	5 mol% Pd(OAc) ₂ , 1 mol% dppp, 2.5 eq. NEt ₃ , 5 eq. vinyl ether, [BMIM][BF ₄], 110°C, 17 h	60
2	5 mol% Ni(COD) ₂ , 5 mol% dppf, 4 eq. dicyclohexylamine, 3 eq. vinyl ether, 1,4-dioxane, 100°C 17 h	89
3	5 mol% Pd(OAc) ₂ , 5.5 mol% dppp, 2 eq. NEt ₃ , 5 eq. vinyl ether, DMF, 80°C, 1 h	91

Table 3.29. Alternative conditions to install the ketone.

Pleasingly, the nickel catalysis and adapted Heck conditions (Entries 2 and 3) both showed significant increases in yield relative to the original Heck reaction (Entry 1). Furthermore, replacing the ionic liquid with DMF removed the necessity for a work up prior to the acidic hydrolysis of the intermediate to the ketone. Although entries 2 and 3 resulted in similar isolated yields, due to the reduced costs and increased availability of palladium versus nickel catalysts, entry 3 offered the preferred conditions and replaced the existing Heck reaction.

Following optimisation of the ketone formation, the synthetic route towards intermediate **3.49** was investigated.

3.3.5.2 Optimisation of a stereoselective ketone reduction to form the WPF shelf of lead compounds 3.37 and 3.131

Chiral aromatic alcohols are common key chiral building blocks in drug-like molecules.²⁰⁵ Although they can be synthesised through chemical processes, due to their specificity and stereoselectivity control, the last decade has seen a surge in the development and use of biocatalysts to obtain such building blocks.²⁰⁶ The aldo-keto reductases (AKR) are a superfamily of enzymes responsible for catalysing redox transformations, with a key role in drug metabolism, detoxification and biosynthesis.²⁰⁷ The AKRs have a large, diverse set of substrates and can function as independent metabolic units or in collaboration with other metabolising enzymes, e.g. cytochrome P450s, as part of a metabolic pathway. A characteristic feature of the AKR superfamily is the transformation of aldehydes and ketones of molecules encountered in drug molecules or those generated endogenously during metabolism.²⁰⁸

3.3.5.2.1 Employing aldo-keto reductases to perform stereoselective ketone reductions

To date, 16 families of AKRs, comprising over 100 enzymes, have been identified. The families are split such that family members share >40% sequence homology and <40% homology with enzymes of other families. The enzymes are present in all phyla, ranging from prokaryotes and yeasts to animals and humans.²⁰⁷ The AKRs have a common conserved structure which contains a conserved pyridine nucleotide binding site. The latter is crucial for the binding of the two forms of nicotinamide adenine dinucleotide cofactor, NADH or NADPH, which act as the hydride source for all AKRs.^{209,210} Whilst biological systems are capable of providing a constant source of the cofactor, through regeneration of oxidised cofactors, extracellular biocatalysis is not able to do this and the reaction will stall once the cofactor is consumed. However, due to the high cost of both cofactors, catalytic rather than stoichiometric quantities are desirable. As such, to mimic biological systems, a second reaction can be used to recycle the oxidised cofactor NAD⁺ or NADP⁺ back to NADH or NADPH respectively.

The catalytic reaction starts upon the binding of cofactor and substrate to the enzyme (Figure 3.30). A hydride ion is transferred from the cofactor to the substrate carbonyl, resulting in an oxidised cofactor and a reduced substrate.²⁰⁷ Subsequent protonation of the oxyanion by the solvent, followed by dissociation of the oxidised cofactor and reduced substrate ends the reaction. This redox reaction involves general acid-base catalysis. Most AKRs have a conserved catalytic tetrad, comprising Tyr, His, Lys and Asp.²⁰⁷

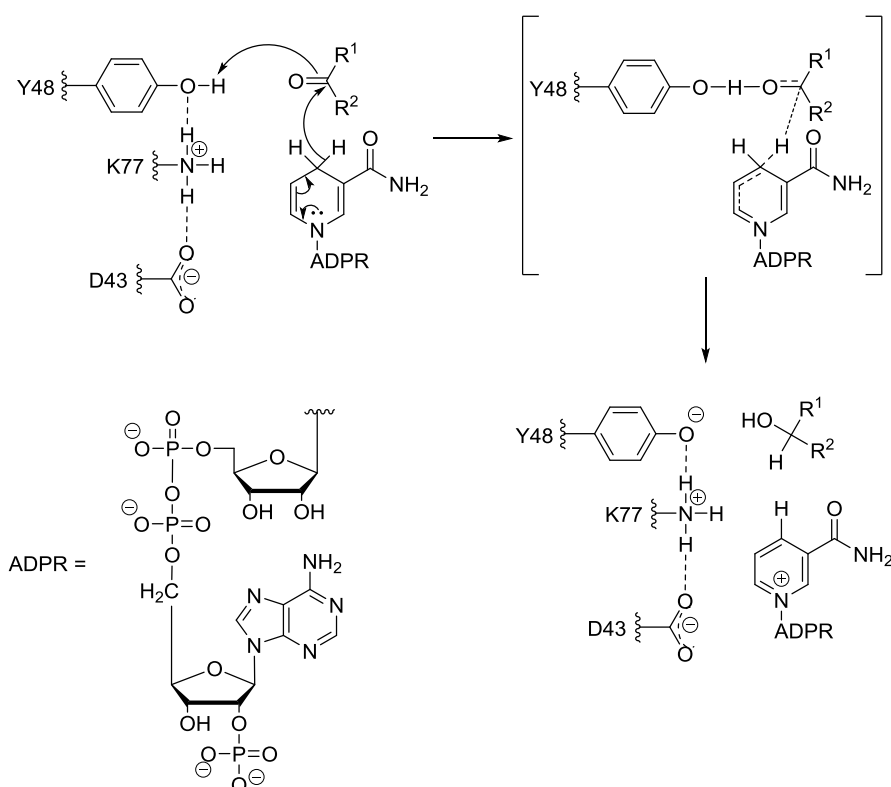
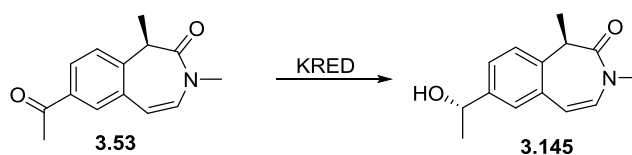


Figure 3.30. Catalytic mechanism of aldo-keto reductases. His-110 (AKR1B1 numbering, not shown) aids the binding of the substrate in the correct orientation.

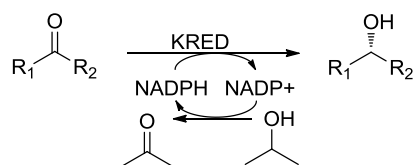
The position of the pyridine nucleotide binding site relative to the substrate binding pocket determines whether the (*R*) or (*S*) alcohol is obtained.²¹⁰ The high stereospecificity and wide substrate scope of the AKRs has seen their use as biocatalysts significantly increase. In particular, AKRs for ketone reductions, more commonly termed ketoreductases or KREDs, are now commercially available. As such, it was thought that a KRED could potentially be used to selectively obtain the (*S*)-enantiomer of the propan-2-ol shelf group **3.145** (Scheme 3.29). This would negate the need for chiral separation of the mixture of diastereomers, thus reducing the loss of material and improving the yield.



Scheme 3.29. A KRED could offer a stereoselective reduction of the ketone to the desired diastereomer **3.145**.

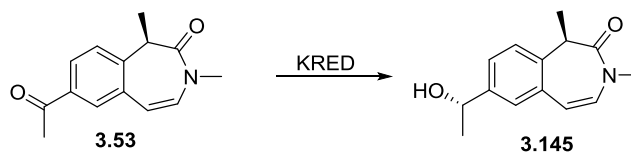
3.3.5.2.2 KRED screen to identify an enzyme to stereoselectively reduce a ketone to the (*S*)-alcohol

To investigate whether a KRED could be used to stereoselectively synthesise the (*S*)-configuration of the propan-2-ol shelf group, a KRED screen was performed. The screen consisted of three 96-well plates that were in-licensed from Codexis. The plates contain a set of KRED variants that have been engineered for enhanced selectivity, activity, substrate range, solvent and temperature stability. Each well contains lysates from the cells in which the enzyme was cultured and therefore, purified enzyme was not utilised but was present in high levels. The lysate eliminates the problems of compound toxicity by removing the need for viable cells, as well as making the running of the screen facile. The KREDs are tolerant to high concentrations of isopropanol (IPA) which is advantageous as it aids solubility of substrates with poor water solubility, as well as acting as a substrate for the recycling of the NADPH cofactor (Scheme 3.30).



Scheme 3.30. The KRED screen is performed in IPA which aids the solubility of compounds and regenerates the NADPH following its oxidation.

Plates 1 and 2 are generally selective towards producing (*R*)-alcohols, whilst Plate 3 tends to synthesise the (*S*)-alcohol. However, this is sometimes substrate dependent and it is recommended that all three plates are screened to increase the chances of success. As such, all three plates were screened using the ketone substrate **3.53** and at 30°C. The results of the KRED screen were analysed by achiral UPLC. The top 100 variants from the three plates were then analysed further by chiral LC to determine the enantioselectivities (Table 3.30-Table 3.32).



Conversion (%) to 3.145													
	1	2	3	4	5	6	7	8	9	10	11	12	
A	93	72	94	93	93	91	53	93	40	44	94	24	12
B	79	94	93	93	80	93	92	17	92	96	97	91	24
C	93	39	3	92	0	95	24	94	68	92	94	86	36
D	95	92	38	85	92	44	23	97	98	93	95	92	48
E	0	0	0	0	93	96	92	97	95	91	93	93	60
F	94	95	94	93	95	96	97	95	96	85	93	94	72
G	58	64	94	80	85	93	25	75	54	95	94	34	84
H	94	94	97	96	92	95	37	90	93	93	93	48	96

ee (%)													
	1	2	3	4	5	6	7	8	9	10	11	12	
A	-	-	-	-	-	-	-	-	-	-	-	-	12
B	-	-	-	-	-	-	-	-	-	-99.0	-99.0	-	24
C	-	-	-	-	-	-	-	-	-	-	-	-	36
D	-	-	-	-	-	-	-	-99.0	-99.0	-	-	-	48
E	-99.0	-99.0	-	-	-	-98.9	-	-98.9	-98.6	-	-	-	60
F	-	-	-	-	-	-99.0	-99.0	-99.0	-98.8	-	-	-	72
G	-	-	-	-	-	-	-	-	-	-	-	-	84
H	-	-	-99.0	-99.0	-	-	-	-	-	-	-	-	96

Table 3.30. The plate map showing conversions of **3.53** to **3.145** (%), determined by achiral UPLC, and the % ee of a selection of variants, determined by chiral LC, for KRED Plate 1.

Conversion (%) to 3.145													
	1	2	3	4	5	6	7	8	9	10	11	12	
A	99	93	95	94	99	93	92	77	93	97	5	94	12
B	82	98	96	95	99	96	88	21	21	95	96	98	24
C	46	95	95	92	94	95	97	97	97	96	95	94	36
D	96	98	97	98	38	96	97	94	96	96	40	94	48
E	0	1	97	95	96	96	96	96	99	94	95	96	60
F	98	97	96	98	97	97	93	99	97	67	28	93	72
G	86	95	44	28	96	97	95	60	97	93	89	98	84
H	98	96	97	96	95	95	97	96	94	88	96	93	96

ee (%)													
	1	2	3	4	5	6	7	8	9	10	11	12	
A	-99.0	-	-	-	-94.9	-	-	-	-	-99.0	-	-	12
B	-	-65.4	-93.0	-75.4	-99.0	-99.0	-	-	-	-	-97.8	-97.2	24
C	-	-	-83.1	-	-	-99.0	-99.0	-99.0	-99.0	-99.0	-99.0	-	36
D	-99.0	-97.7	-93.2	-99.0	-	-99.0	-99.0	-	-99.0	-99.0	-	-	48
E	-	-	-98.7	-98.9	-98.8	-98.9	-99.0	-99.0	-99.0	-	-	-99.0	60
F	-99.0	-99.0	-99.0	-80.7	-99.0	-99.0	-	-99.0	-99.0	-	-	-	72
G	-	-98.8	-	-	-99.0	-99.0	-	-	-99.0	-	-	-99.0	84
H	-99.0	-99.0	-99.0	-98.8	-99.0	-	-99.0	-99.0	-	-	-99.0	-	96

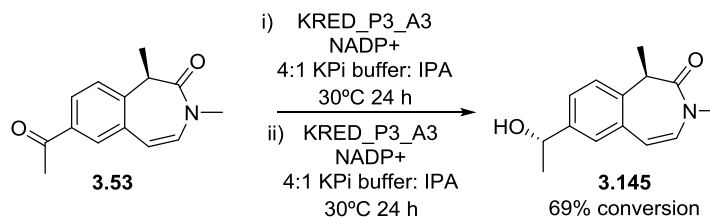
Table 3.31. The plate map showing conversions of **3.53** to **3.145** (%), determined by achiral UPLC, and the % ee of a selection of variants, determined by chiral LC, for KRED Plate 2.

Conversion (%) to 3.145													
	1	2	3	4	5	6	7	8	9	10	11	12	
A	1	99	99	13	21	16	99	1	1	1	1	99	12
B	99	35	95	6	89	1	5	13	99	1	1	1	24
C	99	92	97	99	29	7	1	99	95	1	1	96	36
D	99	81	99	5	4	99	1	3	1	0	0	94	48
E	6	1	2	1	0	0	98	99	99	99	98	97	60
F	99	41	95	75	5	2	1	4	2	0	26	99	72
G	87	64	99	95	1	97	1	9	99	1	96	98	84
H	97	98	98	2	5	13	6	1	98	1	0	98	96

ee (%)													
	1	2	3	4	5	6	7	8	9	10	11	12	
A	-	97.9	97.9	-	-	-	97.8	-	-	-	-	97.8	12
B	97.8	-	97.7	-	-	-	-	-	97.8	-	-	-	24
C	97.8	-	97.8	97.8	-	-	-	97.7	97.7	-	-	97.6	36
D	97.7	-	97.7	-	-	97.8	-	-	-	-	-	-	48
E	-	-	-	-	-	-	-99.0	-99.0	97.6	97.6	97.6	97.6	60
F	97.6	-	-	-	-	-	-	-	-	-	-	97.6	72
G	-	-	97.8	-	-	97.9	-	-	97.7	-	97.7	97.6	84
H	97.6	97.7	97.7	-	-	-	-	-	97.7	-	-	97.7	96

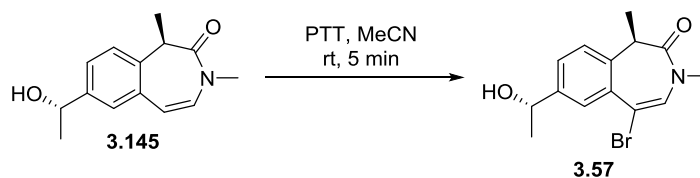
Table 3.32. The plate map showing conversions of **3.53** to **3.145** (%), determined by achiral UPLC, and the % ee of a selection of variants, determined by chiral LC, for KRED Plate 3.

The screen was successful, with over 150 variants showing >90% conversion to the alcohol. Furthermore, the majority of these variants reduced the alcohol with >97% ee, where the negative values correspond to one enantiomer and the positive values to the opposite enantiomer. However, due to a lack of enantiopure markers, it was not possible to determine which plate was generating the desired diastereomer **3.145**. The existing route to the alcohol shelf group involved a chiral separation of the brominated intermediate **3.55** to obtain the enantiopure intermediates **3.56** and **3.57**, thus providing markers for each diastereomer. Therefore, bromination of a product from each plate followed by chiral analysis would identify which enantiomer of the 2-propanol group was being produced on each plate. As Plate 3 is typically selective for producing (*S*)-alcohols, it was decided to scale up a reaction with one variant from this plate first, so that the stereochemistry could be determined. This was completed using enzyme KRED_P3_A3 (KRED in well A3 of Plate 3) as it showed high conversion and ee % and was available in house (Scheme 3.31).



Scheme 3.31. Initial scale up of the enantioselective reduction using KRED_P3_A3.

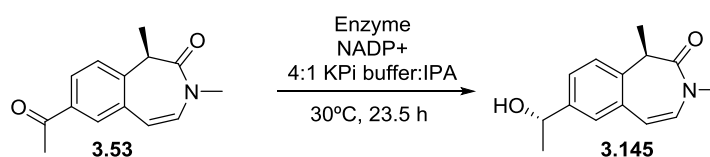
The reaction was completed at a 10 mg/mL concentration of substrate with an equal loading of enzyme. Due to the instability of variants of Plate 3 to high concentrations of IPA, the maximum concentration that can be used is 20% of the overall volume. The insolubility of ketone **3.53** in IPA meant the highest concentration had to be used, therefore resulting in a 4:1 ratio of 100 mM potassium phosphate (KPi) buffer:IPA. Following stirring at 30 °C for 24 hours, ~35% conversion to the desired product (by UPLC and LCMS) was observed. At this point, the reaction was quenched, worked up and the crude starting material/ketone mixture isolated. This reaction was repeated with this crude mixture for a further 24 hours. Interestingly, despite the high conversion observed in the screen, only moderate conversion to the desired product was observed after this time (69% by LCMS). However, as the scale up was only completed on a 50 mg scale, it was decided to isolate the crude material and perform the bromination rather than attempt a purification (Scheme 3.32).



Scheme 3.32. Bromination of the crude mixture of alcohol **3.145** to form **3.57**.

Chiral analysis confirmed that the variant selected from Plate 3, and indeed all of the positive % ee values of the plate maps, afforded the desired diastereomer **3.145**. As such, these initial results suggested that the enantioselective reduction to intermediate **3.145** using a KRED variant was possible. However, as the first scale up reaction showed lower conversion to the desired product than expected, further optimisation was required. It was unknown whether it was the substrate or enzyme concentrations that was hindering the reaction or whether it was the enzyme itself. The enzyme utilised in Scheme 3.31 was a lyophilised powder as opposed to the lysates employed in the plates which may have caused the difference in reactivity. Also available in house were the lyophilised powders of two other enzymes, KRED_P3_C3 and KRED_P3_H9, both of which demonstrated high conversions and ee % in the initial

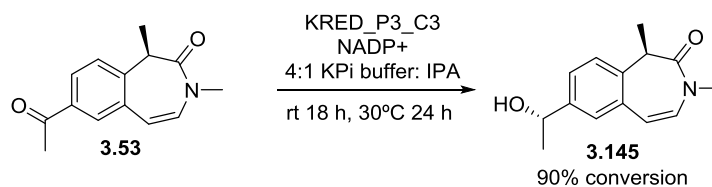
screen. Therefore, a small screen based on these three enzymes and various concentrations was performed (Table 3.33). The conversions quoted for the remainder of this section were determined either by comparing the peak areas observed by UPLC of the starting material and product or by the a/a% by LCMS. Therefore, they are not an accurate measurement of conversion, but rather qualitative methods to provide an idea of whether a low, moderate or high conversion was being achieved. However, as the ketone and product are very similar and as only these two components are present in the reaction mixture and UPLC trace, the conversions stated are very representative of the actual conversion.



Entry	Enzyme	Substrate [mg/mL]	Enzyme [mg/mL]	Conversion (%)
1	KRED_P3_A3	2.5	2.5	42
2	KRED_P3_C3	2.5	2.5	88
3	KRED_P3_H9	2.5	2.5	23
4	KRED_P3_A3	5	5	47
5	KRED_P3_C3	5	5	89
6	KRED_P3_H9	5	5	19
7	KRED_P3_A3	5	10	66
8	KRED_P3_C3	5	10	92
9	KRED_P3_H9	5	10	33
10	KRED_P3_A3	10	10	39
11	KRED_P3_C3	10	10	83
12	KRED_P3_H9	10	10	18

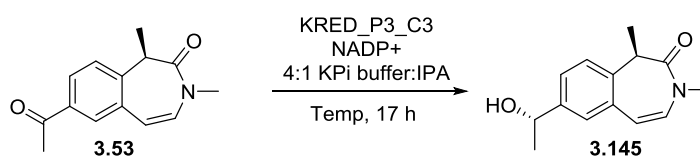
Table 3.33. The results of the small screen based on different enzyme and various concentrations. Conversions (%) were calculate by the ratio of the peak areas observed by UPLC.

Interestingly, enzyme KRED_P3_C3 consistently resulted in high conversions, whilst enzymes KRED_P3_H9 and KRED_P3_A3 afforded low and moderate conversions respectively. The highest conversion for KRED_P3_C3 was observed with a 2:1 enzyme: substrate loading with concentrations of 10 mg/mL and 5 mg/mL respectively (Entry 8). However, high conversions were still observed with a 1:1 substrate: enzyme loading at 10 mg/mL (83%, Entry 11). Although this is a lower conversion, this concentration would significantly reduce the volume of solvent required when scaling up the reaction. Furthermore, it was thought that this conversion could be increased further by elongating the reaction time. Therefore, it was decided to complete a scale up reaction based on the conditions in Entry 11 (Scheme 3.33).



Scheme 3.33. Initial scale up of the enantioselective reduction using KRED_P3_C3.

In contrast to KRED_P3_A3, the small scale up of KRED_P3_C3 afforded high conversion to the desired product. Initially, the reaction was conducted at room temperature, due to a lack of equipment capable of maintaining a temperature of 30°C, the temperature used during the initial screen which resulted in slow conversion to the desired product (by UPLC and LCMS). Once a method was identified, the reaction was then stirred at 30°C for a further 24 hours, after which the reaction stalled at ~90% conversion to the desired product (by LCMS). As the small increase in temperature resulted in a significant increase in conversion to the (*S*)-alcohol, it was decided to investigate further the effects of temperature in an attempt to identify whether the conversion could be improved. Furthermore, it was thought that higher temperatures may increase the solubility of intermediate **3.53** in IPA and, as such, a higher concentration of 20 mg/mL was also investigated (Table 3.34).

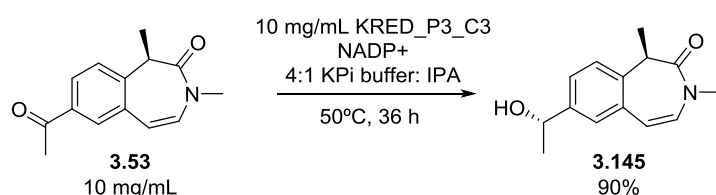


Substrate [mg/mL]	Enzyme [mg/mL]	Temp (°C)	Conversion (%)	ee%
10	10	30	66	99.8
10	10	40	87	99.9
10	10	50	89	99.8
20	20	30	55	99.6
20	20	40	62	99.6
20	20	50	65	99.5

Table 3.34. The effects of temperature on the conversion to the desired product was investigated. Conversions (%) were calculated by the ratio of the peak areas observed by UPLC.

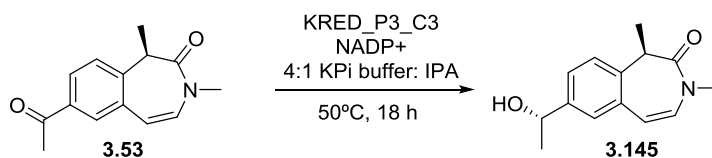
The reactions were performed with a 1:1 substrate: enzyme loading at two concentrations, 10 mg/mL and 20 mg/mL, and three temperatures were investigated, 30°C, 40°C and 50°C. The results indicate that the lower concentration of 10 mg/mL is preferred. Furthermore, an increase in conversion was observed with higher temperatures. Pleasingly, when analysed by chiral LC, the products of all six reactions demonstrated ee >99.5%, suggesting temperature does not impact the enantioselectivities. Therefore, these results suggest that a concentration

of 10 mg/mL and a temperature of 50°C is optimal for this reaction. A small-scale reaction was attempted using these optimised conditions (Scheme 3.34).



Scheme 3.34. Scale up of the enantioselective reduction using an increased temperature.

The improved reaction conditions resulted in a high conversion to the desired product (92 % a/a by LCMS) after 18 hours. However, leaving the reaction for a further 18 hours did not increase the conversion any further, thus suggesting that the reaction stalled at the ~90% conversion. As previously mentioned, variants of Plate 3 present instability in IPA. The stalling of the reactions could be due to this instability causing enzyme denaturation, thus preventing further reaction. If this is the cause, a higher enzyme loading could potentially increase the conversion to product prior to enzyme denaturation. This is supported by the higher conversion observed for the 2:1 enzyme: substrate loading observed in Entry 8, Table 3.33 (*vide supra*). Therefore, enzyme loading between 1-1.5 weight equivalents were investigated (Table 3.35).

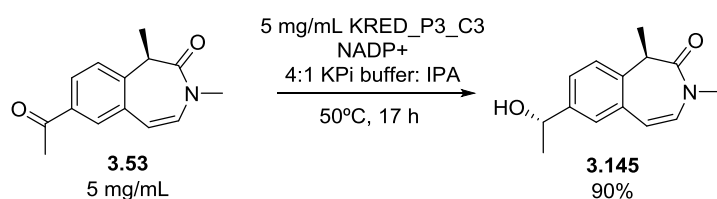


Substrate [mg/mL]	Enzyme [mg/mL]	Conversion (%)
10	10	82
10	11	83
10	12	82
10	13	81
10	14	72
10	15	71

Table 3.35. The effects of enzyme loading on the conversion to the desired product was investigated. Conversions (%) are the % area/area observed by LCMS.

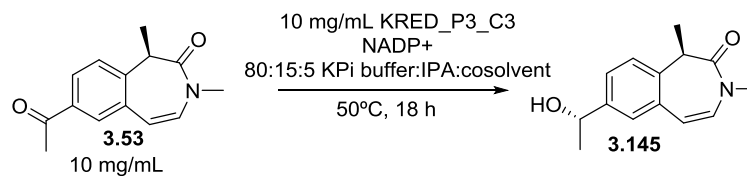
Interestingly, in contrast to the previous results, higher enzyme loadings resulted in reduced conversions. Overall, these investigations suggest that a conversion of ~90% is the optimal

conversion for this reaction. Therefore, the reaction was scaled up per the conditions in Scheme 3.34. Although these conditions gave high conversions on small scale, when replicated on a 1 g scale, minimal conversion to the product was observed. This was thought to be due to the poor solubility of the ketone being more problematic on the large scale. As such, the reaction was repeated with a concentration of 5 mg/mL ketone and 5 mg/mL enzyme (Scheme 3.35).



Scheme 3.35. Large scale up of the enantioselective reduction using the optimised conditions.

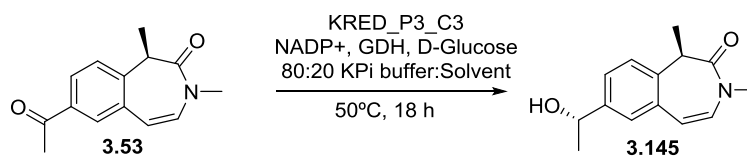
Employing lower concentrations of the enzyme and substrate successfully gave higher conversion to the desired product. Interestingly, the reaction stalled at ~95% conversion to the alcohol (by LCMS and NMR analysis). Despite the addition of fresh enzyme and NADP⁺ cofactor and stirring for an extra two days, no further conversion was observed. As such, column chromatography was required in order to remove the remaining ketone which was undesirable. Therefore, further investigations were undertaken in an attempt to achieve full conversion to the desired alcohol. Firstly, it was hypothesised that increasing the solubility of the ketone, by adding a co-solvent, would drive the reaction to completion. As previously mentioned, due to the instability of the Plate 3 enzymes to organic solvents, they can only form a maximum of 20% of the total volume. In addition, as isopropanol is also the recycling system, only 5% of a co-solvent can be employed. Therefore, five co-solvents were selected and screened based on the known tolerabilities of the Plate 3 KREDs (Table 3.36). The following trials were completed on a 10 mg/mL concentration of the ketone as originally investigated.



Co-solvent	Conversion (%)
THF	21
2-MeTHF	24
Toluene	53
DMSO	29
Methylcyclohexane	22

Table 3.36. The effects of co-solvents on the conversion to the desired alcohol were investigated. Conversions (%) are the % area/area observed by LCMS.

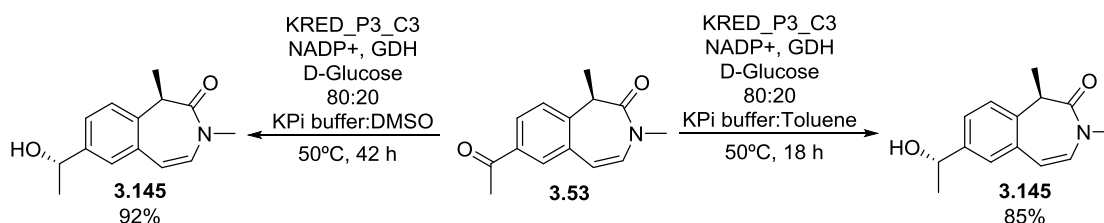
Unfortunately, the addition of co-solvents resulted in significant reduction in conversion to **3.145**. Upon adding the co-solvents to the reaction vials, slurries were formed suggesting poorer solubility of the ketone in the solvent combinations relative to solely isopropanol. Therefore, it was decided to investigate the same solvents in the absence of isopropanol. However, in order to do this, an alternative recycling system was required to replace the role of isopropanol. One such recycling system is the combination of D-glucose and glucose dehydrogenase (GDH). As such, the small solvent screen was completed with D-glucose/GDH as a replacement for isopropanol (Table 3.37).



Co-solvent	Conversion (%)
THF	28
2-MeTHF	7
Toluene	90
DMSO	92
Methylcyclohexane	73

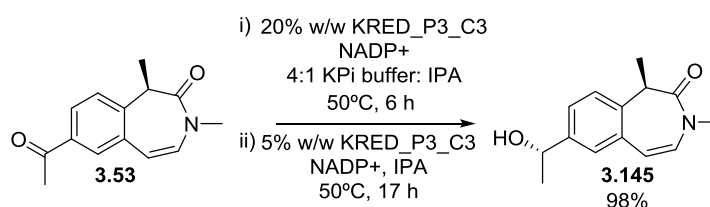
Table 3.37. The effects of alternative solvents and a different recycling system on the conversion to the desired alcohol were investigated. Conversions (%) are the % area/area observed by LCMS.

Pleasingly, comparable conversions to **3.145** were observed when toluene and DMSO were employed, relative to isopropanol, on a small scale. Therefore, it was decided to repeat these reactions on a larger scale to see whether these conversions could be further increased (Scheme 3.36).



Scheme 3.36. Larger scale reduction of **3.53** employing the alternative recycling system.

When these reactions were attempted on a larger scale the rate of conversion to the desired product was much slower. Furthermore, the toluene reaction showed significantly less product after 18 hours of heating than the trial reaction and resulted in a lower yield of 85%. However, the DMSO reaction showed a similar conversion to its trial reaction after 18 hours but this did not increase upon a further 24 hours of heating and afforded a 92% isolated yield. Therefore, although this reaction offers the potential to use an alternative recycling system to isopropanol, it did not achieve full conversion as desired. Consequently, efforts turned back to optimising the isopropanol-based reaction. As aforementioned, isopropanol is oxidised to acetone during the reaction, thus allowing NADPH to be regenerated. Therefore, it was hypothesised that the stalling of the reaction may occur when high levels of acetone are present. At high levels of acetone, further oxidation of isopropanol may become undesirable thus meaning NADPH is not reproduced. As such, removal of the organic layer upon the reaction stalling and reloading the vessel with fresh isopropanol, enzyme and NADP+ could promote further conversion to the product. Furthermore, it was decided to investigate whether this could be achieved with a lower loading of enzyme (Scheme 3.37).



Scheme 3.37. The original KRED reduction conditions with fresh components added once the reaction stalled was investigated.

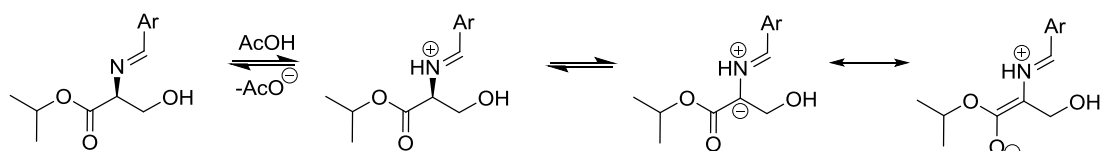
After 6 hours of heating using a 20% weight loading of enzyme, the reaction had stalled at 90% conversion by LCMS. At this stage, the organic layer was removed and fresh components added before a further 17 hours of heating. Pleasingly, this resulted in 100% conversion to the desired product which meant that, following a work up and without a purification, compound **3.145** was isolated in 98% yield. Therefore, the chiral reduction

utilising KRED_P3_C3 using this approach was implemented into the synthetic route of **3.72**.

3.3.5.3 Optimisation of the reductive amination to install the esterase sensitive motif in lead compound **3.37**

The existing route to **3.72** involves a reductive amination of the amino acid ester **2.87** and the pyridine aldehyde **3.43** to form intermediate **3.74**. Although nucleophilic substitution reactions were used to install the ESM in the diazine intermediates, these syntheses involved two synthetic steps compared to the one for a reductive amination. As the synthetic route to final ESM-containing compounds already contains a large number of steps, the one step reaction was desirable. Therefore, it was decided to attempt to optimise the reductive amination first.

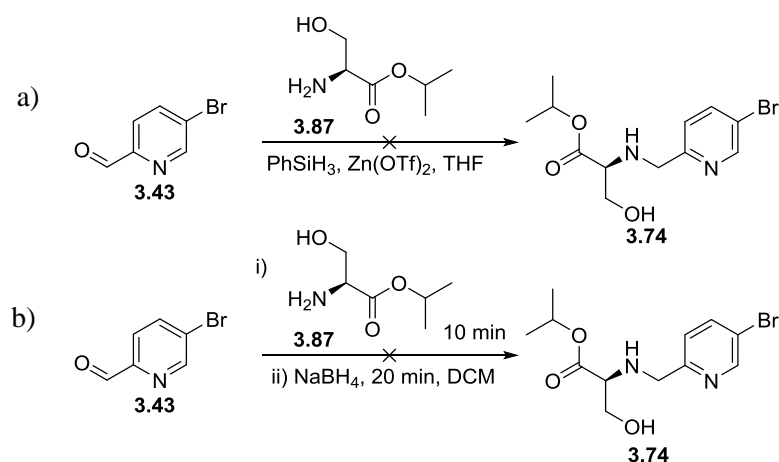
With the isopropyl Ser ESM **2.87**, this sometimes results in partial or full racemisation of the ESM chiral centre. Similar results were published by Yamada *et al* in 1982, who reported the racemisation of optically active amino acids in the presence of acid.²¹¹ The racemisation proceeds through a 1,2-proton shift which is promoted by the presence of acid (Scheme 3.38). Following imine formation, the imine is protonated by the acid to form the iminium ion. The resultant conjugate base abstracts a proton from the α -carbon causing it to go from a tetrahedral geometry to trigonal planar. As such, in the reverse reaction a proton can be delivered with equal chance on either face thus causing racemisation.



Scheme 3.38. Mechanism for the racemisation of amino acid esters in the presence of acid.

Furthermore, acetic acid was shown to result in the fastest racemisation rates out of a range of acids. Acetic acid is present in sodium triacetoxyborohydride and, therefore, could be promoting the observed racemisation when a reductive amination is used to append the ESM. Indeed, when a batch of the building block **3.74**, formed using the reductive amination conditions in Scheme 3.12 by a colleague, was submitted for chiral analysis, it was determined to have an ee of 18%.²¹² This shows a significant amount of racemisation occurred during the reductive amination under these conditions and, as such, alternative

conditions that avoided racemisation were required. As such, alternative reductive aminations were employed to remove the presence of acetic acid (Scheme 3.39). Firstly, a Lewis acid was employed in an attempt to facilitate the imine formation, as well as an alternative hydride source (Scheme 3.39a). Secondly, the imine was pre-formed prior to the addition of sodium borohydride in order to reduce the imine whilst minimising the level of aldehyde reduction (Scheme 3.39b).

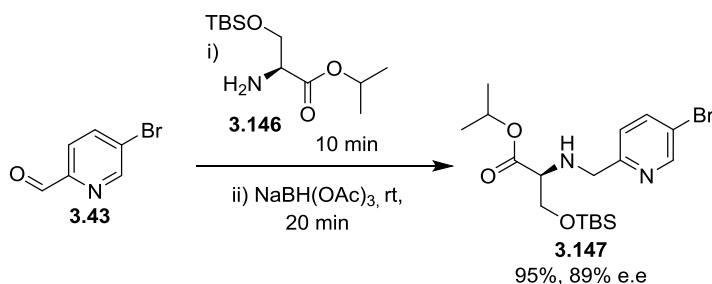


Scheme 3.39. Alternative reductive amination conditions where a) employs a Lewis acid to facilitate the imine formation and reduction in a stereoselective manner with an alternative silane hydride source and b) sodium borohydride reduction following imine formation.

Neither of the sets of conditions afforded the desired product but rather resulted in very messy reaction profiles. Therefore, different conditions were still required. The existing reductive amination conditions (Scheme 3.28, *vide supra*) use salt forms of the amino acid esters and have typical reduction times of 1-4 hours. Therefore, the reaction mixture is subject to large quantities of acid for potentially long periods of times. As such, it was hypothesised that shorter reaction times and using the free base of the amino acid ester would reduce the amount of racemisation observed. Furthermore, it was thought that increasing the steric bulk of the flexible serine chain would reduce the rate of approach of the acetoxy anion and subsequent proton abstraction from the α -carbon.

Consequently, the serine alcohol was protected as a TBS ether in order to increase its steric bulk, with the added advantage that the extra lipophilicity should aid with purification which thus far had been problematic. The intermediate **3.146** was synthesised by a colleague as the free base.²¹² The material was used to perform a reductive amination using the existing conditions (Scheme 3.28, *vide supra*) to form intermediate **3.147**. However, upon the addition of triethylamine a thick sludge was formed which caused slow reduction of the

imine. This meant further equivalents of sodium triacetoxyborohydride was required, totalling 6 equivalents. Full reduction after 6 hours was still not observed and, as such, sodium borohydride also had to be employed. Therefore, the reaction was reattempted with the exclusion of triethylamine and with 5 equivalents of sodium triacetoxyborohydride (Scheme 3.40).

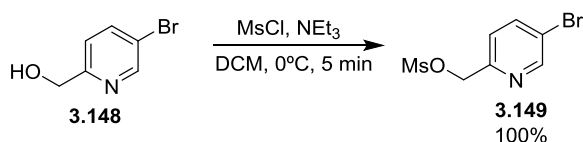


Scheme 3.40. The reductive amination was trialed with the protected Ser ESM.

Full reduction was achieved after twenty minutes with sodium triacetoxyborohydride. Furthermore, the material was obtained in high purity following an aqueous work up, negating the need for a purification. Unfortunately, chiral analysis showed the material to have an ee of 89%. Although this is a significant improvement relative to the starting point, this is not sufficient for the incorporation into target molecules and, as such, needs further improvement. Therefore, it was decided to try an alternative method to forming the C-N bond.

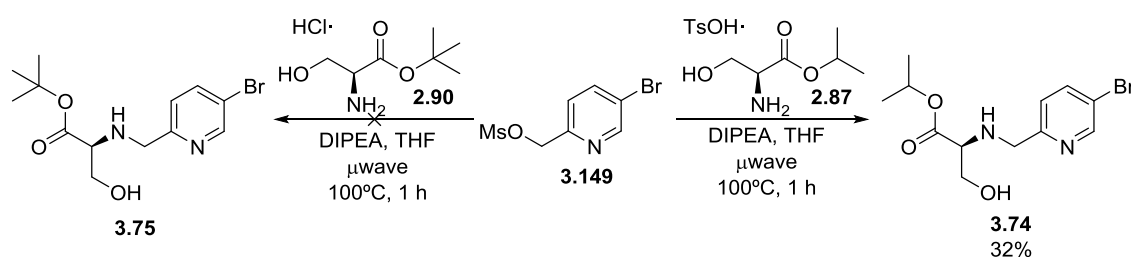
3.3.5.4 Nucleophilic substitutions as an alternative approach to install the esterase sensitive motif in lead compound 3.37

As aforementioned, nucleophilic substitutions are a common method for C-N bond formation. As demonstrated with the second generation diazine analogues, nucleophilic substitution reactions can be used to append the ESM to the relevant heterocycles. Therefore, this approach was applied to the pyridyl analogue **3.72**. Firstly, the mesylate **3.149** was formed through the mesylation of alcohol **3.148** (Scheme 3.41).



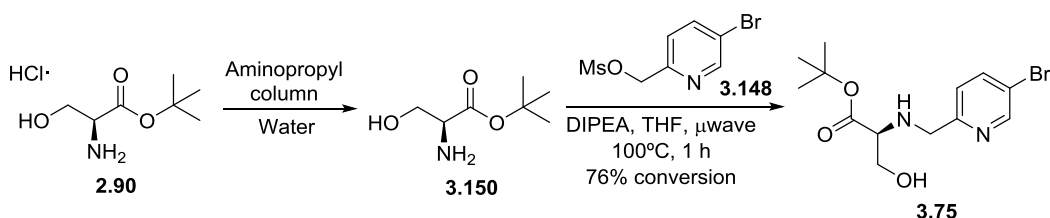
Scheme 3.41. Mesylation conditions employed to form **3.149**.

Initially, the mesylation was completed at room temperature and, although conversion to the desired product was observed, the formation of a side product was also seen in which the chloride ion had displaced the mesylate. However, reducing the temperature to 0°C improved the reaction profile and resulted in complete conversion to the desired mesylate thus negating the need for a purification. Following the isolation of the mesylate, an investigation of the S_N2 reaction with the amino acid ester **2.87** was attempted with a small set of reaction conditions. Of these, THF and DIPEA and the tosic acid salt of the amino acid ester offered the highest conversion to the desired product (Scheme 3.42).



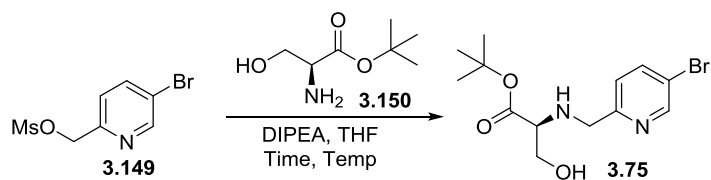
Scheme 3.42. Initial alkylations of the mesylate **3.149**.

Interestingly, while the S_N2 displacement with the isopropyl Ser ESM resulted in the desired product, the same reaction with the *tert*-butyl Ser ESM **2.90** gave only minor conversions to the product. Instead, high conversion to a side product was observed in which the mesylate had been displaced by the chloride of the HCl salt. As such, the *tert*-butyl Ser amino acid ester was desalted to form intermediate **3.150** and the reaction repeated (Scheme 3.43).



Scheme 3.43. Alternative alkylation conditions. Estimated conversion (%) is quoted as the % area/area observed by LCMS.

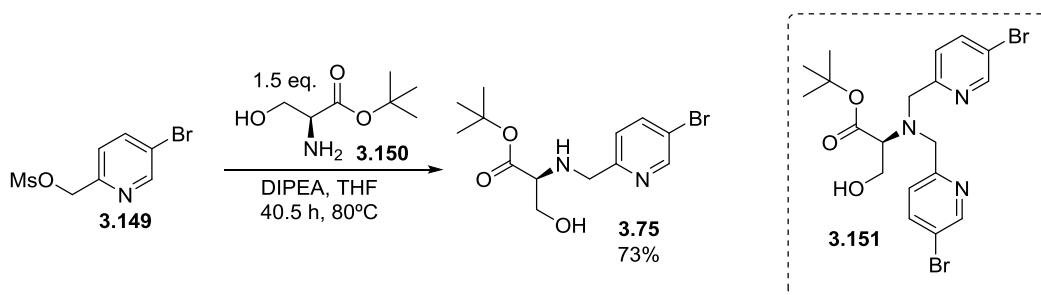
Due to the small scale the product was not isolated but the displacement with the desalted ESM resulted in high conversion to the desired intermediate. However, microwave heating is undesirable for large scale reactions and, as such, further optimisation of these conditions for thermal heating was required. To investigate the optimal temperature for the displacement, a reaction mixture was heated initially at 40°C before the temperature was increased in 10°C increments (Table 3.38). The conversion was monitored at each stage by LCMS analysis.



Temperature (°C)	Time (h)	Conversion (a/a %)	Increase in conversion (a/a %)
40	1.25	2	-
50	2	8	6
60	1.3	14	6
70	2	24	10
80	1	37	13
80	18.5	80	43

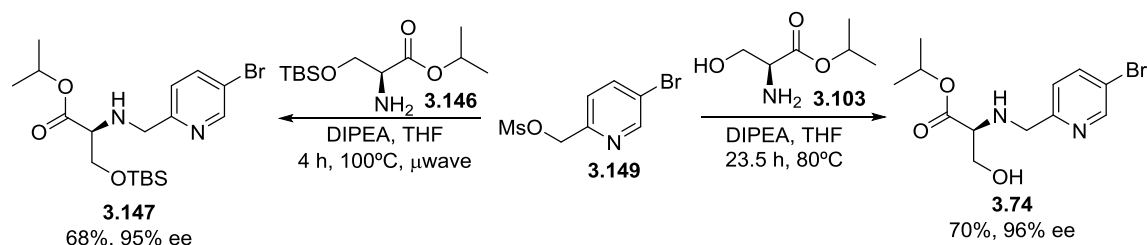
Table 3.38. Initial screen of temperature for the alkylation to form **3.75** using a single reaction mixture that was heated up to higher temperatures at intervals. Estimated conversion (%) is quoted as the % area/area observed by LCMS.

The results showed that significant conversion to the desired product was only achieved at 80°C. Furthermore, despite a longer reaction time, thermal heating overnight produced comparable conversions to microwave heating. As such, thermal heating at 80°C was implemented in the synthetic route, replacing the microwave step. However, whilst high conversions to the desired intermediate were observed, the tertiary amine **3.151**, in which intermediate **3.75** had undergone a second S_N2 reaction with the mesylate **3.149**, was also produced. In an attempt to reduce this side product, the reaction was repeated with an excess of *tert*-butyl Ser ESM (Scheme 3.44).



Scheme 3.44. Alkylation to form **3.75**, employing excess ESM in an attempt to minimise the formation of the side product **3.151**.

These conditions afforded a 90% conversion (by LCMS) to the desired product and isolated yield of 73% with significantly reduced levels of the dialkylated side product. As such, these conditions were applied to the synthesis of the biologically hydrolysable isopropyl Ser amino acid ester **3.74** (Scheme 3.45). To allow comparison to the reductive aminations, the alkylation was also attempted with the protected amino acid ester **3.146**.

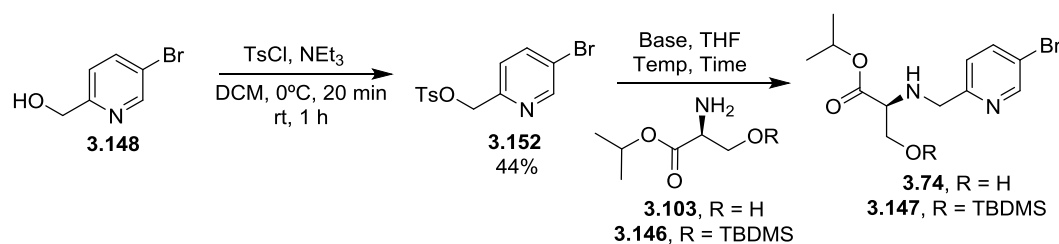


Scheme 3.45. Large scale alkylations to form **3.74** and **3.147**.

The reaction conditions were reproducible when attempted on small scale, however, on larger scale, two equivalents of the amino acid ester and longer heating times were required to push the reaction to completion. Despite this, intermediate **3.74** was obtained in a high yield, over double that of the previous conditions used (Scheme 3.42). The reaction to afford the protected intermediate **3.147** also required longer heating times and it was only obtained in a moderate yield. Chiral analysis determined intermediates **3.74** and **3.147** to have 96% ee and 95% ee respectively, a significant improvement to the ee achieved using reductive aminations (18% ee). However, Ames studies require compounds to have ee > 99.5% and, as such, further improvement was still desired.

Analysis of the amino acid ester showed it to have 100% ee thus suggesting that the minor racemisation was occurring during the reaction. As such, it was thought that increasing the reactivity of the leaving group, which could allow a reduction of the reaction time and the reaction temperature, could improve the ee. Initial investigations focussed on the nosyl group as a replacement for the mesylate. However, the nosyl intermediate was so reactive that it could not be isolated and one-pot procedures resulted in significant side products with minor conversions to the desired intermediate. As such, it was deemed that the nosylate was too reactive and efforts were re-focussed on the tosylate **3.152**.

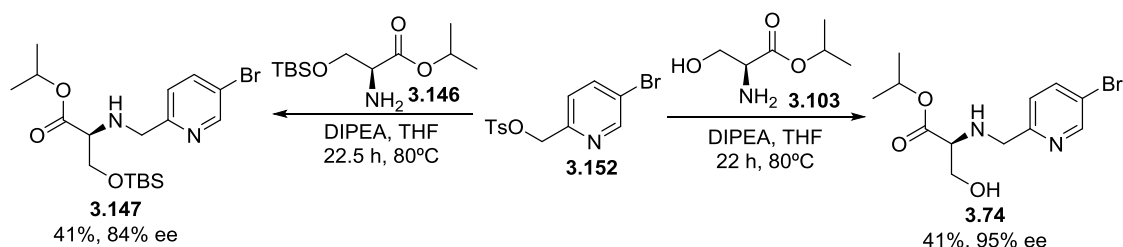
In order to gain a quick insight into base and temperature requirements, the alkylation of **3.152** with the amino acid esters **3.103** and **3.146** were trialled with five different bases and the reaction mixtures were stirred for ~1 hour at room temperature being increased in temperature in 10°C increments with ~1 hour of heating at each temperature. Due to the set-up of the reactions, the maximum temperature possible was 60°C, however, these trial reactions were sufficient to identify whether any of the bases showed increased conversion relative to DIPEA (Table 3.39). The reactions were monitored by LCMS analysis.



		Temp ($^\circ\text{C}$)							
		rt		40		50		60	
Base		OH	OTBS	OH	OTBS	OH	OTBS	OH	OTBS
	DIPEA	0	0	0	2	2	5	7	19
	K_2CO_3	0	0	0	2	3	5	9	18
	2,6-lutidine	0	0	0	1	4	6	4	13
	NaH	0	0	0	0	1	1	12	1
	NEt_3	0	0	0	1	4	6	8	20

Table 3.39. Initial screen of the alkylations on the tosylate **3.152**. Conversions to products **3.74** and **3.147** are quoted as a/a% as seen in LCMS analysis.

Of the temperatures investigated, significant conversion was only observed at 60°C , thus suggesting that, similarly to the mesylate, high temperatures are required to drive the alkylation. In addition, there was no significant difference between the conversions achieved with the various bases, and, as such, they offer no advantages over the original DIPEA base. Interestingly, higher conversions were observed for the protected amino acid ester which suggests that this alkylation could offer reduced reaction times compared to the alkylation with the isopropyl Ser **3.103**. Overall, these results do not imply that an alternative set of conditions to the original conditions (outlined in Scheme 3.45, *vide supra*) will give significant reduction in reaction times or temperatures and, as such, larger scale reactions utilising the original conditions were completed (Scheme 3.46).



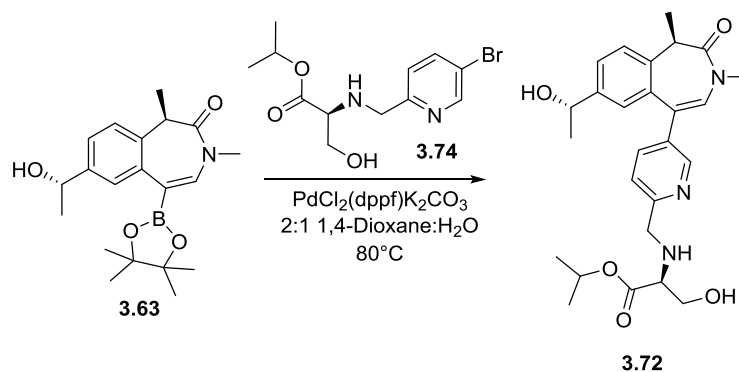
Scheme 3.46. Large scale alkylations of the tosylate **3.152** with the protected and unprotected isopropyl Ser ESMS.

Interestingly, the alkylations employing the TMS protected Ser ESM were consistently lower

yielding than when the unprotected ESM was used. Furthermore, intermediate **3.147** had a significantly lower ee of 84%, which is in line with the results observed during the reductive amination. Overall, through these optimisations, conditions have been developed which afford the desired intermediate in a high ee.

3.3.5.5 Suzuki-Miyaura cross-coupling of boronic ester **3.63** and bromide intermediate **3.74** to form the lead compound **3.37**

The final step of the synthetic route is the Suzuki-Miyaura cross coupling of the boronic ester intermediate **3.63** and bromide intermediate **3.74**. Despite high conversions by LCMS and NMR analysis, low yields were obtained due to poor recovery from purification. Throughout the investigations described in this thesis, purification of ESM-containing final molecules have been low yielding following MDAP or normal phase purification. Therefore, an alternative purification method was desired. It was hypothesised that the poor recovery of material following purification was due to the benzylic amine and pyridyl nitrogen being able to chelate to, and thus be retained on silica. As such, various chromatographic purification methods were investigated that would reduce the capability of this potential interaction (Table 3.40).



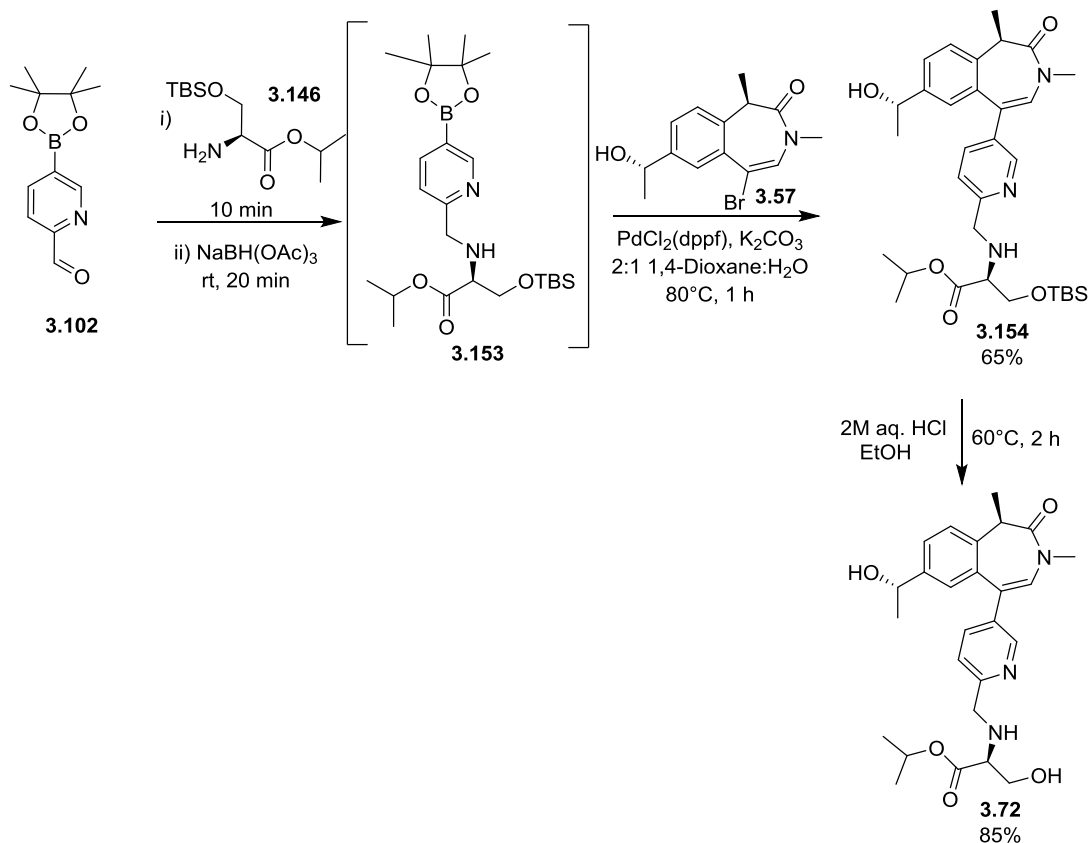
Entry	Purification	Isolated Yield (%)
1	MDAP (HpH)	26
2	Reverse phase (Formic)	0
3	Reverse phase (HpH)	47
4	Normal phase - KP-NH ₂ column	29
5	Normal phase with AcOH flush	0
6	Normal phase with water-saturated EtOAc	64

Table 3.40. Optimisation of the purification method for **3.72**.

Firstly, reverse phase column chromatography was attempted as the original MDAP

purification showed a moderate yield of 26% (entry 1). Whilst the reverse phase chromatography with a formic modifier afforded no product (entry 2), a moderate yield of 47% was obtained with the ammonium carbonate modifier, almost a two-fold improvement (entry 3). As well as reverse phase chromatography, normal phase column chromatography with a KP-NH₂ column was attempted. These columns contain an amine-functionalised silica stationary phase which acts to shield organic amines from acidic silanols and, as such, prevent the amine from chelating to the column. Unfortunately, there was no improvement in the isolated yield when this method was employed (entry 4). Finally, two adaptations of the normal phase column chromatography using silica columns were investigated. The first was flushing the column with five column volumes of acetic acid, prior to running the purification, to ensure full protonation of all of the silica sites and reduce interactions with **3.72**. The second was based on the same principle but using water-saturated ethyl acetate as the eluent so that water would saturate the silica sites.²¹³ Interestingly, the acetic acid flush led to no material being recovered from the column (entry 5). However, the water-saturated ethyl acetate increased the isolated yield to 64% (entry 6). This is a significant improvement on the original conditions and was selected as the optimal purification.

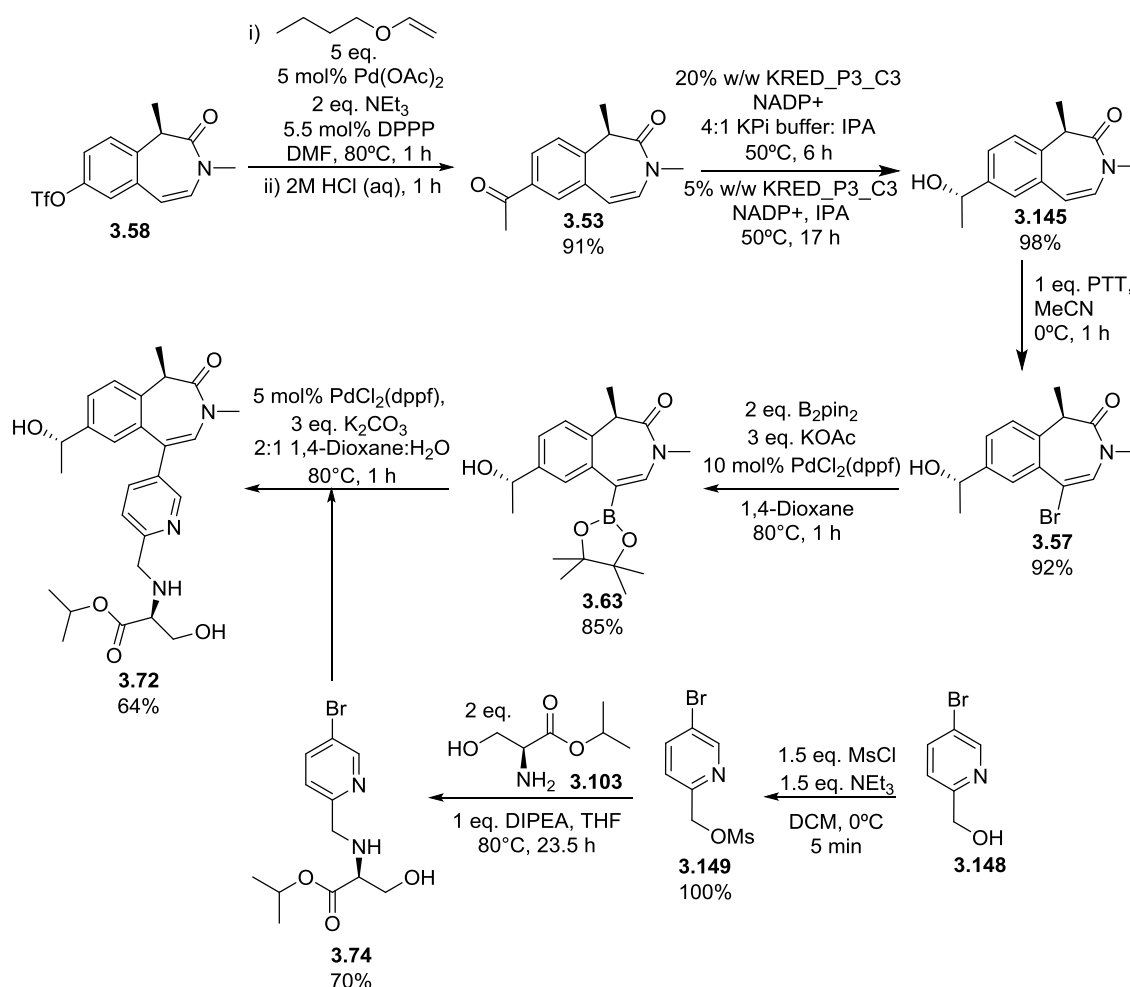
In addition to investigating the purification issues, the synthetic route was also re-examined. The existing route necessitated the BZP intermediate to be the boronic ester as previous attempts at the cross-coupling reaction using the reverse reactivity (i.e. the bromo-BZP and the boronic ester pyridyl intermediate) had failed. This is most likely due to the oxophilicity of boron causing it to interact with the serine hydroxyl group rather than facilitating the cross-coupling. However, as already demonstrated, protection of the serine does not impede the reactivity of the amino acid building block and, as such, it was decided to investigate this further. As aforementioned, the triflate-BZP building block **3.58** is formed from an 8-step synthesis and a further four synthetic steps is required to afford the boronic ester intermediate **3.63**. Therefore, in terms of cost and synthesis times, it would be preferential to use the bromide intermediate **3.57**, which removes a synthetic step and thus increases the amount of material available. To facilitate this, the reductive amination of the protected isopropyl Ser ESM **3.146** and boronic ester **3.102** was completed to afford **3.153** (Scheme 3.47).



Scheme 3.47. Alternative synthetic route to **3.72**.

Using the optimised conditions from Scheme 3.40, the reductive amination of **3.102** and **3.146** afforded intermediate **3.153**. Although the intermediate was isolated in high yield as crude material (91%), the purity was indeterminable due to the presence of the boronic ester and acid in the NMR and LCMS. As such, the crude material was used in the Suzuki-Miyaura cross-coupling without purification in an attempt to identify whether this was an artefact of the intermediate being unstable under LCMS conditions. The LCMS profile of the Suzuki-Miyaura cross-coupling only showed the presence of the starting materials and the product and upon completion, only the product peak. This suggests that intermediate **3.153** was indeed pure but unstable in LCMS analysis, thus fragmenting to several peaks. Pleasingly, **3.154** was afforded in a high yield of 65% over the two steps using the water saturated ethyl acetate purification discussed earlier. This route reduces the number of synthetic steps that the BZP building block **3.58** would have to go through, thus increasing the mass available. Unfortunately, intermediate **3.153** can only be formed through a reductive amination which unfortunately was shown to provide suboptimal e.es. As such, this route is not optimal due to the lower than desired e.e. obtained under these conditions.

In conclusion, significant optimisation to the synthetic route of **3.72** was achieved, with improvements made to several steps (Scheme 3.48).

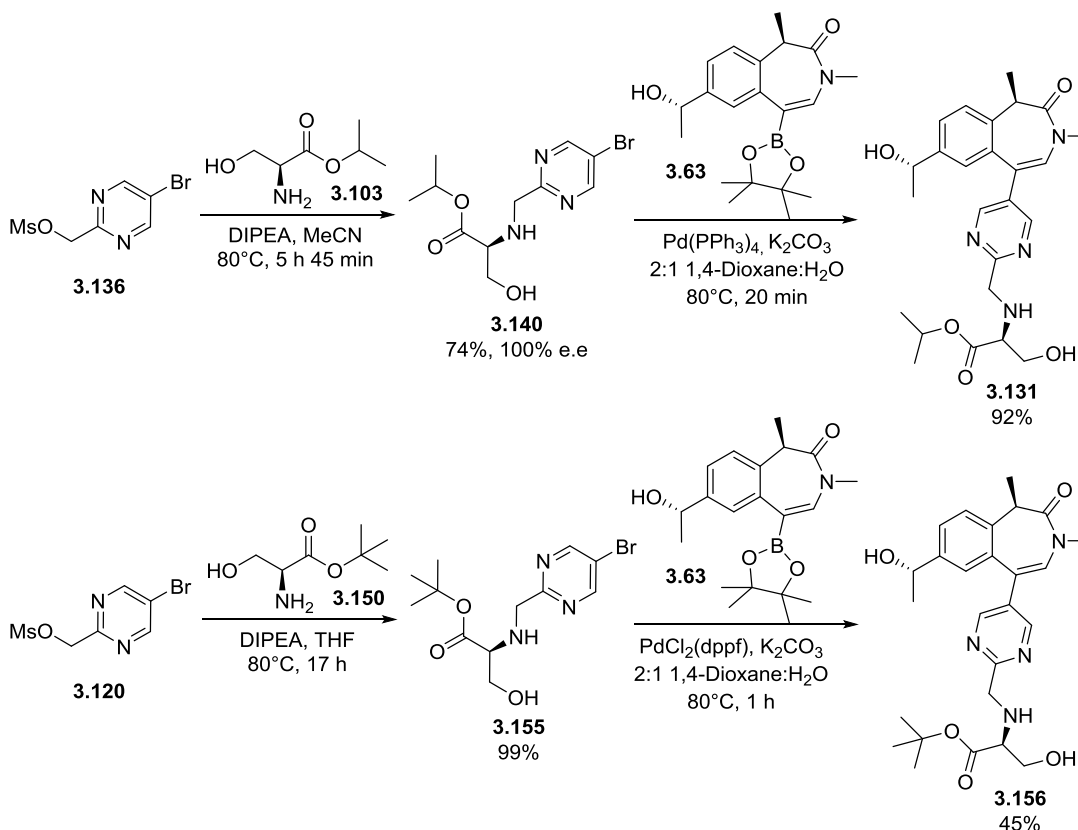


Scheme 3.48. Optimised synthetic route to lead compound **3.72**.

Firstly, minor adaptations to the Heck reaction, including a solvent swap to DMF, saw the yield increase significantly, whilst reducing the reaction time from ~17 hours to 1 hour. Next, a stereoselective enzymatic reduction of the ketone **3.53** replaced the original achiral reduction and chiral separation, thus reducing the loss of material and waiting time, whilst achieving the desired diastereomer **3.145** in high yield and high ee. Furthermore, recrystallisation of this intermediate resulted in 100% ee. Intermediate **3.74** was formed through an alkylation with the isopropyl Ser ESM **3.103** in high ee relative to the original reductive amination (18% ee). Finally, optimisation of the purification of the Suzuki-Miyaura cross coupling to form **3.72** increased the yield from 28% to 64%.

As aforementioned, due to their structural similarity, it was hypothesised that the optimised synthetic route to **3.72** could be directly applied to the synthesis of **3.131**. As such, the synthesis of **3.131** was attempted using the conditions outlined in Scheme 3.48 (Scheme 3.49). Furthermore, the synthesis of the biologically non-hydrolysable *tert*-butyl analogue **3.156** was also synthesised. As intermediate **3.63** is common to both analogues and the

mesylation had been completed previously, only the alkylation and Suzuki-Miyaura cross coupling had to be completed.

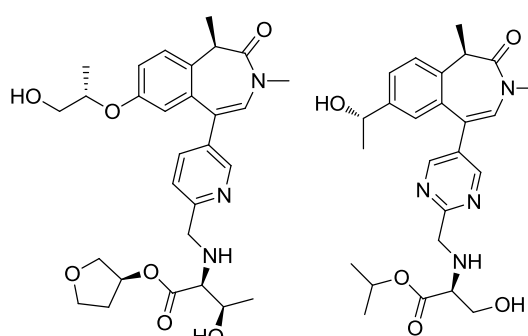


Scheme 3.49. The optimised route to **3.72** was transferable to **3.131**.

The synthetic route was successfully employed to synthesise **3.131** with high yields obtained which highlights the transferability of the route to structurally related molecules. In addition, the route was also applicable to the synthesis of **3.156**. Whilst THF was used as the solvent for the pyridyl intermediate **3.74**, acetonitrile was employed for the synthesis of intermediate **3.140**. Pleasingly, these conditions reduced the reaction time to ~6 h and afforded intermediate **3.140** in 100% ee. Initially, the Suzuki-Miyaura cross-coupling to form **3.131** was completed with PdCl₂(dppf) but minor amounts of ligand co-eluted with the product during column chromatography. As such, the reaction was repeated with Pd(PPh₃)₄ to avoid this problem and, pleasingly, in conjunction with the water-saturated ethyl acetate purification afforded the desired product in >90% yield.

3.3.6 *In vivo* cynomolgus monkey PK studies of lead compounds 3.37 and 3.131

The successful optimisation of the synthetic routes to all three analogues meant the synthesis of large quantities of material was feasible, if required. Furthermore, it also enabled the synthesis of material for *in vivo* and Ames studies. At this stage, analogue 3.72 was retested in the human hepatocyte IVC assay and, unfortunately, demonstrated an increased clearance of 3.3 mL/min/g (82% LBF, n=3) compared to the original value of 2.5 mL/min/g (78% LBF, n=1). This caused the early dose prediction to significantly increase to an undesirable 252 mg QD. As such, this, along with the high human hepatocyte IVC, meant no further studies were performed on this compound. However, analogues 3.37 and 3.131 were progressed into cyno PK studies (Table 3.41).



		3.37	Acid	3.131	Acid
IV 1 mg/kg	CL _{Total} (mL/min/kg)	36.2	-	41.4	-
	V _{SS} (L/kg)	1.3	-	1.45	-
	t _{1/2} (h)	0.7	-	0.35	-
	AUC _{0-t} (h.ng/mL)	226	211	389	248
	Acid: ester ratio	-	0.9:1	-	0.6:1
PO 3 mg/kg	C _{max} (ng/mL)	185	45.0	57.3	291
	Bioavailability (%)	0.6	-	6.0	-
	t _{1/2} (h)	-	-	-	-
	AUC _{0-t} (h.ng/mL)	9.0	78.8	68.0	518
	Acid: ester ratio	-	9:1	-	8:1

Table 3.41. Cynomolgus monkey IV/PO *in vivo* profile based on n=1. It should be noted that the acid was not dosed, but generated *in vivo* from the parent compounds and monitored during the study.

Analogues 3.37 and 3.131 were dosed at 1 mg/kg in the IV portion and 3 mg/kg in the oral portion of the *in vivo* cynomolgus monkey study. The pharmacokinetic parameters for the parent compounds, and their acid metabolite, were monitored following their administration.

Analogue **3.37** exhibited a moderate clearance, in line with what was expected from the *in vitro* hepatocyte clearance, and a low volume of distribution as well as a low AUC for **3.37** in the oral leg which is indicative of poor permeability. The low oral bioavailability is likely due to a combinatorial effect of these parameters. Unfortunately, as a result of the poor bioavailability, no further studies were completed on the compound at this stage. Meanwhile, the second generation diazine analogue **3.131** exhibited higher clearance than expected from the *in vitro* hepatocyte clearance, which contributed to the low half-life observed. Similar levels of **3.131** and its acid metabolite were observed in the IV leg, as shown by the AUCs. However, there were significant difference in the PO leg with a low AUC observed for **3.131** and a high AUC seen for the acid metabolite. This is indicative of the ester being readily absorbed, followed by rapid hydrolysis thus suggesting that the compound is highly turned over by CES-1. These factors resulted in an oral bioavailability of 6%, 10-fold higher than the first generation pyridyl analogue **3.37**. Unfortunately, the oral bioavailability was deemed insufficient for further progression and no further studies were completed. However, the profile did fulfil the hypothesis outlined at the outset of this chapter that reducing the cynomolgus monkey hepatocyte clearance would increase the oral bioavailability relative to the AP-OTS analogue **2.69** (1.1%).

Chapter 4

Conclusions and Future Directions

4.0 Conclusions

This work described in this thesis encapsulates the search for a back-up molecule to the candidate **1.6**. Molecules with desirable profiles have been developed from lipophilic and metabolically unstable starting points in two structurally differentiated series. The aim of the first section of this thesis was to understand whether the ESM could be directed over the WPF shelf to give potent, selective compounds with good physicochemical properties. The lead compound **2.2** displayed high biochemical and cellular activity, with a desirable ΔhWB (+1.3). However, the compound suffered from high HLM and hepatocyte IVC and the acid potency was lower than desired (6.8) (Figure 4.1). As such, compounds with increased metabolic stability and acid potency were desired.

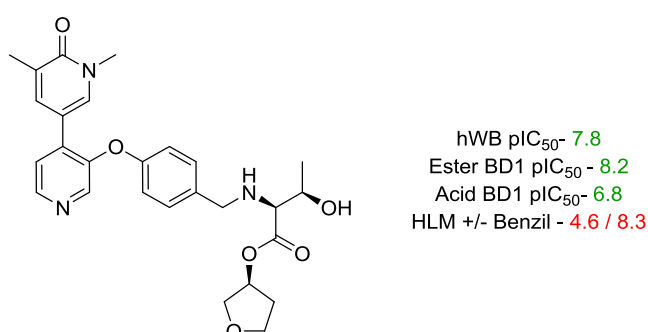


Figure 4.1. Profile of initial lead compound **2.2**.

To achieve this, two approaches were taken (Figure 4.2). The first was to investigate the impact of altering the bond angles to the ESM. Crystal structures of **2.2** in BRD2 BD2 show a hump caused by a methionine residue causes the CH₂NH linker of the ESM to be fixed in position, thus increasing the loss of entropy upon binding. Therefore, it was hypothesised that moving the ESM linker away from this residue, by changing the relative bond angles between the ether and ESM linkages, it would have a higher degree of flexibility and, as such, lead to increased potency. A statistical analysis of bond angle vectors for five-membered rings based on data derived from the Cambridge Structural Database was used to select five-membered rings with angles increasing in 10° increments from 120° to 180°. Due to synthetic tractability, only the 130° and 160° bond angles were accessed. However, the data gathered was sufficient to suggest that the 180° bond angle is the optimal, with both molecules displaying poor biochemical and cellular activity and no improvement in IVC.

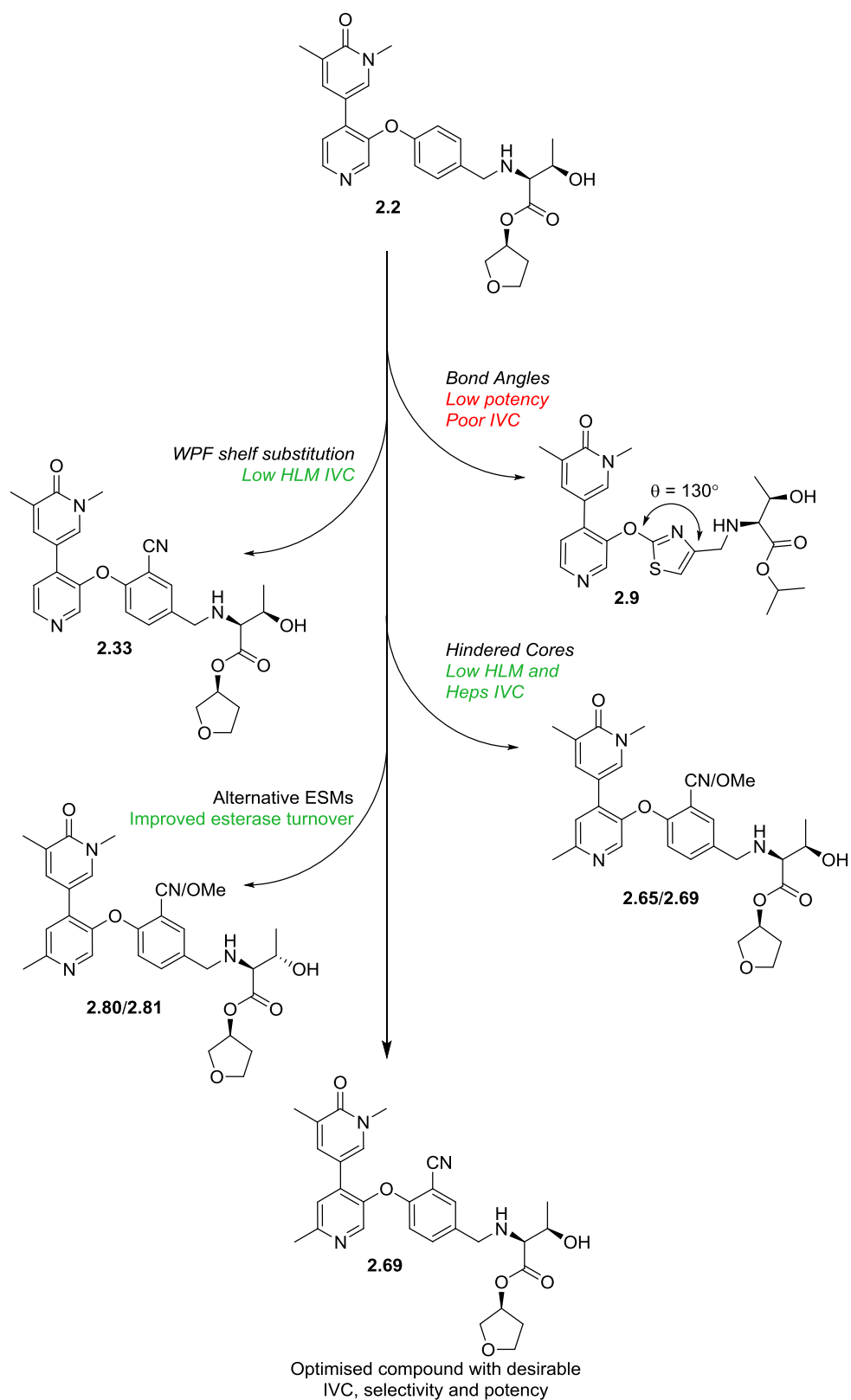


Figure 4.2. Key advancements made in this project.

The second approach investigated the substitution of the WPF shelf group (Figure 4.2., *vide supra*). Crystal structures of **2.1** in BRD2 BD2 indicate a solvent exposed region adjacent to the WPF shelf and the WPF shelf group. As the area is unhindered and at the surface of the bromodomain, it was hypothesised that substitution of the benzene ring of **2.2** would be tolerated. Furthermore, due to the positioning and close proximity of the tryptophan of the WPF shelf and the benzene ring, it was hypothesised that the two rings were interacting through parallel-displaced π - π stacking. A *meta*- σ *meta*- π Craig plot was used to identify substituents to modulate the electronics of the ring, as well as reduce lipophilicity, which were profiled *in silico*. Analysis of the *in silico* data showed the methoxy, methyl and cyano moieties to be the optimal substituents. Initial data indicated the 3-position was sub-optimal for IVC reduction as was the 2-methyl substituent, whilst the 2-OMe and 2-CN analogues, **2.31** and **2.33** respectively, showed improved metabolic stability and similar potencies relative to **2.2**. Interestingly, **2.31** and **2.33** display similar biochemical and cellular activities, showing that modulating the ring electronics does not impact potency and, as such, suggesting the molecules do not interact with the tryptophan of the WPF shelf in a parallel-displaced π - π hydrogen bond.

Although the analogues displayed a lower HLM IVC, a further reduction was required. It was thought the high IVC may be due to the unhindered pyridyl core, moieties which are known to be metabolised by cytochrome P450 enzymes through the interaction of the heme complex and the pyridyl nitrogen. Therefore, by synthesising the sterically encumbered methylpyridine, **2.65** and **2.69**, and 2-pyridyl, **2.76**, analogues, it was theorised that the metabolic stability would be improved due to hindering the coordination of the nitrogen to the Fe and reducing the metabolic turnover. Indeed, the HLM and hepatocyte IVC was reduced to a desirable level for all three analogues. Of the three analogues, **2.65** and **2.69** demonstrated higher biochemical and whole blood ester potency and acid potency, as well as lower lipophilicity, but had low CES-1 turnover. In an attempt to increase turnover by CES-1, alternative ESM groups were incorporated. Interestingly, this was achieved for the isopropyl Ser analogues, **2.88** and **2.89**, and THF *allo*-Thr analogue of **2.65**, **2.63**, but not for the THF *allo*-Thr analogue of **2.69**, **2.64**. Furthermore, whilst the isopropyl Ser analogues **2.88** and **2.89** displayed high human hepatocyte clearance, the THF *allo*-Thr analogues **2.63** and **2.64** achieved the desired levels. As analogues **2.65** and **2.69** were further down the screening cascade, it was decided to progress these analogues into further profiling.

TDI studies revealed that both **2.65** and **2.69** demonstrated time dependent inhibition of CYP3A4, a risk that could be mitigated by a low dose prediction. Further *in vitro* tests

showed both compounds to display high rat and mini pig hepatocyte clearance, whilst having moderate-high dog hepatocyte clearance. The analogues were shown to display high selectivity for BET proteins over other bromodomain-containing proteins, with only a small number of other bromodomains being inhibited. The wider selectivity of the compounds was studied through an enhanced cross-screening panel screen, which showed only two medium risks which were phenotypic flags commonly seen for ESM molecules rather than biological targets. Comparison of the overall profiles of **2.65** and **2.69** at this stage showed **2.69** to have the more desirable profile and, as such, it was selected for further DMPK profiling which facilitated its progression into PK studies. Unfortunately, the compound was shown to exhibit high clearance and a poor bioavailability (1.1%) and at this stage no further studies were completed on the series. However, this series provided a key learning that the target IVC profile was too high to produce a compound with desirable cynomolgus monkey PK. Therefore, this profile was amended and a new target profile generated for the BZP series.

The second part of this thesis focussed on the development of the structurally differentiated BZP series which incorporated an alternative warhead. The aim of the investigation was to understand whether the ESM could be directed through the ZA channel to produce potent, selective compounds with low IVC and desirable physicochemical properties. The starting point **3.4** displayed high whole blood potency and a desirable Δ hWB (+0.9). However, although the compound exhibited desirable lipophilicity, it suffered with high HLM and hepatocyte IVC thus suggesting an underlying metabolic liability (Figure 4.3). As such, compounds that retained the potency but had increased metabolic stability were desired.

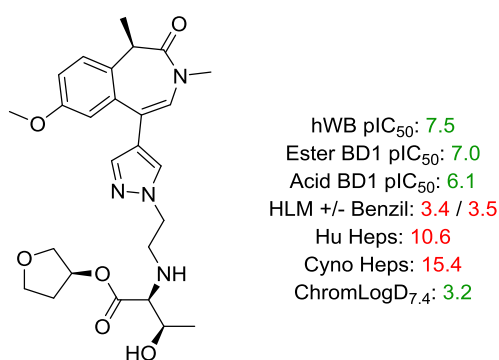


Figure 4.3. Profile of starting point **3.4**.

It was thought that this could be due to the methoxy shelf group substituent, as this moiety is known to be prone to phase I metabolism. Therefore, it was hypothesised that replacing this functionality and further reducing the lipophilicity of the molecule by incorporating polar moieties would reduce the IVC. The BZP series had previously been investigated on a pan-

BET programme elsewhere in GSK and, as such, a wealth of existing SAR surrounding the shelf group was available. A plot of the human hepatocyte clearance versus hWB pIC₅₀ of molecules containing an *N*-methyl pyrazole, analogous to **3.4**, in the vector accessing the ZA channel was generated. Several shelf groups were identified that resulted in the desired potency and IVC and based on *in silico* modelling, three were chosen to be explored within this sub series. Unfortunately, the compounds showed suboptimal potency or a higher than desired IVC and, as such, this sub series was not progressed any further. However, it did highlight two shelf groups which increased the metabolic stability relative to the starting point and these were translated into the other sub series.

The starting point **3.3** displayed exceptional whole blood and biochemical activity, as well as a desirable Δ hWB (+1.3). However, it was very lipophilic and, as such, was not progressed into IVC assays (Figure 4.4). Therefore, similarly to the other sub series, the main aim was to maintain the high activity whilst reducing the lipophilicity and obtaining a desirable IVC profile.

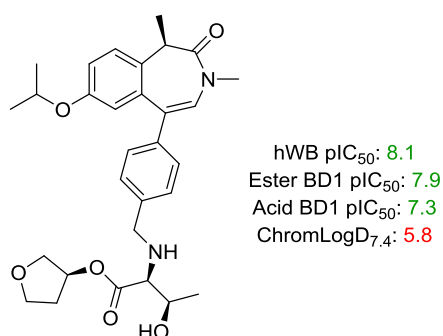


Figure 4.4. Profile of starting point **3.3**.

The compound contains a benzene and isopropyl group, both of which are inherently lipophilic. Therefore, the approach taken was to reduce the lipophilicity by replacing the benzene ring with heteroaromatic alternatives and incorporating polar moieties in place of the isopropyl group (Figure 4.5).

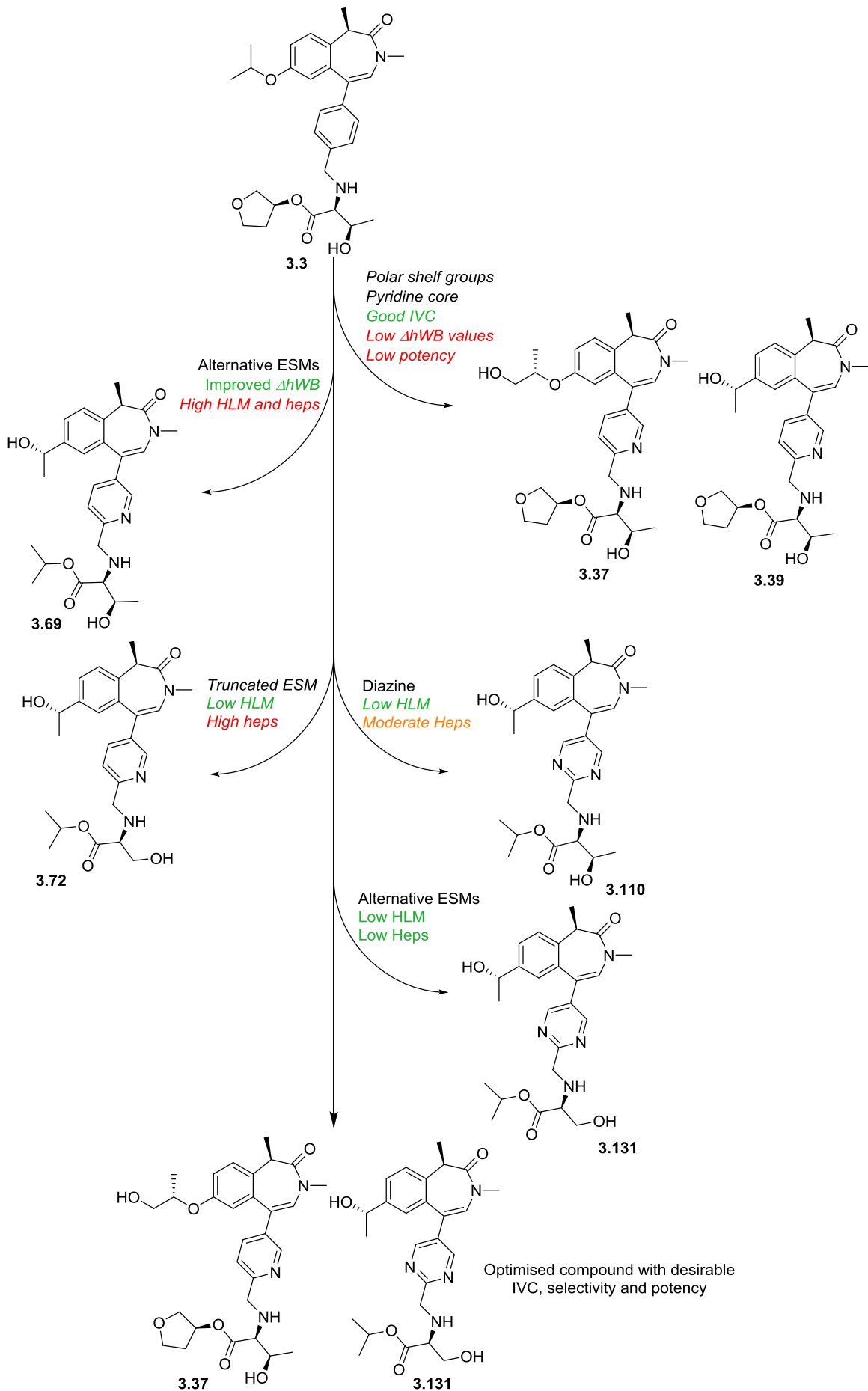


Figure 4.5. Key advancements made in this project.

The first step was to replace the benzene ring with the pyridine and investigate a selection of shelf groups, including the two preferred substituents from the pyrazole sub-series, in the first-generation analogues. This resulted in compounds with reduced lipophilicity and desirable HLM and hepatocyte IVC. Unfortunately, the analogues exhibited low hWB activity and negligible Δ hWB values with the exception of **3.37** which demonstrated excellent hWB potency (8.2) and a Δ hWB = 0.8. The exceptional profile of this compound saw it become the lead molecule for the first-generation series.

As enzymatic turnover can be impacted by steric bulk in close proximity to the site of reaction, it was decided to truncate the THF Thr ESM to isopropyl Thr in the second-generation compounds. It was thought that this would increase CES-1 turnover and therefore increase Δ hWB values relative to the first-generation compounds. Indeed, the second-generation molecules exhibited high whole blood activity and desirable Δ hWB values. Docking of the THF Thr and isopropyl Thr analogues, **3.39** and **3.69** respectively, to CES-1 show that both analogues adopt the same binding mode. However, in order to facilitate the tetrahedral intermediate formed upon the attack of the CES-1 catalytic serine on the ester carbonyl of **3.39**, the THF ring must undergo a conformational change. This is supported by energetic studies which revealed the increased torsional energy of the THF analogue relative to the isopropyl analogue, as well as substantial differences in the electrostatic energies of the molecules, most likely due to the THF oxygen being situated in a lipophilic pocket. As such, the dockings support that **3.39**, the THF ester, is a poorer substrate for CES-1 but mainly due to electrostatics and the need to undergo a conformational change rather than the hypothesised reduced steric bulk.

Furthermore, QSAR modelling was also undertaken to investigate the differences in the Δ hWB values, as well as create predictive models that could be used to design further iterations of compounds. Based on existing SAR, three models were created, one each for the BRD4 BD1 potency, hWB potency and Δ hWB. The results of the models when applied to the test sets revealed the BRD4 BD1 model to be capable of accurately predicting the biochemical potencies while the hWB model was able to rank compounds as having low, medium or high whole blood activity. For each of the models a structural interpretation was also completed which shows fragments that are key or detrimental for potency. Pleasingly, the analyses for the BRD4 BD1 and hWB models both predicted the 1-hydroxyethyl shelf group to be the most important fragment for potency, which correlates with observed data. Furthermore, whilst the BRD4 BD1 structural analysis only had BZP fragments, ESM fragments also appeared in the hWB analysis thus showing the higher whole blood values

are predicted to be from the ESM and, as such, confirming the ESM effect. Interestingly, whilst fragments pertaining to the isopropyl Thr, *allo*-Thr and Ser ESMs were present, there were none relating to the THF Thr ESM fragments thus showing that the model also predicts this ESM is having a low impact on the hWB. This was further supported by the Δ hWB model structural analysis which supports that the isopropyl Thr, *allo*-Thr and Ser ESMs are key for high Δ hWB values, whilst the THF Thr related fragments are of low importance and can actually be detrimental for hWB potency. The physicochemical parameters that were plotted for these fragments suggest that this could be TPSA related, which would reduce permeability and thus the potency in the cellular assay. Overall, the CES-1 dockings and QSAR suggest that the THF Thr is a poorer substrate for CES-1 than the isopropyl ESMs.

Whilst the second-generation analogues displayed high Δ hWB values, Unfortunately, high IVC was also observed due to the increased lipophilicity. Therefore, the Thr ESM was truncated to the isopropyl Ser ESM with the aim of reducing lipophilicity whilst retaining the Δ hWB in the third-generation compounds. Pleasingly, the incorporation of the isopropyl Ser ESM results in compounds **3.72** and **3.73** which retained high whole blood activity whilst demonstrating an increased Δ hWB. Furthermore, **3.72** exhibited a desirable IVC profile, albeit with a slightly higher than desired human hepatocyte clearance (2.5 mg/mL/g), and was selected as a lead molecule. Meanwhile, **3.73**, containing the (*R*)-1-hydroxyethanol shelf group, had decreased metabolic stability relative to **3.72**

In an attempt to further reduce the human hepatocyte clearance of **3.72**, a remining of the human hepatocyte versus hWB pIC₅₀, generated at the start of the project, unveiled two further shelf groups that could be explored (analogues **3.84**, **3.85** and **3.89**). In addition, a third shelf group, the monomethylated diol, was also investigated (analogues **3.86** and **3.87**). The fourth generation analogues monomethylated diols **3.86** and **3.87** exhibited high biochemical and human whole blood activity, unlike analogues **3.84**, **3.85** and **3.89** which were lower than desired. Initially, compound **3.86** could not be submitted IVC assays due the discovery that the isopropyl Ser ESM had epimerised. As such, a new synthetic route was developed which allowed the compound to be progressed down the screening cascade.

In parallel to the third-generation pyridine analogues, investigations into the use of a diazine as the ZA channel group to reduce the IVC of the second-generation analogues were undertaken. As hypothesised, the diazines reduced the lipophilicity of the pyridyl analogue **3.72**, with compounds **3.109** and **3.110** also demonstrated increased metabolic stability. Unfortunately, **3.110** exhibited high cynomolgus monkey hepatocyte clearance, whilst **3.109** had high human hepatocyte clearance. Interestingly, the pyridazine **3.108** and pyrimidine

3.111 exhibited low biochemical and hWB potency, which dockings in BRD4 BD1 suggest is due to a nitrogen lone pair of the diazine clashing with the lone pair of the carbonyl of the proline (Pro371) backbone residue. As such, these diazines were not investigated further.

As observed in the third generation pyridyl analogues, the isopropyl Ser and *allo*-Thr ESMs reduced the IVC and, as such, this was explored with analogues **3.129-3.132**. Indeed, the second generation diazine analogues exhibited increased HLM and hepatocyte metabolic stability. Unfortunately, the human hepatocyte clearance was too high for **3.132** (3.0 mg/mL/g) and analogues **3.129** and **3.130** demonstrated lower than desired hWB potency and, as such, these compounds were not progressed further. However, the pyrimidine analogue **3.131** showed a desirable profile overall and was selected as the lead compound for the diazines and progressed into further profiling.

From the investigation into pyridine and diazines as the ZA channel group, three lead molecules with desirable profiles were identified. They were progressed into further profiling in which they were found to display acceptable TDI, with **3.131** exhibiting no TDI. Furthermore, they were stable in human blood and cynomolgus monkey plasma which would facilitate any *in vivo* studies. To enable such studies, the synthetic routes to the three compounds had to be optimised. While the synthesis of **3.37** was optimised by colleagues, work outlined in this thesis focussed on the optimisation of the synthetic routes to **3.72** and **3.131**. The route to **3.72** contained a moderate yielding Heck reaction to install a ketone which was achirally reduced and brominated prior to a chiral separation to obtain the two diastereomers, thus leading to a further ~50% reduction in yield. Furthermore, the chiral chromatography required was lengthy due to a necessary low loading and, as such, was not desirable for large scale separations. In addition to this, it was found that reductive aminations of the isopropyl Ser amino acid ester **2.87** and pyridine **3.43** resulted in partial racemisation of the chiral centre in the ESM. Finally, despite high conversion to the product by LCMS (>90%), difficulties with purification resulted in a poor yield. Minor amendments to the Heck reaction resulted in a high yield of 91%. Next, a stereoselective reduction was investigated and replaced the original achiral reduction and chiral separation, thus reducing the loss of material and waiting time, whilst achieving the desired enantiomer in quantitative and desirable ee. The reductive amination to form intermediate **3.74** was replaced with an alkylation of the mesylate **3.149** with the isopropyl Ser ESM in high e.e. relative to the original reductive amination (18% ee). Finally, optimisation of the purification of the Suzuki-Miyaura cross coupling to form **3.72** increased the yield from 28% to 64%. Furthermore, this synthetic route was shown to be transferable to the synthesis of **3.131**.

Unfortunately, at this stage, analogue **3.72** was retested in the human hepatocyte IVC assay and demonstrated an increased clearance of 3.45 mL/min/g (82% LBF, n=3) compared to the original value of 2.5 mL/min/g (70% LBF, n=1). This caused the early dose prediction to significantly increase to an undesirable 252 mg QD. As such, this, along with the high human hepatocyte IVC, meant no further studies were completed on the compound at this point. Meanwhile, **3.37** and **3.131** were progressed into cynomolgus monkey PK studies. Unfortunately, **3.37** exhibited poor bioavailability (0.6%), which can most likely be attributed to the poor permeability of the compound limiting its absorption (as suggested by the low ester AUC) and was therefore terminated. Although **3.131** demonstrated a higher bioavailability (6%), it was still insufficient to facilitate an *in vivo* safety study and was also terminated. However, the compound exhibited a high AUC for the acid, suggesting good oral absorption suggesting the poor oral bioavailability was as a result of the high clearance. Furthermore, the compound exhibited a higher oral bioavailability than analogue **2.69** (F% = 1.1%), thus supporting the hypothesis that a further reduced IVC profile would increase the oral bioavailability.

Overall, through the investigations discussed in this report, molecules with improved profiles relative to **2.1** have been developed in the OTS series and to **3.3** in the BZP series. The compounds **2.51**, **3.37**, **3.72** and **3.131** displayed desirable profiles that allowed their progression into late stage studies.

4.1 Future directions

There is existing knowledge surrounding the incorporation of an esterase sensitive motif into small molecule HDAC inhibitors. However, aside from a patent disclosing a previous GSK ESM-iBET series, an ESM-containing small molecule BET inhibitor is yet to be published and remains a novel area.²¹⁴ With the candidate molecule **1.6** currently progressing through the clinic, the identification of a second clinical candidate is still desirable. The work carried out in this thesis provides key knowledge that can be applied to the development of a new series of ESM-containing BET inhibitors.

Firstly, the two series explored in this thesis shows that potent, selective molecules with desirable IVC profiles can be achieved with the ESM directed both through the ZA channel or over the WPF shelf. This knowledge can be used when identifying other potential series as scaffolds only one require one vector to either area of the bromodomain, whereas previous series have been selected based on their capability of directing the ESM through the ZA

channel. Furthermore, both series exemplified that heteroatoms and polar moieties can be tolerated on the WPF shelf, and yield highly potent compounds, despite literature precedent suggesting that only lipophilic groups are tolerated. Consequently, where this has been previously avoided as a result of the hypothesis that only lipophilic groups were tolerated due to the hydrophobic nature of the WPF shelf, such moieties could be further explored. This will provide an alternative method to modulating the physicochemical properties, potentially IVC profiles, which has typically consisted of heteroaromatic rings as ZA channel or WPF shelf groups. In addition, known BET small molecule inhibitors, such as BI 894999 (Figure 4.6a), typically interact with the WPF shelf but do not extend over the shelf. Therefore, to the best of our knowledge the AP OTS series exemplifies the first analogues that exhibit this. As such, the investigation of the bond angles between two vectors to the WPF shelf group is not well preceded outside of this thesis. The work completed in this thesis suggests that a 180° bond angle is optimal, with smaller angles affording low potency compounds (Figure 4.6b). Therefore, future series which incorporate the ESM over the WPF shelf could focus on maintaining the 180° , thus allowing SAR to be more focussed.

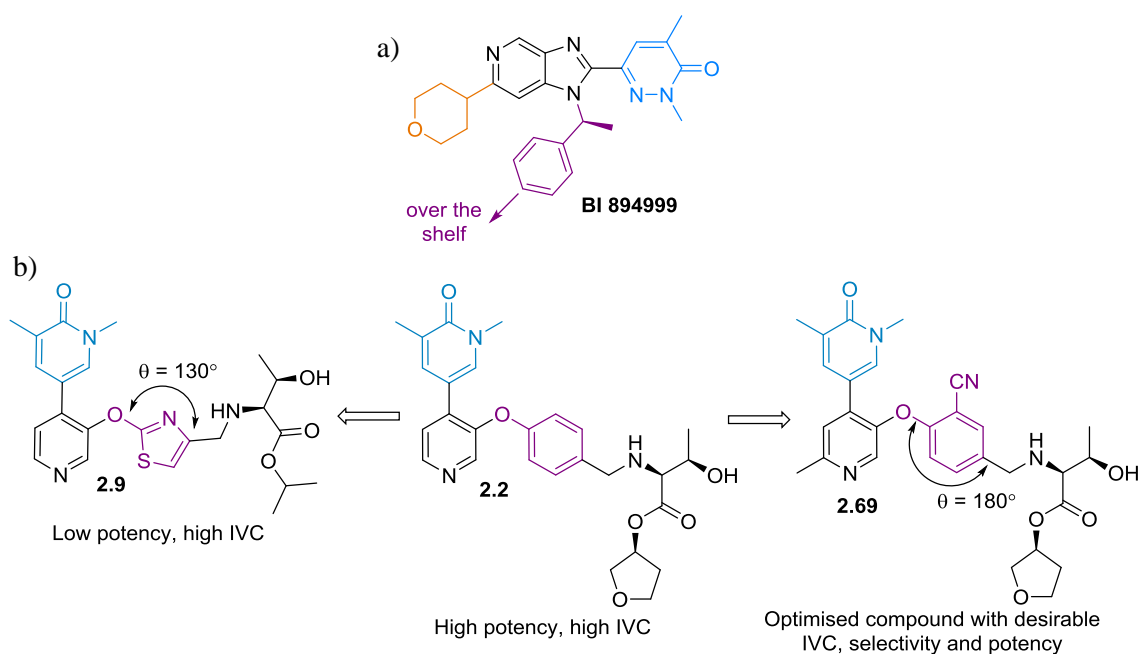


Figure 4.6. a) Clinical candidate BI 894999 is an example of a typical pan-BET small molecule inhibitors which incorporates an acetyl lysine mimetic (blue), a WPF shelf group (purple) and a ZA channel group (orange). To the best of our knowledge, these molecule existing moieties that interact with, but do not extend over the WPF shelf (in the direction of the arrow). b) Work completed within this thesis on the AP OTS series showed that a bond angle of 180° is optimal between the core and the ESM for high potency and low IVC compounds, with smaller angles resulting in reduced potency.

A key determinant in achieving oral bioavailability in cynomolgus monkey is the hepatocyte IVC, as exemplified by the increased oral bioavailability and reduced IVC of analogue **3.131** observed relative to compound **2.69**. Therefore, as an increased oral bioavailability is required, the aims for a future series would need to centre around reducing the cynomolgus monkey and human hepatocyte clearance and building an *in vivo-in vitro* correlation to allow for earlier predictions of oral bioavailability. In addition, the work in this thesis shows that compounds with a TPSA 125\AA^2 exhibited increased permeability and whole blood potency compared to compounds with a higher TPSA. Existing clinical pan-BET inhibitors typically have TPSA 100\AA^2 (Figure 4.7a), whilst molecules throughout this thesis exhibited TPSA >math>100\text{\AA}^2</math> due to the incorporation of the ESM (Figure 4.7b). Molecules with high TPSA and low permeability, such as **2.69**, were shown to have poor oral absorption thus limiting the efficacy achieved by CES-1 hydrolysis and subsequent cell retention. This was also seen for compounds with low CES-1 activity, i.e. a low ΔhWB , as demonstrated by the low acid concentration in the *in vivo* studies of **2.69**. Consequently, when identifying an alternative scaffold, one should be chosen based on its capability to provide a lower TPSA and mw, which could also act to increase oral absorption, as well as a higher ΔhWB .

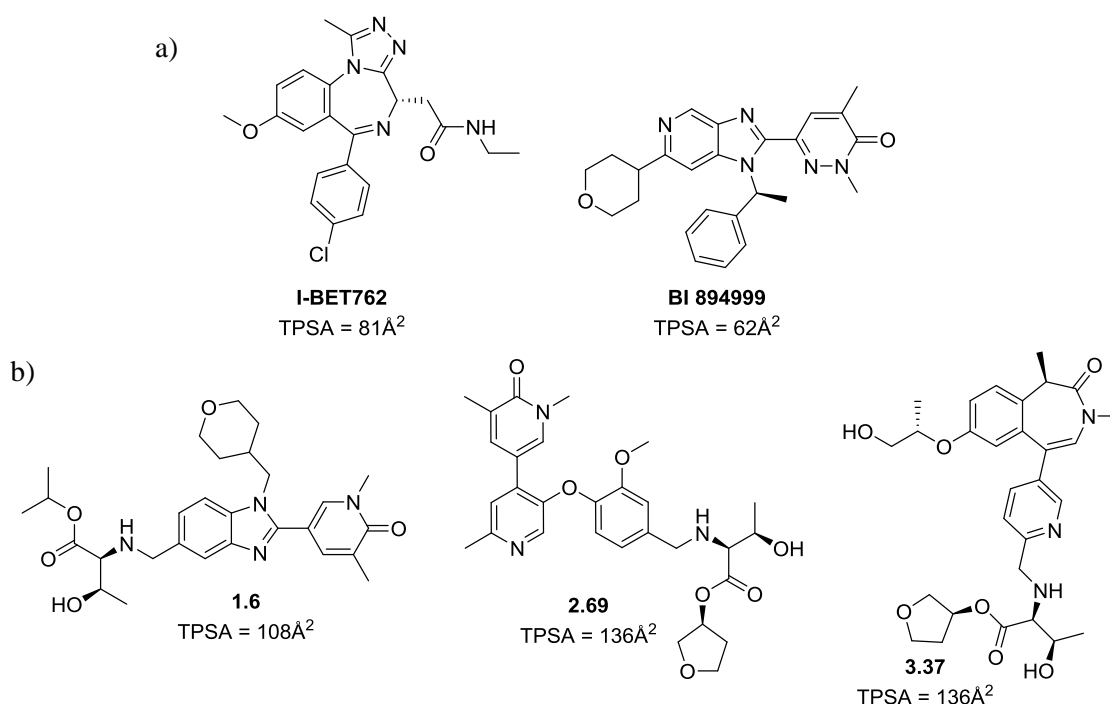


Figure 4.7. a) The majority of existing clinical candidates exhibit TPSA 100\AA^2 for example I-BET762 and BI 984999. b) Incorporation of the ESM increases the TPSA relative to typical drug-like molecules. The isopropyl Thr ESM results in a lower TPSA, as in the clinical candidate **1.6**, whilst the THF Thr ESM significantly increases the TPSA, such as in compounds **2.69** and **3.37**.

SAR gathered within this thesis provided knowledge surrounding the nature of the various ESMs which could easily be transferred to a new series. Firstly, the THF Thr ESM resulted in lower whole blood potency. This can be attributed to a slow CES-1 turnover, supported by the QSAR modelling and CES-1 dockings and as shown by the CES-1 specific activities and low ΔhWB values. Furthermore, this ESM significantly increases the TPSA of the molecules, thus impacting permeability and absorption. Consequently, the THF Thr ESM should not be incorporated into future series unless the compounds are highly turned over, in which case this ESM could be used to decrease CES-1 turnover to a desirable level. Meanwhile, the Ser isopropyl and *allo*-Thr isopropyl ESMs were shown to achieve higher levels of CES-1 hydrolysis, whilst also improving the metabolic stability of compounds and altering their lipophilicities. The knowledge gained from this SAR could be directly applied to a different scaffold, allowing the tuning of molecules from an early stage in the development of the series thus offering an improved pro-drug strategy.

With respect to chemistry, this thesis has shown that enzymatic approaches can be used in conjunction with general synthetic chemistry to synthesise compounds. Although enzymatic transformations are widely reported in the literature, their integration in full synthetic routes is still an emerging area.^{215,216,217} The use of imine reductases to perform reductive aminations has been reported in the literature. However, the exemplars tend to be on molecules outside of drug-like space. Therefore, although the imine reduction was unsuccessful on the AP OTS compounds, the fact that the enzymatic system tolerated the drug-like molecules, i.e. the enzyme did not degrade, this suggests that the enzymatic transformation could be applied more widely within medicinal chemistry. Furthermore, the ketone reductase was shown to stereoselectively reduce an aromatic ketone in the BZP ZA series to achieve high enantiomeric excess and quantitative yield, thus significantly improving upon the traditional synthetic route (Figure 4.8). Typically, enzymatic reactions require narrow pH or temperature ranges in order to progress. However, the KRED screen performed in this thesis showed that KREDs can be utilised at 50°C without diminishing yields or enantiomeric excesses. As such temperatures could aid solubility and reactivity, this could widen the scope of potential substrates for the KRED reduction. Furthermore, as the three KRED screening plates are commercial, this makes the process of identifying a hit more facile and increases the likelihood of success. As benzylic alcohols have high precedent in drug-like molecules, KREDs could be more widely applicable within medicinal chemistry routes than initially suspected and should be considered as an alternative to traditional organic synthetic chemistry for such scaffolds.

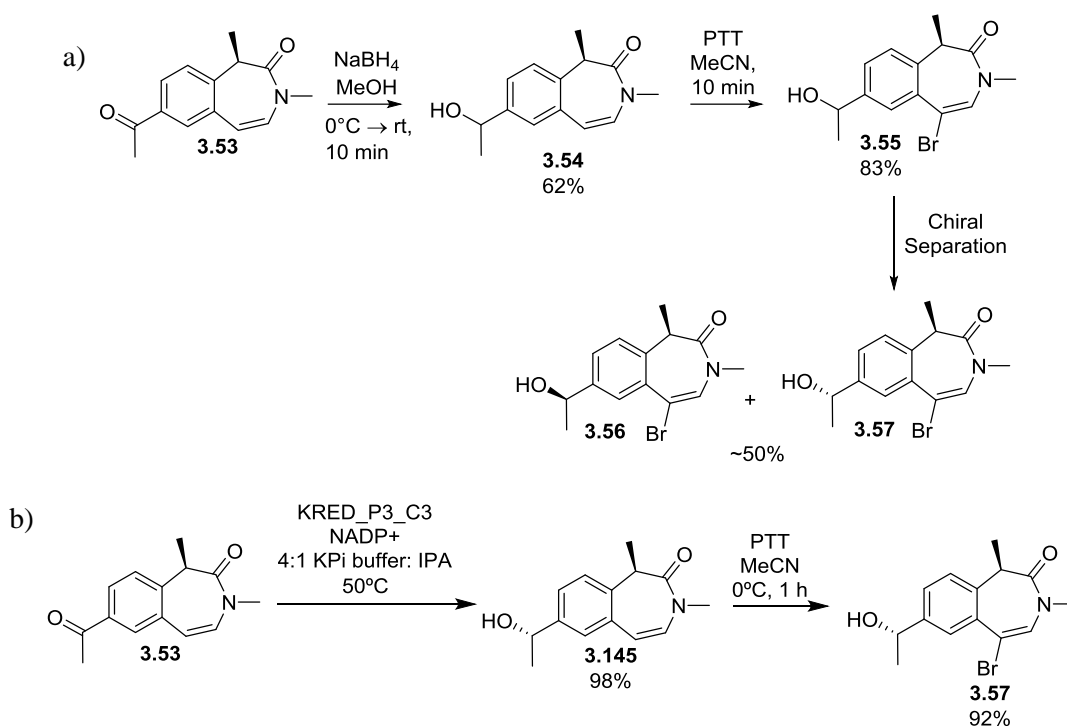


Figure 4.8. a) The traditional synthetic route to **3.57** involves the achiral reduction of ketone **3.53**, followed by bromination and subsequent separation by column chromatography using a chiral stationary phase, which typically takes ~4 weeks. b) An alternative enzymatic approach in which ketone **3.53** is stereoselectively reduced by a KRED to afford the desired diastereomer **3.145** in 98% yield. Subsequent bromination affords intermediate **3.57**. The two step synthesis is significantly higher yielding than the traditional synthetic route.

Finally, CES-1 has a restricted expression profile within the mononuclear myeloid lineage outside of the liver. Therefore, ESM-containing BET inhibitors could be investigated for alternative immuno-inflammatory diseases such as Crohn's disease.²¹⁸ Furthermore, the ESM technology could be applied to any target that has a role within immuno-inflammation and is expressed in these cell types, e.g. CREBBP, thus offering the opportunity to increase the selectivity and efficacy profiles of small molecule inhibitors for such targets.²¹⁸ In addition, the presence of CES-1 in the liver means that ESM-containing small molecule inhibitors could also be investigated for liver indications. In all of these cases, the knowledge gained in this thesis could be directly applied in order to develop molecules with desirable potency, selectivity and CES-1 turnover.

5.0 Experimental

5.1 General experimental details

The names of the compounds cited herein have been obtained using ChemDraw Ultra 12.0. All commercial chemicals and solvents are reagent grade and were used without further purification unless otherwise specified. All reactions except those in aqueous media were carried out with the use of standard techniques for the exclusion of moisture.

Crystal Structures

The crystal structures in this thesis were completed and resolved by Chun-Wa Chung.

LCMS Methodology

Method using formic acid modifier – “LCMS (formic acid)”

LC conditions:

UPLC analysis was conducted on an Acquity UPLC BEH C₁₈ column (50 mm x 2.1 mm, i.d. 1.7 µm packing diameter) at 40°C. The solvents employed were: A = 0.1% v/v solution of formic acid in water; B = 0.1% v/v solution of formic acid in acetonitrile. The gradient (A:B) employed was from 97:3 to 3:97 over 2 min. The UV detection was a summed signal from wavelength of 210 nm to 350 N

MS conditions:

Mass spectrometry was conducted on a Waters ZQ mass spectrometer, with an ionisation mode of alternate-scan positive and negative electrospray. The scan range was 100 to 1000 AMU, the scan time was 0.27 sec and the inter-scan delay was 0.10 sec.

Method using ammonium bicarbonate modifier – “LCMS (HpH)”

LC conditions:

UPLC analysis was conducted on an Acquity UPLC BEH C₁₈ column (50 mm x 2.1 mm, i.d. 1.7 µm packing diameter) at 40°C. The solvents employed were: A = ammonium hydrogen carbonate in water adjusted to pH 10 with ammonia solution; B = acetonitrile. The gradient (A:B) employed was from 99:1 to 0:100 over 2 min. The UV detection was a summed signal from wavelength of 210 nm to 350 nm.

MS conditions:

Mass spectrometry was conducted on a Waters ZQ mass spectrometer, with an ionisation mode of alternate-scan positive and negative electrospray. The scan range was 100 to 1000 AMU, the scan time was 0.27 sec and the inter-scan delay was 0.10 sec.

High Resolution Mass Spectrometry

Chromatography and analysis conditions:

An Agilent 1100 Liquid Chromatograph equipped with a model G1367A autosampler, a model G1312A binary pump and a HP1100 model G1315B diode array detector was used. The method used was generic for all experiments. All separations were achieved using a C₁₈ reversed phase column (100 x 2.1 mm, 3 µm particle size) or equivalent. Gradient elution was carried out with the mobile phases as (A) water containing 0.1% (v/v) TFA and (B) acetonitrile containing 0.1% (v/v) TFA. The conditions for the gradient elution were initially 0% B, increasing linearly to 95% B over 8 min, remaining at 95% B for 0.5 min, then decreasing linearly to 0% B over 0.1 min, followed by an equilibration period of 1.49 min prior to the next injection. The flow rate was 1 mL/min, split to source and the temperature controlled at 40°C with an injection volume of between 2 to 5 µL.

Mass Spectrometry conditions:

Positive ion mass spectra were acquired using a Thermo LTQ–Orbitrap FT mass spectrometer, equipped with an ESI interface, over a mass range of 100 – 1100 Da, with a scan time of 1 sec. The elemental composition was calculated using Xcalibur software and processed using RemoteAnalyzer (Spectral Works Ltd) for the [M+H]⁺ and the mass error quoted as ppm.

MDAP Methodology

Method using formic acid modifier – “MDAP (formic acid)”

LC conditions:

HPLC analysis was conducted on either a Sunfire C₁₈ column (100 mm x 19 mm, i.d 5 µm packing diameter) or a Sunfire C₁₈ column (150 mm x 30 mm, i.d. 5 µm packing diameter) at ambient temperature. The solvents employed were: A = 0.1% v/v solution of formic acid in water; B = 0.1% v/v solution of formic acid in acetonitrile. The purification was run as a gradient (A:B) over either 15 min or 25 min, with a flow rate of 20 mL/min (100 mm x 19

mm, i.d 5 μm packing diameter) or 40 mL/min (150 mm x 30 mm, i.d. 5 μm packing diameter). The UV detection was a summed signal from wavelength of 210 nm to 350 nm.

MS conditions:

Mass spectrometry was conducted on a Waters ZQ mass spectrometer, with an ionisation mode of alternate-scan positive and negative electrospray. The scan range was 100 to 1000 AMU, the scan time was 0.50 secs and the inter-scan delay was 0.20 sec.

Method using ammonium bicarbonate modifier – “MDAP (HpH)”

LC conditions:

HPLC analysis was conducted on either an Xbridge C₁₈ column (100 mm x 19 mm, i.d 5 μm packing diameter) or an Xbridge C₁₈ column (100 mm x 30 mm, i.d. 5 μm packing diameter) at ambient temperature. The solvents employed were: A = 10 mM ammonium bicarbonate in water, adjusted to pH 10 with ammonia solution; B = acetonitrile. The purification was run as a gradient (A:B) over either 15 min or 25 min, with a flow rate of 20 mL/min (100 mm x 19 mm, i.d 5 μm packing diameter) or 40 mL/min (150 mm x 30 mm, i.d. 5 μm packing diameter). The UV detection was a summed signal from wavelength of 210 nm to 350 nm.

MS conditions:

Mass spectrometry was conducted on a Waters ZQ mass spectrometer, with an ionisation mode of alternate-scan positive and negative electrospray. The scan range was 100 to 1000 AMU, the scan time was 0.50 sec and the inter-scan delay was 0.20 sec.

NMR Spectroscopy

Unless otherwise specified, ¹H and ¹³C NMR spectra were recorded using a Bruker DPX400 spectrometer at 400 MHz and 101 MHz, respectively, or using a Bruker Avance 500 spectrometer at 500 MHz and 126 MHz, respectively. Chemical shifts are given in ppm (δ) relative to tetramethylsilane (TMS) as an internal standard. Chemical shifts are given to the nearest 0.01 ppm (¹H NMR) or 0.1 ppm (¹³C NMR) and coupling constants are given to the nearest 0.1 Hz. NMR spectra are recorded at rt unless otherwise stated.

Infrared Spectroscopy

Infra-red (IR) spectra were recorded using a Perkin Elmer Spectrum One FT-IR spectrometer, and key well-defined peaks were recorded in cm^{-1} .

Optical Rotation

Optical rotation measurements were recorded using a Jasco P-1030 polarimeter. The concentration was recorded in g/mL, path length in mm, and temperature in °C.

Melting Point

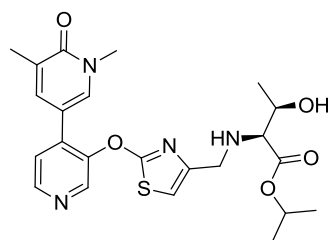
Melting point measurements were recorded using a Stuart SMP10 melting point apparatus.

Compound Purity

The purity of compounds tested in *in vitro* and *in vivo* assays was greater than 95% using interpretation of a combination of LCMS and ¹H NMR data, unless stated otherwise. All compounds were isolated as >90 wt% unless stated.

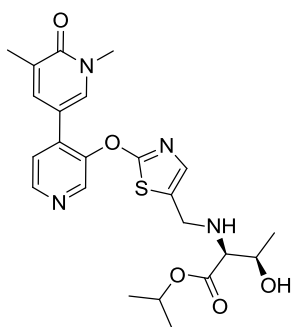
5.2 Procedures

(2*S*, 3*R*)-Isopropyl-2-(((2-(((1,5-dimethyl-6-oxo-1,6-dihydro-(3,4'-bipyridin)-3'-yl)oxy)thiazol-4-yl)methyl)amino)-3-hydroxybutanoate, **2.9**



2-Picoline borane (27.3 mg, 0.26 mmol) was added to a solution of 2-(((1,5-dimethyl-6-oxo-1,6-dihydro-(3,4'-bipyridin)-3'-yl)oxy)thiazole-4-carbaldehyde (**2.23**, 76 mg, 0.23 mmol) and (2*S*,3*R*)-isopropyl 2-amino-3-hydroxybutanoate hydrochloride²¹⁹ (**2.19**, 50.5 mg, 0.26 mmol) in isopropanol (1 mL) and acetic acid (0.11 mL) and the reaction mixture stirred at rt for 4 h under nitrogen. The reaction mixture was purified directly by MDAP (HpH). The relevant fractions were combined and concentrated *in vacuo* to give the title compound (**2.9**, 19.7 mg, 0.04 mmol, 18 % yield) as a brown oil. (α_D)^{20.1°C}_D(c = 1.0, CDCl₃): -5.3°; ν_{\max} (solution in CDCl₃): 3364, 1726, 1655, 1106, 732 cm⁻¹; ¹H NMR (400 MHz, CDCl₃) δ = 8.63 (s, 1H), 8.53 (d, *J* = 4.9 Hz, 1H), 7.60 (d, *J* = 2.4 Hz, 1H), 7.44 (dd, *J* = 1.5, 2.4 Hz, 1H), 7.33 (d, *J* = 4.9 Hz, 1H), 6.63 (s, 1H), 5.00 (spt, *J* = 6.3 Hz, 1H), 3.76 (d, *J* = 14.4 Hz, 1H), 3.72 - 3.66 (m, 1H), 3.64 (d, *J* = 14.4 Hz, 1H), 3.59 (s, 3H), 2.98 (d, *J* = 7.3 Hz, 1H), 2.18 (app. s, 3H), 1.23 (d, *J* = 6.3 Hz, 6H), 1.19 (d, *J* = 6.3 Hz, 3H), NH and OH not observed; ¹³C NMR (101 MHz, CDCl₃) δ = 175.3, 172.3, 171.9, 147.7, 147.6, 144.2, 136.5, 130.1, 123.4, 123.3, 112.1, 109.8, 72.9, 69.2, 67.8, 67.4, 48.4, 38.2, 21.9, 21.7 (2C), 19.5, 17.3; LCMS (HpH): *t*_R = 0.84 min, [M+H⁺] = 473.4 (100 % purity); HRMS: (C₂₃H₂₈N₄O₅S) Requires [M+H⁺] = 473.1859, found [M+H⁺] = 473.1856.

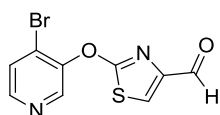
(2*S*,3*R*)-Isopropyl-2-(((2-((1,5-dimethyl-6-oxo-1,6-dihydro-(3,4'-bipyridin)-3'-



yl)oxy)thiazol-5-yl)methyl)amino)-3-hydroxybutanoate, 2.11

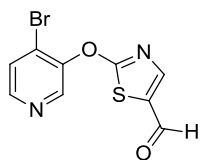
2-Picoline borane (27.3 mg, 0.26 mmol) was added to a solution of 2-((1,5-dimethyl-6-oxo-1,6-dihydro-(3,4'-bipyridin)-3'-yl)oxy)thiazole-4-carbaldehyde (**2.25**, 76 mg, 0.23 mmol) and (2*S*,3*R*)-isopropyl 2-amino-3-hydroxybutanoate hydrochloride²¹⁹ (**2.19**, 50.5 mg, 0.26 mmol) in isopropanol (1 mL) and acetic acid (0.11 mL) and the reaction stirred at rt for 4 h under nitrogen. The reaction mixture was purified by MDAP (HpH). The relevant fractions were combined and concentrated *in vacuo* to afford the title compound (**2.11**, 8.2 mg, 0.02 mmol, 8 % yield) as a brown oil. (α_D)^{19.1°C}_λ(c = 0.5, CDCl₃): -22.7°; ν_{\max} (solution in CDCl₃): 3366, 1724, 1655, 1252, 732 cm⁻¹; ¹H NMR (400 MHz, CDCl₃) δ = 8.61 (s, 1H), 8.54 (d, *J* = 5.1 Hz, 1H), 7.58 (s, 1H), 7.45 (s, 1H), 7.33 (d, *J* = 5.1 Hz, 1H), 6.92 (s, 1H), 5.08 (spt, *J* = 6.3 Hz, 1H), 3.95 (d, *J* = 14.2 Hz, 1H), 3.77 - 3.71 (m, 1H), 3.68 (d, *J* = 14.2 Hz, 1H), 3.59 (s, 3H), 3.11 (br s, 1H), 2.97 (d, *J* = 6.8 Hz, 1H), 2.18 (s, 3H), 1.29 - 1.24 (m, 6H), 1.20 (d, *J* = 6.4 Hz, 3H), NH and OH not observed; ¹³C NMR (101 MHz, CDCl₃) δ = 162.6, 159.2, 147.7, 144.2, 137.1, 136.6, 136.5, 130.0, 123.4, 112.1, 109.9, 77.2, 69.3, 67.8, 67.4, 48.3, 38.2, 21.9, 21.7 (2C), 21.6, 19.5, 17.3; LCMS (HpH): *t*_R = 0.83 min, [M+H⁺] = 473.4 (96 % purity); HRMS: (C₂₃H₂₈N₄O₅S) Requires [M+H⁺] = 473.1859, found [M+H⁺] = 473.1858.

2-((4-Bromopyridin-3-yl)oxy)thiazole-4-carbaldehyde, 2.21



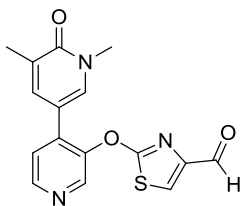
A suspension of 4-bromopyridin-3-ol (**2.13**, 500 mg, 2.87 mmol), potassium carbonate (794 mg, 5.75 mmol) and 2-chlorothiazole-4-carbaldehyde (**2.14**, 636 mg, 4.31 mmol) was heated at 120°C for 16 h. The reaction mixture was concentrated *in vacuo*. The residue was partitioned between ethyl acetate (100 mL), water (100 mL), brine (50 mL) and DCM (100 mL) and allowed to stand overnight after which sodium bicarbonate (50 mL) was added. The entire mixture was filtered, then the organic phase was dried (hydrophobic frit) and concentrated *in vacuo*. The residue was purified by flash column chromatography (silica, 50-75% ethyl acetate in cyclohexane). The appropriate fractions were combined and concentrated *in vacuo* to afford the title compound (**2.21**, 105 mg, 0.34 mmol, 75 wt%, 10% yield) as an orange solid. ¹H NMR (400 MHz, CDCl₃) δ 9.75 (s, 1H), 8.70 (s, 1H), 8.39 (d, *J* = 5.4 Hz, 1H), 7.80 (s, 1H), 7.66 (d, *J* = 5.4 Hz, 1H); LCMS (HpH): *t*_R = 0.82 min, [M+H⁺] = 285.0 / 287.0 (87 % purity).

2-((4-Bromopyridin-3-yl)oxy)thiazole-5-carbaldehyde, 2.22



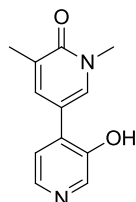
A suspension of 4-bromopyridin-3-ol (**2.13**, 1 g, 5.75 mmol), 2-chlorothiazole-5-carbaldehyde (**2.15**, 1.02 g, 6.90 mmol) and potassium *tert*-butoxide (0.77 g, 6.90 mmol) in acetonitrile (30 mL) was stirred at 70°C for 4 h. The reaction mixture was filtered to remove the precipitate and the filtrate was concentrated *in vacuo*. The residue was partitioned between ethyl acetate (50 mL) and water (50 mL). The layers were separated and the organic phase washed with water (50 mL) before being dried (hydrophobic frit) and concentrated *in vacuo*. The residue was purified by flash column chromatography (silica, 20-50% ethyl acetate in cyclohexane). The appropriate fractions were combined and concentrated *in vacuo* to afford the title compound (**2.22**, 677 mg, 1.66 mmol, 70 wt%, 29 % yield) as an orange sticky solid. ¹H NMR (400 MHz, CDCl₃) δ 9.90 (s, 1H), 8.66 (s, 1H), 8.42 (d, *J* = 5.4 Hz, 1H), 7.88 (s, 1H), 7.68 (d, *J* = 5.4 Hz, 1H); LCMS (formic): *t*_R = 0.84 min, [M+H⁺] = 283.0 / 285.0 (90% purity)

2-((1,5-Dimethyl-6-oxo-1,6-dihydro-(3,4'-bipyridin)-3'-yl)oxy)thiazole-4-carbaldehyde, 2.23



A suspension of 3'-hydroxy-1,5-dimethyl-(3,4'-bipyridin)-6(1*H*)-one (**2.24**, 390 mg, 1.80 mmol), 2-chlorothiazole-4-carbaldehyde (**2.14**, 319 mg, 2.16 mmol) and potassium carbonate (374 mg, 2.71 mmol) in DMF (8 mL) was stirred at 80°C for 4 h. The reaction was concentrated *in vacuo*. The residue purified by MDAP (HpH). The relevant fractions were concentrated *in vacuo* to afford the title compound (**2.23**, 240 mg, 0.73 mmol, 41 % yield) as a yellow oil. ¹H NMR (400MHz, CDCl₃) δ 9.73 (s, 1H), 8.69 (s, 1H), 8.60 (d, *J* = 5.1 Hz, 1H), 7.71 (s, 1H), 7.56 (d, *J* = 2.2 Hz, 1H), 7.44 (dd, *J* = 1.0, 2.2 Hz, 1H), 7.37 (d, *J* = 5.1 Hz, 1H), 3.59 (s, 3H), 2.19 (app. s, 3H); LCMS (HpH): *t*_R = 0.66 min, [M+H⁺] = 328.2 (97 % purity).

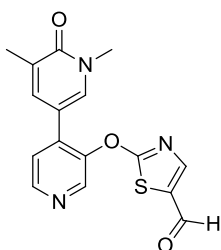
3'-Hydroxy-1,5-dimethyl-(3,4'-bipyridin)-6(1*H*)-one, 2.24



A suspension of 4-bromopyridin-3-ol (**2.13**, 2 g, 11.5 mmol), 1,3-dimethyl-5-(4,4,5,5-tetramethyl-1,3,2-dioxaborolan-2-yl)pyridin-2(1*H*)-one²²⁰ (**2.17**, 5.15 g, 20.7 mmol), palladium(II) acetate (0.13 g, 0.58 mmol) and di(1-adamantyl)-*n*-butylphosphine (206 mg, 0.58 mmol) in 1,4-dioxane (40 mL) and water (8 mL) was degassed with nitrogen for 15 min. To this was added a degassed solution of potassium carbonate (4.77 g, 34.5 mmol) in water (8 mL). The reaction mixture

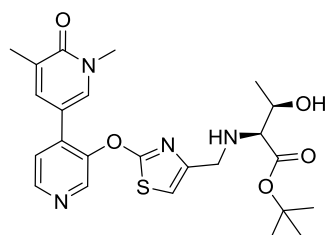
was heated under nitrogen at 40°C for 2 h followed by 100°C for 2 h. Further portions of 1,3-dimethyl-5-(4,4,5,5-tetramethyl-1,3,2-dioxaborolan-2-yl)pyridin-2(1*H*)-one (**2.17**, 1.43 g, 5.75 mmol), palladium(II) acetate (0.13 g, 0.58 mmol) and di(1-adamantyl)-*n*-butylphosphine (0.21 g, 0.58 mmol) were added and the mixture was stirred for a further 2 h. The reaction mixture was filtered over Celite and washed with ethyl acetate (100 mL). The filtrate was passed over an SCX column and the column washed with ethyl acetate followed by (25 % ethanol in ethyl acetate). The product was eluted with 2M ammonia in MeOH and the filtrate concentrated *in vacuo* and dried in a vacuum oven for 5 h to give the title compound (**2.24**, 2.13 g, 9.85 mmol, 86 % yield) as a brown solid. M.pt: 146.3 – 163.4°C; ν_{\max} (solution in CDCl₃): 2905, 1655, 1302, 731 cm⁻¹; ¹H NMR (400 MHz, CDCl₃) δ 8.43 (s, 1H), 8.16 (d, *J* = 5.4 Hz, 1H), 7.95 (d, *J* = 2.0 Hz, 1H), 7.63 (d, *J* = 2.0 Hz, 1H), 7.31 (d, *J* = 5.4 Hz, 1H), 3.51 (s, 3H), 2.26 (s, 3H); ¹³C NMR (101 MHz, CDCl₃) δ = 166.8, 155.6, 146.1, 143.7, 142.5, 142.4, 135.1, 132.2, 127.6, 117.9, 42.6, 22.2; LCMS (HpH): *t*_R = 0.46 min, [M+H⁺] = 217.0 (96 % purity); HRMS: (C₁₂H₁₂N₂O₂) Requires [M+H⁺] = 217.0978, found [M+H⁺] = 217.0977.

2-((1,5-Dimethyl-6-oxo-1,6-dihydro-(3,4'-bipyridin)-3'-yl)oxy)thiazole-5-carbaldehyde, 2.25



A suspension of 3'-hydroxy-1,5-dimethyl-(3,4'-bipyridin)-6(1*H*)-one (**2.11**, 500 mg, 1.97 mmol), 2-chlorothiazole-5-carbaldehyde (**2.15**, 348 mg, 2.36 mmol, 85 wt%) and potassium carbonate (407 mg, 2.95 mmol) were suspended in DMF (8 mL) and stirred at 80°C for 4 h. The reaction mixture was concentrated *in vacuo*. The resultant residue was purified by MDAP (HpH). The relevant fractions were concentrated *in vacuo* to afford the title compound (**2.25**, 140 mg, 0.43 mmol, 22 % yield) as a dark brown oil. ¹H NMR (400MHz, CDCl₃) δ 9.84 (s, 1H), 8.65 (s, 1H), 8.63 (d, *J* = 5.6 Hz, 1H), 7.84 (s, 1H), 7.69 (s, 1H), 7.44 (s, 1H), 7.40 (d, *J* = 5.6 Hz, 1H), 3.60 (s, 3H), 2.19 (s, 3H); LCMS (HpH): *t*_R = 0.72 min, [M+H⁺] = 328.1 (80 % purity).

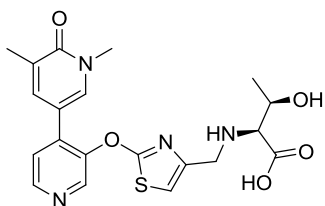
(2*S*,3*R*)-tert-Butyl 2-(((2-((1,5-dimethyl-6-oxo-1,6-dihydro-(3,4'-bipyridin)-3'-yl)oxy)thiazol-4-yl)methyl)amino)-3-hydroxybutanoate, 2.27



2-Picoline borane (27.3 mg, 0.26 mmol) was added to a solution of 2-((1,5-dimethyl-6-oxo-1,6-dihydro-(3,4'-bipyridin)-3'-yl)oxy)thiazole-4-carbaldehyde (**2.23**, 76 mg, 0.23 mmol) and (2*S*,3*R*)-*tert*-butyl 2-amino-3-

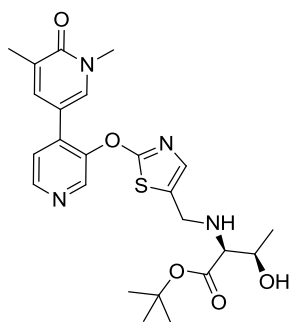
hydroxybutanoate hydrochloride²¹² (**2.26**, 54.1 mg, 0.26 mmol) in isopropanol (1 mL) and acetic acid (0.11 mL) and the reaction mixture stirred at rt for 4 h under nitrogen. The reaction mixture was purified by MDAP (HpH). The relevant fractions were combined and concentrated *in vacuo* to afford the title compound (**2.27**, 27 mg, 0.05 mmol, 28 % yield) as a brown oil. (α_D)^{23.2°C} _{λ} (c = 1.0, CDCl₃): -6.5°; ν_{\max} (solution in CDCl₃): 2977, 1725, 1655, 1233, 1107 cm⁻¹; ¹H NMR (400 MHz, CDCl₃) δ = 8.63 (s, 1H), 8.53 (d, *J* = 4.9 Hz, 1H), 7.59 (d, *J* = 2.4 Hz, 1H), 7.44 (dd, *J* = 1.0, 2.4 Hz, 1H), 7.32 (d, *J* = 4.9 Hz, 1H), 6.62 (t, *J* = 1.0 Hz, 1H), 3.75 (dd, *J* = 1.0, 14.7 Hz, 1H), 3.67 - 3.60 (m, 2H), 3.58 (s, 3H), 2.89 (d, *J* = 7.3 Hz, 1H), 2.18 (app. s, 3H), 1.44 (s, 9H), 1.20 (d, *J* = 6.4 Hz, 3H); ¹³C NMR (101 MHz, CDCl₃) δ = 172.4, 172.1, 162.6, 150.0, 149.9, 147.7, 144.3, 140.0, 136.5, 130.0, 123.4, 112.1, 109.0, 82.0, 77.2, 68.2, 68.1, 48.7, 38.2, 28.1 (s, 3C), 19.4, 17.3; LCMS (HpH): *t*_R = 0.91 min, [M+H⁺] = 487.0 (100 % purity); HRMS: (C₂₄H₃₀N₄O₅S) Requires [M+H⁺] = 487.2016, found [M+H⁺] = 487.2010.

(2*S*,3*R*)-2-(((2-((1,5-Dimethyl-6-oxo-1,6-dihydro-(3,4'-bipyridin)-3'-yl)oxy)thiazol-4-yl)methyl)amino)-3-hydroxybutanoic acid dihydrochloride, 2.28



A solution of (2*S*,3*R*)-*tert*-butyl 2-(((2-((1,5-dimethyl-6-oxo-1,6-dihydro-(3,4'-bipyridin)-3'-yl)oxy)thiazol-4-yl)methyl)amino)-3-hydroxybutanoate (**2.27**, 13.7 mg, 0.03 mmol) in 2M aqueous hydrochloric acid (0.7 mL, 1.41 mmol) was stirred at 60°C for 4 h. The reaction mixture was concentrated *in vacuo* to afford the title compound (**2.28**, 13.8 mg, 0.03 mmol, 97 % yield) as a brown gummy oil. (α_D)^{20.1°C} _{λ} (c = 1.0, H₂O): -30.4°; ν_{\max} (solution in CDCl₃): 3378, 2977, 1725, 1655, 1153 cm⁻¹; ¹H NMR (400 MHz, DMSO-*d*₆) δ = 9.35 (br s, 1H), 9.07 (br s, 1H), 8.79 (s, 1H), 8.61 (d, *J* = 4.9 Hz, 1H), 8.09 (d, *J* = 2.4 Hz, 1H), 7.71 (d, *J* = 4.9 Hz, 1H), 7.62 (dd, *J* = 1.0, 2.4 Hz, 1H), 7.37 (s, 1H), 4.10 (s, 3H), 4.07 - 4.01 (m, 2H), 3.60 - 3.56 (m, 1H), 2.02 (app. s, 3H), 1.11 (d, *J* = 6.8 Hz, 3H), signal for one proton under the broad water peak, NH and OH not observed; ¹³C NMR (101 MHz, CD₃OD) δ = 193.0, 172.8, 164.2, 155.7, 145.1, 140.2, 138.2, 137.1, 128.8, 118.3, 116.4, 112.2, 103.9, 103.7, 65.2, 64.5, 45.2, 37.2, 19.6, 15.8; LCMS (HpH): *t*_R = 0.52 min, [M+H⁺] = 431.4 (100 % purity); HRMS: (C₂₀H₂₂N₄O₅S) Requires [M+H⁺] = 431.139, found [M+H⁺] = 431.1384.

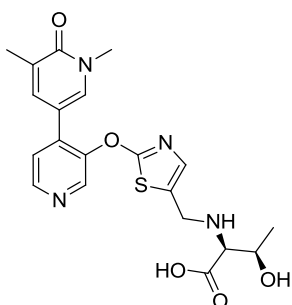
(2*S*,3*R*)-*tert*-Butyl 2-(((2-(((1,5-dimethyl-6-oxo-1,6-dihydro-(3,4'-bipyridin)-3'-yl)oxy)thiazol-5-yl)methyl)amino)-3-hydroxybutanoate, 2.29



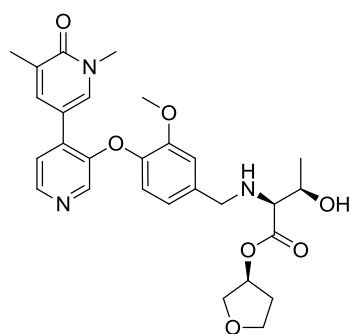
2-Picoline borane (23.0 mg, 0.22 mmol) was added to a solution of 2-(((1,5-dimethyl-6-oxo-1,6-dihydro-(3,4'-bipyridin)-3'-yl)oxy)thiazole-5-carbaldehyde (**2.25**, 64 mg, 0.20 mmol) and (2*S*,3*R*)-*tert*-butyl 2-amino-3-hydroxybutanoate hydrochloride²¹² (**2.26**, 45.5 mg, 0.22 mmol) in isopropanol (1 mL) and acetic acid (0.11 mL) and the reaction mixture stirred at rt for 4 h under nitrogen. The reaction mixture was purified by MDAP (HpH).

The relevant fractions were combined and concentrated *in vacuo* to give the title compound (**2.29**, 5 mg, 0.01 mmol, 5 % yield) as a brown oil. ¹H NMR (400 MHz, CDCl₃) δ = 8.61 (s, 1H), 8.54 (d, *J* = 4.9 Hz, 1H), 7.58 (d, *J* = 2.4 Hz, 1H), 7.45 (dd, *J* = 1.5, 2.4 Hz, 1H), 7.33 (d, *J* = 4.9 Hz, 1H), 6.93 (d, *J* = 1.0 Hz, 1H), 3.95 (dd, *J* = 1.0, 14.2 Hz, 1H), 3.73 - 3.63 (m, 2H), 3.59 (s, 3H), 2.90 (d, *J* = 6.8 Hz, 1H), 2.18 (app. s, 3H), 1.48 (s, 9H), 1.21 (d, *J* = 6.4 Hz, 3H), NH and OH not observed; LCMS (HpH): *t*_R = 0.87 min, [M+H⁺] = 487.4 (99 % purity).

(2*S*,3*R*)-2-(((2-(((1,5-Dimethyl-6-oxo-1,6-dihydro-(3,4'-bipyridin)-3'-yl)oxy)thiazol-5-yl)methyl)amino)-3-hydroxybutanoic acid, 2.30

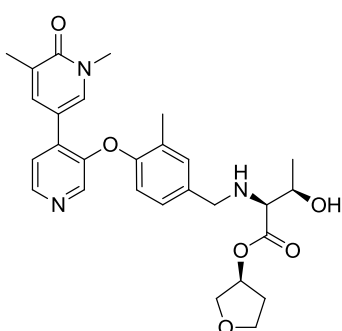


A solution of (2*S*,3*R*)-*tert*-butyl 2-(((2-(((1,5-dimethyl-6-oxo-1,6-dihydro-(3,4'-bipyridin)-3'-yl)oxy)thiazol-5-yl)methyl)amino)-3-hydroxybutanoate (**2.29**, 5 mg, 0.01 mmol) in 2M aqueous hydrochloric acid (360 μL, 0.72 mmol) was stirred at 60°C for 2 h. The reaction mixture was purified by MDAP (HpH). The relevant fraction was concentrated under a stream of nitrogen to afford the title compound (**2.30**, 2 mg, 0.05 mmol, 45 % yield) as an orange gum. ¹H NMR (400MHz, DMSO-d₆) δ 8.65 (d, *J* = 9.3 Hz, 1H), 8.55 - 8.51 (m, 1H), 8.02 (br. s., 1H), 7.59 (br. s., 2H), 7.01 (s, 1H), 3.97 - 3.87 (m, 1H), 3.82 - 3.63 (m, 3H), 3.48 (s, 3H), 3.06 (dd, *J* = 5.5, 11.1 Hz, 1H), 2.02 (s, 2H), 0.89 (d, *J* = 5.5 Hz, 3H); LCMS (HpH): *t*_R = 0.50 min, [M+H⁺] = 431.4 (100 % purity).

(2*S*,3*R*)-(S)-Tetrahydrofuran-3-yl**2-((4-((1,5-dimethyl-6-oxo-1,6-dihydro-(3,4'-****bipyridin)-3'-yl)oxy)-3-methoxybenzyl)amino)-3-hydroxybutanoate, 2.31, Scheme 2.7**

A suspension of 4-((1,5-dimethyl-6-oxo-1,6-dihydro-(3,4'-bipyridin)-3'-yl)oxy)-3-methoxybenzaldehyde (**2.44**, 21.7 mg, 0.06 mmol), (2*S*,3*R*)-(S)-tetrahydrofuran-3-yl 2-amino-3-hydroxybutanoate hydrochloride²²¹ (**2.40**, 28 mg, 0.12 mmol) and triethylamine (26 μ L, 0.19 mmol) in 2-MeTHF (0.5 mL) was stirred at rt for 1.5 h under nitrogen. Sodium triacetoxyborohydride (65.6 mg, 0.31 mmol) was added and

the resulting mixture was stirred for 16.5 h. The mixture was diluted with 2-MeTHF (0.5 mL) and further sodium triacetoxyborohydride (65.6 mg, 0.31 mmol) added. The reaction was stirred for 5 h after which further sodium triacetoxyborohydride (65.6 mg, 0.31 mmol) was added. The reaction was stirred for an hour and then quenched with the dropwise addition of saturated aqueous sodium bicarbonate solution (8 mL) and partitioned with ethyl acetate (8 mL). The aqueous phase was re-extracted with ethyl acetate (3 x 10 mL). The combined organics were dried (hydrophobic frit) and concentrated *in vacuo*. The residue was purified by MDAP (HpH) to give the title compound (**2.31**, 15.1 mg, 0.03 mmol, 47 % yield) as a milky yellow oil. ¹H NMR (400 MHz, CDCl₃) δ = 8.36 (d, *J* = 4.9 Hz, 1H), 8.13 (s, 1H), 7.82 (d, *J* = 2.5 Hz, 1H), 7.60 (dd, *J* = 1.0, 2.5 Hz, 1H), 7.28 (d, *J* = 4.9 Hz, 1H), 7.00 (s, 1H), 6.85 - 6.83 (m, 2H), 5.40 - 5.35 (m, 1H), 3.98 - 3.86 (m, 5H), 3.85 (s, 3H), 3.82 (s, 1H), 3.77 (app. quin, *J* = 6.4 Hz, 1H), 3.68 (d, *J* = 13.2 Hz, 1H), 3.60 (s, 3H), 2.29 - 2.21 (m, 1H), 2.20 (app. s, 3H), 2.06 - 1.98 (m, 1H), 1.25 (d, *J* = 6.4 Hz, 3H), NH and OH not observed; LCMS (HpH): *t*_R = 0.80 min, [M+H⁺] = 524.5 (100 % purity).

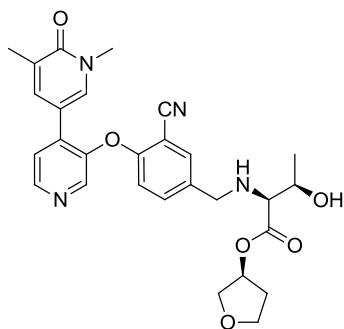
(2*S*,3*R*)-(S)-Tetrahydrofuran-3-yl**2-((4-((1,5-dimethyl-6-oxo-1,6-dihydro-(3,4'-****bipyridin)-3'-yl)oxy)-3-methylbenzyl)amino)-3-hydroxybutanoate, 2.32**

2-Picoline borane (9.75 mg, 0.09 mmol) was added to a solution of 4-((1,5-dimethyl-6-oxo-1,6-dihydro-(3,4'-bipyridin)-3'-yl)oxy)-3-methylbenzaldehyde (**2.47**, 27.7 mg, 0.08 mmol) and (2*S*,3*R*)-(S)-tetrahydrofuran-3-yl 2-amino-3-hydroxybutanoate hydrochloride²²¹ (**2.40**, 37.4 mg, 0.17 mmol) in isopropanol (0.5 mL) and acetic acid (0.06 mL) and the mixture stirred for 1.5 h. The sample was purified by

MDAP (HpH). The relevant fraction was concentrated under a stream of nitrogen to afford the title compound (**2.32**, 4.7 mg, 0.09 mmol, 11 % yield) as a yellow gum. (α_D)^{20.9°C} $\lambda(c =$

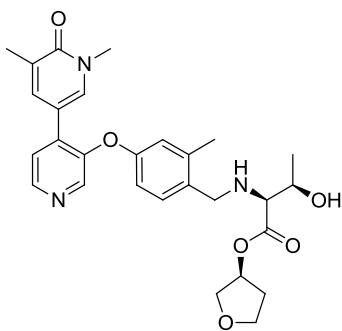
1.0, CDCl₃): -20.3°; ν_{\max} (solution in CDCl₃): 3350, 1726, 1655, 1106 cm⁻¹; ¹H NMR (400MHz, CDCl₃) δ = 8.40 (d, *J* = 4.9 Hz, 1H), 8.15 (s, 1H), 7.69 (d, *J* = 2.6 Hz, 1H), 7.56 (dd, *J* = 1.5, 2.6 Hz, 1H), 7.32 (d, *J* = 4.9 Hz, 1H), 7.22 (d, *J* = 1.5 Hz, 1H), 7.09 (dd, *J* = 2.0, 8.3 Hz, 1H), 6.71 (d, *J* = 8.3 Hz, 1H), 5.37 (m, 1H), 3.98 - 3.79 (m, 5H), 3.73 (app quin, *J* = 6.4 Hz, 1H), 3.65 (d, *J* = 12.7 Hz, 1H), 3.60 (s, 3H), 3.05 (d, *J* = 6.4 Hz, 1H), 2.29 (s, 3H), 2.27 - 2.22 (m, 1H), 2.21 (app. s, 3H), 2.06 - 1.98 (m, 1H), 1.90 (br. s., 2H), 1.24 (d, *J* = 6.4 Hz, 3H), NH and OH not observed; ¹³C NMR (101 MHz, CD₃OD) δ = 167.9, 163.0, 160.1, 157.9, 144.4, 144.3, 139.8, 138.8, 136.9, 134.9, 134.8, 133.4, 130.7, 128.7, 115.3, 111.7, 109.7, 109.1, 102.3, 65.2, 64.7, 55.4, 48.1, 47.9, 45.6, 37.4, 19.5, 15.8; LCMS (HpH): *t*_R = 0.86 min, [M+H⁺] = 508.4 (96 % purity); HRMS: (C₂₈H₃₃N₃O₆) Requires [M+H⁺] = 508.2448, found [M+H⁺] = 508.2449.

(2*S*,3*R*)-(S)-Tetrahydrofuran-3-yl 2-((3-cyano-4-((1,5-dimethyl-6-oxo-1,6-dihydro-(3,4'-bipyridin)-3'-yl)oxy)benzyl)amino)-3-hydroxybutanoate, 2.33



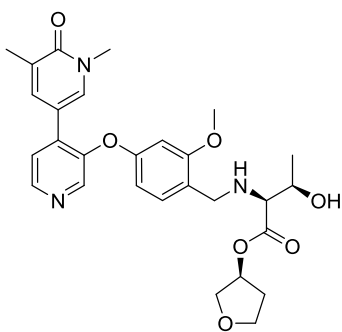
A suspension of 2-((1,5-dimethyl-6-oxo-1,6-dihydro-(3,4'-bipyridin)-3'-yl)oxy)-5-formylbenzonitrile (**2.48**, 44 mg, 0.13 mmol), (2*S*,3*R*)-(S)-tetrahydrofuran-3-yl 2-amino-3-hydroxybutanoate hydrochloride²²⁰ (**2.40**, 34.5 mg, 0.15 mmol) and triethylamine (0.05 mL, 0.38 mmol) in 2-MeTHF (0.9 mL) was stirred for 1.5 h at rt. Sodium triacetoxyborohydride (270 mg, 1.27 mmol) was added and

the reaction mixture was stirred for 6 h, after which further sodium triacetoxyborohydride (135 mg, 0.64 mmol) was added and the reaction stirred for 1.5 h. The reaction mixture was quenched with the addition of saturated aqueous sodium bicarbonate solution (10 mL) and partitioned with ethyl acetate (10 mL). The aqueous phase was re-extracted with ethyl acetate (3 x 10 mL). The combined organics were dried (hydrophobic frit), concentrated *in vacuo* and purified by MDAP (HpH). The relevant fraction was concentrated *in vacuo* to afford the title compound (**2.33**, 16.9 mg, 0.03 mmol, 26 % yield) as a yellow oil. ¹H NMR (400 MHz, CD₃OD) δ = 8.52 (d, *J* = 5.4 Hz, 1H), 8.44 (s, 1H), 7.98 - 7.95 (s, 1H), 7.73 (app. s, 2H), 7.61 (d, *J* = 5.4 Hz, 1H), 7.50 (d, *J* = 8.3 Hz, 1H), 6.72 (d, *J* = 8.3 Hz, 1H), 5.31 - 5.25 (m, 1H), 3.92 (quin, *J* = 6.4 Hz, 1H), 3.88 - 3.75 (m, 5H), 3.61 (d, *J* = 13.9 Hz, 1H), 3.59 (s, 3H), 3.02 (d, *J* = 6.4 Hz, 1H), 2.24 - 2.14 (m, 1H), 2.12 (s, 3H), 2.01 - 1.93 (m, 1H), 1.18 (d, *J* = 6.4 Hz, 3H), NH and OH not observed; LCMS (HpH): *t*_R = 0.80 min, [M+H⁺] = 519.4 (94 % purity).

(2*S*,3*R*)-(S)-Tetrahydrofuran-3-yl**2-((4-((1,5-dimethyl-6-oxo-1,6-dihydro-(3,4'-****bipyridin)-3'-yl)oxy)-2-methylbenzyl)amino)-3-hydroxybutanoate, 2.34**

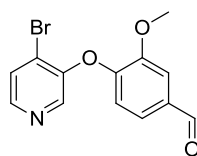
A solution of 4-((1,5-dimethyl-6-oxo-1,6-dihydro-(3,4'-bipyridin)-3'-yl)oxy)-2-methylbenzaldehyde (**2.49**, 53.7 mg, 0.16 mmol), (2*S*,3*R*)-(S)-tetrahydrofuran-3-yl 2-amino-3-hydroxybutanoate hydrochloride²²⁰ (**2.40**, 43.5 mg, 0.19 mmol) in isopropanol (0.7 mL) and acetic acid (0.08 mL) was stirred for 30 min. The reaction vessel was placed under a nitrogen atmosphere, then 2-picoline borane (18.9 mg, 0.18

mmol) was added and the reaction mixture was stirred for 1.5 h. The reaction mixture was purified by MDAP (HpH). The relevant fraction was concentrated *in vacuo*. The sample was combined with some of (2*S*,3*R*)-*tert*-butyl 2-((4-((1,5-dimethyl-6-oxo-1,6-dihydro-(3,4'-bipyridin)-3'-yl)oxy)-3-methoxybenzyl)amino)-3-hydroxybutanoate **2.45**. The resulting mixture was concentrated under a stream of nitrogen. The residue was purified by MDAP (HpH). The relevant fraction was concentrated under a stream of nitrogen to afford the title compound (**2.34**, 8.7 mg, 0.02 mmol, 11 % yield) as a light yellow oil. (α_D)^{20.1°C}_D(c = 0.5, CDCl₃): -40.8°; ν_{\max} (solution in CDCl₃): 3422, 1655, 1562, 904, 724 cm⁻¹; ¹H NMR (400 MHz, CDCl₃) δ = 8.41 (d, *J* = 4.9 Hz, 1H), 8.28 (s, 1H), 7.65 (d, *J* = 2.4 Hz, 1H), 7.51 (dd, *J* = 1.0, 2.4 Hz, 1H), 7.31 (d, *J* = 4.9 Hz, 1H), 7.18 (d, *J* = 8.3 Hz, 1H), 6.75 (d, *J* = 2.9 Hz, 1H), 6.69 (dd, *J* = 2.9, 8.3 Hz, 1H), 5.38 - 5.33 (m, 1H), 3.96 - 3.81 (m, 4H), 3.78 (d, *J* = 12.7 Hz, 1H), 3.71 (qd, *J* = 6.4, 6.8 Hz, 1H), 3.63 (d, *J* = 12.7 Hz, 1H), 3.56 (s, 3H), 3.04 (d, *J* = 6.8 Hz, 1H), 2.33 - 2.31 (m, 3H), 2.27 - 2.19 (m, 1H), 2.17 (app. s, 3H), 2.04 - 1.95 (m, 1H), 1.22 (d, *J* = 6.4 Hz, 3H), NH and OH not observed; ¹³C NMR (101 MHz, CDCl₃) δ = 173.4, 155.9, 145.6, 143.0, 139.1, 136.8, 136.5, 135.9, 132.6, 130.8, 129.6, 122.8, 119.6, 114.9, 112.8, 77.2, 75.8, 73.0, 68.1, 67.4, 67.0, 50.0, 38.2, 32.8, 19.4, 19.2, 19.1, 17.4; LCMS (HpH): *t*_R = 0.88 min, [M+H⁺] = 508.4 (100 % purity); HRMS: (C₂₈H₃₃N₃O₆) Requires [M+H⁺] = 508.2448, found [M+H⁺] = 508.2447.

(2S,3R)-(S)-Tetrahydrofuran-3-yl**2-((4-((1,5-dimethyl-6-oxo-1,6-dihydro-(3,4'-****bipyridin)-3'-yl)oxy)-2-methoxybenzyl)amino)-3-hydroxybutanoate, 2.35**

A suspension of 4-((1,5-dimethyl-6-oxo-1,6-dihydro-(3,4'-bipyridin)-3'-yl)oxy)-2-methoxybenzaldehyde (**2.50**, 56 mg, 0.16 mmol), (2S,3R)-(S)-tetrahydrofuran-3-yl 2-amino-3-hydroxybutanoate hydrochloride²²⁰ (**2.40**, 43.3 mg, 0.19 mmol) and triethylamine (67 μ L, 0.48 mmol) in 2-MeTHF (0.9 mL) was stirred for 30 min under nitrogen. Sodium triacetoxyborohydride (271 mg, 1.28 mmol) was added and

the reaction was stirred for 5 h. Further sodium triacetoxyborohydride (135 mg, 0.64 mmol) was added and the reaction was stirred for 12 h. The reaction mixture was quenched with the addition of saturated aqueous sodium bicarbonate solution (15 mL) and partitioned with ethyl acetate (15 mL). The aqueous phase was re-extracted with ethyl acetate (3 x 15 mL). The combined organics were dried (hydrophobic frit) and concentrated *in vacuo*. The residue was purified by MDAP (HpH). The relevant fraction was concentrated *in vacuo*, to afford the title compound (**2.35**, 45 mg, 0.09 mmol, 54 % yield). (α_D)^{20.1°C} _{λ} (c = 1.0, CDCl₃): -31.2°; ν_{\max} (solution in CDCl₃): 3359, 1730, 1655, 914 cm⁻¹; ¹H NMR (400 MHz, CDCl₃) δ = 8.42 (d, *J* = 4.9 Hz, 1H), 8.29 (s, 1H), 7.64 (s, 1H), 7.52 (s, 1H), 7.32 (d, *J* = 4.9 Hz, 1H), 7.12 (d, *J* = 8.3 Hz, 1H), 6.53 - 6.50 (s, 1H), 6.37 (d, *J* = 8.3 Hz, 1H), 5.23 - 5.17 (m, 1H), 3.91 - 3.82 (m, 3H), 3.79 (s, 3H), 3.77 - 3.68 (m, 3H), 3.62 (app. quin, *J* = 6.4 Hz, 1H), 3.57 (s, 3H), 2.97 (d, *J* = 8.3 Hz, 1H), 2.18 (s, 3H), 2.16 - 2.09 (m, 1H), 1.93 - 1.85 (m, 2H), 1.20 (d, *J* = 6.4 Hz, 3H), NH and OH not observed; ¹³C NMR (101 MHz, CDCl₃) δ = 173.3, 162.6, 159.2, 157.3, 149.5, 145.7, 142.9, 136.7, 136.4, 136.0, 130.8, 129.6, 123.2, 122.9, 112.8, 108.6, 101.2, 75.5, 72.9, 67.9, 67.8, 66.9, 55.5, 48.0, 38.2, 32.7, 19.3, 17.2; LCMS (HpH): t_R = 0.82 min, [M+H⁺] = 524.4 (100 % purity).

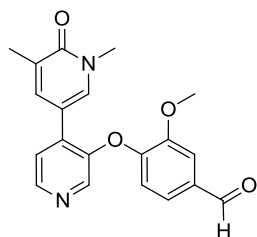
4-((4-Bromopyridin-3-yl)oxy)-3-methoxybenzaldehyde, 2.43, Table 2.7, Entry 5

A suspension of 4-bromopyridin-3-ol (**2.13**, 100 mg, 0.58 mmol), 4-fluoro-3-methoxybenzaldehyde (**2.42**, 266 mg, 1.72 mmol) and potassium carbonate (238 mg, 1.72 mmol) in DMSO (0.8 mL) was stirred in a microwave reactor at 160°C for 1 h. The reaction mixture was partitioned

between ethyl acetate (10 mL), water (5 mL) and brine (5 mL). The aqueous layer was re-extracted with ethyl acetate (3 x 10 mL). The combined organics were dried (hydrophobic frit) and concentrated *in vacuo*. The residue was purified by flash column chromatography (silica, 0-100 % ethyl acetate in cyclohexane followed by 0-10 % ethanol (+1 % NEt₃) in

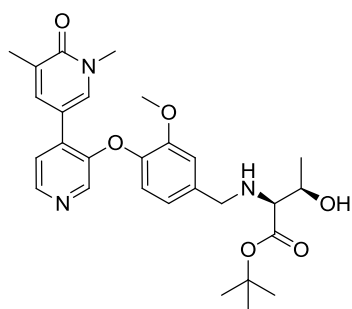
ethyl acetate). The relevant fractions were concentrated *in vacuo* to afford the title compound (**2.43**, 30 mg, 0.10 mmol, 60 wt%, 17 % yield) as an orange oil. ¹H NMR (400 MHz, DMSO-d₆) δ 9.99 (s, 1H), 8.26 (d, *J* = 5.5 Hz, 1H), 8.19 (s, 1H), 7.78 (d, *J* = 5.5 Hz, 1H), 7.67 (d, *J* = 2.0 Hz, 1H), 7.56 (dd, *J* = 2.0, 8.1 Hz, 1H), 7.12 (d, *J* = 8.1 Hz, 1H), 3.91 (s, 3H); LCMS (Formic): *t_R* = 0.96 min, [M+H⁺] = 308.0 / 310.0 (60 % purity).

4-((1,5-Dimethyl-6-oxo-1,6-dihydro-(3,4'-bipyridin)-3'-yl)oxy)-3-methoxybenzaldehyde, 2.44, Table 2.8, Entry 1



A suspension of 4-fluoro-3-methoxybenzaldehyde (**2.42**, 299 mg, 1.94 mmol), 3'-hydroxy-1,5-dimethyl-(3,4'-bipyridin)-6(1*H*)-one (**2.24**, 350 mg, 1.62 mmol) and potassium carbonate (671 mg, 4.86 mmol) in DMF (6 mL) was heated at 80°C for 16 h. The reaction mixture was concentrated *in vacuo*. The residue was partitioned between ethyl acetate (20 mL) and water (20 mL). The aqueous phase was re-extracted with ethyl acetate (3 x 10 mL). The combined organics were dried (hydrophobic frit) and concentrated *in vacuo*. The residue was purified by flash column chromatography (silica, 0-30 % ethanol (+1 % NEt₃) in ethyl acetate). The relevant fractions were concentrated *in vacuo* to give the title compound (**2.44**, 110 mg, 0.31 mmol, 19 % yield) as a black solid. ¹H NMR (400 MHz, CDCl₃) δ = 9.89 (s, 1H), 8.46 (d, *J* = 4.9 Hz, 1H), 8.30 (s, 1H), 7.76 (d, *J* = 2.5 Hz, 1H), 7.53 (dd, *J* = 1.0, 2.5 Hz, 1H), 7.51 (d, *J* = 2.0 Hz, 1H), 7.37 (dd, *J* = 2.0, 8.3 Hz, 1H), 7.33 (d, *J* = 4.9 Hz, 1H), 6.83 (d, *J* = 8.3 Hz, 1H), 3.96 (s, 3H), 3.55 (s, 3H), 2.16 (app. s, 3H); LCMS (HpH): *t_R* = 0.80 min, [M+H⁺] = 351.3 (100 % purity).

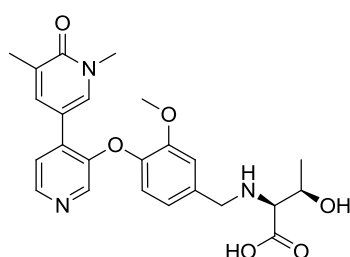
(2*S*,3*R*)-tert-Butyl 2-((4-((1,5-dimethyl-6-oxo-1,6-dihydro-(3,4'-bipyridin)-3'-yl)oxy)-3-methoxybenzyl)amino)-3-hydroxybutanoate, 2.45, Scheme 2.8



4-((1,5-Dimethyl-6-oxo-1,6-dihydro-(3,4'-bipyridin)-3'-yl)oxy)-3-methoxybenzaldehyde (**2.44**, 49 mg, 0.14 mmol) and (2*S*,3*S*)-tert-butyl 2-amino-3-hydroxybutanoate hydrochloride²²¹ (**2.26**, 35.5 mg, 0.17 mmol) were dissolved in isopropanol (1 mL) and acetic acid (0.11 mL) and stirred at rt for 40 min. 2-Picoline borane (15.0 mg, 0.14 mmol) was added and the resulting mixture stirred for 1.5 h. The sample was purified by MDAP (HpH) to afford the title compound (**2.45**, 13.2 mg, 0.03 mmol, 19 % yield) as an orange oil. (α_D)^{19,1°C} λ(c = 0.5, CDCl₃): -27.2°; ν_{max} (solution in CDCl₃): 3331, 2976, 1726, 1655, 1155 cm⁻¹; ¹H NMR (400 MHz, CDCl₃) δ = 8.35 (d, *J* = 4.4 Hz, 1H), 8.12

(s, 1H), 7.82 (d, $J = 2.4$ Hz, 1H), 7.58 (dd, $J = 1.0, 2.4$ Hz, 1H), 7.28 (d, $J = 4.4$ Hz, 1H), 7.04 - 7.02 (m, 1H), 6.87 - 6.81 (m, 2H), 3.90 (d, $J = 13.0$ Hz, 1H), 3.83 (s, 3H), 3.77 - 3.68 (m, 2H), 3.58 (s, 3H), 2.98 (d, $J = 7.3$ Hz, 1H), 2.19 (app. s, 3H), 1.49 (s, 9H), 1.24 (d, $J = 6.4$ Hz, 3H), NH and OH not observed; ^{13}C NMR (101 MHz, CDCl_3) $\delta = 171.9, 162.7, 150.7, 144.5, 143.6, 139.94, 139.87, 137.0, 136.9, 129.4, 121.1, 119.9, 115.5, 113.0, 112.9, 82.5, 77.2, 67.9, 67.7, 56.0, 55.9, 52.0, 38.2, 28.1$ (3C), 19.6, 17.3; LCMS (HpH): $t_R = 1.00$ min, $[\text{M}+\text{H}^+] = 510.4$ (100 % purity); HRMS: ($\text{C}_{28}\text{H}_{35}\text{N}_3\text{O}_6$) Requires $[\text{M}+\text{H}^+] = 510.2605$, found $[\text{M}+\text{H}^+] = 510.2604$.

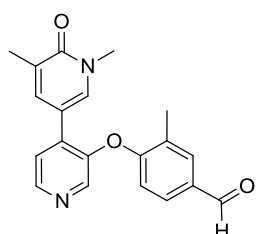
(2*S*,3*R*)-2-((4-((1,5-Dimethyl-6-oxo-1,6-dihydro-(3,4'-bipyridin)-3'-yl)oxy)-3-methoxybenzyl)amino)-3-hydroxybutanoic acid, 2.46, Scheme 2.8



A solution of (2*S*,3*R*)-*tert*-butyl 2-((4-((1,5-dimethyl-6-oxo-1,6-dihydro-(3,4'-bipyridin)-3'-yl)oxy)-3-methoxybenzyl)amino)-3-hydroxybutanoate (**2.45**, 5 mg, 0.10 mmol) in 2M aqueous hydrochloric acid (245 μl , 0.49 mmol) was stirred for 3 h at 50°C. The reaction mixture was concentrated *in vacuo*. The residue was purified by MDAP

(HpH). The relevant fraction was concentrated under a stream of nitrogen to afford the title compound (**2.46**, 2.8 mg, 0.06 mmol, 63 % yield) as a white solid. ^1H NMR (400MHz, DMSO-d_6) δ 8.31 (d, $J = 5.5$ Hz, 1H), 8.04 (s, 1H), 7.94 (d, $J = 2.5$ Hz, 1H), 7.68 (s, 1H), 7.44 (d, $J = 5.5$ Hz, 1H), 7.19 (s, 1H), 6.93 (s, 2H), 3.95 - 3.87 (m, 2H), 3.80 (s, 3H), 3.74 (d, $J = 12.8$ Hz, 1H), 3.52 (s, 3H), 2.97 (br. s., 1H), 2.07 (s, 3H), 1.19 (d, $J = 6.0$ Hz, 3H), exchangeable protons not observed; LCMS (HpH): $t_R = 0.56$ min, $[\text{M}+\text{H}^+] = 454.4$ (100 % purity).

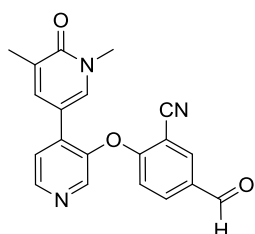
4-((1,5-Dimethyl-6-oxo-1,6-dihydro-(3,4'-bipyridin)-3'-yl)oxy)-3-methylbenzaldehyde, 2.47



A suspension of 4-fluoro-3-methylbenzaldehyde (81 mg, 0.59 mmol), 3'-hydroxy-1,5-dimethyl-(3,4'-bipyridin)-6(1*H*)-one (**2.24**, 106 mg, 0.49 mmol) and potassium carbonate (203 mg, 1.47 mmol) in DMF (1.5 mL) was stirred for 30 h at 80°C. The reaction mixture was diluted with DMF (1.5 mL) and purified by MDAP (HpH). The relevant vial was concentrated *in vacuo* to afford the title compound (**2.47**, 27 mg, 0.08 mmol, 16 % yield) as a black oil. ^1H NMR (400 MHz, CDCl_3) $\delta = 9.89$ (s, 1H), 8.54 (br s, 1H), 8.35 (br s, 1H), 7.78 (d, $J = 2.2$ Hz, 1H), 7.60 (dd, $J = 2.2, 8.3$ Hz, 1H), 7.55 (d, $J = 2.5$

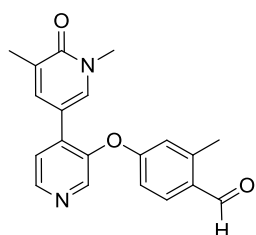
Hz, 1H), 7.47 (dd, $J = 1.2, 2.5$ Hz, 1H), 7.36 (br s, 1H), 6.66 (d, $J = 8.3$ Hz, 1H), 3.54 (s, 3H), 2.42 (s, 3H), 2.15 (app. s, 3H); LCMS (HpH): $t_R = 0.86$ min, $[M+H^+] = 335.3$ (98 % purity).

2-((1,5-Dimethyl-6-oxo-1,6-dihydro-(3,4'-bipyridin)-3'-yl)oxy)-5-formylbenzonitrile, 2.48



Potassium carbonate (575 mg, 4.16 mmol) was added to a solution of 2-fluoro-5-formylbenzonitrile (**2.63**, 207 mg, 1.39 mmol) and 3'-hydroxy-1,5-dimethyl-(3,4'-bipyridin)-6(1*H*)-one (**2.24**, 300 mg, 1.39 mmol) in DMF (6 mL) and the resulting mixture stirred at 80°C for 2.5 h. The reaction mixture was partitioned between saturated aqueous LiCl solution (30 mL) and ethyl acetate (30 mL). The aqueous layer was re-extracted with ethyl acetate (3 x 25 mL). The combined organics were dried (hydrophobic frit) and concentrated *in vacuo*. A yellow solid precipitated during the work up which was purified by flash column chromatography (silica, 0-20 % ethanol (+1 % NEt₃) in ethyl acetate). The relevant fractions were combined and concentrated *in vacuo* to afford the title compound (**2.48**, 158 mg, 0.46 mmol, 33 % yield) as a yellow solid. ¹H NMR (400MHz, CDCl₃) $\delta = 9.91$ (s, 1H), 8.64 (d, $J = 5.1$ Hz, 1H), 8.56 (s, 1H), 8.18 (d, $J = 2.0$ Hz, 1H), 7.94 (dd, $J = 2.0, 8.8$ Hz, 1H), 7.80 (d, $J = 2.4$ Hz, 1H), 7.49 (d, $J = 0.98, 2.4$ Hz, 1H), 7.44 (d, $J = 5.1$ Hz, 1H), 6.76 (d, $J = 8.8$ Hz, 1H), 3.62 (s, 3H), 2.18 (app. s, 3H); LCMS (HpH): $t_R = 0.80$ min, $[M+H^+] = 346.3$ (98 % purity).

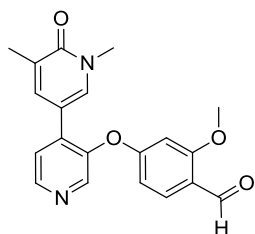
4-((1,5-Dimethyl-6-oxo-1,6-dihydro-(3,4'-bipyridin)-3'-yl)oxy)-2-methylbenzaldehyde, 2.49



A suspension of 4-fluoro-2-methylbenzaldehyde (299 mg, 2.16 mmol), 3'-hydroxy-1,5-dimethyl-(3,4'-bipyridin)-6(1*H*)-one (**2.24**, 390 mg, 1.80 mmol) and potassium carbonate (748 mg, 5.41 mmol) in DMF (6 mL) was heated at 85°C for 64 h. The reaction mixture was concentrated *in vacuo*. The residue was partitioned between ethyl acetate (10 mL) and partitioned with water (10 mL). The aqueous phase was re-extracted with ethyl acetate (3 x 10 mL) and the combined organics dried (hydrophobic frit) and concentrated *in vacuo*. The residue was purified by flash column chromatography (silica, 0-30 % ethanol (+1 % NEt₃) in ethyl acetate). The relevant fractions were concentrated *in vacuo* to afford the title compound (**2.49**, 160 mg, 0.48 mmol, 27 % yield) as a dark brown oil. ¹H NMR (400MHz CDCl₃) $\delta 10.17$ (s, 1H), 8.53 (d, $J = 5.1$ Hz, 1H), 8.41 (s, 1H), 7.77

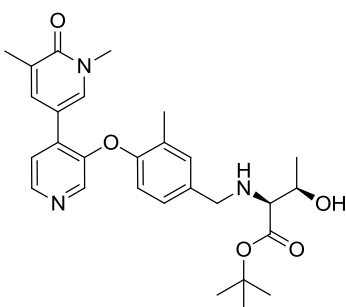
(d, $J = 8.6$ Hz, 1H), 7.59 (d, $J = 2.4$ Hz, 1H), 7.48 (d, $J = 0.98, 2.4$ Hz, 1H), 7.38 (d, $J = 5.1$ Hz, 1H), 6.80 (dd, $J = 2.4, 8.6$ Hz, 1H), 6.75 (d, $J = 2.4$ Hz, 1H), 3.56 (s, 3H), 2.64 (s, 3H), 2.18 (app. s, 3H); LCMS (HpH): $t_R = 0.86$ min, $[M+H^+] = 335.3$ (100 % purity).

4-((1,5-Dimethyl-6-oxo-1,6-dihydro-(3,4'-bipyridin)-3'-yl)oxy)-2-methoxybenzaldehyde, 2.50



3'-Hydroxy-1,5-dimethyl-(3,4'-bipyridin)-6(1*H*)-one **2.24** (300 mg, 1.39 mmol) was dissolved in DMF (6 mL). Methyl 4-fluoro-3-methoxybenzoate (256 mg, 1.39 mmol) was added followed by 4-fluoro-2-methoxybenzaldehyde (257 mg, 1.67 mmol) and potassium carbonate (575 mg, 4.16 mmol). The resulting solution was stirred at 80°C for 15 h. The reaction mixture was concentrated *in vacuo*. The residue was partitioned between ethyl acetate (15 mL) and water (15 mL). The aqueous phase was re-extracted with ethyl acetate (3 x 15 mL) and the combined organics dried (hydrophobic frit) and concentrated *in vacuo*. The residue was purified by flash column chromatography (silica, 0-30 % ethanol (+1 % NEt₃) in ethyl acetate). The relevant fractions were combined and concentrated *in vacuo* to afford the title compound (**2.50**, 108 mg, 0.31 mmol, 22 % yield) as an orange oil. ¹H NMR (400MHz, CDCl₃) $\delta = 10.32$ (s, 1H), 8.52 (d, $J = 5.1$ Hz, 1H), 8.42 (s, 1H), 7.78 (d, $J = 8.6$ Hz, 1H), 7.57 (d, $J = 2.4$ Hz, 1H), 7.47 (dd, $J = 0.98, 2.4$ Hz, 1H), 7.37 (d, $J = 5.1$ Hz, 1H), 6.53 (d, $J = 2.9$ Hz, 1H), 6.41 (dd, $J = 2.9, 8.6$ Hz, 1H), 3.87 (s, 3H), 3.56 (s, 3H), 2.17 (app. s, 3H); LCMS (HpH): $t_R = 0.86$ min, $[M+H^+] = 331.3$ (99 % purity).

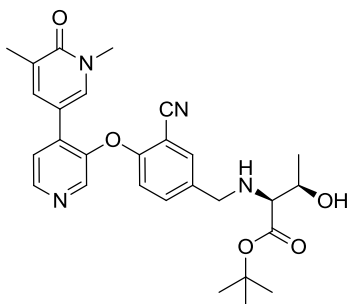
(2*S*,3*R*)-tert-Butyl 2-((4-((1,5-dimethyl-6-oxo-1,6-dihydro-(3,4'-bipyridin)-3'-yl)oxy)-3-methylbenzyl)amino)-3-hydroxybutanoate, 2.52



A solution of 4-((1,5-dimethyl-6-oxo-1,6-dihydro-(3,4'-bipyridin)-3'-yl)oxy)-3-methylbenzaldehyde (**2.47**, 28 mg, 0.08 mmol) and (2*S*,3*S*)-*tert*-butyl 2-amino-3-hydroxybutanoate hydrochloride²²¹ (**2.26**, 21.3 mg, 0.10 mmol) in isopropanol (0.7 mL) and acetic acid (0.08 mL) was stirred for 30 min under nitrogen. 2-Picoline borane (8.96 mg, 0.08 mmol) was added and the reaction was stirred for 1.5 h. The reaction mixture was purified by MDAP (HpH). The relevant fraction was concentrated *in vacuo* to afford the title compound (**2.52**, 14 mg, 0.03 mmol, 34 % yield) as a yellow gum. ¹H NMR (400 MHz, CDCl₃) $\delta = 8.37$ (d, $J = 4.9$ Hz, 1H), 8.12 (s, 1H), 7.68

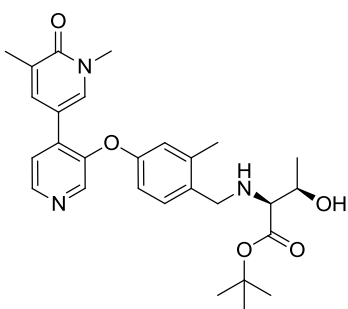
(d, $J = 2.4$ Hz, 1H), 7.55 (dd, $J = 1.5, 2.4$ Hz, 1H), 7.30 (d, $J = 4.9$ Hz, 1H), 7.21 (d, $J = 2.0$ Hz, 1H), 7.08 (dd, $J = 2.0, 8.3$ Hz, 1H), 6.70 (d, $J = 8.3$ Hz, 1H), 3.79 (d, $J = 13.2$ Hz, 1H), 3.64 (qd, $J = 6.4, 7.8$ Hz, 1H), 3.62 (d, $J = 13.2$ Hz, 1H), 3.58 (s, 3H), 2.90 (d, $J = 7.8$ Hz, 1H), 2.27 (s, 3H), 2.19 (app. s, 3H), 1.49 (s, 9H), 1.22 (d, $J = 6.4$ Hz, 3H), NH and OH not observed; LCMS (HpH): $t_R = 1.06$ min, $[M+H^+] = 494.4$ (100 % purity).

(2*S*,3*R*)-tert-Butyl 2-((3-cyano-4-((1,5-dimethyl-6-oxo-1,6-dihydro-(3,4'-bipyridin)-3'-yl)oxy)benzyl)amino)-3-hydroxybutanoate, 2.53



A suspension of 2-((1,5-dimethyl-6-oxo-1,6-dihydro-(3,4'-bipyridin)-3'-yl)oxy)-5-formylbenzonitrile (**2.48**, 74 mg, 0.21 mmol), (2*S*,3*R*)-tert-butyl 2-amino-3-hydroxybutanoate hydrochloride²²¹ (**2.26**, 54.4 mg, 0.26 mmol) and triethylamine (90 μ L, 0.64 mmol) in 2-MeTHF was stirred for 1.5 h under nitrogen. Sodium triacetoxyborohydride (454 mg, 2.14 mmol) was added and the reaction was stirred for 6 h. The reaction mixture was quenched with the addition of saturated aqueous sodium bicarbonate solution (15 mL) and partitioned with ethyl acetate (15 mL). The aqueous phase was re-extracted with ethyl acetate (3 x 15 mL). The combined organics were dried (hydrophobic frit) and concentrated *in vacuo*. The residue was purified by MDAP (HpH). The relevant fraction was concentrated *in vacuo* to afford the title compound (**2.53**, 57 mg, 0.11 mmol, 53 % yield) as a yellow oil. (α_D)^{20,1°C} $\lambda(c = 1.0, \text{CDCl}_3)$: -29.4°; ν_{max} (solution in CDCl_3): 3333, 2980, 1726, 1655, 1592, 1106 cm^{-1} ; $^1\text{H NMR}$ (400 MHz, CDCl_3) $\delta = 8.54$ (d, $J = 4.9$ Hz, 1H), 8.45 (s, 1H), 7.83 (d, $J = 2.5$ Hz, 1H), 7.61 (d, $J = 2.0$ Hz, 1H), 7.50 (dd, $J = 1.0, 2.5$ Hz, 1H), 7.41 (dd, $J = 2.0, 8.3$ Hz, 1H), 7.39 (d, $J = 4.9$ Hz, 1H), 6.63 (d, $J = 8.3$ Hz, 1H), 3.82 (d, $J = 13.7$ Hz, 1H), 3.70 (qd, $J = 6.4, 6.8$ Hz, 1H), 3.62 (s, 3H), 3.61 (d, $J = 13.7$ Hz, 1H), 2.86 (d, $J = 6.8$ Hz, 1H), 2.17 (app. s, 3H), 1.48 (s, 9H), 1.21 (d, $J = 6.4$ Hz, 3H), NH and OH not observed; $^{13}\text{C NMR}$ (101 MHz, CDCl_3) $\delta = 172.5, 162.6, 157.7, 147.5, 147.2, 143.8, 137.1, 137.0, 136.3, 135.3, 134.4, 133.5, 130.2, 123.4, 115.7, 115.2, 111.7, 102.9, 82.3, 68.2, 67.8, 51.0, 38.2, 28.1$ (3C), 19.4, 17.3; LCMS (HpH): $t_R = 0.97$ min, $[M+H^+] = 505.4$, (99 % purity); HRMS: ($\text{C}_{28}\text{H}_{32}\text{N}_4\text{O}_5$) Requires $[M+H^+] = 505.2452$, found $[M+H^+] = 505.2451$.

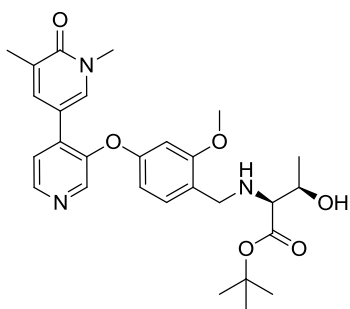
(2*S*,3*R*)-tert-Butyl 2-((4-((1,5-dimethyl-6-oxo-1,6-dihydro-(3,4'-bipyridin)-3'-yl)oxy)-2-methylbenzyl)amino)-3-hydroxybutanoate, 2.54



4-((1,5-Dimethyl-6-oxo-1,6-dihydro-(3,4'-bipyridin)-3'-yl)oxy)-2-methylbenzaldehyde (**2.49**, 49 mg, 0.15 mmol) and (2*S*,3*S*)-tert-butyl 2-amino-3-hydroxybutanoate hydrochloride (**2.26**, 37.2 mg, 0.18 mmol) were dissolved in isopropanol (1 mL) and acetic acid (0.11 mL). The resulting solution was stirred for 30 min, before 2-picoline borane (15.7 mg, 0.15 mmol) was added. The reaction was stirred for 1.5 h. The

reaction mixture was purified directly by MDAP (HpH). The relevant fraction was concentrated *in vacuo*, dissolved in chloroform and concentrated to dryness under a stream of nitrogen to afford the title compound (**2.54**, 15.5 mg, 0.03 mmol, 21 % yield) as an orange gum ¹H NMR (400 MHz, CDCl₃) δ = 8.40 (d, *J* = 4.9 Hz, 1H), 8.28 (s, 1H), 7.66 (d, *J* = 2.4 Hz, 1H), 7.51 (dd, *J* = 1.0, 2.4 Hz, 1H), 7.31 (d, *J* = 4.9 Hz, 1H), 7.20 (d, *J* = 8.3 Hz, 1H), 6.75 (d, *J* = 2.7 Hz, 1H), 6.70 (dd, *J* = 2.7, 8.3 Hz, 1H), 3.78 (d, *J* = 12.7 Hz, 1H), 3.62 (d, *J* = 12.7 Hz, 1H), 3.66 - 3.59 (m, 1H), 3.56 (s, 3H), 2.90 (d, *J* = 7.3 Hz, 1H), 2.32 (s, 3H), 2.18 (app. s, 3H), 1.49 (s, 9H), 1.21 (d, *J* = 6.4 Hz, 3H), NH and OH not observed; LCMS (HpH): *t_R* = 1.07 min, [M+H⁺] = 494.4 (100 % purity).

(2*S*,3*R*)-tert-Butyl 2-((4-((1,5-dimethyl-6-oxo-1,6-dihydro-(3,4'-bipyridin)-3'-yl)oxy)-2-methoxybenzyl)amino)-3-hydroxybutanoate, 2.55

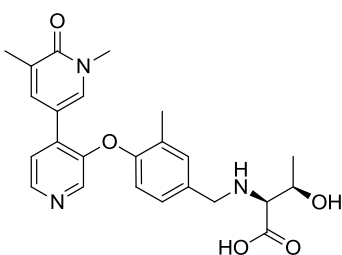


A suspension of 4-((1,5-dimethyl-6-oxo-1,6-dihydro-(3,4'-bipyridin)-3'-yl)oxy)-2-methoxybenzaldehyde (**2.50**, 62.7 mg, 0.18 mmol), (2*S*,3*R*)-tert-butyl 2-amino-3-hydroxybutanoate hydrochloride²²¹ (**2.26**, 45.5 mg, 0.22 mmol) and triethylamine (75 μL, 0.54 mmol) in 2-MeTHF (0.9 mL) was stirred for 30 min under nitrogen. Sodium triacetoxyborohydride (303 mg, 1.43 mmol) was added and

the reaction was stirred for 5 h. Further sodium triacetoxyborohydride (190 mg, 0.90 mmol) was added and the reaction was stirred for 12 h. The reaction mixture was quenched with the addition of saturated aqueous sodium bicarbonate solution (15 mL) and partitioned with ethyl acetate (15 mL). The aqueous phase was re-extracted with ethyl acetate (3 x 15 mL) and the combined organics were dried (hydrophobic frit) and concentrated *in vacuo*. The residue was purified by MDAP (HpH). The relevant fraction was concentrated *in vacuo* to afford the title compound (**2.55**, 48 mg, 0.09 mmol, 52 % yield) as a yellow oil. (α_D)^{20.1°C}_D(c = 1.0, CDCl₃):

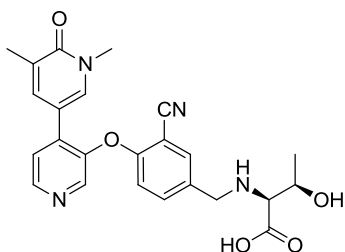
-62.3°; ν_{\max} (solution in CDCl_3): 3418, 2976, 1723, 1655, 1587, 1275 cm^{-1} ; ^1H NMR (400 MHz, CDCl_3) δ = 8.42 (d, J = 4.9 Hz, 1H), 8.30 (s, 1H), 7.64 (d, J = 2.5 Hz, 1H), 7.51 (dd, J = 1.0, 2.5 Hz, 1H), 7.31 (d, J = 4.9 Hz, 1H), 7.14 (d, J = 8.3 Hz, 1H), 6.51 (d, J = 2.4 Hz, 1H), 6.38 (dd, J = 2.4, 8.3 Hz, 1H), 3.79 (s, 3H), 3.74 (app. s, 2H), 3.57 (s, 3H), 3.57 (qd, J = 6.4, 7.8 Hz, 1H), 2.85 (d, J = 7.8 Hz, 1H), 2.18 (app. s, 3H), 1.41 (s, 9H), 1.20 (d, J = 6.4 Hz, 3H), NH and OH not observed; ^{13}C NMR (101 MHz, CDCl_3) δ = 172.7, 162.6, 159.2, 157.3, 149.5, 145.7, 143.0, 136.7, 136.4, 136.0, 130.8, 129.6, 123.4, 122.9, 112.8, 108.6, 101.2, 81.6, 68.6, 68.0, 55.5, 47.9, 38.2, 28.0 (3C), 19.3, 17.3; LCMS (HpH): t_{R} = 1.00 min, $[\text{M}+\text{H}^+]$ = 510.4 (100 % purity); HRMS: ($\text{C}_{28}\text{H}_{35}\text{N}_3\text{O}_6$) Requires $[\text{M}+\text{H}^+]$ = 510.2605, found $[\text{M}+\text{H}^+]$ = 510.2604.

(2*S*,3*R*)-2-((4-((1,5-Dimethyl-6-oxo-1,6-dihydro-(3,4'-bipyridin)-3'-yl)oxy)-3-methylbenzyl)amino)-3-hydroxybutanoic acid, 2.56



A solution of (2*S*,3*R*)-*tert*-butyl 2-((4-((1,5-dimethyl-6-oxo-1,6-dihydro-(3,4'-bipyridin)-3'-yl)oxy)-3-methylbenzyl)amino)-3-hydroxybutanoate (**2.52**, 8.7 mg, 0.02 mmol) in 2M aqueous hydrochloric acid (441 μl , 0.88 mmol) was stirred for 3 h at 50°C. The reaction mixture was concentrated *in vacuo*. The residue was purified by MDAP (HpH). The relevant fraction was concentrated under a stream of nitrogen to afford the title compound (**2.56**, 5.1 mg, 0.01 mmol, 66 % yield) as a white solid. ^1H NMR (400 MHz, $\text{DMSO}-d_6$) δ = 8.41 (d, J = 4.9 Hz, 1H), 8.11 (s, 1H), 8.03 (d, J = 2.4 Hz, 1H), 7.68 (dd, J = 1.5, 2.5 Hz, 1H), 7.56 (d, J = 4.9 Hz, 1H), 7.37 (d, J = 2.0 Hz, 1H), 7.21 (dd, J = 2.0, 8.3 Hz, 1H), 6.69 (d, J = 8.3 Hz, 1H), 4.00 (d, J = 13.2 Hz, 1H), 3.93 (dd, J = 5.4, 6.4 Hz, 1H), 3.88 (d, J = 13.2 Hz, 1H), 3.47 (s, 3H), 3.15 (br d, J = 5.4 Hz, 1H), 2.26 (app. s, 3H), 2.01 (s, 3H), 1.11 (d, J = 6.4 Hz, 3H), exchangeable protons not observed; LCMS (HpH): t_{R} = 0.59 min, $[\text{M}+\text{H}^+]$ = 438.4 (100 % purity).

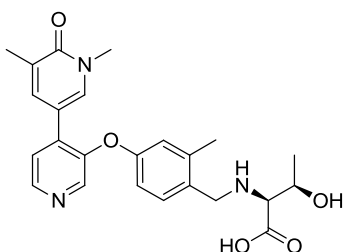
(3-Cyano-4-((1,5-dimethyl-6-oxo-1,6-dihydro-(3,4'-bipyridin)-3'-yl)oxy)benzyl)-L-threonine hydrochloride, 2.57



A solution of (2*S*,3*R*)-*tert*-butyl 2-((3-cyano-4-((1,5-dimethyl-6-oxo-1,6-dihydro-(3,4'-bipyridin)-3'-yl)oxy)benzyl)amino)-3-hydroxybutanoate (**2.53**, 24 mg, 0.05 mmol) in 2M aqueous HCl (1.2 mL, 2.34 mmol) was stirred at 50°C for 3 h. The reaction mixture was concentrated *in vacuo* and subsequently

dried under vacuum at 40°C for four days to afford the title compound (**2.57**, 20 mg, 0.04 mmol, 87 % yield) as a yellow oil. (α_D)^{20.9°C}_λ(c = 1.0, CDCl₃): +189.6°; ν_{\max} (solution in CDCl₃): 3331, 2568, 2232, 1622 cm⁻¹; ¹H NMR (400 MHz, DMSO-d₆) δ = 9.51 (br s, 1H, HCl), 8.78 - 8.68 (m, 2H), 8.14 (br s, 1H), 8.07 (d, *J* = 2.0 Hz, 1H), 7.89 (br s, 1H), 7.77 (dd, *J* = 2.0, 8.8 Hz, 1H), 7.71 (d, *J* = 1.0 Hz, 1H), 6.98 (d, *J* = 8.8 Hz, 1H), 5.91 (br s, 3H), 4.22 (d, *J* = 14.2 Hz, 1H), 4.19 (d, *J* = 14.2 Hz, 1H), 4.10 (dq, *J* = 5.9, 6.4 Hz, 1H), 3.61 (d, *J* = 5.9 Hz, 1H), 3.48 (s, 3H), 2.01 (s, 3H), 1.18 (d, *J* = 6.4 Hz, 3H); ¹³C NMR (101 MHz, CD₃OD) δ = 162.9, 157.8, 145.5, 140.9, 139.8, 137.4, 137.2, 136.5, 136.3, 129.1, 127.8, 126.5, 116.6, 114.4, 111.1, 103.4, 65.4, 65.3, 48.6, 48.1, 47.9, 37.4, 19.7, 15.7; LCMS (HpH): *t*_R = 0.57 min, [M+H⁺] = 449.4 (98 % purity); HRMS: (C₂₄H₂₄N₄O₅) Requires [M+H⁺] = 449.1826, found [M+H⁺] = 449.1821.

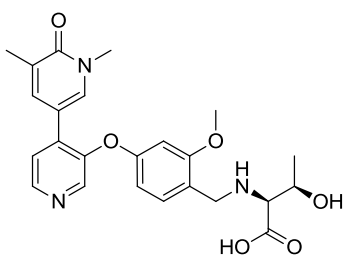
(2*S*,3*R*)-2-((4-((1,5-Dimethyl-6-oxo-1,6-dihydro-(3,4'-bipyridin)-3'-yl)oxy)-2-methylbenzyl)amino)-3-hydroxybutanoic acid, 2.58



A solution of (*2S,3R*)-*tert*-butyl 2-((4-((1,5-dimethyl-6-oxo-1,6-dihydro-(3,4'-bipyridin)-3'-yl)oxy)-2-methylbenzyl)amino)-3-hydroxybutanoate (**2.54**, 9 mg, 0.02 mmol) in 2M aqueous hydrochloric acid (456 μ l, 0.91 mmol) was stirred at 50°C for 3 h. The reaction mixture was concentrated *in vacuo*. The residue was purified by MDAP

(HpH). The relevant fraction was concentrated under a stream of nitrogen to afford the title compound (**2.58**, 3.6 mg, 0.01 mmol, 43 % yield) as a white solid. ¹H NMR (400 MHz, DMSO-d₆) δ = 8.42 (d, *J* = 4.9 Hz, 1H), 8.23 (s, 1H), 8.02 (d, *J* = 2.5 Hz, 1H), 7.66 (dd, *J* = 1.5, 2.5 Hz, 1H), 7.56 (d, *J* = 4.9 Hz, 1H), 7.31 (d, *J* = 8.3 Hz, 1H), 7.12 (br. s, 1H, HCl salt), 6.83 (d, *J* = 2.9 Hz, 1H), 6.74 (dd, *J* = 2.9, 8.3 Hz, 1H), 3.87 (dq, *J* = 5.4, 6.4 Hz, 1H), 3.86 (d, *J* = 13.2 Hz, 1H), 3.69 (d, *J* = 13.2 Hz, 1H), 3.47 (s, 3H), 3.00 (d, *J* = 5.4 Hz, 1H), 2.28 (app. s, 3H), 2.00 (s, 3H), 1.11 (d, *J* = 6.4 Hz, 3H), exchangeable protons not observed; LCMS (HpH): *t*_R = 0.57 min, [M+H⁺] = 438.4 (100 % purity).

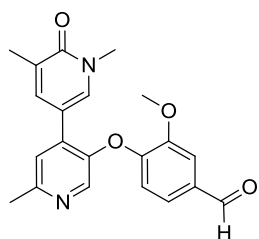
(2*S*,3*R*)-2-((4-((1,5-Dimethyl-6-oxo-1,6-dihydro-(3,4'-bipyridin)-3'-yl)oxy)-2-methylbenzyl)amino)-3-hydroxybutanoic acid, 2.59



A solution of (*2S,3R*)-*tert*-butyl 2-((4-((1,5-dimethyl-6-oxo-1,6-dihydro-(3,4'-bipyridin)-3'-yl)oxy)-2-methylbenzyl)amino)-3-hydroxybutanoate (**2.55**, 9 mg, 0.02 mmol) in 2M aqueous hydrochloric acid (456 μ l, 0.91 mmol)

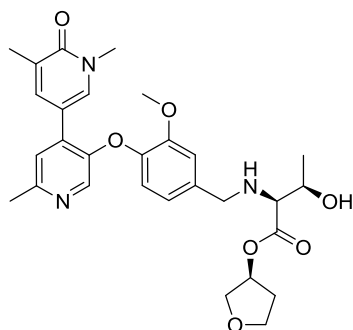
was stirred at 50°C for 3 h. The reaction mixture was concentrated *in vacuo*. The residue was purified by MDAP (HpH). The relevant fraction was concentrated under a stream of nitrogen to afford the title compound (**2.59**, 3.4 mg, 0.01 mmol, 73 % yield) as a white solid. ¹H NMR (400MHz, DMSO-d₆) δ 8.42 (d, *J* = 5.1 Hz, 1H), 8.24 (s, 1H), 8.03 (d, *J* = 2.4 Hz, 1H), 7.66 (d, *J* = 2.4 Hz, 1H), 7.56 (d, *J* = 5.1 Hz, 1H), 7.31 (d, *J* = 8.3 Hz, 1H), 6.83 (d, *J* = 2.7 Hz, 1H), 6.75 (dd, *J* = 2.7, 8.3 Hz, 1H), 3.91 - 3.82 (m, 2H), 3.69 (d, *J* = 13.0 Hz, 1H), 3.47 (s, 3H), 3.00 (d, *J* = 4.9 Hz, 1H), 2.29 (s, 3H), 2.01 (s, 3H), 1.12 (d, *J* = 6.4 Hz, 3H), exchangeable protons not observed; LCMS (HpH): t_R = 0.57 min, [M+H⁺] = 438.4 (100 % purity).

3-Methoxy-4-((1,5,6'-trimethyl-6-oxo-1,6-dihydro-(3,4'-bipyridin)-3'-yl)oxy)benzaldehyde, 2.64



A suspension of 4-fluoro-3-methoxybenzaldehyde (**2.42**, 402 mg, 2.61 mmol), potassium carbonate (1200 mg, 8.69 mmol) and 5'-hydroxy-1,2',5-trimethyl-(3,4'-bipyridin)-6(1*H*)-one¹⁶⁵ (**2.62**, 500 mg, 2.17 mmol) in DMF (10 mL) was heated at 80°C for 16 h. The reaction mixture was concentrated *in vacuo*. The residue was purified by flash column chromatography (silica, 0-100% ethyl acetate in cyclohexane followed by 0-30% ethanol (+1% NEt₃) in ethyl acetate). The relevant fractions were combined and concentrated *in vacuo* to afford the title compound (**2.64**, 685 mg, 1.79 mmol, 82 % yield) as a yellow solid. ¹H NMR (400 MHz, CDCl₃) δ = 9.86 (s, 1H), 8.24 (s, 1H), 7.72 (d, *J* = 2.0 Hz, 1H), 7.51 - 7.48 (m, 2H), 7.32 (dd, *J* = 2.0, 8.1 Hz, 1H), 7.19 (s, 1H), 6.74 (d, *J* = 8.1 Hz, 1H), 3.97 (s, 3H), 3.53 (s, 3H), 2.60 (s, 3H), 2.14 (s, 3H); LCMS (Formic): t_R = 0.63 min, [M+H⁺] = 365.5 (97 % purity).

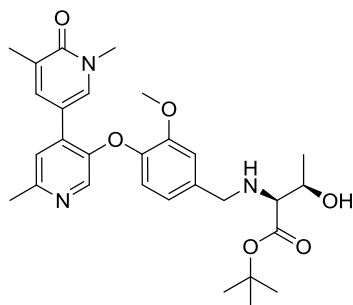
(S)-Tetrahydrofuran-3-yl (3-methoxy-4-((1,5,6'-trimethyl-6-oxo-1,6-dihydro-(3,4'-bipyridin)-3'-yl)oxy)benzyl)-L-threoninate, 2.65



2-Picoline borane (194 mg, 1.811 mmol) was added to a suspension of (*S*)-tetrahydrofuran-3-yl L-threoninate²²⁰ (**2.40**, 170 mg, 0.90 mmol) and 3-methoxy-4-((1,5,6'-trimethyl-6-oxo-1,6-dihydro-(3,4'-bipyridin)-3'-yl)oxy)benzaldehyde (**2.64**, 164 mg, 0.45 mmol) in isopropanol (2 mL), acetic acid (0.2 mL) and DCM (1 mL) and the reaction mixture stirred at rt for 2.5 h under nitrogen. The reaction mixture was quenched with the dropwise addition of water (0.5 mL), then partitioned between DCM

(3 mL) and water (3 mL). The aqueous layer was concentrated to ~1 mL under a stream of nitrogen and then purified directly by MDAP (HpH). The relevant fraction was concentrated *in vacuo* to afford the title compound (**2.65**, 25.9 mg, 0.05 mmol, 11 % yield) as a yellow gum. (α_D)^{22.4°C} _{λ} (c = 0.5, MeOH): -37.1°; ν_{\max} (solution in CDCl₃): 3349, 2925, 1730, 1654, 1593 cm⁻¹; ¹H NMR (400 MHz, DMSO-d₆) δ = 8.03 (d, *J* = 2.4 Hz, 1H), 7.86 (s, 1H), 7.74 (dd, *J* = 1.2, 2.4 Hz, 1H), 7.36 (s, 1H), 7.13 (d, *J* = 1.2 Hz, 1H), 6.88 - 6.82 (m, 2H), 5.26 - 5.20 (m, 1H), 4.71 (d, *J* = 5.6 Hz, 1H), 3.86 - 3.65 (m, 10H), 3.57 (d, *J* = 13.7 Hz, 1H), 3.48 (s, 3H), 3.02 (d, *J* = 4.9 Hz, 1H), 2.45 (s, 3H), 2.19 - 2.07 (m, 1H), 2.02 (app. s, 3H), 1.89 - 1.78 (m, 1H), 1.13 (d, *J* = 6.4 Hz, 3H); ¹³C NMR (101MHz, DMSO-d₆) δ 173.5, 162.0, 153.2, 150.5, 148.7, 143.2, 139.1, 138.1, 137.9, 137.5, 134.5, 127.5, 122.9, 120.7, 119.7, 113.2, 112.5, 75.2, 72.8, 67.9, 66.7, 66.4, 56.2, 51.5, 37.8, 32.8, 23.7, 20.6, 17.5; LCMS (Formic): *t*_R = 0.48 min, [M+H⁺] = 538.2 (100 % purity); HRMS: (C₂₉H₃₅N₃O₇) Requires [M+H⁺] = 538.2548, found [M+H]⁺ 538.2525.

***tert*-Butyl (3-methoxy-4-((1,5,6'-trimethyl-6-oxo-1,6-dihydro-(3,4'-bipyridin)-3'-yl)oxy)benzyl)-L-threoninate, 2.66**

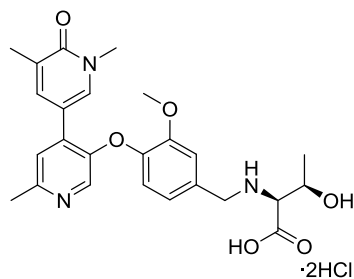


2-Picoline borane (97 mg, 0.91 mmol) was added to a suspension of 3-methoxy-4-((1,5,6'-trimethyl-6-oxo-1,6-dihydro-(3,4'-bipyridin)-3'-yl)oxy)benzaldehyde (**2.64**, 300 mg, 0.82 mmol) and *tert*-butyl L-threoninate hydrochloride²²¹ (**2.26**, 349 mg, 1.65 mmol) in isopropanol (2 mL), acetic acid (0.2 mL) and DCM (1 mL) and the reaction mixture stirred at rt for 2.5 h under nitrogen. The

reaction mixture was quenched with the dropwise addition of water (0.5 mL), then partitioned between DCM (3 mL) and water (3 mL). The organic layer was dried (hydrophobic frit) and concentrated under a stream of nitrogen. The residue was purified by MDAP (HpH). The relevant fraction was concentrated *in vacuo* to afford the title compound (**2.66**, 255 mg, 0.49 mmol, 59 % yield) as a yellow gum. (α_D)^{20.1°C} _{λ} (c = 1.0, CDCl₃): +84.6°; ν_{\max} (solution in CDCl₃): 3372, 1725, 1655, 1507, 1154 cm⁻¹; ¹H NMR (400 MHz, DMSO-d₆) δ = 8.03 (d, *J* = 2.5 Hz, 1H), 7.85 (s, 1H), 7.73 (dd, *J* = 1.2, 2.5 Hz, 1H), 7.36 (s, 1H), 7.13 (s, 1H), 6.87 - 6.82 (m, 2H), 3.82 - 3.74 (m, 6H), 3.56 (d, *J* = 14.7 Hz, 1H), 3.48 (s, 3H), 2.45 (s, 3H), 2.02 (d, *J* = 1.2 Hz, 3H), 1.40 (s, 9H), 1.11 (d, *J* = 6.1 Hz, 3H), NH and OH not observed; ¹³C NMR (101 MHz, CDCl₃) δ = 172.7, 162.7, 153.7, 150.2, 148.1, 144.2, 140.3, 137.0, 136.7, 136.2, 129.2, 122.3, 120.8, 118.8, 113.1, 112.7, 82.0, 68.1, 67.9, 55.9, 52.2, 41.0, 38.2, 28.1 (3C), 23.7, 19.4, 17.3; LCMS (Formic): *t*_R = 0.53 min, [M+H⁺] = 524.4

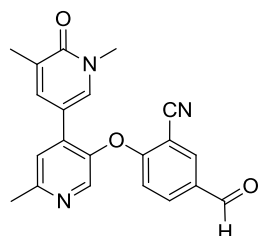
(100 % purity); HRMS: (C₂₉H₃₇N₃O₆) Requires [M+H⁺] = 524.2761, found [M+H⁺] = 524.2760.

3-Methoxy-4-((1,5,6'-trimethyl-6-oxo-1,6-dihydro-(3,4'-bipyridin)-3'-yl)oxy)benzyl)-L-threonine dihydrochloride, 2.67



A solution of *tert*-butyl (3-methoxy-4-((1,5,6'-trimethyl-6-oxo-1,6-dihydro-(3,4'-bipyridin)-3'-yl)oxy)benzyl)-L-threoninate (**2.66**, 11 mg, 0.02 mmol) in 2M aqueous hydrochloric acid (1.0 mL, 2.00 mmol) was heated at 60°C for 2 h. The reaction mixture concentrated *in vacuo* to afford the title compound (**2.67**, 11 mg, 0.02 mmol, 97 % yield) as a yellow gum. ¹H NMR (400 MHz, DMSO-d₆) δ = 9.32 (br s, 2H, 2HCl salt), 8.23 (d, *J* = 1.6 Hz, 1H), 7.99 (s, 1H), 7.81 (dd, *J* = 1.0, 2.5 Hz, 1H), 7.79 (br s, 1H), 7.47 (d, *J* = 1.0 Hz, 1H), 7.09 (d, *J* = 8.3 Hz, 1H), 7.06 (dd, *J* = 1.6, 8.3 Hz, 1H), 4.24 (d, *J* = 12.7 Hz, 1H), 4.17 (d, *J* = 12.7 Hz, 1H), 4.10 (dq, *J* = 5.4, 6.4 Hz, 1H), 3.82 (s, 3H), 3.53 (d, *J* = 5.4 Hz, 1H), 3.50 (s, 3H), 2.60 (s, 3H), 2.04 (app. s, 3H), 1.19 (d, *J* = 6.4 Hz, 3H); LCMS (Formic): t_R = 0.42 min, [M+H⁺] = 468.3 (96 % purity).

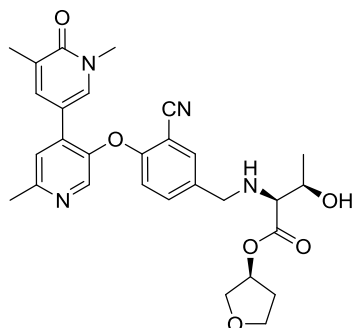
5-Formyl-2-((1,5,6'-trimethyl-6-oxo-1,6-dihydro-(3,4'-bipyridin)-3'-yl)oxy)benzonitrile, 2.68



A suspension of 2-fluoro-5-formylbenzonitrile (**2.63**, 0.78 g, 5.21 mmol), potassium carbonate (1.2 g, 8.69 mmol) and 5'-hydroxy-1,2,5-trimethyl-(3,4'-bipyridin)-6(1*H*)-one²²³ (**2.62**, 1 g, 4.34 mmol) in DMF (15 mL) was heated at 80°C for 16 h. The reaction mixture was partitioned between ethyl acetate (50 mL) and water (50 mL). The aqueous phase was re-extracted with ethyl acetate (50 mL). The combined organic layers dried (hydrophobic frit) and concentrated *in vacuo*. The residue was purified by flash column chromatography (silica, 0-100% ethyl acetate/cyclohexane gradient followed by 0-30% ethanol (+1% NEt₃) in ethyl acetate) to give afford the title compound (**2.68**, 1.25 g, 3.48 mmol, 80 % yield) as a light brown solid. ν_{max} (solution in CDCl₃): 3364, 2720, 1657, 1017 cm⁻¹; ¹H NMR (400 MHz, CDCl₃) δ 9.87 (s, 1H), 8.40 (s, 1H), 8.13 (d, *J* = 2.0 Hz, 1H), 7.89 (d, *J* = 2.0, 8.8 Hz, 1H), 7.72 (d, *J* = 2.5 Hz, 1H), 7.44 (d, *J* = 1.5, 2.5 Hz, 1H), 7.25 (s, 1H), 6.72 (d, *J* = 8.8 Hz, 1H), 3.57 (s, 3H), 2.63 (s, 3H), 2.13 (app. s, 3H); ¹³C NMR (101 MHz, CDCl₃) δ = 188.2, 163.0, 162.5, 157.8, 144.2, 143.6, 137.7, 136.7, 136.0, 136.0, 135.1, 131.4, 130.5, 123.2, 114.6, 114.5, 111.4, 103.3, 38.2, 24.1, 17.2; LCMS (Formic): t_R = 0.75

min, $[M+H^+] = 360.2$ (96 % purity); HRMS: ($C_{21}H_{17}N_3O_3$) Requires $[M+H^+] = 360.1349$, found $[M+H^+] = 360.1348$.

(S)-Tetrahydrofuran-3-yl (3-cyano-4-((1,5,6'-trimethyl-6-oxo-1,6-dihydro-(3,4'-bipyridin)-3'-yl)oxy)benzyl)-L-threoninate, 2.69



Method 1, Scheme 2.9:

A solution of 5-formyl-2-((1,5,6'-trimethyl-6-oxo-1,6-dihydro-(3,4'-bipyridin)-3'-yl)oxy)benzonnitrile (**2.68**, 2.83 g, 7.88 mmol) in isopropanol (19 mL) and DCM (19 mL) was stirred for 10 min at rt. (*S*)-tetrahydrofuran-3-yl L-threoninate hydrochloride²²⁰ (**2.40**, 2.98g, 15.8 mmol) and acetic acid (3 mL) were added and the reaction mixture stirred for 1 h. 2-Picoline borane (0.93 g, 8.66 mmol) was added and the mixture stirred for 1 h at rt. The reaction mixture was quenched with water (10 mL) and concentrated *in vacuo*. The residue was purified by MDAP (HpH). The relevant fractions were combined and concentrated *in vacuo* to afford the title compound (**2.69**, 1.40 g, 2.49 mmol, 32 % yield) as a white solid.

Method 2, Table 2.19

A solution of 5-formyl-2-((1,5,6'-trimethyl-6-oxo-1,6-dihydro-(3,4'-bipyridin)-3'-yl)oxy)benzonnitrile (**2.68**, 100 mg, 0.24 mmol, 85% wt) and (*S*)-tetrahydrofuran-3-yl L-threoninate hydrochloride (**2.40**, 63.1 mg, 0.26 mmol) in isopropanol (1.0 mL) and DCM (0.5 mL) was stirred at rt overnight. The reaction vessel was placed under a nitrogen atmosphere, acetic acid (0.1 mL) and 2-picoline borane (27.8 mg, 0.26 mmol) added and the reaction mixture stirred at rt for 1 hour. The reaction mixture was quenched with water (0.5 mL) and concentrated *in vacuo*. The residue was purified by flash column chromatography (silica, 0-100% ethyl acetate in cyclohexane followed by 0-30% ethanol (+1% NEt_3) in ethyl acetate). The relevant fractions were combined and concentrated *in vacuo* to afford the title compound (**2.69**, 56 mg, 0.10 mmol, 90 wt%, 40 % yield) as a yellow oil.

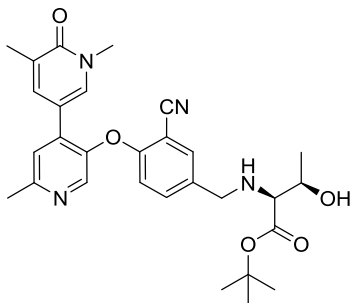
Method 3, Scheme 2.15

5-Formyl-2-((1,5,6'-trimethyl-6-oxo-1,6-dihydro-(3,4'-bipyridin)-3'-yl)oxy)benzonnitrile (**2.68**, 100 mg, 0.28 mmol) and (*S*)-tetrahydrofuran-3-yl L-threoninate hydrochloride (**2.40**, 101 mg, 0.42 mmol) were dissolved THF (1 mL) and DIPEA (0.1 mL, 0.56 mmol) and acetic acid (40 μ L, 0.70 mmol) added. The reaction vessel was placed under a nitrogen

atmosphere and stirred at 40°C for 2 h. The reaction mixture was cooled to rt, sodium triacetoxyborohydride (118 mg, 0.56 mmol) added and the resultant suspension stirred for 1 h. The reaction mixture was quenched with water (1 mL) and purified directly by MDAP (HpH). The relevant fractions were combined and concentrated *in vacuo* to afford the title compound (**2.69**, 125 mg, 0.26 mmol, 84 % yield).

(α_D)^{22.4°C} _{λ} (c = 0.5, MeOH): -28.4°; ν_{\max} (solution in CDCl₃): 3400, 1728, 1652, 1593 cm⁻¹; ¹H NMR (400 MHz, DMSO-d₆) δ = 8.35 (s, 1H), 7.96 (d, *J* = 2.5 Hz, 1H), 7.76 (d, *J* = 2.0 Hz, 1H), 7.62 (dd, *J* = 1.0, 2.5 Hz, 1H), 7.49 (s, 1H), 7.49 (dd, *J* = 2.0, 8.8 Hz, 1H), 6.69 (d, *J* = 8.8 Hz, 1H), 5.19 - 5.14 (m, 1H), 4.68 (d, *J* = 5.4 Hz, 1H), 3.81 (dq, *J* = 5.4, 6.4 Hz, 1H), 3.77 - 3.66 (m, 4H), 3.63 (d, *J* = 13.0 Hz, 1H), 3.54 (d, *J* = 13.0 Hz, 1H), 3.45 (s, 3H), 2.54 (s, 3H), 2.15 - 2.04 (m, 1H), 1.99 (app. s, 3H), 1.86 - 1.78 (m, 1H), 1.08 (d, *J* = 6.4 Hz, 3H), NH and OH not observed; ¹³C NMR (101 MHz, CDCl₃) δ = 173.1, 162.6, 158.2, 156.7, 145.1, 143.3, 137.3, 136.8, 136.3, 134.7, 134.2, 133.4, 130.1, 115.8, 114.7, 111.9, 102.6, 100.0, 75.9, 73.0, 68.2, 67.0, 66.9, 51.1, 38.2, 32.8, 24.0, 19.5, 17.2; LCMS (HpH): *t*_R = 0.83 min, [M+H⁺] = 533.6 (100% purity); HRMS (C₂₉H₃₂N₄O₆) Requires [M+H⁺] = 534.2474, found [M+H⁺] 533.2382.

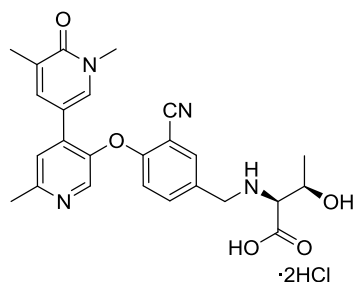
***tert*-Butyl (3-cyano-4-((1,5,6'-trimethyl-6-oxo-1,6-dihydro-(3,4'-bipyridin)-3'-yl)oxy)benzyl)-L-threoninate, 2.70**



A suspension of 5-formyl-2-((1,5,6'-trimethyl-6-oxo-1,6-dihydro-(3,4'-bipyridin)-3'-yl)oxy)benzonitrile (**2.68**, 175 mg, 0.49 mmol) and *tert*-butyl L-threoninate hydrochloride²²¹ (**2.26**, 206 mg, 0.97 mmol) in isopropanol (2 mL), acetic acid (0.2 mL) and DCM (1 mL) was stirred at rt for 2.5 h. The reaction mixture was quenched with the dropwise addition of water (0.5 mL). The reaction mixture was

partitioned between DCM (3 mL) and water (3 mL). The aqueous layer was concentrated to ~1 mL under a stream of nitrogen and then purified by MDAP (HpH) to afford the title compound (**2.70**, 16.4 mg, 0.03 mmol, 6 % yield) as a yellow gum. ¹H NMR (400 MHz, DMSO-d₆) δ = 8.34 (s, 1H), 7.96 (d, *J* = 2.5 Hz, 1H), 7.77 (d, *J* = 2.0 Hz, 1H), 7.62 (dd, *J* = 1.5, 2.5 Hz, 1H), 7.49 (s, 1H), 7.48 (dd, *J* = 2.0, 8.8 Hz, 1H), 6.68 (d, *J* = 8.8 Hz, 1H), 4.57 (d, *J* = 4.9 Hz, 1H), 3.73 (d, *J* = 14.2 Hz, 1H), 3.73 - 3.69 (m, 1H), 3.54 (d, *J* = 14.2 Hz, 1H), 3.45 (s, 3H), 2.53 (s, 3H), 1.99 (app. s, 3H), 1.35 (s, 9H), 1.06 (d, *J* = 6.4 Hz, 3H), NH and OH not observed; LCMS (HpH): *t*_R = 0.64 min, [M+H⁺] = 519.4 (100 % purity).

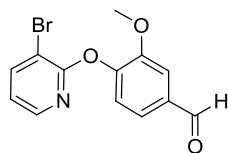
(3-Cyano-4-((1,5,6'-trimethyl-6-oxo-1,6-dihydro-(3,4'-bipyridin)-3'-yl)oxy)benzyl)-L-threonine dihydrochloride, 2.71



A solution of *tert*-butyl (3-cyano-4-((1,5,6'-trimethyl-6-oxo-1,6-dihydro-(3,4'-bipyridin)-3'-yl)oxy)benzyl)-L-threoninate **2.70** (1.5 g, 2.89 mmol) in 2M aqueous HCl (14.5 mL, 28.9 mmol) was heated at 60°C for 2 h. The reaction mixture was concentrated *in vacuo* to afford the title compound (**2.71**, 1.48 g, 2.76 mmol, 96 % yield) as a yellow gum. (α_D)^{20.9°C} λ (c = 1.0, CDCl₃): +364.4°; ν_{\max} (neat): 3252, 2561, 2232,

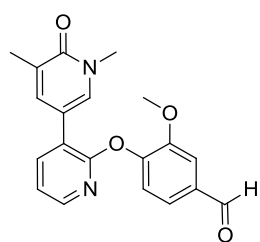
1602 cm⁻¹; ¹H NMR (400 MHz, DMSO-d₆) δ = 8.34 (s, 1H), 7.97 (d, *J* = 2.5 Hz, 1H), 7.78 (d, *J* = 2.0 Hz, 1H), 7.63 (dd, *J* = 1.2, 2.5 Hz, 1H), 7.50 (s, 1H), 7.49 (dd, *J* = 2.0, 8.6 Hz, 1H), 6.69 (d, *J* = 8.6 Hz, 1H), 4.58 (d, *J* = 5.1 Hz, 1H), 3.77 - 3.69 (m, 2H), 3.55 (d, *J* = 14.5 Hz, 1H), 3.46 (s, 3H), 2.82 - 2.75 (m, 1H), 2.54 (s, 3H), 2.37 (br d, *J* = 5.1 Hz, 1H), 2.00 (app. s, 3H), 1.07 (d, *J* = 6.4 Hz, 3H), NH not observed; ¹³C NMR (151 MHz, DMSO-d₆) δ = 169.0, 162.0, 158.6, 146.3, 140.1, 138.4, 138.3, 137.1, 136.3, 128.2, 127.9, 126.0, 116.1, 116.1, 115.9, 110.1, 101.9, 65.6, 64.8, 48.7, 40.6, 39.5, 38.1, 20.7, 17.3; LCMS (HpH): *t*_R = 0.62 min, [M+H⁺] = 463.3 (98 % purity); HRMS: (C₂₅H₂₆N₄O₅) Requires [M+H⁺] = 463.1982, found [M+H⁺] = 463.1976.

4-((3-Bromopyridin-2-yl)oxy)-3-methoxybenzaldehyde, 2.74



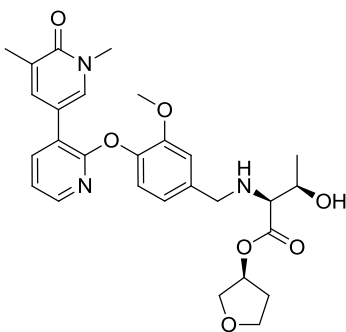
A mixture of 3-bromo-2-chloropyridine (**2.72**, 1 g, 5.20 mmol), 4-hydroxy-3-methoxybenzaldehyde (0.95 g, 6.24 mmol), and cesium carbonate (1.69 g, 5.20 mmol) in DMF (5 mL) was stirred at 140°C for 19 h. The reaction mixture was concentrated *in vacuo*. The residue was partitioned between ethyl acetate (50 mL) and water (50 mL). The organic phase was dried (hydrophobic frit) and concentrated *in vacuo*. The residue was purified by flash column chromatography (silica, 20-75% ethyl acetate in cyclohexane) to afford the title compound (**2.74**, 755 mg, 2.45 mmol, 47 % yield) as a colourless oil. ¹H NMR (400 MHz, CDCl₃) δ = 9.96 (s, 1H), 8.00 (dd, *J* = 1.7, 4.8 Hz, 1H), 7.93 (dd, *J* = 1.7, 7.7 Hz, 1H), 7.53 (d, *J* = 1.7 Hz, 1H), 7.53 (dd, *J* = 1.7, 6.8 Hz, 1H), 7.32 (d, *J* = 6.8 Hz, 1H), 6.90 (dd, *J* = 4.8, 7.7 Hz, 1H), 3.81 (s, 3H); LCMS (Formic): *t*_R = 1.09 min, [M+H⁺] = 308.0 / 310.0 (92 % purity).

4-((1',5'-Dimethyl-6'-oxo-1',6'-dihydro-(3,3'-bipyridin)-2-yl)oxy)-3-methoxybenzaldehyde, 2.75



A mixture of 4-((3-bromopyridin-2-yl)oxy)-3-methoxybenzaldehyde (**2.74**, 512 mg, 1.66 mmol), 1,3-dimethyl-5-(4,4,5,5-tetramethyl-1,3,2-dioxaborolan-2-yl)pyridin-2(1*H*)-one²²³ (**2.17**, 455 mg, 1.83 mmol), potassium carbonate (919 mg, 6.65 mmol) and bis(triphenylphosphine)palladium(II) chloride (117 mg, 0.17 mmol) in ethanol (2.5 mL) and toluene (2.5 mL) was heated in a microwave reactor at 100°C for 1 h. The reaction mixture was diluted with ethyl acetate (25 mL) and filtered over celite. The filtrate was concentrated *in vacuo* and the resultant residue purified by flash column chromatography (silica, 50-100% ethyl acetate in cyclohexane) to afford the title compound (**2.75**, 270 mg, 0.77 mmol, 46 % yield) as a yellow solid. ¹H NMR (400 MHz, CDCl₃) δ = 9.97 (s, 1H), 8.02 (dd, *J* = 2.0, 4.9 Hz, 1H), 7.68 (dd, *J* = 2.0, 7.3 Hz, 1H), 7.67 (d, *J* = 2.6 Hz, 1H), 7.60 (dd, *J* = 1.1, 2.6 Hz, 1H), 7.55 (d, *J* = 1.7 Hz, 1H), 7.53 (dd, *J* = 1.7, 7.8 Hz, 1H), 7.32 (d, *J* = 7.8 Hz, 1H), 7.07 (dd, *J* = 4.9, 7.3 Hz, 1H), 3.84 (s, 3H), 3.62 (s, 3H), 2.22 (app. s, 3H); LCMS (Formic): *t*_R = 0.87 min, [M+H⁺] = 351.2 (96 % purity).

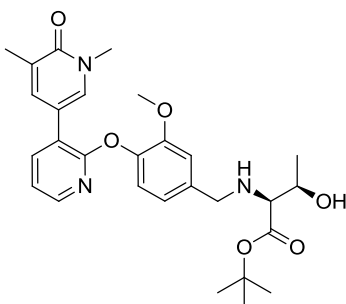
(S)-Tetrahydrofuran-3-yl 4-((1',5'-dimethyl-6'-oxo-1',6'-dihydro-(3,3'-bipyridin)-2-yl)oxy)-3-methoxybenzyl)-L-threoninate, 2.76



(*S*)-Tetrahydrofuran-3-yl L-threoninate²²⁰ (**2.40**, 108 mg, 0.57 mmol) and 4-((1',5'-dimethyl-6'-oxo-1',6'-dihydro-(3,3'-bipyridin)-2-yl)oxy)-3-methoxybenzaldehyde (**2.75**, 100 mg, 0.29 mmol) were suspended in isopropanol (1 mL) and acetic acid (0.1 mL). A couple of drops of triethylamine were added followed by 2-picoline borane (33.6 mg, 0.31 mmol) and the reaction mixture stirred at rt for 2.5 h. The reaction mixture was quenched with the dropwise addition of water (0.5 mL) and purified by MDAP (HpH). The relevant fraction was concentrated *in vacuo* to afford the title compound (**2.76**, 14.8 mg, 0.03 mmol, 10 % yield) as a colourless gum. (α_D)^{22.3°C} λ (c = 0.5, MeOH): -32.9°; ν_{max} (solution in CDCl₃): 3378, 1731, 1655, 1602, 1436 cm⁻¹; ¹H NMR (400 MHz, CDCl₃) δ = 8.01 (dd, *J* = 2.0, 4.9 Hz, 1H), 7.70 (d, *J* = 2.4 Hz, 1H), 7.65 - 7.62 (m, 2H), 7.09 (d, *J* = 7.9 Hz, 1H), 7.03 - 6.99 (m, 2H), 6.93 (dd, *J* = 2.0, 7.9 Hz, 1H), 5.37 - 5.31 (m, 1H), 3.95 - 3.78 (m, 6H), 3.76 (s, 3H), 3.75 - 3.71 (m, 2H), 3.61 (s, 3H), 3.09 (d, *J* = 7.1 Hz, 1H), 2.21 (s, 3H), 2.20 - 2.15 (m, 1H), 2.06 - 1.95 (m, 1H), 1.24 (d, *J* = 6.1 Hz, 3H), NH not observed; ¹³C NMR (101MHz, CDCl₃) δ 173.6, 162.0, 160.2, 151.7, 145.8, 141.20, 138.9, 138.77, 138.2,

137.2, 127.4, 123.5, 120.4, 119.3, 113.3, 112.9, 75.2, 72.8, 68.0, 66.7, 66.5, 60.2, 56.1, 51.6, 37.8, 32.8, 20.6, 17.6; LCMS (Formic): $t_R = 0.57$ min, $[M+H^+] = 524.3$ (100% purity); HRMS ($C_{28}H_{33}N_3O_7$) Requires $[M+H^+] = 524.247$, found $[M+H^+] = 524.3280$.

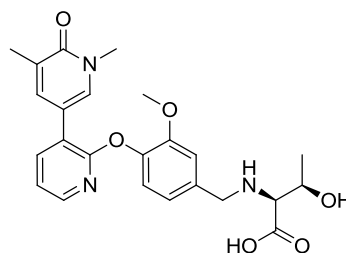
***tert*-Butyl 4-((1',5'-dimethyl-6'-oxo-1',6'-dihydro-(3,3'-bipyridin)-2-yl)oxy)-3-methoxybenzyl)-L-threoninate, 2.77**



4-((1',5'-Dimethyl-6'-oxo-1',6'-dihydro-(3,3'-bipyridin)-2-yl)oxy)-3-methoxybenzaldehyde (**2.75**, 100 mg, 0.29 mmol) and *tert*-butyl L-threoninate hydrochloride²²¹ (**2.26**, 121 mg, 0.57 mmol) were suspended in isopropanol (2 mL) and acetic acid (0.2 mL). A couple of drops of triethylamine and 2-picoline borane (33.6 mg, 0.31 mmol) were added and the reaction mixture stirred at rt for 2.5 h under nitrogen. The

reaction mixture was purified by MDAP (HpH). The relevant fraction was concentrated *in vacuo* to afford the title compound (**2.77**, 91.8 mg, 0.18 mmol, 63 % yield) as a white solid. M.pt: 124.5 – 127.9°C; $(\alpha_D)^{20.9^\circ C} \lambda(c = 1.0, CDCl_3)$: -18.7°; ν_{max} (solution in $CDCl_3$): 3402, 2976, 2350, 1656 cm^{-1} ; 1H NMR (400 MHz, $DMSO-d_6$) $\delta = 7.95$ (dd, $J = 1.8, 4.9$ Hz, 1H), 7.93 (d, $J = 2.5$ Hz, 1H), 7.82 (dd, $J = 1.8, 7.4$ Hz, 1H), 7.76 (dd, $J = 1.2, 2.5$ Hz, 1H), 7.12 (dd, $J = 4.9, 7.4$ Hz, 1H), 7.11 (d, $J = 2.0$ Hz, 1H), 7.08 (d, $J = 8.1$ Hz, 1H), 6.90 (dd, $J = 2.0, 8.1$ Hz, 1H), 4.61 (d, $J = 5.4$ Hz, 1H), 3.84 (dd, $J = 5.4, 13.7$ Hz, 1H), 3.80 - 3.77 (m, 1H), 3.69 (s, 3H), 3.58 (dd, $J = 5.4, 13.7$ Hz, 1H), 3.51 (s, 3H), 2.91 (dd, $J = 5.4, 9.7$ Hz, 1H), 2.32 - 2.27 (m, 1H), 2.05 (app. s, 3H), 1.43 (s, 9H), 1.13 (d, $J = 6.4$ Hz, 3H); ^{13}C NMR (101 MHz, $CDCl_3$) $\delta = 172.9, 162.7, 160.2, 151.5, 145.9, 141.6, 137.9, 137.8, 137.4, 135.9, 129.0, 123.2, 120.7, 120.5, 118.6, 114.4, 112.6, 82.0, 68.1, 68.1, 55.9, 52.4, 38.2, 28.1$ (3C), 19.4, 17.4; LCMS (Formic): $t_R = 0.85$ min, $[M+H^+] = 524.3$ (92 % purity); HRMS: ($C_{28}H_{35}N_3O_6$) Requires $[M+H^+] = 510.2605$, found $[M+H^+] = 510.2604$.

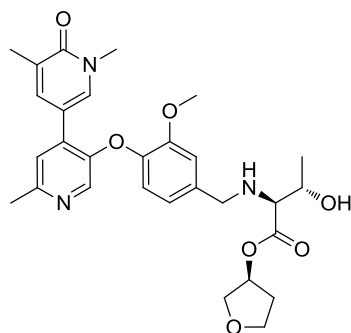
4-((1',5'-Dimethyl-6'-oxo-1',6'-dihydro-(3,3'-bipyridin)-2-yl)oxy)-3-methoxybenzyl)-L-threonine, 2.78



A solution of *tert*-butyl 4-((1',5'-dimethyl-6'-oxo-1',6'-dihydro-(3,3'-bipyridin)-2-yl)oxy)-3-methoxybenzyl)-L-threoninate (**2.77**, 15 mg, 0.029 mmol) in 2M aqueous hydrochloric acid (1 mL, 2.10 mmol) was heated at 60°C for 2 h. The reaction mixture was concentrated *in vacuo*. Separately, 4-((1',5'-dimethyl-6'-oxo-1',6'-dihydro-(3,3'-

bipyridin)-2-yl)oxy)-3-methoxybenzaldehyde (70 mg, 0.20 mmol) and 2-hydroxyethyl L-threoninate hydrochloride (80 mg, 0.40 mmol) were suspended in isopropanol (1 mL) and acetic acid (0.1 mL) under a nitrogen atmosphere. A couple of drops of triethylamine were added, followed by 2-picoline borane (23.5 mg, 0.22 mmol) and the reaction mixture stirred at rt for 2.5 h. The reaction mixture was purified directly by MDAP (HpH) to obtain (4-((1',5'-dimethyl-6'-oxo-1',6'-dihydro-(3,3'-bipyridin)-2-yl)oxy)-3-methoxybenzyl)-L-threonine (12 mg, 0.03 mmol, 13 % yield) as a colourless gum. This material was combined with the product obtained above and purified by MDAP (HpH) to afford the title compound (**2.78**, 5.2 mg, 0.01 mmol, 39 % yield) as a white solid. ¹H NMR (400 MHz, DMSO-d₆) δ = 7.96 (dd, *J* = 1.8, 4.9 Hz, 1H), 7.93 (d, *J* = 2.4 Hz, 1H), 7.83 (dd, *J* = 1.8, 7.5 Hz, 1H), 7.75 (dd, *J* = 1.0, 2.4 Hz, 1H), 7.22 (d, *J* = 1.5 Hz, 1H), 7.15 - 7.11 (m, 2H), 6.98 (br dd, *J* = 1.5, 8.3 Hz, 1H), 4.01 (br d, *J* = 13.4 Hz, 1H), 3.93 - 3.86 (m, 1H), 3.81 (br d, *J* = 13.4 Hz, 1H), 3.70 (s, 3H), 3.51 (s, 3H), 3.00 (d, *J* = 5.1 Hz, 1H), 2.06 (app. s, 3H), 1.16 (d, *J* = 6.4 Hz, 3H), exchangeable protons not observed; LCMS (HpH): *t*_R = 0.56 min, [M+H⁺] = 454.4 (96 % purity).

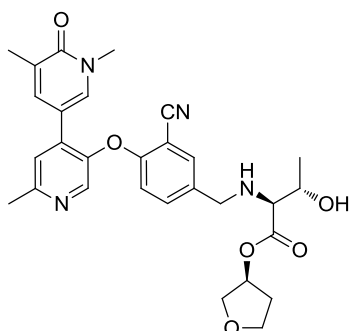
(S)-Tetrahydrofuran-3-yl (3-methoxy-4-((1,5,6'-trimethyl-6-oxo-1,6-dihydro-(3,4'-bipyridin)-3'-yl)oxy)benzyl)-L-allothreoninate, 2.80



A solution of 3-methoxy-4-((1,5,6'-trimethyl-6-oxo-1,6-dihydro-(3,4'-bipyridin)-3'-yl)oxy)benzaldehyde (**2.64**, 170 mg, 0.47 mmol) and (*S*)-tetrahydrofuran-3-yl L-allothreoninate hydrochloride²²⁵ (**2.79**, 211 mg, 0.93 mmol) in isopropanol (2 mL), acetic acid (0.2 mL) and DCM (2 mL) and the mixture was stirred for 1 h at rt. 2-Picoline borane (54.9 mg, 0.51 mmol) was added and the reaction mixture was stirred for 2 h at rt under nitrogen. The reaction mixture was partitioned between water (5 mL) and DCM (5 mL). The aqueous layer re-extracted with ethyl acetate (15 mL) and the organic phase washed with brine (5 mL). The combined organic layers were dried (hydrophobic frit) and concentrated *in vacuo*. The aqueous layer was concentrated *in vacuo* and the resultant residue purified by MDAP (HpH). The relevant fractions were combined to afford the title compound (**2.80**, 32.1 mg, 0.06 mmol, 12 % yield) as a white solid. (α_D)^{22.1°C} λ (*c* = 1.0, MeOH): -19.9°; ν_{\max} (solution in CDCl₃): 3338 1729, 1654, 1592 cm⁻¹; ¹H NMR (400 MHz, CDCl₃) δ = 8.08 (s, 1H), 7.77 (d, *J* = 2.4 Hz, 1H), 7.55 (dd, *J* = 1.2, 2.4 Hz, 1H), 7.13 (s, 1H), 6.98 (d, *J* = 1.7 Hz, 1H), 6.78 (dd, *J* = 1.7, 8.3 Hz, 1H), 6.72 (d, *J* = 8.3 Hz, 1H), 5.41 - 5.35 (m, 1H), 4.05 - 3.98 (m, 1H), 3.96 - 3.86 (m, 3H), 3.86 (s, 3H), 3.85 - 3.79

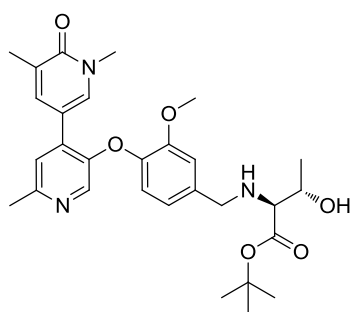
(m, 2H), 3.61 (d, $J = 13.0$ Hz, 1H), 3.56 (s, 3H), 3.29 (d, $J = 4.9$ Hz, 1H), 2.56 (s, 3H), 2.27 - 2.19 (m, 1H), 2.17 (app. s, 3H), 2.06 - 1.99 (m, 2H), 1.15 (d, $J = 6.4$ Hz, 3H), NH not observed; ^{13}C NMR (101MHz, CDCl_3) δ 173.0, 162.7, 153.8, 150.2, 148.1, 144.2, 140.5, 137.3, 136.16, 135.1, 129.2, 122.3, 120.8, 118.6, 113.3, 112.6, 75.6, 73.1, 67.7, 67.0, 65.6, 55.9, 52.3, 38.2, 32.8, 28.1, 23.7, 19.1, 17.3; LCMS (HpH): $t_{\text{R}} = 0.82$ min, $[\text{M}+\text{H}^+] = 538.6$ (95 % purity); HRMS ($\text{C}_{29}\text{H}_{35}\text{N}_3\text{O}_7$) Requires $[\text{M}+\text{H}^+] = 538.2553$, found $[\text{M}+\text{H}^+] = 538.2551$.

(S)-Tetrahydrofuran-3-yl (3-cyano-4-((1,5,6'-trimethyl-6-oxo-1,6-dihydro-(3,4'-bipyridin)-3'-yl)oxy)benzyl)-L-allothreoninate, 2.81



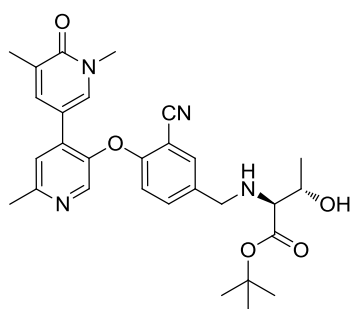
5-Formyl-2-((1,5,6'-trimethyl-6-oxo-1,6-dihydro-(3,4'-bipyridin)-3'-yl)oxy)benzonitrile (**2.68**, 150 mg, 0.42 mmol) was dissolved in isopropanol (1.2 mL) and DCM (0.8 mL) and stirred for 10 min. (S)-tetrahydrofuran-3-yl L-allothreoninate²²⁵ (**2.79**, 158 mg, 0.84 mmol) and acetic acid (0.2 mL) was added and the reaction mixture was stirred for 1 h. The reaction mixture was placed under a nitrogen atmosphere, then 2-picoline borane (49.1 mg, 0.46 mmol) was added and the reaction mixture stirred for 1 h. The mixture was quenched with water (2 mL) and concentrated *in vacuo*. The residue was purified by MDAP (HpH). The relevant fractions were combined and concentrated *in vacuo* to afford the title compound (**2.81**, 114.5 mg, 0.20 mmol, 49 % yield) as a white solid. ^1H NMR (400 MHz, CDCl_3) δ = 8.35 (s, 1H), 7.75 (d, $J = 2.5$ Hz, 1H), 7.59 (d, $J = 2.5$ Hz, 1H), 7.45 (dd, $J = 1.5, 2.5$ Hz, 1H), 7.34 (dd, $J = 2.5, 8.8$ Hz, 1H), 7.21 (s, 1H), 6.57 (d, $J = 8.8$ Hz, 1H), 5.39 - 5.35 (m, 1H), 3.99 (dq, $J = 4.9, 6.4$ Hz, 1H), 3.80 (d, $J = 13.2$ Hz, 1H), 3.95 - 3.77 (m, 4H), 3.60 (s, 3H), 3.56 (d, $J = 13.2$ Hz, 1H), 3.22 (d, $J = 4.9$ Hz, 1H), 2.62 (s, 3H), 2.29 - 2.18 (m, 1H), 2.16 (app. s, 3H), 2.07 - 1.98 (m, 1H), 1.13 (d, $J = 6.4$ Hz, 3H), NH and OH not observed; LCMS (HpH): $t_{\text{R}} = 0.82$ min, $[\text{M}+\text{H}^+] = 533.7$ (100 % purity).

***tert*-Butyl (3-methoxy-4-((1,5,6'-trimethyl-6-oxo-1,6-dihydro-(3,4'-bipyridin)-3'-yl)oxy)benzyl)-L-allothreoninate, 2.83**



2-Picoline borane (54.8 mg, 0.51 mmol) was added to a solution of 3-methoxy-4-((1,5,6'-trimethyl-6-oxo-1,6-dihydro-(3,4'-bipyridin)-3'-yl)oxy)benzaldehyde (**2.64**, 170 mg, 0.47 mmol) and *tert*-butyl L-allothreoninate hydrochloride²²⁶ (**2.82**, 198 mg, 0.93 mmol) in isopropanol (2 mL), acetic acid (0.2 mL) and DCM (2 mL) and the mixture was stirred for 1 h. The reaction mixture was partitioned between water (5 mL) and DCM (5 mL). The aqueous layer was diluted with brine (5 mL) and washed with ethyl acetate (15 mL). The combined organic layers were dried (hydrophobic frit) and concentrated *in vacuo*. The aqueous layer was concentrated *in vacuo* and the resultant residue purified by MDAP (HpH). The relevant fractions were combined to afford the title compound (**2.83**, 123.6 mg, 0.22 mmol, 48 % yield) as a transparent oil. ¹H NMR (400 MHz, CDCl₃) δ = 8.06 (s, 1H), 7.80 (d, *J* = 2.4 Hz, 1H), 7.57 (dd, *J* = 1.0, 2.4 Hz, 1H), 7.14 (s, 1H), 7.00 (d, *J* = 1.7 Hz, 1H), 6.81 (dd, *J* = 1.7, 8.1 Hz, 1H), 6.74 (d, *J* = 8.1 Hz, 1H), 3.99 (s, 1H), 3.86 (d, *J* = 13.0 Hz, 1H), 3.85 (s, 3H), 3.61 (d, *J* = 13.0 Hz, 1H), 3.56 (s, 3H), 3.22 (d, *J* = 4.9 Hz, 1H), 2.55 (s, 3H), 2.17 (app. s, 3H), 1.49 (s, 9H), 1.12 (d, *J* = 6.4 Hz, 3H), NH and OH not observed; LCMS (HpH): *t*_R = 1.00 min, [M+H⁺] = 524.7 (97 % purity).

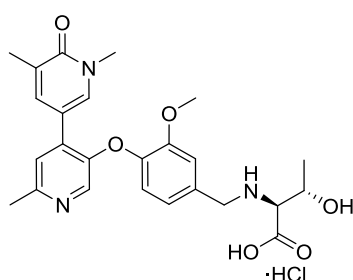
***tert*-Butyl (3-cyano-4-((1,5,6'-trimethyl-6-oxo-1,6-dihydro-(3,4'-bipyridin)-3'-yl)oxy)benzyl)-L-allothreoninate, 2.84**



5-Formyl-2-((1,5,6'-trimethyl-6-oxo-1,6-dihydro-(3,4'-bipyridin)-3'-yl)oxy)benzonitrile (**2.68**, 150 mg, 0.42 mmol) was dissolved in isopropanol (1.2 mL) and DCM (0.8 mL) and stirred for 10 min. *tert*-Butyl L-allothreoninate hydrochloride²²⁶ (**2.82**, 177 mg, 0.84 mmol) and acetic acid (0.2 mL) were added and the reaction mixture was stirred for 1 h. 2-Picoline borane (49.1 mg, 0.46 mmol) was added and the reaction mixture stirred for 1 h. The mixture was quenched with water (2 mL) and concentrated *in vacuo*. The residue was purified by MDAP (HpH) The relevant fractions were combined and concentrated *in vacuo* to afford the title compound (**2.84**, 105 mg, 0.19 mmol, 46 % yield) as a white solid. (α_D)^{20,26} λ (c = 4.0, CDCl₃): -9.9°; ν_{max} (solution in CDCl₃): 3501, 2981, 1655 cm⁻¹; ¹H NMR (400 MHz, CDCl₃) δ 8.35 (s, 1H), 7.78 (d, *J* = 2.5

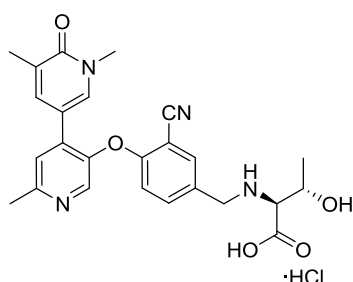
Hz, 1H), 7.60 (d, $J = 2.0$ Hz, 1H), 7.46 (dd, $J = 1.5, 2.4$ Hz, 1H), 7.37 (dd, $J = 2.0, 8.8$ Hz, 1H), 7.22 (s, 1H), 6.59 (d, $J = 8.8$ Hz, 1H), 3.99 (m, 1H), 3.84 (d, $J = 13.2$ Hz, 1H), 3.61 (s, 3H), 3.57 (d, $J = 13.2$ Hz, 1H), 3.16 (d, $J = 4.4$ Hz, 1H), 2.63 (s, 3H), 2.18 (app. s, 3H), 1.49 (s, 9H), 1.10 (d, $J = 6.8$ Hz, 3H), NH and OH not observed; ^{13}C NMR (101 MHz, CDCl_3) $\delta = 172.1, 162.6, 158.1, 156.6, 145.2, 143.3, 137.3, 136.8, 136.3, 135.1, 134.3, 133.5, 130.0, 122.9, 115.8, 114.7, 112.0, 102.5, 82.2, 67.5, 66.0, 51.2, 38.2, 28.1$ (3C), 24.0, 18.8, 17.2; LCMS (HpH): $t_{\text{R}} = 0.99$ min, $[\text{M}+\text{H}^+] = 519.7$ (100 % purity); HRMS: ($\text{C}_{29}\text{H}_{34}\text{N}_4\text{O}_5$) Requires $[\text{M}+\text{H}^+] = 519.2608$, found $[\text{M}+\text{H}^+] = 519.2607$.

(3-Methoxy-4-((1,5,6'-trimethyl-6-oxo-1,6-dihydro-(3,4'-bipyridin)-3'-yl)oxy)benzyl)-L-allothreonine hydrochloride, 2.85



A solution of *tert*-butyl (3-methoxy-4-((1,5,6'-trimethyl-6-oxo-1,6-dihydro-(3,4'-bipyridin)-3'-yl)oxy)benzyl)-L-allothreoninate (**2.83**, 63 mg, 0.12 mmol) in 2M aqueous HCl (4 mL, 8.0 mmol) was heated at 60°C for 2 h. The solvent was concentrated *in vacuo* to afford the title compound (**2.85**, 41.6 mg, 0.08 mmol, 69 % yield) as a yellow solid. M.pt.: 175.8-240.6°C; ($\alpha_{\text{D}}^{20.9^\circ\text{C}}$) $_{\lambda}(c = 2.0, \text{H}_2\text{O})$: -146.4; ν_{max} (solution in CDCl_3): 3336, 2570, 1622, 1490 cm^{-1} ; ^1H NMR (400 MHz, CD_3OD) $\delta = 8.35$ (s, 1H), 8.07 (s, 1H), 8.03 (s, 1H), 7.95 (s, 1H), 7.43 (s, 1H), 7.28 (d, $J = 7.3$ Hz, 1H), 7.16 (d, $J = 7.3$ Hz, 1H), 4.39 (d, $J = 13.7$ Hz, 1H), 4.40 - 4.36 (m, 1H), 4.32 (d, $J = 13.7$ Hz, 1H), 3.97 (d, $J = 3.4$ Hz, 1H), 3.88 (s, 3H), 3.65 (s, 3H), 2.77 (s, 3H), 2.17 (s, 3H), 1.32 (d, $J = 6.8$ Hz, 3H), exchangeable protons not observed; ^{13}C NMR (101 MHz, CD_3OD) $\delta = 167.3, 163.0, 151.1, 150.8, 148.5, 144.0, 143.2, 140.0, 137.0, 129.6, 128.7, 128.6, 126.5, 123.5, 121.5, 115.3, 111.6, 64.7, 63.9, 55.4, 50.0, 37.5, 17.7, 17.5, 15.8$; LCMS (HpH): $t_{\text{R}} = 0.58$ min, $[\text{M}+\text{H}^+] = 468.0$ (100 % purity); HRMS: ($\text{C}_{25}\text{H}_{29}\text{N}_3\text{O}_6$) Requires $[\text{M}+\text{H}^+] = 468.2135$, found $[\text{M}+\text{H}^+] = 468.2132$.

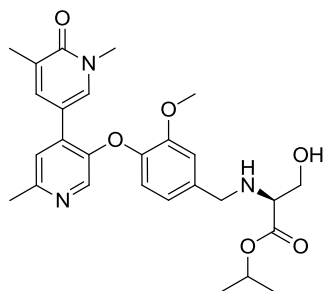
(3-Cyano-4-((1,5,6'-trimethyl-6-oxo-1,6-dihydro-(3,4'-bipyridin)-3'-yl)oxy)benzyl)-L-allothreonine hydrochloride, 2.86



A solution of *tert*-butyl (3-cyano-4-((1,5,6'-trimethyl-6-oxo-1,6-dihydro-(3,4'-bipyridin)-3'-yl)oxy)benzyl)-L-allothreoninate (**2.84**, 22 mg, 0.04 mmol) in 2M aqueous HCl (2 mL, 4.00 mmol) was stirred at 60°C for 1.5 h. The solvent was concentrated *in vacuo* to afford the title

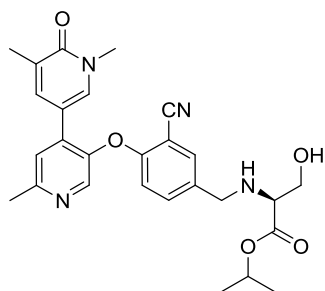
compound (**2.86**, 22 mg, 0.04 mmol, 99 % yield) as a yellow solid. ¹H NMR (400 MHz, DMSO-d₆) δ = 9.38 (br s, 1H, HCl salt), 8.57 (s, 1H), 8.10 (d, *J* = 2.5 Hz, 1H), 8.03 (d, *J* = 2.0 Hz, 1H), 7.77 (s, 1H), 7.72 (dd, *J* = 2.0, 8.8 Hz, 1H), 7.69 (dd, *J* = 1.0, 2.5 Hz, 1H), 6.92 (d, *J* = 8.8 Hz, 1H), 4.29 - 4.22 (m, 1H), 4.17 (app. br s, 2H), 3.85 (m, 1H), 3.48 (s, 3H), 2.63 (s, 3H), 2.01 (app. s, 3H), 1.20 (d, *J* = 6.4 Hz, 3H), exchangeable protons not observed; LCMS (Formic): t_R = 0.58 min, [M+H⁺] = 463.6 (100 % purity).

Isopropyl (3-methoxy-4-((1,5,6'-trimethyl-6-oxo-1,6-dihydro-(3,4'-bipyridin)-3'-yl)oxy)benzyl)-L-serinate, 2.88



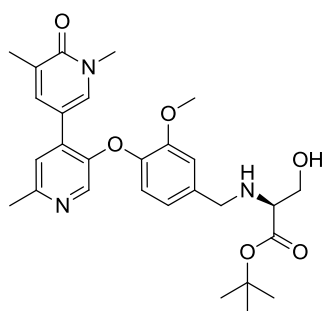
2-Picoline borane (54.9 mg, 0.51 mmol) was added to a solution of 3-methoxy-4-((1,5,6'-trimethyl-6-oxo-1,6-dihydro-(3,4'-bipyridin)-3'-yl)oxy)benzaldehyde (**2.64**, 170 mg, 0.47 mmol) and isopropyl L-serinate, 4-Methylbenzenesulphonic acid salt²²⁵ (**2.87**, 298 mg, 0.93 mmol) in isopropanol (2 mL), acetic acid (0.2 mL) and DCM (2 mL) and the reaction was stirred for 1 h under nitrogen. The reaction mixture was concentrated *in vacuo* and the resultant residue purified by MDAP (HpH). The relevant fractions were combined and concentrated *in vacuo* to afford the title compound (**2.88**, 125.7 mg, 0.24 mmol, 52 % yield) as a transparent oil. (α_D)^{22.0°C}_c(c = 1.0, MeOH): -12.5°; ν_{\max} (solution in CDCl₃): 3324, 2981, 1726, 1654 cm⁻¹; ¹H NMR (400 MHz, CDCl₃) δ = 8.06 (s, 1H), 7.75 (d, *J* = 2.4 Hz, 1H), 7.53 (dd, *J* = 1.2, 2.4 Hz, 1H), 7.12 (s, 1H), 6.97 (d, *J* = 1.7 Hz, 1H), 6.76 (dd, *J* = 1.7, 8.1 Hz, 1H), 6.70 (d, *J* = 8.1 Hz, 1H), 5.07 (spt, *J* = 6.3 Hz, 1H), 3.84 (s, 3H), 3.84 (d, *J* = 12.5 Hz, 1H), 3.76 (dd, *J* = 4.6, 11.0 Hz, 1H), 3.65 (d, *J* = 12.5 Hz, 1H), 3.61 (dd, *J* = 6.4, 11.0 Hz, 1H), 3.54 (s, 3H), 3.29 (dd, *J* = 4.6, 6.4 Hz, 1H), 2.54 (s, 3H), 2.15 (app. s, 3H), 1.25 (app. t, *J* = 6.0 Hz, 6H), NH and OH not observed; ¹³C NMR (101MHz, CDCl₃) δ 172.5, 162.7, 153.7, 150.2, 148.1, 144.1, 140.4, 137.0, 136.6, 136.3, 135.0, 129.1, 122.4, 120.71 118.6, 113.3, 112.6, 68.9, 62.8, 62.0, 55.9, 51.7, 38.2, 23.7, 21.9, 21.8, 17.3; LCMS (HpH): t_R = 0.88 min, [M+H⁺] = 496.6 (100 % purity); HRMS: (C₂₇H₃₃N₃O₆) Requires [M+H⁺] = 496.2448, found [M+H⁺] = 496.2448.

Isopropyl (3-cyano-4-((1,5,6'-trimethyl-6-oxo-1,6-dihydro-(3,4'-bipyridin)-3'-yl)oxy)benzyl)-L-serinate, 2.89



5-Formyl-2-((1,5,6'-trimethyl-6-oxo-1,6-dihydro-(3,4'-bipyridin)-3'-yl)oxy)benzonitrile (**2.68**, 150 mg, 0.42 mmol) was dissolved in isopropanol (1.2 mL), acetic acid (0.2 mL) and DCM (0.8 mL) and stirred for 10 min. Isopropyl L-serinate, 4-methylbenzenesulphonic acid salt²²⁵ (**2.87**, 267 mg, 0.84 mmol) was added to the solution and the reaction mixture was stirred for 1 h. 2-Picoline borane (49.1 mg, 0.46 mmol) was added to and the reaction mixture stirred for a further 1 h. The reaction mixture was quenched with water (3 mL) and concentrated *in vacuo*. The residue was purified by MDAP (HpH). The relevant fractions were combined and concentrated *in vacuo* to afford the title compound (**2.89**, 110.7 mg, 0.21 mmol, 51 % yield) as a transparent oil. ¹H NMR (400 MHz, CDCl₃) δ = 8.35 (s, 1H), 7.75 (d, *J* = 2.4 Hz, 1H), 7.59 (d, *J* = 2.2 Hz, 1H), 7.44 (dd, *J* = 1.2, 2.4 Hz, 1H), 7.35 (dd, *J* = 2.2, 8.8 Hz, 1H), 7.21 (s, 1H), 6.57 (d, *J* = 8.8 Hz, 1H), 5.08 (spt, *J* = 6.3 Hz, 1H), 3.85 (d, *J* = 13.4 Hz, 1H), 3.75 (dd, *J* = 4.6, 10.8 Hz, 1H), 3.64 - 3.58 (m, 5H), 3.24 (dd, *J* = 4.6, 6.4 Hz, 1H), 2.62 (s, 3H), 2.16 (app. s, 3H), 1.27 (app. t, *J* = 6.3 Hz, 6H), NH and OH not observed; LCMS (HpH): *t*_R = 0.88 min, [M+H⁺] = 491.6 (100 % purity).

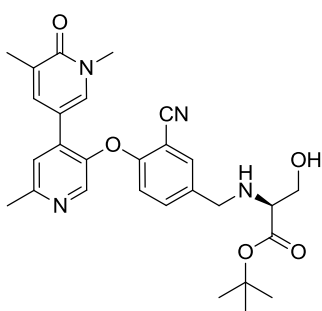
***tert*-Butyl (3-methoxy-4-((1,5,6'-trimethyl-6-oxo-1,6-dihydro-(3,4'-bipyridin)-3'-yl)oxy)benzyl)-L-serinate, 2.91**



2-Picoline borane (54.9 mg, 0.51 mmol) was added to a solution of 3-methoxy-4-((1,5,6'-trimethyl-6-oxo-1,6-dihydro-(3,4'-bipyridin)-3'-yl)oxy)benzaldehyde (**2.64**, 170 mg, 0.47 mmol) and *tert*-butyl L-serinate hydrochloride (**2.90**, 184 mg, 0.93 mmol) in isopropanol (2 mL), acetic acid (0.2 mL) and DCM (2 mL) and the reaction stirred for 1 h. The reaction mixture was concentrated *in vacuo*, dissolved in DMSO (3 mL) and purified by MDAP (HpH). The relevant fractions were combined and concentrated *in vacuo* to afford the title compound (**2.91**, 125.8 mg, 0.24 mmol, 50 % yield) as a transparent oil. (α_D)^{20.9°C} _{λ} (*c* = 4.0, CDCl₃): -5.1°; ν_{max} (solution in CDCl₃): 3332, 1727, 1654, 1594 cm⁻¹; ¹H NMR (400 MHz, CDCl₃) δ = 8.07 (s, 1H), 7.77 (d, *J* = 2.4 Hz, 1H), 7.55 (dd, *J* = 1.0, 2.4 Hz, 1H), 7.13 (s, 1H), 6.98 (d, *J* = 1.7 Hz, 1H), 6.79 (dd, *J* = 1.7, 8.3 Hz, 1H), 6.72 (d, *J* = 8.3 Hz, 1H), 3.85 (s, 3H), 3.85 (d, *J* = 13.0 Hz, 1H), 3.75 (dd, *J* = 4.6, 10.8 Hz, 1H), 3.66 (d,

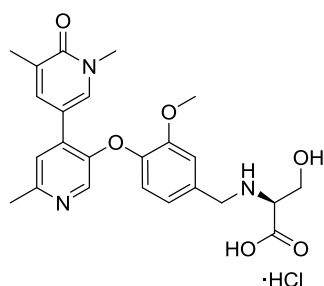
$J = 13.0$ Hz, 1H), 3.59 (dd, $J = 6.5, 10.8$ Hz, 1H), 3.56 (s, 3H), 3.25 (dd, $J = 4.6, 6.5$ Hz, 1H), 2.55 (s, 3H), 2.17 (app. s, 3H), 1.48 (s, 9H), NH and OH not observed; ^{13}C NMR (101 MHz, CDCl_3) $\delta = 171.9, 162.7, 153.8, 150.2, 148.1, 144.3, 140.5, 137.0, 136.6, 136.0, 135.1, 129.2, 122.3, 120.8, 118.6, 113.2, 112.6, 82.1, 62.7, 62.4, 55.9, 51.8, 38.2, 28.1$ (3C), 23.7, 17.3; LCMS (HpH): $t_{\text{R}} = 0.98$ min, $[\text{M}+\text{H}^+] = 510.6$ (100 % purity); HRMS: ($\text{C}_{28}\text{H}_{35}\text{N}_3\text{O}_6$) Requires $[\text{M}+\text{H}^+] = 510.2605$, found $[\text{M}+\text{H}^+] = 510.2604$.

***tert*-Butyl (3-cyano-4-((1,5,6'-trimethyl-6-oxo-1,6-dihydro-(3,4'-bipyridin)-3'-yl)oxy)benzyl)-L-serinate, 2.92**



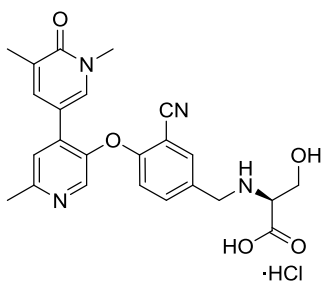
5-Formyl-2-((1,5,6'-trimethyl-6-oxo-1,6-dihydro-(3,4'-bipyridin)-3'-yl)oxy)benzyl nitrile (**2.68**, 150 mg, 0.42 mmol) was dissolved in isopropanol (1.2 mL) and DCM (0.8 mL) and stirred for 10 min. *tert*-Butyl L-serinate hydrochloride (**2.90**, 165 mg, 0.84 mmol) and acetic acid (0.2 mL) were added to the solution and the reaction mixture was stirred for 1 h at rt. 2-Picoline borane (49.1 mg, 0.46 mmol) was added to the reaction mixture and it was stirred for 1 h at rt. The reaction mixture was quenched with water (3 mL) and concentrated *in vacuo*. The residue was purified by MDAP (HpH). The relevant fractions were combined and concentrated *in vacuo*. The residue was purified again by MDAP (HpH). The relevant fractions were combined and concentrated *in vacuo* to afford the title compound (**2.92**, 66.8 mg, 0.13 mmol, 30 % yield) as a transparent oil. ($\alpha_{\text{D}}^{20.9^\circ\text{C}}$) $_{\text{c}} = 2.0$, CDCl_3): -6.0° ; ν_{max} (solution in CDCl_3): 3675, 2232, 1723, 1655, 1595 cm^{-1} ; ^1H NMR (400 MHz, CDCl_3) $\delta = 8.35$ (s, 1H), 7.76 (d, $J = 2.4$ Hz, 1H), 7.59 (d, $J = 2.2$ Hz, 1H), 7.45 (dd, $J = 1.0, 2.4$ Hz, 1H), 7.35 (dd, $J = 2.1, 8.7$ Hz, 1H), 7.21 (s, 1H), 6.57 (d, $J = 8.8$ Hz, 1H), 3.84 (d, $J = 13.7$ Hz, 1H), 3.73 (dd, $J = 4.6, 10.8$ Hz, 1H), 3.62 (d, $J = 13.7$ Hz, 1H), 3.57 (dd, $J = 6.6, 10.8$ Hz, 1H), 3.60 (s, 3H), 3.19 (dd, $J = 4.6, 6.6$ Hz, 1H), 2.62 (s, 3H), 2.16 (app. s, 3H), 1.47 (s, 9H), NH and OH not observed; ^{13}C NMR (101 MHz, CDCl_3) $\delta = 171.9, 162.6, 158.1, 156.6, 145.1, 143.3, 137.3, 136.8, 136.3, 135.0, 134.3, 133.4, 130.0, 122.9, 115.8, 114.7, 112.0, 102.5, 82.2, 62.9, 62.6, 50.7, 38.2, 28.1$ (3C), 24.0, 17.2; LCMS (HpH): $t_{\text{R}} = 0.94$ min, $[\text{M}+\text{H}^+] = 505.6$ (100 % purity); HRMS: ($\text{C}_{28}\text{H}_{32}\text{N}_4\text{O}_5$) Requires $[\text{M}+\text{H}^+] = 505.2452$, found $[\text{M}+\text{H}^+] = 505.2451$.

(3-Methoxy-4-((1,5,6'-trimethyl-6-oxo-1,6-dihydro-(3,4'-bipyridin)-3'-yl)oxy)benzyl)-L-serine hydrochloride, 2.93



A solution of *tert*-butyl (3-methoxy-4-((1,5,6'-trimethyl-6-oxo-1,6-dihydro-(3,4'-bipyridin)-3'-yl)oxy)benzyl)-L-serinate (**2.91**, 45 mg, 0.09 mmol) in 2M aqueous HCl (4 mL, 8.00 mmol) was stirred at 60°C for 2 h. The solvent was concentrated *in vacuo* to afford the title compound (**2.93**, 39.5 mg, 0.08 mmol, 91% yield) as a yellow solid. M.pt.: 193.7-243.3°C; (α_D)^{20.9°C} λ (c = 1.0, H₂O): +112.2°; ν_{\max} (solution in CDCl₃): 3338, 2532, 1978, 1725, 1633 cm⁻¹; ¹H NMR (400 MHz, CD₃OD) δ = 8.34 (d, *J* = 2.5 Hz, 1H), 8.05 - 8.03 (m, 2H), 7.95 (dd, *J* = 1.2, 2.5 Hz, 1H), 7.43 (d, *J* = 2.0 Hz, 1H), 7.28 (d, *J* = 8.3 Hz, 1H), 7.19 (dd, *J* = 2.0, 8.3 Hz, 1H), 4.83 (br s, 1H), 4.36 (s, 2H), 4.12 - 4.07 (m, 3H), 3.89 (s, 3H), 3.65 (s, 3H), 2.77 (s, 3H), 2.17 (app. s, 3H), exchangeable protons not observed; ¹³C NMR (101 MHz, CD₃OD) δ = 168.2, 163.1, 151.1, 150.8, 148.5, 144.0, 143.1, 140.0, 137.0, 130.1, 128.6, 128.6, 126.5, 123.3, 121.4, 115.2, 111.6, 60.7, 58.5, 55.5, 49.2, 37.5, 17.7, 15.8; LCMS (HpH): *t*_R = 0.56 min, [M+H⁺] = 454.6, (100 % purity); HRMS: (C₂₄H₂₇N₃O₆) Requires [M+H⁺] = 454.1979, found [M+H⁺] = 454.1973.

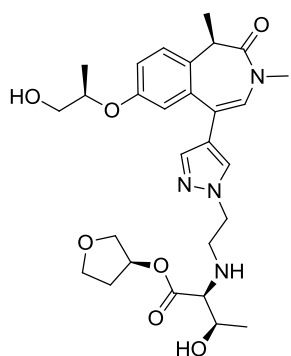
(3-Cyano-4-((1,5,6'-trimethyl-6-oxo-1,6-dihydro-(3,4'-bipyridin)-3'-yl)oxy)benzyl)-L-serine hydrochloride, 2.94



A solution of *tert*-butyl (3-cyano-4-((1,5,6'-trimethyl-6-oxo-1,6-dihydro-(3,4'-bipyridin)-3'-yl)oxy)benzyl)-L-serinate (**2.92**, 12 mg, 0.02 mmol) in 2M aqueous HCl (2 mL, 4.00 mmol) was stirred at 60°C for 1.5 h. The solvent was concentrated *in vacuo* to afford the title compound (**2.94**, 12 mg, 0.02 mmol, 99 % yield) as a yellow solid. ¹H NMR (400 MHz, DMSO-*d*₆) δ 8.66 (s, 1H), 8.17 (d, *J* = 2.4 Hz, 1H), 8.07 (d, *J* = 2.0 Hz, 1H), 7.89 (s, 1H), 7.77 (dd, *J* = 2.0, 8.8 Hz, 1H), 7.72 (dd, *J* = 1.0, 2.4 Hz, 1H), 6.98 (d, *J* = 8.8 Hz, 1H), 4.27 - 3.73 (m, 5H), 3.49 (s, 3H), 2.67 (s, 3H), 2.02 (app. s, 3H), exchangeable protons not observed; LCMS (HpH): *t*_R = 0.56 min, [M+H⁺] = 449.6 (100 % purity).

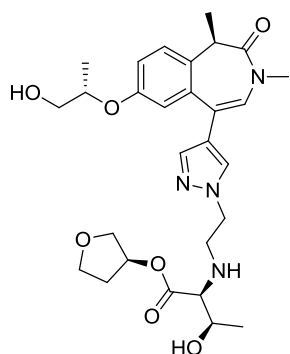
Chapter 3 Experimentals

(S)-Tetrahydrofuran-3-yl (2-(4-((R)-7-(((R)-1-hydroxypropan-2-yl)oxy)-1,3-dimethyl-2-oxo-2,3-dihydro-1H-benzo(d)azepin-5-yl)-1H-pyrazol-1-yl)ethyl)-L-threoninate, 3.7



A solution of (R)-5-(1-(2,2-diethoxyethyl)-1H-pyrazol-4-yl)-7-(((R)-1-hydroxypropan-2-yl)oxy)-1,3-dimethyl-1,3-dihydro-2H-benzo(d)azepin-2-one (**3.28**, 925 mg, 1.46 mmol, 70 wt%) and 2M aqueous hydrochloric acid (5 mL, 10.0 mmol) in THF (3 mL) was stirred at 60°C for 1 h. The reaction mixture was concentrated *in vacuo*. Two thirds of the material (500 mg, 0.87 mmol) and (S)-tetrahydrofuran-3-yl L-threoninate hydrochloride (**2.40**, 420 mg, 1.73 mmol) were dissolved in isopropanol (1 mL) and DCM (0.5 mL). A couple of drops of triethylamine were added and the mixture was stirred for at rt for 2 h. The reaction vessel was placed under a nitrogen atmosphere, acetic acid (0.22 mL) and picoline borane (102 mg, 0.95 mmol) added and the reaction mixture stirred at rt for 1 h. The reaction mixture was quenched with water (0.5 mL) and then purified by MDAP (HpH) to afford the title compound (**3.7**, 58 mg, 0.11 mmol, 12 % yield) as a colourless oil. (α_D)^{23.2°C} λ (c = 1.0, MeOH): +34.2°; ν_{\max} (solution in CDCl₃): 3418, 2977, 1732, 1654, 1492; ¹H NMR (400 MHz, CDCl₃) δ = 7.60 (s, 1H), 7.43 (s, 1H), 7.26 (d, *J* = 8.8 Hz, 1H), 7.00 (dd, *J* = 2.9, 8.8 Hz, 1H), 6.90 (d, *J* = 2.9 Hz, 1H), 6.56 (s, 1H), 5.39 - 5.30 (m, 1H), 4.42 (app. dq, *J* = 3.9, 6.4 Hz, 1H), 4.26 (ddd, *J* = 4.4, 6.8, 14.2 Hz, 1H), 4.14 (ddd, *J* = 4.4, 6.8, 14.2 Hz, 1H), 3.94 - 3.79 (m, 4H), 3.79 - 3.61 (m, 3H), 3.35 (q, *J* = 6.8 Hz, 1H), 3.27 - 3.16 (m, 1H), 3.10 (s, 3H), 2.95 (br q, *J* = 6.8 Hz, 2H), 2.27 - 2.11 (m, 1H), 2.04 - 1.94 (m, 1H), 1.64 (d, *J* = 6.8 Hz, 3H), 1.19 (app. d, *J* = 6.4 Hz, 6H), exchangeable protons not observed; ¹³C NMR (101 MHz, CDCl₃) δ = 172.8, 170.8, 155.9, 138.3, 136.7, 130.7, 129.3, 126.8, 125.1, 121.7, 121.5, 116.4, 115.5, 75.9, 74.9, 73.0, 67.9, 67.8, 67.0, 66.1, 52.6, 48.1, 40.4, 35.1, 32.8, 19.5, 15.7, 12.8; LCMS (HpH): *t*_R = 0.79 min, [M+H⁺] = 543.4, (92% purity); HRMS (C₂₈H₃₈N₄O₇) [M+H⁺] requires 543.2819, found [M+H⁺] 543.2817.

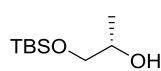
(S)-Tetrahydrofuran-3-yl (2-(4-((R)-7-(((S)-1-hydroxypropan-2-yl)oxy)-1,3-dimethyl-2-oxo-2,3-dihydro-1H-benzo(d)azepin-5-yl)-1H-pyrazol-1-yl)ethyl)-L-threoninate, 3.10



A solution of (R)-5-(1-(2,2-diethoxyethyl)-1H-pyrazol-4-yl)-7-(((S)-1-hydroxypropan-2-yl)oxy)-1,3-dimethyl-1,3-dihydro-2H-benzo(d)azepin-2-one (**3.29**, 930 mg, 1.68 mmol, 80 wt%) and 2M aqueous hydrochloric acid (5 mL, 10.0 mmol) in THF (5 mL) was stirred at 60°C for 1 h. The reaction mixture was

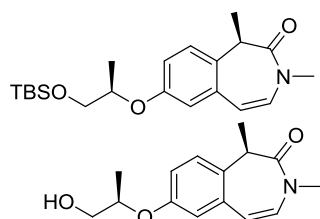
concentrated *in vacuo*. Two thirds of the material and (*S*)-tetrahydrofuran-3-yl L-threoninate hydrochloride (**2.40**, 549 mg, 2.26 mmol) were dissolved in isopropanol (1 mL) and DCM (0.5 mL). A couple of drops of triethylamine were added and the mixture was stirred for at rt for 2 h. The reaction vessel was placed under a nitrogen atmosphere, acetic acid (0.22 mL) and picoline borane (133 mg, 1.24 mmol) added and the reaction mixture stirred at rt for 1 h. The reaction mixture was quenched with water (0.5 mL) and purified by MDAP (HpH) to afford the title compound (**3.10**, 24.3 mg, 0.05 mmol, 4 % yield) as a clear oil. (α_D)^{21.2°C}_D(c = 1.0, CDCl₃): +36.3°; ν_{\max} (solution in CDCl₃): 3368, 2980, 1739, 1664 cm⁻¹; ¹H NMR (400 MHz, CDCl₃) δ = 7.62 (s, 1H), 7.43 (s, 1H), 7.26 (s, 1H), 7.02 (dd, *J* = 2.7, 8.6 Hz, 1H), 6.92 (d, *J* = 2.9 Hz, 1H), 6.57 (s, 1H), 5.38 - 5.33 (m, 1H), 4.36 (app. dquin, *J* = 3.9, 6.4 Hz, 1H), 4.26 (ddd, *J* = 3.9, 6.8, 16.6 Hz, 1H), 4.21 - 4.17 (m, 1H), 3.95 - 3.75 (m, 5H), 3.70 - 3.60 (m, 2H), 3.35 (q, *J* = 6.8 Hz, 1H), 3.33 - 3.29 (m, 1H), 3.11 (s, 3H), 3.06 (d, *J* = 7.8 Hz, 1H), 3.09 - 3.03 (m, 1H), 2.88 - 2.72 (br s, 3H), 2.26 - 2.16 (m, 1H), 2.05 - 1.98 (m, 1H), 1.65 (d, *J* = 6.8 Hz, 3H), 1.24 (d, *J* = 6.4 Hz, 3H), 1.23 (d, *J* = 6.4 Hz, 3H); ¹³C NMR (101 MHz, CD₃OD) δ = 179.3, 167.4, 165.7, 147.3, 145.7, 145.6, 139.4, 139.0, 137.5, 136.6, 134.4, 134.3, 130.2, 130.0, 126.4, 126.2, 123.8, 84.3, 81.6, 75.8, 75.1, 73.8, 56.5, 44.2, 41.7, 29.9, 26.2, 22.4; LCMS (Formic): *t*_R = 0.59 min, [M+H]⁺ = 543.3, (91% purity); HRMS: (C₂₈H₃₈N₄O₇) Requires [M+H]⁺ = 543.2740, found [M+H]⁺ = 543.2817.

((*S*)-1-((*tert*-Butyldimethylsilyloxy)propan-2-ol, **3.21**



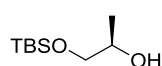
To a solution of (*S*)-propane-1,2-diol (2.32 mL, 31.5 mmol) and 1*H*-imidazole (2.15 g, 31.5 mmol) in DCM (40 mL) was added *tert*-butylchlorodimethylsilane (4.75 g, 31.5 mmol), and the reaction mixture was stirred at rt for 16 h. The reaction mixture was diluted with DCM (100 mL) and washed with water (2 x 50 mL). The combined organic layers were dried (hydrophobic frit) and concentrated *in vacuo*. The crude was purified by flash column chromatography (silica, 0-10% ethyl acetate in cyclohexane) to afford the title compound (**3.21**, 3.76 g, 17.8 mmol, 56% yield) as a colourless oil. ¹H NMR (400 MHz, CDCl₃) δ = 3.86 - 3.76 (m, 1H), 3.59 (dd, *J* = 3.4, 9.8 Hz, 1H), 3.36 (dd, *J* = 7.8, 9.8 Hz, 1H), 2.48 (d, *J* = 3.4 Hz, 1H), 1.12 (d, *J* = 6.4 Hz, 3H), 0.91 (s, 9H), 0.08 (s, 6H).

(R)-7-(((R)-1-((tert-Butyldimethylsilyl)oxy)propan-2-yl)oxy)-1,3-dimethyl-1,3-dihydro-2H-benzo(d)azepin-2-one, 3.22, and (R)-7-(((R)-1-hydroxypropan-2-yl)oxy)-1,3-dimethyl-1,3-dihydro-2H-benzo(d)azepin-2-one



To a mixture of (R)-7-hydroxy-1,3-dimethyl-1,3-dihydro-2H-benzo(d)azepin-2-one²²⁴ (**3.19**, 3.00 g, 14.8 mmol) in toluene (42 mL) was added (S)-1-((tert-butyldimethylsilyl)oxy)propan-2-ol (**3.21**, 3.65 g, 19.2 mmol) and 2-(tributyl-15-phosphanylidene)acetonitrile (4.65 mL, 17.7 mmol). The reaction mixture was split equally between three microwave vials which were sealed and heated in a microwave reactor at 100°C for 4 h. The reaction mixtures were combined and concentrated *in vacuo*. The resultant residue was partitioned between DCM (50 mL) and water (50 mL), the layers were separated and the aqueous layer was washed with DCM (2 x 50 mL). The organic layers were combined and concentrated *in vacuo* to give a brown oil. The oil was purified by flash column chromatography (silica, 0-15% ethyl acetate in cyclohexane). The relevant fractions were combined and concentrated *in vacuo* to give a dark orange oil. The regioisomers were resolved using preparative HPLC employing a 150 x 30mm Sunfire C18 column using a gradient of 75-100% acetonitrile (+0.1% TFA) in water (+0.1% TFA) and a flow rate of 40 mL/min to afford an aqueous solution containing the desired product. The aqueous layer was re-extracted with 9:1 DCM:MeOH (100 mL then 50 mL) and the layers were separated. The combined organic layers were dried (hydrophobic frit) and concentrated *in vacuo* to afford the title compound (**3.22**, 2.65 g, 8.11 mmol, 42% yield) as a white solid. M.pt.: 128.7-133.7°C; (α_D)^{20.9°C} λ (c = 2.0, CDCl₃): +95.7°; ν_{\max} (solution in CDCl₃): 3433, 2978, 1636, 1374 cm⁻¹; ¹H NMR (400 MHz, CDCl₃) δ = 7.21 (d, *J* = 8.6 Hz, 1H), 6.97 (dd, *J* = 2.7, 8.6 Hz, 1H), 6.81 (d, *J* = 2.7 Hz, 1H), 6.34 (d, *J* = 8.8 Hz, 1H), 6.28 (d, *J* = 8.8 Hz, 1H), 4.48 (app. dq, *J* = 3.9, 6.2 Hz, 1H), 3.76 - 3.68 (m, 2H), 3.28 (app. br s, 1H), 3.11 (s, 3H), 2.01 (br s, 1H), 1.61 (d, *J* = 6.8 Hz, 3H), 1.26 (d, *J* = 6.2 Hz, 3H); ¹³C NMR (101 MHz, CDCl₃) δ = 170.3, 156.2, 135.3, 130.5, 129.3, 125.8, 117.0, 116.1, 113.8, 75.1, 66.3, 40.8, 35.6, 15.8, 13.1; LCMS (HpH): *t*_R = 0.83 min, [M+H⁺] = 262.3 (87% purity); HRMS: (C₁₅H₁₉NO₃) [M+H⁺] requires 262.1444, found [M+H⁺] = 262.1437.

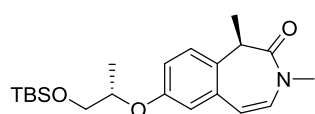
(R)-1-((tert-Butyldimethylsilyl)oxy)propan-2-ol, 3.24



To a mixture of (R)-propane-1,2-diol (1.92 mL, 26.3 mmol) and 1H-imidazole (1.79 g, 26.3 mmol) in DCM (20 mL) was added *tert*-butylchlorodimethylsilane (3.96 g, 26.3 mmol) and the reaction mixture stirred at rt for 16 h.

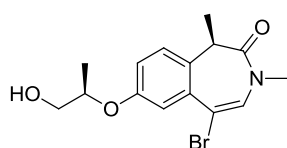
The reaction mixture was diluted with DCM (100 mL) and washed with water (2 x 100 mL). The combined organic layers were dried (hydrophobic frit) and concentrated *in vacuo*. The resultant residue was purified by flash column chromatography (silica, 0-10% ethyl acetate in cyclohexane) to afford the title compound (**3.24**, 3.75 g, 19.7 mmol, 75 % yield) as a colourless liquid. ¹H NMR (400 MHz, CDCl₃) δ = 3.86 - 3.75 (m, 1H), 3.59 (dd, *J* = 3.4, 9.8 Hz, 1H), 3.35 (dd, *J* = 7.8, 9.8 Hz, 1H), 2.45 (s, 1H), 1.12 (d, *J* = 6.4 Hz, 3H), 0.91 (s, 9H), 0.08 (s, 6H).

(*R*)-7-(((*S*)-1-((*tert*-Butyldimethylsilyl)oxy)propan-2-yl)oxy)-1,3-dimethyl-1,3-dihydro-2*H*-benzo(*d*)azepin-2-one, 3.25



To a mixture of (*R*)-1-((*tert*-butyldimethylsilyl)oxy)propan-2-ol (**3.24**, 60.9 mg, 0.32 mmol) in toluene (1 mL) was added (*R*)-7-hydroxy-1,3-dimethyl-1,3-dihydro-2*H*-benzo(*d*)azepin-2-one²²⁶ (**3.19**, 50 mg, 0.25 mmol) and 2-(tributyl-*l*5-phosphanylidene)acetonitrile (0.13 mL, 0.49 mmol) in a microwave vial. The vial was sealed and the mixture heated in a microwave reactor at 100°C for 30 min. The reaction mixture was concentrated under a stream of nitrogen to give a dark brown viscous oil which was purified by MDAP (HpH) to afford the title compound (**3.25**, 52 mg, 0.13 mmol, 90 wt%, 50 % yield) as a yellow oil. ¹H NMR (400 MHz, CDCl₃) δ = 7.19 (d, *J* = 8.8 Hz, 1H), 6.95 (dd, *J* = 2.4, 8.8 Hz, 1H), 6.79 (d, *J* = 2.4 Hz, 1H), 6.33 (d, *J* = 9.3 Hz, 1H), 6.26 (d, *J* = 9.3 Hz, 1H), 4.40 (app. sxt, *J* = 5.9 Hz, 1H), 3.79 (dd, *J* = 5.4, 10.3 Hz, 1H), 3.62 (dd, *J* = 5.4, 10.3 Hz, 1H), 3.22 (app. br s, 1H), 3.11 (s, 3H), 1.61 (br d, *J* = 5.9 Hz, 3H), 1.28 (d, *J* = 5.9 Hz, 3H), 0.88 (s, 9H), 0.07 (s, 3H), 0.04 (s, 3H); LCMS (HpH): *t*_R = 1.57 min, [M+H⁺] = 376.6 (87% purity).

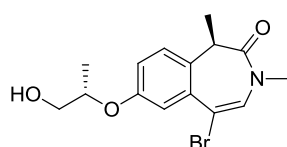
(*R*)-7-(((*R*)-1-Hydroxypropan-2-yl)oxy)-1,3-dimethyl-1,3-dihydro-2*H*-benzo(*d*)azepin-2-one, 3.26



A solution of phenyltrimethylaminotribromide (1.44 g, 3.83 mmol) and (*R*)-7-(((*R*)-1-hydroxypropan-2-yl)oxy)-1,3-dimethyl-1,3-dihydro-2*H*-benzo(*d*)azepin-2-one (**3.22**, 1 g, 3.83 mmol) in acetonitrile (20 mL) was stirred under nitrogen for 1 h. The reaction mixture was partitioned between ethyl acetate (100 mL) and water (100 mL). The aqueous layer was re-extracted with ethyl acetate (100 mL). The combined organic layers were dried (hydrophobic frit) and concentrated *in vacuo* to afford the title compound (**3.26**, 1.26 g, 3.33 mmol, 87 % yield) as an orange solid. M.pt.: 140.9-143.5°C; (α_D)^{20.9°C}_λ(*c* = 2.0, CDCl₃): +66.7°; ν_{max} (solution in CDCl₃): 3433, 2979, 1663, 1487, 1381 cm⁻¹; ¹H NMR (400

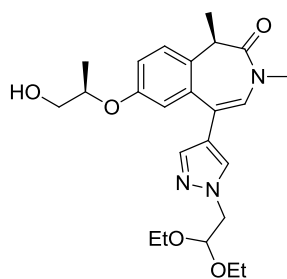
MHz, CDCl₃) δ = 7.26 (d, J = 2.9 Hz, 1H), 7.20 (d, J = 8.8 Hz, 1H), 7.03 (dd, J = 2.9, 8.8 Hz, 1H), 6.82 (s, 1H), 4.52 (app. dquin, J = 3.9, 6.2 Hz, 1H), 3.80 - 3.70 (m, 2H), 3.32 (q, J = 6.8 Hz, 1H), 3.07 (s, 3H), 2.00 (br s, 1H), 1.63 (d, J = 6.8 Hz, 3H), 1.28 (d, J = 6.2 Hz, 3H); ¹³C NMR (101 MHz, CDCl₃) δ = 170.3, 156.4, 135.5, 131.3, 130.2, 125.4, 118.8, 115.1, 111.5, 75.1, 66.3, 40.5, 35.0, 15.6, 12.9; LCMS (HpH): t_R = 0.97 min, [M+H⁺] = 340.2 / 342.2 (92% purity); HRMS: (C₁₅H₁₈BrNO₃) [M+H⁺] requires 340.0549, found [M+H⁺] = 340.0543.

(R)-5-Bromo-7-(((S)-1-hydroxypropan-2-yl)oxy)-1,3-dimethyl-1,3-dihydro-2H-benzo(d)azepin-2-one, 3.27



To a mixture of (R)-7-(((S)-1-((tert-butyl)dimethylsilyl)oxy)propan-2-yl)oxy)-1,3-dimethyl-1,3-dihydro-2H-benzo[d]azepin-2-one (**3.25**, 52 mg, 0.13 mmol) in acetonitrile (1 mL) was added phenyltrimethylaminotribromide (59.3 mg, 0.16 mmol) and the reaction mixture was stirred under nitrogen for 1 h. The reaction mixture was concentrated *in vacuo* and the resultant residue dissolved in ethyl acetate (10 mL) and partitioned with water (10 mL). The layers were separated and the aqueous layer was re-extracted with ethyl acetate (2 x 10 mL). The organic layers were combined (hydrophobic frit) and concentrated *in vacuo* to give an orange solid. The sample was purified by flash column chromatography (silica, 0-30% ethyl acetate in cyclohexane) to afford the title compound (**3.27**, 40 mg, 0.09 mmol, 72 % yield). ¹H NMR (400 MHz, CDCl₃) δ = 7.26 (d, J = 2.9 Hz, 1H), 7.20 (d, J = 8.8 Hz, 1H), 7.03 (dd, J = 2.9, 8.8 Hz, 1H), 6.82 (s, 1H), 4.52 (app. dquin, J = 3.9, 6.2 Hz, 1H), 3.79 - 3.68 (m, 2H), 3.33 (q, J = 6.8 Hz, 1H), 3.07 (s, 3H), 2.08 (app. t, J = 5.4 Hz, 1H), 1.63 (d, J = 6.8 Hz, 3H), 1.29 (d, J = 6.2 Hz, 3H); LCMS (HpH): t_R = 0.98 min, [M+H⁺] = 340.3 / 342.3 (100% purity).

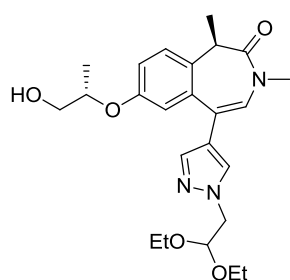
(R)-5-(1-(2,2-Diethoxyethyl)-1H-pyrazol-4-yl)-7-(((R)-1-hydroxypropan-2-yl)oxy)-1,3-dimethyl-1,3-dihydro-2H-benzo(d)azepin-2-one, 3.28



A solution of (R)-5-bromo-7-(((R)-1-hydroxypropan-2-yl)oxy)-1,3-dimethyl-1,3-dihydro-2H-benzo(d)azepin-2-one (**3.26**, 500 mg, 1.47 mmol), 1-(2,2-diethoxyethyl)-4-(4,4,5,5-tetramethyl-1,3,2-dioxaborolan-2-yl)-1H-pyrazole²²⁴ (**3.16**, 684 mg, 2.20 mmol), tetrakis(triphenylphosphine)palladium(0) (85 mg, 0.07 mmol) and potassium carbonate (609 mg, 4.41 mmol) in 1,4-dioxane (5 mL) and water (2.5 mL) was stirred at 80°C for 1 h. The reaction mixture was

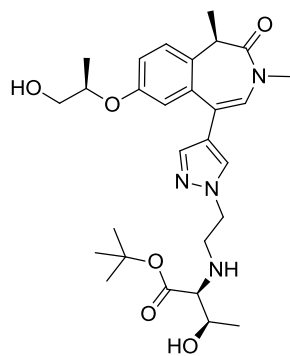
concentrated *in vacuo* to afford the title compound (**3.28**, 927 mg, 1.46 mmol, 70 wt%, 100 % yield) which was used as crude material in the next reaction. ¹H NMR (400 MHz, CDCl₃) δ = 7.55 (s, 1H), 7.46 (s, 1H), 7.28 (d, *J* = 8.3 Hz, 1H), 7.03 (dd, *J* = 2.4, 8.3 Hz, 1H), 6.88 (d, *J* = 2.4 Hz, 1H), 6.56 (s, 1H), 4.83 (t, *J* = 5.6 Hz, 1H), 4.76 (t, *J* = 5.6 Hz, 1H), 4.40 (dq, *J* = 3.7, 6.2 Hz, 1H), 4.22 - 4.19 (m, 3H), 3.78 - 3.64 (m, 7H), 3.35 (q, *J* = 6.8 Hz, 1H), 1.65 (d, *J* = 6.8 Hz, 3H), 1.64 - 1.58 (m, 3H), 1.17 - 1.13 (m, 6H), OH not observed; LCMS (HpH): *t_R* = 0.96 min, [M+H⁺] = 444.4 (83% purity).

(*R*)-5-(1-(2,2-Diethoxyethyl)-1*H*-pyrazol-4-yl)-7-(((*S*)-1-hydroxypropan-2-yl)oxy)-1,3-dimethyl-1,3-dihydro-2*H*-benzo(*d*)azepin-2-one, 3.29



A solution of (*R*)-5-bromo-7-(((*S*)-1-hydroxypropan-2-yl)oxy)-1,3-dimethyl-1,3-dihydro-2*H*-benzo(*d*)azepin-2-one (**3.27**, 635 mg, 1.87 mmol), 1-(2,2-diethoxyethyl)-4-(4,4,5,5-tetramethyl-1,3,2-dioxaborolan-2-yl)-1*H*-pyrazole²²⁴ (**3.16**, 868 mg, 2.80 mmol), tetrakis(triphenylphosphine)palladium(0) (108 mg, 0.09 mmol) and potassium carbonate (774 mg, 5.60 mmol) in 1,4-dioxane (5 mL) and water (2.5 mL) were stirred at 80°C for 1 h. The reaction mixture was concentrated *in vacuo* to afford the title compound (**3.29**, 930 mg, 1.68 mmol, 80 wt%, 90 % yield) which was used as crude material in the next reaction. ¹H NMR (400 MHz, CDCl₃) δ = 7.57 (s, 1H), 7.45 (s, 1H), 7.26 (s, 1H), 7.02 (dd, *J* = 2.4, 8.8 Hz, 1H), 6.89 (d, *J* = 2.4 Hz, 1H), 6.55 (s, 1H), 4.83 (t, *J* = 5.6 Hz, 1H), 4.39 (dq, *J* = 3.7, 6.2 Hz, 1H), 4.22 - 4.19 (m, 2H), 3.78 - 3.70 (m, 2H), 3.65 (br s, 2H), 3.53 - 3.42 (m, 2H), 3.35 (q, *J* = 6.8 Hz, 1H), 3.11 (s, 3H), 2.00 (s, 3H), 1.69 (br s, 1H), 1.65 (d, *J* = 6.8 Hz, 3H), 1.19 - 1.17 (m, 6H); LCMS (HpH): *t_R* = 0.98 min, [M+H⁺] = 444.5 (80% purity).

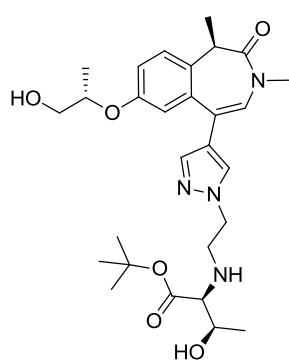
***tert*-Butyl (2-(4-((*R*)-7-(((*R*)-1-hydroxypropan-2-yl)oxy)-1,3-dimethyl-2-oxo-2,3-dihydro-1*H*-benzo(*d*)azepin-5-yl)-1*H*-pyrazol-1-yl)ethyl)-*L*-threoninate, 3.32**



A solution of (*R*)-5-(1-(2,2-diethoxyethyl)-1*H*-pyrazol-4-yl)-7-(((*R*)-1-hydroxypropan-2-yl)oxy)-1,3-dimethyl-1,3-dihydro-2*H*-benzo(*d*)azepin-2-one (**3.29**, 925 mg, 1.46 mmol, 70 wt%) and 2M aqueous hydrochloric acid (5 mL, 10.0 mmol) in THF (3 mL) was stirred at 60°C for 1 h. The reaction mixture was concentrated *in vacuo*. A third of the material and *tert*-butyl *L*-threoninate hydrochloride (**2.26** 236 mg, 1.04 mmol) were dissolved in isopropanol (1 mL) and DCM (0.5 mL). A couple of drops of

triethylamine were added and the mixture was stirred for at rt for 2 h. The reaction vessel was placed under a nitrogen atmosphere, acetic acid (0.22 mL) and picoline borane (61.0 mg, 0.57 mmol) added and the reaction mixture stirred at rt for 1 h. The reaction mixture was quenched with water (0.5 mL) and purified directly by MDAP (HpH) to afford the title compound (**3.32**, 31.2 mg, 0.06 mmol, 11 % yield) as a colourless oil. (α_D)^{23.2°C}_D(c = 1.0, MeOH): +84.9°; ν_{\max} (solution in CDCl₃): 3368, 2974, 1724, 1655, 1492 cm⁻¹; ¹H NMR (400 MHz, CDCl₃) δ = 7.61 (d, *J* = 1.0 Hz, 1H), 7.41 (d, *J* = 1.0 Hz, 1H), 7.26 (d, *J* = 8.8 Hz, 1H), 7.00 (dd, *J* = 2.7, 8.8 Hz, 1H), 6.89 (d, *J* = 2.7 Hz, 1H), 6.55 (s, 1H), 4.43 (app. dquin, *J* = 3.9, 6.4 Hz, 1H), 4.27 (br ddd, *J* = 3.9, 6.1, 14.2 Hz, 1H), 4.11 (ddd, *J* = 3.9, 7.8, 14.2 Hz, 1H), 3.68 (dd, *J* = 3.9, 12.0 Hz, 1H), 3.64 (dd, *J* = 6.4, 12.0 Hz, 1H), 3.61 (qd, *J* = 6.4, 7.4 Hz, 1H), 3.35 (q, *J* = 6.8 Hz, 1H), 3.22 (ddd, *J* = 3.9, 6.1, 12.7 Hz, 1H), 3.10 (s, 3H), 2.93 (ddd, *J* = 3.9, 7.8, 12.7 Hz, 1H), 2.81 (d, *J* = 7.8 Hz, 1H), 1.64 (d, *J* = 6.8 Hz, 3H), 1.47 (s, 9H), 1.19 (d, *J* = 6.4 Hz, 3H), 1.18 (d, *J* = 6.4 Hz, 3H), exchangeable protons not observed; ¹³C NMR (101 MHz, CDCl₃) δ = 172.8, 170.8, 156.0, 138.4, 136.7, 130.8, 129.3, 126.8, 125.1, 121.7, 121.5, 116.4, 115.5, 75.9, 74.9, 73.0, 67.9, 67.8, 67.0, 66.1, 52.3, 48.1, 40.4, 35.1, 32.8, 19.5, 15.7, 12.8; LCMS (HpH): *t*_R = 0.95 min, [M+H⁺] = 529.4, (99% purity); HRMS (C₂₈H₄₀N₄O₆) [M+H⁺] requires 529.3027, found [M+H⁺] 529.3023.

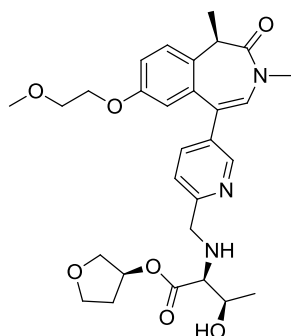
tert*-Butyl (2-(4-((*R*)-7-(((*S*)-1-hydroxypropan-2-yl)oxy)-1,3-dimethyl-2-oxo-2,3-dihydro-1*H*-benzo(*d*)azepin-5-yl)-1*H*-pyrazol-1-yl)ethyl)-*L*-threoninate, **3.33*



A solution of (*R*)-5-(1-(2,2-diethoxyethyl)-1*H*-pyrazol-4-yl)-7-(((*S*)-1-hydroxypropan-2-yl)oxy)-1,3-dimethyl-1,3-dihydro-2*H*-benzo(*d*)azepin-2-one (**3.29**, 930 mg, 1.68 mmol, 80 wt%) and 2M aqueous hydrochloric acid (5 mL, 10.0 mmol) in THF (5 mL) was stirred at 60°C for 1 h. The reaction mixture was concentrated *in vacuo*. A third of the material (300 mg, 0.52 mmol) and *tert*-butyl *L*-threoninate hydrochloride (**2.26**, 236 mg, 1.04 mmol) were dissolved in isopropanol (1 mL) and DCM (0.5 mL). A couple of drops of triethylamine were added and the mixture was stirred for at rt for 2 h. The reaction vessel was placed under a nitrogen atmosphere, acetic acid (0.22 mL) and picoline borane (61.0 mg, 0.57 mmol) added and the reaction mixture stirred at rt for 1 h. The reaction mixture was quenched with water (0.5 mL) and purified directly by MDAP (HpH) to afford the title compound (**3.33**, 20.4 mg, 0.04 mmol, 7 % yield) as a colourless oil. (α_D)^{23.2°C}_D(c = 1.0, MeOH): +117.7°; ν_{\max} (solution in CDCl₃): 3372, 2968, 1725, 1655, 1490 cm⁻¹; ¹H NMR (400 MHz, CDCl₃) δ = 7.61 (d, *J* = 1.0 Hz, 1H), 7.43 (d, *J* = 1.0 Hz, 1H),

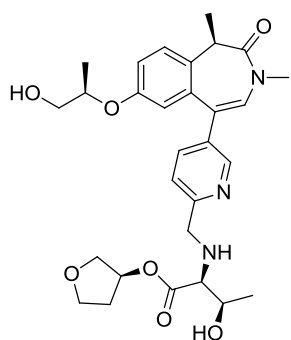
7.26 (d, $J = 8.8$ Hz, 1H), 7.02 (dd, $J = 2.4, 8.8$ Hz, 1H), 6.92 (d, $J = 2.4$ Hz, 1H), 6.57 (s, 1H), 4.36 (app. dq, $J = 3.9, 6.4$ Hz, 1H), 4.28 (ddd, $J = 4.4, 6.4, 14.2$ Hz, 1H), 4.19 (ddd, $J = 3.9, 7.4, 14.2$ Hz, 1H), 3.69 (qd, $J = 6.4, 7.4$ Hz, 1H), 3.67 (dd, $J = 3.9, 12.0$ Hz, 1H), 3.63 (dd, $J = 6.4, 12.0$ Hz, 1H), 3.35 (q, $J = 6.8$ Hz, 1H), 3.29 (ddd, $J = 3.9, 6.4, 12.7$ Hz, 1H), 3.10 (s, 3H), 3.02 (ddd, $J = 3.9, 7.8, 12.7$ Hz, 1H), 2.90 (d, $J = 7.8$ Hz, 1H), 1.65 (d, $J = 6.8$ Hz, 3H), 1.48 (s, 9H), 1.24 (d, $J = 6.4$ Hz, 3H), 1.21 (d, $J = 6.4$ Hz, 3H), exchangeable protons not observed; ^{13}C NMR (101 MHz, CDCl_3) $\delta = 173.1, 159.3, 159.1, 157.3, 134.6, 132.6, 130.9, 127.7, 125.8, 125.6, 124.8, 116.3, 112.8, 77.2, 75.9, 73.0, 71.0, 68.2, 67.6, 67.3, 67.0, 59.2, 52.0, 40.9, 35.8, 32.8, 19.6, 12.9$; LCMS (Formic): $t_R = 0.91$ min, $[\text{M}+\text{H}^+] = 529.3$, (91% purity); HRMS ($\text{C}_{28}\text{H}_{40}\text{N}_4\text{O}_6$) $[\text{M}+\text{H}^+]$ requires 529.3027, found $[\text{M}+\text{H}^+] = 529.3024$.

(S)-Tetrahydrofuran-3-yl ((5-((R)-7-(2-methoxyethoxy)-1,3-dimethyl-2-oxo-2,3-dihydro-1H-benzo(d)azepin-5-yl)pyridin-2-yl)methyl)-L-threoninate, 3.35



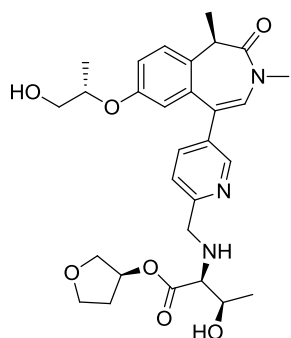
A solution of (*R*)-7-(2-methoxyethoxy)-1,3-dimethyl-5-(4,4,5,5-tetramethyl-1,3,2-dioxaborolan-2-yl)-1,3-dihydro-2*H*-benzo(d)azepin-2-one (**3.59**, 75 mg, 0.19 mmol), (*S*)-tetrahydrofuran-3-yl ((5-bromopyridin-2-yl)methyl)-L-threoninate (**3.46**, 83 mg, 0.23 mmol), $\text{Pd}(\text{PPh}_3)_4$ (22.4 mg, 0.02 mmol) and potassium carbonate (80 mg, 0.58 mmol) in 1,4-dioxane (1.3 mL) and water (0.65 mL) was stirred at 80°C for 1 h. The reaction mixture was partitioned between ethyl acetate (20 mL), water (20 mL) and brine (2 mL) was added. The aqueous layer was washed with further ethyl acetate (20 mL). The combined organic layers were dried (hydrophobic frit), concentrated *in vacuo* and purified by MDAP (HpH) to afford the title compound (**3.35**, 51 mg, 0.09 mmol, 46% yield) as white gum. (α_D) $^{20.9^\circ\text{C}}$ $_{\lambda}(c = 2.0, \text{CDCl}_3)$: +66.0°; ν_{max} (solution in CDCl_3): 2880, 2249, 1730, 1375 cm^{-1} ; ^1H NMR (400 MHz, CDCl_3) $\delta = 8.55$ (d, $J = 2.5$ Hz, 1H), 7.57 (dd, $J = 2.5, 8.3$ Hz, 1H), 7.31 (d, $J = 8.3$ Hz, 1H), 7.30 (d, $J = 8.8$ Hz, 1H), 7.03 (dd, $J = 2.9, 8.8$ Hz, 1H), 6.55 (s, 1H), 6.53 (d, $J = 2.9$ Hz, 1H), 5.39 - 5.34 (m, 1H), 4.07 (d, $J = 14.2$ Hz, 1H), 4.03 - 3.77 (m, 8H), 3.65 (t, $J = 4.9$ Hz, 2H), 3.38 (s, 3H), 3.37 (q, $J = 6.8$ Hz, 1H), 3.17 (s, 3H), 3.15 (d, $J = 7.2$ Hz, 1H), 2.26 - 2.17 (m, 1H), 2.07 - 1.99 (m, 1H), 1.69 (d, $J = 6.8$ Hz, 3H), 1.25 (d, $J = 6.4$ Hz, 3H); ^{13}C NMR (101 MHz, CDCl_3) $\delta = 173.2, 170.7, 158.1, 157.1, 149.0, 137.3, 136.1, 134.7, 130.7, 129.4, 127.2, 125.3, 121.8, 116.1, 113.6, 75.7, 73.0, 70.9, 68.1, 67.7, 67.4, 67.0, 59.1, 53.4, 40.6, 35.4, 32.9, 19.6, 12.9$; LCMS (HpH): $t_R = 0.90$ min, $[\text{M}+\text{H}^+] = 540.3$ (97% purity); HRMS: ($\text{C}_{29}\text{H}_{37}\text{N}_3\text{O}_7$) $[\text{M}+\text{H}^+]$ requires 540.2710, found $[\text{M}+\text{H}^+] = 540.2709$.

(S)-Tetrahydrofuran-3-yl ((5-((R)-7-(((R)-1-hydroxypropan-2-yl)oxy)-1,3-dimethyl-2-oxo-2,3-dihydro-1H-benzo(d)azepin-5-yl)pyridin-2-yl)methyl)-L-threoninate, 3.36



A solution of (*R*)-7-(((*R*)-1-hydroxypropan-2-yl)oxy)-1,3-dimethyl-5-(4,4,5,5-tetramethyl-1,3,2-dioxaborolan-2-yl)-1,3-dihydro-2*H*-benzo(*d*)azepin-2-one (**3.60**, 75 mg, 0.19 mmol), (*S*)-tetrahydrofuran-3-yl ((5-bromopyridin-2-yl)methyl)-L-threoninate (**3.46**, 83 mg, 0.23 mmol), Pd(PPh₃)₄ (22.4 mg, 0.02 mmol) and potassium carbonate (80 mg, 0.58 mmol) in 1,4-dioxane (1.3 mL) and water (0.65 mL) was stirred at 80°C for 1 h. The reaction mixture was partitioned between ethyl acetate (20 mL), water (20 mL) and brine (2 mL) was added. The aqueous layer was washed with further ethyl acetate (20 mL). The combined organic layers were dried (hydrophobic frit), concentrated *in vacuo* and purified by MDAP (HpH) to afford the title compound (**3.36**, 38 mg, 0.06 mmol, 33 % yield) as a yellow solid. ¹H NMR (400 MHz, CDCl₃) δ = 8.55 (d, *J* = 2.5 Hz, 1H), 7.59 (dd, *J* = 2.5, 8.3 Hz, 1H), 7.32 (d, *J* = 8.3 Hz, 1H), 7.31 (d, *J* = 8.8 Hz, 1H), 7.04 (dd, *J* = 2.4, 8.8 Hz, 1H), 6.56 (s, 1H), 6.52 (d, *J* = 2.4 Hz, 1H), 5.37 - 5.32 (m, 1H), 4.36 (dq, *J* = 2.4, 6.4, 12.7 Hz, 1H), 4.06 (d, *J* = 14.2 Hz, 1H), 3.95 - 3.78 (m, 6H), 3.67 - 3.60 (m, 2H), 3.37 (q, *J* = 6.8 Hz, 1H), 3.17 (s, 3H), 3.13 (d, *J* = 7.3 Hz, 1H), 2.26 - 2.16 (m, 1H), 2.05 - 2.00 (m, 1H), 1.69 (d, *J* = 6.8 Hz, 3H), 1.24 (d, *J* = 6.4 Hz, 3H), 1.14 (d, *J* = 6.4 Hz, 3H), exchangeable protons not observed; LCMS (HpH): *t*_R = 0.83 min, [M+H⁺] = 540.34 (95% purity).

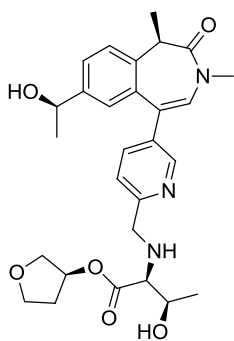
(S)-Tetrahydrofuran-3-yl ((5-((R)-7-(((S)-1-hydroxypropan-2-yl)oxy)-1,3-dimethyl-2-oxo-2,3-dihydro-1H-benzo(d)azepin-5-yl)pyridin-2-yl)methyl)-L-threoninate, 3.37



A solution of (*R*)-7-(((*S*)-1-hydroxypropan-2-yl)oxy)-1,3-dimethyl-5-(4,4,5,5-tetramethyl-1,3,2-dioxaborolan-2-yl)-1,3-dihydro-2*H*-benzo(*d*)azepin-2-one (**3.61**, 52 mg, 0.13 mmol), (*S*)-tetrahydrofuran-3-yl ((5-bromopyridin-2-yl)methyl)-L-threoninate (**3.46**, 48 mg, 0.13 mmol), Pd(PPh₃)₄ (8.6 mg, 7.44 μmol) and potassium carbonate (56.5 mg, 0.41 mmol) in 1,4-dioxane (1 mL) and water (0.5 mL) was stirred at 80°C for 2 h. The reaction mixture was diluted with 9:1 DCM:MeOH (10 mL) and partitioned with water (10 mL). The aqueous layer was re-extracted with 9:1 DCM:MeOH (3 x 10 mL). The combined organic layers were dried (hydrophobic frit) and concentrated *in vacuo* to afford a yellow oil. The oil was purified by flash column chromatography (silica, 0-10% MeOH in DCM) to afford the title compound (**3.37**, 12 mg, 0.02 mmol, 17 % yield). ¹H NMR (400 MHz, CDCl₃) δ = 8.55

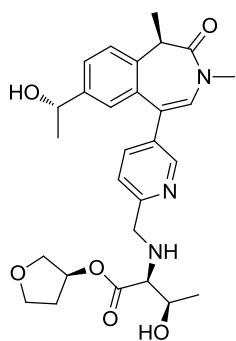
(d, $J = 2.0$ Hz, 1H), 7.59 (dd, $J = 2.0, 8.3$ Hz, 1H), 7.32 (d, $J = 8.3$ Hz, 1H), 7.30 (d, $J = 8.8$ Hz, 1H), 7.03 (dd, $J = 2.4, 8.8$ Hz, 1H), 6.56 (s, 1H), 6.53 (d, $J = 2.4$ Hz, 1H), 5.39 - 5.33 (m, 1H), 4.37 - 4.28 (m, 1H), 4.08 (d, $J = 14.2$ Hz, 1H), 3.97 - 3.75 (m, 8H), 3.37 (q, $J = 6.8$ Hz, 1H), 3.17 (s, 3H), 3.12 (d, $J = 7.3$ Hz, 1H), 2.27 - 2.16 (m, 1H), 2.08 - 1.99 (m, 1H), 1.69 (d, $J = 6.8$ Hz, 3H), 1.24 (d, $J = 6.4$ Hz, 3H), 1.21 (d, $J = 6.4$ Hz, 3H), exchangeable protons not observed; LCMS (HpH): $t_R = 0.56$ min, $[M+H]^+ = 540.42$ (95 % purity).

(S)-Tetrahydrofuran-3-yl ((5-((R)-7-((R)-1-hydroxyethyl)-1,3-dimethyl-2-oxo-2,3-dihydro-1H-benzo(d)azepin-5-yl)pyridin-2-yl)methyl)-L-threoninate, 3.38



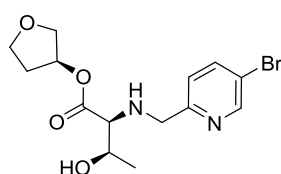
A solution of (*R*)-7-((*R*)-1-hydroxyethyl)-1,3-dimethyl-5-(4,4,5,5-tetramethyl-1,3,2-dioxaborolan-2-yl)-1,3-dihydro-2*H*-benzo(*d*)azepin-2-one (**3.62**, 160 mg, 0.40 mmol, 90 wt%), (*S*)-tetrahydrofuran-3-yl ((5-bromopyridin-2-yl)methyl)-L-threoninate (**3.46**, 174 mg, 0.48 mmol), Pd(PPh₃)₄ (23.3 mg, 0.02 mmol) and potassium carbonate (167 mg, 1.21 mmol) in 1,4-dioxane (2.5 mL) and water (1.25 mL) were stirred at 80°C for 10 min. The reaction mixture was partitioned between ethyl acetate (20 mL) and water (20 mL). The aqueous phase was extracted with 8:2 DCM:MeOH (20 mL). The organic layers were dried (hydrophobic frit), concentrated *in vacuo* and purified by MDAP (HpH) to afford the title compound (**3.38**, 64 mg, 0.13 mmol, 31 % yield) as a yellow gummy oil. (α_D)^{23.2°C}_D(c = 1.0, MeOH): +78.4°; ν_{max} (solution in CDCl₃): 3366, 2978, 1732, 1664, 1451 cm⁻¹; ¹H NMR (400 MHz, CDCl₃) $\delta = 8.54$ (d, $J = 2.2$ Hz, 1H), 7.61 (dd, $J = 2.2, 8.1$ Hz, 1H), 7.46 (dd, $J = 2.0, 8.3$ Hz, 1H), 7.38 (d, $J = 8.3$ Hz, 1H), 7.33 (d, $J = 8.1$ Hz, 1H), 6.99 (d, $J = 2.0$ Hz, 1H), 6.59 (s, 1H), 5.40 - 5.33 (m, 1H), 4.79 (q, $J = 6.4$ Hz, 1H), 4.11 (d, $J = 14.3$ Hz, 1H), 4.00 - 3.79 (m, 6H), 3.40 (q, $J = 6.8$ Hz, 1H), 3.19 (d, $J = 7.3$ Hz, 1H), 3.16 (s, 3H), 2.27 - 2.15 (m, 1H), 2.08 - 1.99 (m, 1H), 1.71 (d, $J = 6.8$ Hz, 3H), 1.39 (d, $J = 6.4$ Hz, 3H), 1.26 (d, $J = 6.4$ Hz, 3H), exchangeable protons not observed; ¹³C NMR (101 MHz, CDCl₃) $\delta = 172.1, 170.4, 156.4, 148.9, 144.3, 137.5, 137.0, 135.3, 135.0, 129.6, 127.1, 126.8, 124.6, 124.5, 122.1, 76.1, 72.9, 69.8, 67.8, 67.5, 67.0, 52.8, 41.2, 35.4, 32.8, 25.4, 19.8, 12.8$; LCMS (HpH): $t_R = 0.79$ min, $[M+H]^+ = 510.4$ (99% purity); HRMS (C₂₈H₃₅N₃O₆) $[M+H]^+$ requires 510.2605, found $[M+H]^+ 510.2600$.

(S)-Tetrahydrofuran-3-yl ((5-((R)-7-((S)-1-hydroxyethyl)-1,3-dimethyl-2-oxo-2,3-dihydro-1H-benzo(d)azepin-5-yl)pyridin-2-yl)methyl)-L-threoninate, 3.39



A solution of (*R*)-7-((*S*)-1-hydroxyethyl)-1,3-dimethyl-5-(4,4,5,5-tetramethyl-1,3,2-dioxaborolan-2-yl)-1,3-dihydro-2*H*-benzo(*d*)azepin-2-one (**3.63**, 160 mg, 0.38 mmol, 85 wt%), (*S*)-tetrahydrofuran-3-yl ((5-bromopyridin-2-yl)methyl)-L-threoninate (**3.46**, 164 mg, 0.46 mmol), Pd(PPh₃)₄ (22.0 mg, 0.02 mmol) and potassium carbonate (158 mg, 1.14 mmol) in 1,4-dioxane (2.5 mL) and water (1.25 mL) were stirred at 80°C for 10 min. The reaction mixture was partitioned between ethyl acetate (20 mL) and water (20 mL). The aqueous phase was re-extracted with 8:2 DCM:MeOH (20 mL). The organic layer was dried (hydrophobic frit) and concentrated *in vacuo*. The residue was purified by MDAP (HpH) to afford the title compound (**3.39**, 73 mg, 0.14 mmol, 38 % yield) as a yellow gummy oil. (α_D)^{21.2°C} (c = 1.0, CDCl₃): +56.4°; ν_{\max} (solution in CDCl₃): 3409, 2976, 1731, 1662, 1387 cm⁻¹; ¹H NMR (400 MHz, CDCl₃) δ = 8.53 (d, *J* = 2.5 Hz, 1H), 7.61 (dd, *J* = 2.5, 8.3 Hz, 1H), 7.43 (dd, *J* = 2.0, 8.3 Hz, 1H), 7.37 (d, *J* = 8.3 Hz, 1H), 7.33 (d, *J* = 8.3 Hz, 1H), 7.01 (d, *J* = 2.0 Hz, 1H), 6.59 (s, 1H), 5.39 - 5.33 (m, 1H), 4.80 (q, *J* = 6.4 Hz, 1H), 4.11 (d, *J* = 14.7 Hz, 1H), 3.96 (d, *J* = 14.7 Hz, 1H), 3.94 - 3.79 (m, 5H), 3.40 (q, *J* = 6.8 Hz, 1H), 3.20 (d, *J* = 7.3 Hz, 1H), 3.16 (s, 3H), 2.26 - 2.15 (m, 1H), 2.08 - 1.98 (m, 1H), 1.71 (d, *J* = 6.8 Hz, 3H), 1.39 (d, *J* = 6.4 Hz, 3H), 1.25 (d, *J* = 6.4 Hz, 3H), exchangeable protons not observed; ¹³C NMR (101 MHz, CDCl₃) δ = 172.4, 170.4, 156.9, 148.9, 144.3, 137.3, 136.9, 135.2, 135.1, 129.6, 127.2, 126.8, 124.6, 124.4, 122.1, 76.0, 73.0, 69.8, 67.9, 67.6, 67.0, 52.9, 41.2, 35.4, 32.8, 25.2, 19.7, 12.8; LCMS (HpH): *t*_R = 0.81 min, [M+H⁺] = 510.4 (97% purity); HRMS: (C₂₈H₃₅N₃O₆) [M+H⁺] requires 510.2605, found [M+H⁺] = 510.2608.

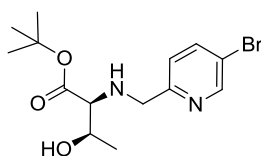
(S)-Tetrahydrofuran-3-yl ((5-bromopyridin-2-yl)methyl)-L-threoninate, 3.46



5-Bromopicolinaldehyde (500 mg, 2.69 mmol) and (*S*)-tetrahydrofuran-3-yl L-threoninate hydrochloride (**2.40**, 978 mg, 4.03 mmol) were dissolved THF (10 mL) and DIPEA (0.94 mL, 5.38 mmol) and acetic acid (0.39 mL, 6.72 mmol) added. The reaction vessel was placed under a nitrogen atmosphere and stirred at 40°C for 2 h. The reaction mixture was cooled to rt, sodium triacetoxyborohydride (1.42 mg, 6.72 mmol) added and the resultant suspension stirred for 2 h. The reaction mixture was quenched with water (10 mL), then diluted with THF (100 mL) and partitioned with water (100 mL). The aqueous layer was extracted with 8:2 DCM:MeOH (100 mL). The combined organic layers

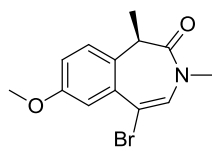
were dried (hydrophobic frit) and concentrated *in vacuo*. The residue was purified by flash column chromatography (silica, 0-100% ethyl acetate in cyclohexane). The relevant fractions were combined and concentrated *in vacuo* to afford the title compound (**3.46**, 482 mg, 1.34 mmol, 50 % yield). ¹H NMR (400 MHz, CDCl₃) δ = 8.60 (d, *J* = 2.4 Hz, 1H), 7.78 (dd, *J* = 2.4, 8.3 Hz, 1H), 7.24 (d, *J* = 8.3 Hz, 1H), 5.34 - 5.29 (m, 1H), 3.92 - 3.75 (m, 7H), 3.07 (d, *J* = 6.8 Hz, 1H), 2.25 - 2.14 (m, 1H), 2.01 - 1.90 (m, 1H), 1.22 (d, *J* = 6.4 Hz, 3H), NH and OH not observed; LCMS (HpH) *t*_R = 0.78, [M+H⁺] = 359.2 / 361.2 (98% purity).

***tert*-Butyl ((5-bromopyridin-2-yl)methyl)-L-threoninate, 3.47**



5-Bromopicolinaldehyde (500 mg, 2.69 mmol) and *tert*-butyl L-threoninate hydrochloride (**2.26**, 854 mg, 4.03 mmol) were dissolved THF (10 mL) and DIPEA (0.94 mL, 5.38 mmol) and acetic acid (0.39 mL, 6.72 mmol) added. The reaction vessel was placed under a nitrogen atmosphere and stirred at 40°C for 2 h. The reaction mixture was cooled to rt, sodium triacetoxyborohydride (1424 mg, 6.72 mmol) added and the resultant suspension stirred for 2 h. The reaction mixture was quenched with water (10 mL), then diluted with THF (100 mL) and partitioned with water (100 mL). The aqueous layer was extracted with 8:2 DCM:MeOH (100 mL). The combined organic layers were dried (hydrophobic frit) and concentrated *in vacuo*. The residue was purified by flash column chromatography (silica, 0-100% ethyl acetate in cyclohexane). The relevant fractions were combined and concentrated *in vacuo* to afford the title compound (**3.47**, 793 mg, 2.30 mmol, 85 % yield). ¹H NMR (400 MHz, CDCl₃) δ = 8.61 (d, *J* = 2.5 Hz, 1H), 7.78 (dd, *J* = 2.4, 8.3 Hz, 1H), 7.25 (d, *J* = 8.3 Hz, 1H), 3.96 (d, *J* = 14.7 Hz, 1H), 3.81 (d, *J* = 14.7 Hz, 1H), 3.76 - 3.67 (m, 1H), 3.62 (br s, 2H), 2.95 (d, *J* = 6.8 Hz, 1H), 1.47 (s, 9H), 1.23 (d, *J* = 6.4 Hz, 3H); LCMS (HpH) *t*_R = 1.03 min, [M+H⁺] = 345.2 / 347.2 (96% purity).

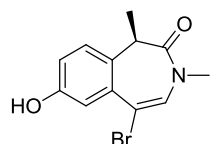
(*R*)-5-Bromo-7-methoxy-1,3-dimethyl-1,3-dihydro-2*H*-benzo(*d*)azepin-2-one, 3.49



A solution of phenyltrimethylaminotribromide (19.03 g, 50.6 mmol) and (*R*)-7-methoxy-1,3-dimethyl-1,3-dihydro-2*H*-benzo(*d*)azepin-2-one²¹⁸ (**3.48**, 10 g, 46.0 mmol) in acetonitrile (100 mL) was stirred under nitrogen for 1 h. The reaction mixture was partitioned between ethyl acetate (200 mL) and water (200 mL). The aqueous layer was re-extracted with ethyl acetate (200 mL). The combined organics were dried (hydrophobic frit) and concentrated *in vacuo* to afford the title compound (**3.49**, 12.3 g, 41.5 mmol, 90 % yield) as a white solid. M.pt.: 96.3-110.8°C; (α_D)^{20.9°C} _λ(*c* = 2.0, CDCl₃): +132.8°; ν_{max} (solution in CDCl₃): 2979, 1669,

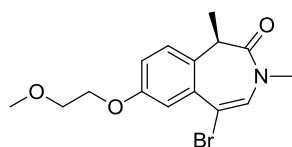
1354 cm^{-1} ; ^1H NMR (400 MHz, CDCl_3) δ = 7.22 (d, J = 2.9 Hz, 1H), 7.20 (d, J = 8.8 Hz, 1H), 7.01 (dd, J = 2.9, 8.8 Hz, 1H), 6.82 (s, 1H), 3.83 (s, 3H), 3.32 (q, J = 6.8 Hz, 1H), 3.06 (s, 3H), 1.63 (d, J = 6.8 Hz, 3H); ^{13}C NMR (101 MHz, CDCl_3) δ = 170.3, 158.3, 135.3, 131.2, 129.7, 125.3, 117.3, 112.5, 111.7, 55.5, 40.4, 35.0, 12.9; LCMS (HpH): t_{R} = 1.13 min, $[\text{M}+\text{H}^+] = 296.1 / 298.1$ (98% purity); HRMS: ($\text{C}_{13}\text{H}_{14}\text{BrNO}_2$) $[\text{M}+\text{H}^+]$ requires 296.0287, found $[\text{M}+\text{H}^+] = 296.0280$.

(R)-5-Bromo-7-hydroxy-1,3-dimethyl-1,3-dihydro-2H-benzo(d)azepin-2-one, 3.50



Boron tribromide (1M in DCM) (73.9 mL, 73.9 mmol) was added slowly to a solution of (*R*)-5-bromo-7-methoxy-1,3-dimethyl-1,3-dihydro-2H-benzo(*d*)azepin-2-one (**3.49**, 7.3 g, 24.7 mmol) in DCM (70.4 mL) under nitrogen at -78°C and the resultant solution stirred at -78°C for 1 h. The solution was then stirred at rt for 15 min before being quenched with water (20 mL). The reaction mixture was diluted with 5:2 DCM:MeOH (240 mL) and partitioned with water (300 mL). The layers were separated and the aqueous layer re-extracted with 5:2 DCM:MeOH (240 mL). The combined organic layers were dried (hydrophobic frit) and concentrated *in vacuo* to afford the title compound (**3.50**, 5.80 g, 20.6 mmol, 83 % yield) as a cream solid. M.pt.: $195.4\text{--}215.6^\circ\text{C}$; (α_{D}) $^{22.9^\circ\text{C}}$ $\lambda(c = 1.0, \text{CDCl}_3)$: $+40.9^\circ$; ν_{max} (solution in CDCl_3): 3251, 2924, 1645, 1493 cm^{-1} ; ^1H NMR (400 MHz, DMSO-d_6) δ = 9.64 (s, 1H), 7.10 (s, 1H), 7.09 (d, J = 8.3 Hz, 1H), 7.04 (d, J = 2.4 Hz, 1H), 6.90 (dd, J = 2.4, 8.3 Hz, 1H), 3.23 (q, J = 6.8 Hz, 1H), 2.99 (s, 3H), 1.46 (d, J = 6.8 Hz, 3H); ^{13}C NMR (101 MHz, CDCl_3) δ = 154.4, 131.1, 129.5, 125.5, 118.2, 114.3, 111.4, 40.4, 35.1, 31.0, 12.9, 0.0; LCMS (HpH) t_{R} = 0.88 min, $[\text{M}+\text{H}^+] = 282.1 / 284.1$ (97% purity); HRMS: ($\text{C}_{12}\text{H}_{12}\text{BrNO}_2$) $[\text{M}+\text{H}^+]$ requires 282.0100, found $[\text{M}+\text{H}^+] = 282.0125$.

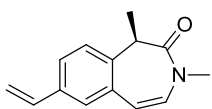
(R)-5-Bromo-7-(2-methoxyethoxy)-1,3-dimethyl-1,3-dihydro-2H-benzo(d)azepin-2-one, 3.51



A suspension of (*R*)-5-bromo-7-hydroxy-1,3-dimethyl-1,3-dihydro-2H-benzo(*d*)azepin-2-one (**3.50**, 1 g, 3.54 mmol), 1-bromo-2-methoxyethane (1.0 mL, 10.6 mmol) and potassium carbonate (1.47 g, 10.6 mmol) in DMF (5 mL) was heated in the microwave at 100°C for 3 h. The mixture was partitioned between ethyl acetate (100 mL) and water (100 mL). The aqueous layer was re-extracted with ethyl acetate (2 x 100 mL). The combined organic layers were dried (hydrophobic frit) and concentrated *in vacuo* to afford the title compound (**3.51**, 1.16 g, 3.41 mmol, 96 % yield) as a cream solid. ^1H NMR

(400 MHz, CDCl₃) δ = 7.25 (d, J = 2.9 Hz, 1H), 7.19 (d, J = 8.8 Hz, 1H), 7.04 (dd, J = 2.9, 8.8 Hz, 1H), 6.81 (s, 1H), 4.17 - 4.13 (m, 2H), 3.78 - 3.73 (m, 2H), 3.45 (s, 3H), 3.32 (q, J = 6.8 Hz, 1H), 3.07 (s, 3H), 1.63 (d, J = 6.8 Hz, 3H); LCMS (HpH): t_R = 1.12 min, [M+H⁺] = 340.2 / 342.2 (97% purity).

(R)-1,3-Dimethyl-7-vinyl-1,3-dihydro-2H-benzo(d)azepin-2-one, 3.52



Method 1, Scheme 3.7

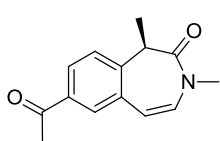
Bis(triphenylphosphine)palladium(II) chloride (0.33 g, 0.47 mmol) was added to a stirred solution of (R)-7-bromo-1,3-dimethyl-1,3-dihydro-2H-benzo(d)azepin-2-one²¹⁹ (**3.20**, 5 g, 18.8 mmol), vinylboronic anhydride pyridone complex (6.33 g, 26.3 mmol), and potassium carbonate (10.4 g, 75.0 mmol) in 1,2-dimethoxyethane (150 mL) and water (35 mL). The reaction mixture was refluxed for 4 h under nitrogen. The cooled reaction mixture was diluted with ethyl acetate (200 mL). The organic phase was dried (hydrophobic frit) and concentrated *in vacuo*. The residue was purified by flash column chromatography (silica, 0-30% ethyl acetate in cyclohexane) to afford the title compound (**3.52**, 4.08g, 15.3 mmol, 80 wt%, 81 % yield), as a yellow solid.

Method 2, Scheme 3.16

PdCl₂(PPh₃)₂ (138.6 mg, 0.20 mmol) was added to a stirring solution of (R)-7-bromo-1,3-dimethyl-1,3-dihydro-2H-benzo(d)azepin-2-one²¹⁹ (**3.20**, 2.00 g, 7.50 mmol), vinylboronic anhydride pyridine complex (2.77 g, 11.5 mmol) and potassium carbonate (4.12 g, 29.8 mmol) in 1,2-dimethoxyethane (60 mL) and water (15 mL). The reaction mixture was stirred at 80°C for 5 h. Further vinylboronic anhydride pyridine complex (0.83 g, 3.45 mmol) was added to the reaction mixture which was stirred at 80°C overnight. Further vinylboronic anhydride pyridine complex (904 mg, 3.76 mmol) was added to the reaction mixture which was stirred at 80°C for 6 h. More PdCl₂(PPh₃)₂ (0.13 g, 0.19 mmol) was added to the reaction mixture which was stirred at 80°C for 1 h. The cooled reaction mixture was diluted with ethyl acetate (60 mL) and the organic layer was separated and dried (hydrophobic frit) before being concentrated *in vacuo* to afford a dark brown oil. The oil was purified by flash column chromatography (silica, 0-30 % ethyl acetate in cyclohexane). The fractions were combined and concentrated *in vacuo* to afford a light yellow solid which was dried in a vacuum oven overnight to afford the title compound (**3.52**, 1.21 g, 5.65 mmol, 85 wt%, 75 % yield), a light yellow solid. ¹H NMR (400 MHz, CDCl₃) δ = 7.45 (dd, J = 2.0, 8.3 Hz, 1H), 7.29 (d, J = 2.0 Hz, 1H), 7.27 (d, J = 8.3 Hz, 1H), 6.72 (dd, J = 10.8, 17.6 Hz, 1H), 6.43 (d, J = 9.3 Hz, 1H), 6.31 (d, J = 9.3 Hz, 1H), 5.75 (d, J = 17.6 Hz, 1H), 5.26 (d, J = 10.8 Hz,

1H), 3.31 (app. br s, 1H), 3.13 (s, 3H), 1.65 (d, $J = 6.8$ Hz, 3H); LCMS (HpH): $t_R = 1.13$ min, $[M+H^+] = 214.32$, (86 % purity).

(R)-7-Acetyl-1,3-dimethyl-1,3-dihydro-2H-benzo(d)azepin-2-one, 3.53, Scheme 3.7



Method 1, Scheme 3.7

To (R)-1,3-dimethyl-7-vinyl-1,3-dihydro-2H-benzo(d)azepin-2-one (**3.52**, 4.08 g, 19.3 mmol, 80 wt%) in a microwave vial was added palladium(II) chloride (0.34 g, 1.91 mmol), benzoquinone (2.28 g, 21.0 mmol), methanol (56 mL) and water (8 mL). The reaction was stirred at 80°C for 3 h under nitrogen. The reaction volume was reduced *in vacuo* to approximately 20 mL, then partitioned between 2M aqueous HCl (20 mL), water (50 mL) and ethyl acetate (100 mL). The phases were separated and the aqueous layer re-extracted with ethyl acetate (2 x 50 mL). The combined organic layers were filtered through Celite, dried (hydrophobic frit) and concentrated *in vacuo* to give a yellow-brown oil, which was purified by flash column chromatography (silica, 0 - 50% ethyl acetate in cyclohexane) to afford the title compound (**3.53**, 2.54 g, 7.75 mmol, 41 % yield).

Method 2, Scheme 3.8

To a solution of (R)-7-bromo-1,3-dimethyl-1,3-dihydro-2H-benzo(d)azepin-2-one²²⁶ (**3.20**, 5.50 g, 20.7 mmol) in toluene (200 mL) was added tributyl(1-ethoxyvinyl)stannane (7.67 mL, 22.7 mmol) and reaction mixture was degassed with nitrogen for 10 min. Then bis(triphenylphosphine)palladium(II) chloride (0.73 g, 1.03 mmol) was added and mixture was again degassed for a further 10 min and then heated at 100°C for 16 h. The reaction mixture was treated with 2M aqueous HCl (400 mL). The organic layer was separated and the aqueous layer was re-extracted with ethyl acetate (2 x 500 mL). The combined organic layers were dried (hydrophobic frit) and concentrated *in vacuo* to give a yellow oil which was purified by flash column chromatography (silica, 10-30% ethyl acetate in cyclohexane). During elution of the product, it began to precipitate upon coming out of the machine. This caused the machine to become blocked. The fractions containing product were combined and concentrated *in vacuo* to afford the title compound (**3.53** Batch 1, 1.37 g, 5.68 mmol, 28 % yield) as a white solid. The waste from the column was concentrated *in vacuo* to afford the title compound (**3.53** Batch 2, 400 mg, 1.48 mmol, 85 wt%, 7 % yield) as a white solid. DCM (500 mL) was manually pumped through the silica column and the eluent concentrated *in vacuo* to afford the title compound (**3.53** Batch 3, 1.46 g, 6.05 mmol, 29 % yield).

Method 3, Scheme 3.9

(*R*)-1,3-Dimethyl-2-oxo-2,3-dihydro-1*H*-benzo(*d*)azepin-7-yltrifluoromethane sulfonate²²⁶ (**3.58**, 3 g, 8.95 mmol), palladium(II) acetate (0.10 g, 0.45 mmol), *n*-butyl vinyl ether (5.79 mL, 44.7 mmol) and triethylamine (3.12 mL, 22.4 mmol) were stirred in 1-butyl-3-methylimidazolium tetrafluoroborate (10 mL) under nitrogen at 110°C for 17 h in a sealed vial. The reaction mixture was concentrated under reduced pressure to give a black liquid. The liquid was partitioned between ethyl acetate (100 mL) and water (100 mL). A 2M aqueous LiCl solution (20 mL) was added. The layers were separated and the aqueous layer was re-extracted with ethyl acetate (100 mL). The organic layers were combined, dried (hydrophobic frit) and concentrated under reduced pressure to give a red oil. The oil was taken up in MeOH (10 mL) and 2M aqueous HCl (20 mL) added. The reaction mixture was stirred for 30 min at rt. The reaction mixture was diluted with DCM (90 mL) and water (60 mL) and 2M aqueous LiCl (20 mL) was added. The aqueous layer was re-extracted with 9:1 DCM:MeOH (50 mL). The organic layers were combined, dried (hydrophobic frit) and concentrated under reduced pressure to give a yellow solid. The solid was purified by flash column chromatography (silica, 0-100% ethyl acetate in cyclohexane) to afford the title compound (**3.53**, 1.23 g, 5.37 mmol, 60% yield) as a white solid.

Method 4, Table 3.29 Entry 2

Under nitrogen, (*R*)-1,3-dimethyl-2-oxo-2,3-dihydro-1*H*-benzo(*d*)azepin-7-yl trifluoromethanesulfonate²²⁶ (**3.58**, 100 mg, 0.30 mmol), dppf (8.27 mg, 0.02 mmol) and dicyclohexylamine (0.24 mL, 1.19 mmol) were dissolved in 1,4-dioxane (1.5 mL). *n*-Butyl vinyl ether (0.12 mL, 0.90 mmol) and bis(1,5-cyclooctadiene)nickel(0) (4.10 mg, 0.02 mmol) were added and the mixture was stirred at 100°C for 17 h. The reaction was cooled to rt and 6M HCl (3.00 mL, 18.00 mmol) added. The final mixture was stirred for 1 h. The reaction mixture was diluted with ethyl acetate (20 mL). The organic layers were combined, dried (hydrophobic frit) and concentrated under reduced pressure to give an orange oil. The oil was purified by flash column chromatography (silica, 0-50% ethyl acetate in cyclohexane) to afford the title compound (**3.53**, 61 mg, 0.27 mmol, 89 % yield) as a white solid.

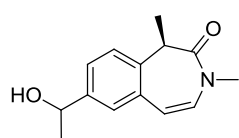
Method 5, Table 3.29 Entry 3

A solution of (*R*)-1,3-dimethyl-2-oxo-2,3-dihydro-1*H*-benzo(*d*)azepin-7-yl trifluoromethanesulfonate²¹⁶ (**3.58**, 1.50 g, 4.47 mmol), palladium(II) acetate (0.05 g, 0.22 mmol) and 1,3-bis(diphenylphosphaneyl)propane (0.10 g, 0.25 mmol) in DMF (10 mL) was

put under a nitrogen atmosphere. *n*-Butyl vinyl ether (2.89 mL, 22.4 mmol) and triethylamine (1.25 mL, 8.95 mmol) were added and the resultant solution was stirred under nitrogen at 80°C for 1 h. The reaction mixture was cooled to rt, 2M aqueous HCl (10 mL) added and the mixture left to stir for 1 h. The liquid was partitioned between ethyl acetate (100 mL) and water (100 mL). The layers were separated. The aqueous was re-extracted with ethyl acetate (100 mL). The organic layers were combined, dried (hydrophobic frit) and concentrated under reduced pressure to give an orange oil. The oil was purified by flash column chromatography (silica, 0-50% ethyl acetate in cyclohexane) to afford the title compound (**3.53**, 932 mg, 4.06 mmol, 91 % yield) as a white solid.

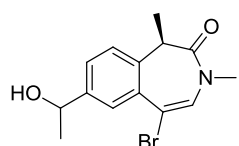
M.pt: 123.64 – 126.81°C; (α_D)^{20.9°C}_D(c = 1.0, CDCl₃): +85.7°; ν_{\max} (solution in CDCl₃): 2938, 1660, 1461, 1152 cm⁻¹; ¹H NMR (400 MHz, CDCl₃) δ = 7.95 (dd, *J* = 2.0, 8.3 Hz, 1H), 7.86 (d, *J* = 2.0 Hz, 1H), 7.41 (d, *J* = 8.3 Hz, 1H), 6.48 (d, *J* = 9.3 Hz, 1H), 6.37 (d, *J* = 9.3 Hz, 1H), 3.34 (app. br s, 1H), 3.14 (s, 3H), 2.61 (s, 3H), 1.68 (d, *J* = 6.4 Hz, 3H); ¹³C NMR (101 MHz, CDCl₃) δ = 197.5, 140.7, 140.6, 135.5, 131.3, 131.2, 128.3, 126.9, 115.7, 115.7, 77.2, 35.7, 26.6, 13.1; LCMS (HpH) *t*_R = 0.87 min, [M+H]⁺ = 230.3 (100% purity); HRMS: (C₁₄H₁₅NO₂) [M+H]⁺ requires 230.1168, found [M+H]⁺ = 230.1173.

(1R)-7-(1-Hydroxyethyl)-1,3-dimethyl-1,3-dihydro-2H-benzo(d)azepin-2-one, 3.54



To a solution of (*R*)-7-acetyl-1,3-dimethyl-1,3-dihydro-2H-benzo(*d*)azepin-2-one (**3.53**, 1.27 g, 5.54 mmol) in methanol (15 mL) at 0°C was carefully added sodium borohydride (0.42 g, 11.1 mmol). The reaction was removed from the ice bath and stirred at rt for 10 min. The reaction mixture was quenched with water (100 mL) and extracted with ethyl acetate (2 x 100 mL). The combined organic layers were dried (hydrophobic frit) and concentrated under reduced pressure to the title compound (**3.54**, 1.14 g, 4.93 mmol, 89 % yield) as a white solid. ¹H NMR (400 MHz, DMSO-*d*₆) δ = 8.58 (s, 1H), 7.95 (d, *J* = 8.3 Hz, 1H), 7.42 (d, *J* = 8.3 Hz, 1H), 6.64 (d, *J* = 9.3 Hz, 1H), 6.60 (d, *J* = 9.3 Hz, 1H), 3.16 (app. br s, 1H), 3.05 (s, 3H), 2.58 (s, 3H), 1.53 (d, *J* = 6.8 Hz, 3H), OH not observed; LCMS (HpH): *t*_R = 0.79 min, [M+H]⁺ = 232.3 (95% purity).

(1R)-5-Bromo-7-(1-hydroxyethyl)-1,3-dimethyl-1,3-dihydro-2H-benzo(d)azepin-2-one, 3.55

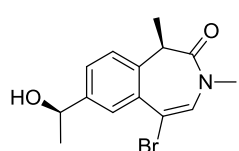


To a mixture of (*1R*)-7-(1-hydroxyethyl)-1,3-dimethyl-1,3-dihydro-2H-benzo(*d*)azepin-2-one (**3.54**, 1.14 g, 4.93 mmol) in acetonitrile (25

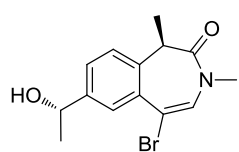
mL) was added phenyltrimethylaminotribromide (1.85 g, 4.93 mmol) and the reaction mixture was stirred under nitrogen for 10 min. The reaction mixture was diluted with ethyl acetate (100 mL) and partitioned with water (100 mL). The aqueous layer was re-extracted with ethyl acetate (100 mL). The combined organic layers were dried (hydrophobic frit) and evaporated under reduced pressure. The resultant residue was purified by flash column chromatography (silica, 0-100% ethyl acetate in cyclohexane) to afford the title compound (**3.55**, 1.27 g, 4.09 mmol, 83 % yield) as a yellow oil. ¹H NMR (400 MHz, CDCl₃) δ = 7.26 (d, *J* = 2.5 Hz, 1H), 7.20 (d, *J* = 8.8 Hz, 1H), 7.03 (dd, *J* = 2.5, 8.8 Hz, 1H), 6.82 (s, 1H), 4.52 (dq, *J* = 3.0, 6.4 Hz, 1H), 3.33 (q, *J* = 6.8 Hz, 1H), 3.07 (s, 3H), 1.98 (app. br s, 1H), 1.63 (d, *J* = 6.8 Hz, 3H), 1.29 (d, *J* = 6.4 Hz, 3H); LCMS (HpH): *t*_R = 0.95 min, [M+H⁺] = 310.1 / 312.1 (100% purity).

(*R*)-5-Bromo-7-((*R*)-1-hydroxyethyl)-1,3-dimethyl-1,3-dihydro-2*H*-benzo(*d*)azepin-2-one, **3.56 and (*R*)-5-bromo-7-((*S*)-1-hydroxyethyl)-1,3-dimethyl-1,3-dihydro-2*H*-benzo(*d*)azepin-2-one, **3.57****

Chiral resolution of (*1R*)-5-bromo-7-(1-hydroxyethyl)-1,3-dimethyl-1,3-dihydro-2*H*-benzo(*d*)azepin-2-one was carried out using a 250mm x 30mm Chiralpak column, 400-500uL injection volume and eluting with 20% ethanol/heptane at a flow rate of 42.5ml/min. The appropriate fractions for each isomer were combined and evaporated under reduced pressure to give the title compounds.



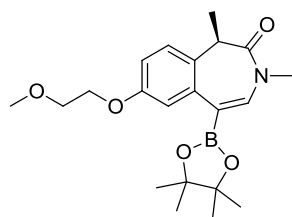
3.56 M.pt.: 73.9-105.4°C; (α_D)^{20.9°C} λ (c = 1.0, CDCl₃): +112.5°; ν_{\max} (solution in CDCl₃): 3435, 1659, 1382, 1271 cm⁻¹; ¹H NMR (400 MHz, CDCl₃) δ = 7.72 (d, *J* = 2.0 Hz, 1H), 7.47 (dd, *J* = 2.0, 8.3 Hz, 1H), 7.28 (d, *J* = 8.3 Hz, 1H), 6.84 (s, 1H), 4.95 (q, *J* = 6.4 Hz, 1H), 3.37 (q, *J* = 6.8 Hz, 1H), 3.07 (s, 3H), 1.65 (d, *J* = 6.8 Hz, 3H), 1.51 (d, *J* = 6.4 Hz, 3H), OH not observed; ¹³C NMR (101 MHz, CDCl₃) δ = 170.0, 144.6, 136.3, 134.4, 131.1, 127.6, 125.2, 124.3, 111.9, 69.9, 41.0, 35.0, 25.3, 12.8; LCMS (HpH): *t*_R = 0.95 mins, [M+H⁺] = 310.1 / 312.1 (97% purity); HRMS: (C₁₄H₁₆BrNO₂) [M+H⁺] requires = 310.0443, found [M+H⁺] = 310.0435.



3.57 M.pt.: 43.2-69.1°C; (α_D)^{20.9°C} λ (c = 2.0, CDCl₃): +62.00; ν_{\max} (solution in CDCl₃): 3350, 1670, 1381, 1230 cm⁻¹; ¹H NMR (400 MHz, CDCl₃) δ = 7.73 (d, *J* = 2.0 Hz, 1H), 7.46 (dd, *J* = 2.0, 8.3 Hz, 1H), 7.29 (d, *J* = 8.3 Hz, 1H), 6.84 (s, 1H), 4.95 (dq, *J* = 2.9, 6.4 Hz,

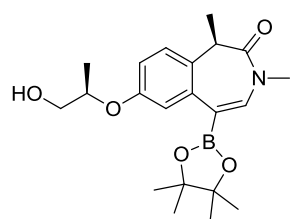
1H), 3.37 (q, $J = 6.8$ Hz, 1H), 3.08 (s, 3H), 1.82 (d, $J = 2.9$ Hz, 1H), 1.66 (d, $J = 6.8$ Hz, 3H), 1.51 (d, $J = 6.4$ Hz, 3H); ^{13}C NMR (101 MHz, CDCl_3) $\delta = 169.9, 144.6, 136.2, 134.4, 131.1, 127.6, 125.2, 124.3, 111.9, 69.9, 41.0, 35.0, 25.2, 12.7$; LCMS (HpH): $t_R = 0.96$ mins, $[\text{M}+\text{H}^+] = 310.1 / 312.1$ (90% purity); HRMS: ($\text{C}_{14}\text{H}_{16}\text{BrNO}_2$) $[\text{M}+\text{H}^+]$ requires = 310.0443, found $[\text{M}+\text{H}^+] = 310.0439$.

(*R*)-7-(2-Methoxyethoxy)-1,3-dimethyl-5-(4,4,5,5-tetramethyl-1,3,2-dioxaborolan-2-yl)-1,3-dihydro-2*H*-benzo(*d*)azepin-2-one, 3.59



A solution of (*R*)-5-bromo-7-(2-methoxyethoxy)-1,3-dimethyl-1,3-dihydro-2*H*-benzo(*d*)azepin-2-one (**3.51**, 500 mg, 1.47 mmol), bis(pinacolato)diboron (746 mg, 2.94 mmol), potassium acetate (433 mg, 4.41 mmol) and $\text{PdCl}_2(\text{dppf})\cdot\text{DCM}$ adduct (108 mg, 0.15 mmol) in 1,4-dioxane (8 mL) was stirred at 70°C for 16 h. The reaction mixture was filtered through Celite, then partitioned between water (50 mL) and ethyl acetate (50 mL). The aqueous layer was extracted with further ethyl acetate (50 mL). The organic layers were dried (hydrophobic frit), concentrated *in vacuo* and purified by flash column chromatography (silica, 0-30% ethyl acetate in cyclohexane) to afford the title compound (**3.59**, 491 mg, 1.21 mmol, 82 % yield) as a white solid. M.pt.: $110.5\text{-}126.7^\circ\text{C}$; (α_D) $^{20.9^\circ\text{C}}$ $\lambda(c = 1.0, \text{CDCl}_3)$: $+121.7^\circ$; ν_{max} (solution in CDCl_3): 2978, 1676, 1605, 1410 cm^{-1} ; ^1H NMR (400 MHz, CDCl_3) $\delta = 7.17$ (d, $J = 8.6$ Hz, 1H), 7.17 (d, $J = 2.7$ Hz, 1H), 7.00 (s, 1H), 6.96 (dd, $J = 2.7, 8.6$ Hz, 1H), 4.13 (dd, $J = 4.4, 5.4$ Hz, 2H), 3.75 (dd, $J = 4.4, 5.4$ Hz, 2H), 3.45 (s, 3H), 3.17 (q, $J = 6.8$ Hz, 1H), 3.13 (s, 3H), 1.59 (d, $J = 6.8$ Hz, 3H), 1.34 (app. d, $J = 8.8$ Hz, 12H); ^{13}C NMR (101 MHz, CDCl_3) $\delta = 171.4, 156.9, 141.2, 137.0, 129.4, 124.7, 115.4, 113.5, 83.9, 71.1, 67.3, 59.2, 40.7, 35.6, 25.1, 25.1$ (4 C), 24.6, 12.9; LCMS (HpH): $t_R = 1.26$ min, $[\text{M}+\text{H}^+] = 388.4$ (84 % purity). Boronic acid $t_R = 0.70$ min, $[\text{M}+\text{H}^+] = 306.2$ (15 % purity); HRMS: ($\text{C}_{21}\text{H}_{30}\text{BNO}_5$) $[\text{M}+\text{H}^+]$ requires 388.2332, found $[\text{M}+\text{H}^+] = 388.2295$.

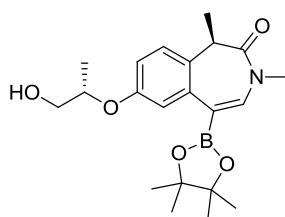
(*R*)-7-(((*R*)-1-Hydroxypropan-2-yl)oxy)-1,3-dimethyl-5-(4,4,5,5-tetramethyl-1,3,2-dioxaborolan-2-yl)-1,3-dihydro-2*H*-benzo(*d*)azepin-2-one, 3.60



A solution of (*R*)-5-bromo-7-(((*R*)-1-hydroxypropan-2-yl)oxy)-1,3-dimethyl-1,3-dihydro-2*H*-benzo(*d*)azepin-2-one (**3.26**, 385 mg, 1.13 mmol), bis(pinacolato)diboron (575 mg, 2.23 mmol), potassium acetate (333 mg, 3.39 mmol) and $\text{PdCl}_2(\text{dppf})\cdot\text{DCM}$ adduct (83 mg, 0.11 mmol) in 1,4-dioxane (5.7 mL) was stirred at

70°C for 16 h. The reaction mixture was filtered through Celite and washed with ethyl acetate (20 mL). The solution was concentrated *in vacuo* and purified by flash column chromatography (silica, 0-50% ethyl acetate in cyclohexane) to afford the title compound (**3.60**, 366.2 mg, 0.85 mmol, 75 % yield) as a gum. (α_D)^{20.9°C}_D(c = 10.0, CDCl₃): +165.1°; ν_{\max} (solution in CDCl₃): 3449, 2978, 1662, 1606, 1412 cm⁻¹; ¹H NMR (400 MHz, CDCl₃) δ = 7.19 (d, *J* = 2.7 Hz, 1H), 7.18 (d, *J* = 8.6 Hz, 1H), 7.02 (s, 1H), 6.95 (dd, *J* = 2.7, 8.6 Hz, 1H), 4.48 (dq, *J* = 2.4, 6.4, 12.2 Hz, 1H), 3.79 - 3.69 (m, 2H), 3.17 (q, *J* = 6.8 Hz, 1H), 3.13 (s, 3H), 1.93 (app. br s, 1H), 1.60 (d, *J* = 6.8 Hz, 3H), 1.34 (d, *J* = 8.3 Hz, 12H), 1.30 (d, *J* = 6.4 Hz, 3H); ¹³C NMR (101 MHz, CDCl₃) δ = 171.4, 155.6, 141.3, 137.0, 129.5, 124.9, 116.9, 114.3, 83.9, 82.9, 75.0, 74.6, 66.4, 40.7, 35.6, 25.1, 24.8, 24.6, 24.6, 15.5, 12.9; LCMS (HpH): *t*_R = 1.15 min, [M+H⁺] = 388.39 (95% purity); HRMS: (C₂₁H₃₀BNO₅) [M+H⁺] requires 388.2332, found [M+H⁺] = 388.2294.

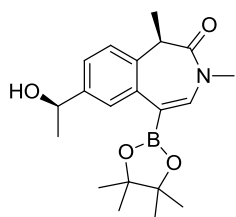
(R)-7-(((S)-1-Hydroxypropan-2-yl)oxy)-1,3-dimethyl-5-(4,4,5,5-tetramethyl-1,3,2-dioxaborolan-2-yl)-1,3-dihydro-2H-benzo(d)azepin-2-one, 3.61



(*R*)-5-Bromo-7-(((*S*)-1-hydroxypropan-2-yl)oxy)-1,3-dimethyl-1,3-dihydro-2*H*-benzo(*d*)azepin-2-one (**3.27**, 650 mg, 1.91 mmol), bis(pinacolato)diboron (968 mg, 3.81 mmol), potassium acetate (565 mg, 5.76 mmol) and PdCl₂(dppf)·DCM adduct (158 mg, 0.19 mmol) were stirred in 1,4-dioxane (8 mL) at 60°C for 2

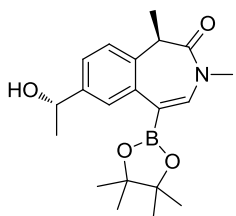
h. The reaction was quenched with 9:1 DCM:MeOH (10 mL), filtered over Celite and washed with 9:1 DCM:MeOH (10 mL). The filtrate was partitioned with water (20 mL). The aqueous layer was re-extracted with a further two portions of 9:1 DCM:MeOH (2 x 20 mL). The combined organic layers were dried (hydrophobic frit) and concentrated *in vacuo* to afford a brown oil. The residue was purified using flash column chromatography (silica, 30-60 % ethyl acetate in cyclohexane) to afford the title compound (**3.61**, 735 mg, 1.90 mmol, 99 % yield). ¹H NMR (400 MHz, CDCl₃) δ = 7.18 (d, *J* = 8.8 Hz, 1H), 7.19 (d, *J* = 2.9 Hz, 1H), 7.01 (s, 1H), 6.95 (dd, *J* = 2.9, 8.8 Hz, 1H), 4.46 (dq, *J* = 3.5, 6.4, 13.0 Hz, 1H), 3.83 - 3.67 (m, 2H), 3.18 (q, *J* = 6.8 Hz, 1H), 3.13 (s, 3H), 1.60 (d, *J* = 6.8 Hz, 3H), 1.35 (app. d, *J* = 7.8 Hz, 12H), 1.30 (d, *J* = 6.4 Hz, 3H), OH not observed; LCMS (HpH): *t*_R = 1.13 min, [M+H⁺] = 388.40 (89 % purity).

(R)-7-((R)-1-Hydroxyethyl)-1,3-dimethyl-5-(4,4,5,5-tetramethyl-1,3,2-dioxaborolan-2-yl)-1,3-dihydro-2H-benzo(d)azepin-2-one, 3.62



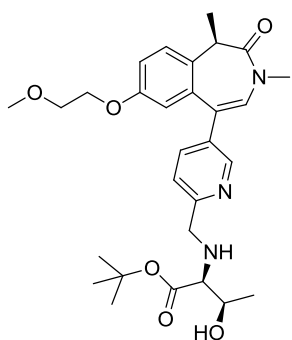
PdCl₂(dppf) (118 mg, 0.16 mmol) was added to a stirred mixture of (R)-5-bromo-7-((R)-1-hydroxyethyl)-1,3-dimethyl-1,3-dihydro-2H-benzo(d)azepin-2-one (**3.56**, 500 mg, 1.61 mmol), bis(pinacolato)diboron (819 mg, 3.22 mmol) and potassium acetate (475 mg, 4.84 mmol) in 1,4-dioxane (10 mL). The reaction mixture was stirred at 70°C for 4 h under nitrogen. The reaction mixture was cooled to rt and partitioned between ethyl acetate (100 mL) and water (100 mL). The aqueous phase was re-extracted with ethyl acetate (2 x 50 mL). The combined organics were dried (hydrophobic frit) and concentrated *in vacuo*. The residue was purified by flash column chromatography (silica, 0-100% ethyl acetate in cyclohexane) to afford the title compound (**3.62**, 577 mg, 1.45 mmol, 90 wt%, 90 % yield) as a brown oil. ¹H NMR (400 MHz, CDCl₃) δ = 7.58 (d, *J* = 2.0 Hz, 1H), 7.38 (dd, *J* = 2.0, 8.3 Hz, 1H), 7.28 (d, *J* = 8.3 Hz, 1H), 7.02 (s, 1H), 4.92 (q, *J* = 6.4 Hz, 1H), 3.22 (q, *J* = 6.8 Hz, 1H), 3.13 (s, 3H), 1.89 (s, 1H), 1.62 (d, *J* = 6.8 Hz, 3H), 1.51 (d, *J* = 6.4 Hz, 3H), 1.35 (app. d, *J* = 10.3 Hz, 12H); LCMS (HpH): t_R: 1.07 min, [M+H⁺] = 358.3 (89% purity).

(R)-7-((S)-1-Hydroxyethyl)-1,3-dimethyl-5-(4,4,5,5-tetramethyl-1,3,2-dioxaborolan-2-yl)-1,3-dihydro-2H-benzo(d)azepin-2-one, 3.63



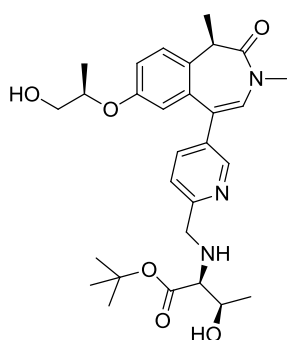
PdCl₂(dppf) (113 mg, 0.15 mmol) was added to a stirred mixture of (R)-5-bromo-7-((S)-1-hydroxyethyl)-1,3-dimethyl-1,3-dihydro-2H-benzo(d)azepin-2-one (**3.57**, 479 mg, 1.54 mmol), bis(pinacolato)diboron (784 mg, 3.09 mmol) and potassium acetate (455 mg, 4.63 mmol) in 1,4-dioxane (15 mL). The reaction mixture was stirred at 70°C for 1 h under nitrogen. The reaction mixture was cooled to rt and partitioned between ethyl acetate (100 mL) and water (100 mL). The aqueous phase was re-extracted with ethyl acetate (2 x 50 mL). The combined organics were dried (hydrophobic frit) and concentrated *in vacuo*. The residue was purified by flash column chromatography (silica, 0-100% ethyl acetate in cyclohexane) to afford the title compound (**3.63**, 546 mg, 1.30 mmol, 85 wt%, 84 % yield) as a brown oil which solidified into a brown solid upon standing. ¹H NMR (400 MHz, CDCl₃) δ = 7.59 (d, *J* = 2.0 Hz, 1H), 7.38 (dd, *J* = 2.0, 8.3 Hz, 1H), 7.27 (d, *J* = 8.3 Hz, 1H), 7.02 (s, 1H), 4.90 (q, *J* = 6.4 Hz, 1H), 3.22 (q, *J* = 6.8 Hz, 1H), 3.13 (s, 3H), 1.62 (d, *J* = 6.8 Hz, 3H), 1.51 (d, *J* = 6.4 Hz, 3H), 1.35 (app. d, *J* = 10.3 Hz, 12H); LCMS (HpH): t_R = 1.09 min, [M+H⁺] = 358.4 (87% purity).

***tert*-Butyl ((5-((*R*)-7-(2-methoxyethoxy)-1,3-dimethyl-2-oxo-2,3-dihydro-1*H*-benzo(*d*)azepin-5-yl)pyridin-2-yl)methyl)-*L*-threoninate, 3.64**



A solution of (*R*)-7-(2-methoxyethoxy)-1,3-dimethyl-5-(4,4,5,5-tetramethyl-1,3,2-dioxaborolan-2-yl)-1,3-dihydro-2*H*-benzo(*d*)azepin-2-one (**3.59**, 75 mg, 0.19 mmol), *tert*-butyl ((5-bromopyridin-2-yl)methyl)-*L*-threoninate (**3.47**, 80 mg, 0.23 mmol), Pd(PPh₃)₄ (22.4 mg, 0.02 mmol) and potassium carbonate (80 mg, 0.58 mmol) in 1,4-dioxane (1.3 mL) and water (0.65 mL) was stirred at 80°C for 1 h. The reaction mixture was partitioned between ethyl acetate (20 mL), water (20 mL) and brine (2 mL) was added. The aqueous layer was washed with further ethyl acetate (20 mL). The combined organic layers were dried (hydrophobic frit), concentrated *in vacuo* and purified by MDAP (Formic). The relevant fractions were concentrated under a stream of nitrogen to afford the title compound (**3.64**, 11 mg, 0.02 mmol, 10 % yield) as a white gum. ¹H NMR (400 MHz, CDCl₃) δ = 8.56 (d, *J* = 2.2 Hz, 1H), 7.56 (dd, *J* = 2.2, 8.1 Hz, 1H), 7.32 (d, *J* = 8.8 Hz, 1H), 7.30 (d, *J* = 8.1 Hz, 1H), 7.03 (dd, *J* = 2.4, 8.8 Hz, 1H), 6.55 (s, 1H), 6.53 (d, *J* = 2.4 Hz, 1H), 4.07 (d, *J* = 14.7 Hz, 1H), 4.03 - 3.93 (m, 2H), 3.89 (d, *J* = 14.7 Hz, 1H), 3.74 (qd, *J* = 6.4, 7.6 Hz, 1H), 3.65 (app. t, *J* = 4.9 Hz, 2H), 3.38 (s, 3H), 3.37 (q, *J* = 6.8 Hz, 1H), 3.16 (s, 3H), 3.01 (d, *J* = 7.6 Hz, 1H), 1.69 (d, *J* = 6.8 Hz, 3H), 1.50 (s, 9H), 1.25 (d, *J* = 6.4 Hz, 3H), NH and OH not observed; LCMS (HpH): t_R = 1.10 min, [M+H⁺] = 526.38 (98% purity).

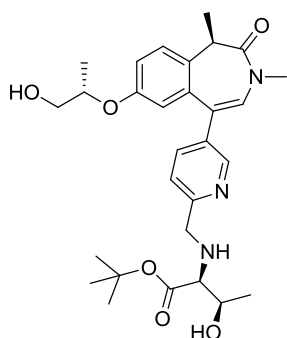
***tert*-Butyl ((5-((*R*)-7-(((*R*)-1-hydroxypropan-2-yl)oxy)-1,3-dimethyl-2-oxo-2,3-dihydro-1*H*-benzo(*d*)azepin-5-yl)pyridin-2-yl)methyl)-*L*-threoninate, 3.65**



A solution of (*R*)-7-(((*R*)-1-hydroxypropan-2-yl)oxy)-1,3-dimethyl-5-(4,4,5,5-tetramethyl-1,3,2-dioxaborolan-2-yl)-1,3-dihydro-2*H*-benzo(*d*)azepin-2-one (**3.60**, 75 mg, 0.16 mmol), *tert*-butyl ((5-bromopyridin-2-yl)methyl)-*L*-threoninate (**3.47**, 64.2 mg, 0.19 mmol), Pd(PPh₃)₄ (17.9 mg, 0.02 mmol) and potassium carbonate (64.2 mg, 0.47 mmol) in 1,4-dioxane (1.3 mL) and water (0.65 mL) was stirred at 80°C for 1 h. The reaction mixture was partitioned between ethyl acetate (20 mL) and water (20 mL). Brine (2 mL) was added. The aqueous layer was washed with further ethyl acetate (20 mL). The combined organic layers were dried (hydrophobic frit), concentrated *in vacuo* and purified by MDAP (Formic). The relevant fractions were concentrated under a stream of nitrogen and purified by MDAP (HpH). The relevant fractions were concentrated under a

stream of nitrogen afford the title compound (**3.65**, 10 mg, 0.02 mmol, 12 % yield) as a white gum. (α_D)^{20.9°C}_D(c = 2.0, CDCl₃): +60.0°; ν_{\max} (solution in CDCl₃): 3419, 2934, 2245, 1724, 1662 cm⁻¹; ¹H NMR (400 MHz, CDCl₃) δ = 8.57 (d, *J* = 2.2 Hz, 1H), 7.59 (dd, *J* = 2.2, 8.1 Hz, 1H), 7.34 (d, *J* = 8.1 Hz, 1H), 7.30 (d, *J* = 8.8 Hz, 1H), 7.04 (dd, *J* = 2.4, 8.8 Hz, 1H), 6.56 (s, 1H), 6.52 (d, *J* = 2.4 Hz, 1H), 4.39 - 4.31 (m, 1H), 4.07 (d, *J* = 14.7 Hz, 1H), 3.89 (d, *J* = 14.7 Hz, 1H), 3.73 (qd, *J* = 6.4, 7.6 Hz, 1H), 3.68 - 3.60 (m, 2H), 3.37 (q, *J* = 6.8 Hz, 1H), 3.17 (s, 3H), 2.99 (d, *J* = 7.6 Hz, 1H), 1.69 (d, *J* = 6.8 Hz, 3H), 1.50 (s, 9H), 1.24 (d, *J* = 6.4 Hz, 3H), 1.14 (d, *J* = 6.4 Hz, 3H), exchangeable protons not observed; ¹³C NMR (101 MHz, CDCl₃) δ = 172.6, 170.7, 158.4, 156.0, 149.0, 137.1, 136.3, 134.6, 131.0, 129.4, 127.2, 125.4, 121.8, 117.5, 115.3, 82.0, 75.0, 68.6, 68.2, 66.1, 40.6, 35.4, 28.1 (3C), 19.4, 15.7, 12.9, 1.0; LCMS (HpH): *t*_R = 1.01 min, [M+H⁺] = 526.39 (97% purity); HRMS: (C₂₉H₃₉N₃O₆) [M+H⁺] requires 526.2918, found [M+H⁺] = 526.2918.

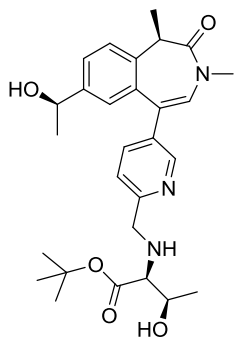
tert*-Butyl ((5-((*R*)-7-(((*S*)-1-hydroxypropan-2-yl)oxy)-1,3-dimethyl-2-oxo-2,3-dihydro-1*H*-benzo(*d*)azepin-5-yl)pyridin-2-yl)methyl)-L-threoninate, **3.66*



A solution of (*R*)-7-(((*S*)-1-hydroxypropan-2-yl)oxy)-1,3-dimethyl-5-(4,4,5,5-tetramethyl-1,3,2-dioxaborolan-2-yl)-1,3-dihydro-2*H*-benzo(*d*)azepin-2-one (**3.61**, 56.3 mg, 0.15 mmol), *tert*-butyl ((5-bromopyridin-2-yl)methyl)-L-threoninate (**3.47**, 53.1 mg, 0.15 mmol), Pd(PPh₃)₄ (10.2 mg, 8.83 μ mol) and potassium carbonate (63.4 mg, 0.46 mmol) in 1,4-dioxane (1 mL) and water (0.5 mL) was stirred at 80°C for 1 h. 9:1 DCM:MeOH (10 mL) was added to the cooled reaction mixture which was partitioned with water (10 mL). The aqueous layer was re-extracted with 9:1 DCM:MeOH (2 x 10 mL). The combined organic layers were dried (hydrophobic frit) and concentrated *in vacuo* to afford an orange oil. The oil was purified using MDAP (Formic). The fractions were diluted with brine (60 mL) and were partitioned with ethyl acetate (40 mL). The organic layer was dried (hydrophobic frit) and concentrated *in vacuo* to afford a light yellow solid. The solid was purified again by MDAP (Formic). The relevant fractions were combined, diluted with sodium bicarbonate (40 mL) and partitioned with ethyl acetate (70 mL). The organic layer was concentrated *in vacuo* to afford the title compound (**3.66**, 2.5 mg, 4.76 μ mol, 3 % yield). ¹H NMR (400 MHz, CDCl₃) δ = 8.57 (d, *J* = 2.5 Hz, 1H), 7.60 (dd, *J* = 2.5, 8.3 Hz, 1H), 7.35 (d, *J* = 8.3 Hz, 1H), 7.31 (d, *J* = 8.8 Hz, 1H), 7.03 (dd, *J* = 2.5, 8.8 Hz, 1H), 6.57 (s, 1H), 6.54 (d, *J* = 2.5 Hz, 1H), 4.38 - 4.29 (m, 1H), 4.08 (d, *J* = 14.2 Hz, 1H), 3.89 (d, *J* = 14.2 Hz, 1H), 3.72 (qd, *J* = 6.4, 7.6 Hz, 1H), 3.63 (d, *J* = 5.4 Hz, 2H), 3.37 (q, *J* = 6.8 Hz, 1H), 3.18 (s, 3H), 2.98 (d, *J* =

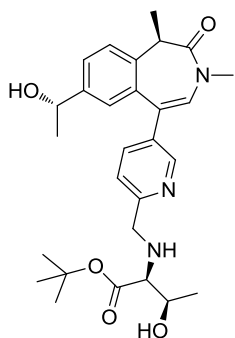
7.6 Hz, 1H), 1.70 (d, $J = 6.8$ Hz, 3H), 1.51 (s, 9H), 1.24 (d, $J = 6.4$ Hz, 3H), 1.21 (d, $J = 6.4$ Hz, 3H), exchangeable protons not observed; LCMS (HpH): $t_R = 1.02$ min, $[M+H^+] = 526.4$ (97 % purity).

***tert*-Butyl ((5-((*R*)-7-((*R*)-1-hydroxyethyl)-1,3-dimethyl-2-oxo-2,3-dihydro-1*H*-benzo(*d*)azepin-5-yl)pyridin-2-yl)methyl)-*L*-threoninate, 3.67**



A solution of (*R*)-7-((*R*)-1-hydroxyethyl)-1,3-dimethyl-5-(4,4,5,5-tetramethyl-1,3,2-dioxaborolan-2-yl)-1,3-dihydro-2*H*-benzo(*d*)azepin-2-one (**3.62**, 50 mg, 0.13 mmol), *tert*-butyl ((5-bromopyridin-2-yl)methyl)-*L*-threoninate (**3.47**, 52.2 mg, 0.15 mmol), Pd(PPh₃)₄ (7.28 mg, 6.30 μmol) and potassium carbonate (52.2 mg, 0.38 mmol) in 1,4-dioxane (0.75 mL) and water (0.38 mL) were stirred at 80°C for 10 min. The reaction mixture was partitioned between ethyl acetate (20 mL) and water (20 mL). The aqueous phase was re-extracted with 8:2 DCM:MeOH (20 mL). The organic layer was dried (hydrophobic frit) and concentrated *in vacuo*. The residue was purified by MDAP (HpH) to afford the title compound (**3.67**, 22 mg, 0.04 mmol, 35 % yield) as a yellow gummy oil. ¹H NMR (400 MHz, CDCl₃) $\delta = 8.55$ (d, $J = 2.2$ Hz, 1H), 7.58 (dd, $J = 2.2, 8.3$ Hz, 1H), 7.47 (dd, $J = 2.0, 8.3$ Hz, 1H), 7.38 (d, $J = 8.3$ Hz, 1H), 7.34 (d, $J = 8.3$ Hz, 1H), 6.99 (d, $J = 2.0$ Hz, 1H), 6.58 (s, 1H), 4.80 (q, $J = 6.4$ Hz, 1H), 4.07 (d, $J = 14.2$ Hz, 1H), 3.89 (d, $J = 14.2$ Hz, 1H), 3.77 - 3.69 (m, 1H), 3.40 (q, $J = 6.8$ Hz, 1H), 3.16 (s, 3H), 3.00 (d, $J = 7.3$ Hz, 1H), 1.71 (d, $J = 6.8$ Hz, 3H), 1.50 (s, 9H), 1.39 (d, $J = 6.8$ Hz, 3H), 1.24 (d, $J = 6.4$ Hz, 3H), exchangeable protons not observed; LCMS (HpH): $t_R = 0.96$ min, $[M+H^+] = 496.4$ (94% purity).

***tert*-Butyl ((5-((*R*)-7-((*S*)-1-hydroxyethyl)-1,3-dimethyl-2-oxo-2,3-dihydro-1*H*-benzo(*d*)azepin-5-yl)pyridin-2-yl)methyl)-*L*-threoninate, 3.68**

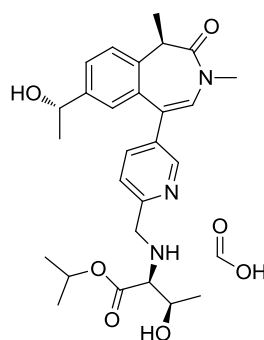


A solution of (*R*)-7-((*S*)-1-hydroxyethyl)-1,3-dimethyl-5-(4,4,5,5-tetramethyl-1,3,2-dioxaborolan-2-yl)-1,3-dihydro-2*H*-benzo(*d*)azepin-2-one (**3.63**, 50 mg, 0.12 mmol), *tert*-butyl ((5-bromopyridin-2-yl)methyl)-*L*-threoninate (**3.47**, 49.3 mg, 0.14 mmol), Pd(PPh₃)₄ (6.87 mg, 5.95 μmol) and potassium carbonate (49.3 mg, 0.36 mmol) in 1,4-dioxane (0.75 mL) and water (0.38 mL) were stirred at 80°C for 10 min. The reaction mixture was partitioned between ethyl acetate (20 mL) and water (20 mL). The aqueous phase was re-extracted with 8:2 DCM:MeOH (20 mL). The organic layer was dried (hydrophobic frit) and concentrated *in vacuo*. The residue

was purified by MDAP (HpH) to afford the title compound (**3.68**, 23 mg, 0.05 mmol, 39 % yield) as a yellow gummy oil. (α_D)^{20.9°C} λ (c = 2.0, CDCl₃): +4.5°; ν_{\max} (solution in CDCl₃): 3389, 2976, 1724, 1667, 1369 cm⁻¹; ¹H NMR (400 MHz, CDCl₃) δ = 8.54 (d, *J* = 2.5 Hz, 1H), 7.58 (dd, *J* = 2.5, 8.3 Hz, 1H), 7.45 (dd, *J* = 2.0, 8.3 Hz, 1H), 7.38 (d, *J* = 8.3 Hz, 1H), 7.34 (d, *J* = 8.3 Hz, 1H), 7.01 (d, *J* = 2.0 Hz, 1H), 6.58 (s, 1H), 4.80 (q, *J* = 6.4 Hz, 1H), 4.07 (d, *J* = 14.7 Hz, 1H), 3.88 (d, *J* = 14.7 Hz, 1H), 3.73 (qd, *J* = 6.4, 7.6 Hz, 1H), 3.40 (q, *J* = 6.8 Hz, 1H), 3.16 (s, 3H), 3.00 (d, *J* = 7.6 Hz, 1H), 1.71 (d, *J* = 6.8 Hz, 3H), 1.49 (s, 9H), 1.40 (d, *J* = 6.4 Hz, 3H), 1.24 (d, *J* = 6.4 Hz, 3H), exchangeable protons not observed; ¹³C NMR (101 MHz, CDCl₃) δ = 172.7, 162.6, 159.2, 157.3, 149.5, 145.7, 143.0, 136.8, 136.4, 136.0, 130.8, 129.6, 123.4, 122.9, 112.8, 108.6, 101.2, 81.6, 68.6, 68.0, 55.5, 47.9, 38.2, 28.0 (3C), 19.3, 17.3; LCMS (HpH): *t*_R = 0.95 min, [M+H⁺] = 496.4 (85% purity); HRMS: (C₂₈H₃₇N₃O₅) [M+H⁺] requires 497.2888, found [M+H⁺] = 496.2811.

Isopropyl

((5-((*R*)-7-((*S*)-1-hydroxyethyl)-1,3-dimethyl-2-oxo-2,3-dihydro-1*H*-benzo(*d*)azepin-5-yl)pyridin-2-yl)methyl)-L-threoninate, formic acid salt, **3.69**

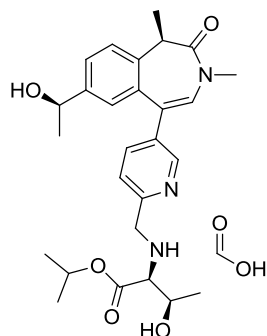


A solution of (*R*)-7-((*S*)-1-hydroxyethyl)-1,3-dimethyl-5-(4,4,5,5-tetramethyl-1,3,2-dioxaborolan-2-yl)-1,3-dihydro-2*H*-

benzo(*d*)azepin-2-one (**3.63**, 50 mg, 0.12 mmol), isopropyl ((5-bromopyridin-2-yl)methyl)-L-threoninate (**3.71**, 47 mg, 0.14 mmol), Pd(PPh₃)₄ (6.87 mg, 5.95 μmol) and potassium carbonate (49.3 mg, 0.36 mmol) in 1,4-dioxane (1 mL) and water (0.50 mL) were stirred

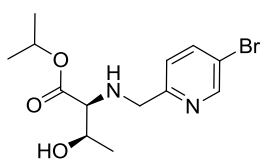
at 80°C for 10 min. The reaction mixture was concentrated *in vacuo* and purified by MDAP (HpH) to afford the title compound (**3.69**, 28.8 mg, 0.06 mmol, 46 % yield) as a yellow gummy oil. (α_D)^{23.2°C} λ (c = 1.0, MeOH): +31.9°; ν_{\max} (solution in CDCl₃): 3408, 1726, 1662, 1455, 1105 cm⁻¹; ¹H NMR (400 MHz, CDCl₃) δ = 8.55 (s, 1H), 7.59 (d, *J* = 7.8 Hz, 1H), 7.45 (d, *J* = 8.3 Hz, 1H), 7.39 (d, *J* = 8.3 Hz, 1H), 7.33 (d, *J* = 7.8 Hz, 1H), 7.01 (s, 1H), 6.59 (s, 1H), 5.09 (app. spt, *J* = 6.4 Hz, 1H), 4.81 (q, *J* = 6.4 Hz, 1H), 4.09 (d, *J* = 14.2 Hz, 1H), 3.94 (d, *J* = 14.2 Hz, 1H), 3.84 - 3.75 (m, 1H), 3.40 (q, *J* = 6.8 Hz, 1H), 3.17 (s, 3H), 3.11 (d, *J* = 7.8 Hz, 1H), 1.72 (d, *J* = 6.4 Hz, 3H), 1.40 (d, *J* = 6.8 Hz, 3H), 1.28 (app dd, *J* = 2.0, 6.4 Hz, 6H), 1.25 (br d, *J* = 6.4 Hz, 3H), exchangeable protons not observed; ¹³C NMR (101 MHz, CDCl₃) δ = 172.7, 170.4, 149.1, 149.0, 149.0, 146.7, 144.2, 137.3, 137.1, 136.9, 135.2, 129.5, 126.7, 124.7, 124.4, 92.8, 77.2, 69.9, 69.1, 68.1, 41.2, 35.4, 25.2, 21.9, 21.8, 19.4, 12.8; LCMS (HpH): *t*_R = 0.92 min, [M+H⁺] = 482.7 (100% purity); HRMS (C₂₇H₃₅N₃O₅) [M+H⁺] requires 482.2656, found [M+H⁺] 482.2652.

Isopropyl ((5-((*R*)-7-((*R*)-1-hydroxyethyl)-1,3-dimethyl-2-oxo-2,3-dihydro-1*H*-benzo(*d*)azepin-5-yl)pyridin-2-yl)methyl)-L-threoninate formic acid salt, 3.70



A solution of (*R*)-7-((*R*)-1-hydroxyethyl)-1,3-dimethyl-5-(4,4,5,5-tetramethyl-1,3,2-dioxaborolan-2-yl)-1,3-dihydro-2*H*-benzo(*d*)azepin-2-one (**3.62**, 50 mg, 0.13 mmol), isopropyl ((5-bromopyridin-2-yl)methyl)-L-threoninate (**3.71**, 50.1 mg, 0.15 mmol), Pd(PPh₃)₄ (7.28 mg, 6.30 μmol) and potassium carbonate (52.2 mg, 0.38 mmol) in 1,4-dioxane (1 mL) and water (0.50 mL) were stirred at 80°C for 10 min. The reaction mixture was concentrated *in vacuo* and purified by MDAP (HpH) to afford the title compound (**3.70**, 33 mg, 0.06 mmol, 50 % yield) as a yellow gummy oil. (α_D)^{23.2°C} (*c* = 1.0, CDCl₃): +75.7°; ν_{\max} (solution in CDCl₃): 3247, 2979, 1663, 1375, 1104 cm⁻¹; ¹H NMR (400 MHz, CDCl₃) δ = 8.58 (d, *J* = 2.0 Hz, 1H), 8.08 (br s, 1H, formic acid salt), 7.67 (dd, *J* = 2.0, 8.3 Hz, 1H), 7.48 (dd, *J* = 2.0, 8.3 Hz, 1H), 7.40 (d, *J* = 8.3 Hz, 1H), 7.38 (d, *J* = 8.3 Hz, 1H), 6.99 (d, *J* = 2.0 Hz, 1H), 6.62 (s, 1H), 5.11 (app. spt, *J* = 6.4 Hz, 1H), 4.80 (q, *J* = 6.4 Hz, 1H), 4.15 (d, *J* = 14.2 Hz, 1H), 3.98 (d, *J* = 14.2 Hz, 1H), 3.87 (qd, *J* = 6.4, 7.3 Hz, 1H), 3.40 (q, *J* = 6.8 Hz, 1H), 3.18 (s, 3H), 3.16 (d, *J* = 7.3 Hz, 1H), 1.72 (d, *J* = 6.8 Hz, 3H), 1.41 (d, *J* = 6.4 Hz, 3H), 1.29 (app. dd, *J* = 2.9, 6.4 Hz, 6H), 1.27 (d, *J* = 6.4 Hz, 3H), exchangeable protons not observed; ¹³C NMR (101 MHz, CDCl₃) δ = 172.8, 170.4, 158.2, 149.0, 144.2, 137.1, 137.0, 135.1, 134.7, 129.4, 127.4, 126.7, 124.6, 124.5, 121.9, 69.9, 68.9, 68.1, 68.1, 53.4, 41.2, 35.4, 25.4, 21.9, 21.8, 19.4, 12.84; LCMS (HpH): *t*_R = 0.92 min, [M+H⁺] = 482.7 (100% purity); HRMS (C₂₇H₃₆N₃O₅) [M+H⁺] requires 482.2656, found [M+H⁺] 482.2654.

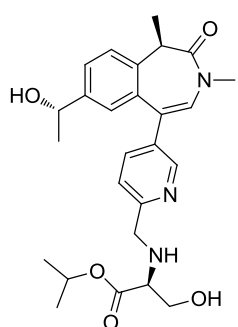
Isopropyl ((5-bromopyridin-2-yl)methyl)-L-threoninate, 3.71



A solution of 5-bromopicolinaldehyde (500 mg, 2.69 mmol), isopropyl L-threoninate hydrochloride (**2.19**, 797 mg, 4.03 mmol), DIPEA (0.94 mL, 5.38 mmol) and acetic acid (0.39 mL, 6.72 mmol) in THF (10 mL) was stirred at 40°C for 2 h. The solution was left to cool to rt, then sodium triacetoxyborohydride (1.42 g, 6.72 mmol) was added and the reaction mixture was stirred at rt for 30 min. The reaction mixture was quenched with water (30 mL) and the aqueous layer was extracted with 8:2 DCM in MeOH (100 mL). The organic layer was dried (hydrophobic frit) and concentrated *in vacuo*. The residue was purified by flash column chromatography (silica, 0-100% ethyl acetate in cyclohexane) to afford the title compound (**3.71**, 683 mg, 1.96 mmol, 73 % yield) as an oil. (α_D)^{20.9°C} (*c* = 2.0,

CDCl₃): -25.9°; ν_{\max} (solution in CDCl₃): 3323, 2980, 1726, 1467, 1186 cm⁻¹; ¹H NMR (400 MHz, CDCl₃) δ = 8.60 (d, J = 2.5 Hz, 1H), 7.78 (dd, J = 2.4, 8.3 Hz, 1H), 7.24 (d, J = 8.3 Hz, 1H), 5.05 (app. spt, J = 6.3 Hz, 1H), 3.96 (d, J = 14.7 Hz, 1H), 3.82 (d, J = 14.7 Hz, 1H), 3.74 (qd, J = 6.4, 7.3 Hz, 1H), 3.01 (d, J = 7.3 Hz, 1H), 1.25 (d, J = 6.3 Hz, 6H), 1.22 (d, J = 6.3 Hz, 3H), NH and OH not observed; ¹³C NMR (101 MHz, CDCl₃) δ = 172.8, 157.6, 150.3, 139.1, 123.4, 119.1, 68.9, 68.1, 67.8, 53.2, 21.9, 21.8, 19.3; LCMS (Formic): t_R = 0.61 min, [M+H⁺] = 331.05 / 333.06 (98% purity); HRMS: (C₁₃H₁₉BrN₂O₃) [M+H⁺] requires 331.0658, found [M+H⁺] = 331.0653.

Isopropyl ((5-((*R*)-7-((*S*)-1-hydroxyethyl)-1,3-dimethyl-2-oxo-2,3-dihydro-1*H*-benzo(*d*)azepin-5-yl)pyridin-2-yl)methyl)-L-serinate, 3.72



Method 1, Scheme 3.12

5-((*R*)-7-((*S*)-1-Hydroxyethyl)-1,3-dimethyl-2-oxo-2,3-dihydro-1*H*-benzo(*d*)azepin-5-yl)picolinaldehyde (**3.76**, 8.3 mg, 0.03 mmol) and isopropyl L-serinate tosic acid salt²²⁵ (**2.87**, 11.8 mg, 0.04 mmol) were dissolved in DCM (0.5 mL) and stirred at rt for 1 h. Triethylamine (10.32 μ l, 0.07 mmol) and sodium triacetoxyborohydride (10.5 mg, 0.05 mmol) were added and the reaction mixture was stirred for 4 h.

The reaction mixture was quenched with water (5 mL) and partitioned with 9:1 DCM:MeOH (5 mL). The layers were separated and the organic layer was re-extracted with 9:1 DCM:MeOH (5 mL). The combined organic layers were dried (hydrophobic frit) and concentrated under reduced pressure. The residue was purified by MDAP (HpH) to afford the title compound (**3.72**, 3.0 mg, 6.42 μ mol, 26 % yield) as a yellow oil.

Method 2, Scheme 3.14

A solution of (*R*)-7-((*S*)-1-hydroxyethyl)-1,3-dimethyl-5-(4,4,5,5-tetramethyl-1,3,2-dioxaborolan-2-yl)-1,3-dihydro-2*H*-benzo(*d*)azepin-2-one (**3.63**, 100 mg, 0.24 mmol), isopropyl ((5-bromopyridin-2-yl)methyl)-L-serinate²²⁵ (**3.74**, 91 mg, 0.29 mmol), Pd(PPh₃)₄ (13.8 mg, 0.01 mmol) and potassium carbonate (99 mg, 0.71 mmol) in 1,4-dioxane (2 mL) and water (1.00 mL) was stirred at 80°C for 10 min. The reaction mixture was diluted with water (5 mL) and partitioned with 9:1 DCM:MeOH (10 mL). The layers were separated and the organic layer was re-extracted with 9:1 DCM:MeOH (10 mL). The combined organic layers were concentrated under a stream of nitrogen and the resultant residue purified by flash column chromatography (KP-NH column, 0-100% ethyl acetate in cyclohexane

followed by 0-30% ethanol in ethyl acetate) to afford the title compound (**3.72**, 32 mg, 0.07 mmol, 29 % yield) as a yellow gummy oil.

Method 3, Table 3.40 Entry 6

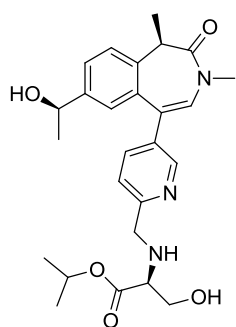
To a solution of (*R*)-7-((*S*)-1-hydroxyethyl)-1,3-dimethyl-5-(4,4,5,5-tetramethyl-1,3,2-dioxaborolan-2-yl)-1,3-dihydro-2*H*-benzo(*d*)azepin-2-one (**3.63**, 50 mg, 0.08 mmol), PdCl₂(dppf)·DCM adduct (3.14 mg, 3.85 μmol) and isopropyl ((5-bromopyridin-2-yl)methyl)-*L*-serinate (**3.74**, 24.4 mg, 0.08 mmol) in 1,4-dioxane (1 mL) was added a solution of potassium carbonate (31.9 mg, 0.23 mmol) in water (0.50 mL). The resultant solution was stirred at 80°C for 1 h. The reaction mixture was diluted with water (10 mL) and partitioned with 9:1 DCM:MeOH (10 mL). The layers were separated and the organic layer was re-extracted with 9:1 DCM:MeOH (10 mL). The combined organic layers were dried (hydrophobic frit) and concentrated under reduced pressure. The residue was purified by flash column chromatography (silica, 0-100% water-saturated ethyl acetate in cyclohexane, 0-30% ethanol in water saturated ethyl acetate) to afford the title compound (**3.72**, 23 mg, 0.05 mmol, 64 % yield) as a yellow oil.

Method 4, Scheme 3.47

A solution of isopropyl *O*-(*tert*-butyldimethylsilyl)-*N*-((5-((*R*)-7-((*S*)-1-hydroxyethyl)-1,3-dimethyl-2-oxo-2,3-dihydro-1*H*-benzo(*d*)azepin-5-yl)pyridin-2-yl)methyl)-*L*-serinate (**3.154**, 10 mg, 0.02 mmol) in 2M aqueous hydrochloric acid (0.5 mL, 1.00 mmol) and ethanol (0.5 mL) was stirred at 60°C for 2 h. The reaction mixture was neutralised to ~pH 8 with saturated aqueous sodium bicarbonate and partitioned with DCM (5 mL). The aqueous layer was re-extracted with 9:1 DCM:MeOH. The combined organic layers were dried (hydrophobic frit) and concentrated under reduced pressure to afford the title compound (**3.72**, 6.8 mg, 0.02 mmol, 85 % yield) as a yellow gum.

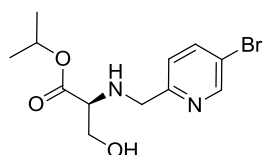
¹H NMR (400 MHz, CDCl₃) δ = 8.54 (d, *J* = 2.2 Hz, 1H), 7.58 (dd, *J* = 2.2, 8.1 Hz, 1H), 7.45 (dd, *J* = 2.0, 8.3 Hz, 1H), 7.38 (d, *J* = 8.3 Hz, 1H), 7.31 (d, *J* = 8.3 Hz, 1H), 7.00 (d, *J* = 2.0 Hz, 1H), 6.58 (s, 1H), 5.09 (app. spt, *J* = 6.3 Hz, 1H), 4.80 (q, *J* = 6.4 Hz, 1H), 4.12 (d, *J* = 14.7 Hz, 1H), 3.93 (d, *J* = 14.7 Hz, 1H), 3.83 (dd, *J* = 4.4, 11.0 Hz, 1H), 3.69 (dd, *J* = 6.6, 11.0 Hz, 1H), 3.49 (dd, *J* = 4.4, 6.6 Hz, 1H), 3.40 (q, *J* = 6.8 Hz, 1H), 3.17 (s, 3H), 1.72 (d, *J* = 6.8 Hz, 3H), 1.40 (d, *J* = 6.4 Hz, 3H), 1.28 (app. dd, *J* = 4.9, 6.3 Hz, 6H), exchangeable protons not observed; LCMS (Formic): t_R = 0.58 min, [M+H⁺] = 468.4 (100% purity).

Isopropyl ((5-((R)-7-((R)-1-hydroxyethyl)-1,3-dimethyl-2-oxo-2,3-dihydro-1H-benzo(d)azepin-5-yl)pyridin-2-yl)methyl)-L-serinate, 3.73



5-((R)-7-((R)-1-Hydroxyethyl)-1,3-dimethyl-2-oxo-2,3-dihydro-1H-benzo(d)azepin-5-yl)picolinaldehyde (**3.77**, 40 mg, 0.12 mmol) and isopropyl L-serinate tosic acid salt²²⁵ (**2.87**, 57.0 mg, 0.18 mmol) were dissolved in DCM (0.5 mL) and stirred at rt for 1 h. Triethylamine (0.05 mL, 0.36 mmol) and sodium triacetoxyborohydride (50.4 mg, 0.24 mmol) were added and the reaction mixture was stirred for 4 h. The reaction mixture was quenched with water (5 mL) and partitioned with 9:1 DCM:MeOH (5 mL). The layers were separated and the organic layer was re-extracted with 9:1 DCM:MeOH (5 mL). The combined organic layers were dried (hydrophobic frit) and concentrated under reduced pressure. The residue was purified by MDAP (HpH) to afford the title compound (**3.73**, 20 mg, 0.04 mmol, 36 % yield) as a yellow oil. (α_D)^{20.9°C} λ (c = 1.0, CDCl₃): +93.0°; ν_{max} (solution in CDCl₃): 3405, 1728, 1660, 1376, 1195, cm⁻¹; ¹H NMR (400 MHz, CDCl₃) δ = 8.55 (d, *J* = 2.2 Hz, 1H), 7.59 (dd, *J* = 2.2, 8.1 Hz, 1H), 7.47 (dd, *J* = 2.0, 8.1 Hz, 1H), 7.39 (d, *J* = 8.1 Hz, 1H), 7.32 (d, *J* = 8.1 Hz, 1H), 6.98 (d, *J* = 2.0 Hz, 1H), 6.58 (s, 1H), 5.09 (app. spt, *J* = 6.4 Hz, 1H), 4.80 (q, *J* = 6.4 Hz, 1H), 4.12 (dd, *J* = 5.0, 14.7 Hz, 1H), 3.94 (dd, *J* = 3.0, 14.7 Hz, 1H), 3.84 (ddd, *J* = 2.9, 4.4, 10.8 Hz, 1H), 3.70 (dd, *J* = 6.8, 10.8 Hz, 1H), 3.50 (dd, *J* = 4.4, 10.8 Hz, 1H), 3.40 (q, *J* = 6.8 Hz, 1H), 3.16 (s, 3H), 1.72 (d, *J* = 6.8 Hz, 3H), 1.39 (d, *J* = 6.4 Hz, 3H), 1.28 (app. dd, *J* = 4.4, 6.4 Hz, 6H), exchangeable protons not observed; ¹³C NMR (101 MHz, CDCl₃) δ = 172.2, 170.4, 158.4, 149.0, 144.3, 137.2, 137.0, 135.1, 134.8, 129.4, 127.4, 126.7, 124.6, 124.4, 122.0, 69.9, 69.1, 62.8, 62.6, 52.6, 41.2, 35.4, 25.4, 21.9, 21.8, 12.8; LCMS (HpH): *t*_R = 0.86 min, [M+H⁺] = 468.4 (99% purity); HRMS: (C₂₆H₃₃N₃O₅) [M+H⁺] requires 468.2578, found [M+H⁺] = 468.2496.

Isopropyl ((5-bromopyridin-2-yl)methyl)-L-serinate, 3.74



Method 1, Scheme 3.13

A solution of 5-bromopicolinaldehyde (248 mg, 1.33 mmol), (*S*)-isopropyl 2-amino-3-hydroxypropanoate tosic acid salt²²⁵ (**2.87**, 639 mg, 2.00 mmol) and triethylamine (0.37 mL, 2.67 mmol) in DCM (15 mL) was stirred at 40°C for 2.5 h. The reaction mixture was cooled to rt before sodium triacetoxyborohydride (698 mg, 3.29 mmol) was added. The reaction mixture was left to stir at rt for 2 h and was then left with no stirring overnight. The reaction mixture was quenched by the slow addition of water (30 mL) and partitioned with 9:1 DCM:MeOH (15 mL). The

aqueous layer was re-extracted with 9:1 DCM:MeOH (2 x 15 mL). The combined organic layers were washed with sodium bicarbonate (30 mL), dried (hydrophobic frit) and concentrated *in vacuo* to afford a yellow oil. The oil was left to dry in a vacuum oven at 45°C to afford the title compound (**3.74**, 356 mg, 1.12 mmol, 84 % yield), a yellow solid.

Method 2, Scheme 3.42

A solution of (5-bromopyridin-2-yl)methyl methanesulfonate (**3.149**, 50 mg, 0.19 mmol), isopropyl L-serinate 4-methylbenzenesulfonate²²⁵ (**2.87**, 90 mg, 0.28 mmol) and DIPEA (0.33 mL, 1.88 mmol) in THF (0.5 mL) was stirred at 100°C in a microwave reactor for 1 h. The reaction mixture was passed over an aminopropyl column and washed with methanol (5 mL). The filtrate was concentrated under reduced pressure then dissolved in ethyl acetate (10 mL) and was partitioned with water (10 mL). The aqueous layer was re-extracted with ethyl acetate (3 x 10 mL). The combined organic layers were dried (hydrophobic frit) before being concentrated *in vacuo* to afford a yellow oil. The oil was purified by flash column chromatography (alumina, 0-100 % ethyl acetate in cyclohexane then 0-30 % ethanol in ethyl acetate) to afford the title compound (**3.74**, 19 mg, 0.06 mmol, 32 % yield) as a yellow solid.

Method 3, Scheme 3.45

A solution of (5-bromopyridin-2-yl)methyl methanesulfonate (**3.149**, 500 mg, 1.88 mmol), isopropyl L-serinate (**3.103**, 415 mg, 2.82 mmol) and DIPEA (0.33 mL, 1.88 mmol) in THF (20 mL) was stirred at 80°C for 16.5 h. Further isopropyl L-serinate (138 mg, 0.94 mmol) in THF (2 mL) was added to the reaction mixture and the resultant solution was stirred at 80°C for 7 h. The reaction mixture was left to stand at rt for 63.75 h. The reaction mixture was diluted with DCM:MeOH (20 mL) and was partitioned with water (20 mL). The aqueous layer was re-extracted with DCM:MeOH (3 x 20 mL). The combined organic layers were dried (hydrophobic frit) and concentrated *in vacuo* to afford an orange oil. The oil was purified by flash column chromatography (C18 silica, 15-55 % acetonitrile in aqueous ammonium bicarbonate pH 10) to afford the title compound (**3.74**, 438 mg, 1.38 mmol, 74 % yield) as an orange oil. Chiral analysis conducted on a 250 mm x 46 mm Chiralpak ID 5µm column, eluting with a gradient of 20% ethanol in heptane (+0.1% isopropylamine) at a flow rate of 1 mL/min showed the compound to have an e.e of 98%.

Method 4, Scheme 3.46

A solution of (5-bromopyridin-2-yl)methyl 4-methylbenzenesulfonate (**3.152**, 50 mg, 0.15 mmol), isopropyl L-serinate (**3.103**, 32.3 mg, 0.22 mmol) and DIPEA (26 μ L, 0.15 mmol) in THF (2 mL) was stirred at 80°C for 22 h. The reaction mixture was diluted with 9:1 DCM:MeOH (10 mL) and partitioned with water (10 mL). The aqueous layer was re-extracted with 9:1 DCM:MeOH (3 x 10 mL). The combined organic layers were dried (hydrophobic frit) and concentrated *in vacuo* to afford a light brown oil. The oil was purified by flash column chromatography (silica, 0-100 % water saturated ethyl acetate in cyclohexane). The fraction was concentrated *in vacuo* to afford the title compound (**3.74**, 19 mg, 0.06 mmol, 41 % yield) as an oil. Chiral analysis conducted on a 250 mm x 46 mm Chiralpak ID 5 μ m column, eluting with a gradient of 20% ethanol in heptane (+0.1% isopropylamine) at a flow rate of 1 mL/min showed the compound to have an e.e of 95%.

(α_D)^{20.9°C} _{λ} (c = 2.0, CDCl₃): -10.8°; ν_{\max} (solution in CDCl₃): 3319, 2976, 1728, 1364 cm⁻¹; ¹H NMR (400 MHz, CDCl₃) δ = 8.61 (d, *J* = 2.5 Hz, 1H), 7.78 (dd, *J* = 2.5, 8.3 Hz, 1H), 7.23 (d, *J* = 8.3 Hz, 1H), 5.07 (app. spt, *J* = 6.3 Hz, 1H), 4.02 (d, *J* = 14.7 Hz, 1H), 3.87 (d, *J* = 14.7 Hz, 1H), 3.81 (dd, *J* = 4.2, 11.0 Hz, 1H), 3.67 (dd, *J* = 6.4, 11.0 Hz, 1H), 3.44 (dd, *J* = 4.2, 6.4 Hz, 1H), 2.88 - 2.76 (br s, 2H), 1.26 (app. dd, *J* = 3.9, 6.4 Hz, 6H); ¹³C NMR (101 MHz, CDCl₃) δ = 172.1, 157.7, 150.4, 139.2, 123.4, 119.1, 69.1, 62.6, 62.5, 52.5, 21.8, 21.8; LCMS (HpH): *t*_R = 0.85 min, [M+H⁺] = 317.1 / 319.2 (96 % purity); HRMS: (C₁₂H₁₇BrN₂O₂) [M+H⁺] requires 317.0502, found [M+H⁺] = 317.0496.

***tert*-Butyl ((5-bromopyridin-2-yl)methyl)-L-serinate, 3.75, Scheme 3.44**



Method 1, Scheme 3.44

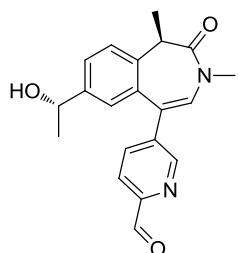
A solution of (5-bromopyridin-2-yl)methyl methanesulfonate (**3.149**, 600 mg, 2.26 mmol), *tert*-butyl L-serinate (**3.150**, 727 mg, 4.51 mmol) and DIPEA (0.39 mL, 2.26 mmol) in THF (20 mL) was stirred at 80°C for 40.5 h. The reaction mixture was diluted with 9:1 DCM:MeOH (20 mL) and partitioned with water (30 mL). The aqueous layer was re-extracted with 9:1 DCM:MeOH (3 x 20 mL). The combined organic layers were dried (hydrophobic frit) before being concentrated *in vacuo* to afford an orange oil. The oil was purified by flash column chromatography (C18 silica, 15-55 % acetonitrile in aqueous ammonium bicarbonate pH 10) to afford the title compound (**3.75**, 546 mg, 1.65 mmol, 73 % yield) as white needles.

Method 2, Scheme 3.13

A solution of 5-bromopicolinaldehyde (254 mg, 1.37 mmol), *tert*-butyl *L*-serinate hydrochloride (**2.90**, 400 mg, 2.02 mmol) and triethylamine (0.38 mL, 2.73 mmol) in DCM (15 mL) was stirred at 40°C for 2.5 h. The reaction mixture was allowed to cool to rt before sodium triacetoxyborohydride (727 mg, 3.43 mmol) was added. The reaction mixture was left to stir for 1.5 h at rt. The reaction mixture was quenched by the slow addition of water (30 mL) and partitioned with 9:1 DCM:MeOH (15 mL). The aqueous layer was re-extracted with 9:1 DCM:MeOH (2 x 15 mL). The combined organic layers were washed with sodium bicarbonate (30 mL), dried (hydrophobic frit) and concentrated *in vacuo* to afford a yellow solid. The solid was left to dry in a vacuum oven at 45°C overnight afford the title compound (**3.75**, 389 mg, 1.17 mmol, 86 % yield) as a yellow solid.

M.pt.: 95.2-98.8°C; (α_D)^{20.9°C}_D(c = 1.0, CDCl₃): -26.0°; ν_{max} (solution in CDCl₃): 3319, 2978, 1728, 1368, 1156 cm⁻¹; ¹H NMR (400 MHz, CDCl₃) δ = 8.61 (d, *J* = 2.4 Hz, 1H), 7.77 (dd, *J* = 2.4, 8.3 Hz, 1H), 7.23 (d, *J* = 8.3 Hz, 1H), 4.00 (d, *J* = 14.7 Hz, 1H), 3.84 (d, *J* = 14.7 Hz, 1H), 3.77 (dd, *J* = 4.4, 11.0 Hz, 1H), 3.62 (dd, *J* = 6.6, 11.0 Hz, 1H), 3.36 (dd, *J* = 4.4, 6.6 Hz, 1H), 2.94 (br s, 1H), 2.47 (br s, 1H), 1.47 (s, 9H); ¹³C NMR (101 MHz, CDCl₃) δ = 171.9, 158.0, 150.4, 139.2, 123.4, 119.0, 103.7, 82.0, 77.2, 63.0, 62.7, 52.6, 28.1; LCMS (HpH): *t*_R = 0.92 min, [M+H⁺] = 331.2 / 333.2 (100 % purity); HRMS: (C₁₃H₁₉BrN₂O₃) [M+H⁺] requires 331.0658, found [M+H⁺] = 331.0653.

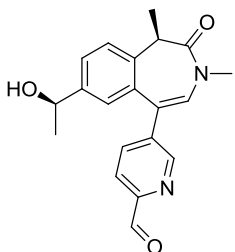
5-((*R*)-7-((*S*)-1-Hydroxyethyl)-1,3-dimethyl-2-oxo-2,3-dihydro-1*H*-benzo(*d*)azepin-5-yl)picolinaldehyde, 3.76



A solution of (*R*)-7-((*S*)-1-hydroxyethyl)-1,3-dimethyl-5-(4,4,5,5-tetramethyl-1,3,2-dioxaborolan-2-yl)-1,3-dihydro-2*H*-benzo(*d*)azepin-2-one (**3.63**, 50 mg, 0.12 mmol), 5-bromopicolinaldehyde (26.6 mg, 0.14 mmol), Pd(PPh₃)₄ (6.87 mg, 5.95 μ mol) and potassium carbonate (49.3 mg, 0.36 mmol) in 1,4-dioxane (1 mL) and water (0.50 mL) were stirred at 80°C for 10 min. The reaction mixture was diluted with water (5 mL) and partitioned with 9:1 DCM:MeOH (10 mL). The layers were separated and the organic layer was re-extracted with 9:1 DCM:MeOH (10 mL). The combined organic layers were concentrated under a stream of nitrogen and the resultant residue purified by MDAP (HpH) to afford the title compound (**3.76**, 8.8 mg, 0.03 mmol, 22 % yield) as an orange gummy oil. ¹H NMR (400 MHz, CDCl₃) δ = 10.11 (d, *J* = 1.0 Hz, 1H), 8.77 (d, *J* = 2.0 Hz, 1H), 7.98 (dd, *J* = 1.0, 8.3 Hz, 1H), 7.82 (dd, *J* = 1.0, 8.3 Hz, 1H), 7.49

(dd, $J = 2.0, 8.3$ Hz, 1H), 7.41 (d, $J = 8.3$ Hz, 1H), 7.00 (d, $J = 2.0$ Hz, 1H), 6.72 (s, 1H), 4.82 (br q, $J = 6.4$ Hz, 1H), 3.42 (q, $J = 6.8$ Hz, 1H), 3.21 (s, 3H), 1.73 (d, $J = 6.8$ Hz, 3H), 1.40 (d, $J = 6.4$ Hz, 3H); LCMS (HpH): $t_R = 0.83$ min, $[M+H^+] = 337.3$ (73% purity), Hydrate $t_R = 0.54$ mins, $[M+H^+] = 353.3$ (10% purity).

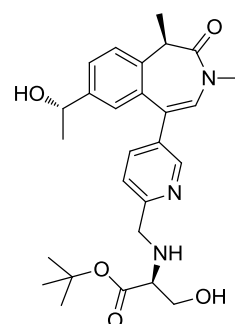
5-((*R*)-7-((*R*)-1-Hydroxyethyl)-1,3-dimethyl-2-oxo-2,3-dihydro-1*H*-benzo(*d*)azepin-5-yl)picolinaldehyde, 3.77



A solution of (*R*)-7-((*R*)-1-hydroxyethyl)-1,3-dimethyl-5-(4,4,5,5-tetramethyl-1,3,2-dioxaborolan-2-yl)-1,3-dihydro-2*H*-benzo(*d*)azepin-2-one (**3.62**, 100 mg, 0.24 mmol), 5-bromopicolinaldehyde (53.1 mg, 0.29 mmol), Pd(PPh₃)₄ (13.8 mg, 0.01 mmol) and potassium carbonate (99 mg, 0.71 mmol) in 1,4-dioxane (1 mL) and water (0.50 mL) were stirred at 80°C for 10 min. The reaction mixture was diluted with

water (5 mL) and partitioned with 9:1 DCM:MeOH (10 mL). The layers were separated and the organic layer was re-extracted with 9:1 DCM:MeOH (10 mL). The combined organic layers were concentrated under a stream of nitrogen and the resultant residue purified by MDAP (HpH) to afford the title compound (**3.77**, 66 mg, 0.20 mmol, 82 % yield) as an orange gummy oil. ¹H NMR (400 MHz, CDCl₃) $\delta = 10.15$ (s, 1H), 8.80 (d, $J = 2.0$ Hz, 1H), 8.01 (d, $J = 8.3$ Hz, 1H), 7.84 (dd, $J = 2.5, 8.6$ Hz, 1H), 7.52 (dd, $J = 2.5, 8.3$ Hz, 1H), 7.45 (s, 1H), 7.01 (d, $J = 2.0$ Hz, 1H), 6.74 (s, 1H), 4.84 (q, $J = 6.4$ Hz, 1H), 3.45 (q, $J = 6.8$ Hz, 1H), 3.23 (s, 3H), 1.76 (d, $J = 6.8$ Hz, 3H), 1.42 (d, $J = 6.4$ Hz, 3H); LCMS (HpH): $t_R = 0.83$ min, $[M+H^+] = 337.3$ (95% purity).

***tert*-Butyl ((5-((*R*)-7-((*S*)-1-hydroxyethyl)-1,3-dimethyl-2-oxo-2,3-dihydro-1*H*-benzo(*d*)azepin-5-yl)pyridin-2-yl)methyl)-*L*-serinate, 3.78**

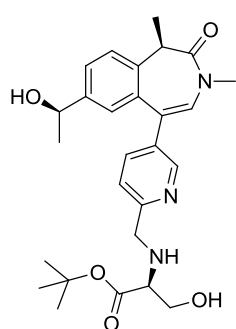


A stirrer hot plate was pre-heated to 80°C. A solution of potassium carbonate (49.3 mg, 0.36 mmol) in water (1.00 mL) was added to a solution of (*R*)-7-((*S*)-1-hydroxyethyl)-1,3-dimethyl-5-(4,4,5,5-tetramethyl-1,3,2-dioxaborolan-2-yl)-1,3-dihydro-2*H*-benzo(*d*)azepin-2-one (**3.63**, 50 mg, 0.12 mmol), *tert*-butyl ((5-bromopyridin-2-yl)methyl)-*L*-serinate (**3.75**, 47.3 mg, 0.14 mmol) and Pd(PPh₃)₄ (6.87 mg, 5.95 μ mol) in 1,4-dioxane (2 mL) and were stirred at 80°C for 10

min. The reaction mixture was diluted with water (5 mL) and partitioned with 9:1 DCM:MeOH (10 mL). The layers were separated and the organic layer was re-extracted with 9:1 DCM:MeOH (10 mL). The combined organic layers were concentrated under reduced

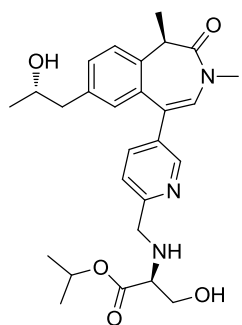
pressure to give an orange oil. The oil was purified by flash column chromatography (basic alumina, 0-100% ethyl acetate in cyclohexane followed by 0-30% ethanol in ethyl acetate) to afford the title compound (**3.78**, 30.3 mg, 0.06 mmol, 53 % yield) as an orange gummy oil. $^1\text{H NMR}$ (400 MHz, CDCl_3) δ = 8.55 (d, J = 2.0 Hz, 1H), 7.58 (dd, J = 2.0, 8.3 Hz, 1H), 7.45 (dd, J = 1.5, 8.3 Hz, 1H), 7.39 (d, J = 8.3 Hz, 1H), 7.32 (d, J = 8.3 Hz, 1H), 7.00 (d, J = 1.5 Hz, 1H), 6.58 (s, 1H), 4.81 (q, J = 6.4 Hz, 1H), 4.12 (d, J = 14.7 Hz, 1H), 3.92 (d, J = 14.7 Hz, 1H), 3.83 - 3.76 (m, 1H), 3.72 (q, J = 6.8 Hz, 1H), 3.68 - 3.62 (m, 1H), 3.46 - 3.37 (m, 1H), 3.17 (s, 3H), 1.72 (d, J = 6.8 Hz, 3H), 1.49 (s, 9H), 1.40 (d, J = 6.4 Hz, 3H), exchangeable protons not observed; LCMS (HpH): t_{R} = 0.91 min, $[\text{M}+\text{H}^+]$ = 482.4 (95% purity).

tert*-Butyl ((5-((*R*)-7-((*R*)-1-hydroxyethyl)-1,3-dimethyl-2-oxo-2,3-dihydro-1*H*-benzo(*d*)azepin-5-yl)pyridin-2-yl)methyl)-*L*-serinate, **3.79*



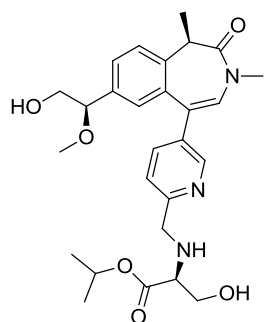
5-((*R*)-7-((*R*)-1-Hydroxyethyl)-1,3-dimethyl-2-oxo-2,3-dihydro-1*H*-benzo(*d*)azepin-5-yl)picolinaldehyde (**3.77**, 25 mg, 0.07 mmol) and *tert*-butyl *L*-serinate hydrochloride (**2.90**, 14.7 mg, 0.07 mmol) were dissolved DCM (0.5 mL) and stirred at rt for 1 h. Triethylamine (0.03 mL, 0.22 mmol) and sodium triacetoxyborohydride (31.5 mg, 0.15 mmol) were added and the reaction mixture was stirred for 4 h. The reaction mixture was quenched with water (5 mL) and partitioned with 9:1 DCM:MeOH (5 mL). The layers were separated and the organic layer was re-extracted with 9:1 DCM:MeOH (5 mL). The combined organic layers were dried (hydrophobic frit) and concentrated under reduced pressure. The residue was purified by MDAP (HpH) to afford the title compound (**3.79**, 18.0 mg, 0.04 mmol, 50 % yield) as a yellow oil. (α_{D}) $^{20.9^\circ\text{C}}$ λ (c = 1.0, CDCl_3): +96.7 $^\circ$; ν_{max} (solution in CDCl_3): 3405, 2978, 1727, 1391 cm^{-1} ; $^1\text{H NMR}$ (400 MHz, CDCl_3) δ = 8.54 (d, J = 2.2 Hz, 1H), 7.59 (dd, J = 2.2, 8.1 Hz, 1H), 7.47 (dd, J = 1.5, 8.1 Hz, 1H), 7.38 (d, J = 8.1 Hz, 1H), 7.32 (d, J = 8.1 Hz, 1H), 6.98 (d, J = 1.5 Hz, 1H), 6.56 (s, 1H), 4.79 (q, J = 6.4 Hz, 1H), 4.10 (dd, J = 5.0, 14.7 Hz, 1H), 3.92 (dd, J = 1.5, 14.7 Hz, 1H), 3.85 - 3.79 (m, 1H), 3.67 (dd, J = 6.4, 10.8 Hz, 1H), 3.45 - 3.41 (m, 1H), 3.39 (q, J = 6.8 Hz, 1H), 3.16 (s, 3H), 1.71 (d, J = 6.8 Hz, 3H), 1.49 (s, 9H), 1.39 (d, J = 6.4 Hz, 3H), exchangeable protons not observed; $^{13}\text{C NMR}$ (101 MHz, CDCl_3) δ = 171.9, 170.3, 158.4, 149.0, 144.3, 137.2, 136.9, 135.1, 134.7, 129.4, 127.4, 126.7, 124.7, 124.4, 121.9, 82.1, 69.8, 63.2, 62.7, 52.7, 41.2, 35.4, 28.1 (3C), 25.4, 12.8; LCMS (HpH): t_{R} = 0.93 min, $[\text{M}+\text{H}^+]$ = 482.4 (92% purity); HRMS: ($\text{C}_{27}\text{H}_{35}\text{N}_3\text{O}_5$) $[\text{M}+\text{H}^+]$ requires 482.2656, found $[\text{M}+\text{H}^+]$ = 482.2577.

Isopropyl ((5-((*R*)-7-((*S*)-2-hydroxypropyl)-1,3-dimethyl-2-oxo-2,3-dihydro-1*H*-benzo(*d*)azepin-5-yl)pyridin-2-yl)methyl)-L-serinate, 3.84



A solution of potassium carbonate (50.3 mg, 0.36 mmol) in water (1 mL) was added to a suspension of (*R*)-7-((*S*)-2-hydroxypropyl)-1,3-dimethyl-5-(4,4,5,5-tetramethyl-1,3,2-dioxaborolan-2-yl)-1,3-dihydro-2*H*-benzo(*d*)azepin-2-one (**3.95**, 50 mg, 0.12 mmol), isopropyl ((5-bromopyridin-2-yl)methyl)-L-serinate (**3.74**, 46.1 mg, 0.15 mmol) and PdCl₂(dppf) (4.43 mg, 6.06 μmol) in 1,4-dioxane (2 mL) and the resultant suspension heated on a pre-heated stirrer hot plate at 80°C for 20 min. Further PdCl₂(dppf) (4.43 mg, 6.06 μmol) was added and the suspension heated for 10 min. The reaction mixture was diluted with water (5 mL) and partitioned with 9:1 DCM:MeOH (10 mL). The layers were separated and the organic layer was re-extracted with 9:1 DCM:MeOH (10 mL). The combined organic layers were concentrated under a stream of nitrogen and the resultant residue purified by flash column chromatography (alumina, 0-100% ethyl acetate in cyclohexane followed by 0-30% ethanol in ethyl acetate) to afford the title compound (**3.84**, 23.1 mg, 0.05 mmol, 40 % yield) as a yellow gummy oil. (α_D)^{22.9°C} $\lambda(c = 1.0, \text{CDCl}_3)$: +74.6°; ν_{max} (solution in CDCl₃): 3404, 2978, 1728, 1663, 1560 cm⁻¹; ¹H NMR (400 MHz, CDCl₃) δ = 8.56 (d, *J* = 1.5 Hz, 1H), 7.60 - 7.55 (m, 1H), 7.35 (d, *J* = 8.3 Hz, 1H), 7.33 - 7.29 (m, 2H), 6.83 (d, *J* = 2.0 Hz, 1H), 6.58 (s, 1H), 5.09 (app. spt, *J* = 6.4 Hz, 1H), 4.12 (dd, *J* = 5.9, 14.7 Hz, 1H), 3.94 (dd, *J* = 2.9, 14.7 Hz, 1H), 3.92 - 3.80 (m, 2H), 3.70 (dd, *J* = 6.4, 10.8 Hz, 1H), 3.54 - 3.47 (m, 1H), 3.39 (q, *J* = 6.8 Hz, 1H), 3.18 (s, 3H), 2.69 (ddd, *J* = 1.5, 4.4, 13.7 Hz, 1H), 2.59 (dd, *J* = 7.8, 13.7 Hz, 1H), 1.71 (d, *J* = 6.8 Hz, 3H), 1.28 (dd, *J* = 4.4, 6.4 Hz, 6H), 1.17 (d, *J* = 6.4 Hz, 3H), exchangeable protons not observed; ¹³C NMR (101 MHz, CDCl₃) δ = 172.2, 170.5, 158.4, 149.0, 149.0, 137.2, 136.9, 136.1, 135.2, 134.8, 130.8, 129.3, 128.6, 127.3, 124.4, 121.9, 69.0, 68.7, 62.8, 62.6, 52.6, 45.1, 41.1, 35.4, 22.9, 21.9, 21.8; LCMS (HpH): t_R = 0.87 min, [M+H⁺] = 482.4 (100% purity); HRMS: (C₂₇H₃₅N₃O₂) [M+H⁺] requires 482.2656, found [M+H⁺] = 482.2652.

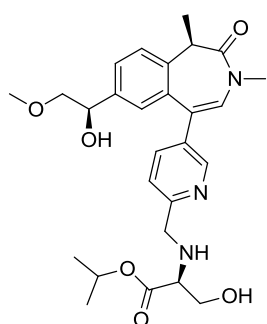
Isopropyl ((5-((*R*)-7-((*R*)-2-hydroxy-1-methoxyethyl)-1,3-dimethyl-2-oxo-2,3-dihydro-1*H*-benzo(*d*)azepin-5-yl)pyridin-2-yl)methyl)serinate, 3.86



A solution of potassium carbonate (63.4 mg, 0.46 mmol) in water (0.75 mL) was added to a solution of (*R*)-5-bromo-7-((*R*)-2-hydroxy-1-methoxyethyl)-1,3-dimethyl-1,3-dihydro-2*H*-benzo(*d*)azepin-2-one (**3.100**, 52 mg, 0.15 mmol, 88 wt%), isopropyl ((5-(4,4,5,5-tetramethyl-1,3,2-dioxaborolan-2-yl)pyridin-

2-yl)methyl)-L-serinate (**3.101**, 55.7 mg, 0.15 mmol, 90 wt%) and PdCl₂(dppf)·DCM adduct (6.24 mg, 7.64 μmol) in 1,4-dioxane (1.5 mL) and the resulting solution was stirred at 80°C for 2 h. The reaction mixture was diluted with 9:1 DCM:MeOH (10 mL) and was partitioned with water (10 mL). The aqueous layer was re-extracted with 9:1 DCM:MeOH (3 x 10 mL). The combined organic layers were dried (hydrophobic frit), before being concentrated *in vacuo* to afford a brown oil. The brown oil was re-dissolved in 1,4 dioxane (1.5 mL) along with PdCl₂(dppf)·DCM adduct (6.24 mg, 7.64 μmol) and isopropyl ((5-(4,4,5,5-tetramethyl-1,3,2-dioxaborolan-2-yl)pyridin-2-yl)methyl)-L-serinate (**3.86**, 37 mg, 0.10 mmol). To this solution, a solution of potassium carbonate (63.4 mg, 0.46 mmol) in water (0.75 mL) was added and the resultant solution was stirred at 80°C for 1 h. The reaction mixture was diluted with 9:1 DCM:MeOH (10 mL) and was partitioned with water (10 mL). The aqueous layer was re-extracted with 9:1 DCM:MeOH (3 x 10 mL). The combined organic layers were dried (hydrophobic frit), before being concentrated *in vacuo* to afford a brown oil. The oil was purified by MDAP (HpH) to afford the title compound (7 mg, 0.01 mmol, 9 % yield) as a pale yellow film. Chiral analysis conducted on a 250mm x 30mm Chiralpak ID column, eluting with 40% ethanol in heptane (+0.1% isopropylamine) at a flowrate of 1 mL/min showed the sample to be a 51:49 ratio of diastereomers from the racemisation of the ESM chiral centre. ¹H NMR (400 MHz, CDCl₃) δ = 8.56 (d, *J* = 2.0 Hz, 1H), 7.57 (dd, *J* = 2.0, 7.8 Hz, 1H), 7.42 (d, *J* = 7.8 Hz, 1H), 7.39 (dd, *J* = 1.5, 8.3 Hz, 1H), 7.33 (d, *J* = 8.3 Hz, 1H), 6.93 (s, 1H), 6.62 (d, *J* = 1.5 Hz, 1H), 5.10 (app. spt, *J* = 6.4 Hz, 1H), 4.21 (dd, *J* = 4.4, 7.8 Hz, 1H), 4.17 - 4.09 (m, 1H), 3.99 - 3.91 (m, 1H), 3.88 - 3.81 (m, 1H), 3.74 - 3.68 (m, 1H), 3.62 - 3.47 (m, 3H), 3.40 (q, *J* = 6.8 Hz, 1H), 3.21 (s, 3H), 3.19 (s, 3H), 1.73 (d, *J* = 6.8 Hz, 3H), 1.28 (app. dd, *J* = 4.4, 6.4 Hz, 6H), exchangeable protons not observed; LCMS (HpH): *t_R* = 0.82 min, [M+H⁺] = 498.4 (100 % purity).

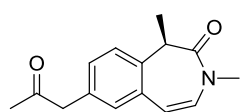
Isopropyl ((5-((*R*)-7-((*R*)-1-hydroxy-2-methoxyethyl)-1,3-dimethyl-2-oxo-2,3-dihydro-1*H*-benzo(*d*)azepin-5-yl)pyridin-2-yl)methyl)-L-serinate, **3.87, Scheme 3.20**



A solution of potassium carbonate (48.7 mg, 0.35 mmol) in water (0.50 mL) was added to a solution of (*R*)-5-bromo-7-((*R*)-1-hydroxy-2-methoxyethyl)-1,3-dimethyl-1,3-dihydro-2*H*-benzo(*d*)azepin-2-one (**3.99**, 40 mg, 0.12 mmol), isopropyl ((5-(4,4,5,5-tetramethyl-1,3,2-dioxaborolan-2-yl)pyridin-2-yl)methyl)-L-serinate (**3.101**, 47 mg, 0.13 mmol) and PdCl₂(dppf)·DCM adduct (4.80 mg, 5.88 μmol) in 1,4-dioxane (1 mL) and the solution was stirred at 80°C for 2.5 h. Further isopropyl ((5-(4,4,5,5-tetramethyl-1,3,2-dioxaborolan-2-

yl)pyridin-2-yl)methyl)-L-serinate (10 mg, 0.03 mmol) was added and the reaction mixture stirred at 80°C for 15 min. The reaction mixture was left standing at rt for 1 h. The reaction mixture was diluted with 9:1 DCM:MeOH (10 mL) and passed over a Celite cartridge. The filtrate was partitioned with water (10 mL) and the aqueous layer was re-extracted with 9:1 DCM:MeOH (2 x 10 mL). The combined organic layers were dried (hydrophobic frit) before being concentrated *in vacuo* to afford a brown oil. The oil was dissolved in 1,4-dioxane (1 mL) and PdCl₂(dppf)-DCM adduct (7 mg, 8.57 μmol) and isopropyl ((5-(4,4,5,5-tetramethyl-1,3,2-dioxaborolan-2-yl)pyridin-2-yl)methyl)-L-serinate (**3.101**, 20 mg, 0.06 mmol) added. To this solution, a solution of potassium carbonate (48.7 mg, 0.35 mmol) in water (0.5 mL) was added and the resulting solution was stirred at 80°C for 1.5 h. The reaction mixture was diluted with 9:1 DCM:MeOH (10 mL) and was partitioned with water (10 mL). The aqueous layer was re-extracted with 9:1 DCM:MeOH (3 x 10 mL). The combined organic layers were dried (hydrophobic frit) before being concentrated *in vacuo* to afford a brown oil. The oil was purified by MDAP (HpH) to afford the title compound (**3.87**, 11 mg, 0.02 mmol, 19 % yield) as a yellow film. Chiral analysis conducted on a 250mm x 30mm Chiralpak ID column, eluting with 40% ethanol in heptane (+0.1% isopropylamine) at a flowrate of 1 mL/min showed the sample to be a 37:63 ratio of diastereomers from the racemisation of the ESM. ¹H NMR (400 MHz, CDCl₃) δ = 8.56 (d, *J* = 2.2 Hz, 1H), 7.57 (dd, *J* = 2.2, 8.1 Hz, 1H), 7.45 (dd, *J* = 1.5, 7.8 Hz, 1H), 7.39 (d, *J* = 7.8 Hz, 1H), 7.31 (d, *J* = 8.1 Hz, 1H), 7.03 (d, *J* = 1.5 Hz, 1H), 6.59 (s, 1H), 5.09 (app. spt, *J* = 6.3 Hz, 1H), 4.79 (dd, *J* = 3.2, 8.6 Hz, 1H), 4.17 - 4.07 (m, 1H), 3.97 - 3.90 (m, 1H), 3.87 - 3.80 (m, 1H), 3.70 (dd, *J* = 6.4, 11.2 Hz, 1H), 3.53 - 3.40 (m, 3H), 3.37 (s, 3H), 3.36 - 3.29 (m, 1H), 3.17 (s, 3H), 1.71 (d, *J* = 6.8 Hz, 3H), 1.28 (dd, *J* = 4.4, 6.3 Hz, 6H), exchangeable protons not observed; LCMS (HpH): *t_R* = 0.82 min, [M+H⁺] = 498.4 (98 % purity).

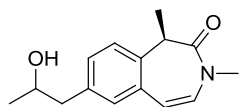
(R)-1,3-Dimethyl-7-(2-oxopropyl)-1H-benzo(d)azepin-2(3H)-one, 3.90



A suspension of (*R*)-7-bromo-1,3-dimethyl-1*H*-benzo(*d*)azepin-2(3*H*)-one²¹⁹ (**3.20**, 1.0 g, 3.76 mmol), palladium(II) acetate (51 mg, 0.23 mmol), cesium carbonate (2.45 g, 7.52 mmol) and Xantphos (0.22 g, 0.38 mmol) in 1,4-dioxane (15 mL) and propan-2-one (3.86 mL, 52.6 mmol) were heated in a sealed vial at 80°C for 2 h. The reaction mixture was filtered over Celite and the column washed with ethyl acetate (100 mL). The resultant solution was concentrated under reduced pressure to afford a brown oil. The oil was purified by flash column chromatography (silica, 10-70% ethyl acetate in cyclohexane) to afford the title compound (**3.90**, 842 mg, 3.46 mmol, 92 % yield) as yellow oil. ¹H NMR (400 MHz, CDCl₃) δ = 7.28 (d, *J* = 7.8 Hz, 1H),

7.22 (dd, $J = 1.5, 7.8$ Hz, 1H), 7.09 (d, $J = 1.5$ Hz, 1H), 6.38 (d, $J = 8.8$ Hz, 1H), 6.30 (d, $J = 8.8$ Hz, 1H), 3.70 (s, 2H), 3.27 (app. br s, 1H), 3.12 (s, 3H), 2.16 (s, 3H), 1.63 (d, $J = 6.8$ Hz, 3H); LCMS (HpH): $t_R = 0.88$ min, $[M+H^+] = 244.3$ (99 % purity).

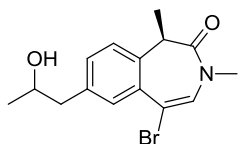
(1R)-7-(2-Hydroxypropyl)-1,3-dimethyl-1,3-dihydro-2H-benzo(d)azepin-2-one, 3.91



To a solution of (*R*)-1,3-dimethyl-7-(2-oxopropyl)-1,3-dihydro-2H-benzo(*d*)azepin-2-one (**3.90**, 842 mg, 3.46 mmol) in methanol (15 mL) at 0°C was carefully added sodium borohydride (262 mg, 6.92 mmol).

The reaction was removed from the ice bath and stirred at rt for 10 min. The reaction mixture was quenched with water (100 mL) and extracted with ethyl acetate (2 x 100 mL). The combined organic layers were dried (hydrophobic frit) and concentrated under reduced pressure to afford the title compound (**3.91**, 642 mg, 2.62 mmol, 76 % yield) as a white solid. ¹H NMR (400 MHz, CDCl₃) $\delta = 7.28 - 7.22$ (m, 2H), 7.11 (d, $J = 1.0$ Hz, 1H), 6.40 (d, $J = 9.4$ Hz, 1H), 6.29 (d, $J = 9.4$ Hz, 1H), 4.02 (app. sxt, $J = 6.4$ Hz, 1H), 3.27 (app. br s, 1H), 3.12 (s, 3H), 2.79 (ddd, $J = 1.5, 4.9, 13.4$ Hz, 1H), 2.69 (ddd, $J = 1.5, 8.3, 13.4$ Hz, 1H), 1.64 (d, $J = 6.8$ Hz, 3H), 1.49 (br s, 1H), 1.25 (d, $J = 6.4$ Hz, 3H); LCMS (HpH): $t_R = 0.98$ min, $[M+H^+] = 246.3$ (95% purity).

(1R)-5-Bromo-7-(2-hydroxypropyl)-1,3-dimethyl-1,3-dihydro-2H-benzo(d)azepin-2-one, 3.92

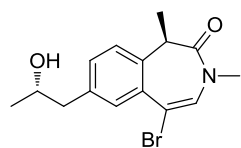


To a mixture of (*1R*)-7-(2-hydroxypropyl)-1,3-dimethyl-1,3-dihydro-2H-benzo(*d*)azepin-2-one (**3.91**, 642 mg, 2.62 mmol) in acetonitrile (25 mL) was added phenyltrimethylaminotribromide (984 mg, 2.62 mmol) and the reaction mixture was stirred under nitrogen for 10 min. The reaction mixture

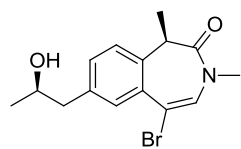
was diluted with ethyl acetate (100 mL) and partitioned with water (100 mL). The aqueous layer was re-extracted with ethyl acetate (100 mL). The combined organic layers were dried (hydrophobic frit) and evaporated under reduced pressure. The resultant residue was purified by flash column chromatography (silica, 0-100% ethyl acetate in cyclohexane) to afford the title compound (**3.92**, 824 mg, 2.54 mmol, 97 % yield) as a yellow oil. ¹H NMR (400 MHz, CDCl₃) $\delta = 7.56$ (s, 1H), 7.31 (dd, $J = 2.0, 8.8$ Hz, 1H), 7.23 (d, $J = 8.8$ Hz, 1H), 6.83 (d, $J = 2.0$ Hz, 1H), 4.09 - 3.99 (m, 1H), 3.94 - 3.87 (m, 1H), 3.36 (q, $J = 6.8$ Hz, 1H), 3.07 (s, 2H), 2.87 - 2.78 (m, 1H), 2.77 - 2.70 (m, 1H), 1.65 (d, $J = 6.8$ Hz, 3H), 1.26 (d, $J = 6.4$ Hz, 3H), OH not observed; LCMS (HpH): $t_R = 1.00$ min, $[M+H^+] = 324.2 / 326.2$ (100% purity).

(R)-5-Bromo-7-((S)-2-hydroxypropyl)-1,3-dimethyl-1,3-dihydro-2H-benzo(d)azepin-2-one, 3.93 and **(R)-5-bromo-7-((R)-2-hydroxypropyl)-1,3-dimethyl-1,3-dihydro-2H-benzo(d)azepin-2-one, 3.94**

Chiral resolution of (1R)-5-bromo-7-(2-hydroxypropyl)-1,3-dimethyl-1,3-dihydro-2H-benzo(d)azepin-2-one **3.92** was carried out using a 250mm x 30mm Chiralpak AD-H column, eluting with 10% ethanol/heptane at a flow rate of 30 mL/min. The appropriate fractions for each isomer were combined and evaporated under reduced pressure to give the title compounds.

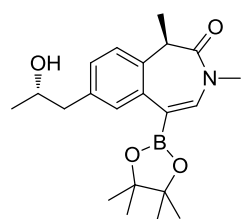


3.93: $^1\text{H NMR}$ (400 MHz, CDCl_3) δ = 7.56 (d, J = 1.5 Hz, 1H), 7.31 (dd, J = 1.5, 8.3 Hz, 1H), 7.24 (d, J = 8.3 Hz, 1H), 6.83 (s, 1H), 4.05 (app. sxt, J = 6.4 Hz, 1H), 3.36 (q, J = 6.8 Hz, 1H), 3.08 (s, 3H), 2.84 (dd, J = 4.9, 13.2 Hz, 1H), 2.73 (dd, J = 8.3, 13.2 Hz, 1H), 1.65 (d, J = 6.8 Hz, 3H), 1.45 (br s, 1H), 1.26 (d, J = 6.4 Hz, 3H); LCMS (HpH): t_R = 1.00 min, $[\text{M}+\text{H}^+]$ = 324.1 / 326.1 (98% purity)



3.94: $^1\text{H NMR}$ (400 MHz, CDCl_3) δ = 7.56 (d, J = 1.5 Hz, 1H), 7.31 (dd, J = 1.5, 8.3 Hz, 1H), 7.24 (d, J = 8.3 Hz, 1H), 6.82 (s, 1H), 4.08 - 3.99 (m, 1H), 3.36 (q, J = 6.8 Hz, 1H), 3.08 (s, 3H), 2.82 (dd, J = 4.9, 13.8 Hz, 1H), 2.73 (dd, J = 8.1, 13.8 Hz, 1H), 1.65 (d, J = 6.8 Hz, 3H), 1.51 (br s, 1H), 1.26 (d, J = 6.4 Hz, 3H); LCMS (HpH): t_R = 1.00 min, $[\text{M}+\text{H}^+]$ = 324.1 / 326.1 (95% purity).

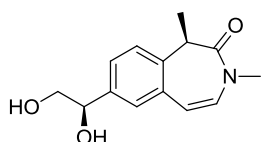
(R)-7-((S)-2-Hydroxypropyl)-1,3-dimethyl-5-(4,4,5,5-tetramethyl-1,3,2-dioxaborolan-2-yl)-1,3-dihydro-2H-benzo(d)azepin-2-one, 3.95



$\text{PdCl}_2(\text{dppf})$ (83 mg, 0.11 mmol) was added to a stirred mixture of (R)-5-bromo-7-((S)-2-hydroxypropyl)-1,3-dimethyl-1,3-dihydro-2H-benzo(d)azepin-2-one (**3.93**, 368 mg, 1.14 mmol), bis(pinacolato)diboron (576 mg, 2.27 mmol) and potassium acetate (334 mg, 3.41 mmol) in 1,4-dioxane (10 mL). The reaction mixture was stirred at 80°C for 1 h under nitrogen. The reaction mixture was cooled to rt and partitioned between ethyl acetate (100 mL) and water (100 mL). The aqueous phase was extracted with ethyl acetate (2 x 50 mL). The combined organics were dried (hydrophobic frit) and concentrated *in vacuo*. The residue was purified by flash column chromatography (silica, 0-100% ethyl acetate in cyclohexane) to afford the title compound (**3.95**, 310 mg, 0.84 mmol, 74 % yield), as a brown oil which turned into a brown solid upon standing. $^1\text{H NMR}$ (400 MHz, CDCl_3) δ = 7.41 (d, J = 1.5 Hz, 1H), 7.24 (d, J = 8.3 Hz, 1H), 7.20 (dd, J =

1.5, 8.3 Hz, 1H), 7.01 (s, 1H), 4.03 - 3.94 (m, 1H), 3.22 (q, $J = 6.8$ Hz, 1H), 3.14 (s, 3H), 2.79 (dd, $J = 4.4, 13.8$ Hz, 1H), 2.69 (dd, $J = 8.1, 13.8$ Hz, 1H), 1.91 (br s, 1H), 1.62 (d, $J = 6.8$ Hz, 3H), 1.36 (s, 6H), 1.33 (s, 6H), 1.27 (d, $J = 6.8$ Hz, 3H); LCMS (HpH): $t_R = 1.14$ min, $[M+H^+] = 372.4$ (92% purity).

(R)-7-((R)-1,2-Dihydroxyethyl)-1,3-dimethyl-1,3-dihydro-2H-benzo(d)azepin-2-one, 3.96, Scheme 3.16

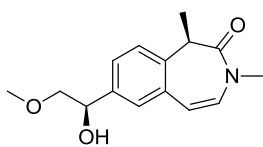


A solution of (*R*)-1,3-dimethyl-7-vinyl-1,3-dihydro-2*H*-benzo(*d*)azepin-2-one (**3.52**, 1.14 g, 4.54 mmol, 85 wt%) and AD-mix- β (6.40 g, 4.54 mmol) in IPA (40 mL) and water (40 mL) was stirred at rt for 18 h. The reaction was quenched by adding saturated sodium sulfite (150 mL) and stirring the resultant solution for 0.5 h. The mixture was partitioned with ethyl acetate (100 mL). The aqueous layer was re-extracted with ethyl acetate (2 x 100 mL). The combined organic layers were dried (hydrophobic frit) before being concentrated *in vacuo* to afford a yellow oil. The oil was purified by flash column chromatography (silica, 60-100% ethyl acetate in cyclohexane) to afford the title compound (**3.96**, 693 mg, 2.80 mmol, 62 % yield) as a white solid. ^1H NMR (400 MHz, CDCl_3) $\delta = 7.37$ (dd, $J = 2.0, 8.3$ Hz, 1H), 7.31 (d, $J = 8.3$ Hz, 1H), 7.29 (d, $J = 2.0$ Hz, 1H), 6.42 (d, $J = 9.3$ Hz, 1H), 6.32 (d, $J = 9.3$ Hz, 1H), 4.84 (td, $J = 3.4, 7.8$ Hz, 1H), 3.78 (ddd, $J = 3.4, 7.3, 11.2$ Hz, 1H), 3.67 (ddd, $J = 4.9, 7.8, 11.2$ Hz, 1H), 3.29 (app. br s, 1H), 3.12 (s, 3H), 2.47 (d, $J = 3.4$ Hz, 1H), 1.96 (dd, $J = 4.9, 7.3$ Hz, 1H), 1.64 (d, $J = 6.8$ Hz, 3H); LCMS (Formic) $t_R = 0.59$ min, $[M+H^+] = 248.3$ (100 % purity).

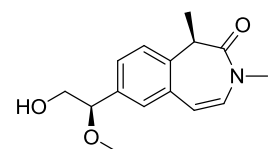
(R)-7-((R)-1-Hydroxy-2-methoxyethyl)-1,3-dimethyl-1,3-dihydro-2H-benzo(d)azepin-2-one compound, 3.97 and (R)-7-((R)-2-hydroxy-1-methoxyethyl)-1,3-dimethyl-1,3-dihydro-2H-benzo(d)azepin-2-one, 3.98, Scheme 3.17

To a stirring solution of (*R*)-7-((*R*)-1,2-dihydroxyethyl)-1,3-dimethyl-1,3-dihydro-2*H*-benzo(*d*)azepin-2-one (**3.96**, 476 mg, 1.93 mmol) and iodomethane (0.12 mL, 1.93 mmol) in DMF (10 mL), sodium hydride (85 mg, 2.12 mmol) was added and the resulting solution was stirred at rt for 1.25 h. The reaction was quenched by the slow addition of water (10 mL) before being partitioned with 9:1 DCM:MeOH (20 mL), brine (5 mL) was added to aid in separation. The aqueous layer was re-extracted with 9:1 DCM:MeOH (3 x 20 mL). The combined organic layers were dried (hydrophobic frit) before being concentrated *in vacuo* to afford a yellow oil. The yellow oil was purified using flash column chromatography (silica, 60-85 % ethyl acetate in cyclohexane) to afford a mixture of the monomethylated products.

Chiral resolution was carried out using a 250mm x 30mm Chiralpak AD-H column, eluting with 25% ethanol (+0.2% isopropylamine) / heptane (+0.2% isopropylamine) at a flow rate of 30 mL/min. The appropriate fractions for each isomer were combined and evaporated under reduced pressure to give the title compounds.

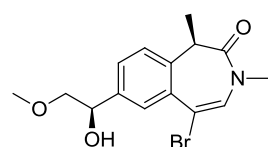


3.97: $^1\text{H NMR}$ (400 MHz, DMSO-d_6) δ = 7.37 (dd, J = 1.6, 8.3 Hz, 1H), 7.30 (d, J = 1.6 Hz, 1H), 7.21 (d, J = 8.3 Hz, 1H), 6.53 (d, J = 9.3 Hz, 1H), 6.48 (d, J = 9.3 Hz, 1H), 5.31 (d, J = 4.9 Hz, 1H), 4.73 - 4.67 (m, 1H), 3.44 - 3.34 (m, 2H), 3.24 (s, 3H), 3.18 (app. br s, 1H), 3.02 (s, 3H), 1.49 (d, J = 6.8 Hz, 3H); LCMS (HpH): t_{R} = 0.75 min, $[\text{M}+\text{H}^+]$ = 262.3 (96 % purity)



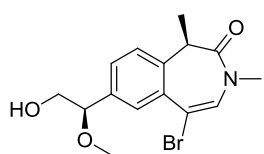
3.98: $^1\text{H NMR}$ (400 MHz, DMSO-d_6) δ = 7.32 (dd, J = 2.0, 8.1 Hz, 1H), 7.25 (d, J = 8.1 Hz, 1H), 7.24 (d, J = 2.0 Hz, 1H), 6.54 (d, J = 9.3 Hz, 1H), 6.49 (d, J = 9.3 Hz, 1H), 4.76 (dd, J = 5.4, 6.4 Hz, 1H), 4.20 (dd, J = 4.9, 6.8 Hz, 1H), 3.53 (ddd, J = 5.4, 6.8, 11.2 Hz, 1H), 3.40 (ddd, J = 4.9, 6.4, 11.2 Hz, 1H), 3.21 (app. br s, 1H), 3.17 (s, 3H), 3.03 (s, 3H), 1.50 (d, J = 6.8 Hz, 3H); LCMS (HpH): t_{R} = 0.75 min, $[\text{M}+\text{H}^+]$ = 262.3 (98 % purity).

(R)-5-Bromo-7-((R)-1-hydroxy-2-methoxyethyl)-1,3-dimethyl-1,3-dihydro-2H-benzo(d)azepin-2-one, 3.99, Scheme 3.18



A solution of (*R*)-7-((*R*)-1-hydroxy-2-methoxyethyl)-1,3-dimethyl-1,3-dihydro-2*H*-benzo(*d*)azepin-2-one (**3.97**, 90 mg, 0.34 mmol) and phenyltrimethylaminotribromide (129 mg, 0.34 mmol) in acetonitrile (1.5 mL) was stirred at rt, under nitrogen, for 10 min. The solution was diluted with 9:1 DCM:MeOH (10 mL) and was partitioned with water (10 mL). The aqueous layer was re-extracted with a further two portions of 9:1 DCM:MeOH (2 x 10 mL). The combined organic layers were dried (hydrophobic frit) before being concentrated *in vacuo* to afford the title compound (**3.99**, 85 mg, 0.25 mmol, 73 % yield) as a yellow oil. $^1\text{H NMR}$ (400 MHz, CDCl_3) δ = 7.75 (d, J = 2.0 Hz, 1H), 7.46 (dd, J = 2.0, 8.3 Hz, 1H), 7.29 (d, J = 8.3 Hz, 1H), 6.84 (s, 1H), 4.93 (dd, J = 3.4, 8.8 Hz, 1H), 3.94 (br s, 1H), 3.57 (dd, J = 3.4, 9.8 Hz, 1H), 3.46 - 3.40 (m, 4H), 3.37 (q, J = 6.8 Hz, 1H), 3.07 (s, 3H), 1.65 (d, J = 6.8 Hz, 3H); LCMS (HpH): t_{R} = 0.88 min, $[\text{M}+\text{H}^+]$ = 340.1 / 342.1 (94 % purity).

(R)-5-Bromo-7-((R)-2-hydroxy-1-methoxyethyl)-1,3-dimethyl-1,3-dihydro-2H-benzo(d)azepin-2-one, 3.100



Method 1, Scheme 3.18

A solution of (R)-7-((R)-2-hydroxy-1-methoxyethyl)-1,3-dimethyl-1,3-dihydro-2H-benzo(d)azepin-2-one (**3.98**, 45 mg, 0.17 mmol) and phenyltrimethylaminotribromide (64.7 mg, 0.17 mmol) in acetonitrile (1.5 mL) was stirred at rt under nitrogen for 20 min. Further phenyltrimethylaminotribromide (7 mg, 0.02 mmol) was added and the reaction mixture was stirred at rt under nitrogen for 20 min. The solution was diluted with ethyl acetate (10 mL) and was partitioned with water (10 mL). The aqueous layer was re-extracted with a further portion of ethyl acetate (10 mL). In parallel, a solution of (R)-7-((R)-2-hydroxy-1-methoxyethyl)-1,3-dimethyl-1,3-dihydro-2H-benzo(d)azepin-2-one (**3.98**, 36 mg, 0.14 mmol) and phenyltrimethylaminotribromide (51.8 mg, 0.14 mmol) in acetonitrile (1.5 mL) was stirred at rt, under nitrogen, for 20 min. The solution was diluted with ethyl acetate (10 mL) and was partitioned with water (10 mL). The aqueous layer was re-extracted with a further portion of ethyl acetate (10 mL). The organic layers from each work up were combined, dried (hydrophobic frit) and concentrated *in vacuo* to afford the title compound (**3.100**, 57 mg, 0.17 mmol, 88 wt%, 54 % yield). ¹H NMR (400 MHz, CDCl₃) δ = 7.65 (d, *J* = 1.5 Hz, 1H), 7.39 (dd, *J* = 1.5, 8.3 Hz, 1H), 7.31 (d, *J* = 8.3 Hz, 1H), 6.85 (s, 1H), 4.35 (dd, *J* = 4.9, 7.3 Hz, 1H), 3.67 - 3.63 (m, 2H), 3.38 (q, *J* = 6.8 Hz, 1H), 3.32 (s, 3H), 3.09 (s, 3H), 1.66 (d, *J* = 6.8 Hz, 3H), OH not observed; LCMS (HpH): t_R = 0.88 min, [M+H⁺] = 340.2 / 342.2 (88% purity).

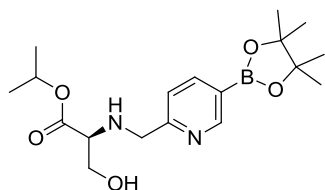
Method 2, Scheme 3.21

A solution of (R)-7-((R)-1-methoxy-2-(trityloxy)ethyl)-1,3-dimethyl-1,3-dihydro-2H-benzo[d]azepin-2-one (**3.105**, 615 mg, 1.10 mmol) and phenyltrimethylaminotribromide (413 mg, 1.10 mmol) in acetonitrile (20 mL) was stirred at rt for 3 h 30 min. Acetic acid (4 mL) was added to the reaction mixture which was stirred at rt for 1 h. An extra portion of acetic acid (2 mL) was added to the reaction mixture which was stirred at rt for 2 h. 9:1 DCM:MeOH (20 mL) was added to the reaction mixture which was partitioned with water (30 mL). The aqueous layer was re-extracted with 9:1 DCM:MeOH (3 x 20 mL). The combined organic layers were dried (hydrophobic frit) before being concentrated *in vacuo* to afford a yellow oil. The oil was dissolved in acetonitrile (15 mL) and acetic acid (7.5 mL) was added and was stirred for 1 h at rt. Water (20 mL) was added to the reaction mixture and was extracted with ethyl acetate (40 mL). The aqueous layer was re-extracted with two

further portions of ethyl acetate (2 x 30 mL). The combined organic layers were dried (hydrophobic frit) and were concentrated *in vacuo* to afford a yellow solid. The solid was dissolved in acetonitrile (20 mL) and was stirred with acetic acid (5 mL) and triethylsilane (0.18 mL, 1.10 mmol) for 19 h 30 min. Ethyl acetate (30 mL) was added to the reaction mixture which was partitioned with water (30 mL). The aqueous layer was re-extracted with ethyl acetate (3 x 30 mL). The combined organic layers were dried (hydrophobic frit) and concentrated *in vacuo* to afford an off-white solid. The solid was purified by flash column chromatography (silica, 0-100 % water saturated ethyl acetate in cyclohexane) to afford the title compound (**3.100**, 255 mg, 0.75 mmol, 68 % yield) as white oil.

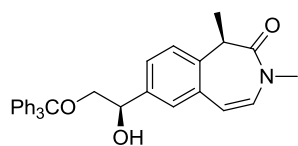
¹H NMR (400 MHz, CDCl₃) δ = 7.65 (d, *J* = 1.7 Hz, 1H), 7.39 (dd, *J* = 1.7, 8.3 Hz, 1H), 7.31 (d, *J* = 8.3 Hz, 1H), 6.85 (s, 1H), 4.35 (dd, *J* = 4.9, 6.8 Hz, 1H), 3.69 - 3.62 (m, 2H), 3.38 (q, *J* = 6.8 Hz, 1H), 3.32 (s, 3H), 3.09 (s, 3H), 2.19 (dd, *J* = 4.9, 7.8 Hz, OH), 1.66 (d, *J* = 6.8 Hz, 3H); LCMS (Formic): *t_R* = 0.86 min, [M+H⁺] = 340.2 / 342.2 (100 % purity).

Isopropyl ((5-(4,4,5,5-tetramethyl-1,3,2-dioxaborolan-2-yl)pyridin-2-yl)methyl)-L-serinate, 3.101



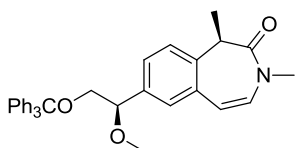
A solution of 5-(4,4,5,5-tetramethyl-1,3,2-dioxaborolan-2-yl)picolinialdehyde (200 mg, 0.86 mmol), isopropyl L-serinate (**3.103**, 200 mg, 1.36 mmol) and triethylamine (0.24 mL, 1.72 mmol) in DCM (5 mL) was stirred at rt for 2 h, then the reaction mixture was left standing at rt for 15 h. Sodium triacetoxyborohydride (546 mg, 2.57 mmol) was added to the reaction mixture which was then stirred at rt for 2 h. The reaction was quenched by the addition of water (10 mL) and was partitioned with 9:1 DCM:MeOH (10 mL), brine (10 mL) was added to aid the separation. The aqueous layer was re-extracted with 9:1 DCM:MeOH (2 x 10 mL). The combined organic layers were dried (hydrophobic frit) and were concentrated *in vacuo* to afford the title compound (**3.101**, 147 mg, 0.40 mmol, 90 wt%, 47 % yield) as a yellow oil. ¹H NMR (400 MHz, CDCl₃) δ = 8.88 (d, *J* = 1.7 Hz, 1H), 8.02 (dd, *J* = 1.7, 7.6 Hz, 1H), 7.28 (d, *J* = 7.6 Hz, 1H), 5.06 (spt, *J* = 6.4 Hz, 1H), 4.09 (d, *J* = 15.2 Hz, 1H), 3.92 (d, *J* = 15.2 Hz, 1H), 3.79 (dd, *J* = 4.4, 11.2 Hz, 1H), 3.67 (dd, *J* = 6.4, 11.2 Hz, 1H), 3.44 (dd, *J* = 4.4, 6.4 Hz, 1H), 1.35 (s, 12H), 1.26 (d, *J* = 6.4 Hz, 6H); LCMS (HpH): *t_R* 0.44 min, [M+H⁺] = 283.3 (76 % purity).

(R)-7-((R)-1-Hydroxy-2-(trityloxy)ethyl)-1,3-dimethyl-1,3-dihydro-2H-benzo[d]azepin-2-one, 3.104



A solution of (R)-7-((R)-1,2-dihydroxyethyl)-1,3-dimethyl-1,3-dihydro-2H-benzo[d]azepin-2-one (**3.96**, 669 mg, 2.71 mmol), trityl chloride (754 mg, 2.71 mmol) and triethylamine (0.45 mL, 3.25 mmol) in DCM (30 mL) was stirred at rt for 4 h 30 min. The reaction mixture was partitioned with water (30 mL). The aqueous layer was re-extracted with 9:1 DCM:MeOH (3 x 20 mL). The combined organic layers were dried (hydrophobic frit) before being concentrated *in vacuo* to afford a pale yellow film. The film was purified by flash column chromatography (silica, 0-100 % ethyl acetate in cyclohexane). The relevant fractions were combined and concentrated *in vacuo* to afford the title compound (**3.104**, 800 mg, 1.63 mmol, 60 % yield) as a white gum. ¹H NMR (400 MHz, CDCl₃) δ = 7.43 - 7.38 (m, 6H), 7.32 - 7.26 (m, 6H), 7.25 - 7.18 (m, 6H), 6.37 (d, *J* = 9.3 Hz, 1H), 6.27 (d, *J* = 9.3 Hz, 1H), 4.77 (ddd, *J* = 2.4, 3.8, 8.3 Hz, 1H), 3.34 (dd, *J* = 3.8, 9.8 Hz, 1H), 3.27 (dd, *J* = 8.3, 9.8 Hz, 1H), 3.21 (app. br s, 1H), 3.09 (s, 3H), 2.74 (d, *J* = 2.4 Hz, 1H), 1.61 (d, *J* = 6.8 Hz, 3H); LCMS (HpH) *t*_R = 1.42 min, [M+H⁺] = 490.2 (100 % purity).

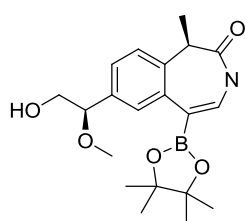
(R)-7-((R)-1-Methoxy-2-(trityloxy)ethyl)-1,3-dimethyl-1,3-dihydro-2H-benzo[d]azepin-2-one, 3.105



To a stirring solution of (R)-7-((R)-1-hydroxy-2-(trityloxy)ethyl)-1,3-dimethyl-1,3-dihydro-2H-benzo[d]azepin-2-one (**3.104**, 825 mg, 1.69 mmol) and iodomethane (0.11 mL, 1.69 mmol) in DMF (15 mL), sodium hydride (74.1 mg, 1.85 mmol) was added and the resulting solution was stirred at rt for 2 h 45 min. Further sodium hydride (27.0 mg, 0.67 mmol) and iodomethane (42 μL, 0.67 mmol) were added and the reaction mixture stirred at rt for 1 h 30 min. Further sodium hydride (27.0 mg, 0.67 mmol) and iodomethane (42 μL, 0.67 mmol) were added and the resulting solution was stirred at rt for 17 h. Extra portions of sodium hydride (13.5 mg, 0.34 mmol) and iodomethane (21 μL, 0.34 mmol) were added to the reaction mixture which was stirred at rt for 2 h. The reaction was quenched by the dropwise addition of water (10 mL). The suspension was extracted with 9:1 DCM:MeOH (40 mL). Extra water (10 mL) and brine (10 mL) were added to aid the separation. The aqueous layer was re-extracted with three further portions of 9:1 DCM:MeOH (3 x 30 mL). The combined organic layers were dried (hydrophobic frit) before being concentrated *in vacuo* to afford a yellow liquid. The liquid was dissolved in 9:1 DCM:MeOH (20 mL) and partitioned with 5 % LiCl (aq) (50 mL). The organic layer was dried (hydrophobic frit) and

concentrated *in vacuo* to afford a yellow liquid. The same procedure was repeated again to remove the residual DMF. Upon concentration a yellow oil was afforded, this was further dried in a vacuum oven at 45°C overnight to afford the title compound (**3.105**, 639 mg, 1.27 mmol, 75 % yield) as a yellow oil. ¹H NMR (400 MHz, CDCl₃) δ = 7.38 - 7.32 (m, 6H), 7.26 - 7.13 (m, 12H), 6.39 (d, *J* = 9.3 Hz, 1H), 6.29 (d, *J* = 9.3 Hz, 1H), 4.25 (dd, *J* = 4.9, 6.8 Hz, 1H), 3.39 (dd, *J* = 6.8, 9.8 Hz, 1H), 3.30 (s, 3H), 3.24 (br s, 1H), 3.15 (dd, *J* = 4.9, 9.8 Hz, 1H), 3.12 (s, 3H), 1.64 (d, *J* = 6.4 Hz, 3H); LCMS (Formic): *t*_R = 1.54 min, [M+H⁺] = 504.4 (96% purity).

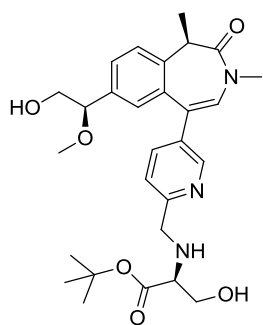
(*R*)-7-((*R*)-2-Hydroxy-1-methoxyethyl)-1,3-dimethyl-5-(4,4,5,5-tetramethyl-1,3,2-dioxaborolan-2-yl)-1,3-dihydro-2*H*-benzo[*d*]azepin-2-one, 3.106



A solution of (*R*)-5-bromo-7-((*R*)-2-hydroxy-1-methoxyethyl)-1,3-dimethyl-1,3-dihydro-2*H*-benzo[*d*]azepin-2-one (**3.100**, 255 mg, 0.75 mmol), bispinacolatodiboron (381 mg, 1.50 mmol), potassium acetate (221 mg, 2.25 mmol) and PdCl₂(dppf)·DCM adduct (61.2 mg, 0.08 mmol) in 1,4-dioxane (10 mL) was stirred at 60°C for 2 h 10 min.

The mixture was diluted with 9:1 DCM:MeOH (20 mL) and partitioned with water (30 mL). The aqueous layer was re-extracted with 9:1 DCM:MeOH (3 x 20 mL). The combined organic layers were passed over celite and concentrated *in vacuo* to afford a brown oil. The oil was purified by flash column chromatography (silica, 0-100 % ethyl acetate in cyclohexane) to afford the title compound (**3.106**, 168 mg, 0.37 mmol, 49 % yield) as a yellow oil. ¹H NMR (400MHz, CDCl₃) δ = 7.52 (s, 1H), 7.30 - 7.27 (m, 2H), 7.03 (s, 1H), 4.35 (app. t, *J* = 6.1 Hz, 1H), 3.66 - 3.60 (m, 2H), 3.35 (s, 3H), 3.23 (q, *J* = 6.8 Hz, 1H), 3.14 (s, 3H), 1.63 (d, *J* = 6.8 Hz, 3H), 1.36 (s, 6H), 1.33 (s, 6H), OH not observed; LCMS (HpH) *t*_R = 1.05 min, [M+H⁺] = 388.4 (90% purity).

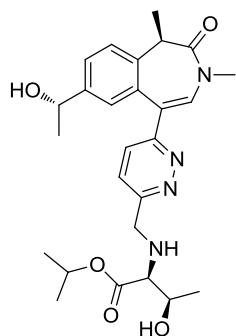
***tert*-Butyl ((5-((*R*)-7-((*R*)-2-hydroxy-1-methoxyethyl)-1,3-dimethyl-2-oxo-2,3-dihydro-1*H*-benzo[*d*]azepin-5-yl)pyridin-2-yl)methyl)-*L*-serinate, 3.107**



A solution of potassium carbonate (44.2 mg, 0.32 mmol) in water (1 mL) was added to a solution of (*R*)-7-((*R*)-2-hydroxy-1-methoxyethyl)-1,3-dimethyl-5-(4,4,5,5-tetramethyl-1,3,2-dioxaborolan-2-yl)-1,3-dihydro-2*H*-benzo[*d*]azepin-2-one (**3.106**, 55 mg, 0.11 mmol, 75 wt%), *tert*-butyl ((5-bromopyridin-2-yl)methyl)-*L*-serinate (**3.75**, 35.3 mg, 0.11 mmol) and PdCl₂(dppf)·DCM adduct (8.70 mg, 10.65 μmol) in 1,4-dioxane (2

mL) and the resulting solution was stirred at 80°C for 20 min. The reaction mixture was diluted with 9:1 DCM:MeOH (10 mL) and was partitioned with water (10 mL). The aqueous layer was re-extracted with three further portions of 9:1 DCM:MeOH (3 x 10 mL). The combined organic layers were dried (hydrophobic frit) before being concentrated *in vacuo* to afford a brown oil. The oil was purified by flash column chromatography (silica, 0-100 % water-saturated ethyl acetate in cyclohexane). The fractions were concentrated *in vacuo* to afford the title compound (**3.107**, 25 mg, 0.05 mmol, 46 % yield) as a yellow oil. ¹H NMR (400 MHz, CDCl₃) δ = 8.56 (d, *J* = 2.0 Hz, 1H), 7.56 (dd, *J* = 2.0, 8.1 Hz, 1H), 7.42 - 7.38 (m, 2H), 7.33 (d, *J* = 8.1 Hz, 1H), 6.92 (d, *J* = 2.0 Hz, 1H), 6.61 (s, 1H), 4.21 (dd, *J* = 4.2, 7.6 Hz, 1H), 4.13 (d, *J* = 14.2 Hz, 1H), 3.94 (d, *J* = 14.2 Hz, 1H), 3.82 (dd, *J* = 4.2, 11.0 Hz, 1H), 3.68 (dd, *J* = 6.4, 10.8 Hz, 1H), 3.60 - 3.49 (m, 2H), 3.43 (dd, *J* = 4.4, 6.8 Hz, 1H), 3.40 (q, *J* = 6.8 Hz, 1H), 3.21 (s, 3H), 3.19 (s, 3H), 2.81 (br s, 3H), 1.72 (d, *J* = 6.8 Hz, 3H), 1.49 (s, 9H); LCMS (Formic): *t*_R = 0.62 min, [M+H⁺] = 512.5 (98 % purity).

Isopropyl ((6-((*R*)-7-((*S*)-1-hydroxyethyl)-1,3-dimethyl-2-oxo-2,3-dihydro-1*H*-benzo(*d*)azepin-5-yl)pyridazin-3-yl)methyl)-L-threoninate, 3.108

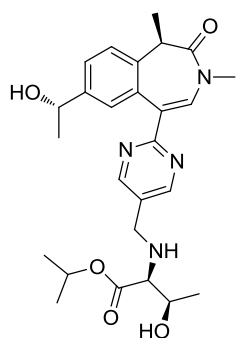


A solution of (*R*)-7-((*S*)-1-hydroxyethyl)-1,3-dimethyl-5-(4,4,5,5-tetramethyl-1,3,2-dioxaborolan-2-yl)-1,3-dihydro-2*H*-benzo(*d*)azepin-2-one (**3.63**, 50 mg, 0.12 mmol), isopropyl ((6-chloropyridazin-3-yl)methyl)-L-threoninate (**3.120**, 41.1 mg, 0.14 mmol), Pd(PPh₃)₄ (6.87 mg, 5.95 μmol) and potassium carbonate (49.3 mg, 0.36 mmol) in 1,4-dioxane (1 mL) and water (0.50 mL) were stirred at 80°C for 10 min.

The reaction mixture was diluted with water (5 mL) and partitioned with 9:1 DCM:MeOH (10 mL). The layers were separated and the organic layer was re-extracted with 9:1 DCM:MeOH (10 mL). The combined organic layers were concentrated under a stream of nitrogen and the resultant residue purified by MDAP (HpH) to afford the title compound (**3.108**, 21.1 mg, 0.04 mmol, 37 % yield) as an orange gummy oil. (α_D)^{23.2°C}_D(c = 1.0, CDCl₃): +229.6°; ν_{max} (solution in CDCl₃): 2981, 1687, 1660, 1597, 1236 cm⁻¹; ¹H NMR (400 MHz, CDCl₃) δ = 7.52 - 7.42 (m, 3H), 7.39 (d, *J* = 7.8 Hz, 1H), 7.36 (d, *J* = 7.8 Hz, 1H), 7.12 (s, 1H), 5.10 (app. spt, *J* = 6.4 Hz, 1H), 4.84 (q, *J* = 6.4 Hz, 1H), 4.27 (d, *J* = 14.7 Hz, 1H), 4.06 (d, *J* = 14.7 Hz, 1H), 3.80 (qd, *J* = 6.3, 7.0 Hz, 1H), 3.41 (q, *J* = 6.8 Hz, 1H), 3.24 - 3.18 (m, 3H), 3.13 (d, *J* = 7.0 Hz, 1H), 1.71 (d, *J* = 6.8 Hz, 3H), 1.42 (d, *J* = 6.4 Hz, 3H), 1.32 - 1.26 (m, 6H), 1.24 (d, *J* = 6.3 Hz, 3H), exchangeable protons not observed; ¹³C NMR (101 MHz, CDCl₃) δ = 172.7, 170.3, 159.5, 159.1, 144.3, 137.0, 133.7, 132.5, 127.4, 126.8, 125.9, 125.1, 124.6, 123.9, 69.9, 69.1, 68.2, 67.7, 52.0, 41.4, 35.8, 25.3, 21.9,

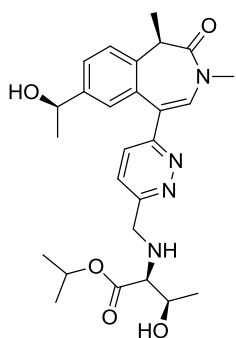
under a stream of nitrogen and the resultant residue purified by MDAP (HpH) to afford the title compound (**3.110**, 3.2 mg, 6.63 μ mol, 6 % yield) as an orange gummy oil. ^1H NMR (400 MHz, CDCl_3) δ = 8.66 (s, 2H), 7.47 (dd, J = 1.5, 8.3 Hz, 1H), 7.40 (d, J = 8.3 Hz, 1H), 6.99 (d, J = 1.5 Hz, 1H), 6.60 (s, 1H), 5.08 (spt, J = 6.3 Hz, 1H), 4.82 (q, J = 6.4 Hz, 1H), 4.18 (d, J = 15.8 Hz, 1H), 4.11 (d, J = 15.8 Hz, 1H), 3.79 (qd, J = 6.4, 7.8 Hz, 1H), 3.39 (q, J = 6.8 Hz, 1H), 3.18 (s, 3H), 3.11 (d, J = 7.8 Hz, 1H), 1.73 (d, J = 6.8 Hz, 3H), 1.41 (d, J = 6.4 Hz, 3H), 1.28 (d, J = 6.3 Hz, 6H), 1.24 (d, J = 6.4 Hz, 3H), exchangeable protons not observed; LCMS (HpH): t_{R} = 0.88 min, $[\text{M}+\text{H}^+]$ = 483.7 (100% purity).

Isopropyl ((2-((*R*)-7-((*S*)-1-hydroxyethyl)-1,3-dimethyl-2-oxo-2,3-dihydro-1*H*-benzo(*d*)azepin-5-yl)pyrimidin-5-yl)methyl)-*L*-threoninate, 3.111



A solution of (*R*)-7-((*S*)-1-hydroxyethyl)-1,3-dimethyl-5-(4,4,5,5-tetramethyl-1,3,2-dioxaborolan-2-yl)-1,3-dihydro-2*H*-benzo(*d*)azepin-2-one (**3.63**, 50 mg, 0.12 mmol), isopropyl ((2-chloropyrimidin-5-yl)methyl)-*L*-threoninate (**3.123**, 41.1 mg, 0.14 mmol), $\text{Pd}(\text{PPh}_3)_4$ (6.87 mg, 5.95 μ mol) and potassium carbonate (49.3 mg, 0.36 mmol) in 1,4-dioxane (1 mL) and water (0.50 mL) were stirred at 80°C for 10 min. The reaction mixture was diluted with water (5 mL) and partitioned with 9:1 DCM:MeOH (10 mL). The layers were separated and the organic layer was re-extracted with 9:1 DCM:MeOH (10 mL). The combined organic layers were concentrated under a stream of nitrogen and the resultant residue purified by MDAP (HpH) to afford the title compound (**3.111**, 18 mg, 0.04 mmol, 31 % yield) as an orange gummy oil. (α_{D}) $^{20.9^\circ\text{C}}$ $_{\lambda}(\text{c} = 1.0, \text{CDCl}_3)$: +156.8°; ν_{max} (solution in CDCl_3): 3431, 2979, 1663, 1425 cm^{-1} ; ^1H NMR (400 MHz, CDCl_3) δ = 8.69 (s, 2H), 7.79 (s, 1H), 7.46 (dd, J = 2.0, 8.3 Hz, 1H), 7.39 (d, J = 2.0 Hz, 1H), 7.37 (d, J = 8.3 Hz, 1H), 5.12 (app. spt, J = 6.4 Hz, 1H), 4.87 (q, J = 6.4 Hz, 1H), 3.93 (d, J = 13.7 Hz, 1H), 3.78 (qd, J = 6.4, 6.8 Hz, 1H), 3.68 (d, J = 13.7 Hz, 1H), 3.42 (q, J = 6.8 Hz, 1H), 3.23 (s, 3H), 3.02 (d, J = 6.8 Hz, 1H), 1.67 (d, J = 6.8 Hz, 3H), 1.46 (d, J = 6.4 Hz, 3H), 1.29 (app. t, J = 6.4 Hz, 6H), 1.24 (d, J = 6.4 Hz, 3H), exchangeable protons not observed; ^{13}C NMR (101 MHz, CDCl_3) δ = 172.8, 170.9, 164.9, 157.1 (2C), 143.5, 136.7, 135.3, 133.5, 129.4, 126.6, 126.4, 125.6, 124.1, 70.2, 69.2, 68.2, 67.2, 47.4, 41.5, 36.0, 25.0, 22.0, 21.8, 19.4, 12.7; LCMS (HpH): t_{R} = 0.89 mins, $[\text{M}+\text{H}^+]$ = 483.7 (100% purity); HRMS: ($\text{C}_{26}\text{H}_{34}\text{N}_4\text{O}_5$) $[\text{M}+\text{H}^+]$ requires 483.2608, found $[\text{M}+\text{H}^+]$ = 483.2601.

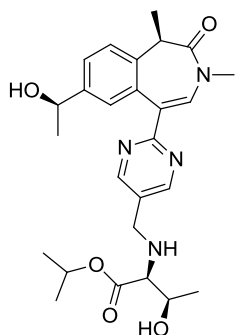
((6-((*R*)-7-((*R*)-1-hydroxyethyl)-1,3-dimethyl-2-oxo-2,3-dihydro-1*H*-benzo(*d*)azepin-5-yl)pyridazin-3-yl)methyl)-*L*-threoninate, 3.112



A solution of (*R*)-7-((*R*)-1-hydroxyethyl)-1,3-dimethyl-5-(4,4,5,5-tetramethyl-1,3,2-dioxaborolan-2-yl)-1,3-dihydro-2*H*-benzo(*d*)azepin-2-one (**3.62**, 50 mg, 0.13 mmol), isopropyl ((6-chloropyridazin-3-yl)methyl)-*L*-threoninate (**3.120**, 43.5 mg, 0.15 mmol), Pd(PPh₃)₄ (7.28 mg, 6.30 μmol) and potassium carbonate (52.2 mg, 0.38 mmol) in 1,4-dioxane (1 mL) and water (0.50 mL) were stirred at 80°C for 10 min.

The reaction mixture was diluted with water (5 mL) and partitioned with 9:1 DCM:MeOH (10 mL). The layers were separated and the organic layer was re-extracted with 9:1 DCM:MeOH (10 mL). The combined organic layers were concentrated under a stream of nitrogen and the resultant residue purified by MDAP (HpH) to afford the title compound (**3.112**, 16 mg, 0.03 mmol, 26 % yield) as a yellow gummy oil. (α_D)^{21.2°C}_c (c = 1.0, CDCl₃): +199.8°; ν_{\max} (solution in CDCl₃): 3406, 2979, 1725, 1667, 1374 cm⁻¹; ¹H NMR (400 MHz, CDCl₃) δ = 7.51 (s, 1H), 7.50 (d, *J* = 8.1 Hz, 1H), 7.49 (dd, *J* = 2.0, 8.1 Hz, 1H), 7.40 (d, *J* = 8.3 Hz, 1H), 7.35 (d, *J* = 8.8 Hz, 1H), 7.10 (d, *J* = 2.0 Hz, 1H), 5.10 (app. spt, *J* = 6.3 Hz, 1H), 4.83 (q, *J* = 6.4 Hz, 1H), 4.28 (d, *J* = 14.2 Hz, 1H), 4.06 (d, *J* = 14.2 Hz, 1H), 3.80 (qd, *J* = 6.4, 7.1 Hz, 1H), 3.41 (q, *J* = 6.8 Hz, 1H), 3.22 (s, 3H), 3.13 (d, *J* = 7.1 Hz, 1H), 1.71 (d, *J* = 6.8 Hz, 3H), 1.42 (d, *J* = 6.4 Hz, 3H), 1.29 (app. dd, *J* = 4.2, 6.3 Hz, 6H), 1.25 (d, *J* = 6.4 Hz, 3H), exchangeable protons not observed; ¹³C NMR (101 MHz, CDCl₃) δ = 172.7, 170.3, 159.5, 159.1, 144.3, 137.1, 133.7, 132.5, 127.5, 126.7, 125.9, 125.1, 124.7, 123.9, 69.9, 69.1, 68.2, 67.7, 52.0, 41.5, 35.8, 25.4, 21.9, 21.8, 19.4, 12.8; LCMS (HpH): *t*_R = 0.84 min, [M+H⁺] = 483.4 (100% purity); HRMS: (C₂₆H₃₄N₄O₅) [M+H⁺] requires 483.2608, found [M+H⁺] = 483.2607.

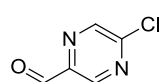
Isopropyl ((2-((*R*)-7-((*R*)-1-hydroxyethyl)-1,3-dimethyl-2-oxo-2,3-dihydro-1*H*-benzo(*d*)azepin-5-yl)pyrimidin-5-yl)methyl)-*L*-threoninate, 3.115



A solution of (*R*)-7-((*R*)-1-hydroxyethyl)-1,3-dimethyl-5-(4,4,5,5-tetramethyl-1,3,2-dioxaborolan-2-yl)-1,3-dihydro-2*H*-benzo(*d*)azepin-2-one (**3.62**, 50 mg, 0.13 mmol), isopropyl ((2-chloropyrimidin-5-yl)methyl)-*L*-threoninate (**3.123**, 43.5 mg, 0.15 mmol), Pd(PPh₃)₄ (7.28 mg, 6.30 μmol) and potassium carbonate (52.2 mg, 0.38 mmol) in 1,4-dioxane (1 mL) and water (0.50 mL) were stirred at 80°C for 10 min. The reaction mixture was diluted with water (5 mL) and partitioned with 9:1 DCM:MeOH (10 mL). The layers were separated and the

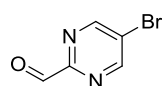
organic layer was re-extracted with 9:1 DCM:MeOH (10 mL). The combined organic layers were concentrated under a stream of nitrogen and the resultant residue purified by MDAP (HpH) to afford the title compound (**3.115**, 23.5 mg, 0.05 mmol, 39 % yield) as a yellow gummy oil. (α_D)^{20.9°C}_D(c = 1.0, CDCl₃): +174.5°; ν_{\max} (solution in CDCl₃): 3432, 2979, 1670, 1425 cm⁻¹; ¹H NMR (400 MHz, CDCl₃) δ = 8.69 (s, 2H), 7.79 (s, 1H), 7.46 (dd, *J* = 2.0, 8.3 Hz, 1H), 7.39 (d, *J* = 2.0 Hz, 1H), 7.37 (d, *J* = 8.3 Hz, 1H), 5.12 (spt, *J* = 6.3 Hz, 1H), 4.87 (q, *J* = 6.4 Hz, 1H), 3.93 (d, *J* = 13.7 Hz, 1H), 3.78 (app. quin, *J* = 6.4 Hz, 1H), 3.68 (d, *J* = 13.7 Hz, 1H), 3.42 (q, *J* = 6.8 Hz, 1H), 3.23 (s, 3H), 3.09 (br s, 1H), 3.02 (d, *J* = 6.4 Hz, 1H), 2.05 (br s, 1H), 1.71 (br s, 1H), 1.67 (d, *J* = 6.8 Hz, 3H), 1.46 (d, *J* = 6.4 Hz, 3H), 1.29 (t, *J* = 6.4 Hz, 6H), 1.24 (d, *J* = 6.3 Hz, 3H); ¹³C NMR (101 MHz, CDCl₃) δ = 172.8, 170.9, 164.9, 157.0 (2C), 143.5, 136.7, 135.2, 133.5, 129.4, 126.6, 126.5, 125.5, 124.1, 70.2, 69.2, 68.2, 67.2, 47.4, 41.5, 36.0, 25.1, 22.0, 21.8, 19.4, 12.7; LCMS (HpH): *t*_R = 0.88 mins, [M+H⁺] = 483.7 (99% purity); HRMS: (C₂₆H₃₄N₄O₅) [M+H⁺] requires 482.2608, found [M+H⁺] = 483.2608.

5-Chloropyrazine-2-carbaldehyde, 3.118



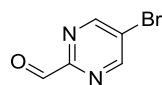
A solution of (5-chloropyrazin-2-yl)methanol (1.00 g, 6.92 mmol) and manganese(IV) oxide (7.22 g, 83.0 mmol) in chloroform (35 mL) was stirred under nitrogen at 55°C for 22 h. The reaction mixture was filtered over Celite, diluted with MeOH (50 mL) and concentrated *in vacuo* to afford the title compound (**3.118**, 250 mg, 1.75 mmol, 25 % yield) as a cream solid. ¹H NMR (400 MHz, CDCl₃) δ = 10.14 (s, 1H), 8.95 (s, 1H), 8.75 (s, 1H); LCMS (HpH): *t*_R = 0.48 min, [M+H⁺] not observed (92% purity).

5-Bromopyrimidine-2-carbaldehyde, 3.119



A solution of (5-bromopyrimidin-2-yl)methanol (250 mg, 1.32 mmol) and manganese(IV) oxide (1.38 g, 15.9 mmol) in chloroform (15 mL) was stirred under nitrogen at 55°C for 22 h. The reaction mixture was filtered over Celite, diluted with MeOH (50 mL) and concentrated *in vacuo* to afford 5-bromopyrimidine-2-carbaldehyde (**3.119**, 94 mg, 0.50 mmol, 38 % yield) as a cream solid. ¹H NMR (400 MHz, CDCl₃) δ = 10.09 (s, 1H), 9.04 (s, 2H); LCMS (HpH): *t*_R = 0.41 min, [M+H⁺] not observed (100% purity).

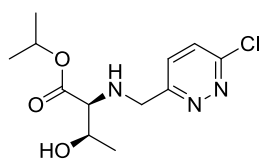
5-Bromopyrimidine-2-carbaldehyde, 3.119



A solution of (5-bromopyrimidin-2-yl)methanol (253 mg, 1.34 mmol) and manganese(IV) oxide (1.39 g, 16.0 mmol) in chloroform (15 mL) was stirred

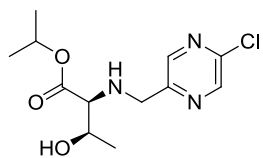
at 55°C under nitrogen overnight. The reaction mixture was diluted with methanol (15 mL) and was passed over Celite with 1:1 DCM:MeOH washings (~70 mL). The filtrate was concentrated *in vacuo* to afford 5-bromopyrimidine-2-carbaldehyde (**3.119**, 156 mg, 0.83 mmol, 62 % yield), light yellow solid. ¹H NMR (400MHz, DMSO-d₆) δ = 9.96 (s, 1H), 9.28 (s, 2H); LCMS (HpH): t_R = 0.41 min, [M+H⁺] 186.2 / 188.1 (94 % purity).

Isopropyl ((6-chloropyridazin-3-yl)methyl)-L-threoninate, **3.120**



6-Chloropyridazine-3-carbaldehyde (200 mg, 1.40 mmol) and isopropyl L-threoninate hydrochloride (**2.19**, 447 mg, 2.11 mmol) were dissolved THF (1 mL) and DIPEA (0.49 mL, 2.81 mmol) and acetic acid (0.20 mL, 3.51 mmol) added. The reaction vessel was placed under a nitrogen atmosphere and stirred at 40°C for 2 h. The reaction mixture was cooled to rt, sodium triacetoxyborohydride (595 mg, 2.81 mmol) added and the resultant suspension stirred for 2 h. The reaction mixture was quenched with water (10 mL) and partitioned with 9:1 DCM:MeOH (10 mL). The layers were separated and the aqueous layer was re-extracted with 9:1 DCM:MeOH (10 mL). The combined organics were dried (hydrophobic frit) and concentrated *in vacuo* to afford the title compound (**3.120**, 205 mg, 0.64 mmol, 46 % yield) as a yellow oil. (α_D)^{20.9°C}_D(c = 1.0, CDCl₃): -30.7°; ν_{\max} (solution in CDCl₃): 3340, 2981, 1725, 1375 cm⁻¹; ¹H NMR (400 MHz, CDCl₃) δ = 7.58 (d, J = 8.8 Hz, 1H), 7.49 (d, J = 8.8 Hz, 1H), 5.06 (app. spt, J = 6.3 Hz, 1H), 4.23 (d, J = 14.7 Hz, 1H), 4.03 (d, J = 14.7 Hz, 1H), 3.79 (qd, J = 6.4, 6.8 Hz, 1H), 3.04 (d, J = 6.8 Hz, 1H), 1.27 (app. dd, J = 4.4, 6.3 Hz, 6H), 1.22 (d, J = 6.4 Hz, 3H), NH and OH not observed; ¹³C NMR (101 MHz, CDCl₃) δ = 172.6, 160.6, 156.1, 128.5, 128.3, 69.2, 68.1, 67.4, 51.5, 21.9, 21.8, 19.4; LCMS (HpH): t_R = 0.76 min, [M+H⁺] = 288.4 (88% purity); HRMS: (C₁₂H₁₈ClN₃O₃) [M+H⁺] requires 288.1116, found [M+H⁺] = 288.1109.

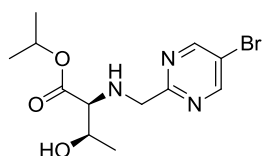
Isopropyl ((5-chloropyrazin-2-yl)methyl)-L-threoninate, **3.121**



5-Chloropyrazine-2-carbaldehyde (100 mg, 0.70 mmol) and isopropyl L-threoninate hydrochloride (**2.19**, 208 mg, 1.05 mmol) were dissolved THF (1 mL) and DIPEA (0.25 mL, 1.40 mmol) and acetic acid (0.10 mL, 1.75 mmol) added. The reaction vessel was placed under a nitrogen atmosphere and stirred at 40°C for 2 h. The reaction mixture was cooled to rt, sodium triacetoxyborohydride (297 mg, 1.40 mmol) added and the resultant suspension stirred for 2 h. The reaction mixture was quenched with water (10 mL) and partitioned with 9:1 DCM:MeOH (10 mL). The layers were separated and the aqueous layer

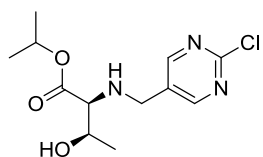
was re-extracted with 9:1 DCM:MeOH (10 mL). The combined organics were dried (hydrophobic frit) and concentrated *in vacuo*. The resultant residue was purified by flash column chromatography (silica, 0-100% ethyl acetate in in cyclohexane). The relevant fractions were combined and concentrated *in vacuo* to afford the title compound (**3.121**, 44 mg, 0.15 mmol, 22 % yield) as a yellow oil. (α_D)^{20.9°C}_D(c = 2.0, CDCl₃): +65.9°; ν_{\max} (solution in CDCl₃): 3384, 2979, 1732, 1662, 1457 cm⁻¹; ¹H NMR (400 MHz, CDCl₃) δ = 8.55 (s, 1H), 8.40 (s, 1H), 5.06 (spt, *J* = 6.4 Hz, 1H), 4.03 (d, *J* = 14.7 Hz, 1H), 3.89 (d, *J* = 14.7 Hz, 1H), 3.77 (qd, *J* = 6.4, 6.8 Hz, 1H), 3.04 (d, *J* = 6.8 Hz, 1H), 1.26 (d, *J* = 6.4 Hz, 6H), 1.23 (d, *J* = 6.4 Hz, 3H), NH and OH not observed; ¹³C NMR (101 MHz, CDCl₃) δ = 152.7, 151.2, 144.5, 143.4, 143.2, 142.7, 94.6, 72.4, 55.3, 50.6, 28.0 (2C); LCMS (HpH) *t*_R = 0.88 min, [M+H⁺] = 288.2 (95% purity); HRMS: (C₁₃H₂₀ClN₃O₅) [M+H⁺] requires 302.1272, found [M+H⁺] = 302.1267.

Isopropyl ((5-bromopyrimidin-2-yl)methyl)-L-threoninate, **3.122**



5-Bromopyrimidine-2-carbaldehyde (94 mg, 0.50 mmol) and isopropyl L-threoninate hydrochloride (**2.19**, 149 mg, 0.75 mmol) were dissolved THF (1 mL) and DIPEA (0.18 mL, 1.01 mmol) and acetic acid (0.07 mL, 1.26 mmol) added. The reaction vessel was placed under a nitrogen atmosphere and stirred at 40°C for 2 h. The reaction mixture was cooled to rt, sodium triacetoxyborohydride (213 mg, 1.01 mmol) added and the resultant suspension stirred for 2 h. The reaction mixture was quenched with water (10 mL) and partitioned with 9:1 DCM:MeOH (10 mL). The layers were separated and the aqueous layer was re-extracted with 9:1 DCM:MeOH (10 mL). The combined organics were dried (hydrophobic frit) and concentrated *in vacuo*. The resultant residue was purified by flash column chromatography (silica, 0-100% ethyl acetate in in cyclohexane). The relevant fractions were combined and concentrated *in vacuo* to afford the title compound (**3.122**, 47 mg, 0.14 mmol, 28 % yield) as a yellow oil. ¹H NMR (400 MHz, CDCl₃) δ = 8.75 (s, 2H), 5.05 (spt, *J* = 6.3 Hz, 1H), 4.05 (d, *J* = 2.4 Hz, 2H), 3.76 (qd, *J* = 6.3, 7.5 Hz, 1H), 3.08 (d, *J* = 7.5 Hz, 1H), 1.26 (d, *J* = 6.3 Hz, 6H), 1.23 (d, *J* = 6.3 Hz, 3H), NH and OH not observed; LCMS (HpH) *t*_R = 0.86 min, [M+H⁺] = 332.1 / 334.1 (96% purity).

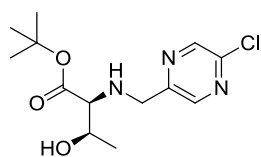
Isopropyl ((2-chloropyrimidin-5-yl)methyl)-L-threoninate, **3.123**



2-Chloropyrimidine-5-carbaldehyde (200 mg, 1.40 mmol) and isopropyl L-threoninate hydrochloride (**2.19**, 447 mg, 2.11 mmol) were dissolved THF (1 mL) and DIPEA (0.49 mL, 2.81 mmol) and

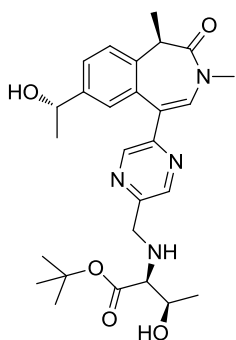
acetic acid (0.20 mL, 3.51 mmol) added. The reaction vessel was placed under a nitrogen atmosphere and stirred at 40°C for 2 h. The reaction mixture was cooled to rt, sodium triacetoxyborohydride (595 mg, 2.81 mmol) added and the resultant suspension stirred for 2 h. The reaction mixture was quenched with water (10 mL) and partitioned with 9:1 DCM:MeOH (10 mL). The layers were separated and the aqueous layer was re-extracted with 9:1 DCM:MeOH (10 mL). The combined organics were dried (hydrophobic frit) and concentrated *in vacuo*. The resultant residue was purified by flash column chromatography (silica, 0-100% ethyl acetate in cyclohexane). The relevant fractions were combined and concentrated *in vacuo* to the title compound (**3.123**, 313 mg, 1.09 mmol, 78% yield). $(\alpha_D)^{20.9^\circ C} (c = 2.0, \text{CDCl}_3): -27.5^\circ$; ν_{max} (solution in CDCl_3): 3427, 2981, 1724, 1552, 1394 cm^{-1} ; $^1\text{H NMR}$ (400 MHz, CDCl_3) $\delta = 8.60$ (s, 2H), 5.10 (app. spt, $J = 6.3$ Hz, 1H), 3.92 (d, $J = 14.2$ Hz, 1H), 3.80 (quin, $J = 6.4$ Hz, 1H), 3.68 (d, $J = 14.2$ Hz, 1H), 2.98 (d, $J = 6.4$ Hz, 1H), 1.29 (app. dd, $J = 5.3, 6.3$ Hz, 6H), 1.23 (d, $J = 6.4$ Hz, 3H), NH and OH not observed; $^{13}\text{C NMR}$ (101 MHz, CDCl_3) $\delta = 172.6, 160.6, 159.5, 131.2, 69.3, 68.2, 67.1, 46.8, 21.9, 21.8$ (2C), 19.5; LCMS (HpH) $t_R = 0.81$ min, $[\text{M}+\text{H}^+] = 288.4$ (95% purity); HRMS: ($\text{C}_{12}\text{H}_{18}\text{ClN}_3\text{O}_3$) $[\text{M}+\text{H}^+]$ requires 288.1116, found $[\text{M}+\text{H}^+] = 288.1107$.

***tert*-Butyl ((5-chloropyrazin-2-yl)methyl)-L-threoninate, 3.124**



5-Chloropyrazine-2-carbaldehyde (100 mg, 0.70 mmol) and *tert*-butyl L-threoninate hydrochloride (**2.26**, 223 mg, 1.02 mmol) were dissolved THF (1 mL) and DIPEA (0.25 mL, 1.40 mmol) and acetic acid (0.10 mL, 1.75 mmol) added. The reaction vessel was placed under a nitrogen atmosphere and stirred at 40°C for 2 h. The reaction mixture was cooled to rt, sodium triacetoxyborohydride (297 mg, 1.40 mmol) added and the resultant suspension stirred for 2 h. The reaction mixture was quenched with water (10 mL) and partitioned with 9:1 DCM:MeOH (10 mL). The layers were separated and the aqueous layer was re-extracted with 9:1 DCM:MeOH (10 mL). The combined organics were dried (hydrophobic frit) and concentrated *in vacuo*. The resultant residue was purified by flash column chromatography (silica, 0-100% ethyl acetate in cyclohexane) to afford the title compound (**3.124**, 68 mg, 0.23 mmol, 32 % yield) as a yellow oil. $^1\text{H NMR}$ (400 MHz, CDCl_3) $\delta = 8.53$ (d, $J = 1.5$ Hz, 1H), 8.41 (d, $J = 1.5$ Hz, 1H), 4.03 (d, $J = 14.7$ Hz, 1H), 3.88 (d, $J = 14.7$ Hz, 1H), 3.74 (app. quin, $J = 6.4$ Hz, 1H), 2.97 (d, $J = 6.4$ Hz, 1H), 1.47 (s, 9H), 1.24 (d, $J = 6.4$ Hz, 3H), NH and OH not observed; LCMS (HpH): $t_R = 0.95$ min, $[\text{M}+\text{H}^+] = 302.2$ (96% purity).

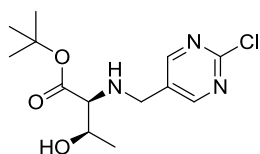
***tert*-Butyl ((5-((*R*)-7-((*S*)-1-hydroxyethyl)-1,3-dimethyl-2-oxo-2,3-dihydro-1*H*-benzo[*d*]azepin-5-yl)pyrazin-2-yl)methyl)-*L*-threoninate, 3.125**



A solution of (*R*)-7-((*S*)-1-hydroxyethyl)-1,3-dimethyl-5-(4,4,5,5-tetramethyl-1,3,2-dioxaborolan-2-yl)-1,3-dihydro-2*H*-benzo[*d*]azepin-2-one (**3.63**, 50 mg, 0.13 mmol), *tert*-butyl ((5-chloropyrazin-2-yl)methyl)-*L*-threoninate (**3.124**, 45.6 mg, 0.15 mmol), Pd(PPh₃)₄ (7.28 mg, 6.30 μmol) and potassium carbonate (52.2 mg, 0.38 mmol) in 1,4-dioxane (1 mL) and water (0.5 mL) were stirred at 80°C for 10 min. The reaction mixture was diluted with water (5 mL) and partitioned

with 9:1 DCM:MeOH (10 mL). The layers were separated and the organic layer was re-extracted with 9:1 DCM:MeOH (10 mL). The combined organic layers were concentrated under a stream of nitrogen and the resultant residue purified by MDAP (HpH) to afford the title compound (**3.125**, 11 mg, 0.02 mmol, 18 % yield) as a yellow gummy oil. (α_D)^{20.9°C}_c (c = 1.0, CDCl₃): +89.5°; ν_{\max} (solution in CDCl₃): 3422, 2976, 1724, 1664, 1368 cm⁻¹; ¹H NMR (400 MHz, CDCl₃) δ = 8.61 (d, *J* = 1.5 Hz, 1H), 8.46 (d, *J* = 1.5 Hz, 1H), 7.48 (dd, *J* = 1.5, 8.3 Hz, 1H), 7.40 (d, *J* = 8.3 Hz, 1H), 7.30 (s, 1H), 7.22 (d, *J* = 1.5 Hz, 1H), 4.85 (q, *J* = 6.4 Hz, 1H), 4.08 (d, *J* = 14.7 Hz, 1H), 3.91 (d, *J* = 14.7 Hz, 1H), 3.74 (qd, *J* = 6.4, 7.3 Hz, 1H), 3.40 (q, *J* = 6.8 Hz, 1H), 3.21 (s, 3H), 3.01 (d, *J* = 7.3 Hz, 1H), 1.71 (d, *J* = 6.8 Hz, 3H), 1.48 (s, 9H), 1.44 (d, *J* = 6.4 Hz, 3H), 1.25 (d, *J* = 6.4 Hz, 3H), exchangeable protons not observed; ¹³C NMR (101 MHz, CDCl₃) δ = 172.5, 170.5, 152.5, 151.5, 144.3, 143.7, 143.1, 137.0, 133.5, 132.4, 126.8, 125.3, 124.6, 124.2, 82.2, 69.9, 68.5, 68.2, 51.3, 41.4, 35.8, 28.1 (3C), 25.2, 19.42, 12.8; LCMS (HpH): *t*_R = 0.96 mins, [M+H⁺] = 497.4 (98% purity); HRMS: (C₂₇H₃₆N₄O₅) [M+H⁺] requires 497.2765, found [M+H⁺] = 497.2764.

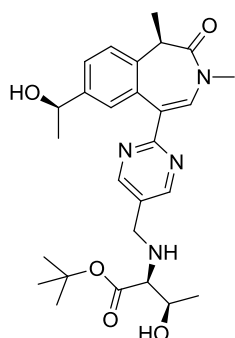
***tert*-Butyl ((2-chloropyrimidin-5-yl)methyl)-*L*-threoninate, 3.127**



2-Chloropyrimidine-5-carbaldehyde (100 mg, 0.70 mmol) and *tert*-butyl *L*-threoninate hydrochloride (**2.26**, 223 mg, 1.05 mmol) were dissolved THF (10 mL) and DIPEA (0.25 mL, 1.40 mmol) and acetic acid (0.1 mL, 1.75 mmol) added. The reaction vessel was placed under a nitrogen atmosphere and stirred at 40°C for 2 h. The reaction mixture was cooled to rt, sodium triacetoxyborohydride (372 mg, 1.75 mmol) added and the resultant suspension stirred for 2 h. The reaction mixture was quenched with water (10 mL) and partitioned with 9:1 DCM:MeOH (10 mL). The layers were separated and the aqueous layer was re-extracted with 9:1 DCM:MeOH (10 mL). The combined organics were dried (hydrophobic frit) and concentrated *in vacuo*. The resultant residue was purified by flash column chromatography

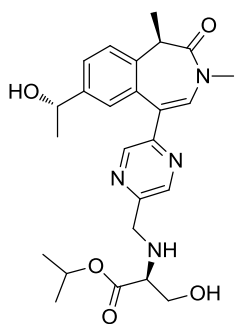
(silica, 0-100% ethyl acetate in in cyclohexane) to afford the title compound (**3.127**, 192 mg, 0.60 mmol, 86 % yield) as a yellow oil. ¹H NMR (400 MHz, CDCl₃) δ = 8.60 (s, 2H), 3.90 (d, *J* = 13.7 Hz, 1H), 3.76 (app. quin, *J* = 6.4 Hz, 1H), 3.68 (d, *J* = 13.7 Hz, 1H), 2.90 (d, *J* = 6.4 Hz, 1H), 1.49 (s, 9H), 1.23 (d, *J* = 6.4 Hz, 3H), NH and OH not observed; LCMS (HpH) *t_R* = 0.90 min, [M+H⁺] = 302.4 (93% purity).

tert*-Butyl ((2-((*R*)-7-((*R*)-1-hydroxyethyl)-1,3-dimethyl-2-oxo-2,3-dihydro-1*H*-benzo[*d*]azepin-5-yl)pyrimidin-5-yl)methyl)-*L*-threoninate, **3.128*



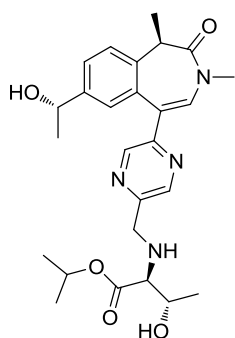
A solution of (*R*)-7-((*R*)-1-hydroxyethyl)-1,3-dimethyl-5-(4,4,5,5-tetramethyl-1,3,2-dioxaborolan-2-yl)-1,3-dihydro-2*H*-benzo[*d*]azepin-2-one (**3.62**, 50 mg, 0.13 mmol), *tert*-butyl ((2-chloropyrimidin-5-yl)methyl)-*L*-threoninate (**3.127**, 45.6 mg, 0.15 mmol), Pd(PPh₃)₄ (7.28 mg, 6.30 μmol) and potassium carbonate (52.2 mg, 0.38 mmol) in 1,4-dioxane (1 mL) and water (0.5 mL) were stirred at 80°C for 10 min. The reaction mixture was diluted with water (5 mL) and partitioned with 9:1 DCM:MeOH (10 mL). The layers were separated and the organic layer was re-extracted with 9:1 DCM:MeOH (10 mL). The combined organic layers were concentrated under a stream of nitrogen and the resultant residue purified by MDAP (HpH) to afford the title compound (**3.128**, 21.5 mg, 0.04 mmol, 34 % yield) as a yellow gummy oil. (α_D)^{20.9°C}_{λ(c = 1.0, H₂O)}: +98.6°; ν_{max} (solution in CDCl₃): 3431, 2977, 1633, 1368 cm⁻¹; ¹H NMR (400 MHz, CDCl₃) δ = 8.70 (s, 2H), 7.79 (s, 1H), 7.47 (dd, *J* = 2.0, 8.3 Hz, 1H), 7.40 (d, *J* = 2.0 Hz, 1H), 7.37 (d, *J* = 8.3 Hz, 1H), 4.88 (q, *J* = 6.4 Hz, 1H), 3.92 (d, *J* = 13.7 Hz, 1H), 3.74 (qd, *J* = 6.4, 6.8 Hz, 1H), 3.68 (d, *J* = 13.7 Hz, 1H), 3.42 (q, *J* = 6.8 Hz, 1H), 3.23 (s, 3H), 3.08 (br s, 1H), 2.94 (d, *J* = 6.8 Hz, 1H), 1.90 (br s, 1H), 1.68 (d, *J* = 6.8 Hz, 3H), 1.62 (br s, 1H), 1.51 (s, 9H), 1.47 (d, *J* = 6.4 Hz, 3H), 1.24 (d, *J* = 6.4 Hz, 3H); ¹³C NMR (101 MHz, CDCl₃) δ = 172.5, 170.9, 164.8, 157.0 (2C), 143.5, 136.7, 135.2, 133.5, 129.5, 126.6, 126.5, 125.5, 124.1, 82.5, 70.2, 68.2, 67.8, 47.4, 41.5, 36.0, 28.2 (3C), 25.1, 19.4, 12.7; LCMS (HpH): *t_R* = 0.95 mins, [M+H⁺] = 497.7 (100% purity); HRMS: (C₂₇H₃₆N₄O₅) [M+H⁺] requires 497.2765, found [M+H⁺] = 497.2762.

Isopropyl ((5-((*R*)-7-((*S*)-1-hydroxyethyl)-1,3-dimethyl-2-oxo-2,3-dihydro-1*H*-benzo(*d*)azepin-5-yl)pyrazin-2-yl)methyl)-L-serinate, 3.129



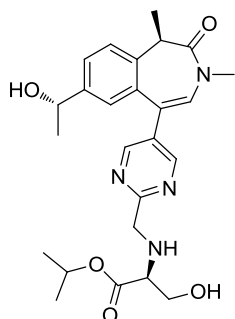
A solution of potassium carbonate (39.5 mg, 0.29 mmol) in water (0.50 mL) was added to a suspension of (*R*)-7-((*S*)-1-hydroxyethyl)-1,3-dimethyl-5-(4,4,5,5-tetramethyl-1,3,2-dioxaborolan-2-yl)-1,3-dihydro-2*H*-benzo(*d*)azepin-2-one (**3.63**, 40 mg, 0.10 mmol), isopropyl ((5-bromopyrazin-2-yl)methyl)-L-serinate (**3.138**, 30.3 mg, 0.10 mmol) and PdCl₂(dppf) (3.48 mg, 4.76 μmol) in 1,4-dioxane (1 mL) and the reaction mixture was stirred on a pre-heated stirrer hot plate at 80°C for 10 min. The reaction mixture was diluted with water (5 mL) and partitioned with 9:1 DCM:MeOH (10 mL). The layers were separated and the organic layer was re-extracted with 9:1 DCM:MeOH (10 mL). The combined organic layers were concentrated under a stream of nitrogen and the resultant residue purified by flash column chromatography (alumina, 0-100% ethyl acetate in cyclohexane, 0-30% ethanol in ethyl acetate) to afford a yellow gummy oil. The oil was further purified by MDAP (HpH) to afford the title compound (**3.129**, 15 mg, 0.03 mmol, 34 % yield) as a yellow gum. (α_D)^{20.9°C}_λ(*c* = 1.0, CDCl₃): +212.1°; ν_{\max} (solution in CDCl₃): 3415, 2979, 1669, 1625, 1270 cm⁻¹; ¹H NMR (400 MHz, CDCl₃) δ = 8.60 (d, *J* = 1.5 Hz, 1H), 8.47 (d, *J* = 1.5 Hz, 1H), 7.48 (dd, *J* = 1.8, 8.3 Hz, 1H), 7.41 (d, *J* = 8.3 Hz, 1H), 7.30 (s, 1H), 7.21 (d, *J* = 1.8 Hz, 1H), 5.09 (app. spt, *J* = 6.3 Hz, 1H), 4.85 (q, *J* = 6.4 Hz, 1H), 4.13 (d, *J* = 14.7 Hz, 1H), 3.96 (d, *J* = 14.7 Hz, 1H), 3.84 (dd, *J* = 4.4, 10.8 Hz, 1H), 3.69 (dd, *J* = 6.4, 10.8 Hz, 1H), 3.48 (s, 1H), 3.41 (q, *J* = 6.8 Hz, 1H), 3.22 (s, 3H), 1.71 (d, *J* = 6.8 Hz, 3H), 1.44 (d, *J* = 6.4 Hz, 3H), 1.28 (app. t, *J* = 6.3 Hz, 6H), exchangeable protons not observed; ¹³C NMR (101 MHz, CDCl₃) δ = 172.1, 170.5, 152.5, 151.6, 144.3, 143.7, 143.1, 137.0, 133.5, 132.4, 126.8, 125.3, 124.6, 124.2, 124.1, 69.9, 62.7, 62.6, 50.6, 41.4, 35.8, 25.2, 21.9, 21.8, 12.7; LCMS (HpH): *t*_R = 0.82 min, [M+H⁺] = 469.4 (99% purity); HRMS: (C₂₅H₃₂N₄O₅) [M+H⁺] requires 469.2452, found [M+H⁺] = 469.2447.

Isopropyl ((5-((R)-7-((S)-1-hydroxyethyl)-1,3-dimethyl-2-oxo-2,3-dihydro-1H-benzo(d)azepin-5-yl)pyrazin-2-yl)methyl)-L-allothreoninate, 3.130



A solution of potassium carbonate (74.0 mg, 0.54 mmol) in water (0.62 mL) was added to a solution of (R)-7-((S)-1-hydroxyethyl)-1,3-dimethyl-5-(4,4,5,5-tetramethyl-1,3,2-dioxaborolan-2-yl)-1,3-dihydro-2H-benzo(d)azepin-2-one (**3.63**, 75 mg, 0.18 mmol), isopropyl ((5-bromopyrazin-2-yl)methyl)-L-allothreoninate (**3.139**, 143 mg, 0.34 mmol) and PdCl₂(dppf) (6.53 mg, 8.92 μmol) in 1,4-dioxane (1.25 mL) and the resulting solution was stirred at 80°C for 1.75 h, after which the reaction was left standing at rt overnight. To the reaction mixture 9:1 DCM:MeOH (10 mL) was added and was partitioned with water (10 mL). The aqueous layer was re-extracted with 9:1 DCM:MeOH (3 x 10 mL). The combined organic layers were dried (hydrophobic frit) and concentrated *in vacuo* to afford a dark orange oil. The oil was purified by flash column chromatography (alumina, 0-100 % ethyl acetate in cyclohexane, flushed with ethanol). The relevant fractions were combined and concentrated *in vacuo* to afford an orange oil. The oil was purified again by MDAP (Formic) to afford the title compound (**3.130**, 3.3 mg, 6.84 μmol, 4 % yield) as a colourless oil. ¹H NMR (400 MHz, CDCl₃) δ = 8.61 (d, *J* = 1.5 Hz, 1H), 8.46 (d, *J* = 1.5 Hz, 1H), 7.47 (dd, *J* = 1.5, 8.3 Hz, 1H), 7.40 (d, *J* = 8.3 Hz, 1H), 7.30 (s, 1H), 7.21 (d, *J* = 1.5 Hz, 1H), 5.11 (app. spt, *J* = 6.3 Hz, 1H), 4.85 (q, *J* = 6.4 Hz, 1H), 4.14 (d, *J* = 14.2 Hz, 1H), 4.08 (dq, *J* = 4.4, 6.4 Hz, 1H), 3.91 (d, *J* = 14.2 Hz, 1H), 3.43 (d, *J* = 4.4 Hz, 1H), 3.41 (q, *J* = 6.8 Hz, 1H), 3.22 (s, 3H), 1.71 (d, *J* = 6.8 Hz, 3H), 1.44 (d, *J* = 6.4 Hz, 3H), 1.28 (app. dd, *J* = 6.3, 7.8 Hz, 6H), 1.15 (d, *J* = 6.4 Hz, 3H), exchangeable protons not observed; LCMS (HpH): t_R = 0.87 min, [M+H⁺] = 483.4 (100 % purity).

Isopropyl ((5-((R)-7-((S)-1-hydroxyethyl)-1,3-dimethyl-2-oxo-2,3-dihydro-1H-benzo(d)azepin-5-yl)pyrimidin-2-yl)methyl)-L-serinate, 3.131



Method 1, Table 3.25

To a solution of (R)-7-((S)-1-hydroxyethyl)-1,3-dimethyl-5-(4,4,5,5-tetramethyl-1,3,2-dioxaborolan-2-yl)-1,3-dihydro-2H-benzo(d)azepin-2-one (**3.63**, 100 mg, 0.25 mmol), PdCl₂(dppf) (9.22 mg, 0.01 mmol) and isopropyl ((5-bromopyrimidin-2-yl)methyl)-L-serinate (**3.140**, 104 mg, 0.28 mmol) in 1,4-dioxane (2 mL) was added a solution of potassium carbonate (104 mg, 0.76 mmol) in water (1.00 mL). The resultant solution was stirred at 80°C for 1 h. The reaction mixture was diluted with water

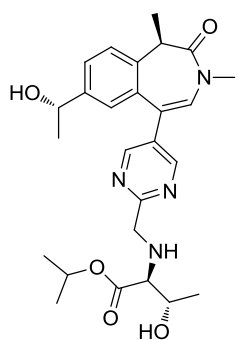
(10 mL) and partitioned with 9:1 DCM:MeOH (10 mL). The layers were separated and the organic layer was re-extracted with 9:1 DCM:MeOH (10 mL). The combined organic layers were dried (hydrophobic frit) and concentrated under reduced pressure. The residue was purified by MDAP (HpH) to afford the title compound (**3.131**, 23.0 mg, 0.05 mmol, 19 % yield) as a yellow oil.

Method 2, Scheme 3.49

To a solution of (*R*)-7-((*S*)-1-hydroxyethyl)-1,3-dimethyl-5-(4,4,5,5-tetramethyl-1,3,2-dioxaborolan-2-yl)-1,3-dihydro-2*H*-benzo[*d*]azepin-2-one (**3.63**, 600 mg, 0.92 mmol), tetrakis(triphenylphosphine)palladium(0) (53.4 mg, 0.05 mmol) and isopropyl ((5-bromopyrimidin-2-yl)methyl)-*L*-serinate (**3.140**, 294 mg, 0.92 mmol) in 1,4-dioxane (10 mL) was added a solution of potassium carbonate (383 mg, 2.77 mmol) in water (5 ml). The resultant solution was stirred at 80°C for 20 min. The reaction mixture was diluted with water (10 mL) and partitioned with 9:1 DCM:MeOH (10 mL). The layers were separated and the organic layer was re-extracted with 9:1 DCM:MeOH (10 mL). The combined organic layers were dried (hydrophobic frit) and concentrated under reduced pressure. The residue was purified by flash column chromatography (silica, 0-100% water-saturated ethyl acetate in cyclohexane then holding at 100% water-saturated ethyl acetate). The relevant fractions were concentrated under reduced pressure to a minimal volume at which point the product precipitated. Filtration afforded batch 1 of the title compound (**3.131**, 252 mg, 0.54 mmol, 58 % yield) as a white solid. The filtrate was concentrated under reduced pressure to afford batch 2 of the title compound (**3.131**, 150 mg, 0.32 mmol, 34 % yield) as a yellow oil which solidified to a yellow solid upon standing.

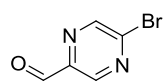
M.pt: 108.9 - 118.5°C (collected on a solid batch); (α_D)^{20.9°C}_D(c = 1.0, CDCl₃): +75.6°; ν_{\max} (solution in CDCl₃): 3404, 2797, 1729, 1667, 1376 cm⁻¹; ¹H NMR (400 MHz, CDCl₃) δ = 8.67 (s, 2H), 7.46 (dd, *J* = 1.5, 8.3 Hz, 1H), 7.40 (d, *J* = 8.3 Hz, 1H), 7.00 (d, *J* = 1.5 Hz, 1H), 6.62 (s, 1H), 5.10 (app. spt, *J* = 6.3 Hz, 1H), 4.82 (q, *J* = 6.4 Hz, 1H), 4.30 (d, *J* = 16.1 Hz, 1H), 4.17 (d, *J* = 16.1 Hz, 1H), 3.90 (dd, *J* = 3.9, 11.2 Hz, 1H), 3.76 (dd, *J* = 6.4, 11.2 Hz, 1H), 3.60 (dd, *J* = 3.9, 6.4 Hz, 1H), 3.39 (q, *J* = 6.8 Hz, 1H), 3.19 (s, 3H), 1.73 (d, *J* = 6.8 Hz, 3H), 1.40 (d, *J* = 6.4 Hz, 3H), 1.28 (app. dd, *J* = 4.0, 6.3 Hz, 6H), exchangeable protons not observed; ¹³C NMR (101 MHz, CDCl₃) δ = 171.5, 170.3, 166.6, 156.7 (2C), 144.7, 136.9, 134.2, 132.3, 130.2, 127.1, 124.7, 124.1, 123.9, 69.7, 69.3, 62.8, 62.3, 53.0, 41.3, 35.6, 25.2, 21.8, 21.8, 12.8; LCMS (HpH): *t*_R = 0.81 min, [M+H⁺] = 469.4 (95% purity); HRMS: (C₂₅H₃₂N₄O₅) [M+H⁺] requires 469.2452, found [M+H⁺] = 469.2446.

Isopropyl ((5-((*R*)-7-((*S*)-1-hydroxyethyl)-1,3-dimethyl-2-oxo-2,3-dihydro-1*H*-benzo(*d*)azepin-5-yl)pyrimidin-2-yl)methyl)-L-allothreoninate, 3.132



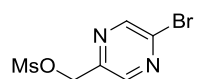
A solution of potassium carbonate (81 mg, 0.59 mmol) in water (0.50 mL) was added to a solution of (*R*)-7-((*S*)-1-hydroxyethyl)-1,3-dimethyl-5-(4,4,5,5-tetramethyl-1,3,2-dioxaborolan-2-yl)-1,3-dihydro-2*H*-benzo(*d*)azepin-2-one (**3.63**, 82 mg, 0.20 mmol), PdCl₂(dppf)·DCM adduct (7.97 mg, 9.75 μmol) and isopropyl ((5-bromopyrimidin-2-yl)methyl)-L-allothreoninate (**3.141**, 64.8 mg, 0.20 mmol) in 1,4-dioxane (1 mL) and the resulting solution was stirred at 80°C for 1 h. The reaction mixture was diluted with 9:1 DCM:MeOH (10 mL) and was partitioned with water (10 mL). The aqueous layer was re-extracted with 9:1 DCM:MeOH (3 x 10 mL) and the combined organic layers were dried (hydrophobic frit) before being concentrated *in vacuo* to afford a dark brown oil. The oil was purified by flash column chromatography (alumina, 0-100 % ethyl acetate in cyclohexane, 0-20 % ethanol in ethyl acetate). The fractions were combined *in vacuo* to afford a brown oil. The oil was purified by MDAP (HpH) to afford the title compound (**3.132**, 35 mg, 0.07 mmol, 37 % yield) as an orange oil. ¹H NMR (400 MHz, CDCl₃) δ = 8.65 (s, 2H), 7.44 (dd, *J* = 1.5, 8.1 Hz, 1H), 7.38 (d, *J* = 8.1 Hz, 1H), 6.99 (d, *J* = 1.5 Hz, 1H), 6.61 (s, 1H), 5.09 (app. spt, *J* = 6.3 Hz, 1H), 4.81 (q, *J* = 6.4 Hz, 1H), 4.26 (d, *J* = 16.1 Hz, 1H), 4.09 (dq, *J* = 3.9, 6.4 Hz, 1H), 4.04 (d, *J* = 16.1 Hz, 1H), 3.48 (d, *J* = 3.9 Hz, 1H), 3.39 (q, *J* = 6.8 Hz, 1H), 3.17 (s, 3H), 1.72 (d, *J* = 6.8 Hz, 3H), 1.39 (d, *J* = 6.4 Hz, 3H), 1.28 (app. t, *J* = 6.3 Hz, 6H), 1.14 (d, *J* = 6.4 Hz, 3H), exchangeable protons not observed; LCMS (HpH): t_R = 0.84 min, [M+H⁺] = 483.4 (97 % purity).

5-Bromopyrazine-2-carbaldehyde^e, 3.134



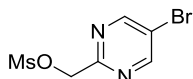
A solution of (5-bromopyrazin-2-yl)methanol (250 mg, 1.32 mmol) and manganese(IV) oxide (1.38 g, 15.9 mmol) in chloroform (15 mL) was stirred at 55°C for 6 h. The reaction mixture was diluted with methanol (15 mL) and was passed over Celite with copious washings of 1:1 MeOH:DCM (~250 mL). The filtrate was dried (hydrophobic frit) before being concentrated *in vacuo* to afford 5-bromopyrazine-2-carbaldehyde (**3.134**, 223 mg, 1.19 mmol, 90 % yield) as a yellow oil. ¹H NMR (400MHz, DMSO-d₆) δ = 10.06 (s, 1H), 9.11 (d, *J* = 1.5 Hz, 1H), 8.94 (d, *J* = 1.5 Hz, 1H); LCMS (HpH): t_R = 0.52 min, [M+H⁺] = not observed (100 % purity).

(5-Bromopyrazin-2-yl)methyl methanesulfonate, 3.135



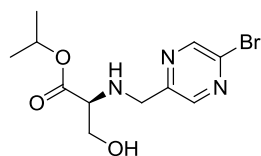
Methanesulfonyl chloride (0.29 mL, 3.69 mmol) was added to a stirring solution of (5-bromopyrazin-2-yl)methanol (465 mg, 2.46 mmol) and triethylamine (0.51 mL, 3.69 mmol) in DCM (5 mL). The reaction mixture was stirred at rt for 10 min. To the reaction mixture 9:1 DCM:MeOH (10 mL) was added and the solution was partitioned with water (15 mL). The aqueous layer was re-extracted with 9:1 DCM:MeOH (3 x 10 mL). The combined organic layers were dried and were concentrated *in vacuo* to afford the title compound (**3.135**, 561 mg, 1.76 mmol, 84 wt%, 72 % yield) as a pale yellow oil. ν_{\max} (solution in CDCl_3): 3449, 2977, 1677, 1602, 1353 cm^{-1} , $^1\text{H NMR}$ (400 MHz, CDCl_3) δ = 8.69 (d, J = 1.5 Hz, 1H), 8.52 (d, J = 1.5 Hz, 1H), 5.33 (s, 2H), 3.13 (s, 3H); $^{13}\text{C NMR}$ (101 MHz, CDCl_3) δ = 140.9, 136.1, 129.2, 128.9, 124.1, 84.0; LCMS (HpH): t_{R} = 0.73 min, $[\text{M}+\text{H}^+]$ not observed (84 % purity); HRMS: ($\text{C}_6\text{H}_7\text{BrN}_2\text{O}_3\text{S}$) $[\text{M}+\text{H}^+]$ requires 266.9440, found $[\text{M}+\text{H}^+] = 266.9438$.

(5-Bromopyrimidin-2-yl)methyl methanesulfonate, 3.136



A solution of (5-bromopyrimidin-2-yl)methanol (200 mg, 1.06 mmol) and triethylamine (0.22 mL, 1.59 mmol) in DCM (3 mL) was cooled to 0°C. To this solution, methanesulfonyl chloride (0.12 mL, 1.59 mmol) was added dropwise and the resultant solution was stirred at 0°C for 5 min. The reaction mixture was diluted with 9:1 DCM:MeOH (10 mL) and partitioned with water (20 mL). The aqueous layer was re-extracted with three further portions of 9:1 DCM:MeOH (3 x 10 mL). The combined organic layers were dried (hydrophobic frit) before being concentrated *in vacuo* to afford the title compound (**3.136**, 280 mg, 1.05 mmol, 99 % yield) as an orange solid. $^1\text{H NMR}$ (400MHz, CDCl_3) δ = 8.84 (s, 2H), 5.40 (s, 2H), 3.21 (s, 3H); LCMS (HpH): t_{R} = 0.68 min, $[\text{M}+\text{H}^+] = 267.2 / 269.2$ (98 % purity).

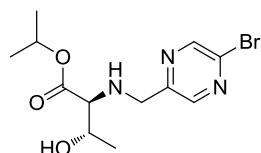
Isopropyl ((5-bromopyrazin-2-yl)methyl)-L-serinate, 3.138



(5-Bromopyrazin-2-yl)methyl methanesulfonate (**3.135**, 160 mg, 0.48 mmol, 80 wt%), triethylamine (0.20 mL, 1.44 mmol) and isopropyl L-serinate (**3.103**, 70.5 mg, 0.48 mmol) were stirred in ethanol (2 mL) under nitrogen at 80°C for 20 min. The reaction mixture was concentrated under reduced pressure to afford an orange oil. The oil was dissolved in DCM (5 mL) and partitioned with water (5 mL). The organic phase was dried (hydrophobic frit) and concentrated under reduced pressure. The resultant oil was purified by flash column chromatography (alumina, 50-100% ethyl acetate in cyclohexane followed by

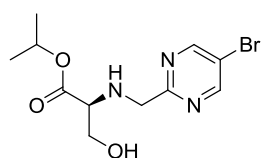
0-30% ethanol in ethyl acetate) to afford the title compound (**3.138**, 30 mg, 0.09 mmol, 20 % yield) as a yellow oil. ¹H NMR (400 MHz, CDCl₃) δ = 8.63 (d, *J* = 1.5 Hz, 1H), 8.39 (d, *J* = 1.5 Hz, 1H), 5.08 (app. t, *J* = 6.3 Hz, 1H), 4.06 (d, *J* = 14.7 Hz, 1H), 3.89 (d, *J* = 14.7 Hz, 1H), 3.84 - 3.78 (m, 1H), 3.71 - 3.66 (m, 1H), 3.43 (dd, *J* = 4.4, 6.3 Hz, 1H), 1.27 (dd, *J* = 5.1, 6.3 Hz, 6H), NH and OH not observed; LCMS (HpH): *t*_R = 0.80 min, [M+H⁺] = 316.1 / 318.1, (100% purity).

Isopropyl ((5-bromopyrazin-2-yl)methyl)-L-allothreoninate, **3.139**



A solution of (5-bromopyrazin-2-yl)methyl methanesulfonate (**3.135**, 386 mg, 1.21 mmol, 84 wt%), isopropyl L-allothreoninate (**3.137**, 167 mg, 14 mmol) and triethylamine (0.43 mL, 3.11 mmol) in ethanol was stirred at 80°C for 2 h. The reaction mixture was cooled to rt and was concentrated *in vacuo* to afford a brown oil. The oil was dissolved in 9:1 DCM:MeOH (10 mL) and partitioned with water (10 mL). The aqueous layer was re-extracted with 9:1 DCM:MeOH (3 x 10 mL). The combined organic layers were dried (hydrophobic frit) and being concentrated *in vacuo* to afford the title compound (**3.139**, 193 mg, 0.44 mmol, 42 % yield) as a brown oil. ¹H NMR (400 MHz, CDCl₃) δ = 8.63 (d, *J* = 1.5 Hz, 1H), 8.40 (d, *J* = 1.5 Hz, 1H), 5.09 (app. spt, *J* = 6.3 Hz, 1H), 4.10 - 4.01 (m, 2H), 3.84 (d, *J* = 14.7 Hz, 1H), 3.37 (d, *J* = 4.4 Hz, 1H), 1.28 (d, *J* = 6.3 Hz, 3H), 1.26 (d, *J* = 6.3 Hz, 3H), 1.13 (d, *J* = 6.4 Hz, 3H), NH and OH not observed; LCMS (HpH): *t*_R = 0.87 min, [M+H⁺] = 332.1 / 334.1 (78 % purity).

Isopropyl ((5-bromopyrimidin-2-yl)methyl)-L-serinate, **3.140**, Table 3.24



Method 1, Table 3.24

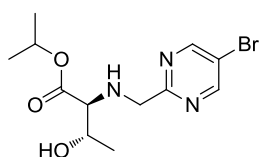
(5-Bromopyrimidin-2-yl)methyl methanesulfonate (**3.136**, 235 mg, 0.53 mmol, 60 wt%), triethylamine (0.22 mL, 1.58 mmol) and isopropyl L-serinate (**3.103**, 78 mg, 0.53 mmol) were stirred in ethanol (2 mL) under nitrogen at 80°C for 1 h. The reaction mixture was concentrated under reduced pressure. The resultant oil was dissolved in DCM (5 mL) and partitioned with water (5 mL). The aqueous phase was re-extracted with DCM (5 mL). The combined organic layers were dried (hydrophobic frit) and concentrated under reduced pressure to afford the title compound (**3.140**, 182 mg, 0.29 mmol, 50 wt%, 54 % yield).

Method 2, Scheme 3.49

A solution of (5-bromopyrimidin-2-yl)methyl methanesulfonate (**3.136**, 50 mg, 0.19 mmol), isopropyl L-serinate (**3.103**, 41.3 mg, 0.28 mmol) and DIPEA (0.03 mL, 0.19 mmol) in acetonitrile (2 mL) was stirred at 80°C for 5 h 45 min. The reaction mixture was diluted with 9:1 DCM:MeOH (10 mL) and partitioned with water (10 mL). The aqueous layer was re-extracted with 9:1 DCM:MeOH (3 x 10 mL). The combined organic layers were dried (hydrophobic frit) and concentrated *in vacuo* to afford a yellow oil. The oil was purified by flash column chromatography (silica, 0-100 % water saturated ethyl acetate in cyclohexane) to afford the title compound (**3.140**, 44 mg, 0.14 mmol, 74 % yield) as a yellow solid. Chiral analysis conducted on a 250 mm x 46 mm Chiralpak AD 10µm column, eluting with a gradient of 30% ethanol in heptane at a flow rate of 1 mL/min showed the compound to have an e.e of 100%.

(α_D)^{20.9°C}_λ(c = 2.0, CDCl₃): -19.5; ν_{\max} (solution in CDCl₃): 3161, 2979, 1722, 1543, 1423 cm⁻¹; ¹H NMR (400 MHz, CDCl₃) δ = 8.75 (s, 2H), 5.07 (app. spt, *J* = 6.3 Hz, 1H), 4.14 (d, *J* = 16.1 Hz, 1H), 4.04 (d, *J* = 16.1 Hz, 1H), 3.83 (dd, *J* = 4.4, 11.3 Hz, 1H), 3.69 (dd, *J* = 6.4, 11.3 Hz, 1H), 3.48 (dd, *J* = 4.4, 6.4 Hz, 1H), 1.26 (app. dd, *J* = 3.7, 6.3 Hz, 6H); ¹³C NMR (101 MHz, CDCl₃) δ = 172.0, 166.7, 157.8 (2C), 118.5, 69.1, 62.7, 62.6, 53.0, 21.83, 21.79; LCMS (Formic): *t*_R = 0.40 min, [M+H⁺] = 318.2 / 320.2 (100% purity); HRMS: (C₁₁H₁₆BrN₃O₃) [M+H⁺] requires 318.0454, found [M+H⁺] = 318.0454.

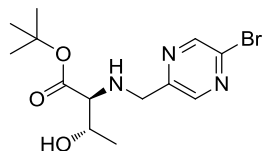
Isopropyl ((5-bromopyrimidin-2-yl)methyl)-L-allothreoninate, 3.141



A solution of (5-bromopyrimidin-2-yl)methyl methanesulfonate (**3.136**, 286 mg, 1.07 mmol), isopropyl L-allothreoninate (**3.137**, 259 mg, 1.61 mmol) and sodium bicarbonate (270 mg, 3.21 mmol) in acetonitrile (12 mL) was stirred at 70°C for 14 h. The reaction mixture was diluted with 9:1 DCM:MeOH (20 mL) and was partitioned with water (25 mL). The aqueous layer was re-extracted with 9:1 DCM:MeOH (3 x 20 mL). The combined organic layers were dried (hydrophobic frit) and concentrated *in vacuo* to afford a yellow oil. The oil was purified by column chromatography (alumina, 0-100 % ethyl acetate in cyclohexane, 10-20 % ethanol in ethyl acetate). The column was flushed with 100% ethanol. The fractions were combined and concentrated *in vacuo* to afford a pale yellow solid. The solid was purified by MDAP (Formic). The fractions were combined and concentrated *in vacuo* to afford a solid. The solid was dissolved in methanol (~10 mL) and was passed over a 5 g aminopropyl cartridge with methanol (~40 mL). The filtrate was concentrated *in vacuo* to

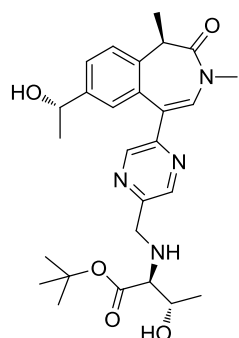
the title compound (**3.141**, 167 mg, 0.50 mmol, 50 wt%, 47 % yield) as a white solid. ¹H NMR (400 MHz, CDCl₃) δ = 8.75 (s, 2H), 5.07 (app. spt, *J* = 6.3 Hz, 1H), 4.14 (d, *J* = 16.1 Hz, 1H), 4.07 (dd, *J* = 4.4, 6.4 Hz, 1H), 3.99 (d, *J* = 16.1 Hz, 1H), 3.45 (d, *J* = 4.4 Hz, 1H), 3.10 (br s, 2H), 1.26 (app. dd, *J* = 5.3, 6.3 Hz, 6H), 1.14 (d, *J* = 6.4 Hz, 3H); LCMS (HpH): *t_R* = 0.81 min, [M+H⁺] = 332.2 / 334.1 (96 % purity).

***tert*-Butyl ((5-bromopyrazin-2-yl)methyl)-L-allothreoninate, 3.143**



A solution of (5-bromopyrazin-2-yl)methyl methanesulfonate (**3.135**, 95 mg, 0.30 mmol), *tert*-butyl L-allothreoninate (**3.142**, 52.4 mg, 0.30 mmol) and triethylamine (0.13 mL, 0.90 mmol) in ethanol (2 mL) was stirred at 80°C for 2 h. The reaction mixture was cooled and concentrated *in vacuo* to afford a brown oil. The oil was dissolved in 9:1 DCM:MeOH (10 mL) and was partitioned with water (10 mL). The aqueous layer was re-extracted with three further portions of 9:1 DCM:MeOH (3 x 10 mL). The combined organic layers were dried (hydrophobic frit) before being concentrated *in vacuo* to afford a light brown oil. The oil was purified by flash column chromatography (silica, 60-80 % ethyl acetate in cyclohexane). The relevant fractions were combined and concentrated *in vacuo* to afford the title compound (**3.143**, 46 mg, 0.13 mmol, 42 % yield) as a white solid. ¹H NMR (400 MHz, CDCl₃) δ = 8.64 (d, *J* = 1.5 Hz, 1H), 8.41 (d, *J* = 1.5 Hz, 1H), 4.09 - 4.01 (m, 2H), 3.85 (d, *J* = 14.7 Hz, 1H), 3.32 (d, *J* = 4.4 Hz, 1H), 2.80 (d, *J* = 9.3 Hz, 1H), 2.44 (br s, 1H), 1.49 (s, 9H), 1.13 (d, *J* = 6.4 Hz, 3H); LCMS (HpH): *t_R* = 0.96 min, [M+H⁺] = 346.2 / 348.2 (97 % purity).

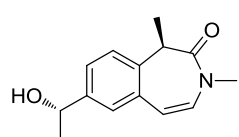
***tert*-Butyl ((5-((*R*)-7-((*S*)-1-hydroxyethyl)-1,3-dimethyl-2-oxo-2,3-dihydro-1*H*-benzo[*d*]azepin-5-yl)pyrazin-2-yl)methyl)-L-allothreoninate, 3.144**



A solution of potassium carbonate (53.3 mg, 0.39 mmol) in water (0.63 mL) was added to a solution of (*R*)-7-((*S*)-1-hydroxyethyl)-1,3-dimethyl-5-(4,4,5,5-tetramethyl-1,3,2-dioxaborolan-2-yl)-1,3-dihydro-2*H*-benzo[*d*]azepin-2-one (**3.63**, 54 mg, 0.13 mmol), *tert*-butyl ((5-bromopyrazin-2-yl)methyl)-L-allothreoninate (**3.143**, 46 mg, 0.13 mmol) and PdCl₂(dppf)·DCM adduct (5.25 mg, 6.42 μmol) in 1,4-dioxane (1.25 mL) and the resulting solution was stirred at 80°C for 0.25 h, after which the reaction was left standing at rt for 1 h. The reaction mixture was diluted with 9:1 DCM:MeOH (10 mL) and partitioned with water (10 mL). The aqueous layer was re-extracted 9:1 DCM:MeOH (3 x 10 mL). The combined organic layers were

dried (hydrophobic frit) before being concentrated *in vacuo* to afford a brown oil. The oil was purified by MDAP (HpH) to afford the title compound (**3.144**, 28 mg, 0.06 mmol, 44 % yield) as a light brown solid. ¹H NMR (400 MHz, CDCl₃) δ = 8.60 (d, *J* = 1.5 Hz, 1H), 8.46 (d, *J* = 1.5 Hz, 1H), 7.47 (dd, *J* = 1.5, 8.3 Hz, 1H), 7.40 (d, *J* = 8.3 Hz, 1H), 7.29 (s, 1H), 7.21 (d, *J* = 1.5 Hz, 1H), 4.84 (q, *J* = 6.4 Hz, 1H), 4.13 (d, *J* = 14.2 Hz, 1H), 4.04 (dq, *J* = 4.4, 6.4 Hz, 1H), 3.88 (d, *J* = 14.2 Hz, 1H), 3.41 (q, *J* = 6.8 Hz, 1H), 3.36 (d, *J* = 4.4 Hz, 1H), 3.21 (s, 3H), 1.71 (d, *J* = 6.8 Hz, 3H), 1.48 (s, 9H), 1.43 (d, *J* = 6.8 Hz, 3H), 1.13 (d, *J* = 6.4 Hz, 3H), exchangeable protons not observed; LCMS (HpH): *t*_R = 0.95 min, [M+H⁺] = 497.4 (95 % purity).

(R)-7-((S)-1-Hydroxyethyl)-1,3-dimethyl-1,3-dihydro-2H-benzo[d]azepin-2-one, 3.145,



Method 1, Scheme 3.34

A suspension of (*R*)-7-acetyl-1,3-dimethyl-1,3-dihydro-2*H*-benzo(*d*)azepin-2-one (**3.53**, 100 mg, 0.44 mmol) in IPA (2 mL) was sonicated for 10 min. Following this, a solution of NADP⁺ (10 mg, 0.01 mmol) and KRED_P3_C3 (100 mg, 0.44 mmol) in 0.1 M potassium phosphate buffer pH 7 (8 mL, 0.44 mmol) was added and the resultant suspension stirred at 50°C for 18 h. The reaction mixture was then stirred at 50°C for a further 18 h after which acetonitrile (10 mL) was added and the mixture stirred rapidly for 10 min. The mixture was vortexed for 2 min and left for 10 min to settle before it was filtered over Celite and washed with acetonitrile (20 mL). The filtrate was concentrated under reduced pressure until the organic solvents were removed. The aqueous layer was diluted with water (10 mL) and partitioned with ethyl acetate (10 mL). The aqueous layer was re-extracted with ethyl acetate (20 mL). The combined organic layers were concentrated under reduced pressure to afford the title compound (**3.145**, 91 mg, 0.39 mmol, 90 % yield).

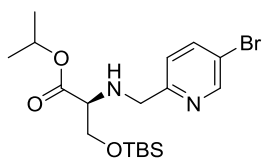
Method 2, Scheme 3.37

A suspension of (*R*)-7-acetyl-1,3-dimethyl-1,3-dihydro-2*H*-benzo(*d*)azepin-2-one (**3.53**, 50 mg, 0.22 mmol) in IPA (1 mL) was sonicated for 10 min. Following this, a solution of NADP⁺ (4 mg, 5.11 μmol) and KRED_P3_C3 (10 mg, 0.218 mmol) in 0.1 M potassium phosphate buffer pH 7 (4 mL, 0.218 mmol) was added and the resultant suspension stirred at 50°C for 6 h. The reaction mixture was concentrated to remove the organic layer, then fresh IPA (1 mL), KRED_P3_C3 (2.5 mg, 0.02 mmol) and NADP⁺ (1 mg, 1.28 μmol) and mixture stirred at 50°C for 17 h. Acetonitrile (5 mL) was added and the reaction mixture stirred for 1 h. The mixture was filtered over Celite and washed with acetonitrile (10 mL).

The filtrate was concentrated *in vacuo* to remove the organic layer and partitioned with ethyl acetate (10 mL). The aqueous layer was re-extracted with ethyl acetate (10 mL) and the combined organic layers were dried (hydrophobic frit) and concentrated *in vacuo* to afford the title compound (**3.145**, 49.4 mg, 0.21 mmol, 98 % yield).

(α_D)^{20.9°C} _{λ} (c = 1.0, CDCl₃): +61.5°; ν_{\max} (solution in CDCl₃): 3435, 2974, 1644, 1376 cm⁻¹; ¹H NMR (400 MHz, CDCl₃) δ = 7.37 (dd, *J* = 1.7, 8.1 Hz, 1H), 7.28 (d, *J* = 8.1 Hz, 1H), 7.27 (d, *J* = 1.7 Hz, 1H), 6.42 (d, *J* = 9.3 Hz, 1H), 6.29 (d, *J* = 9.3 Hz, 1H), 4.89 (q, *J* = 6.4 Hz, 1H), 3.25 (app. br s, 1H), 3.10 (s, 3H), 2.17 (br s, 1H), 1.63 (d, *J* = 6.8 Hz, 3H), 1.48 (d, *J* = 6.4 Hz, 3H); ¹³C NMR (101 MHz, CDCl₃) δ = 144.1, 135.2, 130.4, 125.9, 123.7, 123.6, 116.3, 77.4, 77.2, 70.0, 35.6, 25.2, 13.1, 0.0; LCMS (HpH): *t*_R = 0.75 min, [M+H⁺] = 232.2 (96 % purity); HRMS: (C₁₄H₁₇NO₂) [M+H⁺] requires 232.1338, found [M+H⁺] = 232.1332.

Isopropyl *N*-((5-bromopyridin-2-yl)methyl)-*O*-(*tert*-butyldimethylsilyl)-L-serinate, **3.147**



Method 1, Scheme 3.40

A solution of 2-formyl-5-bromopyridine (100 mg, 0.54 mmol) and isopropyl *O*-(*tert*-butyldimethylsilyl)-L-serinate²¹⁶ (**3.146**, 169 mg, 0.65 mmol) in DCM (5 mL) was stirred for 10 min before sodium triacetoxyborohydride (570 mg, 2.69 mmol) was added and the mixture was stirred at rt for 20 min. The reaction mixture was quenched with water (10 mL) and diluted with DCM (5 mL). The organic layer was separated and the aqueous layer was re-extracted with 9:1 DCM:MeOH (10 mL). The combined organic layers were concentrated under reduced pressure to afford the title compound (**3.147**, 221 mg, 0.51 mmol, 95 % yield) as a yellow oil. Chiral analysis conducted on a 250 mm x 46 mm Chiralpak AD-H 5 μ m column, eluting with a gradient of 3% ethanol in heptane (+0.1% isopropylamine) at a flow rate of 1 mL/min showed the compound to have an e.e of 89%.

Method 2, Scheme 3.45

A solution of (5-bromopyridin-2-yl)methyl methanesulfonate (**3.149**, 50 mg, 0.19 mmol), isopropyl *O*-(*tert*-butyldimethylsilyl)-L-serinate²¹⁶ (**3.146**, 73.7 mg, 0.28 mmol) and DIPEA (0.03 mL, 0.19 mmol) in THF (2 mL) was stirred at 100°C in a microwave reactor for 4 h. The reaction mixture was diluted with ethyl acetate (5 mL) and was concentrated *in vacuo* to afford a yellow oil. The oil was purified by flash column chromatography (silica, 0-100 % ethyl acetate in cyclohexane) to afford the title compound (**3.147**, 61 mg, 0.13 mmol, 68 % yield) as a yellow oil. Chiral analysis conducted on a 250 mm x 46 mm Chiralpak AD-H

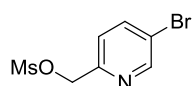
5 μ m column, eluting with a gradient of 3% ethanol in heptane (+0.1% isopropylamine) at a flow rate of 1 mL/min showed the compound to have an e.e of 95%.

Method 3, Scheme 3.46

A solution of (5-bromopyridin-2-yl)methyl 4-methylbenzenesulfonate (**3.152**, 50 mg, 0.15 mmol), isopropyl *O*-(*tert*-butyldimethylsilyl)-L-serinate²¹⁶ (**3.146**, 57.3 mg, 0.22 mmol) and DIPEA (26 μ L, 0.15 mmol) in THF (2 mL) was stirred at 80°C for 22.5 h. The reaction mixture was diluted with 9:1 DCM:MeOH (10 mL) and partitioned with water (10 mL). The aqueous layer was re-extracted with 9:1 DCM:MeOH (3 x 10 mL). The combined organic layers were dried (hydrophobic frit) and concentrated *in vacuo* to afford a yellow oil. The oil was purified by flash column chromatography (silica, 0-100 % ethyl acetate in cyclohexane) to afford the title compound (**3.147**, 26 mg, 0.06 mmol, 41% yield) as a pale yellow oil. Chiral analysis conducted on a 250 mm x 46 mm Chiralpak AD-H 5 μ m column, eluting with a gradient of 3% ethanol in heptane (+0.1% isopropylamine) at a flow rate of 1 mL/min showed the compound to have an e.e of 84%.

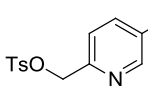
¹H NMR (400 MHz, CDCl₃) δ = 8.59 (d, *J* = 2.4 Hz, 1H), 7.76 (dd, *J* = 2.5, 8.3 Hz, 1H), 7.32 (d, *J* = 8.3 Hz, 1H), 5.06 (app. spt, *J* = 6.3 Hz, 1H), 4.01 (d, *J* = 14.7 Hz, 1H), 3.88 (dd, *J* = 4.7, 9.8 Hz, 1H), 3.84 (dd, *J* = 4.7, 9.8 Hz, 1H), 3.82 (d, *J* = 14.7 Hz, 1H), 3.35 (app. t, *J* = 4.7 Hz, 1H), 2.29 (br s, 1H), 1.25 (app. dd, *J* = 2.9, 6.3 Hz, 6H), 0.88 (s, 9H), 0.05 (s, 3H), 0.04 (s, 3H); LCMS (HpH): *t*_R = 1.56 min, [M+H⁺] = 431.3 / 433.3 (99% purity).

(5-Bromopyridin-2-yl)methyl methanesulfonate²²⁷, 3.149



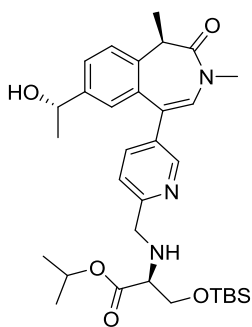
A solution of (5-bromopyridin-2-yl)methanol (500 mg, 2.66 mmol) and triethylamine (0.56 mL, 3.99 mmol) in DCM (12 mL) was cooled to 0°C. To this solution, methanesulfonyl chloride (0.31 mL, 3.99 mmol) was added dropwise and the resultant solution was stirred at 0°C for 5 min. The reaction mixture was diluted with 9:1 DCM:MeOH (10 mL) and partitioned with water (20 mL). The aqueous layer was re-extracted with 9:1 DCM:MeOH (3 x 20 mL). The combined organic layers were dried (hydrophobic frit), concentrated *in vacuo* and dried in a vacuum oven (45°C) overnight to afford the title compound (**3.149**, 709 mg, 2.66 mmol, 100 % yield) as a dark brown solid. ¹H NMR (400 MHz, CDCl₃) δ = 8.67 (d, *J* = 2.5 Hz, 1H), 7.89 (dd, *J* = 2.5, 8.3 Hz, 1H), 7.38 (d, *J* = 8.3 Hz, 1H), 5.28 (s, 2H), 3.09 (s, 3H); LCMS (HpH): *t*_R = 0.81 min, [M+H⁺] = 266.1 / 268.1 (100 % purity).

(5-Bromopyridin-2-yl)methyl 4-methylbenzenesulfonate, **3.152**



A solution of (5-bromopyridin-2-yl)methanol (500 mg, 2.66 mmol) and triethylamine (0.56 mL, 3.99 mmol) in DCM (12 mL) was cooled to 0°C. To this solution 4-methylbenzenesulfonyl chloride (760 mg, 3.99 mmol) was added slowly and the resultant solution was stirred at 0°C for 20 min then at rt for 1 h. The solution was concentrated *in vacuo* to afford a light orange solid. The solid was dissolved in 9:1 DCM:MeOH (10 mL) and partitioned with water (10 mL). The aqueous layer was re-extracted with 9:1 DCM:MeOH (3 x 10 mL). The combined organic layers were dried (hydrophobic frit) and concentrated *in vacuo* to afford a dark red oil. The oil was purified by flash column chromatography (silica, 0-30 % ethyl acetate in cyclohexane) to afford the title compound (**3.152**, 400 mg, 1.17 mmol, 44 % yield) as a white solid. ¹H NMR (400MHz, CDCl₃) δ = 8.56 (d, *J* = 2.0 Hz, 1H), 7.84 - 7.79 (m, 3H), 7.39 - 7.30 (m, 3H), 5.09 (s, 2H), 2.45 (s, 3H); LCMS (HpH): *t*_R = 1.17 min, [M+H⁺] = 342.0 / 344.0 (95% purity).

Isopropyl *O*-(*tert*-butyldimethylsilyl)-*N*-((5-((*R*)-7-((*S*)-1-hydroxyethyl)-1,3-dimethyl-2-oxo-2,3-dihydro-1*H*-benzo(*d*)azepin-5-yl)pyridin-2-yl)methyl)-*L*-serinate, **3.154**

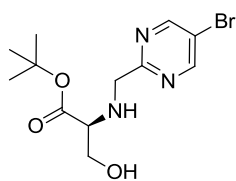


A solution of 5-(4,4,5,5-tetramethyl-1,3,2-dioxaborolan-2-yl)picolinaldehyde (100 mg, 0.43 mmol) and isopropyl *O*-(*tert*-butyldimethylsilyl)-*L*-serinate²¹⁶ (**3.146**, 135 mg, 0.52 mmol) in DCM (5 mL) was stirred for 10 min before sodium triacetoxyborohydride (455 mg, 2.15 mmol) was added and the mixture was stirred at rt for 20 min. The reaction mixture was quenched with water (10 mL) and diluted with DCM (5 mL). The organic layer was separated and the aqueous layer was re-extracted with 9:1 DCM:MeOH (10 mL). The combined organic layers were concentrated under reduced pressure to afford crude (*S*)-(6-(((3-((*tert*-butyldimethylsilyl)oxy)-1-isopropoxy-1-oxopropan-2-yl)amino)methyl)pyridin-3-yl)boronic acid, **3.153**, as a yellow oil.

To a solution of the oil (22.8 mg, 0.07 mmol), PdCl₂(dppf)·DCM adduct (3.00 mg, 3.68 μmol) and isopropyl *O*-(*tert*-butyldimethylsilyl)-*N*-((5-(4,4,5,5-tetramethyl-1,3,2-dioxaborolan-2-yl)pyridin-2-yl)methyl)-*L*-serinate (35.2 mg, 0.07 mmol) in 1,4-dioxane (1 mL) was added a solution of potassium carbonate (30.5 mg, 0.22 mmol) in water (0.50 mL). The resultant solution was stirred at 80°C for 1 h. The reaction mixture was diluted with water (100 mL) and partitioned with 9:1 DCM:MeOH (100 mL). The layers were separated and the organic layer was re-extracted with 9:1 DCM:MeOH (2 x 100 mL). The combined organic layers were dried (hydrophobic frit) and concentrated under reduced pressure. The

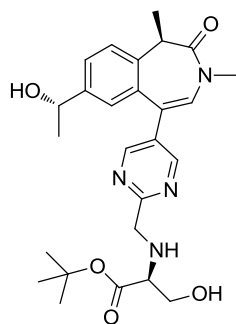
residue was purified by flash column chromatography (silica, 0-100% water saturated ethyl acetate in cyclohexane, 0-30% ethanol in water saturated ethyl acetate) to afford the title compound (**3.154**, 30.4 mg, 0.05 mmol, 65 % yield). ¹H NMR (400 MHz, CDCl₃) δ = 8.53 (d, *J* = 2.5 Hz, 1H), 7.56 (dd, *J* = 2.4, 8.3 Hz, 1H), 7.47 (dd, *J* = 2.0, 8.3 Hz, 1H), 7.40 (d, *J* = 8.3 Hz, 1H), 7.39 (d, *J* = 8.3 Hz, 1H), 7.00 (d, *J* = 2.0 Hz, 1H), 6.57 (s, 1H), 5.08 (app. spt, *J* = 6.3 Hz, 1H), 4.80 (q, *J* = 6.4 Hz, 1H), 4.09 (d, *J* = 14.7 Hz, 1H), 3.94 - 3.86 (m, 3H), 3.43 (t, *J* = 4.9 Hz, 1H), 3.40 (q, *J* = 6.8 Hz, 1H), 3.17 (s, 3H), 1.72 (d, *J* = 6.8 Hz, 3H), 1.40 (d, *J* = 6.4 Hz, 3H), 1.28 (app. dd, *J* = 3.4, 6.3 Hz, 6H), 0.89 (s, 9H), 0.06 (s, 3H), 0.06 (s, 3H), NH and NH not observed; LCMS (Formic): t_R = 0.96 min, [M+H⁺] = 581.5 (95% purity).

***tert*-Butyl ((5-bromopyrimidin-2-yl)methyl)-L-serinate, 3.155**



A solution of (5-bromopyrimidin-2-yl)methyl methanesulfonate (**3.136**, 50 mg, 0.19 mmol), *tert*-butyl L-serinate (60.4 mg, 0.37 mmol) and DIPEA (33 μL, 0.19 mmol) in THF (2 mL) was stirred at 80°C for 17 h. 9:1 DCM:MeOH (20 mL) was added to the reaction mixture which was partitioned with water (30 mL). The aqueous layer was re-extracted with 9:1 DCM:MeOH (3 x 20 mL). The combined organic layers were dried (hydrophobic frit) and concentrated *in vacuo* to afford the title compound (**3.155**, 68.2 mg, 0.19 mmol, 99 % yield) as an orange oil. ¹H NMR (400 MHz, CDCl₃) δ = 8.75 (s, 2H), 4.13 (d, *J* = 16.1 Hz, 1H), 4.03 (d, *J* = 16.1 Hz, 1H), 3.80 (dd, *J* = 4.4, 10.8 Hz, 1H), 3.64 (dd, *J* = 6.8, 10.8 Hz, 1H), 3.41 (dd, *J* = 4.4, 6.8 Hz, 1H), 1.47 (s, 9H); LCMS (Formic): t_R = 0.46 min, [M+H⁺] = 332.4 / 334.4 (97 % purity).

***tert*-Butyl ((5-((*R*)-7-((*S*)-1-hydroxyethyl)-1,3-dimethyl-2-oxo-2,3-dihydro-1*H*-benzo[*d*]azepin-5-yl)pyrimidin-2-yl)methyl)-L-serinate, 3.156**



To a solution of (*R*)-7-((*S*)-1-hydroxyethyl)-1,3-dimethyl-5-(4,4,5,5-tetramethyl-1,3,2-dioxaborolan-2-yl)-1,3-dihydro-2*H*-benzo[*d*]azepin-2-one (**3.63**, 120 mg, 0.19 mmol), PdCl₂(dppf)·DCM adduct (7.54 mg, 9.24 μmol) and *tert*-butyl ((5-bromopyrimidin-2-yl)methyl)-L-serinate (**3.155**, 68.2 mg, 0.19 mmol) in 1,4-dioxane (2 mL) was added a solution of potassium carbonate (77 mg, 0.55 mmol) in water (1 mL). The resultant solution was stirred at 80°C for 1 h. The reaction mixture was diluted with water (100 mL) and partitioned with 9:1 DCM:MeOH (100 mL). The layers were separated and the organic layer was re-extracted with 9:1 DCM:MeOH (2 x 100 mL). The combined organic layers were dried (hydrophobic frit) and concentrated under reduced

pressure. The residue was purified by flash column chromatography (silica, 0-100% water-saturated ethyl acetate in cyclohexane then 0-30% ethanol in water saturated ethyl acetate) to afford the title compound (**3.156**, 40.3 mg, 0.08 mmol, 45 % yield). ¹H NMR (400 MHz, CDCl₃) δ = 8.67 (s, 2H), 7.47 (dd, *J* = 2.0, 8.3 Hz, 1H), 7.40 (d, *J* = 8.3 Hz, 1H), 7.00 (d, *J* = 2.0 Hz, 1H), 6.61 (s, 1H), 4.82 (q, *J* = 6.4 Hz, 1H), 4.26 (d, *J* = 16.1 Hz, 1H), 4.10 (d, *J* = 16.1 Hz, 1H), 3.83 (dd, *J* = 4.2, 11.3 Hz, 1H), 3.67 (dd, *J* = 6.6, 11.2 Hz, 1H), 3.46 (dd, *J* = 4.2, 6.6 Hz, 1H), 3.39 (q, *J* = 6.8 Hz, 1H), 3.19 (s, 3H), 1.73 (d, *J* = 6.8 Hz, 3H), 1.49 (s, 9H), 1.41 (d, *J* = 6.4 Hz, 3H), exchangeable protons not observed; LCMS (Formic): *t*_R = 0.64 min, [M+H⁺] = 463.4 (99% purity).

6.0 References

- (1) El-Gabalawy, H.; Guenther, L.; Bernstein, C. N. *J. Rheumatol.*, **2010**, *85*, 2.
- (2) Adapa, D.; Sai, Y.; Anand, Y.; Mehaboobi, S. *J. Clin. Cell. Immunol.*, **2011**, *11*, 2.
- (3) Elenkov, I. J.; Iezzoni, D. G.; Daly, A.; Harris, A. G.; Chrousos, G. P. *Neuroimmunomodulation*, **2005**, *12*, 255.
- (4) Zhang, J. M.; An, J. *Int. Anesthesiol. Clin.*, **2007**, *45*, 27.
- (5) Gabay, C. *Arthritis Res. Ther.*, **2006**, *8*, S3.
- (6) Watson, J. D. C., F. H. C. *Nature Education* **2008**, *1*, 100.
- (7) Jackson, S. P.; Bartek, J. *Nature*, **2009**, *461*, 1071.
- (8) Watson, J. D. *Nature*, **1953**, *4356*, 737.
- (9) Pary, L. *Nature Education*, **2008**, *1*, 1.
- (10) International Human Genome Sequencing Consortium, *Nature*, **2004**, *431*, 931.
- (11) Annunziato, A. *Nature Education*, **2008**, *1*, 26.
- (12) Baker, M. *Nat. Methods*, **2011**, *8*, 717.
- (13) Hahn, S. *Nat. Struct. Mol. Biol.*, **2004**, *11*, 394.
- (14) Clancy, S. B. *Nature Education*, **2008**, *1*, 101.
- (15) Furdas, S. D.; Carlino, L.; Sippl, W.; Jung, M. *Med. Chem. Commun.*, **2012**, *3*, 123.
- (16) Wray, J.; Kalkan, T.; Smith, A. G. *Biochem. Soc. Trans.*, **2010**, *38*, 1027.
- (17) Hoffmann, M. J.; Schulz, W. A. *Biochem. Cell Biol.*, **2005**, *83*, 296.
- (18) Jaenisch, R.; Bird, A. *Nat. Genet.*, **2003**, *33*, 245.
- (19) Simpson, S. J.; Sword, G. A.; Lo, N. *Curr. Biol.*, **2011**, *21*, 738.
- (20) Burris, H. H.; Baccarelli, A. A. *J. Appl. Toxicol.*, **2014**, *34*, 2904.
- (21) Sims, R. J.; Reinberg, D. *Nat. Rev.*, **2008**, *9*, 815.
- (22) Yoo, C. B.; Jones, P. A. *Nat. Rev. Drug Discov.*, **2006**, *5*, 37.
- (23) Burgess, D. J. *Nat. Rev. Gen.*, **2014**, *15*, 707.
- (24) Law, J. A.; Jacobsen, S. E. *Nat. Rev. Gen.*, **2010**, *11*, 204.
- (25) Hackenberg, M.; Barturen, G.; Carpena, P.; Luque-Escamilla, P. L.; Previti, C.; Oliver, J. L. *BMC Genomics*, **2010**, *11*, 327.
- (26) PubMed 'Epigenetic' Search Results, <https://www.ncbi.nlm.nih.gov/pubmed/?term=epigenetic> (accessed Apr 5, 2018)
- (27) Yoo, J.; Kim, J. H.; Robertson, K. D.; Medina-Franco, J. L. In *Advances in Protein Chemistry and Structural Biology*; Academic Press: 2012; Vol. Volume 87, p 219.
- (28) Zhang, W.; Xu, J. *Biomark. Res.*, **2017**, *5*, 1.
- (29) Chen, T.; Li, E. *Curr. Top. Dev. Biol.* **2004**, *60*, 55.
- (30) Chen, T.; Hevi, S.; Gay, F.; Tsujimoto, N.; He, T.; Zhang, B.; Ueda, Y.; Li, E. *Nat Gen.*, **2007**, *39*, 391.
- (31) Subramaniam, D.; Thombre, R.; Dhar, A.; Anant, S. *Front. Oncol.*, **2014**, *4*, 80.
- (32) Brown, K. D.; Robertson, K. D. *Nat. Gen.*, **2007**, *39*, 289.
- (33) Jones, P. A.; Baylin, S. B. *Cell*, **2007**, *128*, 683.
- (34) Bygren, L. O.; Tinghög, P.; Carstensen, J.; Edvinsson, S.; Kaati, G.; Pembrey, M. E.; Sjöström, M. *BMC Genetics*, **2014**, *15*, 12.
- (35) Issa, J. P.; Kantarjian, H. M. *Clin. Cancer Res.*, **2009**, *15*, 3938.
- (36) Philips, T. *Nature Education*, **2008**, *1*, 116.
- (37) Stressemann, C.; Lyko, F. *Int. J. Cancer*, **2008**, *123*, 8.
- (38) Zhang, W.; Xu, J. *Biomark. Res.*, **2017**, *5*, 1.
- (39) Wild, L.; Flanagan, J. M. *Biochim. Biophys. Acta Rev. Cancer*, **2010**, *1806*, 50.
- (40) Bayer. An Open-label, Non-randomized, Multicenter Phase I Dose Escalation Study to Characterize Safety, Tolerability, Pharmacokinetics and Maximum Tolerated Dose of BAY 1238097 in Subjects With Advanced Malignancies. In: [ClinicalTrials.gov](https://clinicaltrials.gov) [Internet]. [cited 2017 Mar 15] <https://clinicaltrials.gov/ct2/show/NCT02369029>. NLM Identifier: NCT02369029.

- (41) Choudhary, C.; Kumar, C.; Gnad, F.; Nielsen, M. L.; Rehman, M.; Walther, T. C.; Olsen, J. V.; Mann, M. *Science*, **2009**, *325*, 834.
- (42) Ferguson, L. R.; Tatham, A. L.; Lin, Z.; Denny, W. A. *Curr. Cancer Drug Targ.*, **2011**, *11*, 199.
- (43) Arrowsmith, C. H.; Bountra, C.; Fish, P. V.; Lee, K.; Schapira, M. *Nat. Rev. Drug Discov.*, **2012**, *11*, 384.
- (44) Chakravarty, S.; Pathak, S. S.; Maitra, S.; Khandelwal, N.; Chandra, K. B.; Kumar, A. In *International Review of Neurobiology*; Pandey, S. C., Ed.; Academic Press: 2014; Vol. 115, p 117.
- (45) Yang, X. J.; Seto, E. *Oncogene*, **2007**, *26*, 5310.
- (46) Lee, K. K.; Workman, J. L. *Nat. Rev. Mol. Cell Biol.*, **2007**, *8*, 284.
- (47) Denis, G. V.; Nikolajczyk, B. S.; Schnitzler, G. R. *FEBS letters*, **2010**, *584*, 3260.
- (48) Lombardi, P. M.; Cole, K. E.; Dowling, D. P.; Christianson, D. W. *Curr. Opin. Struct. Biol.*, **2011**, *21*, 735.
- (49) Michaelides, M. R.; Kluge, A.; Patane, M.; Van Drie, J. J.; Wang, C. T.; Hansen, M.; Risi, R. M.; Mantei, R.; Hertel, C.; Karukurichi, K.; Nesterov, A.; McElligott, D.; De Bries, P.; Langston, J. W.; Cole, P. A.; Marmorstein, R.; Lui, H.; Lasko, L.; Bromberg, K. D.; Lai, A.; Kesicki, E. A. *ACS Med. Chem. Lett.*, **2018**, *9*, 28.
- (50) Gallinari, P.; Di Marco, S.; Jones, P.; Pallaoro, M.; Pallaoro, M.; Steinkuhler, C.; Steinkuhler, C. *Cell Res.*, **2007**, *2*, 1748.
- (51) Baur, J. A.; Pearson K.; Price, N. L.; Price, N.; Jamieson, H. A.; Jamieson, H.; Lerin, C.; Kalra, A.; Prabhu, V. V.; Allard, J. S.; Allard, K.; Lopez, L.; Lewis, K.; Pistell P.; Poosala, S.; Becker, K. G.; Boss, O.; Gwinn, D.; Wang, M.; Ramaswamy, S.; Fishbein, K. W.; Spencer, R. G.; Lakatta, E. G.; Le Couteur, D.; Shaw, R. J.; Navas, P.; Puigserver, P.; Ingram, D. K.; de Cabo, R.; Sinclair, D. A. *Nature*, **2006**, *444*, 337.
- (52) Mann, B. S.; Johnson Jr; Cohen M.; Justice, R.; Pazdur, R. *Oncologist*, **2007**, *12*, 1247.
- (53) Bubna, A. K. *Indian J. Dermatol.*, **2015**, *60*, 419.
- (54) Lauffer, B. E.; Mintzer, R.; Fong R.; Mukund, S.; Tam, C.; Zilberleyb, I.; Flicke, A.; Ritscher, A.; Fedorowicz, G.; Vallerio, R.; Ortwine, D.; Gunzner, J.; Modrusan, Z.; Neumann, L.; Koth, C.; Lupardus, P.; Kaminker, J; Heise, C.; Steiner, P. *J. Biol. Chem.*, **2013**, *288*, 26926.
- (55) Tamkun, J. W.; Deuring, R.; Scott, M. P.; Kissinger, M.; Pattatucci, A. M.; Kaufman, T. C.; Kennison, J. A. *Cell*, **1992**, *68*, 561.
- (56) Muller, S.; Filippakopoulos, P.; Knapp, S. *Expert Rev. Mol. Med.*, **2011**, *13*, 29.
- (57) Sanchez, R.; Zhou, M. M. *Curr. Opin. Drug Discov. Devel.*, **2009**, *12*, 659.
- (58) Smith, S. G.; Sanchez, R.; Zhou, M. M. *Chem. Biol.*, **2014**, *21*, 573.
- (59) Filippakopoulos, P.; Knapp, S. *Nat. Rev. Drug Discov.*, **2014**, *13*, 337.
- (60) Dawson, M. A.; Prinjha, R. K.; Dittman, A.; Giotopoulos, G.; Bantscheff, M.; Chan, W. I.; Robson, S. C.; Chung, C. W.; Hopf, C.; Savitski, M. M.; Huthmacher, C.; Gudgin, E.; Lugo, D.; Beinke, S.; Chapman, T. D.; Roberts, E. J.; Soden, P. E.; Auger, K. R.; Mirguet, O.; Doehner, K.; Delwel, R.; Burnett, A. K.; Jeffrey, P.; Drewes, G.; Lee, K.; Huntly, B. J. P.; Kouzarides, T. *Nature*, **2011**, *478*, 529.
- (61) Filippakopoulos, P.; Knapp, S. *FEBS Letters*, **2012**, *586*, 2692.
- (62) Nicodeme, E.; Jeffrey, K. L.; Schaefer, U.; Beinke, S.; Dewell, S.; Chung, C. W.; Chandwani, R.; Marazzi, I.; Wilson, P.; Coste, H.; White, J.; Kirilovsky, J.; Rice, C. M.; Lora, J. M.; Prinjha, R. K.; Lee, K.; Tarakhovskiy, A. *Nature*, **2010**, *468*, 1119.
- (63) Romero, F. A.; Taylor, A. M.; Crawford, T. D.; Tsui, V.; Cote, A.; Magnuson, S. *J. Med. Chem.*, **2016**, *59*, 1271.
- (64) Galdeano, C.; Ciulli, A. *Future Med. Chem.*, **2016**, *8*, 1655.

- (65) Picaud, S.; Wells, C.; Felletar, I.; Brotherton, D.; Martin, S.; Savitsky, P.; Diez-Dacal, B.; Philpott, M.; Bountra, C.; Lingard, H.; Fedorov, O.; Muller, S.; Brennan, P.; Knapp, S.; Filippakopoulos, P. *Prot. Natl. Acad. Sci. USA*. **2013**, *110*, 19745.
- (66) Gacias, M.; Gerona-Navarro, G.; Plotnikov, A. N.; Zhang, G.; Zeng, L.; Kaur, J.; Moy, G.; Rusinova, E.; Rodriguez, Y.; Matikainen, B.; Vincek, A.; Joshua, J.; Casaccia, P.; Zhou, M. M. *Chem. Biol.*, **2014**, *21*, 841.
- (67) Chaidos, A.; Caputo, V.; Karadimitris, A. *Ther. Adv. Hematol.*, **2015**, *6*, 128.
- (68) LeRoy, G.; Rickards, B.; Flint, S. *Mol. Cell*, **2008**, *30*, 51.
- (69) Itzen, F.; Greifenberg, A. K.; Böskén, C. A.; Geyer, M. *Nucleic Acids Res.*, **2014**, *42*, 7577.
- (70) Schroder, S.; Cho, S.; Zeng, L.; Zhang, Q.; Kaehlcke, K.; Mak, L.; Lau, J.; Bisgrove, D.; Schnolzer, M.; Verdin, E.; Zhou, M. M.; Ott, M. *J. Biol. Chem.*, **2012**, *287*, 1090.
- (71) Mitsubishi Tanabe Pharma Corporation, *Annual Report (2009)*, p.37.
- (72) Kempen, H. J.; Bellus, D.; Fedorov, O.; Nicklisch, S.; Filippakopoulos, P.; Picaud, S.; Knapp, S. *Lipid Insights* **2013**, *6*, 47.
- (73) Jennings, L. E.; Measures, A. R.; Wilson, B. G.; Conway, S. J. *Future Med. Chem.*, **2014**, *6*, 179.
- (74) Chung, C. W.; Coste, H.; White, J. H.; Mirguet, O.; Wilde, J.; Gosmini, R. L.; Delves, C.; Magny, S. M.; Woodward, R.; Hughes, S. A.; Boursier, E. V.; Flynn, H.; Bouillot, A. M.; Bamborough, P.; Brusq, J. M.; Gellibert, F. J.; Jones, E. J.; Riou, A. M.; Homes, P.; Martin, S. L.; Uings, I. J.; Toum, J.; Clement, C. A.; Boullay, A. B.; Grimley, R. L.; Blandel, F. M.; Prinjha, R. K.; Lee, K.; Kirilovsky, J.; Nicodeme, E. *J. Med. Chem.*, **2011**, *54*, 3827.
- (75) Zhao, Y.; Yang, C. Y.; Wang, S. *J. Med. Chem.*, **2013**, *56*, 7498.
- (76) Klein, K.; Kabala, P. A.; Grabiec, A. M.; Gay, R. E.; Kolling, C.; Lin, L. L.; Gay, S.; Tak, P. P.; Prinjha, R. K.; Ospelt, C.; Reedquist, K. A. *Ann. Rheum. Dis.* **2014**, *0*, 1.
- (77) Liu, T.; Lin, X.; Yu, H. *Gene*, **2015**, *571*, 97.
- (78) Innala, L.; Sjöberg, C.; Möller, B.; Ljung, L.; Smedby, T.; Södergren, A.; Magnusson, S.; Rantapää-Dahlqvist, S.; Wållberg-Jonsson, S. *Arthritis Res. Ther.*, **2016**, *18*, 33.
- (79) Donahue, K. E.; Gartlehner, G.; Jonas, D. E. *Ann. J. Med.*, **2008**, *148*, 124.
- (80) Myasoedova, E.; Crowson, C. S.; Kremers, H. M.; Therneau, T. M.; Gabriel, S. E. *Arthritis Rheum.*, **2010**, *62*, 1576.
- (81) Alamanos, Y.; Voulgari, P. V.; Drosos, A. A. *Sem. Arthritis Rheum.*, **2006**, *36*, 182.
- (82) Shichikawa, K.; Inoue, K.; Hirota, S.; Maeda, A.; Ota, H.; Kimura, M.; Ushiyama, T.; Tsujimoto, M. *Ann. Rheum. Dis.*, **1999**, *58*, 751.
- (83) Kaipainen-Seppanen, O.; Aho, K. *J. Rheumatol.* **2000**, *27*, 94.
- (84) Abhishek, A.; Doherty, M.; Kuo, C. F.; Mallen, C. D.; Zhang, W.; Grainge, M. J. *Rheumatology*, **2017**, *56*, 736.
- (85) Guo, Q.; Wang, Y.; Xu, D.; Nossent, J.; Pavlos, N. J. *Bone Res.*, **2018**, *6*, 15.
- (86) Lacroix, B. D.; Karlsson, M. O.; Friberg, L. E. *CPT: Pharmacometrics Syst. Pharmacol.*, **2014**, *3*, 143.
- (87) Felson, D. T.; LaValley, M. P. *Arthritis Res. Ther.*; **2014**, *16*, 101.
- (88) Noss, E. H.; Brenner, M. B. *Immunol. Rev.*, **2008**, *223*, 252.
- (89) Chang, S. K.; Gu, Z.; Brenner, M. B. *Immunol. Rev.*, **2010**, *233*, 256.
- (90) Firestein, G. S. *Nature*, **2003**, *423*, 356.
- (91) Strand, V.; Kimberly, R.; Isaacs, J. D. *Nat. Rev. Drug Discov.*, **2007**, *6*, 75.
- (92) Tran, C. N.; Lundy, S. K.; Fox, D. A. *Pathophysiology*, **2005**, *12*, 183.
- (93) Feldmann, M.; Maini, R. N. *Immunol. Rev.*, **2008**, *223*, 7.
- (94) Issekutz, A. C.; Meager, A.; Otterness, I.; Issekutz, T. B. *Clin. Exp. Immunol.*, **1994**, *97*, 26.

- (95) Piguet, P. F.; Grau, G.; Vesin, C.; Loetscher, H.; Gentz, R.; Lesslauer, W. *Immunology*, **1992**, *77*, 510.
- (96) Uson, J.; Balsa, A.; Pascual-Salcedo, D.; Cabezas, J.; Gonzalez-Tarrio, J.; Martin-Mola, E.; Fontan, G. *J. Rheumatol.*, **1997**, *24*, 2069.
- (97) Alonzi, T.; Fattori, E.; Lazzaro, D.; Costa, P.; Probert, L.; Kollias, G.; De Benedetti, F.; Poli, V.; Ciliberto, G. *J. Exp. Med.*, **1998**, *187*, 461.
- (98) Hayashida, K.; Nanki, T.; Girschick, H.; Yavuz, S.; Ochi, T.; Lipsky, P. E. *Arthritis Res.*, **2001**, *3*, 118.
- (99) Weinblatt, M. E. *Rheumatology*, **1995**, *19*, 43.
- (100) Salliot, C.; Van Der Heijde, D. *Ann. Rheum. Dis.* **2009**, *68*, 1100.
- (101) Segal, R.; Yaron, M.; Tartakovsky, B. *Sem. Arthritis Rheum.*, **1990**, *20*, 190.
- (102) Kremer J. M.; Lee J. K. *Arthritis Rheum.*, **2005**, *29*, 822.
- (103) Bathon, J. M.; Martin, R. W.; Fleischmann, R. M.; Tesser, J. R.; Schiff, M. H.; Keystone, E. C.; Genovese, M. C.; Wasko, M. C.; Moreland, L. W.; Weaver, A. L.; Markenson, J.; Finck, B. K. *N. Eng. J. Med.*, **2000**, *343*, 1586.
- (104) Breedveld F. C.; Weisman, M. H.; Kavanaugh A. F.; Cohen S. B.; Pavelka, K.; Vollenhoven R. V.; Sharp, J.; Perez J. L.; Spencer-Green G. T. *Arthritis Rheum.*, **2005**, *54*, 26.
- (105) Blix, H. S.; Viktil, K. K.; Moger, T. A.; Reikvam, A. *J. Pharm. Pract.*, **2010**, *8*, 50.
- (106) Khmelnsky, Y. L.; Mozhaev, V. V.; Cotterill, I. C.; Michels, P. C.; Boudjabi, S.; Khlebnikov, V.; Madhava Reddy, M.; Wagner, G. S.; Hansen, H. C. *Eur. J. Med. Chem.*, **2013**, *64*, 121.
- (107) Hewings, D. S.; Fedorov, O.; Filippakopoulos, P.; Martin, S.; Picaud, S.; Tumber, A.; Wells, C.; Olcina, M. M.; Freeman, K.; Gill, A.; Ritchie, A. J.; Sheppard, D. W.; Russell, A. J.; Hammond, E. M.; Knapp, S.; Brennan, P. E.; Conway, S. J. *J. Med. Chem.*, **2013**, *56*, 3217.
- (108) Fish, P. V.; Filippakopoulos, P.; Bish, G.; Brennan, P. E.; Bunnage, M. E.; Cook, A. S.; Federov, O.; Gerstenberger, B. S.; Jones, H.; Knapp, S.; Marsden, B.; Nocka, K.; Owen, D. R.; Philpott, M.; Picaud, S.; Primiano, M. J.; Ralph, M. J.; Sciammetta, N.; Trzuppek, J. D. *J. Med. Chem.*, **2012**, *55*, 9831.
- (109) Doroshow, D. B.; Eder, J. P.; LoRusso, P. M. *Ann. Oncol.*, **2017**, *28*, 1776.
- (110) Mirguet, O.; Gosmini, R.; Toum, J.; Clement, C. A.; Barnathan, M.; Brusq, J. M.; Mordaunt, J. E.; Grimes, R. M.; Crowe, M.; Pineau, O.; Ajakane, M.; Daugan, A.; Jeffrey, P.; Cutler, L.; Haynes, A. C.; Smithers, N. N.; Chung, C. W.; Bamborough, P.; Uings, I. J.; Lewis, A.; Witherington, J.; Parr, N.; Prinjha, R. K.; Nicodeme, E. *J. Med. Chem.*, **2013**, *56*, 7501.
- (111) Siebel, A. L.; Trinh, S. K.; Formosa, M. F.; Mundra, P. A.; Natoli, A. K.; Reddy-Luthmoodoo, M.; Huynh, K.; Khan, A. A.; Carey, A. L.; Van Hall, G.; Cobelli, C.; Dalla-Man, C.; Otvos, J. D.; Rye, K. A.; Johansson, J.; Gordon, A.; Wong, N. C.; Sviridov, D.; Barter, P.; Duffy, S. J.; Meikle, P. J.; Kingwell, B. A. *Metabolism*, **2016**, *65*, 904.
- (112) Coudé, M.-M.; Braun, T.; Berrou, J.; Dupont, M.; Bertrand, S.; Masse, A.; Raffoux, E.; Itzykson, R.; Delord, M.; Riveiro, M. E.; Herait, P.; Baruchel, A.; Dombret, H.; Gardin, C. *Oncotarget*, **2015**, *6*, 17698.
- (113) Stathis, A.; Zucca, E.; Bekradda, M.; Gomez-Roca, C.; Delord, J. P.; de La Motte Rouge, T.; Uro-Coste, E.; de Braud, F.; Pelosi, G.; French, C. A. *Cancer Discov.* **2016**, *6*, 492.
- (114) Albrecht, B. K.; Gehling, V. S.; Hewitt, M. C.; Vaswani, R. G.; Côté, A.; Leblanc, Y.; Nasveschuk, C. G.; Bellon, S.; Bergeron, L.; Campbell, R.; Cantone, N.; Cooper, M. R.; Cummings, R. T.; Jayaram, H.; Joshi, S.; Mertz, J. A.; Neiss, A.; Normant, E.; O'Meara, M.; Pardo, E.; Poy, F.; Sandy, P.; Supko, J.; Sims, R. J.; Harmange, J. C.; Taylor, A. M.; Audia, J. E. *J. Med. Chem.*, **2016**, *59*, 1330.

- (115) Roche, H. L. 2013. Hoffmann-La Roche. A Two-Part, Phase I, Multicenter, Open-Label Study of RO6870810/TEN-010 Given Subcutaneously: Part A: A Dose-Escalation Study in Patients With Advanced Solid Tumors. Part B: An Expansion Cohort in Patients With Selected Malignancies. In: ClinicalTrials.gov [Internet]. [cited 2017 Mar 15]. <https://clinicaltrials.gov/ct2/show/NCT01987362>. NLM Identifier: NCT01987362.
- (116) Finley, A.; Copeland, R. A. *Chem. Biol.*, **2014**, *21*, 1196.
- (117) Bolden, J. E.; Tasdemir, N.; Dow, L. E.; Van Es, J. H.; Wilkinson, J. E.; Zhao, Z.; Clevers, H.; Lowe, S. W. *Cell Reports*, **2014**, *8*, 1919.
- (118) Fahmy, T. M.; Fong, P. M.; Goyal, A.; Saltzman, W. M. *Mater. Today*, **2005**, *8*, 18.
- (119) Bae, Y. H.; Park, K. *J. Control. Release*, **2011**, *153*, 198.
- (120) Singh, R.; Lillard, J. W. *Exp. Mol. Pathol.*, **2009**, *86*, 215.
- (121) Deckert, P. M. *Curr. Drug Targets*, **2009**, *10*, 158.
- (122) Lamprecht, A.; Ubrich, N.; Yamamoto, H.; Schafer, U.; Takeuchi, H.; Maincent, P.; Kawashima, Y.; Lehr, C. M. *J. Pharmacol. Exp. Ther.*, **2001**, *299*, 775.
- (123) Scott, R. C.; Crabbe, D.; Krynska, B.; Ansari, R.; Kiani, M. F. *Exp. Opin. Drug Deliv.* **2008**, *5*, 459.
- (124) Gabizon, A.; Martin, F. *Drugs*, **1997**, *54*, 15.
- (125) Srinivasarao, M.; Low, P. S. *Chem. Rev.*, **2017**, *117*, 12133.
- (126) Park, J. W.; Hong, K.; Kirpotin, D. B.; Colbern, G.; Shalaby, R.; Baselga, J.; Shao, Y.; Nielsen, U. B.; Marks, J. D.; Moore, D.; Papahadjopoulos, D.; Benz, C. C. *Clin. Cancer Res.*, **2002**, *8*, 1172.
- (127) Olayioye, M. A.; Neve, R. M.; Lane, H. A.; Hynes, N. E. *The EMBO Journal*, **2000**, *19*, 3159.
- (128) Drozd, E.; Krzyszton-Russjan, J.; Gruber, B. *Cancer Geno. Proteom.*, **2016**, *13*, 161
- (129) Kratz, F. *Exp. Opin. Invest. Drugs*, **2007**, *16*, 855.
- (130) Schluep, T.; Gunawan, P.; Ma, L.; Jensen, G.; Durringer, J.; Hinton, S.; Richter, W.; Hwang, J. *Clin. Cancer Res.* **2009**, *15*, 181.
- (131) Khalil, M. W.; Sasse, F.; Lunsdorf, H.; Elnakady, Y.; Reichenbach, H. *Chem. Biochem.* **2006**, *7*, 678.
- (132) Leamon, C. P.; Reddy, J. A.; Vetzal, M.; Dorton, R.; Westrick, E.; Parker, N.; Wang, Y.; Vlahov, I. *Cancer Res.*, **2008**, *68*, 9839.
- (133) Reddy, J. A.; Bloomfield, A.; Nelson, M.; Dorton, R.; Vetzal, M.; Leamon, C. P. *Cancer Res.*, **2014**, *74*, 832.
- (134) Han, H. *AAPS Pharmsci*, **2000**, *2*, 1.
- (135) Damber, J. E.; Aus, G. *Lancet*, **2008**, *12*, 1474.
- (136) De Wit, R. *BJU Int.* **2008**, *101*, 11.
- (137) Kratz, F.; Müller-Driver, R.; Hofmann, I.; Drevs, J.; Clemens, U. *J. Med. Chem.*, **2000**, *43*, 1253.
- (138) Kratz, F. *Expert Opin. Investig. Drugs*, **2007**, *16*, 855.
- (139) Kratz, F.; Warnecke, A.; Scheuermann, K.; Stockmar, C.; Schwab, J.; Lazar, P.; Drückes, P.; Esser, N.; Drevs, J.; Rognan, D.; Bissantz, C.; Hinderling, C.; Folkers, G.; Fichtner, I.; Unger, C. *J. Med. Chem.*, **2002**, *45*, 5523.
- (140) Davidson, A. H.; Patel, S. R.; Mazzei, F. A.; Davies, S. J.; Drummond, A. H.; Moffat, D. F. C.; Baker, K. W. J.; Donald, A. D. G. Enzyme Inhibitors. PCT/GB2006/001605 (WO 2006/117549), 2006.
- (141) Needham, L. A.; Davidson, A. H.; Bawden, L. J.; Belfield, A.; Bone, E. A.; Brotherton, D. H.; Bryant, S.; Charlton, M. H.; Clark, V. L.; Davies, S. J.; Donald, A.; Day, F. A.; Krige, D.; Legris, V.; McDermott, J.; McGovern, Y.; Owen, J.; Patel, S. R.; Pintat, S.; Testar, R. J.; Wells, G. M.; Moffat, D.; Drummond, A. H. *J. Pharmacol. Exp. Ther.*, **2011**, *339*, 132.
- (142) Mai, T. I. *J. Pharm. Exp. Ther.*, **2006**, *21*, 176.

- (143) Holmes, R. S.; Wright, M. W.; Laulederkind, S. J.; Cox, L. A.; Hosokawa, M.; Imai, T.; Ishibashi, S.; Lehner, R.; Miyazaki, M.; Perkins, E. J.; Potter, P. M.; Redinbo, M. R.; Robert, J.; Satoh, T.; Yamashita, T.; Yan, B.; Yokoi, T.; Zechner, R.; Maltais, L. *J. Mamm. Genome*, **2010**, *21*, 427.
- (144) Hosokawa, M.; *Molecules*, **2008**, *13*, 412.
- (145) Laizure, S. C.; Herring, V.; Hu, Z.; Witbrodt, K.; Parker, R. B. *Pharmacotherapy*, **2013**, *33*, 210.
- (146) Bencharit, S.; Morton, C. L.; Xue, Y.; Potter, P. M.; Redinbo, M. R. *Nat. Struct. Biol.*, **2003**, *10*, 349.
- (147) Bencharit, S.; Morton, C. L.; Hyatt, J. L.; Kuhn, P.; Danks, M. K.; Potter, P. M.; Redinbo, M. R. *Chem. Biol.*, **2003**, *10*, 341.
- (148) Encinas, L.; O'Keefe, H.; Neu, M.; Remuñán, M. J.; Patel, A. M.; Guardia, A.; Davie, C. P.; Pérez-Macías, N.; Yang, H.; Convery, M. A.; Messer, J. A.; Pérez-Herrán, E.; Centrella, P. A.; Álvarez-Gómez, D.; Clark, M. A.; Huss, S.; O'Donovan, G. K.; Ortega-Muro, F.; McDowell, W.; Castañeda, P.; Arico-Muendel, C. C.; Pajk, S.; Rullás, J.; Angulo-Barturen, I.; Álvarez-Ruíz, E.; Mendoza-Losana, A.; Ballell-Pages, L.; Castro-Pichel, J.; Evindar, G. *J. Med. Chem.*, **2014**, *57*, 1276.
- (149) Buller, F.; Mannocci, L.; Scheuermann, J.; Neri, D. *Bioconjugate Chem.*, **2010**, *21*, 1571.
- (150) Hofrichter, M.; Bublitz, F.; Fritsche, W. *J. Basic Microbiol.*, **1995**, *35*, 303.
- (151) Xu Luo, L.; Warren, M. K.; Rose Wendy, L.; Gong, W.; Wang Ji, M. *J. Leukoc. Biol.*, **1996**, *60*, 365.
- (152) Alex, A.; Millan, D. S.; Perez, M.; Wakenhut, F.; Whitlock, G. A. *Med. Chem. Comm.*, **2011**, *2*, 669.
- (153) Murray, C. W.; Erlanson, D. A.; Hopkins, A. L.; Keserü, G. M.; Leeson, P. D.; Rees, D. C.; Reynolds, C. H.; Richmond, N. J. *ACS Med. Chem. Lett.*, **2014**, *5*, 616.
- (154) Guengerich, F. P. *Chem. Res. Toxicol.* **2008**, *21*, 70.
- (155) Meunier, B.; De Visser, S. P.; Shaik, S. *Chem. Rev.*, **2004**, *104*, 3947.
- (156) He, K.; Iyer, K. R.; Hayes, R. N.; Sinz, M. W.; Woolf, T. F.; Hollenberg, P. F. *Chem. Res. Toxicol.*, **1998**, *11*, 252.
- (157) Satoh, T.; Hosokawa, M. *Chem. Biol. Interact.* **2006**, *162*, 195.
- (158) Urick, A. K.; Hawk, L. M. L.; Cassel, M. K.; Mishra, N. K.; Liu, S.; Adhikari, N.; Zhang, W.; Dos Santos, C. O.; Hall, J. L.; Pomerantz, W. C. K. *ACS Chem. Biol.*, **2015**, *10*, 2246.
- (159) Jung, M.; Philpott, M.; Muller, S.; Schulze, J.; Badock, V.; Eberspacher, U.; Moosmayer, D.; Bader, B.; Schmees, N.; Fernandez-Montalvan, A.; Haendler, B. *J. Biol. Chem.*, **2014**, *289*, 9304.
- (160) Alavijeh, M. S.; Chishty, M.; Qaiser, M. Z.; Palmer, A. M. *NeuroRx*, **2005**, *2*, 554.
- (161) Smith, D.; Fox, F.; Alex, A.; Metabolism, Pharmacokinetics and Toxicity of Functional Groups, 1st Ed.; RSC: 2010.
- (162) Thomas, P.; Unpublished work, GSK, **2016**.
- (163) Craig, P. N. *J. Med. Chem.*, **1971**, *14*, 680.
- (164) Kaiser, J. P.; Feng, Y.; Bollag, J. M. *Microbiol. Rev.*, **1996**, *60*, 483.
- (165) Sevrioukova, I. F.; Poulos, T. L. *J. Med. Chem.*, **2013**, *56*, 3733.
- (166) Koduri, B.; Unpublished work, GVK, **2016**.
- (167) Perez-Palau, M.; Unpublished work, GSK, **2016**.
- (168) Watson, R.; Unpublished work, GSK, **2016**.
- (169) Benkovic, S. J.; Hammes-Schiffer, S. *Science*, **2003**, *301*, 1196.
- (170) Berg JM, T. J., Stryer L. The Michaelis-Menten Model Accounts for the Kinetic Properties of Many Enzymes. In *Biochemistry*, 5th ed.; New York: W H Freeman: 2002.
- (171) Ghislieri, D.; Turner, N. J. *Topics in Catalysis*, **2014**, *57*, 284.

- (172) Lenz, M.; Borlinghaus, N.; Weinmann, L.; Nestl, B. M. *World J. Microbiol. Biotech.*, **2017**, *33*, 199.
- (173) Matzel, P.; Gand, M.; Hohne, M. *Green Chem.*, **2017**, *19*, 385.
- (174) Mangas-Sanchez, J.; France, S. P.; Montgomery, S. L.; Aleku, G. A.; Man, H.; Sharma, M.; Ramsden, J. I.; Grogan, G.; Turner, N. J. *Curr. Opin. Chem. Biol.*, **2017**, *37*, 19.
- (175) Huber, T.; Schneider, L.; Präg, A.; Gerhardt, S.; Einsle, O.; Müller, M. *Chem. Cat. Chem.*, **2014**, *6*, 2248.
- (176) Aleku, G. A.; France, S. P.; Man, H.; Mangas-Sanchez, J.; Montgomery, S. L.; Sharma, M.; Leipold, F.; Hussain, S.; Grogan, G.; Turner, N. J. *Nature Chem.*, **2017**, *9*, 961.
- (177) Maugeri, Z.; Rother, D. *J. Biotech.*, **2017**, *258*, 167.
- (178) Van de Waterbeemd, H.; Smith, D. A.; Jones, B. C. *J. Comput. Aided Mol. Des.* **2001**, *15*, 273.
- (179) Ramgren, S. D.; Garg, N. K. *Org. Lett.*, **2014**, *16*, 824.
- (180) Howard, O.; Israel, E.; Unpublished work, GSK, **2017**.
- (181) Mo, J.; Xu, L.; Xiao, J. *J. Am. Chem. Soc.*, **2005**, *127*, 751.
- (182) Thomas, P.; Unpublished work, GSK, 2017
- (183) Hansch, C.; Maloney, P. P.; Fujita, T.; Muir, R. M. *Nature*, **1962**, *194*, 178.
- (184) Cherkasov, A.; Muratov, E. N.; Fourches, D.; Varnek, A.; Baskin, I. I.; Cronin, M.; Dearden, J.; Gramatica, P.; Martin, Y. C.; Todeschini, R.; Consonni, V.; Kuz'min, V. E.; Cramer, R.; Benigni, R.; Yang, C.; Rathman, J.; Terfloth, L.; Gasteiger, J.; Richard, A.; Tropsha, A. *J. Med. Chem.*, **2014**, *57*, 4977.
- (185) Tropsha, A. *Mol. Inf.*, **2010**, *29*, 476.
- (186) Nantasenamat, C.; Isarankura-Na-Ayudhya, C.; Prachayasittikul, V. *Exp. Opin. Drug Discov.*, **2010**, *5*, 633.
- (187) Katritzky, A. R.; Gordeeva, E. V. *J. Chem. Inf. Comput. Sci.*, **1993**, *6*, 835.
- (188) Gozalbes, R.; Doucet, J. P.; Derouin, F. *Curr. Drug Targets Infect. Disord.*, **2002**, *2*, 93.
- (189) Larsson, M.; Kumar Mishra, B.; Tysklind, M.; Linusson, A.; Andersson, P. L. *SAR QSAR Environ. Res.* **2013**, *24*, 461.
- (190) Labute, P. *J. Mol. Graph. Model.*, **2000**, *18*, 464.
- (191) Mitchell, J. B. O. *Wiley Interdiscip. Rev. Comput. Mol. Sci.* **2014**, *4*, 468.
- (192) Frimayanti, N.; Yam, M. L.; Lee, H. B.; Othman, R.; Zain, S. M.; Rahman, N. A. *Int. J. Mol. Sci.* **2011**, *12*, 8626.
- (193) Polishchuk, P. G.; Kuz'min, V. E.; Artemenko, A. G.; Muratov, E. N. *Mol. Inf.* **2013**, *32*, 843.
- (194) Luscombe, C. Unpublished Work, GSK, **2017**.
- (195) Cox, R.; Green, D. V. S.; Luscombe, C. N.; Malcolm, N.; Pickett, S. D. *J. Comp. Aided Mol. Design*, **2013**, *27*, 321.
- (196) Kuroda, M. *J. Chem. Inform.*, **2017**, *9*, 1.
- (197) Owen, J. R.; Nabney, I. T.; Medina-Franco, J. L.; López-Vallejo, F. *J. Chem. Inf. Model.*, **2011**, *51*, 1552.
- (198) Rogers, D.; Hahn, M. *J. Chem. Inf. Model.*, **2010**, *50*, 742.
- (199) Wold, S.; Sjöström, M.; Eriksson, L. *Chem. Int. Lab. Sys.*, **2001**, *58*, 109.
- (200) Abdi, H. *Wiley Interdiscip. Rev: Comp. Stat.*, **2010**, *2*, 97.
- (201) Cereto-Massagué, A.; Ojeda, M. J.; Valls, C.; Mulero, M.; Garcia-Vallvé, S.; Pujadas, G., *Methods*, **2015**, *71*, 58.
- (202) Lavecchia, A. *Drug Discov. Today*, **2015**, *20*, 318.
- (203) Svetnik, V.; Liaw, A.; Tong, C.; Culberson, J. C.; Sheridan, R. P.; Feuston, B. P. *J. Chem. Inf. Comp. Sci.*, **2003**, *43*, 1947.
- (204) Gøgsig, T. M.; Kleimark, J.; Nilsson Lill, S. O.; Korsager, S.; Lindhardt, A. T.; Norrby, P. O.; Skrydstrup, T. *J. Am. Chem. Soc.*, **2012**, *134*, 443.

- (205) Cabri, W.; Bedeschi, A. *J. Org. Chem.*, **1990**, *55*, 3655.
- (206) Chang, X.; Yang, Z.; Zeng, R.; Yang, G.; Yan, J. *Chi. J. Chem. Eng.*, **2010**, *18*, 1029.
- (207) Barski, O. A.; Tipparaju, S. M.; Bhatnagar, A. *Drug Met. Rev.*, **2008**, *40*, 553.
- (208) Bachur, N. R. *Science*, **1976**, *193*, 595.
- (209) Fujii, Y.; Watanabe K.; Hayashi, H.; Urade, Y.; Kuramitsu S.; Kagamiyama, H.; Hayaishi, O. *J. Biol. Chem.*, **1990**, *17*, 9914.
- (210) Scoble, J.; McAlister, A. D.; Fulton, Z.; Troy, S.; Byres, E.; Vivian, J. P.; Brammananth, R.; Wilce, M. C. J.; Le Nours, J.; Zaker-Tabrizi, L.; Coppel, R. L.; Crellin, P. K.; Rossjohn, J.; Beddoe, T. *J. Mol. Biol.*, **2010**, *398*, 26.
- (211) Grigg, R.; Gunaratne, H. Q. N. *Tet. Lett.*, **1983**, *24*, 4457.
- (212) Bit, R.; Unpublished work, GSK, **2016**.
- (213) Kirkland, J. J.; Snyder, L. R. *Introduction to Modern Liquid Chromatography*, 2nd ed., Wiley-Interscience, New York, 1979, p374-383.
- (214) Bit, R. A.; Brown, J. A.; Humphreys, P. G.; Jones, K. L. *Benzimidazole Derivatives as Bromodomain Inhibitors*, PCT/EP2016/055792 (WO 2016/146738 A1), **2016**
- (215) Hudlicky, T.; *Chem. Rev.* **2011**, *111*, 3995.
- (216) Ghislieri, D.; Green, A. P.; Pontini, M.; Willies, S. C.; Rowles, I.; Frank, A.; Grogan, G.; Turner, N. J.; *J. Am. Chem. Soc.*, **2013**, *135*, 10863.
- (217) Brand, M.; Measures, A. M.; Wilson, B. G.; Cortopassi, W. A.; Alexander, A.; Höss, M.; Hewings, D. S.; Rooney, T. P. C.; Paton, R. S.; Conway, S. J.; *ACS Chem. Biol.*, **2015**, *10*, 22.
- (218) Piatnitski Chekler, E. L.; Pellergrino, A.; Lanz, T. A.; Denny, R. A.; Flick, A. C.; Coe, J.; Langille, J.; Basak, A.; Liu, S.; Stock, I. A.; Sahasrabudha, P.; Bonin, P. D.; Lee, K.; Pletcher, M. T.; Jones, L. H. *Chem. Biol.*, **2015**, *22*, 1588.
- (219) Vanaparti, L.; Unpublished work, GVK, **2016**.
- (220) Koduri, B.; Unpublished work, GVK, **2016**.
- (221) Alajangi, T.; Unpublished work, GVK, **2016**.
- (222) Watson, R.; Unpublished work, GSK, **2018**.
- (223) Subbaramireddy, S.; Unpublished work, GVK, **2017**.
- (224) Unpublished work, WuXi Apptech, **2017**.
- (225) Beech, M.; Unpublished work, GSK, **2015**.
- (226) Sreenivasreddy, M, Unpublished, GVK, **2017**.
- (227) Friedle, S.; Kodanko, J. J.; Morys, A. J.; Takahiro, H.; Moenne-Loccoz, P.; Lippard, S. J. *J. Am. Chem. Soc.*, **2009**, *131*, 14508.

7.0 Appendix 1: Assay protocols

Brd4 BD1 FRET Assay

50 nL of test compounds in DMSO were serially diluted 1:3 into a Greiner 384 well low-volume assay plate. To each well was added 5 μ L of protein/ligand solution (to an assay buffer of 50 mM HEPES, 150 mM NaCl, 1 mM CHAPS pH7.4, 5% glycerol and 1 mM DTT pH7.4 (using NaOH) was added the fluoroprobe and BRD4-Y390A protein). The assay plate was centrifuged at 1000 rpm for 60 seconds then incubated at RT for 30 min. To each well was added 5 μ L of anti-His Eu solution (in assay buffer). The assay plate was centrifuged at 1000 rpm for 60 seconds then incubated at RT for 30 min. The assay plates were read using a Perkin Elmer Envision 2104 reader (emission 1: 665 nm, emission 2: 615 nm).

Human Whole Blood (hWB) MCP-1 Assay

0.5 μ L of compounds in 3 mM DMSO were serially diluted (1:3) into a Greiner 96 well flat, clear bottom plate. 130 μ L of human whole blood (with added sodium heparin, 10 μ L/mL) was added to the compound wells, the plates incubated (37°C, 5% CO₂) for 30 min, and 10 μ L of 2.8 μ g/mL LPS diluted in PBS was added. The plates are then incubated at 37°C, 5% CO₂ overnight. 140 μ L of PBS was added to the compound plate and the plates are centrifuged at 1800 rpm for 10 min. 20 μ L of the supernatant was transferred to an anti-MCP1 antibody coated 96 well MSD plates and incubated for 1.5 h on a plate shaker. 20 μ L of 1X sulfo-TAG anti-MCP1 antibody was then added to each well and the plates were incubated for 1 h at RT whilst shaking. The plates were then washed three times with PBS and 0.05% Tween 20 using a plate washer and 150 μ L read buffer P/T (2X) was added to the plate. The plates were read using an MSD reader.

ChromLogD_{7.4}

The compound, 10 mM in DMSO, was diluted with methanol. The sample was analysed on a LUNA 5 μ , C18 (50 x 3.0 mm) column on a Agilent 1100 system using a mobile phase of 50 mM ammonium acetate adjusted to pH7.4, using concentrated ammonia solution and acetonitrile.

Solubility (CLND)

The aqueous solubility of compounds was determined using chemiluminescent nitrogen detection (CLND) as a quantification method. Stock solutions of 10 mM compounds in DMSO were serially diluted in phosphate buffered saline (pH7.4) and analysed by HPLC (Agilent 1100 HPLC system; mobile phase 90% methanol, 10% water; flow rate 0.2 mL/min) using CLND (Antek 8060C chemiluminescent nitrogen detector).

AMP

3.5 µL of lipid solution (1.8% phosphatidylcholine in 1% cholesterol decan solution) was added to a filter plate (Millicell-96-well cell culture plate), the plate shaken for 12 seconds, and then 250 µL of buffer (50 mM phosphate buffer with 0.5% encapsin, pH at 7.4) added to donor side and 100 µL added to the receiver side. The assay plate was shaken for 45 min before adding the test compound (2.5 µL) to the donor side. The assay plates are then incubated at rt for 3 h. The donor and receiver solution were then analysed by HPLC.

HLM IVC - This was carried out by Cyprotex using their Microsomal Stability assay and Hepatocyte Stability assay using the following protocol

Microsomes (final protein concentration 0.5 mg/mL), 50 mM potassium phosphate buffer pH7.4 and NADPH (final concentration 1 mM) were pre-incubated at 37°C prior to the addition of the test compound (final substrate concentration 0.5 µM; final DMSO concentration 0.25%) to initiate the reaction. The final incubation volume is 500 µL. For the + Benzil assays, Benzil (50 µM) is included in the buffer in the pre-incubation stage. A control is included for each compound tested where 50 mM phosphate buffer pH 7.4 is added instead of NADPH (minus NADPH). All incubations are performed singularly for each test compound. Each compound is incubated for 45 min and 50 µL samples were taken at 0, 5, 15, 30 and 45 min. The control (minus NADPH) is sampled at 45 min only. The reactions are stopped by the addition of 100 µL acetonitrile containing internal standard to the sample. The terminated samples are centrifuged at 2500 rpm for 20 min at 4°C to precipitate the protein. and added to the stop solution wells. Samples were analysed by LCMS/MS.

TDI – This was carried out by Cyprotex using their Cytochrome P450 time dependent inhibition (IC₅₀ shift) assay using the following protocol

Human liver microsomes (0.1 mg/mL) and test compound (2, 5, 20, 50, 200, 500 µM final DMSO concentration 0.25%) or DMSO were pre-incubated for 0 min or incubated in the absence and presence of NADPH for 30 min. The probe substrate midazolam (2.5 µM) and NADPH (1 mM) were then added to the incubations (final DMSO concentration 0.26%). Following incubation for 5 min, the reaction was terminated by the addition of an aliquot of the incubation into methanol. The samples were centrifuged at 2500 rpm for 30 min at 4°C, and aliquots of the supernatant were diluted with formic acid in deionised water containing internal standard (final formic acid concentration 0.1%). The samples were analysed by LCMS/MS. The time dependent CYP3A4 inhibitor, mifepristone, was screened alongside the test compounds as a positive control.

Whole Blood Half Life

995 µL of blood was spiked with 5 µL of a 200 µg/mL test compound solution at 37°C to produce a 1000 ng/mL incubation solution. An aliquote of spiked blood (25 µL) was removed from the incubation at multiple time points (0, 2, 5, 10, 15, 20, 40, 60, 120, 180 and 240 minutes). Samples were subjected to protein precipitation with organic solvent containing an internal standard prior to analysis using LCMS/MS.

Cynomolgus Monkey Plasma Half Life

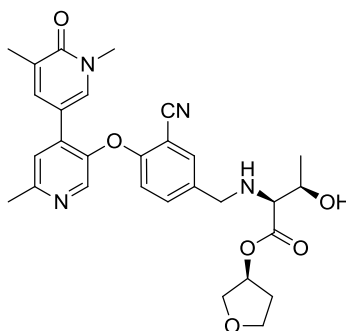
995 µL of plasma was spiked with 5 µL of a 200 µg/mL test compound solution 37°C to produce a 1000 ng/mL incubation solution. An aliquote of spiked blood (25 µL) was removed from the incubation at multiple time points (0, 2, 5, 10, 15, 20, 40, 60, 120 and 180). Samples were subjected to protein precipitation with organic solvent containing an internal standard prior to analysis using LCMS/MS.

Bromoscan – This was carried out by DiscoverX using the following protocol

Bromodomain assays. T7 phage strains displaying bromodomains were grown in parallel in 24-well blocks in an *E. coli* host derived from the BL21 strain. *E. coli* were grown to log-phase and infected with T7 phage from a frozen stock (multiplicity of infection = 0.4) and incubated with shaking at 32°C until lysis (90-150 minutes). The lysates were centrifuged

(5,000 x g) and filtered (0.2 μ m) to remove cell debris. Streptavidin-coated magnetic beads were treated with biotinylated small molecule or acetylated peptide ligands for 30 minutes at room temperature to generate affinity resins for bromodomain assays. The liganded beads were blocked with excess biotin and washed with blocking buffer (SeaBlock (Pierce), 1 % BSA, 0.05 % Tween 20, 1 mM DTT) to remove unbound ligand and to reduce non-specific phage binding. Binding reactions were assembled by combining bromodomains, liganded affinity beads, and test compounds in 1x binding buffer (16 % SeaBlock, 0.32x PBS, 0.02%BSA, 0.04 % Tween 20, 0.004% Sodium azide, 7.9 mM DTT). Test compounds were prepared as 1000X stocks in 100% DMSO and subsequently diluted 1:25 in monoethylene glycol (MEG). The compounds were then diluted directly into the assays such that the final concentrations of DMSO and MEG were 0.1% and 2.4%, respectively. All reactions were performed in polypropylene 384-well plates in a final volume of 0.02 ml. The assay plates were incubated at room temperature with shaking for 1 hour and the affinity beads were washed with wash buffer (1x PBS, 0.05% Tween 20). The beads were then re-suspended in elution buffer (1x PBS, 0.05% Tween 20, 2 μ M non-biotinylated affinity ligand) and incubated at room temperature with shaking for 30 minutes. The bromodomain concentration in the eluates was measured by qPCR.

8.0 Appendix 2: Measured IC₅₀ values of compound 2.69 against closely related bromodomains



Target	IC ₅₀ (nM)	Selectivity (fold)
BRD4(1)	1.5	-
CREBBP	1900	1267
EP300	2600	1733
BAZ2A	4000	2667
BRPF1	370	247

Table 8.1. Measured IC₅₀s of compound 2.69 against bromodomain-containing proteins that exhibited >80% inhibition in the single shot panel.

9.0 Appendix 3: *In vivo* PK data

Parameter	Monkey (Cynomolgus) (n=4)		Monkey (Cynomolgus) (n=3)	
	1.6	Acid	2.69	Acid
IV dose (mg/kg)	1.0 ± 0.0	-	1.0 ± 0.0	-
CL _{Total} (mL/min/kg)	35 ± 6	-	80.7 ± 20.7	-
[Range]	[27-41]	-	[57.2-95.5]	-
V _{ss} (L/kg)	1.1 ± 0.5	-	1.98 ± 4.2	-
[Range]	[0.8-1.9]	-	[1.51-2.28]	-
t _{1/2} (h)	0.4 ± 0.2	0.9 ± 0.2 ²	0.28 ± 0.13	0.33 ± 0.0 ⁴
[Range]	[0.3-0.7]	[0.7-1.1]	[0.15-0.30]	-
C _{max} (ng/mL)	483 ± 155	34.2 ± 8.3	272 ± 47.7	66.3 ± 16.0
[Range]	[276-652]	[25.8-44.5]	[240-327]	[48.1-77.9]
AUC _∞ (ng.h/mL)	502 ± 90.6	82.6 ± 15.5 ²	209 ± 49.4	54.2 ± 9.6 ¹
[Range]	[414-328]	[68.5-99.3]	[178-266]	[43.8-62.1]
Acid: ester ratio	-	0.1 ± 0.1	-	0.25 ± 0
[Range]	-	[0.1-0.2]	-	-
PO dose (mg/kg)	3.1 ± 0.0	-	3.0 ± 0.0	-
C _{max} (ng/mL)	173 ± 143	33.6 ± 13.0	14.9 ± 13.5	13.0 ± 4.2
[Range]	[66.0-373]	[20.3-51.4]	[3.09-29.6]	[8.8-17.2]
Bioavailability (%)	24 ± 12	-	1.17 ± 0.0 ³	-
[Range]	[15-42]	-	[1.01-1.34]	-
AUC _∞ (ng.h/mL)	364 ± 172	104 ± 25.0 ²	8.76 ± 0.0 ³	8.2 ± 2.9 ¹
[Range]	[267-621]	[76.1-125]	[5.4-12.1]	[4.9-10.3]
t _{1/2} (h)	1.2 ± 1.7	1.5 ± 0.7 ²	0.27 ± 0.02 ³	NR
[Range]	[0.3-3.7]	[0.9-2.3]	[0.25-0.28]	NR
Acid: ester ratio	-	0.4 ± 0.1 ¹	0.93	0.93 ± 0
[Range]	-	[0.2-0.5]	-	-

Table 9.1. *In vivo* cynomolgus monkey PK data. Values are mean, ± SD unless otherwise stated. IV dose 1 h infusion in DMSO and 10% (w/v) Kleptose HPB in saline (2:98 (v/v)). PO dose vehicle: 1% (w/v) methylcellulose (400 cps) (aq), Acid: ester ratio calculated using AUC_∞ unless otherwise stated, ¹Acid: ester ratio calculated using AUC_t, ²n=3, ³n=2, ⁴n=1

10.0 Appendix 4: QSAR modelling supplementary information

10.1 All methods used to build the models

Splitting methods: No Split, Individual clusters, Random 80, Systematic every 5th

Descriptor subsets: FCFP_4, ECFP_4, Physchem_largeset, Simple Physchem, estates

Model Types: R PLS, PP RP Forest, PP GFA, R SVM

10.2 BRD4 BD1 QSAR model information

	Training	Validation	Test
Correlation Coefficient	0.90	0.71	0.87
Determination Coefficient	0.81	0.51	0.76
Kendall Tau	0.77	0.56	0.76
Bias	0.00	0.00	-0.13
RMSE	0.27	0.43	0.33
SCE	12.88	34.03	4.89
Size	183	183	46

Table 10.1. Statistical parameters for the QSAR model

Names	Values
Model Type	R PLS
Split Id	Random_80
Descriptor Subset	ECFP_4
Parameter Set	Small data sets <250 (Public)
Created On	12/05/2017 12:59
Model Parameters	
R PLS Multiselect Numeric Scaling	Mean-Centre and Scale
R PLS Model Type	Kemel
R PLS Model Domain Fingerprint	FCFP_2
R PLS Additional Properties	
R PLS Seed	12345
R PLS Optimal Component Decay	1
R PLS Convert Fingerprints To	Fixed -Length Array of Counts
R PLS Fingerprint Distance Function	Tanimoto
R PLS Numeric Distance Function	Euclidean
R PLS NumberOfVariable	3;5;7
R PLS Fixed Length	256

Table 10.2. Build parameters for the QSAR model

10.3 Human whole blood QSAR model information

	Training	Validation	Test
Correlation Coefficient	0.86	0.57	0.78
Determination Coefficient	0.73	0.33	0.62
Kendall Tau	0.69	0.40	0.60
Bias	0.00	0.02	0.10
RMSE	0.37	0.62	0.43
SCE	21.55	60.50	12.32
Size	156	156	67

Table 10.3. Statistical parameters of the QSAR model

Names	Values
Model Type	R PLS
Split Id	IndivClusters_80
Descriptor Subset	FCFP_4
Parameter Set	Parameter Set small data sets <250 (Public)
Created On	12/05/2017 14:24
Model Parameters	
R PLS Multiselect Numeric Scaling	Mean-Centre and Scale
R PLS Model Type	Kemel
R PLS Model Domain Fingerprint	FCFP_2
R PLS Additional Properties	
R PLS Seed	12345
R PLS Optimal Component Decay	0.995
R PLS Convert Fingerprints To	Fixed -Length Array of Counts
R PLS Fingerprint Distance Function	Tanimoto
R PLS Numeric Distance Function	Euclidean
R PLS NumberOfVariable	3;5;7
R PLS Fixed Length	256

Table 10.4. Build parameters for the QSAR model

10.4 Δ hWB QSAR model information

	Training	Validation	Test
Correlation Coefficient	0.85	0.64	0.82
Determination Coefficient	0.72	0.41	0.67
Kendall Tau	0.70	0.39	0.63
Bias	0.00	-0.01	-0.14
RMSE	0.27	0.37	0.30
SCE	4.14	7.76	1.29
Size	58	58	14

Table 10.5. Statistical parameters of the QSAR model

Names	Values
Model Type	PP RP Forest
Split Id	Systematic_every_5th
Descriptor Subset	Physchem_LargeSet
Parameter Set	Small data sets <250 (Public)
Created On	12/05/2017 15:43
PP RP Forest Weighting Method	By Class
PP RP Forest Maximum Lookahead Depth	0
PP RP Forest Number of Trees	500
PP RP Forest Maximum Generic Depth	0
PP RP Forest Generic Node Weighting	1.5
PP RP Forest Maximum Tree Depth	5
PP RP Forest Number of Descriptors	Fixed Number
PP RP Forest Minimum Samples Per Node	5
PP RP Forest Equalize Class Sizes	FALSE
PP RP Forest Ensemble Method	Bagging
PP RP Forest Optimize Cutoff	FALSE
PP RP Forest Number of Descriptors	Sqrt(D)
PP RP Forest Number of Lookahead Alternatives	3
PP RP Forest Number of Descriptors Fraction	0.33
PP RP Forest Min Samples Is	Absolute Minimum
PP RP Forest Random Seed	12345
PP RP Forest Maximum Knots Per Property	50
PP RP Forest Fingerprint Distance Function	Tanimoto
PP RP Forest Split Method	Gini
PP RP Forest Multiselect Numeric Scaling	Mean-Center and Scale
PP RP Forest Numeric Distance Function	Euclidean
PP RP Forest Model Domain Fingerprint	FCFP_2
PP RP Forest Preferred	Class
PP RP Forest Model Type	Regression

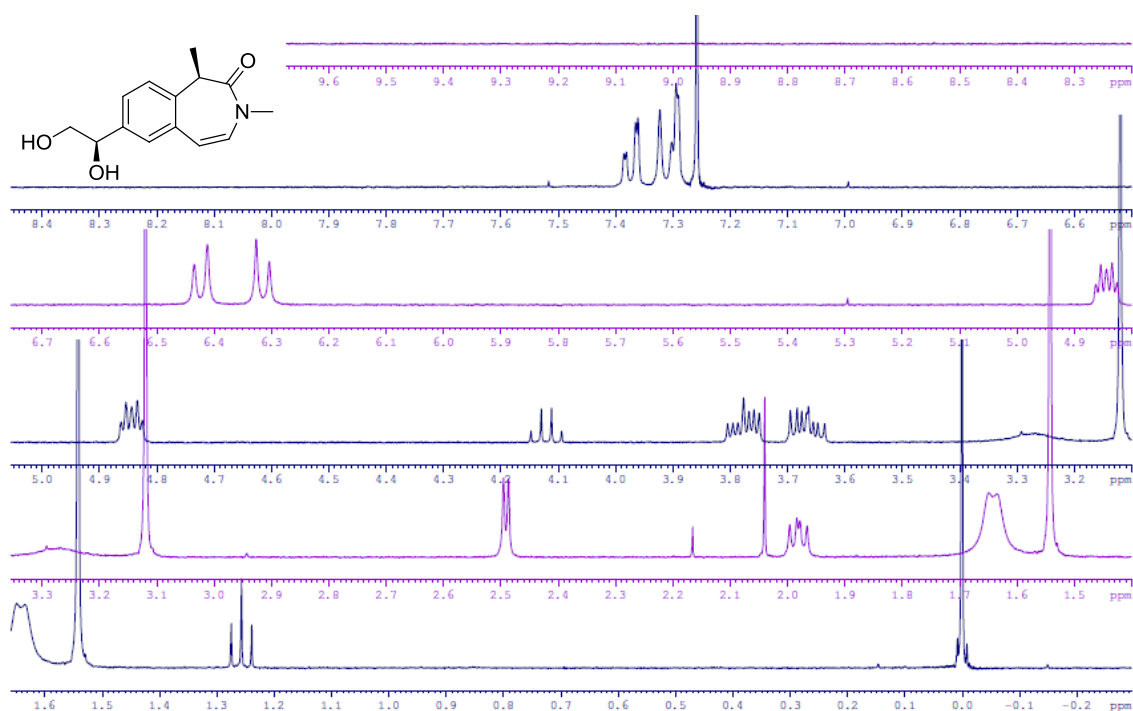
Table 10.6. Build parameters for the QSAR model.

Num_Chain Assesmblies	Molecular_FractionalPolarSASA	VSA_AlogP5
SC_3_C	ALogP_MR	Num_DoubleBonds
Gskhba	CHI_1	VSA_MR3
LipinskiDrug Like	Kappa_1	Gskacidclass
Num_H_Acceptors	Num_RingBonds	V_DIST_mag
NumLipinski Violations	VSA_MR8	PEOE_VSA_FPPOS
VSA_Partial Charge 3	CHI_V_3_C	SC_0
VSA_Partial Charge 4	V_DIST_equ	PEOE_PCNEG
VSA_MR7	V_ADJ_equ	VSA_AlogP1
VSA_AlogP9	PHI	Zagreb
VSA_AlogP7	Num_RingAssemblies	CHI_V_2
CHI_3_C	Kappa_1_AM	VSA_MR2
Num_Atom Classes	Molecular_Solubility	VSA_Partial Charge10
E_ADJ_mag	VSA_AlogP8	VSA_Partial Charge6
SC_3_P	ChargeVSA_PartialCharge7	IAC_Total
E_DIST_mag	Fraction_RotatableBonds	Num_Single Bonds
Petitjean_Ratio	VSA_AlogP3	Num_H_Acceptors Lipinski
CHI_2	JX	V_ADJ_mag
VSA_Partial Charge 2	Wiener	PEOE_VSA_POS
SC_2	Kappa_2_AM	VSA_Partial Charge 1
PEOE_RPC NEG	PEOE_VSA_FPOL	CHI_3_P
VSA_MR5	JY	VSA_Partial Charge 8
Num_H_Donors	VSA_AlogP4	CHI_0
Num_H_Donors_Lipinski	VSA_MR4	Petitjean_Diameter
IC	PEOE_VSA_NEG	VSA_AlogP6
CIC	gskhbd	Kappa_3
SIC	QED	CHI_V_3_38
SC_1	VSA_Partial Charge9	E_ADJ_equ
PEOE_VSA_FPOS	PEOE_VSA_FPNEG	PEOE_VSA_HYD
IAC_Mean	ALogP	Molecular_SAVol
PEOE_VSA_PNEG	PEOE_VSA_FHYD	CHI_V_1
VSA_PartialCharge11	Num_AromaticBonds	Molecular_Weight
VSA_PartialCharge14	BIC	Molecular_PolarsurfaceArea
Petitjean_Radius	PEOE_VSA_POL	CHI_V_0
VSA_AlogP2	VSA_PartialCharge12	Num_StereoAtoms
Molecular_Density	VSA_MR6	E_DIST_equ
Molecular_SurfaceArea	PEOE_RPC_POS	Kappa_3_AM
Molecular_PolarSASA	PEOE_VSA_FNEG	Num_RotatableBonds
VSA_MR1	Kappa_2	VSA_MR4
Molecular_SASA	Num_Bonds	Molecular_Fractional PolarSurfaceArea

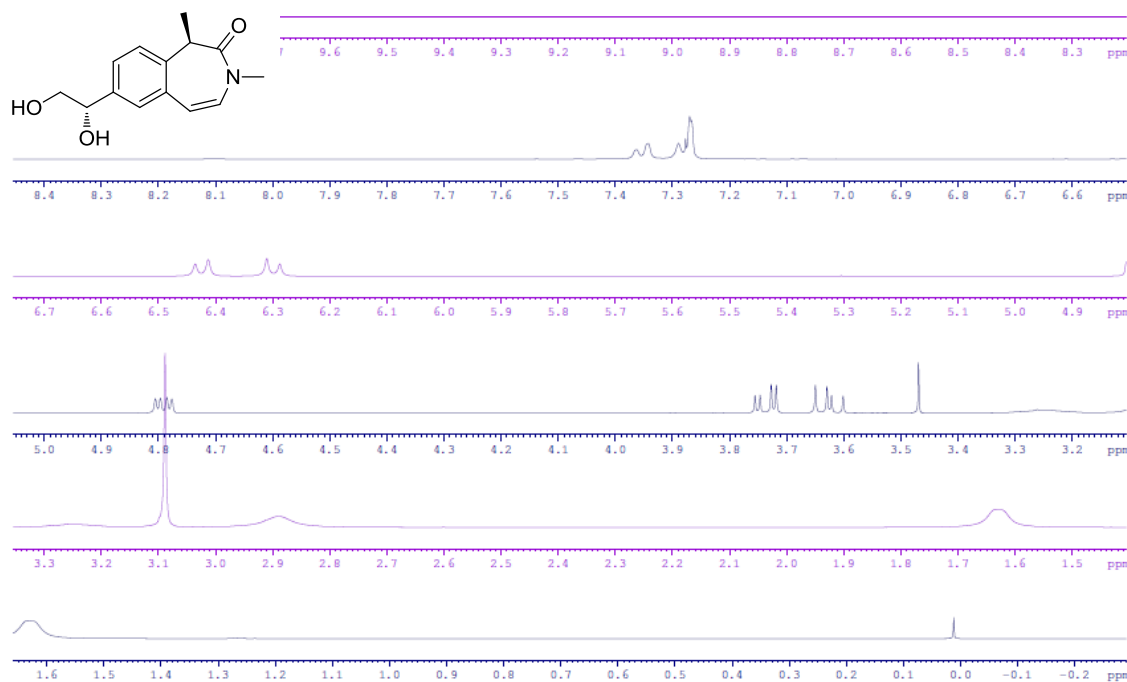
Table 10.7. PhysChem Descriptor Set applied to the Δ hWB dataset

11.0 Appendix 5: NMR analyses of intermediate 3.96 and the corresponding diastereomer containing the (*S*)-configuration of the diol

11.1 NMR of the (*R*)-configuration of the diol synthesised in Scheme 3.16.

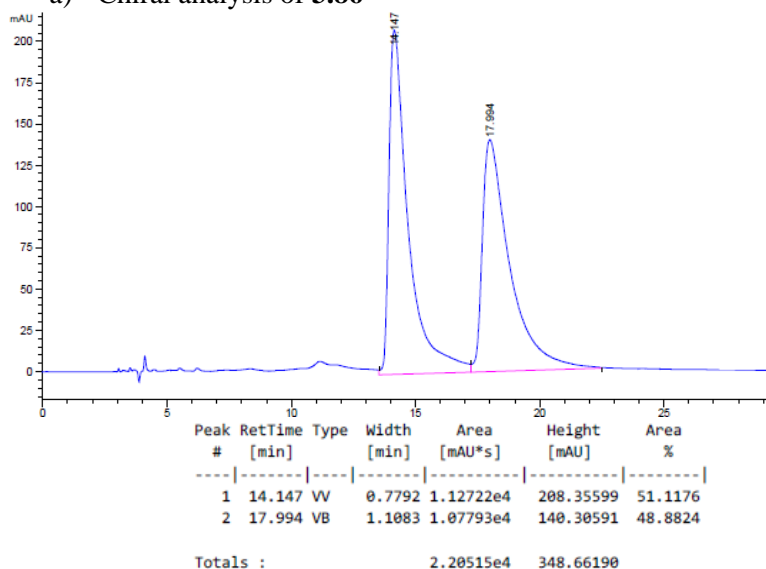


11.2 NMR of the (*S*)-configuration of the diol synthesised by a colleague

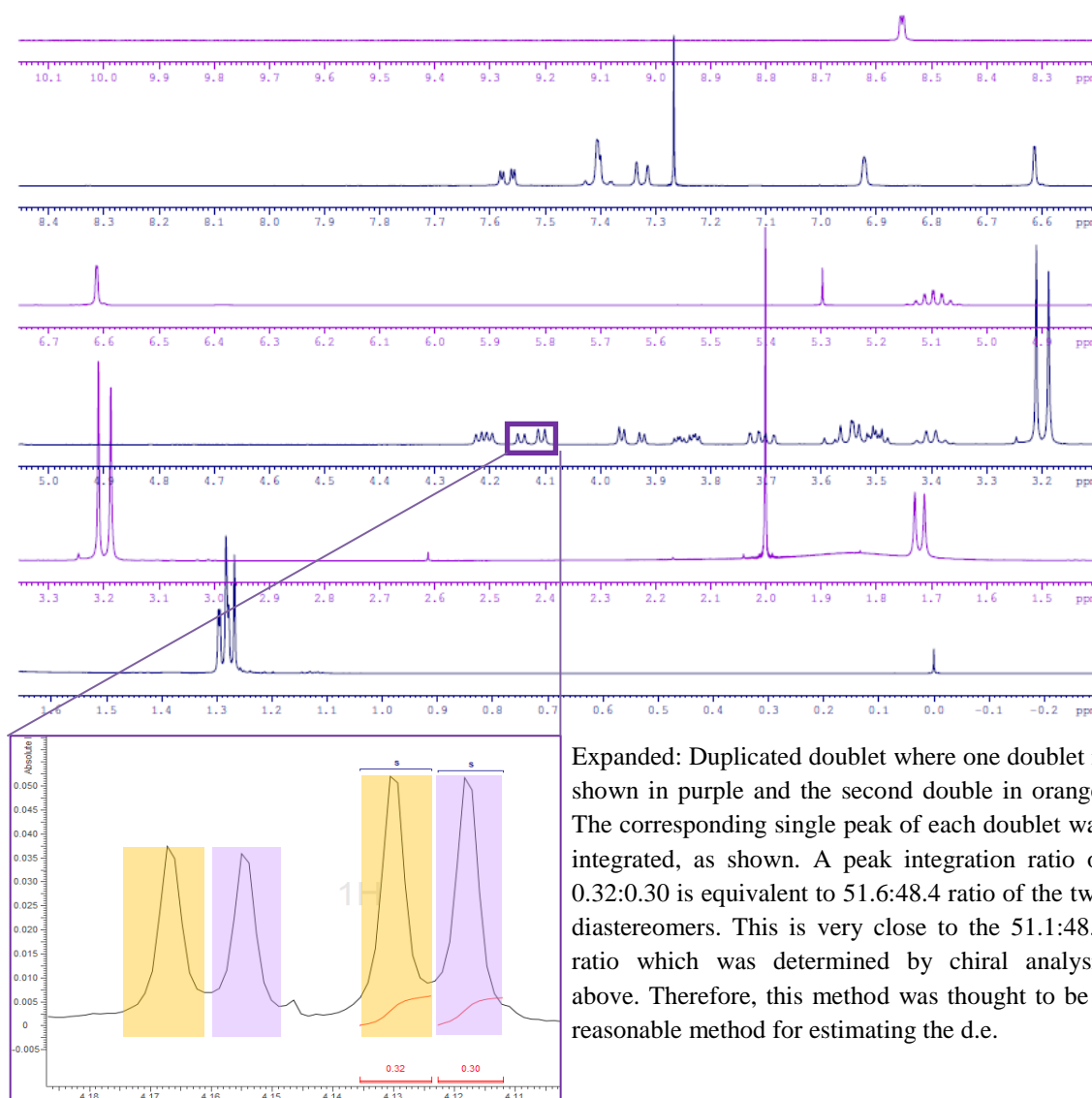


12.0 Appendix 6: Chiral analysis and NMR interpretation of Intermediate 3.86

a) Chiral analysis of **3.86**

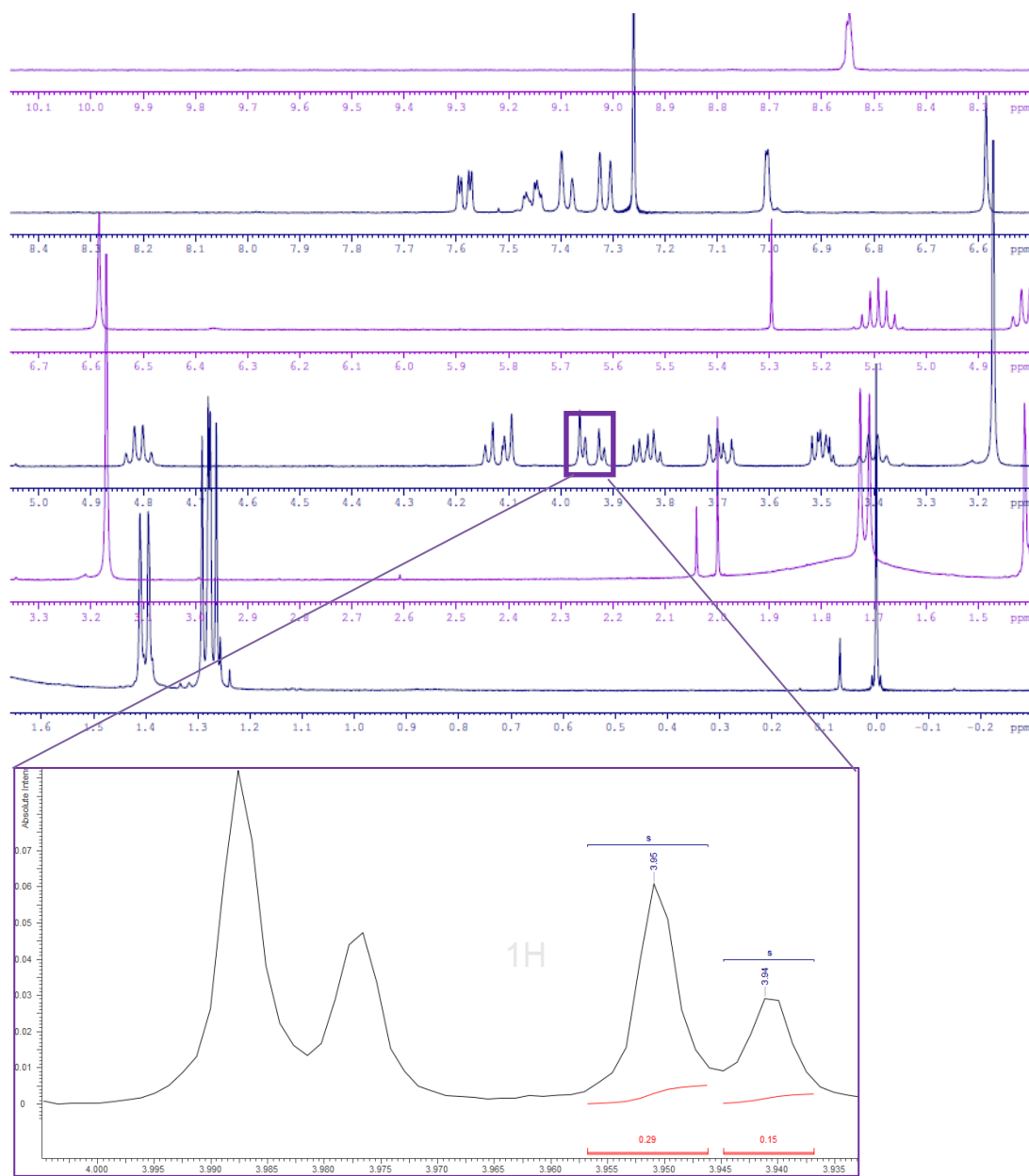


b) NMR analysis of **3.86**

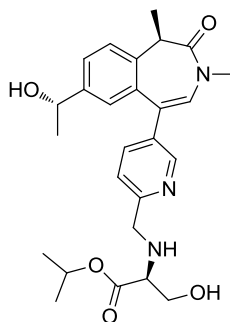


13.0 Appendix 7: NMR analyses to estimate diastereomeric excess

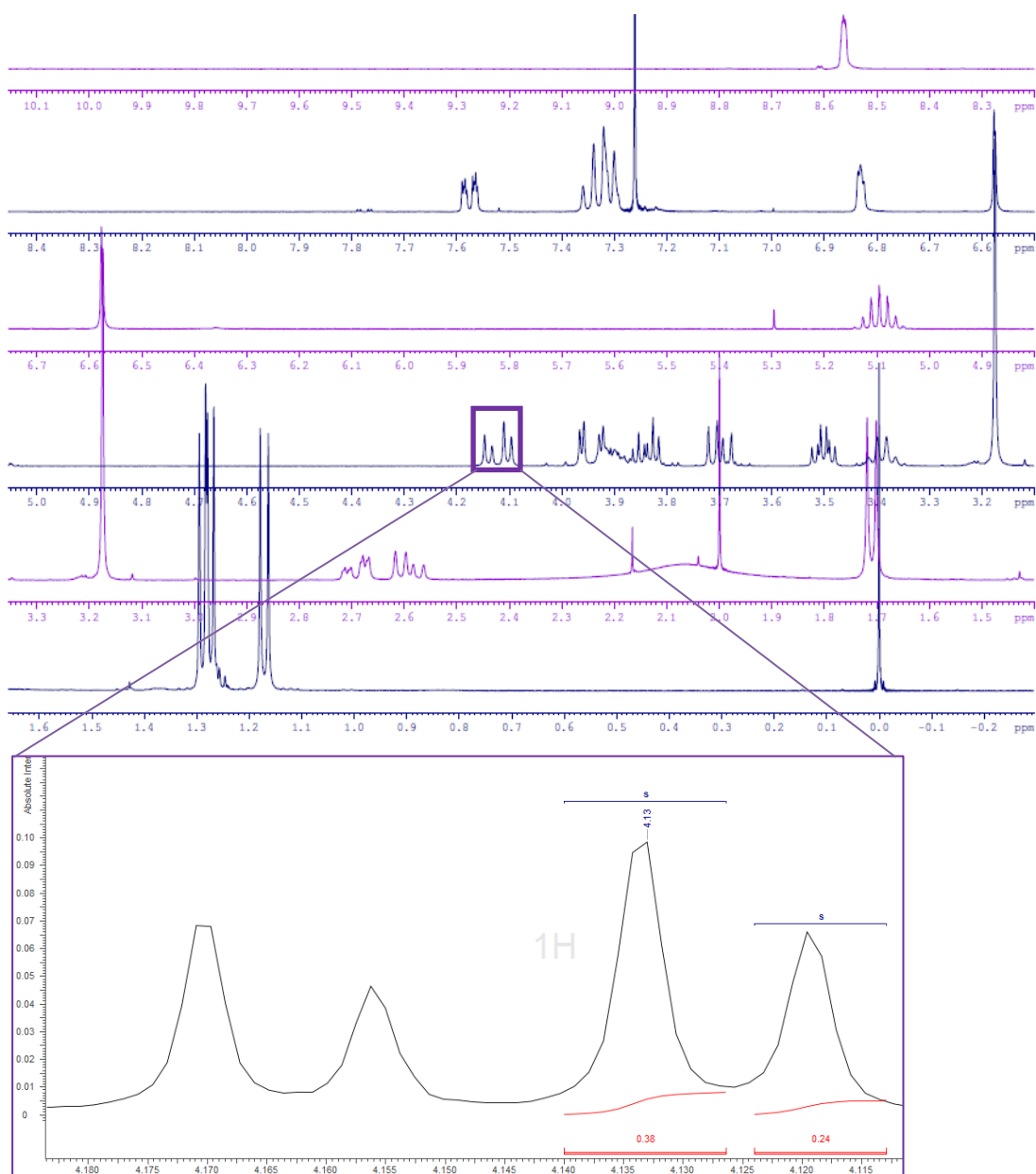
a) Compound **3.72** prior to route optimisation



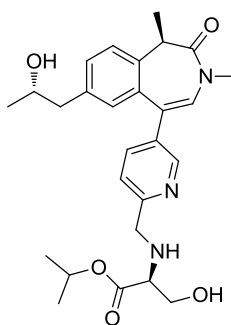
Peak ratio of 0.29:0.15 corresponds to d.r. ~ 65.9:34.1



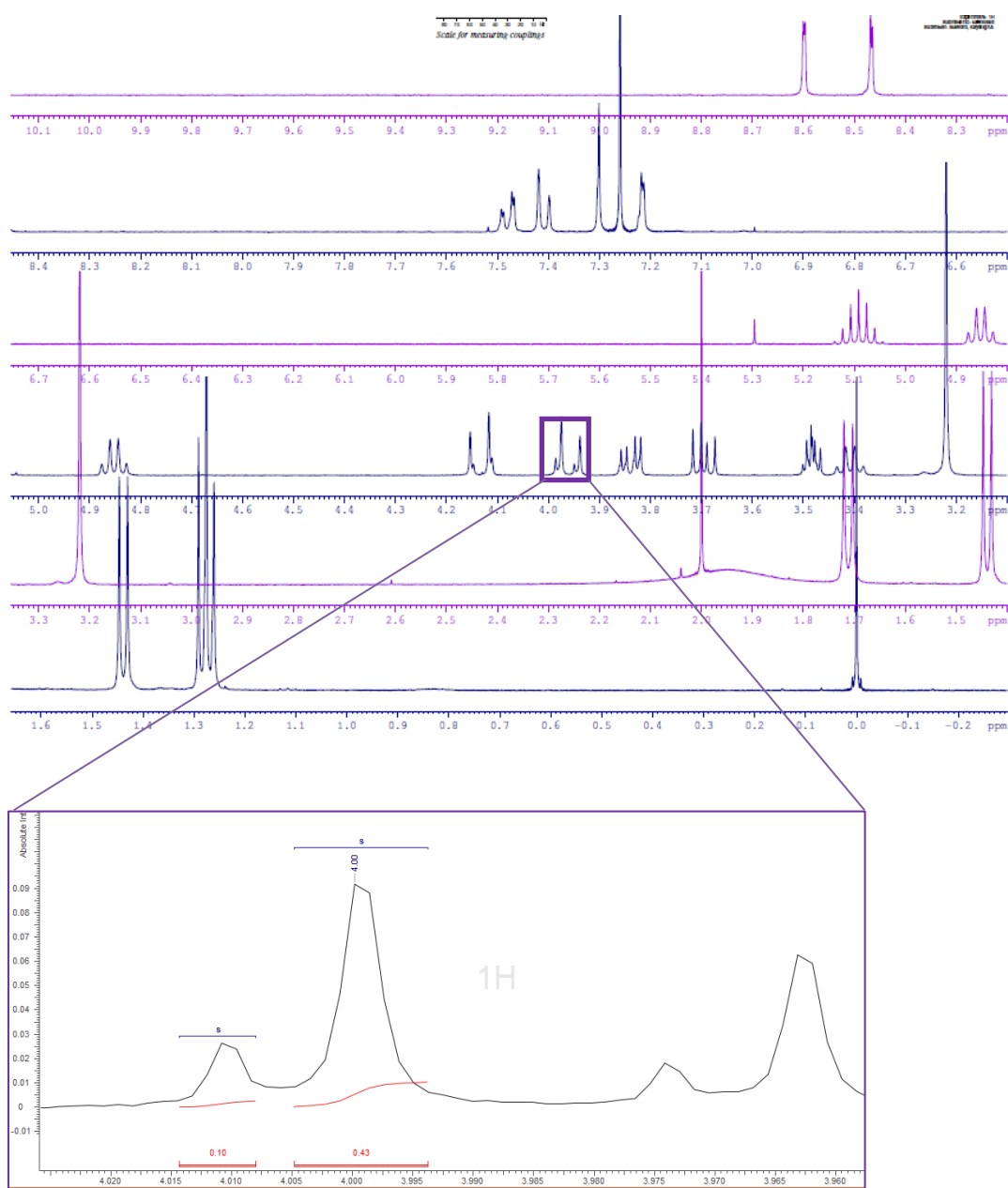
b) Compound **3.84**



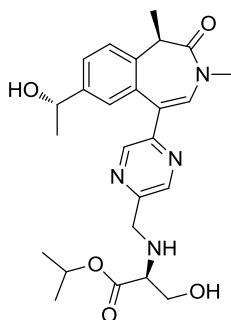
Peak ratio of 0.38:0.24 corresponds to d.r. ~ 61.3:38.7



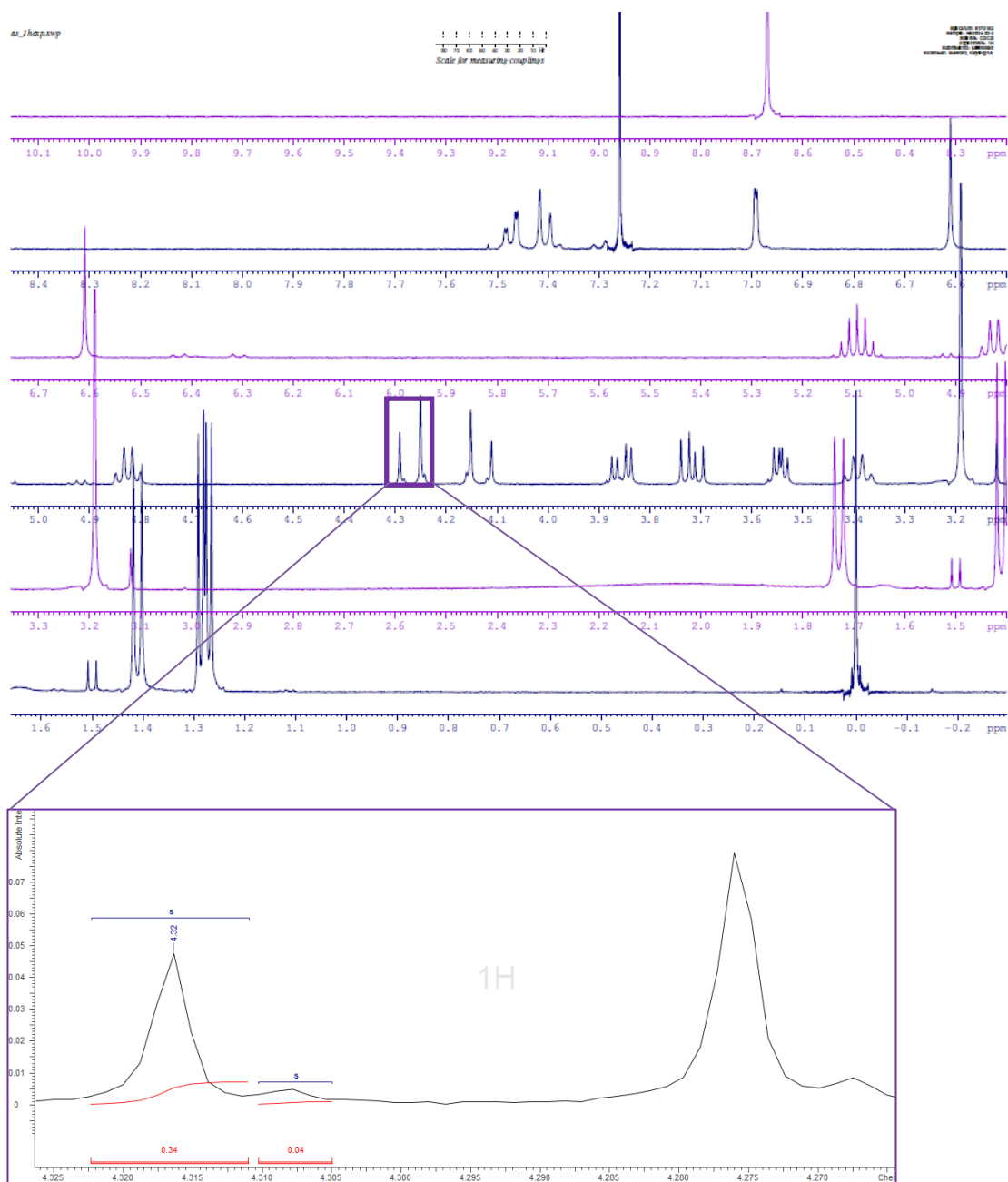
c) Compound **3.129**



Peak ratio of 0.10:0.43 corresponds to d.r. ~ 18.9:91.1



d) Compound **3.131** prior to route optimisation



Peak ratio of 0.34:0.04 corresponds to d.r. ~ 89.7:10.3

